Ph.D. Program in Civil, Chemical and Environmental Engineering

Curriculum in Structural and Geotechnical Engineering, Mechanics and Materials

Department of Civil, Chemical and Environmental Engineering

Polytechnic School, University of Genoa, Italy.

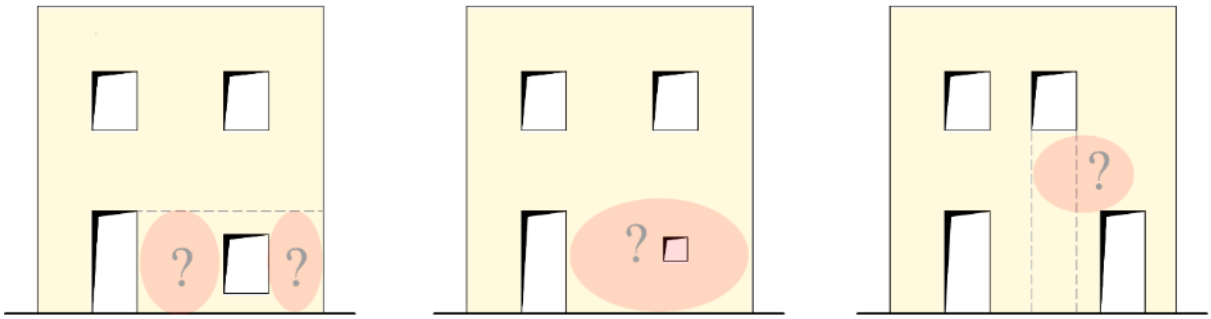

Equivalent Frame modelling of URM buildings: numerical validation and rules

Daniela Camilletti

EQUIVALENT FRAME MODELLING OF URM BUILDINGS: NUMERICAL VALIDATION AND RULES

BY

DANIELA CAMILLETTI

Dissertation discussed in partial fulfillment of
the requirements for the Degree of

DOCTOR OF PHILOSOPHY

Civil, Chemical and Environmental Engineering
curriculum in Structural and Geotechnical Engineering, Mechanics and Materials
Department of Civil, Chemical and Environmental Engineering, University of Genoa, Italy

March, 2019

Advisers:
Prof. Sergio Lagomarsino – Department of Civil, Chemical and Environmental Engineering, University of Genoa
Prof. Serena Cattari – Department of Civil, Chemical and Environmental Engineering, University of Genoa

External Reviewers:
Prof. Jan Rots – Faculty of Civil Engineering and Geosciences, Delft University of Technology
Prof. Vincenzo Sepe – Department of Engineering and Geology, University "G. D'Annunzio" of Chieti-Pescara

Examination Committee:
Prof. Gianni Bartoli – Department of Civil and Environmental Engineering, University of Florence
Prof. Anna Saetta – Department of Architecture, Construction and Conservation, IUAV University of Venice
Prof. Roberta Sburlati – Department of Civil, Chemical and Environmental Engineering, University of Genoa

Ph.D. program in Civil, Chemical and Environmental Engineering

Curriculum in Structural and Geotechnical Engineering, Mechanics and Materials

Cycle XXXI

A chi ha sempre creduto in me,
strappandomi un sorriso anche nei momenti "no".

Alla mia famiglia, alle mie tre S. e al mio D.,
che sono quanto di più caro io abbia nella mia vita.

"Se comprendere è impossibile,
conoscere è necessario."
(Primo Levi)

ABSTRACT

Within the context of the seismic analysis of masonry buildings, the application of verification procedures based on nonlinear analyses is now widespread and requires reliable and computationally efficient modelling strategies.

Among other possible techniques, the so-called “Equivalent Frame Method” (EFM) is one of the most used, especially in practice engineering. This simplified approach allows to describe the global in-plane behavior of the building and is based on the assumption that the nonlinear response of each wall is concentrated in specific masonry panels which are defined *a priori* (piers – vertical panels and spandrels –masonry beams that connect piers), while the remaining portions of the wall are usually idealized as rigid nodes.

Despite of the large use of these models, there are many aspects that should be considered in order to verify their actual reliability, especially with regard to their application to existing masonry buildings. These last, indeed, are characterized by many irregularities that represent very hard-to-model features, making the application of the EFM complicated and even questionable: presence of flexible diaphragms (vaults, timber floors), different quality of the connection between the orthogonal walls, complex geometries and irregular opening patterns that are the result of several modifications during the years. All these aspects lead to several modelling uncertainties, which are not adequately addressed by the seismic codes, even if most of them explicitly suggest the use of the EFM for the seismic analysis of masonry buildings. Regarding these aspects, the collaboration to research projects developed at national scale has allowed to directly experience the not negligible consequences of the adoption of different plausible modelling choices on the outcomes of the seismic design and assessment of masonry buildings.

Within this context, the objective of the present research is to provide a validation of the Equivalent Frame approach with regard to some of the critical issues related to its application.

In particular, the attention is focused on the first step to deal with when applying this modelling approach, that is the *a priori* identification of the structural elements geometry. This last is usually related to the opening pattern of the considered wall: although it is rather straightforward in presence of regular walls with openings perfectly aligned, it may result difficult and arbitrary in presence of irregular opening patterns. The criteria proposed in the literature to this aim are mainly empirical and have never been validated in a robust way, especially with regard to their application to walls with irregular opening layouts. Furthermore, since no standardized rules are provided by the codes, professional engineers can use different criteria for the identification of piers and spandrels, thus potentially obtaining different outcomes of the seismic assessment.

Hence, the research here presented firstly provides a systematic comparison between the different criteria available in the literature when applied to walls with different types of irregularity in the opening layout, aiming to explore their potentialities and their limits. To this aim, nonlinear static analyses are performed on case-studies structures represented by two-story walls, making comparisons in terms of global and local response as well as damage pattern between EF models and more accurate Finite Element models, whose results are considered as the reference solution. The obtained results are useful to provide specific indications about the rules for the EF schematization to be used (or avoided) depending on the types of irregularity characterizing the wall; moreover, some possible refinements are discussed, and specific original rules are outlined.

Furthermore, since the seismic design and assessment of real buildings require to perform the analyses on 3D models, where the modelling of the connections between the orthogonal walls comes into play, the deepening of this aspect is deemed necessary in the view of a robust validation of the EF model. Indeed, as highlighted also by some preliminary analyses, the modelling of the flange effect may significantly affect, depending on the adopted assumptions, the obtained structural response. Therefore, some preliminary insights about this issue have been addressed. The obtained results, even if still at initial phase, already allow to highlight some potentialities and limits of the strategies commonly used by current EF models for the modelling of URM piers with flanges, outlining possible improvements and representing the starting point for future researches.

INDEX

INTRODUCTION

The assessment of the seismic vulnerability of existing masonry buildings is today a relevant issue for all the earthquake prone countries, and a proper evaluation of their seismic behavior is therefore needed. This underlines the necessity to have good representative structural models, able to provide reliable results and at the same time associated to a reasonable computational burden, which is fundamental to make these tools available and exploitable not only at research level but also at engineering practice.

As known, masonry buildings under the seismic actions may exhibit different types of response: a global response, mainly associated to the activation of a box-like behavior and to an in-plane response of walls, and the local response of single parts, usually subjected to out-of-plane mechanisms.

The work developed in this thesis is focused on the study of the global in-plane response of masonry buildings, provided that the analysis and the verification of the local mechanisms is separately realized through specific analysis methods, models and verification procedures.

Among the models developed in literature for the analysis of the global response of masonry buildings, the so-called "Equivalent Frame Model" represents nowadays one of the most diffused. This simplified approach is based on the assumption that the nonlinear response of each wall is concentrated in specific masonry panels which are defined *a priori* (piers – vertical panels and spandrels –masonry beams that connect piers), while the remaining portions of the wall are idealized as rigid nodes. Thanks to the simplicity of implementation it requires and to its computational efficiency, in the last decades the Equivalent Frame (EF) approach has met great success not only at research level but also for practice engineering aims. The requisite of the computational efficiency is particularly relevant for the execution of nonlinear analyses, that in case of masonry structures, which show a nonlinear behaviour even at early stages of seismic loading due to the low tensile strength of masonry, are usually required. Moreover, the great spread of such a modelling strategy is promoted by the fact that the EF idealization is explicitly recommended by several national and international codes (NTC08 (2008), Eurocode 8 (CEN (2005)).

Despite of the large use of these models, there are many aspects that should be considered in order to improve their reliability and that have not yet been validated in a robust way. Indeed, the seismic codes do not provide specific indications about all the possible modelling choices the EF idealization implies, like as: the identification of the structural elements, the modelling of the diaphragms and of the flange effect, the effective length of the r.c. tie beams, the loading scheme of the floors. Furthermore, a dedicated and specific technical literature, available also to practitioners and to which the professional engineers can refer for properly applying this approach, does not exist. As a consequence, many uncertainties arise, leading to a quite arbitrary application of the method on behalf of the professionals and the analysists who commonly work with it.

For these reasons, the problem of the reliability and the correct use of these models represents nowadays a topic of great concern that is discussed in literature by several authors (Marques and Lourenço (2011), Calderoni et al (2015), De Falco et al (2017), Cattari et al (2018a)).

Within this context, the present research aims to improve the reliability of the EF approach with regard to specific problems, proposing, if necessary, some developments or defining proper indications which should accompany its application.

In particular, among the aforementioned critical issues, the attention is here focused on the problem of the *a priori* identification of the effective geometry of the structural elements (piers and spandrels), which represents the first step to deal with in the application of this modelling approach. The criteria commonly used to this aim are related to the opening pattern of the considered wall; in presence of regular walls, with openings perfectly aligned, the identification of the structural components of the frame is in general straightforward. However, it may result difficult and arbitrary in presence of irregular opening patterns (openings of different size and misaligned in the vertical and horizontal direction), thus representing a significant source of uncertainty in the application of the EF method. The current practice in this field is to consider empirical rules based on the observation of damage after past earthquakes and/or calibrated on few experimental tests or on a small number of numerical simulations, but never validated in a robust way and by considering different opening layouts.

Hence, the work here developed aims to realize a systematic comparison between the rules available in the literature, which are mainly meant for almost regular walls, when applied to walls with an irregular opening pattern, in order to explore their potentialities and their limits, and to introduce, where necessary, some specific and targeted rules.

The importance of deepening the problem of the EF schematization is stressed not only by works available in the literature (Augenti e Romano (2008), Marques and Lourenço (2011), Bracchi et al (2015)) but also by the results obtained within a research program I was involved in during these years: the "Task 4.3 - Analysis of Benchmark URM Structures" carried out within the ReLUIS 2014-2018 project – *Topic: Masonry Structures* (Cattari et al (2018a)), which showed that this modelling assumption actually affects the obtained global response, with potential repercussions on the outcomes of the seismic verifications.

The reference model adopted in the thesis for the validation of the EF approach with regard to the identification of the structural elements in presence of an irregular opening layout is based on the execution of numerical nonlinear analyses and considers as reference solution the results provided by a Finite Element (FE) model where masonry is modelled as a continuum equivalent material. Since the two employed modelling strategies work at different scales (material scale in the case of the FE model and structural element scale in the case of the EF model), a preliminary calibration of the parameters the two models are based on, performed at the scale of single panels, is necessary, in order to ensure consistency between them. To this aim, a specific procedure is defined.

After that, several case studies structures, represented by two-storey masonry walls with different irregular opening layouts, are introduced and parametric nonlinear static analyses are performed on them, making comparisons (in terms of global response, local response and damage pattern) between the results provided by EF models defined according to various assumptions with regard to the structural elements geometry and the corresponding FE model. More specifically, three different problems regarding the identification of the structural elements are faced, each one connected to specific types of irregularity in the opening pattern of the wall: the problem of the identification of the pier effective height, which is of concern especially when dealing with openings of different height at the same storey, the problem of the presence

of little openings and the problem of the identification of spandrels in walls with vertically misaligned openings or a different number of openings per storey.

Before starting with the study of the irregular walls, the introduced numerical validation procedure is applied to a regular masonry wall, in order to test it on a wall configuration where a lower scatter on the obtained results is expected.

The defined wall configurations are aimed to promote a *strong spandrel-weak pier* behavior type, thus focusing the attention mainly on masonry piers. The choice is motivated by the fact that, in addition to the problem of the definition of their effective geometry, there are still many open issues in literature on the modelling of spandrel elements, starting from the determination of proper strength criteria. Thus, to face all these critical issues at the same time it would not have allowed to achieve conclusive results even in the case of masonry piers. Anyhow, the spandrels, even if resistant, come into play as deformable elements, so that it is possible to make some considerations about their identification, providing indications which may be useful for these specific cases.

Furthermore, it is worth highlighting that in this work the aspect of the seismic verification is not directly faced, being the attention focused on the modelling in all its aspects. However, it is evident that the availability of a numerical model able to provide accurate results in terms of both local and global response represents the essential preliminary step for the execution of the seismic verifications needed for the assessment and the design of the masonry buildings.

After the in-depth validation of the EF approach with respect to the above mentioned aspects, being aware that the seismic design and assessment of real buildings require to perform the analyses on 3D models, where the modelling of the connections between the orthogonal walls comes into play, some preliminary insights about the problem of the modelling of the flange effect have been addressed.

The necessity to deepen this topic is further motivated by the results obtained within both the previous cited research project and another research activity I had the possibility to join, the RINTC project (Manzini et al (2018), Cattari et al (2018b)). In particular, the latter showed that the adoption of different modelling hypotheses in the EF models about how the flange effect is managed has not negligible repercussions on the outcomes of the seismic assessment and design of masonry buildings. Therefore, the deepening of this issue, even if in a preliminary way, is deemed necessary in the view of a robust validation of the EF model.

In this case, in particular, the aim is to investigate the simplified modelling strategies commonly adopted in the EF models for the description of the behavior of URM piers with flanges, highlighting their potentialities and, if present, their limits.

The adopted methodology always refers to the introduced numerical validation approach; therefore, it is based on the execution of numerical analyses and on comparisons with the results of FE models, considered as the reference “exact” solution. Even if for the moment no codified modelling rules are proposed regarding this issue, the obtained results already allow to suggest some possible strategies of improvement that could be included in the EF models and that will represent the starting point for future researches on this topic.

Finally, the structure of the thesis is outlined.

In **Chapter 1** a general overview of the modelling strategies for the seismic analysis of masonry structures is provided, focusing on models commonly adopted for the analysis of the global response, and in particular on the Equivalent Frame approach. Regarding this last, a state of the art about the different critical issues involved in its application, including an overview of the available rules for the EF schematization as well as a literature survey on the issues related to the modelling of walls with flanges, is provided.

In **Chapter 2** the relevant experiences of the two above cited research projects I was involved in are described, underlining those aspects and results which were more significant for addressing the insights and the analyses made in this thesis.

In **Chapter 3** the numerical approach adopted for the validation of the EF method is detailed, describing in particular both: the procedure applied for the calibration of the parameters in the Finite Element Model adopted as reference solution; and the criteria used to carry out the comparison at global (pushover curve, damage pattern) and local (in terms of generalized forces and drift on panels) scales.

While in Chapter 3 the procedure is at first applied to a regular URM wall, in **Chapter 4** the discussion of the main results on the irregular wall configurations is presented.

In **Chapter 5** the results of the analyses on the masonry piers with flanges as well as the generalization of specific modelling rules concerning pier elements are presented. The latter are aimed to deepen some specific issues that have come out from the analysis of the irregular walls presented in Chapter 4.

At last, in **Chapter 6** the conclusions and the outlooks for future researches are discussed.

CHAPTER 1

1 MODELLING THE SEISMIC RESPONSE OF URM BUILDINGS

The modelling of the seismic response of masonry buildings represents today one of the most important field of research in civil and conservation engineering area.

Despite of the efforts of the scientific community, there are still strong uncertainties when dealing with structural behavior of masonry, much larger than for steel or reinforced concrete constructions. The difficulty in modelling such structures depends on several peculiar factors which characterize masonry buildings, differentiating them from other structural typologies.

First of all, one of the main issues is represented by the composite nature of masonry, which is a heterogeneous material made up of a complex system of blocks and joints. For this reason, its behavior strongly depends on both mechanical characteristics of constituents (stiffness and strength of blocks and joints) and rules of construction of the assemblage. It is worth noting that many different types of materials can be used: typical units are bricks, blocks, ashlars, adobes, irregular stones and others, while mortar joints (when present) can be made of clay, bitumen, chalk, lime/cement-based mortar, glue or other materials. Moreover, also the techniques that may be adopted for assembling together the materials are numerous, and the quality of the execution may vary depending on the skills and care of manufacturers (e.g. mortar joints perfectly or not perfectly filled). As a consequence, many typologies of masonry can be found, especially when dealing with existing buildings, generated by different possible combinations of the geometry, nature and arrangement of units as well as the characteristics of mortar. As an example, there may be regular masonries made of bricks and perfectly-executed bed and head mortar joints but also irregular masonries characterized by stones with variable shape and dimension, assembled together with or without mortar joints. Still, masonry is characterized by a significantly large variability of mechanical properties, due to workmanship and to the use of natural materials, which both make it less standardized with respect to other construction materials (Figure 1.1).

In addition, the mechanical behavior of the different types of masonry has generally a common feature: a very low tensile strength, which causes the onset of cracking phenomena for low levels of stress and, therefore, a nonlinear behavior even at early stages of external actions such as the seismic loading. As known, masonry buildings are characterized by a significant seismic vulnerability, showed during recent and past earthquakes occurred in many different countries all over the world, including Italy ((D'Ayala and Paganoni (2011), Cattari et al (2012), Brandonisio et al (2013), Penna et al (2014a), Fragomeli et al (2017), Sorrentino et al (2018)). As a consequence, when dealing with the seismic design and assessment of masonry structures nonlinear analyses should be adopted (Lagomarsino and Cattari (2015a)); indeed, they actually represent the most suitable tool for the description of the behavior of such structures under horizontal actions. It is worth noting that, in the last decade, the achievement of performance-based earthquake engineering concepts has led to an increasing utilization of analysis methods and verification procedures based on the execution of nonlinear analyses for the evaluation of the seismic performances of masonry buildings.

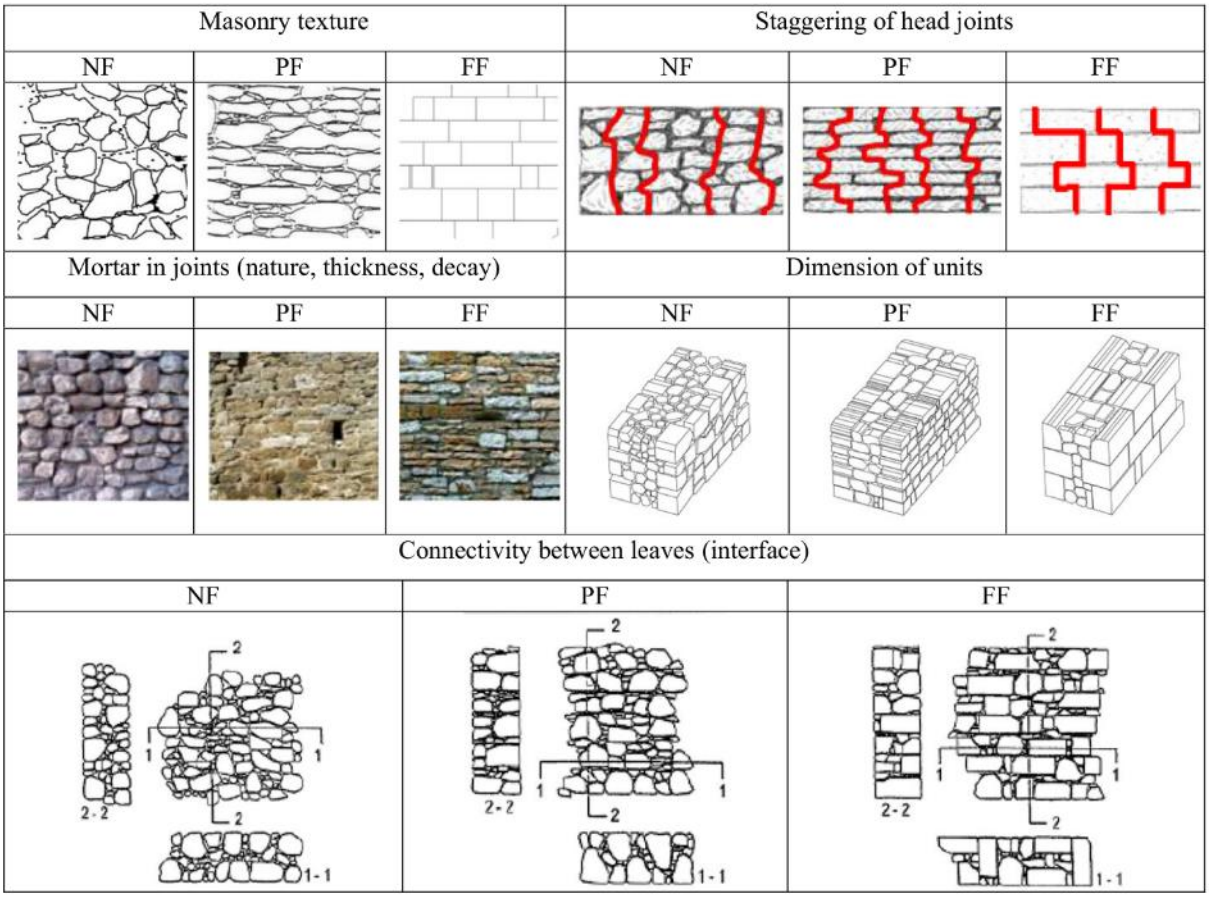

Figure 1.1 - Classification of masonry following visual inspection according to the RELUIS methodology for the assessment of the quality of built masonry, where: *NF* refer to Non-Favourable type of masonry; *PF*- Partly-Favourable type of masonry and *FF*- Fully-Favourable type of masonry (after Giuffrè (1993); Borri (2006); Binda and Cardani (2007); Lagomarsino and Magenes (2009); Bosiljkov et al (2010)); from Kržan et al (2015).

They mainly refer to incremental static procedures, but also nonlinear dynamic analyses can be adopted (as recently suggested in CNR-DT 212/2013 (2014) for a probabilistic assessment). The nonlinear static procedures (Coefficient Method (ASCE/SEI (2014)), Capacity Spectrum Method (Freeman (1998), N2 Method (Fajfar (2000), Eurocode 8, Part 1 (CEN (2004a), synthetically named in the following EC8-1), NTC08 (2008)) are in general the most widely diffused, being suggested also in several seismic codes. As well-known, these procedures are based on a comparison between the displacement capacity of the structure and the displacement demand of the predicted earthquake, which depends on the dynamic properties of structure, subsoil and site. Definition of the displacement capacity requires the evaluation of a force-displacement curve ("pushover" curve) able to describe the structural global response to horizontal forces and to provide essential information on the structural behavior in terms of stiffness, overall strength and ultimate displacement capacity. This curve can be obtained by subjecting the structure, idealized through an adequate model, to static distribution of lateral loads (simulating the seismic inertial forces). Further details about the nonlinear static analysis and other methods commonly adopted for the seismic analysis of masonry buildings are provided in Chapter 2 (section 2.2).

From these considerations, it is evident the need of models capable to describe the seismic response of masonry structures until very high states of damage, and providing a good balance between accuracy and

efficiency, which means that they should describe the nonlinear behavior of masonry with a reasonable computational burden. This is fundamental also to make these tools available and exploitable not only at research level but also in engineering practice. However, it is not an easy task.

During the years, several methods and computational tools have been developed for the seismic analysis of masonry buildings, based on different theories and approaches and resulting in different levels of complexity. Concerning them, it is important to highlight that a complex analysis tool does not necessarily provide better results than a simple tool (Lourenço (2002)). Indeed, on one hand there are "theoretical" approaches able to describe in a very detailed way the material behavior at the micro-scale but unable to solve problems at the scale of the construction (due to the complexity and the computational effort required, especially when nonlinearity is included). On the other hand, there are "engineering-based" approaches that, by describing the behavior of the material through a phenomenological approach, allow to perform analyses at the scale of the construction but may provide unreliable results for certain structural and load configurations; furthermore, in most cases they are based on very simplified hypotheses, so that the reliability of their predictions depends on the consistency between such hypotheses and the structure actually examined. Some approaches require only few input parameters but provide a rough representation of the structure; on the contrary, some others are able to give an accurate description of the nonlinear behavior but require a large number of constitutive parameters, and often some of them do not have a clear physical meaning and are therefore difficult to calibrate.

Another important aspect which has to be taken into account when modelling masonry structures, especially in the case of the existing ones, is the geometric complexity of the configurations. Indeed, existing masonry buildings are often the product of several transformations occurred during the years, such as expansions, demolitions of specific parts, introduction of new openings in the walls or infilling of existing ones, formation of complex building aggregates, addition of further levels. For this reason, masonry buildings often appear as complex structures in which it is difficult even to identify a clear structural scheme. Therefore, specific *in-situ* investigations are essential when dealing with the assessment of existing structures, as explicitly suggested in the instructions for the application of the Italian building code (MIT (2009)), where a precise methodological path with specific rules to properly guide and address the knowledge process is imposed. However, the complexity of the real situations inevitably poses several issues about the correct way to model specific aspects and structural details, thus leading to many uncertainties in the definition of the structural models (as discussed in section 1.3 and in Chapter 2, within the context of the Equivalent Frame models, that represent the focus of this thesis).

With regard to the actual behavior of masonry buildings under the seismic actions, damage survey after past earthquakes showed that in presence of walls with good masonry quality (namely where chaotic failures of the walls can be neglected), two main and different types of response can occur, as illustrated in Figure 1.2:

- the global seismic response of the structure, mainly associated to the activation of a box-like behavior and to an in-plane response of walls (the so-called "second mode" mechanisms (Giuffrè (1993));
- the local response of single parts (usually subjected to out-of-plane mechanisms, also called "first mode" mechanisms).

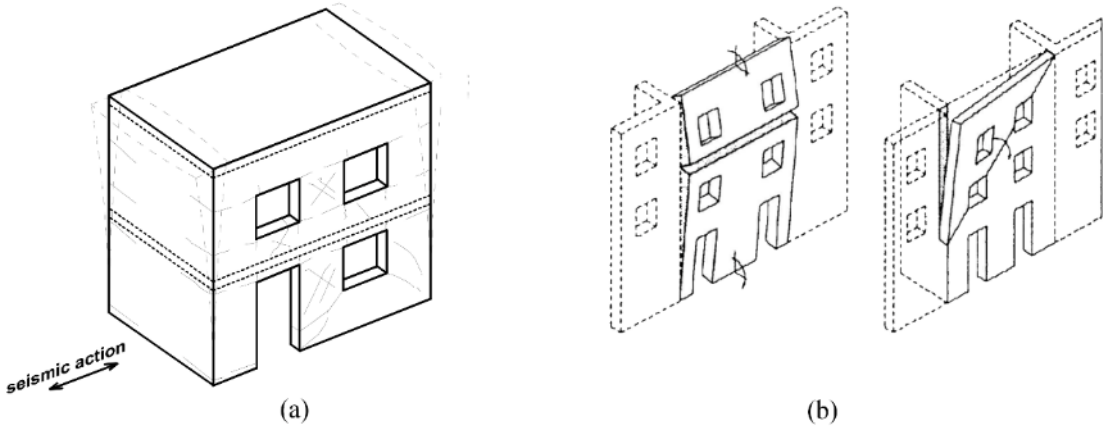

Figure 1.2 – Global (a) and local (b) response of a masonry building (adapted from Magenes (2006) and D'Ayala & Speranza (2003)).

It is evident that during an earthquake both these types of response may simultaneously occur, and that an exhaustive seismic verification would take into account both of them. However, it is generally recognized - and adopted in common practice in the literature and codes – that a satisfactory assessment may be obtained by analysing them separately, neglecting the interactions that may occur. This assumption is effective especially in the cases where the out-of-plane response is characterized by the activation of overturning mechanisms involving limited portions of the walls.

In particular, the "first mode" mechanisms are often referred to as "local mechanisms", in the sense that they are usually associated to the local response of structural elements/macroelements, which could in turn generate a global collapse but can be studied in first instance without recurring to a global structural model of the whole structure. Conversely, in case of global seismic response, where the resistance of the building to horizontal actions is provided by the combined effect of the in-plane capacity of walls and the connection and load-transfer capacity of floors, a 3D model is in general necessary.

Moreover, the study of the two types of response is usually conducted through different analysis and modelling approaches. In the case of the global response the analysis methods which is possible to adopt may be linear and nonlinear, static and dynamic, applied to the 3D model of the building (a more detailed description of these methods can be found in Chapter 2, section 2.2). On the other hand, with specific reference to the analysis methods for local mechanisms, the Italian building code (hereinafter referred to as NTC08 (NTC08 (2008)) proposes the adoption of a kinematic linear and nonlinear approach, basically founded on the Equilibrium Limit Analysis.

The work developed in this thesis is focused on the study of the global in-plane response of unreinforced masonry (URM) buildings, faced through the adoption of 3D structural models, provided that the analysis and the verification of the local mechanisms is separately realized through specific analysis methods, models and verification procedures. Considering that, in the following (section 1.1) a general overview of the modelling strategies which can be adopted for the seismic analysis of masonry structures is provided, focusing on models commonly adopted for the analysis of the global response (section 1.2). Among them, particular attention is given to the Equivalent Frame (EF) approach, which represents the framework

towards which the research here developed is addressed. More specifically, the main features of this modelling technique as well as the hypotheses on which it is based are discussed; then (section 1.3) the attention is focused on specific critical issues and modelling uncertainties involved in the application of the EF approach, with emphasis on the aspects investigated in this thesis, i.e. the EF idealization of masonry walls (for which a detailed review of the state of the art is proposed (section 1.3.1) and the modelling of the connections between the orthogonal walls.

1.1 MODELLING STRATEGIES FOR URM BUILDINGS: OVERVIEW

Several models are proposed in literature for the modelling of masonry structures, characterized by different levels of simplifications (Lourenço (2002), Roca et al (2010)).

These models can be classified (Calderini et al (2010)) following two criteria (Figure 1.3): scale of analysis (whether material or structural element one) and type of description of masonry continuum (whether continuous or discrete). It is evident that this classification is not exhaustive, since not all the models available in the literature can be included in the considered classes and hybrid cases are always possible.

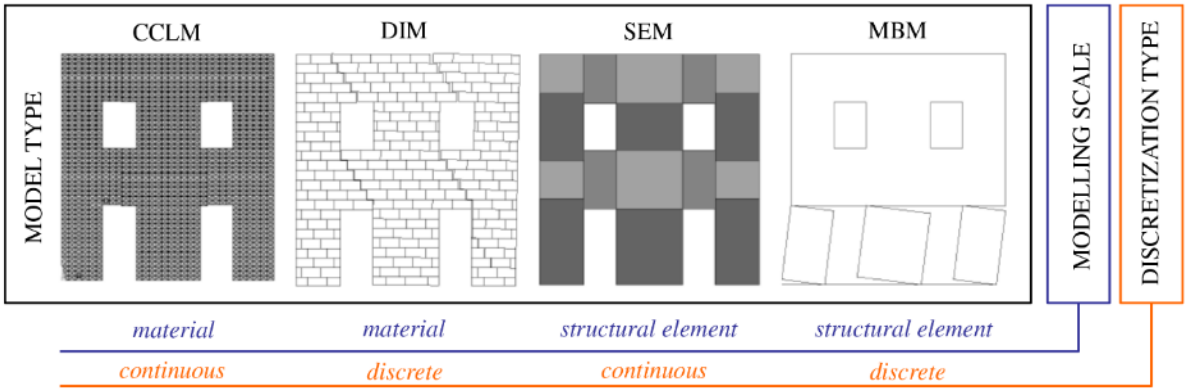

Figure 1.3 – Classification of modelling strategies for masonry buildings (from Lagomarsino and Cattari (2015b)).

Models developed at *material scale* are oriented to describe in an accurate way the complex behavior of masonry solids. At this scale, a fundamental role is played by the composite nature of the material, which may be considered whether like heterogeneous or homogenous, thus obtaining two types of models:

- Discrete Interface Models (DIM), where the material is considered as heterogeneous (*discrete approach*);
- Continuum Constitutive Law Models (CCLM), where the material is considered as homogeneous (*continuous approach*).

In particular, the use of Discrete Interface Models (also referred to as "micro-models") represents a very accurate approach, where the description of the behavior of the material is faced without adopting any simplification: each single constituent (blocks and mortar joints) is modelled separately and then assembled with the others by means of interface elements. The primary aim of this modelling approach is to closely represent masonry from the knowledge of the properties of each constituent and the interface. Within this

context, also more simplified approaches are possible, in which only units and joints elements, reduced to zero-thickness interfaces, are present (commonly referred to as "simplified micro-modelling approaches", Roca et al (2010)). However, these techniques require a large computational effort and their use is in general limited to small substructures.

In the Continuum Constitutive Law Models (usually defined as "macro-models"), the interaction between units and mortar is neglected and a more synthetic description of the masonry material, regarded as an equivalent homogeneous material, is provided through continuum constitutive laws. Despite being less detailed, such models may be extended to larger structural portions and represent a valid option also for complex geometries. However, since for a reliable representation of the structural behaviour the use of nonlinear constitutive laws is needed, the problem of the significant computational effort is still present.

Moving to the models developed at *element scale*, in this case the driving idea is to identify, within the masonry continuum, portions of structure subjected to recurrent damage modes: to this aim, post-earthquake damage observation is a remarkable source of information. The masonry structure is thus not seen as a "blurred" continuum but a set of bodies with common mechanical behaviors. Also at this scale of analysis, two different approaches are usually adopted, thus leading to two families of models:

- Macro-Block Models (MBM), based on a *discrete approach*;
- Structural Elements Models (SEM), based on a *continuous approach.*

More specifically, in the Macro-Block Models the behavior of a set of masonry bodies, connected through interfaces, is considered. The shape of each body is defined on the basis of recurrent crack patterns observed in the observation of damage occurred after past earthquakes. Each masonry body is commonly assumed as rigid and nonlinear behavior is concentrated at the interfaces, which are assumed as non-resisting tension joints, capable, in some cases, to transfer frictional forces.

In the Structural Element Models (also referred to as "macroelement models") the identification of macroscopic structural elements, whose behavior is described through a limited number of static and kinematic variables, is required. The macroelements represent damage, cracking, sliding and rotations in predefined zones which are characterised based on mechanical assumptions and implementation of more or less sophisticated nonlinear constitutive laws. The Structural Element Models, in which the Equivalent Frame models are included, have the advantage of being characterized by few parameters and by a reduced computational effort regarding the modelling and the structural analysis phases. Nevertheless, they assume that the damage of elements can occur only in the concentrated zones established by the user before the analysis, while the other elements remain undamaged.

The choice of the modelling strategy to use, among those now discussed, depends in general on the type of the building seismic response (Calderini et al (2010), Lagomarsino and Cattari (2015b)), which, as previously introduced, can be characterized by in-plane and out-of-plane mechanisms. More in detail, for both of these two types of response (global and local) models with different degree of accuracy may be adopted. Even if this distinction has not to be intended in a strict way, in general discrete models (MBM and DIM) are used to describe local mechanisms, while continuous models (SEM and CCLM) are particularly suitable to analyse the global response of buildings. Indeed, regarding in particular the study

of the global response, the adoption of Discrete Interface Models, that are in principle applicable to whole buildings, in most of the cases leads to a computational effort which is not feasible from an engineering point of view; on the other hand, discrete Macro-Block Models seem to be applicable only in extreme cases in which the global response turns out in fully independent masonry walls that can be analysed separately.

Since this work is oriented to the analysis of the global response of URM buildings, in the following the attention will be focused on the Continuum Constitutive Laws Models (CCLM) and on the Structural Elements Models (SEM), providing also a critical comparison between these two approaches, based on different modelling scales. It is stressed that the two constitutive models adopted for the parametric analyses performed in this thesis belong to these two types of approaches, and are used, as better explained in Chapter 3, with different aims: one (the Equivalent Frame model) is the object of the investigation, while the other (the Continuum Constitutive Law Model) is the tool used for its validation.

1.2 MODELS FOR GLOBAL RESPONSE

As afore introduced, the global response of a masonry building is strictly related to both the in-plane capacity of vertical structural elements (walls) and the connection and load transfer effect due to horizontal structural elements (floors). As a consequence, the structural analysis requires 3D models.

1.2.1 Continuum Constitutive Law Models

In general, the Continuum Constitutive Law Models (CCLM) allow to simulate the response of masonry structures with a degree of accuracy greater than Structural Element Models. In these models, masonry is considered as a fictitious homogeneous material while the structure is described by means of a continuous mesh of 2D or 3D Finite Elements. Regarding the definition of the continuum constitutive laws aimed to describe the behavior of the material, many different formulations have been developed and are proposed in the literature; they are substantially represented by nonlinear constitutive laws, which, as before introduced, are actually the most suitable for the description of masonry behavior.

It is stressed that a comprehensive review of the nonlinear continuum models proposed in the literature for masonry material is beyond the scope of this thesis, being these models here used as validation tools and not as the object of investigation. Therefore, in the following a general overview of the most diffused and different types of approaches is reported; a detailed review of these type of models can be found in Calderini et al (2010) and in Roca et al (2010).

First of all, depending on the assumptions on which they are based, the continuum constitutive laws can be classified as isotropic or anisotropic. With reference to this aspect, it is stressed that the adoption of an anisotropic or of an isotropic constitutive law should depend, in general, on the features of the masonry under consideration. Indeed, as previously introduced, masonry is characterized by a huge variety of typologies: there may be regular masonries, made up of a regular arrangement of bricks and mortar joints, whose behavior is strongly anisotropic, but also irregular masonries, characterized by a chaotic arrangement of blocks and joints, such as in the case of stone irregular masonry, whose behavior is almost isotropic.

Moreover, in order to define the continuum constitutive laws, two approaches are commonly adopted: a phenomenological or a micromechanical approach.

In the micromechanical approach the global mechanical response of the composite material is usually obtained by adopting homogenization procedures, that is studying a representative volume element (RVE) of the heterogeneous material and then determining the constitutive laws of the homogenized equivalent material. This approach is used in general in case of regular and periodic masonry, where the identification of the RVE is rather simple. Another possibility in this field is to describe the response of the continuum material through multi-scale techniques, which consist in the structural modelling through different scales. Within this context, in general, two scales are used: one at the continuum mechanics structural level and the other at the material level. However, the use of these techniques is rather complex since it requires to solve the micromechanical problem and to adopt the obtained results in order to perform the structural analysis, involving processes of upscaling (in order to move from the micro-scale to the macro-scale) and downscaling (used for passing from the macro-scale to the micro-scale). Simplified multi-scale techniques, in which the microstructural behavior of masonry is related to the continuum through simplified micromechanical analysis, have been presented by Gambarotta and Lagomarsino (1997b) and by Calderini and Lagomarsino (2008). These two models, in particular, have been specifically developed for describing the behavior of brick masonry, and are therefore particularly suitable in case of regular masonry with a strong anisotropy. The first one, which is a continuum damage model based on the mortar joint model described in Gambarotta and Lagomarsino (1997a), refers to the hypothesis of plane stress condition and considers only the inelastic strains in the mortar bed joints and in brick units, thus ignoring the mechanisms of inelastic deformation involving the head joints together with the bed joints. In Calderini and Lagomarsino (2008) the contribution of the mechanisms of inelasticity involving the head joints (opening and closing) is introduced, thus giving the possibility to describe also stair-stepped shear failure modes (due to sliding along bed and head joints).

Moving to the phenomenological approach, in this case the behavior of the material is defined on the basis of experimental tests on large-scale specimens, which directly provide stress-strain relationships and limit domain. Within this context models can be based on plasticity, damage, smeared cracking or a combination of these. Since they are not based on a model of the microstructure, they usually need a careful calibration of the parameters. The phenomenological models adopted for masonry are usually borrowed from those developed for concrete, in most cases represented by isotropic constitutive laws, particularly suitable to model non-periodic and irregular masonry (for which the application of homogenization techniques is difficult). The smeared crack approach, in particular, was originally developed for the study of the fracture behavior of reinforced concrete structures that may exhibit diffuse crack pattern (De Borst et al (1993)). It is based on the idea to represent the crack opening as an equivalent strain; therefore, the cracked solid remains continuum, and its discretization is fixed during the whole analysis. A crack in a point is initiated orthogonally to the direction of the maximum principal stress when it overcomes the tensile strength and is not localized in a specific line, but it is spread, literally ‘smeared’, over a finite region; then, the cracking effects are described in terms of stress–strain law.

In the field of plasticity laws, an isotropic model which uses concepts of damaged elasticity in combination with tensile and compressive plasticity is the Concrete Damaged Plasticity (CDP) model developed by Lubliner et al (1989). Always considering the field of plasticity laws, in Lourenço et al (1997) a phenomenological orthotropic model capable of predicting independent inelastic responses along the

material axes and whose parameters can be determined through targeted experimental tests (Lourenço et al (1998)) is proposed.

In the light of these considerations the selection of the continuum model to use may depend on several factors: first of all the type of masonry which has to be considered in the numerical simulations, that can be regular or irregular (and, therefore, with a prevailing anisotropic or isotropic behavior, respectively), the availability of experimental data necessary for the determination of the constitutive parameters, the associated computational burden as well as the capacity of convergence also for advanced nonlinear phase, which is fundamental in case of masonry in order to fully understand failure mechanisms and reliably assess the structural safety (especially considering the necessities of the performance based design and assessment).

Regarding the choice of the continuum constitutive model to use for the analyses here performed, it is worth noting that, for the aim here pursued, which is to perform a validation of the Equivalent Frame approach when applied to specific critical situations, the simulation of a specific masonry typology is not strictly necessary. Indeed, the fundamental aspect is, once defined the masonry type to take as reference, to adopt as much as possible the same hypotheses and boundary conditions in the two considered models and to assume coherent parameters in the two modelling strategies (through a proper calibration, as better explained in Chapter 3), in order to focus the attention only on the aspects under examination. Moreover, since for this research it is important to investigate the response of masonry buildings up to collapse, a fundamental prerequisite is to use constitutive laws and convergence algorithms able to explore increasing damage levels and computationally efficient, in order to perform the parametric analyses needed. For these reasons the isotropic Concrete Damaged Plasticity (CDP) model previously introduced was adopted, whose good performances in describing the response of the masonry material until high level of damage have been proved in several previous studies, including the simulation of complex historical masonry structures (Milani and Valente (2015), Valente and Milani (2016), Casolo et al (2016), D'Altri et al (2017), Fortunato et al (2017), Milani et al (2017), Castellazzi et al (2018), Degli Abbati et al (2019)).

1.2.2 Structural Element Models

Even if the CCLM allow to simulate the response of masonry structures with a degree of accuracy greater than structural elements models, their employment in practice presents some problems, first of all for the large computational burden they require. Therefore, often the use of SEM is preferred, especially at engineering practice: these approaches, indeed, allow to perform nonlinear analyses (both static and dynamic) with a reasonable computational effort and to govern "better" the response due to the limited number of mechanical properties involved.

As previously introduced, the technique is based on the identification in each wall of macroscopic structural elements (masonry portions defined as "piers" and "spandrels"), defined from a geometrical and kinematic point of view through finite elements (shells or frames) and from a static point of view through their internal forces. The static equilibrium of the element can be formulated with reference to the internal force resultants instead of the continuum stress. Piers are the principal vertical resisting elements for both dead and seismic loads; spandrels, which are intended to be those parts of the walls between two vertically

aligned openings, are secondary horizontal elements (for what concerns vertical loads), coupling the response of adjacent piers in case of seismic loads.

Among the Structural Element Models, the so-called Equivalent Frame models are the most widely diffused. They consider the walls as an idealized frame, in which deformable elements (piers alone or piers and spandrels), where the nonlinear response is concentrated, connect rigid nodes (parts of the wall that are not usually subjected to damage). The modelling of the whole structure is obtained by assembling masonry walls (idealized as 2D frames), of which, in most of the cases, only in-plane response is modelled, and horizontal floors (that may be assumed as rigid or deformable, as discussed in section 1.3). Figure 1.4 illustrates a sketch aiming at representing the wall idealisation into an assemblage of structural elements. In particular, in this figure different solutions are shown: i) simplified models, in which only the pier elements are modelled, and ii) the actual Equivalent Frame models, that consider both pier and spandrel elements.

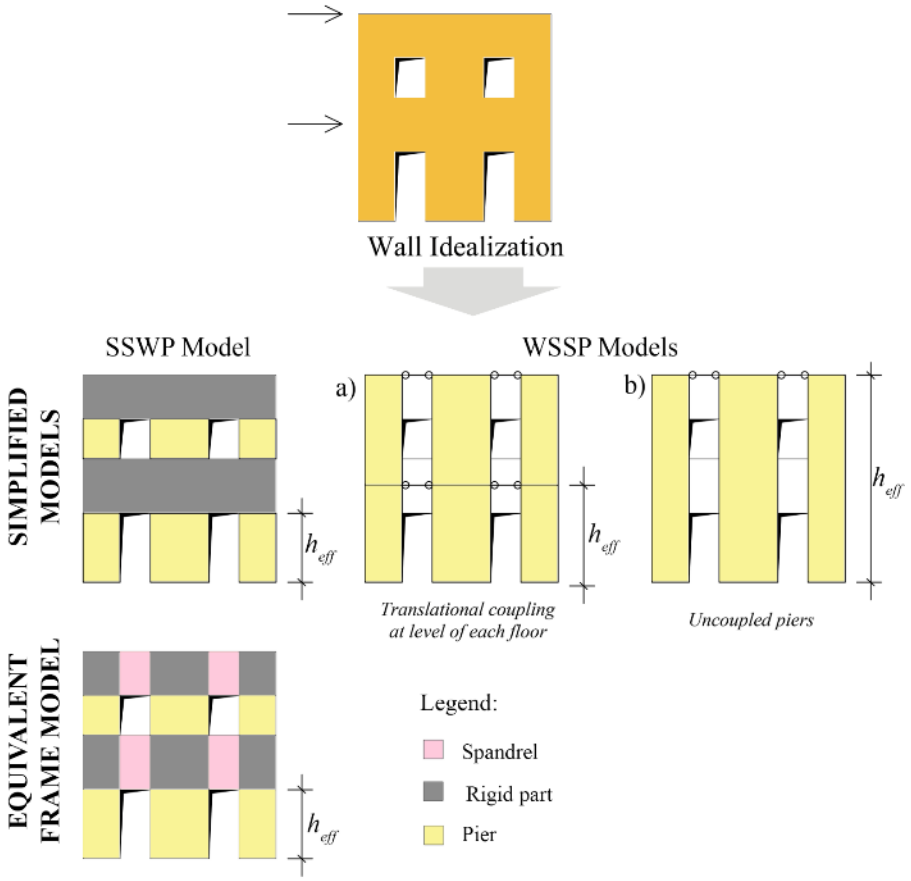

Figure 1.4 – URM wall idealization according to simplified and Equivalent Frame models (adapted from Cattari and Lagomarsino (2009)).

Regarding in particular the models listed at point i), it is stressed that the modelling of spandrels may result even unrequested, since on their behavior some a priori simplified assumptions are made: this is the case of the simplified models explicitly suggested by international codes such as FEMA 356 (2000) and FEMA 306 (1998). In particular, in the idealisation as a "strong spandrel-weak pier" model (SSWP in Figure 1.4) it is assumed that piers crack first, thus averting the failure of spandrels, which are usually considered as infinitely stiff portions assuring a complete coupling between piers. This corresponds to the

imposition of a fixed rotation boundary condition at the piers extremities, and it is also known as "storey mechanism"; it is therefore consistent with the POR method (Tomaževič (1978)), one of the first modelling approaches inspired to a frame discretization of masonry walls which was largely adopted in Italy after the 1980 Irpinia earthquake.

On the contrary, in case of "weak spandrel-strong pier" model (WSSP in Figure 1.4), the hypothesis of both null strength and null stiffness of spandrels is adopted, thus assuming the piers as uncoupled (i.e., cantilever idealization, see WSSP – case a) in Figure 1.4). However, in most cases it is licit to assume that the horizontal displacements of the vertical resistant elements are at least coupled at the floor levels due to the presence of the horizontal diaphragms (see WSSP – case b) in Figure 1.4). It is evident that, as highlighted in Figure 1.4, the use of different models implies also the use of different effective heights for the piers (h_{eff}). The choice between SSWP and WSSP models, which actually correspond to two extreme idealizations, should follow a preliminary reconnaissance about the features characterizing the spandrels in the building under examination. In particular, it should be assessed: a) the state of damage characterizing these elements and b) the presence of specific constructive details.

Referring to point a), some indications are traced in FEMA 306 (1998), which specifically deals with the evaluation of earthquake damaged buildings. In particular, this code addresses the choice of SSWP models when there is no spandrel damage, and of WSSP models when the spandrels are fully cracked.

With reference to point b), as a rule, the assumption which SSWP model is based on seems consistent with new buildings, where masonry spandrels are always connected to lintels, tie beams and slabs made of iron or reinforced concrete. In fact, these elements, being stiff and tensile resistant, are usually able to ensure a consistent coupling between piers, making the contribution of masonry negligible. On the contrary, in historical and existing buildings spandrels are in many cases intrinsically weak elements. Indeed, lintels are usually made of wood or masonry, tie beams are often absent and floors are flexible (e.g. due to the presence of vaults or wooden floors); these reasons therefore justify the adoption of WSSP models.

In the Italian building code (NTC08 (2008)), the WSSP model is assumed as the simplest allowed modelling technique (cantilever models), while the SSWP hypothesis (storey mechanism) is no more allowed for the analysis of multi-storey masonry buildings.

Despite the advantage of adopting very simplified and manageable models, since they are based on an aprioristic choice, some troublesome issues arise. First of all, it is conceivable that both of these limiting cases are inappropriate for certain walls, which may display both types of response in different regions or which can be involved in a different idealisation progressing the nonlinear response of the structure. Moreover, it is not at all a foregone conclusion that the presence of certain constructive details (e.g. r.c. beams interposed inside the spandrels), not supported by a quantitative evaluation of their effectiveness, is sufficient to assure the achievement of the hypotheses which these simplified models are based on. All these issues highlight the need to refer to more detailed models, where both pier and spandrel elements are modelled, so that the transition between different boundary conditions can be directly obtained from the progressive damage of elements. In this way, the behavior as "strong" or "weak" spandrels can come out through the analysis rather than through *a priori* considerations, which may be erroneous.

For these reasons, the modelling strategy based on the idealisation of the structure through an "Equivalent Frame" appears as the most suitable for the analysis of standard masonry buildings. Moreover, thanks to

the simplicity of implementation it requires and to its computational efficiency (even for nonlinear analyses), in the last decades the EF method has met great success not only at research level but also in practice engineering, being explicitly recommended by several national and international codes (NTC08 (2008), Eurocode 8, Part 3 (CEN (2005)), synthetically named in the following EC8-3) and guidelines (CNR DT-212 (2014)).

Once having idealized the masonry wall into an assemblage of structural elements, the reliable prediction of its overall behavior mainly depends on the proper interpretation of the single panel response. Regarding this aspect, several formulations are proposed in literature for the description of the nonlinearity in the masonry panels. A general description of different possible models has been recently carried out in in Calderini et al (2010) and in Marques and Lourenço (2011).

A fundamental prerequisite of the models proposed for the masonry structural elements is that they should be able to properly simulate the main in-plane failures characterizing a masonry panel subjected to horizontal and vertical loads. Observations of seismic damage in complex masonry walls, as well as laboratory experimental tests, have shown that it may undergo two typical types of behavior (that is, flexural and shear), to which different failure modes are associated (approximatively represented in Figure 1.5): rocking and crushing (flexural behavior); sliding shear failure and diagonal cracking (shear behavior). As known, the occurrence of different failure modes depends on several parameters: the geometry of the panel; the boundary conditions; the acting axial load; the mechanical characteristics of the masonry constituents; the masonry geometrical characteristics (block aspect ratio, in-plane and cross-section masonry pattern). Moreover, mixed failure modes are also possible.

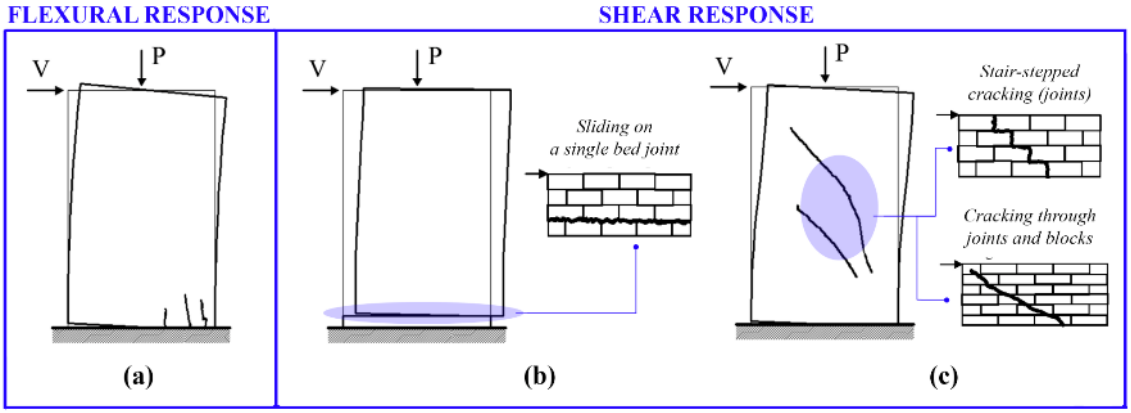

Figure 1.5 – Main in-plane failure mechanisms of a masonry panel: (a) flexural failure, (b) shear sliding failure and (c) shear diagonal failure.

The flexural failure mode (Figure 1.5-a) is associated to the rocking of the masonry portion in its own plane. The loss in bearing capacity is associated to the onset and propagation of cracking in the tensile zone and/or to the crushing of the panel in the compressed zone. The sliding shear failure mode (Figure 1.5-b) is associated to the sliding of the masonry panel in its own plane. In this case, the loss of bearing capacity is associated to the formation of cracks parallel to the bed joints. The diagonal shear failure mode (Figure 1.5-c) is associated to the loss of bearing capacity of the masonry panel due to excessive shear and to the consequent formation of diagonal cracks along the directions of the principal compression stresses.

Moreover, the diagonal crack may develop only through joints (sliding along head and bed joints, typically activated when mortar joints are weaker than units) or, alternatively, through units and joints.

As it is possible to see from Figure 1.6, these different failure types activate different behaviors on the associated masonry panel in terms of displacement capacity (interpreted through values of drift, as better discussed in Chapter 3) and hysteretic response.

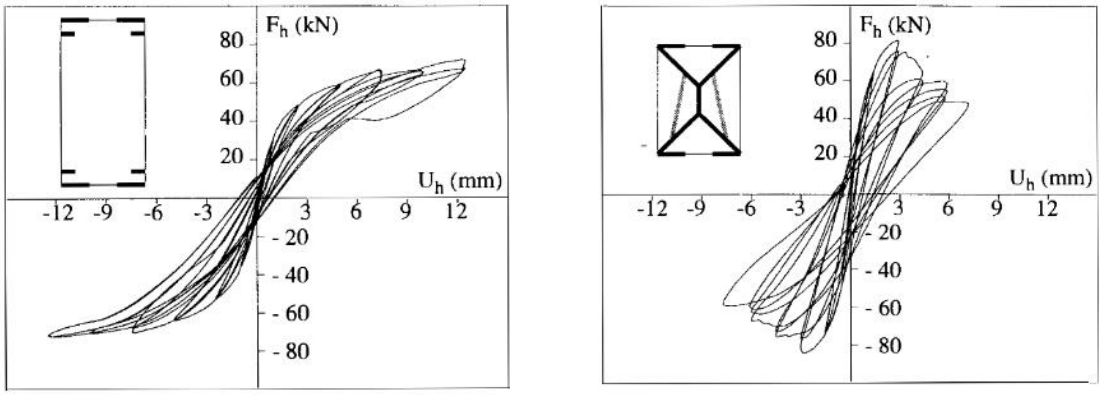

Figure 1.6 – Hysteretic response of: (a) a panel undergoing flexural failure and (b) a panel undergoing shear failure (from Anthoine et al (1995)).

A first classification between the different models proposed for masonry panels in the literature may be done by considering that masonry elements where the nonlinear response is concentrated can be described as one-dimensional or two-dimensional structural elements, by means of more or less detailed models.

Regarding the class of one-dimensional models (also referred to as "frame elements"), a first possibility is represented by the equivalent strut idealization proposed in Calderoni et al (1987) and Calderoni et al (1989), according to which masonry panels are schematized as "variable geometry" struts, whose orientation and stiffness reproduce the behavior of the entire panel. Another possibility is the use of nonlinear beam models, according to which masonry panels are described as shear-deformable beams with nonlinear behavior. In most cases, the description of the nonlinear behavior is directly faced in terms of global stiffness, strength and ultimate displacement capacity by assuming a proper shear-drift relationship.

In this field, an example is represented by the simplified nonlinear beam element implemented in TREMURI Program (Lagomarsino et al (2013)); in this case, it is assumed that masonry panel behavior is given by a bilinear relation with cut-off in strength (without hardening) and stiffness decay in nonlinear phase (for non-monotonic action). Another nonlinear beam model proposed in the literature is the one described in Grande et al (2011), which includes also the possibility to simulate the presence of fiber-reinforced plastic (FRP) materials, that can be eventually introduced in the masonry elements for strengthening purposes.

In general, the modelling of the inelastic behavior of the structural elements can be faced through two different approaches, i.e. lumped plasticity and spread plasticity models. In the lumped plasticity approach inelasticity occurs in limited portions of the structural elements; in this case, linear shear-deformable beams are connected by inelastic links (defined also as plastic hinges) in which damage, cracking, sliding and rotations are concentrated, as in the two-nodes frame element formulated in Magenes and Della Fontana

(1998), in the nonlinear beam model afore introduced (Lagomarsino et al (2013)) and in the approach proposed in Penelis (2006). Conversely, in the spread plasticity approach the basic idea is that the mechanical nonlinearity of masonry is included over the whole length of the pier and spandrel elements, as for example in the model proposed in Belmouden and Lestuzzi (2007). Another model based on concepts of spread plasticity has been developed by Raka et al (2014); in particular, the model adopts a fiber discretization of the associated cross-sections, that is used to simulate the axial and flexural behaviors and automatically accounts for their interaction. This model also considers the shear response by adding a nonlinear spring (whose behavior is described through a phenomenological nonlinear shear force - deformation constitutive law) to the fiber-section frame element.

However, some limitations in the use of frame-type elements can be identified, namely due to the inaccurate simulation of the interaction between macroelements (spandrels are connected to the piers at a point, while in reality there is a more complex stress transfer mechanism between horizontal and vertical elements that takes place over the node), to the difficulties that arise for complex geometries and to the weak modelling of the cracked condition of panels.

Another possibility that can be taken into consideration is therefore the adoption of two-dimensional macroelements. This class of models, in particular, includes both macroelements assuming “no tension” hypothesis (D’Asdia and Viskovic (1994), Braga et al (1998)) and more accurate models aimed to provide a synthetic mechanical description of main deformation, damage and dissipation mechanisms of panels.

In particular, focusing the attention on the second group of models, the macroelement model proposed in Penna et al (2014b) allows, with a limited number of degrees of freedom (8 in total) to represent the main in-plane masonry failure modes. The model presents a mechanics based formulation in which the panel response is not governed by predetermined values of strength and stiffness, but it depends instead on mechanical properties, their possible deterioration, actual boundary conditions and applied forces, that may vary in each step of the analysis. The model described in Penna et al (2014b) provides a refinement of a previously developed macroelement model (Gambarotta and Lagomarsino (1996), Brencich and Lagomarsino (2008)); in particular, a nonlinear degrading model for rocking damage which permits to keep into account the effect of limited compressive strength (toe-crushing) is included. The macroelement model is a two-node element provided with two additional internal degrees of freedom; it is composed by three parts: a central body where only shear deformation can occur and two interfaces (where the external degrees of freedom are placed) that can be considered as infinitely rigid in shear and with a negligible thickness. The model includes a nonlinear shear stress-strain cyclic relation that is derived by the macroscopic integration of the continuous model introduced in Gambarotta and Lagomarsino (1997b) (as originally proposed in Gambarotta and Lagomarsino (1996), Brencich et al (1998)) as well as a nonlinear description of the coupled relation between flexural and axial degrees of freedom, which allows to explicitly evaluate the cracking effects on the rocking motion (uplift effect).

Recently, an improved version of the macroelement developed in Penna et al (2014b), which solves some of the limitations still present in this model, has been presented in Bracchi et al (2018).

Further studies propose the use of nonlinear springs for simulating the failure mechanisms of masonry panels: in Chen et al (2008) nonlinear shear springs in series with rotational springs are adopted in order to

reproduce both shear and flexural response, while in Rinaldin et al (2016) piers and spandrels are described utilising multi-spring nonlinear elements.

Other modelling strategies based on assemblies of rigid bodies and nonlinear springs present intermediate capabilities between distinct element and macroelement modelling. More specifically, in Casolo and Peña (2007) a "rigid-body spring model" (RBSM) specifically formulated with the aim to approximate the macroscopic behavior of masonry walls with reduced degrees of freedom is proposed. The basic idea is to model the solid material as an assembly of plane quadrilateral rigid elements connected to each other by two normal springs and one shear spring at each side.

Another model which involves the use of nonlinear springs is the one proposed by Caliò et al (2012). This macroelement consists of a pinned quadrilateral made with four rigid edges, in which two diagonal springs are connected to the corners to simulate the shear behavior. The flexural and sliding shear behavior is simulated through discrete distributions of springs located in correspondence of the sides of the quadrilateral, capable to simulate its interaction with the adjacent macroelements. It is stressed that each panel may be modelled by recurring to different mesh solutions (it means that each panel can be discretized through one or more elements); moreover, differently from the classical EF models, no distinction is made between nonlinear elements and rigid portions, since the introduced marcoelements can be used for the discretization of the whole wall.

Some of the above described formulations are already implemented in software codes specifically dedicated to the analysis of masonry buildings, such as the programs ANDILWall/SAM II (Magenes and Della Fontana (1998), Manzini et al (2006)), TREMURI (Lagomarsino et al (2013), STA Data (2017)), 3DMacro (Caliò et al (2012)). Moreover, the nonlinear beam model can be easily and effectively implemented also in general purpose software packages, as for example SAP 2000 (Kappos et al (2002), Salonikos et al (2002), Pasticier et al (2008)).

In the following Chapter (section 2.1) a detailed comparison between several EF models based on different formulations and implemented in specific commercial software is discussed.

1.2.3 Comparison between Continuum Models and Equivalent Frame models

Since the two modelling approaches now described for the study of the global response of masonry buildings (Continuum Constitutive Law Models and, in the framework of Structural Element Models, the Equivalent Frame method) work at different scales, some differences between them can be highlighted, which are of particular interest with a view to the comparisons between these two models performed in the present research.

In particular, these differences are about:

i) the discretization of the structure (mesh);
ii) the definition of the constitutive laws;
iii) the definition of the mechanical parameters to be adopted.

With reference to point i), in EF models it is necessary to realize an *a-priori* identification of the structural elements where the nonlinear response is concentrated, which leads, consequently, to the determination of the extension of the rigid nodes. As widely explained in section 1.3.1, this is usually guided by the

observation of damage occurred in past earthquakes, which helps to identify the portions of the wall which are most commonly subjected to damage. On the contrary, in CCLM the structure is modelled as a nonlinear continuum discretized into a number of finite elements, so that no simplification about the localization of the masonry damage pattern and the structure geometry is made. This aspect makes this kind of models particularly suitable for the validation of the Equivalent Frame approach with regard to the proper definition of the geometry of the structural elements, which is actually one of the main purposes of this thesis, and contributes to justify the choice of a continuum model as a validation tool.

With reference to point ii), in CCLM constitutive models are referred to the material and are expressed in terms of stress-strain relationships, defined whether through a phenomenological approach or homogenization procedures. Conversely, in the EF models the constitutive laws are usually referred to masonry panels and are expressed in terms of force-drift relationships, defined through more or less detailed approaches. One of the possibilities, suggested also by the Italian building code (NTC08 (2008)), is to consider elastic-plastic laws where the stiffness is evaluated by adopting the beam theory (computing both the contributions in terms of shear and flexural behavior), the strength is obtained by referring to simplified resistance criteria (associated to different failure modes) and the ultimate displacement capacity is expressed in terms of drift (defined as a function of the occurred failure mode on the basis of available experimental tests or literature data). However, also more refined multilinear constitutive laws can be adopted, as suggested in CNR-DT 212 (2014) (Figure 1.7). In this case the post-peak behavior of the masonry elements is described through a progressive strength degradation occurring in correspondence of fixed drift thresholds associated to increasing Damage Levels (DLs), thus representing a more faithful description of the actual behavior of masonry panels observed during experimental tests. As indicated in Figure 1.7-b, according to CNR-DT 212 (2014) it is possible to identify, on the softening branch of the shear – drift (V-θ) curves, three different Damage Levels, which correspond to specific performance conditions characterizing the panels: severe damage (indicated as DL3 in Figure 1.7-b), very severe damage (DL4) and collapse (DL5). These Damage Levels refer to the degrees of damage usually used in modern macro-seismic scales (EMS98, Grünthal (1998)). Values of drift that correspond to the first two levels of damage are recommended by national and international standards. Damage Level 5 corresponds to a condition where the masonry pier completely loses the ability to carry the horizontal loads.

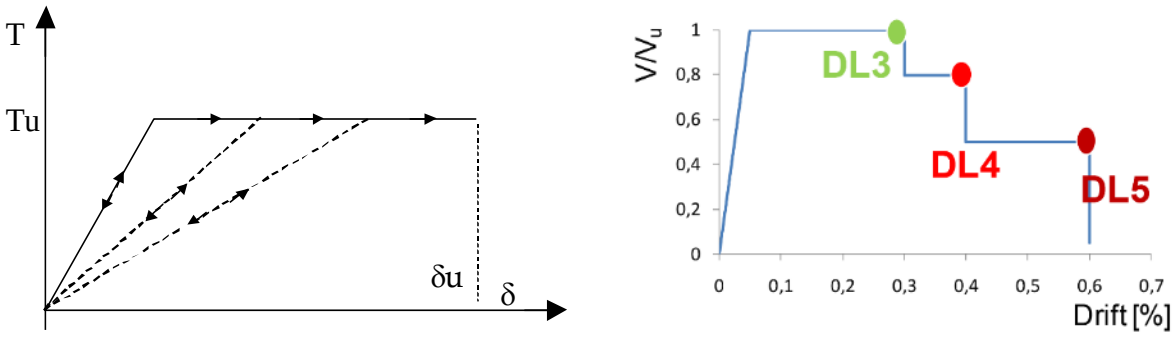

(a) **(b)**

Figure 1.7 – Possible force-drift relationships for masonry panels: (a) elastic-plastic behavior (from Cattari et al (2005)) and (b) multilinear constitutive law with strength degradation in correspondence of fixed drift thresholds associated to performance levels (Damage Levels, DLs) (from CNR – DT 212 (2014)).

As far as the mechanical parameters to be adopted are concerned (point iii)), the following differences between the two modelling approaches can be identified. Concerning *stiffness*, in CCLM it is possible to take into account its progressive reduction due to damage (according to the constitutive laws formulated at material scale). On the contrary, in EF models, in particular in those cases in which simplified models are adopted for structural elements (like as nonlinear beam ones), such stiffness reduction can be taken into account only in a very simplified way. Concerning this point, codes and recommendations (EC8, NTC08) propose to adopt reduced inelastic stiffness properties, representing damaged conditions of the material; more specifically, a reduction of 50% of the initial elastic moduli is suggested, in absence of more refined evaluations. An alternative suggested in Lagomarsino et al (2013) is to take into account this reduction by using empirical formulations that correlate the stiffness value with the actual compressive state.

When more detailed models are adopted, such as models based on the fiber approach or the macroelement proposed in Penna et al (2014b), it is possible to better describe the stiffness degradation process. However, in this last case, it is necessary to define inelastic compliance parameters able to describe the damage progress directly at the scale of the structural element (which is not always an easy task since a detailed calibration would require suitable experimental test results performed on masonry panels).

Regarding *strength*, in CCLM it is possible to take into account the actual non homogeneous stress state produced by the acting forces: the admissibility of the stress state is assessed in all points of the structural elements with reference to strength criteria of the material. In the EF models the strength is assessed with reference to simplified strength criteria of structural elements, related to the failure mechanisms that may occur. The most common simplified models present in the literature and codes (discussed in Magenes and Calvi (1997) and Calderini et al (2009a)) are based on the approximate evaluation of the local/mean stress state produced by the applied forces on predefined points/sections of the panel and the assessment of its admissibility with reference to the limit strength domain of the material (usually idealised through simple schematizations based on few mechanical parameters, as the compressive strength of masonry, diagonal tensile strength of masonry, cohesion and friction of mortar joints).

In order to conclude this comparison, some considerations about the issues related to the execution of the seismic verifications required by the codes when adopting these two types of models are necessary. In general, the seismic codes (NTC08, EC8) provide limit conditions that, both in case of strength and displacement capacity, refer to quantities and parameters associated to the scale of masonry panels: generalized forces, in case of strength, and drift values, in case of deformation and displacement capacity. Regarding this last aspect, it is stressed that the performance-based design requires to associate given limit states to specific performance conditions characterizing the structure under consideration. As an example, when the seismic analysis is performed in the form of nonlinear static analysis, it is necessary to identify the limit states on the capacity curve obtained by the pushover analysis. The attainment of such limit states is in general associated with the attainment of predefined drift thresholds in the structural elements. It is evident that in the EF models the evaluation of the quantities and the parameters required for the verifications is straightforward, being the modelling directly faced at the structural element scale. Conversely, if a continuum FE model is adopted for the structural analysis, an additional effort is required: indeed, the elements on which the drift parameter related to the limit states is monitored should be identified

after the analysis and also generalized stresses and strains should be calculated *ex-post* (Calderini et al 2009b).

In the light of these considerations it is stressed that, when a continuum model is used for the execution of the seismic analysis, it is necessary first of all to ensure that the adopted model is able to reproduce in terms of strength and displacement capacity the behavior at the scale of the panel as observed in experimental tests and according to the criteria proposed in the codes. Indeed, the mechanical properties to be assumed as reference for a specific masonry type (found in codes or in the literature, as result of experimental tests) are usually referred to the scale of masonry panels rather than to the scale of the material; this implies a preliminary phase aimed to calibrate the parameters of the constitutive law of the continuum material, defined in the stress-strain domain, with those referring to the structural element scale (this issue is discussed in detail in Chapter 3, section 3.2).

Then it is necessary to *ex-post* evaluate the reaching of the limit conditions by examining specific sections of the structure under study. Even if this procedure requires an additional effort with respect to the use of structural element models, it is evident that the results obtained in such way derive from a more accurate modelling, referring to the material scale. In this sense, they can be used as a reference solution and the continuum model can be regarded as a validation tool for the more simplified structural element approach. These considerations are at the base of the methodological approach adopted in this thesis for the validation of the EF method, which is described in detail in Chapter 3.

1.3 EQUIVALENT FRAME MODELS: CRITICAL ISSUES

Despite of the large use of the Equivalent Frame (EF) models, especially at practice engineering level, there are many aspects that should be considered in order to improve their reliability and that have not yet been validated in a robust way. Recently, in Quagliarini et al (2017) a critical review of the Equivalent Frame approach, considering in particular its application to existing URM buildings, has been carried out, underlining the most recurrent critical issues that should be deeper investigated and developed.

It is worth noting that the seismic codes, even if explicitly suggest the adoption of this modelling technique for the seismic assessment and design of masonry buildings, do not provide specific indications about all the possible modelling choices the EF idealization implies. Furthermore, a dedicated and specific technical literature, available also to practitioners and to which the professional engineers can refer for properly applying this approach, does not actually exist. As a consequence, many uncertainties arise, leading to a quite arbitrary application of the method on behalf of the professionals and the analysists who commonly work with it.

For these reasons, the problem of the reliability and the correct use of these models represents nowadays a topic of great concern, as discussed in literature by several authors (Marques and Lourenço (2011), Calderoni et al (2015), De Falco et al (2017), Cattari et al (2018a)).

Assuming the capability to properly describe the response of single URM panels, that indeed is not completely solved in literature, in particular in the case of spandrels (as further discussed in the following), some of the most common critical issues as well as modelling uncertainties involved in the application of the EF approach deal with:

i) the identification of the geometry of the structural elements;
ii) the modelling of the out-of-plane response of the walls;
iii) the modelling of the diaphragms;
iv) the modelling of the spandrel elements;
v) the modelling of the flange effect;
vi) the determination of the effective length of the r.c. tie beams;
vii) the assumption of the loading scheme for the floors.

These modelling uncertainties and critical issues come into play both in the modelling of the new masonry buildings and, even more, when considering the existing ones. In this case, indeed, the hypotheses on which the EF method is based (box-like behavior, aligned opening patterns, regularity in plan and elevation) are often not verified, and the presence of many hard-to-model features makes the application of this approach complicated and even questionable: presence of flexible diaphragms (vaults, timber floors), different quality of the connection between the walls, complex geometries and irregular opening patterns that are the result of several modifications during the years. Several works available in the literature have contributed to highlight that these modelling uncertainties may actually affect the final result in terms of global pushover curves (Rota et al (2014), Bracchi et al (2015)).

With reference to the critical aspects above listed, in the following a brief description of each one of the aforementioned issues is provided, with the aim to underline the aspects which still represent open problems in the literature, discussing also the possible modelling choices that can be adopted in these cases.

With regard to the problem of the correct identification of the structural elements (point i)), it actually represents the main topic which this thesis is based on and among the first ones that the EF models require to face. It is deepened in detail in the following sections: in particular, first of all a comprehensive review of the criteria proposed in literature for the identification of the structural elements in the EF models is provided (section 1.3.1), followed by a general overview of the studies already carried out on irregular masonry walls and mainly focused on the validation of the EF approach when applied to these “critical” cases (section 1.3.2).

In general, it is fundamental to observe that, as already introduced in the previous section, the EF models are meant to study the global in-plane response of URM buildings; therefore, out-of-plane mechanisms have to be always verified separately through modelling approaches that are more suitable for assessing them. Once made this assumption, a first simplification that is in general carried out when using EF models (point ii)) is to ignore the out-of-plane stiffness and strength of the walls, assuming it as negligible. However, some specific structural element models (ANDILWall - Magenes et al (2006), Manzini et al (2006); MIDAS Gen (2018); AEDES.PCM (2016); 3DMacro - Caliò et al (2012)), already implemented in computer programs for the analysis of masonry buildings, are capable to include also this contribution, thus giving the possibility to estimate the “error” associated to the previously cited hypothesis. In general, when the out-of-plane contribution is neglected, an underestimation of the global initial stiffness and peak strength may be obtained, which could be quite relevant in the cases where a significant thickness of walls is present. This is evidenced also by some comparative works between EFM and more accurate CCLM models (e.g. Cattari et al (2015)).

A further important issue that has to be considered when dealing with 3D models is related to the modelling of the diaphragms (point iii)), whose main role is to contribute to the load redistribution between the bearing walls. The modelling of floors is usually faced in the EF models by considering strongly simplified hypotheses. In general, a linear elastic behavior is assumed for these elements, and this represents a first simplification. Indeed, during an earthquake the diaphragm could actually be interested by damage (e.g. significant angular deformations may occur), causing ductile or fragile failures that may affect its capacity to transfer loads between the bearing walls. However, up to now no sufficient data for supporting the introduction of a proper modelling of the nonlinear response of the diaphragms are present in the literature, as highlighted also in CNR-DT 212 (2014).

A further simplification which is commonly adopted in the EF models regarding the modelling of the diaphragms is to consider only their in-plane stiffness. This last (in particular the shear elastic modulus) affects the mutual co-operation between the walls: rigid diaphragms are able to redistribute the actions between the walls as a function of their stiffness and position in plan, while very flexible floors cannot ensure a proper load redistribution between the walls during the analysis, thus emphasising their independent behavior. As a result, different assumptions about the diaphragm in-plane stiffness may significantly affect the overall response of a masonry building, as recently highlighted in (Marino (2018), Marino et al (2019)).

Regarding the determination of the diaphragm in-plane stiffness, many of the available commercial codes assume floors as infinitely rigid in their plane. However, this assumption cannot be always considered as effective, especially in case of existing buildings, where old construction techniques are often present (wooden diaphragms, vaults). For this reason, in some cases (like in Lagomarsino et al (2013)) floors are modelled as orthotropic membrane finite elements with the possibility to take into account their actual finite stiffness. Concerning this, it seems important noting that the evaluation of the stiffness properties may be rather simply identified in some floor typologies, ascribing it to the structural role of some specific elements (as an example, the shear stiffness of a r.c. floor with beams and slab is mainly given by the slab). However, in other cases, such as in presence of vaults, the stiffness strongly depends on many factors such as shape, geometrical proportion (e.g., rise-to-span ratio), thickness and material properties. So, the definition of the elastic moduli to be attributed to the equivalent plane element may be highly arbitrary. In Cattari et al (2008) the definition of equivalent stiffness properties has been proposed for some types of vaults (barrel, cross and cloister vaults). In case of timber floors, specific indications were already suggested in NZSEE (2006), and some experimental tests on specimens refurbished by using different techniques are presented in Piazza et al (2008). Furthermore, recently some authors carried out a critical review of the formulae proposed in the literature and codes (Brignola et al (2012)), stressing the importance to take into account not only the contribution offered by the single structural elements (such as panel sheathing or beams) but also that of connectors (in the wall-to-diaphragm connection), and proposing a simplified analytical approach for the evaluation of the in-plane stiffness properties of few types of timber diaphragms. The behavior of timber floors has been more recently investigated through both experimental campaigns and numerical methods in (Casagrande et al (2018), Giongo et al (2018)).

However, even if it is usually neglected in the EF models, the out-of-plane stiffness of the diaphragms may provide an additional stiffness to the walls of the examined structure. With the aim to conventionally take into account this contribution without explicitly modelling the out-of-plane stiffness of the diaphragms

some authors (RINTC Workgroup (2018)), in presence of buildings with r.c. tie beams and rigid floors, increase the stiffness of the r.c. tie beams to account for a pertinence influence area of diaphragms expected to interact with the vertical walls.

Furthermore, it is worth noting that the simplified hypotheses above discussed and usually adopted in the EF models concerning the modelling of diaphragms make not possible to account for the local interaction phenomena occurring between the floors and the spandrels, which however may have an important role in the actual structural response of the 3D building. On the contrary, the use of FE models allows to realize a more accurate modelling of these elements and their possible interaction, and the kinematic coupling that may activate, especially when in presence of rigid floors, can produce an effect similar to the presence of "tie rods" on the spandrels. It is evident that this effect cannot be captured through the EF models due to the adopted simplifications.

Another prominent issue in the EF models concerns the modelling of spandrels (point iv)). In the past, experimental campaigns and numerical studies were mainly focused on piers and only few works were conducted on spandrels (Calderoni et al (2007)); as a consequence, most of the simplified models proposed in the literature are specifically meant for pier elements. This is motivated by the fact that, traditionally classified in the hierarchy of structural walls as secondary elements, spandrels have lately been recognized to play a significant role in the seismic response of masonry buildings. Indeed, they actually affect the boundary conditions of piers (i.e. fixed-fixed or cantilever), with great repercussions on the predictions of their load-bearing capacity. Therefore, in the last decade increasing attention has been paid also to the study of spandrels, both from an experimental (e.g. Beyer and Dazio (2012), Graziotti et al (2012) and Parisi et al (2014)) and from a numerical point of view (Lagomarsino and Cattari (2008), Milani et al (2009), Beyer and Mangalathu (2014)).

All the recent studies performed on spandrels are fundamental for starting a better understanding of the complex behavior of these elements and are useful to fill some gaps present in the literature about the topic; however, the process is still at the beginning, since the experimental tests on spandrels are still limited and, *de facto*, the literature in this field is not as well consolidated as in the case of pier panels. For this reason, the modelling of spandrels in the EF models still poses serious problems not only for the determination of proper constitutive laws for these elements, but also for the definition of adequate strength criteria.

With reference to this last aspect, the common practice adopted in most of the seismic codes is to use the same models developed for piers, assuming the spandrel behavior as that of a pier rotated by 90°. More precisely, NTC08 makes a distinction in the strength criterion to be adopted for spandrels as a function of the acting axial load (if known or unknown from the analysis). It is worth noting that, due to the very low axial loads that usually characterize spandrels (in particular when tensile resistant elements coupled to them are absent), the adoption of a failure criterion for flexural response analogous to that of piers may lead to a significant underestimation of the actual strength associated to this mechanism. The consequence is that, very often, in EF models that simulate the response of panels as nonlinear beams, spandrels are ineffective just from the beginning of the analysis, thus inducing the cantilever conditions of piers.

However, the recent developed studies have shown that spandrels present some specific features that differentiate them from piers and that affect their force-displacement response, such as the interlocking of bricks at the end-sections with the contiguous masonry portions, the type of lintels if present (able to

significantly affect also the residual strength capacity of the spandrel-lintel system) and the axial restraint provided by other structural elements (e.g. reinforced concrete beams, steel tie-rods or adjacent piers).

More sophisticated and representative strength criteria, specific for spandrels (in general made of brick masonry), have been recently proposed in the literature, as for example in Beyer (2012) (these criteria have been adopted in NZSEE (2015)), and, for what concerns flexural strength, in Cattari and Lagomarsino (2008). In this last case, in particular, the basic idea is that, thanks to the aforementioned interlocking phenomena, spandrels may rely on the contribution of an "equivalent tensile strength" that alters the flexural strength domain usually adopted for piers (based on the beam theory, neglecting the tensile strength of the material). The use of this criterion is suggested in CNR-DT 212 (2014).

In Cattari and Beyer (2015) a quantitative assessment of the effects of adopting different strength criteria for spandrels in EF models is presented, showing how much these choices can affect the global response of URM buildings.

Another critical issue about the spandrels is represented by the evaluation of the axial load acting in these elements, which may influence their strength. Indeed, it is stressed that the reliable estimation of this quantity is not an easy task in the EF models, due to several reasons (CNR DT 212 (2014)). First of all, as afore mentioned, in most cases the hypothesis of infinitely stiff diaphragms is adopted, and therefore the axial load acting in the spandrels cannot be evaluated from the analysis. When a diaphragm with finite stiffness is considered, other factors contribute to make questionable the provided estimate of the axial load in the spandrels, such as the approximate application of the horizontal equivalent static forces in the pushover procedure (which is based on the lumped masses approach) and the approximate modelling of the interaction between spandrels, tensile-resistant elements and floors. For these reasons, in CNR-DT 212 (2014) it is explicitly suggested to take into account the contribution to the spandrel strength given by the acting axial load only if the estimate provided by the numerical model is considered as sufficiently reliable. Regarding this aspect, it is worth noting that also in the commentary of the new Italian building code (NTC18 (2018)), where the proposed strategy for modelling the spandrel strength is to consider the contribution of the equivalent tensile strength, it is suggested to use the estimate corresponding to an axial load equal to zero, thus implicitly assuming as not sufficiently reliable the axial load computed by the numerical models.

Further practical critical issues involved in the modelling of spandrel elements in EF models are discussed in Chapter 2 (section 2.1), on the basis of the results of a comparison between different software codes adopted for the analysis of a simple structure.

In order to build the 3D model and perform the global analyses, walls have to be properly connected. With reference to this aspect (point v)) it is underlined that, even if masonry piers are usually considered as rectangular cross-sections for the computation of their strength, stiffness and ductility properties, in a real masonry building the walls are connected to each other, thus forming piers with L-, C-, T-, or I-shaped cross sections. The presence of such flanges can influence the in-plane response of the walls in terms of failure modes, maximum strength and displacement capacity and therefore also the performances of the whole building, as highlighted by experimental campaigns conducted both at the scale of single masonry panels (Russell and Ingham (2008), Russell and Ingham (2010), Russell et al (2014), Khanmohammadi et

al (2014), Sajid et al (2018)) and at the structural level (Tomaževič et al (1993), Costley and Abrams (1996), Paquette and Bruneau (2003), Moon et al (2006)).

For these reasons, it is fundamental to include a proper modelling of the connections between the walls in the numerical models employed for the design or the assessment. Nevertheless, it still represents a critical issue, first of all for the determination of the effective width to consider for the flange as well as for the definition of strength criteria referred to non-rectangular cross sections.

Regarding the first aspect, little research on unreinforced masonry (URM) walls is present in the literature, being most of the studies concentrated on the determination of the effective flange width in reinforced concrete and reinforced masonry shear walls (Priestly and He (1995), Hassan and EI-Tawil (2003), Shi and Wang (2016)). Moreover, the definitions proposed for reinforced concrete or reinforced masonry cannot be simply extended to URM walls, since the rationales employed are different for the different materials (Yi (2004)). For example, previous research has shown that with increasing lateral drifts, the effective flange width of a reinforced concrete shear wall will increase due to yielding of reinforcement. Obviously, this cannot be applied to brittle URM walls.

A simple geometric approach for the identification of the effective flange width in URM walls is proposed in Yi (2004), based on the so-called "rule of the 45°" (Figure 1.8). Moreover, some indications are provided by the codes (Eurocode 6, Part 1-1 (CEN (2004b), MSJC (2008)) and mainly depend on the geometry of the involved walls; however, no specifications about how to include flanges in the strength verification are given.

In the literature, an analytical model to evaluate the in-plane response of URM piers with single flange and fixed-free condition was developed by Yi (2004). In this work, in particular, in order to investigate the effects of flanges on the lateral strength of a non-rectangular section URM pier, a specific pier model is developed, through a proper modification of a model termed "effective pier model" previously introduced by the Author. Then, on the basis of this "modified" effective pier model, the maximum strengths corresponding to four primary failure modes (rocking, bed-joint sliding, toe crushing and diagonal tension) for the cantilever pier are calculated, leading to four corresponding failure criteria.

This model was successively revised for piers with flanges in both ends by Khanmohammadi et al (2014). Furthermore, in Mordant (2016) a simplified expression for the computation of the compressive length in presence of flanged sections is proposed.

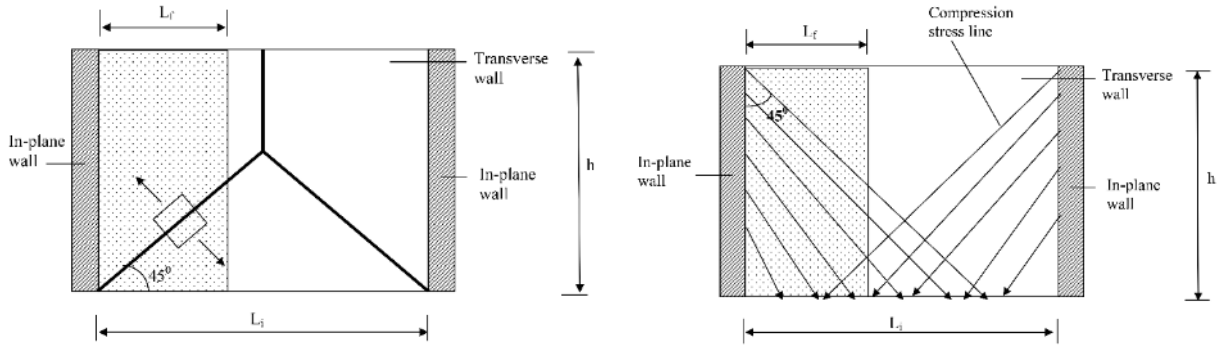

Figure 1.8 – Effective width for the tension flange (left) and for the compression flange (right) according to the rule proposed byn Yi et al (2004); from Yi et al (2004).

Within this framework, in the EF models the presence of flanges is usually modelled in a simplified way and by considering the presence of the flange only with respect to the computation of the normal stress redistribution, while the strength verification is made on the rectangular section responding in-plane. However, a systematic consideration of the effective width of flanges depending on their dimensions is not included. The connection between the orthogonal walls is usually managed through the perfect coupling of the vertical component or with rigid links, regardless the dimension of the flange; this may lead to an overestimation of the flange effect in presence of flanges with significant width, where it seems unrealistic to consider all the width as effective. Some software allow also the use of beams characterized by a proper stiffness in order to simulate different degrees of connection between the orthogonal walls (until the complete decoupling) (Figure 1.9), but there are no specific indications in the literature about how to properly calibrate the stiffness of these beams, which is usually determined through empirical approaches. The implications of different assumptions about the modelling of the connection between the orthogonal walls in the EF models are illustrated, referring to the results obtained through the analysis of specific case studies, in Chapter 2.

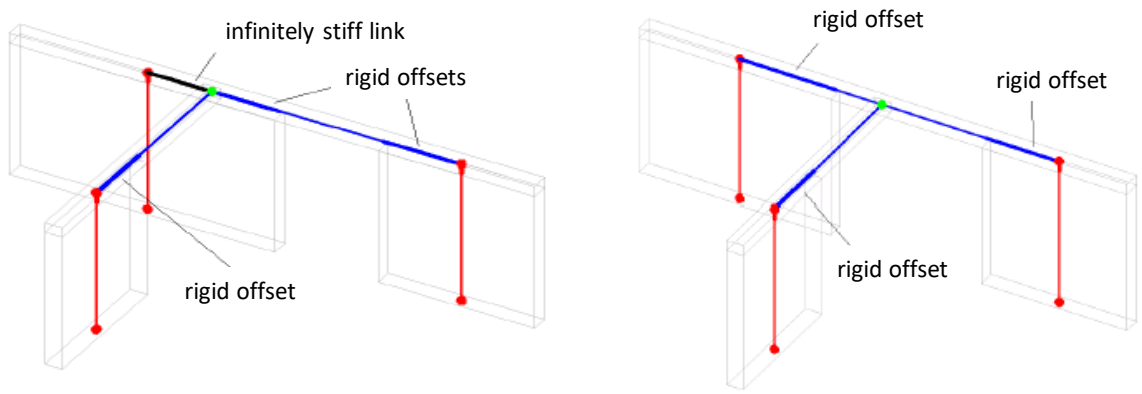

Figure 1.9 – Strategies for modelling the flange effect in EF models (from Manzini et al (2006)).

Concerning the definition of the structural model of a URM building, some specific modelling uncertainties that may arise refer to both the loading scheme to adopt for the floors (point vi)) and the effective length of the r.c. tie beams (point vii)). The first aspect deals with the possibility to consider for the diaphragm an unidirectional (i.e., the load is transferred only along the principal direction) or a bidirectional behavior (i.e.: part of the load is transferred in the secondary direction). Regarding the second aspect, it is underlined that the choice of the effective length of the r.c. tie beams is, *de facto*, arbitrary. It is observed that r.c. tie beams in real buildings are actually continuous along the length of the corresponding walls; however, their effective length should account for the more or less effective coupling between masonry panels, as also testified in the experimental work done by Beyer and Dazio (2012). The two extreme conditions that can be used in this case are an effective length equal to the total length of the wall or equal to the net width of the corresponding opening. The effect on the global response of different assumptions about these modelling choices is discussed in detail in Chapter 2 (section 2.2).

1.3.1 Rules for the identification of piers and spandrels

The *a priori* identification of the geometry characterizing the structural elements (piers and spandrels) represents the first step to deal with when applying the EF approach. The criteria commonly used to this aim are mainly function of the opening pattern of the considered wall; this is consistent with the earthquake damage observation, that shows in most of the cases a concentration of damage and failure modes in the masonry portions located between the openings aligned in the horizontal and vertical direction.

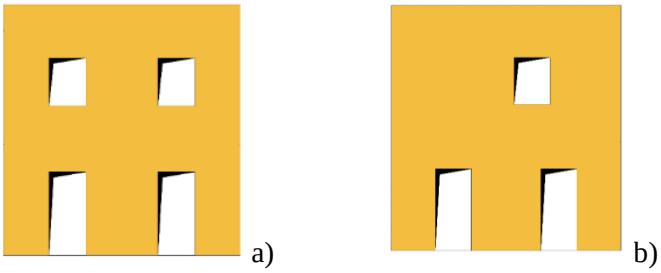

Figure 1.10 - Example of: a) *regular* masonry wall and b) *irregular* masonry wall.

Moreover, depending on the features of its opening layout, a masonry wall can be defined as *regular* or *irregular*. In particular, a *regular wall* presents openings of the same size at each storey and perfectly aligned in both the orthogonal directions, while an *irregular wall* is characterized by the presence of openings with different geometries, misaligned in the horizontal and/or vertical direction or even by a variable number of openings per story (Figure 1.10).

Figure 1.11 - Examples of irregular opening layouts in masonry walls. Photos by S. Cattari and S. Marino.

Differently from the new buildings, which are designed with regularly distributed openings in order to be conforming to the regularity rules imposed by the seismic codes, the existing masonry buildings are often the result of several modifications during the years, that in most of the cases have led to very complex geometries, even when considering the opening layout: the most recurrent geometric irregularities related to the opening pattern are usually determined by staircase openings, misaligned floors, window and door openings at the same storey as well as creation/closure of some openings (Figure 1.11).

In presence of *regular walls*, the identification of the structural components of the equivalent frame is in general straightforward, being based on the horizontal and vertical alignments between the openings, and it can be easily obtained by extending their contours. As for example, in Figure 1.12 an exemplification of the main steps of the frame idealization procedure in a regular masonry wall is illustrated (Lagomarsino et al (2013)): from the identification of spandrels and piers (steps 1-2) to that of nodes (step 3).

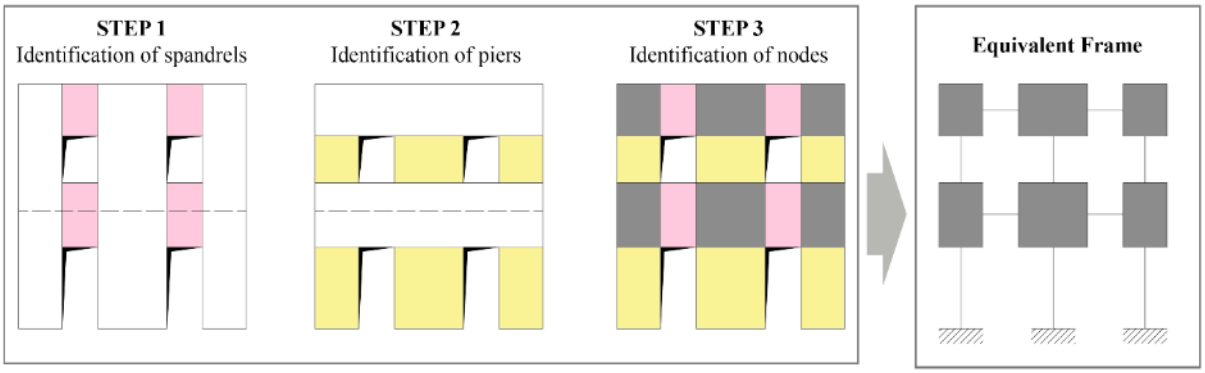

Figure 1.12 – Example of equivalent frame idealization in case of regularly distributed openings (adapted from Lagomarsino et al 2013).

On the other hand, when considering *irregular walls* the a priori identification of piers and spandrels becomes more difficult and ambiguous, thus leading to arbitrary and conventional choices.

In general, the rules adopted for the identification of piers and spandrels are empirical or based on limited experimentations and\or few numerical simulations; moreover, until now they have never been systematically validated through specific and dedicated parametric analyses and by considering different opening layouts.

The analysis of the literature highlights that while several criteria are proposed for the definition of the geometry of piers, on the contrary for spandrels only few indications are available.

More in detail, the geometry of the spandrel elements in presence of *regular* walls can be easily obtained by considering the portions of masonry included between two vertically aligned openings. However, in case of not perfectly aligned openings no specific and systematic rules supported by numerical or experimental research can be found.

An empirical criterion which provides indications also in presence of irregularity in the opening pattern of the wall is proposed in Lagomarsino et al (2013). According to this rule the idea is to conventionally assume a mean value for the effective length L_{eff} of spandrel elements as a function of the overlapping part between the openings at the two levels; when no overlap is present or the opening lacks at all, it is suggested

to assume that portion of masonry as a rigid area (Figure 1.13). However, further studies, based on both experimental testing and numerical research, should be performed in order to validate the capability of the presented procedure for different types of opening layout.

Moving to masonry piers, the principal problem is the definition of their effective height h_{eff}, that represents, as widely recognized in the literature, a key modelling parameter in the EF models. Indeed, the geometry of pier panels usually plays a crucial role in the structural response, since they represent the main resisting elements devoted to counteract seismic actions and to transfer all the loads to the foundation system. Concerning the determination of their effective height, several uncertainties may arise when dealing with walls characterized by irregularly arranged openings, especially in presence of openings with different size at the same floor or in the case of external piers, where the formation of inclined cracks starting from the opening corners, documented by the observed damage, should be taken into account.

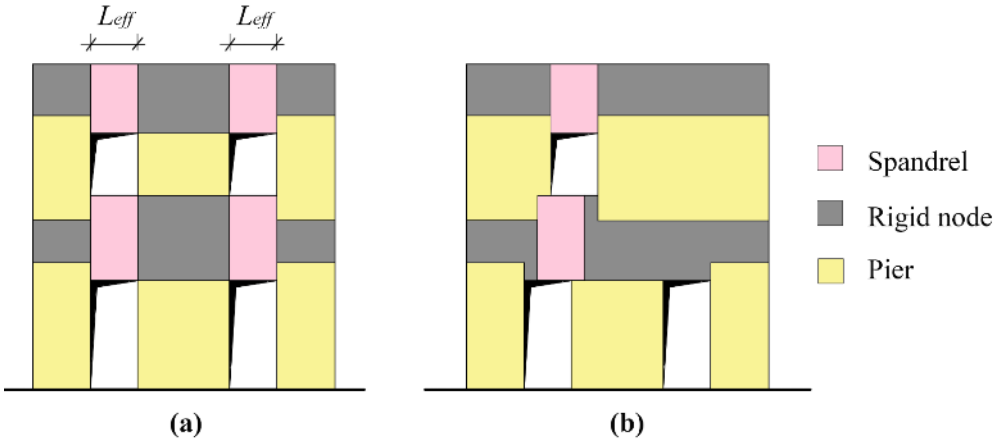

Figure 1.13 – Identification of the geometry of the spandrels (L_{eff} = effective length) according to the criterion proposed in Lagomarsino et al (2013) in presence of: (a) a regular wall; (b) an irregular wall with vertical misalignment between the openings located at two consecutive storeys.

Regarding this aspect, there are several criteria proposed in the literature and based on different principles. Some first proposals suggested the use of the openings edges as reference. The deformable height of piers was assumed equal to the distance between the extensions of the horizontal edges of the adjacent openings. Two alternatives were accepted in case of adjacent openings with different heights, namely to take the closest (minimum clear height) or the farthest distance between their horizontal edge lines. These simple rules were generally used in the application of the POR method (Tomaževič (1978)). Moreover, the criterion of the minimum clear height still represents today a possible choice adopted by professional engineers in presence of walls with openings of different size at the same story (Bracchi et al (2015)). However, these criteria may lead to an erroneous evaluation of the pier stiffness: too high the former and too low the latter (Dolce (1991)).

In FEMA 356 (2000) it is suggested to model masonry walls by taking into account the effect of spandrels only in terms of boundary conditions for piers; more specifically, as a function of spandrel rigidity, it is required to consider masonry piers as fixed-fixed (coupled) or cantilevered (uncoupled), defining the effective height of each pier as the height of the adjacent openings. This scheme presumes the assumption of a great rigidity for the spandrels and it may be reasonable when considering the *strong spandrels-weak*

piers (SSWP) behavior type (typical in case of new buildings, where often the spandrels are coupled to r.c. tie beams); however, it appears not suitable in presence of weak spandrels without tensile resistant elements and well-anchored lintels, that are common when dealing with existing buildings. In these walls, indeed, the spandrels fail before the piers and thus cannot be used to define their height (Moon et al (2006)). For this reason, some authors (Moon et al (2006)) recommend to assume the piers effective height equal to the interstorey height for a better reproduction of uncoupled piers (*weak spandrel – strong pier (WSSP)* behavior type). It is also stressed that the FEMA 356 (2000) approach fails in the case of walls with openings of different heights, even if spandrels can be considered as strong elements.

Another approach based on the consideration of the spandrels effects on the stiffness of piers is represented by the proposal formulated by Dolce (1991), which tries to overcome the above discussed shortcomings. In particular, in this case the idea is to take into account not only the equivalent stiffness of each pier, but also the mutual interaction with the surrounding spandrels; indeed, the state of deformation affecting the spandrels may result in a variable elastic restraint for the piers, thus inducing a considerable variation of their actual stiffness. On the basis of a series of Finite Element (FE) analyses on 20 different pier–spandrel systems characterized by varying geometry and boundary conditions, Dolce proposed a simplified formula, derived through a statistic evaluation of the equivalent stiffness of these modules. In particular, the values of stiffness obtained with the FE models were assumed as the reference solution and compared with those computed by considering the theory of the Timoshenko beam, with both shear and flexural deformability. In addition, an upper bound slope of 30° was found for segments simulating masonry cracks that start at the right or left corner of the openings and propagate toward the opposite pier edges.

The proposed formula is the following:

$$h_{eff} = h' + \delta \frac{B(h_w - h')}{h'} \qquad (1.2)$$

where: h_w is the interstorey height, δ is a coefficient equal to 1/3 that was properly calibrated by Dolce through the performed numerical simulations, B is the width of the pier and h' is a geometrical parameter (see Figure 1.14-a1) defined as the distance between the midpoints of the lines connecting the vertices of two consecutive openings; according to what observed about the cone diffusion of the cracks, these lines have a limit inclination of 30°. The final effective height of the pier (h_{eff}) is then obtained by properly modifying h' according to equation 1.2, which takes into account the global geometry of the wall level under consideration.

This criterion has met during the years a great success among the researchers working on masonry structures with the EF approach and today it still represents, even with some simplifications, the main reference for the frame discretization proposed by the most common EF models currently available for the analysis of URM walls.

In the Tremuri software (Lagomarsino et al (2013)) a criterion similar to the Dolce's proposal but without the limitation on the maximum inclination of cracks has been implemented. More specifically, according to this criterion pier elements are defined starting from the height of adjacent openings: when these latter are perfectly aligned, the height is assumed equal to that of the openings, while in presence of openings with different heights or external piers, it is assumed as the average of the heights of the adjacent openings or the average of the interstorey height and the height of the opening, respectively (Figure 1.14-b).

Some other works adopt a criterion similar to that proposed in Tremuri but with the limitation of the cone diffusion proposed by Dolce (Bracchi et al (2015), Rota et al (2014)).

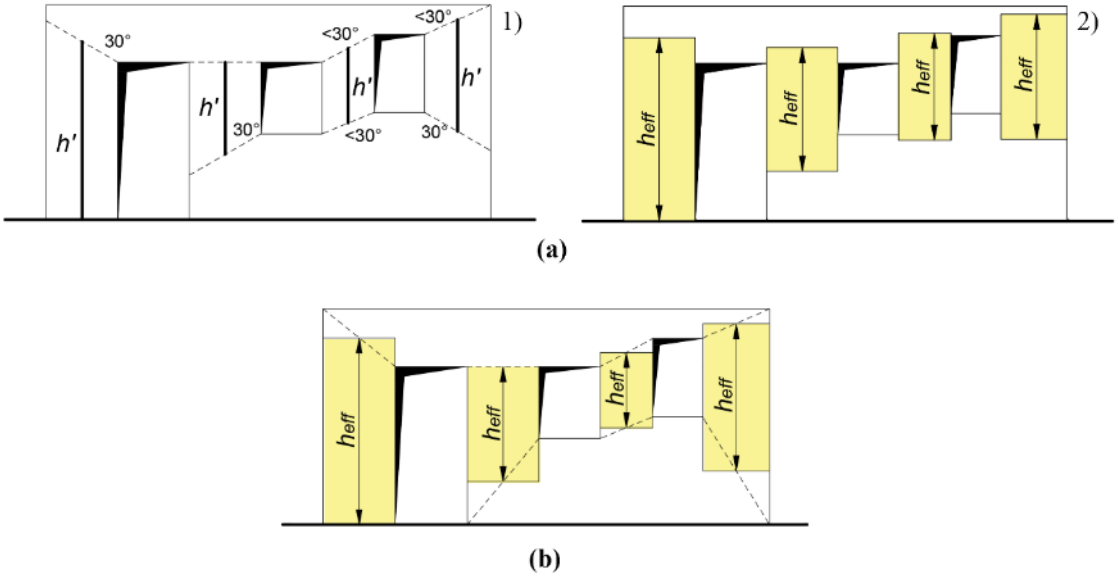

Figure 1.14 – Proposals for the identification of the pier effective height (h_{eff}) by: (a) Dolce (1991) (1) determination of *h'*, included in equation 1.2 for determining the final height of the pier; 2) final height of the pier) and (b) Lagomarsino et al. (2013).

It is worth noting that the above discussed criteria for the definition of the pier effective height are not related to the direction of the seismic action; consequently, a unique capacity model is considered for studying the in-plane behavior of a given masonry wall. However, other rules available in the literature take into account that the cyclic nature of the earthquake motion can induce a different failure pattern depending on the direction of the seismic forces, thus leading to a pier geometry which changes with the loading orientation (Figure 1.15).

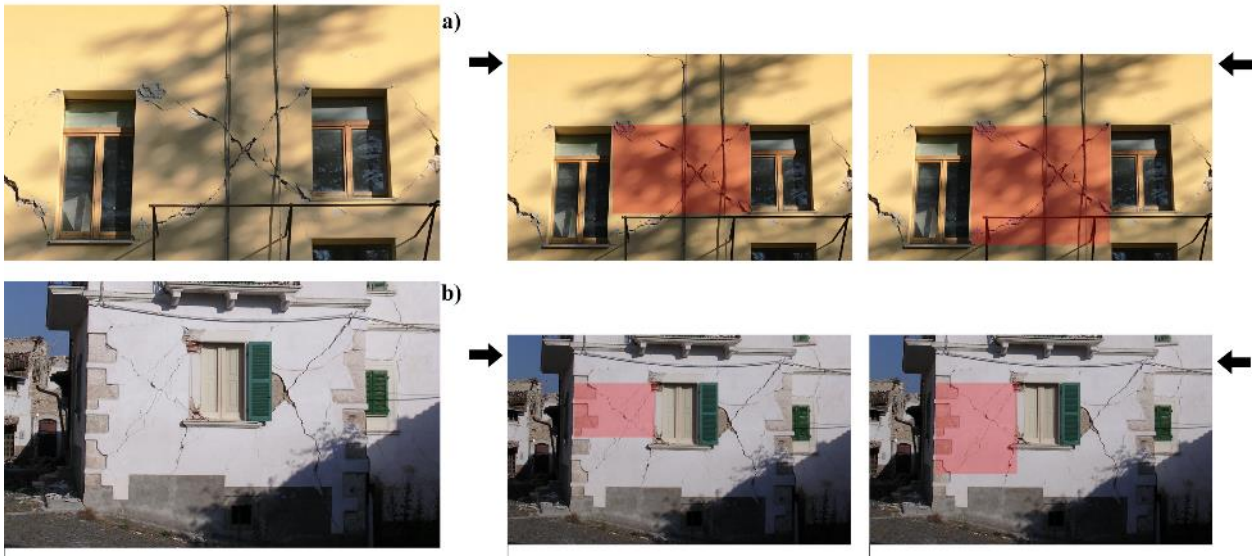

Figure 1.15– URM walls with shear failure of piers showing different effective heights, depending on the orientation of the seismic forces (a) 2016 central Italy earthquake b) 2009, L'Aquila, Italy, earthquake); photos by S. Cattari.

In particular, in Augenti (2006), on the basis of the observation of the damage occurred in residential and school masonry buildings after past earthquakes, it is proposed to assume the pier effective height equal to the height of the opening which follows the pier in the direction of the seismic load (Figure 1.16-a). This criterion has found helpful confirmations both in on-site inspections on cultural heritage buildings destroyed by the 2009 L'Aquila (Italy) earthquake (Augenti and Parisi (2010)) and in experimental tests carried out on masonry building prototypes in terms of damage distribution (Paquette and Bruneau (2003)).

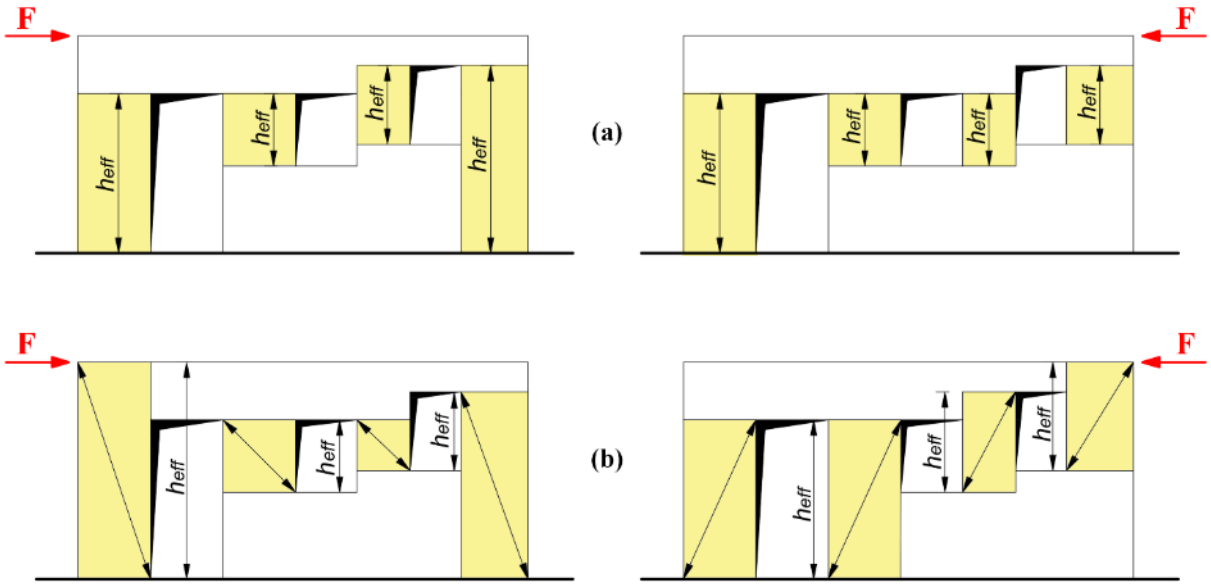

Figure 1.16 – Proposals for the identification of the pier effective height (h_{eff}) depending on the orientation of the seismic actions: (a) Augenti (2006) and (b) Moon et al (2006).

In addition, considering the results of a quasi-static lateral loading tests on a full-scale 2-story URM building (Yi et al (2006)), Moon et al (2006) proposed a pier effective height equal to the height over which a compression strut is likely to develop (Figure 1.16-b). The compression strut is defined by assuming that cracks can develop either horizontally or at 45°. Moreover, the strut is assumed to develop at the steepest possible angle; that is, the likely compression strut is taken as the strut which offers the minimum lateral resistance. This criterion, which correctly predicts all the flexural cracks described by Yi et al (2006), is already suggested in some National Standards (NZSEE (2015)) and was recently used for comparative analysis of simplified macroelement methods (Marques and Lourenço (2011)); however, it seems more related to a flexural failure rather than to a diagonal shear cracking.

As shown in Figure 1.16, the adoption of the criteria proposed by Augenti (2006) and by Moon et al (2006) may lead, especially when irregular opening patterns are considered, to two different capacity models for the same wall, depending on the considered direction of the seismic forces.

Finally, a further modelling strategy, obtained as a combination of those discussed above, is proposed in Parisi et al (2013), referring to a simple system represented by a single masonry wall with an opening (trilith) subjected to lateral loads. The suggested rule, which is derived through analytical-numerical comparisons on lateral stiffness of single piers, assigns the effective height proposed by Dolce (1991) to

the pier located on the side of the lateral action, while for the opposite pier it is proposed to assume an effective height equal to the adjacent opening or equal to the height of the applied lateral force, depending on whether it is uncracked or cracked, respectively.

This criterion is based on the consideration of the normal stress distribution acting on the spandrel and accounts for the damage occurring in this panel. However, it results quite complex to be implemented in a numerical model since it provides for each pier an effective height that may vary depending not only on its location with respect to the applied seismic action, but also on the considered performance level. Moreover, it has been developed for a specific and very simple configuration, represented by a trilith with prevailing rocking response, and its extension to other more complex configurations (multi-storey walls, walls with more than one opening per storey, irregular opening patterns, ...) should be properly assessed.

Within this heterogeneous framework, the building codes do not provide specific indications about the criteria to use. On the contrary, they are quite ambiguous on the matter: EC8 (CEN (2004a)) and NTC08 state that "unreinforced masonry buildings should have vertically aligned openings" (note that no horizontal alignment is specified) and that "in absence of more accurate evaluations, only the wall portions with vertical continuity from the analysed level to the foundation system should be considered in the structural model". These provisions are useful for the design of new buildings, favouring regular solutions, but do not mention alternative methodologies in the case of the assessment of existing buildings with irregular walls. Moreover, the problem of the discretization of the irregular walls is pointed out only in rather general terms and an exhaustive consideration of all the possible sources of irregularity in the opening pattern is not present. Indeed, only the vertical misalignment between openings at different storeys is taken into account, while the other types of irregularities, including the presence of openings with different heights (i.e., doors and windows) at one or more stories, are disregarded, even if they are clearly of concern for structural modelling of walls.

For what concerns spandrel elements, the indications provided are even less: in NTC08 it is stated that spandrel elements can be included into the model only if supported by lintels adequately bonded to the adjoining walls; however, no specific rules are provided for their identification when they have to be included in the structural models.

This literature review highlights that, since the seismic codes are not exhaustive and in literature many different criteria (or a very low number in case of spandrels) are available, the EF idealization of a given masonry wall is quite arbitrary. As a consequence, given the same architectural configuration it is possible to obtain, depending on the chosen criterion, different structural models. Although these differences are more evident when considering *irregular* walls, even in a *regular* wall some uncertainties may arise, mainly regarding the effective height of the external piers (Figure 1.17).

It is evident that when different structural models are considered for the same wall, different global responses can be obtained (in terms of stiffness, strength and displacement capacity): this may imply critical issues on the outcomes of the seismic verifications that, in case of masonry buildings, are performed on the global pushover curve. In particular, in Chapter 2 (section 2.1), some sensitivity analyses on a simple

structure devoted to understand the repercussions of the adoption of different rules for the geometry of the structural elements on the outcomes of pushover analyses are presented.

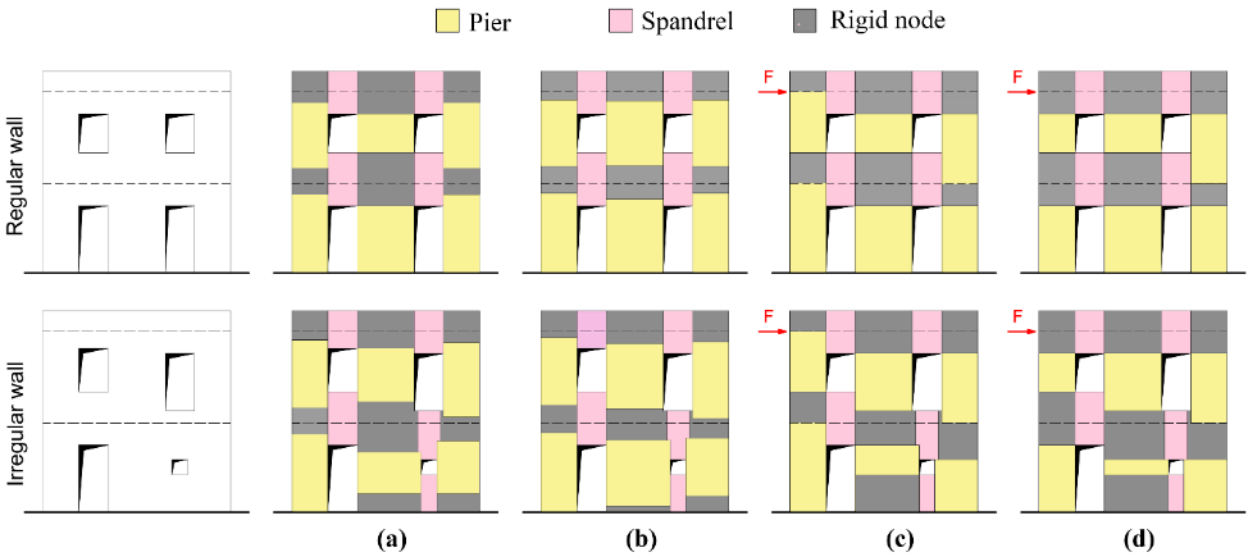

Figure 1.17- Different EF idealizations in case of a regular and of an irregular masonry wall. Pier effective height according to: (a) Lagomarsino et al (2013), (b) Dolce (1991), (c) Moon et al (2006), (d) Augenti (2006); spandrel effective length according to Lagomarsino et al (2013).

Furthermore, in Bracchi et al (2015) the Authors performed a comparative analysis (using nonlinear static analyses) on eight building prototypes considering different possible modelling assumptions, and among them different criteria for the wall discretization: minimum clear height; Lagomarsino et al (2013); and Lagomarsino et al (2013) with cone diffusion limitation. From this work, the assumptions made on the wall discretization seem to affect not only the global initial stiffness but, above all and largely, the ultimate displacement of the equivalent system. This clearly shows the importance to correctly define specific and validated criteria to be used in the EF models for the schematization of URM walls.

It is also stressed that all the discussed criteria on wall discretization have been mainly developed for masonry buildings with quite regular opening patterns, and not enough and exhaustive comparative studies justify those schematizations for existing buildings with very irregular opening layouts or with specific types of irregularity, such as the presence of very little openings, as the one at the ground floor in the irregular wall illustrated in Figure 1.17. In these cases, their application should be carefully assessed in order to avoid erroneous predictions on the seismic capacity of the given walls.

All these considerations motivate the need of a systematic comparison between the different criteria when applied to irregular walls as well as the necessity of a proper evaluation of their reliability in predicting the effective structural response in presence of different opening layouts, which are actually the main objectives of this thesis.

1.3.2 Studies on irregular URM walls

While the problem of irregular openings in two-dimensional structures has been widely studied in literature for reinforced concrete (r.c.) walls, both experimentally and numerically (Berti et al (2017)), on

the contrary, in case of URM walls the research is yet at a preliminary stage, and the works focusing on this problem are all quite recent. Some of these studies are aimed to understand how much the presence of irregularities in the opening pattern affects the seismic vulnerability of the walls, while others are focused on the evaluation of the accuracy of the EF models in these cases.

More specifically, one of the first works in this field is the one by Parisi and Augenti (2013). Here a systematic classification of the most recurrent types of irregularities that can affect masonry walls is provided, proposing also geometric indexes for quantifying them. In particular, four basic irregularity types are identified, basing on simple geometric modifications with respect to a regular scheme represented by a two-story wall with four openings (two horizontal and two vertical alignments):

(1) *Horizontal irregularity*: the wall has openings with different heights at the same story and equal widths along the height (Figure 1.18-a)
(1) *Vertical irregularity*: the wall has openings with equal heights at the same story and different widths along the height (Figure 1.18-b).
(2) *Offset irregularity*: the wall has horizontal and/or vertical offsets between openings with equal or different sizes. (Figure 1.18-c).
(3) *Variable openings number irregularity*: the wall has different number of openings per story (Figure 1.18-d).

The first three basic irregularities are here defined for single couples of openings, whereas the last irregularity is defined for couples of stories.

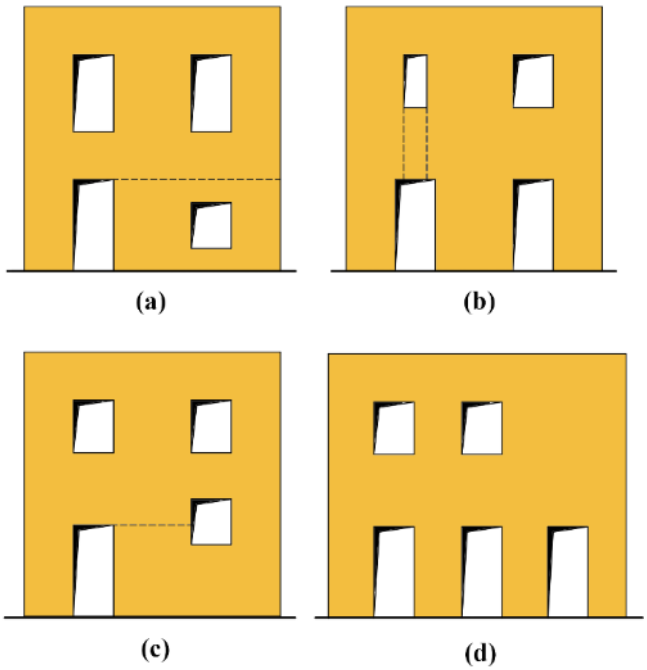

Figure 1.18 – Types of irregularities characterizing the opening pattern of masonry walls according to Parisi and Augenti (2013): (a) horizontal irregularity; (b) vertical irregularity; (c) offset irregularity; (d) variable openings number irregularity.

The Authors also performed, by using EF models, parametric analyses on walls with horizontal and vertical irregularity, with the aim to evaluate the effects of such irregularities on some key parameters of

the seismic response (elastic vibration period, ultimate shear force, ultimate displacement, ductility) with respect to the regular wall. Then, through regression analyses, some simplified models for assessing each capacity parameter as a function of the introduced irregularity indexes were obtained. However, in these studies the attention is focused on the evaluation of the seismic vulnerability of irregular masonry walls, assuming that the EF approach can provide reliable results also when applied to these cases.

In Parisi et al (2015) a similar work is carried out on walls with vertical opening offset, this time through analyses performed with a continuous FE model; in particular, in addition to the capacity parameters previously introduced, also the stress/strain fields characterizing the examined irregular walls are evaluated, and the performed analyses highlight limitations and need for modification of current rules for simplified macroelement analysis of masonry buildings.

Other more recent works deal with the effects produced by the irregularities on the modelling accuracy of the EF approach, making comparisons with more accurate modelling techniques (in general FE models where masonry is modelled as a continuum material or through micro-modelling approaches), and considering both analyses in linear and nonlinear field. In these studies, the FE models represent the reference solution, so that the accuracy of the EF approach is estimated in terms of percentage error with respect to the results of the FE models. In general, with increasing irregularity, the accuracy of the EF models decreases.

Within this context, in Berti et al (2017) there is an attempt to define a limit for the applicability of the EF approach as a function of the entity of the irregularity characterizing the opening pattern of a given wall; in particular, it is proposed to introduce a confidence factor aimed to penalize the application of the EF approach to walls with significant irregularities. However, both Berti et al (2017) and Parisi and Augenti (2013) do not consider different possible criteria for the EF idealization of the analysed walls: they assume a fixed criterion (the one proposed by Dolce (1991) and the one proposed by Augenti (2006), respectively). Nevertheless, the uncertainties in the EF idealization should be included in this kind of evaluations since, as mentioned in the previous section and demonstrated also in the analyses discussed in Augenti and Romano (2008), in presence of irregularities the adoption of different criteria for the identification of piers and spandrels may significantly affect the obtained response.

Other works are aimed to evaluate the accuracy of the EF modelling technique not only in presence of irregular walls, as a function of the level of irregularity, (Siano et al (2017a), Siano et al (2017b)) but also for regular walls, characterized by openings still aligned but with varying dimensions (Siano et al (2017a), Siano et al (2018)). In this last case, the parameter of interest is the relative geometry of piers and spandrels, that may lead, in extreme cases, to the so-called by Authors *non frame-like* walls, where the consistency between the wall geometry and the ideal frame configuration is low, so that the applicability of the EF approach may result questionable.

Differently from the before mentioned studies, in all these works two possible criteria for the definition of the pier effective height are considered: the one proposed by Dolce (1991) and the other by Augenti (2006). Comparisons between EF and FE models are realized by using both linear and nonlinear analyses, finding that the accuracy of the EF approach tends to decrease with the introduction of the irregularities and, in case of regular walls, when the geometrical affinity with an ideal frame configuration decreases. On the

basis of the obtained results, also in this case it is proposed to define specific limits of applicability for the EF approach.

Even if these studies represent a first attempt to perform the validation of the EF approach when applied to irregular masonry walls, however the evaluation of the reliability of this modelling technique appears to be not exhaustive, since the comparisons performed with more refined models are limited to the global response or to some checks on the obtained damage patterns, while a systematic and in-depth analysis also in terms of local response is still lacking.

In Calderoni et al (2017) some suggestions for the schematization of the Equivalent Frame in presence of specific irregular wall configurations are provided, and even in this case comparisons between EF models and more accurate FE models are employed, however mainly in the linear field (in terms of top displacements and elastic stiffness). In particular, some real existing walls belonging to historical old masonry buildings and with rather complex opening patterns are considered, and some targeted modelling strategies for these cases are proposed (Figure 1.19).

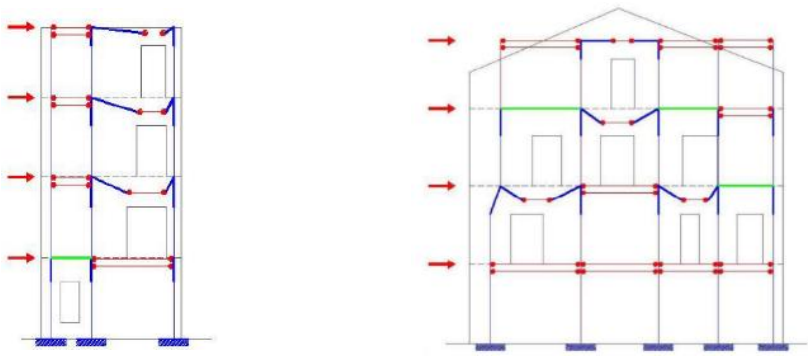

Figure 1.19 – Solutions for the application of the EF schematization to specific irregular masonry walls proposed in Calderoni et al (2017) (from Calderoni et al (2017)).

The suggested strategies refer to the types of irregularities encountered in the analysed walls (mainly the presence of a different number of piers at each storey, of vertically misaligned openings and of a variable height of the wall – i.e. presence of gables). Even if these suggestions may represent possible solutions to take into consideration for these types of irregularities, they appear to be non-systematic. Indeed, they have been meant for the specific considered cases, so that their application to different wall configurations is not immediate and requires (as also recognized by the Authors) an accurate and rational modelling process to be performed by an expert judgement with a deep knowledge of the problems affecting the behavior of masonry walls.

All the aforementioned contributions demonstrate the increasing interest which is developing, especially in the last years, in the application of the EF approach to the study of the seismic behavior of irregular masonry walls and in the problems connected with the identification of the structural elements of the frame in these cases. This clearly contributes to contextualize the research activity carried out in this thesis, underlining the relevance of the topic it is based on.

Even though employing different methodologies, the presented studies substantially confirm the importance of correctly including the irregularities characterizing the opening patterns within the capacity models of the walls, since they in general lead to a non-uniform distribution of the gravity loads between the masonry panels and also to a significant damage localization, thus influencing the seismic response of the considered structure and increasing its vulnerability. Moreover, it emerged that the piers geometry represents a key parameter in the EF modelling, since it can strongly influence the outcomes of the analyses. In particular, it came out that the types of irregularity which mostly affect both the vulnerability of the wall and the accuracy of the obtained results are those where the changing dimension is the pier effective height: (Parisi and Augenti (2013), Siano et al (2017a)). These aspects clearly highlight the need of a careful calibration of this parameter to improve the capability of the EF models to describe URM walls performances. In addition, also the problem of the correct identification of the spandrel elements in presence of vertically misaligned openings arise, since no systematically validated rules are available to this aim.

Nevertheless, it is important to stress that all the illustrated studies underline the presence of some difficulties and critical issues in the application of the EF approach to irregular masonry walls but do not provide specific indications about how to proceed in these cases and do not make systematic investigations about the potentialities and the limits of the rules available for the EF idealization in presence of different opening layouts. Also, the numerical validation of the approach when applied to irregular walls appears to be not exhaustive and further detailed comparisons with more refined models, especially in terms of local response, are required, thus motivating the work here carried out.

CHAPTER 2

2 DESIGN AND ASSESSMENT OF URM BUILDINGS: RELEVANT EXPERIENCES

In this Chapter some of the results obtained within the ambit of two different research projects I had the possibility to participate to, as a part of the Research Unit of the University of Genoa, are illustrated.

These experiences actually represent the preliminary and introductory studies to the research that is the main object of this thesis. Indeed, both the research projects refer, even if with different aims, to the use of the Equivalent Frame approach, and were useful to deepen different aspects of this modelling technique. More specifically, the participation to these researches allowed on one hand to understand the repercussions on the seismic assessment and design of modelling choices that can be made when using this kind of models and on the other to directly experience and identify the strengths and the weaknesses of this approach as well as the most critical aspects that characterize it.

In particular, the two projects are: the "Task 4.3 - Analysis of Benchmark URM Structures" carried out within the ReLUIS 2014-2018 project – *Topic: Masonry Structures* (described in section 2.1) and the RINTC project (described in section 2.2).

After a brief description of the specific objectives of these projects, in the next sections the attention will be mainly focused on those aspects and results which are more significant for addressing the insights and the analyses that were made in the PhD work thesis.

2.1 ANALYSIS OF BENCHMARK STRUCTURES

The results described in this section refer to the research activities of "Task 4.3- Analysis of Benchmark Structures*"* carried out within the ReLUIS 2014-2018 project – *Topic: Masonry Structures* (Coord. Proff. S. Lagomarsino, G. Magenes and C. Modena), founded by the Italian Department of Civil Protection (DPC). Starting from 2014, this research program (Cattari et al (2016)) has involved several Italian universities, (University of Chieti-Pescara - UniCH coordinated by Proff. E. Spacone and G. Camata, University of Catania - UniCT coordinated by Prof. I. Caliò, University of Bologna - UniBO coordinated by Prof. S. De Miranda, University of Naples - UniNA coordinated by Proff. B. Calderoni, University of Pavia- UniPV coordinated by Prof. G. Magenes, University of Rome – UniRM3 coordinated by Prof. G. De Felice, University of Venice – IUAV coordinated by Prof. A. Saetta), including the University of Genoa (coordinated by S. Cattari). The whole research group that participated to this activity is briefly referred to in the following as "Task 4.3 Work Group". The activity has been coordinated by Prof. Guido Magenes and Serena Cattari.

The final objective of this research, which is still in progress, is to produce scientific reports that can be useful tools for professionals, as well as to make users more aware of the correct use of software programs by providing them analytical tools and a methodologic approach for the critical analysis of the obtained results. The research is motivated by the awareness that nowadays computer programs represent one of the

essential tools adopted by analysts and engineers for the seismic analysis of new and existing buildings. However, since the outcomes of the seismic vulnerability evaluations significantly affect not only the design of strengthening interventions at the scale of single buildings but also the plan of mitigation policies at large scale, the problem of the reliability and the correct use of these software codes arises.

The research activity was organized by defining various benchmark structures of increasing complexity (single panel, trilith, 2D wall, single-unit two-story building, real 3D buildings – see Figure 2.1), each accompanied by data sheets which contain all the input information necessary to reproduce the structures by a third party, too. The considered structural typologies were specifically designed providing, where possible, analytical solutions as reference, procedures for checking the results or approximate estimates of the expected range of variation through simplified approaches.

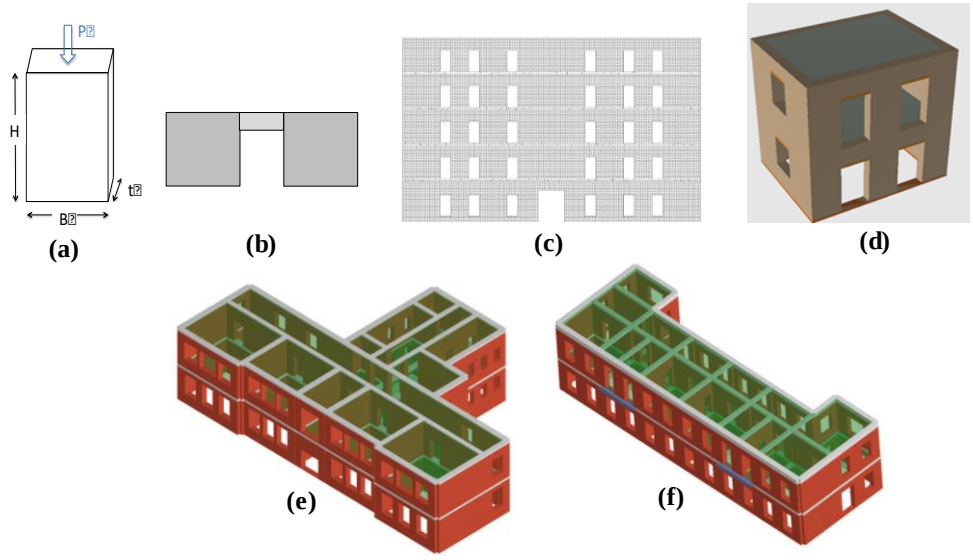

Figure 2.1– Benchmark structures defined in the research project: (a) single panel; (b) trilith; (c) multi-storey wall; (d) 2-story building; (e) real building located in Visso (MC), Italy); (f) real building located in Pizzoli, (AQ), Italy.

As widely discussed in Chapter 1, different modelling techniques can be adopted for the seismic analysis of masonry buildings; within this context, the modelling strategies considered in the project are aimed to cover a rather wide group of the different possible methods among which the professional engineers can choose. In particular, the introduced benchmark structures were analysed by the involved research units through NonLinear Static Analysis and by using different computer programs based on Continuum Finite Element, Discrete Element and Structural Element modelling approaches.

Among the Structural Element modelling approaches, particular attention was given to the Equivalent Frame (EF) method, which is one of the most used. Indeed, it has been implemented in many computer programs specifically oriented to the analysis of masonry buildings; moreover, it can be just as effectively implemented in general purpose software packages directly by the analysts. This has led to a huge variety of options, but also to a potential scattering of the achievable results, as testified also in literature (Marques and Lourenço (2011), Marques and Lourenço (2014), Calderoni et al (2015), De Falco et al (2017)).

Since within the "Task 4.3- Analysis of Benchmark Structures" several computer programs based on the Equivalent Frame approach were used, the research activity represented also an opportunity to actually

evaluate the variability and the scattering of the attainable results when different implementation strategies of this modelling approach are used.

In particular, the participation to this comparison among various software allowed to directly experience the model uncertainty. This last, indeed, implies the adoption of specific assumptions that can differ from case to case and that should be known by the user, in order to correctly interpret the results.

Therefore, the benchmarking of different models belonging to the EF approach allowed to:

- identify, through parametric analyses, the most critical modelling issues involved within the use of these models;
- directly experience how specific modelling aspects (modelling of spandrels, of flange effect, of stiffness degradation, of different failure modes) are treated in the different models and the related consequences on the seismic response of the analysed structure;
- understand if, under the same hypotheses and by sharing some modelling choices, it is possible to obtain a relatively low scatter of the results.

Among the wide set of benchmark case studies analysed within the project, in the following sections only the results related to the single-unit two-story building are presented (Figure 2.1-d). Indeed, even if rather simple, this case-study allows to highlight, through a series of parametric analyses, several specific and interesting modelling aspects as well as critical issues that are useful to motivate and contextualize some choices made in this work.

A more detailed description of the results obtained through the analysis of the other benchmark structures can be found in Cattari et al (2016) and in Cattari et al (2017).

2.1.1 Two-story URM benchmark configurations

The analysed benchmark structure is represented by a single-unit two-story masonry building with rigid diaphragms, for which a total of seven configurations were obtained by varying the layout of the openings characterizing the walls and the structural details, as better explained in the following.

The specific features of each defined configuration are meant to deepen some critical aspects related to the modelling of the masonry buildings, such as the role of the axial load variation on the pier strength, the effects of the interaction between the structural elements (piers and spandrels), the aspect of the geometry adopted for them and the effects induced by the presence of tensile resistant elements coupled to the spandrels, with respect to the criteria now proposed in the Italian building code (NTC08). Moreover, the analysis of this 3D structure allows to study the effects of the stress redistribution in presence of walls with different stiffness as well as the influence of torsional and flange effects.

In Figure 2.2 the geometry of the conceived configurations is shown.

With regard to the opening pattern of the walls characterizing the analysed structures, three different geometries were considered, hereinafter referred to as A-type wall, B-type wall and C-type wall (as indicated in Figure 2.2). It is underlined that the geometry characterizing the A-type wall reproduces the so-called *Door Wall* tested in the laboratory of the University of Pavia in 1994 with a pseudo-static cyclic test (Calvi and Magenes (1994)).

These different wall types were assembled in various ways in order to obtain three different geometrical configurations (Figure 2.2):

- structure I: the bearing walls (oriented in the X direction, according to the coordinate system indicated in Figure 2.2) are represented by two equal A-type walls, thus providing a regular and symmetrical structure; side walls are without openings;
- structure II: it is defined starting from structure I and substituting one of the A-type walls with a B-type one, thus obtaining an asymmetrical structure;
- structure III: it is obtained starting from structure II and substituting one of the side walls with a C-Type wall.

For all the considered structures the wall thickness was assumed equal to 0.25 m, while the floor slabs (each one carrying a live load of 10 kN/ m^2) are perpendicular to the walls oriented in the X direction.

Concerning the structural details, four different configurations were considered:

- case a): absence of tensile resistant elements coupled to the spandrels (aimed to promote a *weak spandrel-strong pier* behaviour type);
- case b): presence of steel tie rods coupled to the spandrels;
- case c) presence of reinforce concrete (r.c.) tie beams coupled to the spandrels;
- case d): starting from case c) and imposing fixed rotations at each floor level (*shear type* idealization).

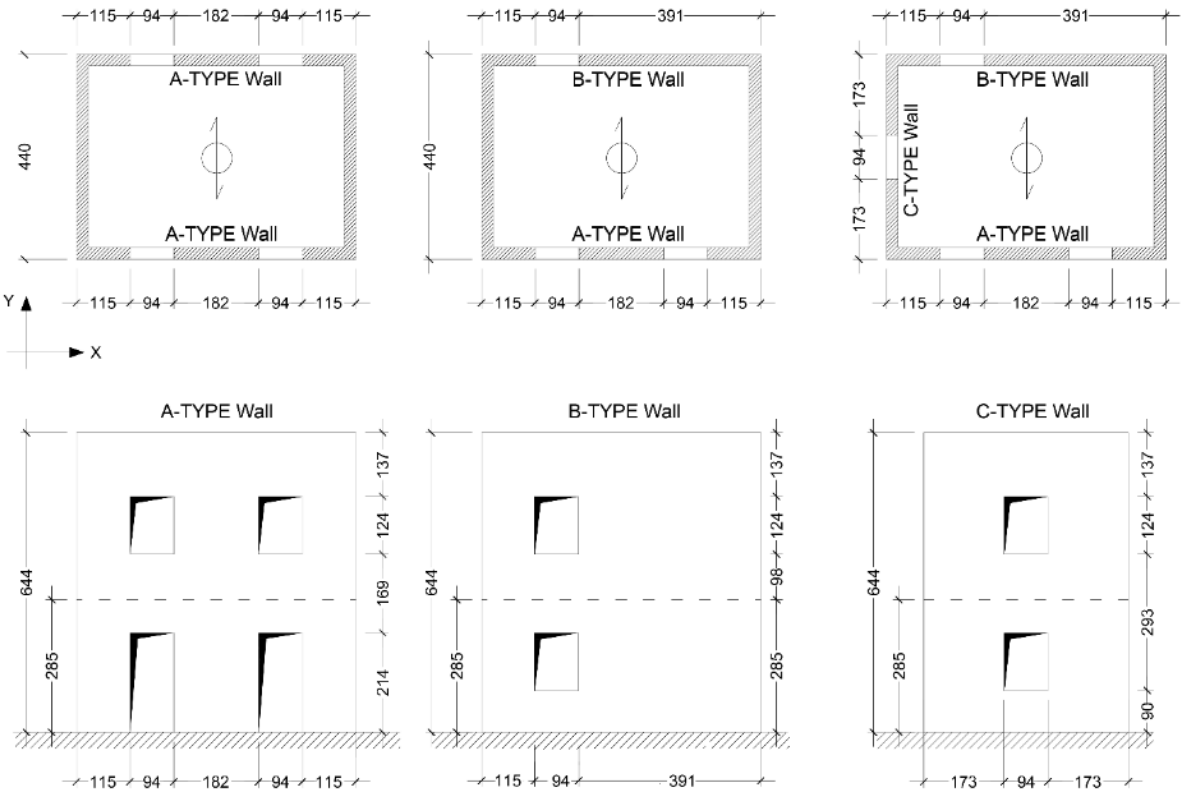

Figure 2.2 - Plans and façades of the analysed benchmark structure (measures in cm); the dashed lines indicate the interstorey height.

By combining the three abovementioned structures (I, II and III) and the different possibilities regarding the structural details, seven final configurations were obtained and then analysed. In the following, for the sake of brevity, the attention will be focused only on the results related to structure I and II. In the case of structure I only two options were considered for what concerns the structural details, namely option a) and option b), while for structure II all the options were examined. The obtained configurations are identified in the following with the acronyms Ia, Ib, IIa, IIb, IIc, IId.

As far as the mechanical parameters are concerned, the adopted values are reported in Table 2.1. In particular, the parameters used for masonry are representative of a brick masonry characterized by clay bricks and lime mortar. Some of these parameters were derived from the experimental campaign which the benchmark structure is inspired to (Anthoine et al (1995)). The elastic moduli of masonry shown in Table 2.1 refer to the initial elastic condition. In case of nonlinear beam idealization of masonry panels with elastic-perfectly plastic constitutive law, in order to obtain the parameters representative of the cracked condition they were reduced by using a coefficient equal to 0.5. The yielding strength of piers was computed as the minimum between: the Turnsek and Cacovic model (1971), assumed for interpreting the diagonal shear cracking failure mode (as proposed in §C.8.7.1.5 of the Instruction for application of the NTC08 (MIT 2009)) and the criterion proposed in NTC08, based on the beam theory that neglects the tensile strength of the material and assumes a stress block normal stress distribution at the compressed toe, for interpreting the flexural failure mode. The collapse of panels was determined by assuming a drift limit value equal to 0.4% and 0.6% in the case of the shear and flexural failure modes, respectively. For spandrels, the criteria proposed in NTC08 were assumed as reference.

In the case of b) configurations, tie rods have a diameter of 20 mm and are placed at the floor level (preloaded with 10 kN), while in c) configuration the dimensions of the r.c tie beams are 0.25x0.25 m^2. Moreover, each r.c tie beam is reinforced with 4ϕ16 longitudinal rebars (2 at the extrados and 2 at the intrados) and ϕ10 stirrups with 200 mm spacing.

The diaphragms are assumed as rigid; when in the considered software the assumption of infinite stiffness for the diaphragms is not available, it has been assumed to consider a r.c. slab with 0.2 m thickness.

Table 2.1- Mechanical properties of the materials adopted for the single unit two-story masonry building.

	f_c [MPa]	τ_0 [MPa]	E_m [MPa]	G_m [MPa]	w [kN/m^3]
Masonry	6.20	0.163	1800	600	17.50
Steel		**Tie rods** S235 – f_{yk} = 235 MPa		**Tie beams rebars** B450C – f_{yk} = 450 MPa	
Concrete	Class C25/30 – f_{ck} = 25 MPa				

Notes: f_m masonry compressive strength; τ_0 masonry shear strength; E_m masonry elastic modulus; G_m masonry shear modulus; w masonry specific weight; f_{yk} characteristics yield strength of steel; f_{ck} characteristic cylindrical compressive strength of concrete.

Where the presence of r.c. tie beams is considered (configuration IIc), their effective length was assumed equal to the opening width, locating them at the level of the diaphragm.

As widely discussed in section 1.3.1, in the EF modelling approach the choice of the geometry to adopt for the structural elements actually represents a critical issue; indeed, seismic codes do not provide specific and standardized indications, so that it may represent a first source of uncertainty and a potential cause for differences on the obtained results.

In this context, in a first set of analyses it was decided to neglect the effect of this epistemic modelling uncertainty, and the same geometry for the structural elements (piers and spandrels) was adopted for all the considered software based on the EF modelling approach. The adopted discretization (based on the rules proposed in Lagomarsino et al (2013)) and the numbering used in the following for the identification of the elements are shown in Figure 2.3 in case of the walls composing structure II. The same applies also to structure I, that is obtained by simply substituting the B-type wall with another A-type wall.

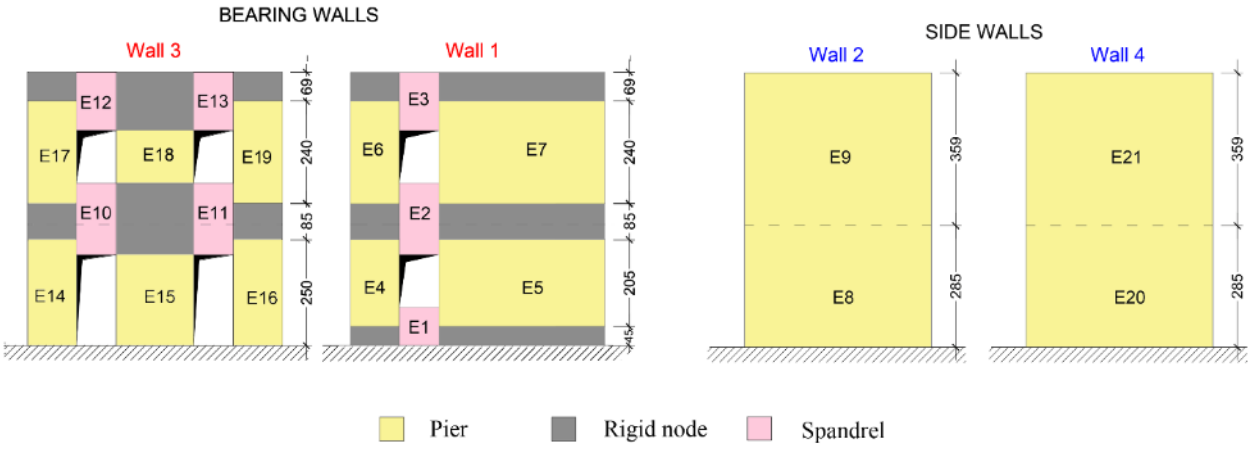

Figure 2.3 – Structure II: adopted element numbering and EF idealization used in all the examined software for the A-type and the B-type walls.

For this first set of analyses the results of eight EF models are available from activities of Task 4.3 Work Group. In particular, among these eight Structural Elements models six software describe the response of structural elements through a nonlinear beam with lumped plasticity (3Muri distributed by STA.Data (2017) and developed by Lagomarsino et al (2013); Aedes.PCM (2018); ANDILWall developed by Magenes et al (2006) and Manzini et al (2006); CDSWin OpenSees© (2018) based on the hinge formulation proposed in Spacone et al (2007); MIDAS Gen (2018); SAP2000), one software is based on a fiber model (MIDAS Gen (2016) based on the model proposed in Spacone et al (1996)) and one adopts a macro-element formulation, in which the different failure modes (flexural and shear) are managed through nonlinear springs (3DMacro developed by Caliò et al (2009) and Caliò et al (2012)). In particular, the analyses have been executed: in case of 3Muri by the RU of UniGE; in case of Aedes.PCM, CDSWin OpenSees© and MIDAS Gen by the RU of UniCH; in case of SAP2000 by the RU of UniNa; in case of ANDILWall by the RU of UniPV; in case of 3DMacro by the RU of UniCT.

In this first phase, the modelling process was faced by adopting, when possible, the same common assumptions: the same equivalent frame idealization for the geometry of piers and spandrels (see Figure

2.3) was shared and the same hypothesis on the out-of-plane contribution of the walls was considered (that is, when possible, it was neglected). This choice reflects the will to reduce the influences of both the different characteristics of the software and of the arbitrariness of analysts in the definition of the models (which would produce a greater dispersion of the results).

Then, in a second phase, further investigations were realized in the case of the EF model realized by adopting 3Muri program, addressed to the specific scopes of this PhD thesis. In particular, for structure IIc, the influence of different possible assumptions regarding: i) the effective height of piers and ii) the modelling of the connection between the orthogonal walls were explored. With reference to point i), in addition to the aforementioned mesh, three other EF idealizations were considered for the walls of the analysed building, defined on the basis of different criteria available in the literature and introduced in section 1.3.1.

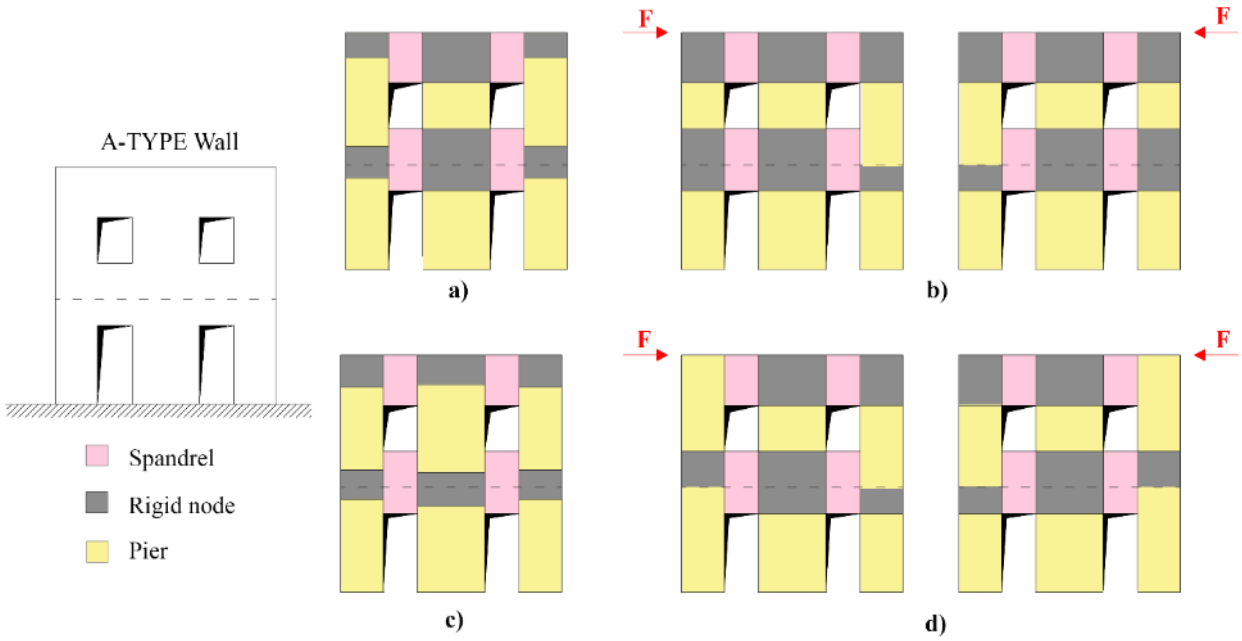

Figure 2.4 – EF idealization of the A-type wall according to different criteria employed for studying the sensitivity to the adopted structural element geometry (pier effective height: a) Lagomarsino et al (2013); b) Augenti (2006) c) Dolce (1991); d) Moon et al (2006); spandrel effective length: Lagomarsino et al (2013)).

In particular, since the openings of the considered walls (A-type and B-type walls) are perfectly aligned at the two consecutive storeys, no specific uncertainties are present in the identification of spandrels, for which the criterion proposed in Lagomarsino et al (2013) was adopted. Regarding the determination of the pier effective height, the considered rules are those presented in Dolce (1991), Augenti (2006) and Moon et al (2006). It is recalled that according to the criteria suggested in Augenti (2006) and in Moon et al (2006) the pier effective height is a function of the direction of the seismic action; therefore, in these cases two different structural models are considered, depending on the verse of the performed analysis.

The comparison between the different introduced idealizations is illustrated in Figure 2.4 in case of the A-type wall (indicated also as “Wall 3”) and in Figure 2.5 for the B-type wall (indicated also as “Wall 1”). It is possible to see that the choice of different criteria actually leads to quite significant differences in the geometry of piers and, consequently, in the extension of the rigid nodes. This clearly affects the final

deformability of the considered wall and may actually have not negligible repercussions on the stiffness, strength and displacement capacity of the single structural elements.

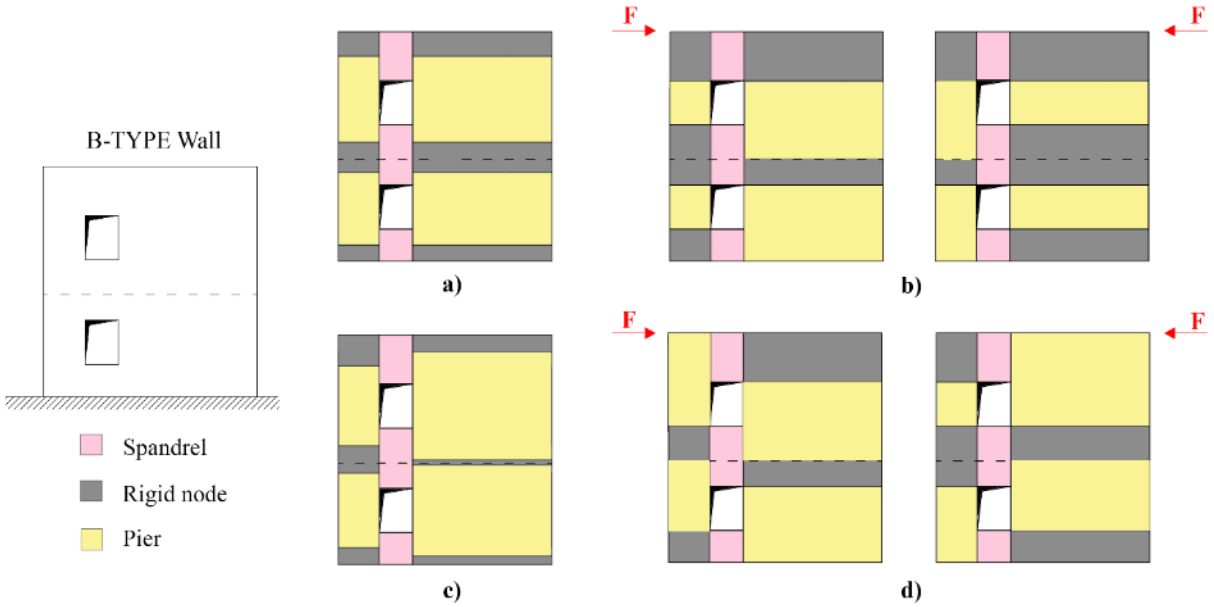

Figure 2.5 – EF idealization of the B-type wall according to different criteria employed for studying the sensitivity to the adopted structural element geometry (pier effective height: a) Lagomarsino et al (2013); b) Augenti (2006) c) Dolce (1991); d) Moon et al (2006); spandrel effective length: Lagomarsino et al (2013)).

In Table 2.2 the effective height h_{eff} of the pier elements as well as their aspect ratio λ are reported, considering all the EF idealizations previously introduced.

Table 2.2 – Effective height (h_{eff}) and aspect ratios (λ) obtained for the piers of A-type and B-type walls of structure II according to the considered criteria. See Figure 2.3 for element numbering.

			Lagomarsino et al. (2013)	Dolce (1991)	Moon et al (2006)		Augenti (2006)	
					Pos	Neg	Pos	Neg
B-type (Wall 1)	E4	h_{eff} [m]	2.05	2.09	1.95	2.14	1.24	2.14
		λ [-]	1.78	1.82	1.70	1.86	1.08	1.86
	E5	h_{eff} [m]	2.05	2.56	2.14	1.95	2.14	1.24
		λ [-]	0.52	0.65	0.55	0.50	0.55	0.32
	E6	h_{eff} [m]	2.40	2.24	2.61	2.22	1.24	2.22
		λ [-]	2.09	1.95	2.27	1.93	1.08	1.93
	E7	h_{eff} [m]	2.40	3.05	2.22	2.61	2.22	1.24
		λ [-]	0.61	0.78	0.57	0.68	0.57	0.32
A-type (Wall 3)	E14	h_{eff} [m]	2.50	2.53	2.85	2.14	2.14	2.14
		λ [-]	2.17	2.2	2.48	1.86	1.86	1.86
	E15	h_{eff} [m]	2.14	2.34	2.14	2.14	2.14	2.14
		λ [-]	1.18	2.03	1.18	1.18	1.18	1.18
	E16	h_{eff} [m]	2.50	2.53	2.14	2.85	2.14	2.14
		λ [-]	2.17	2.20	1.86	2.47	1.86	1.86
	E17	h_{eff} [m]	2.40	2.24	2.61	2.22	1.24	2.22
		λ [-]	2.09	1.95	2.27	1.93	1.86	1.93
	E18	h_{eff} [m]	1.24	2.39	1.24	1.24	1.24	1.24
		λ [-]	0.68	1.31	0.68	0.68	0.68	0.68
	E19	h_{eff} [m]	2.40	2.24	2.22	2.61	2.22	1.24
		λ [-]	2.09	1.94	1.93	2.27	1.93	1.08

2.1.2 Standardized criteria adopted for the comparison

The examined single-unit two-story building was modelled according to the different considered approaches and then analysed through nonlinear static analyses performed by assuming a uniform distribution of lateral forces acting in the X direction (see Figure 2.2).

The global response of the structure is clearly influenced by various aspects, such as:

- the variation at each step of the analysis of the axial force in the masonry structural elements, governing their shear strength;
- the combined interaction between masonry piers and spandrels, implying, as an example, the modification of the static scheme of the panels due to plasticization of the masonry beams;
- the interaction between the masonry beams and horizontal elements of other materials with tensile strength eventually coupled to the spandrels, such as steel tie rods or r.c. tie beams;
- the constitutive laws of materials (masonry, concrete, steel);
- the in-plane stiffness of the floor slabs (flexible-rigid diaphragms);
- the quality of the connection among walls and between walls and horizontal structures;
- the sensitivity of the linear/non-linear transition phase of the structural elements to parameters governing the numerical convergence (e.g. tolerance, maximum number of iterations, etc.).

With reference to the first set of analyses (carried out by the Task 4.3 Work Group), in order to deeply investigate these aspects and their influence on the predictions of the adopted models, a series of specific comparisons between them was defined. Some of these comparisons refer to the global scale response, in terms of capacity curves both of the whole structure and of each one of the structural walls oriented in the direction of the seismic action (Wall 1 and Wall 3, as indicated in Figure 2.3).

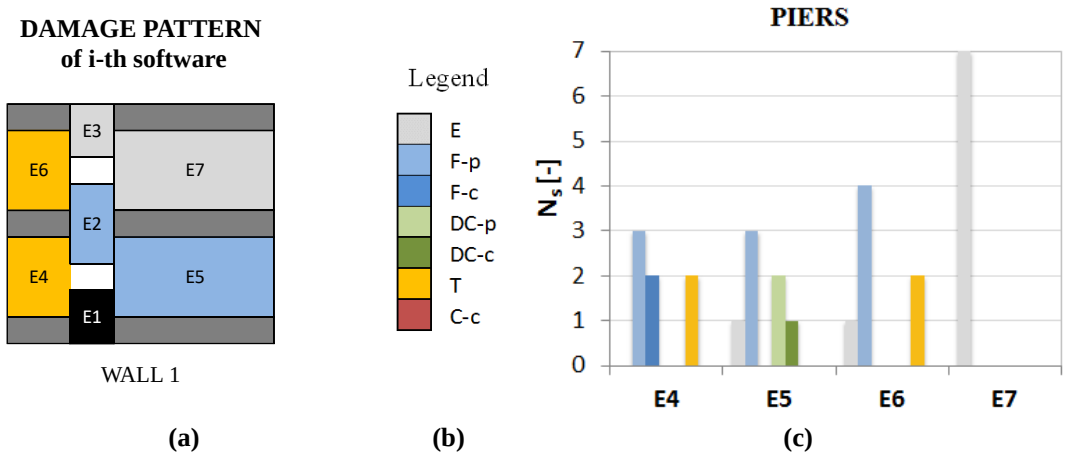

Figure 2.6 - Criterion adopted for the comparison of the damage distribution: (a) Example of damage distribution in a wall obtained by a i-th software; (b) Legend of failure mechanisms: E: Elastic; F-p: Flexural-plastic; F-c: Flexural-collapse; DC-p: Diagonal Cracking-plastic; Diagonal Cracking-collapse; T: Tension; C-c: Compression-collapse; (c) Synthesis of the comparison of the predicted failure mechanisms among software.

Other more accurate checks refer to the local scale and are represented by: i) the variation of both the axial load and the shear force at the base of the masonry panels at the ground level; ii) the failure mechanism

predicted for each structural element by the software and the corresponding damage distribution in the walls at different significant steps of the analysis (at gravity loads application; at 0.5 times the maximum base shear; at maximum base shear; at life-safety limit state, defined according to NTC08, at maximum displacement). In particular, the comparison of the damage distributions in the walls predicted by the software was conducted, as illustrated in Figure 2.6, by counting for each structural element the predicted occurrences of the considered failure mechanisms.

In addition, some significant parameters of the structural response (referred to as SRPs, i.e. Structural Response Parameters) were identified and compared according to the criteria explained in the following.

The identified SRPs are the three parameters describing the equivalent bilinear curve corresponding to the global capacity curve of the structure (K_s, $d_{u,s}$ and $V_{y,s}$), as defined in the Explicative Notes of NTC08 (MIT 2009) (Figure 2.7). In particular:

- the equivalent stiffness, K_s, is evaluated at a base shear level equal to 0.7 times the maxim value;
- the ultimate displacement, $d_{u,s}$, corresponds to an overall base shear decay not less than 0.2 times the maximum value;
- the yielding equivalent base shear, $V_{y,s}$, is evaluated imposing the equivalence of the areas under the capacity curve and the equivalent bi-linear curve.

For each SRP, the ratio between the value obtained from each software and the corresponding average value, calculated by considering the results provided by all the software, was evaluated, since it was not possible to differentiate the level of reliability of each one (Figure 2.7).

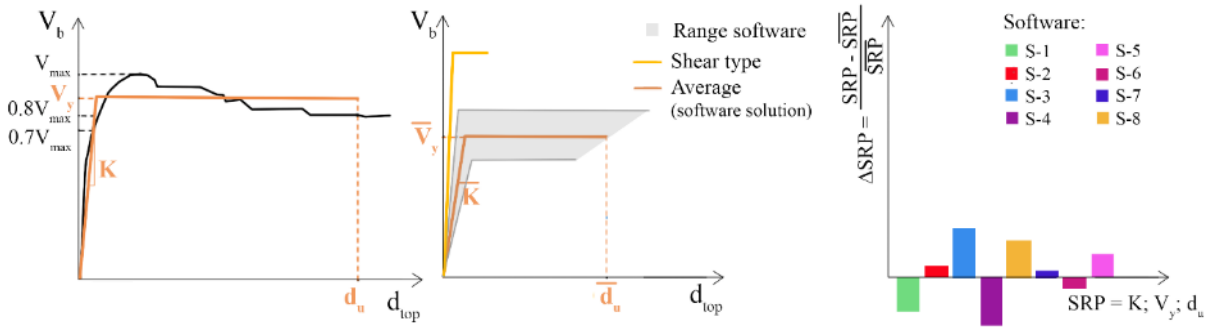

(a) (b) (c)

Figure 2.7 – Exemplification of the procedure adopted for: (a) conversion of the pushover curve into an equivalent bilinear curve (rules defined in NTC08 (2008)); (b) computation of the average values of the SRPs (K_s, V_y, d_u) and (c) computation, for each software, of the scatter with respect to the average values of the SRPs.

Moving to the second set of analyses, similar types of comparisons were conducted, considering again the obtained global response (with reference both to the pushover curves and to the SRPs associated to the equivalent bilinear curves), the local response and the damage pattern predicted by the models associated to the different examined modelling assumptions.

2.1.3 Main results

In this section some of the most relevant results obtained through the performed nonlinear static analyses are illustrated. In particular, at first the results of the analyses performed with the different software codes

and by adopting, as much as possible, the same modelling hypotheses, are presented (section 2.1.3.1), as obtained from Task 4.3 Work Group; subsequently, the results attained by using only 3Muri software and by varying the geometry of the structural elements (section 2.1.3.2) and the assumptions about the connection between the orthogonal walls (section 2.1.3.3) are discussed.

It is stressed that the results coming from Task 4.3 Work Group are reported and commented without any explicit reference to the software; for this reason, each one has been anonymously associated to a label and to a colour. These latter results are already published in Cattari et al (2018a), as the outcome obtained by the Task 4.3 Work Group. This work has been adopted as reference for further developments and comparisons made for the specific purposes of this thesis and described in the above mentioned sections 2.1.3.2 and 2.1.3.3.

2.1.3.1 Results from different software codes by adopting the same modelling hypotheses

The nonlinear static analyses were performed by assuming a uniform distribution of lateral forces acting in the X direction (see Figure 2.2); in the following only the results referring to the analyses in the positive verse are discussed.

It is stressed that, being the present research activity still work in progress, for some of the analysed configurations the results of the analyses with specific software codes are not available for the moment.

In Table 2.3 a synthesis of the available results for each analysed configuration is shown.

Table 2.3 – Synthesis of the available results for each analysed configuration.

Models\Config.	**Ia**	**Ib**	**IIa**	**IIb**	**IIc**	**IId**
EF-a						
EF-b						
EF-c						
EF-d						
EF-e						
EF-f						
EF-g						
EF-h						
LEGEND						
	Available				Not available	

In general, all the considered software were able to catch the variations in the global response that the defined configurations were meant to activate.

Figure 2.8 illustrates, as an example for one of the examined software, the global base shear-top displacement curves obtained for structure II and those associated to the A-type wall in case of both structure I and II. As expected, starting from configuration a (*weak spandrel-strong pier* behaviour type) and moving to the ideal shear type one (configuration d) through the configuration c (strong spandrel-weak pier behaviour type), both the global stiffness and the base shear progressively increase, while the displacement capacity decreases (Figure 2.8-a).

With regard to the single wall, for each type of configuration (i.e. configuration a, b, c or d) the same behaviour is observed, except for negligible differences mainly ascribable to a different redistribution of the stresses when moving from structure I, which is symmetric (being both of the bearing walls of type A) to structure II, which is asymmetric, or moving through various configurations (b, c and d), where the presence of different structural details produces a different coupling among elements inside the same wall.

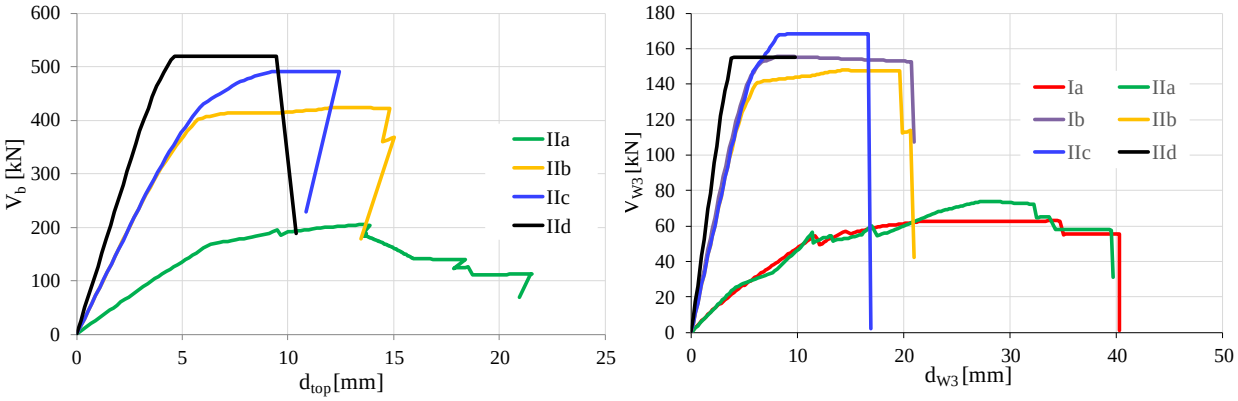

(a) **(b)**

Figure 2.8 - Global pushover curves (a) and pushover curves for the A-type wall (b) obtained with software EF-a considering the different analysed configurations for structure I and II.

After this general consideration, in the following more detailed comparisons between the results obtained with the different software are illustrated, according to the criteria previously introduced.

Global pushover curves and SRPs related to the bilinear curves

Figure 2.9 shows, for all the configurations of structure I (Ia and Ib) the global *pushover* curves obtained with the different software, while Figure 2.10 illustrates the pushover curves obtained for the corresponding configurations of structure II (IIa, IIb) together with their idealizations in bilinear curves. These bilinear curves, in particular, provide the data which are necessary for the calculation of the SRPs and their scatter with respect to the mean value, as illustrated in Figure 2.11 for all the configurations defined from structure II.

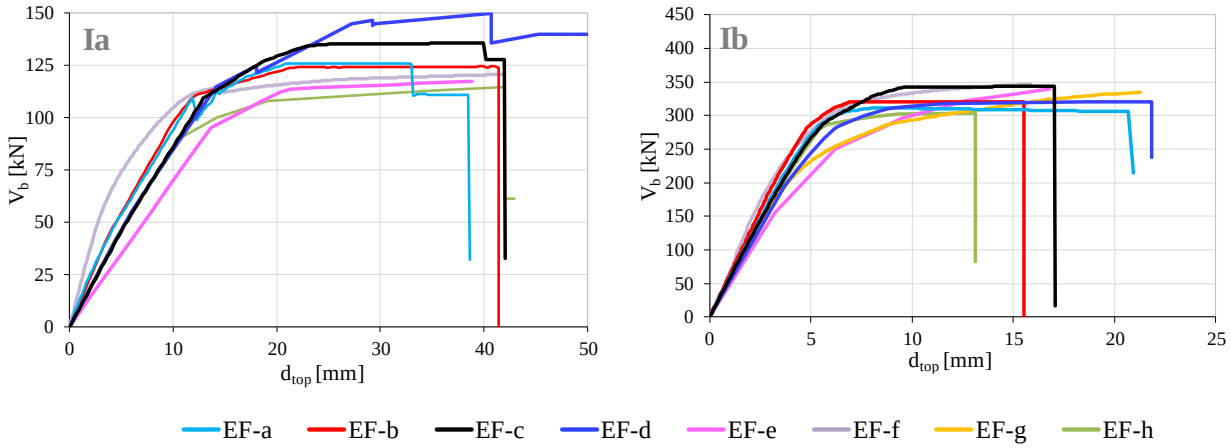

Figure 2.9 - Global pushover curves obtained for structure I.

Considering the global pushover curves obtained with software C, the black dot in Figure 2.10 indicates the step of the analysis corresponding to the activation of a plastic hinge associated to the flexural failure of pier E5. The reaching of this specific condition was explicitly indicated since it emerged that in this software, differently than in the other cases, after the activation of the hinge the normal force and the bending moment become independent (i.e. the bending moment remains constant even if the normal stress changes during the analysis).

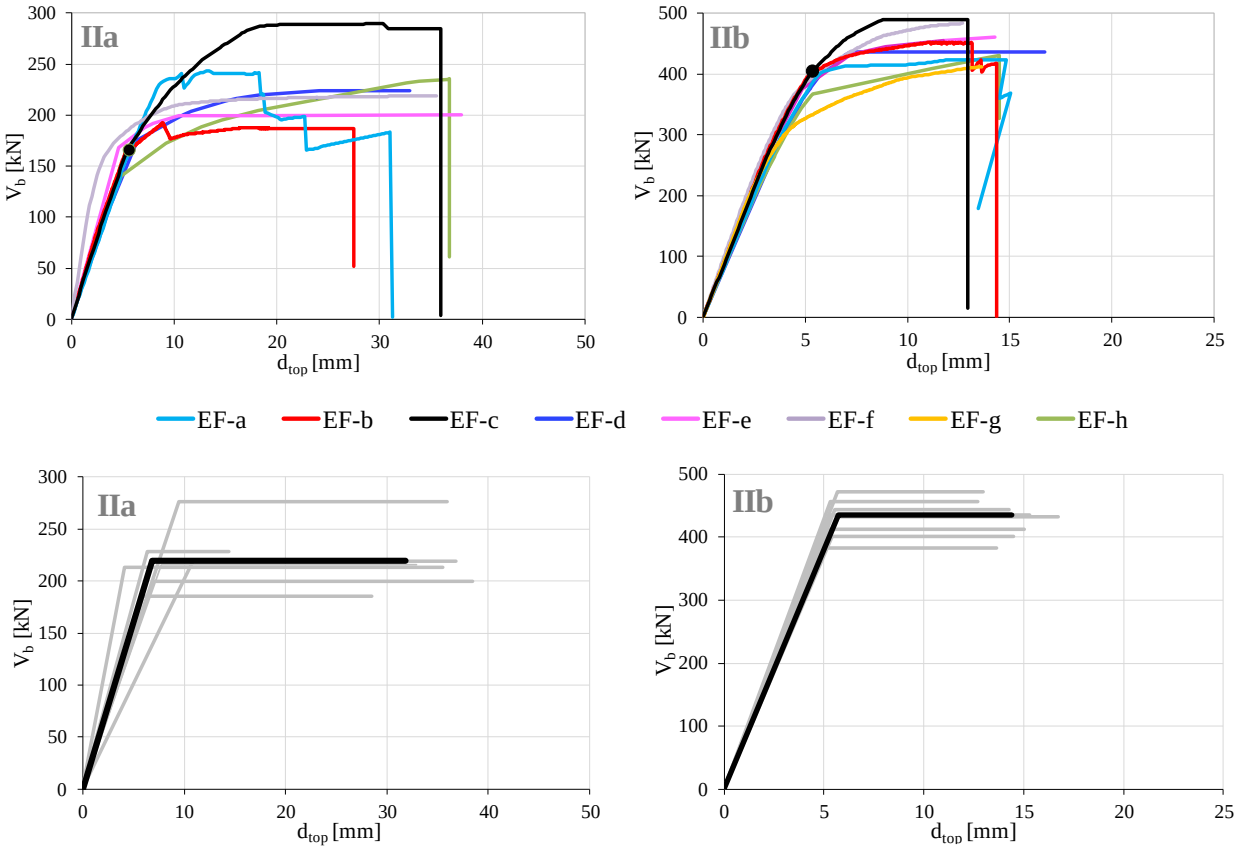

Figure 2.10 - Global pushover curves and related equivalent bilinear curves for structure II (in the graphs representing the bilinear curves the black line indicates the mean curve used as reference for the calculation of the scatter of the SRPs).

Moving to the analysis of the data derived from the bilinear curves, it is observed that the significant scatter of the results associated to the configuration with weak spandrels (IIa) (approximatively around 20-30%, except for few cases of specific programs, where it is even higher) progressively decreases moving to the shear-type configuration (IId), where it is lower than 10%. Moreover, in the case of configuration IId it is possible to analytically calculate an estimate of the solution, and the numerical results are substantially in good agreement with it (Cattari et al (2016)).

From the analysis of structure II, and more in general considering also the other case-studies examined by the research group within the ReLUIS project, it was observed that the configurations characterized by weak spandrels are the most sensitive to the algorithms and the solutions implemented in the software and to the possible modelling choices adopted by the users. Some of the aspects which affect the response in this specific case are:

- the possibility for the software to calculate the actual normal force acting on the spandrels; regarding this issue, it is reminded that NTC08 allows two possible alternatives for the definition of the failure criteria to adopt for the spandrels: one of them has to be used when the normal force is known from the analysis, while the other when it is unknown. Regarding this, it is important to take into account the criterion adopted by the different computer programs about the modelling of the diaphragms (fully rigid diaphragms or characterized by a finite stiffness);
- the effects of the interaction between the masonry panels and the diaphragms when these last are explicitly modelled: for example, a high axial stiffness of the diaphragms can produce the same effect of a tie rod on the spandrels, even if a specific tensile resisting element is not coupled to them;
- in the case of the fiber approach, the role of the tensile strength of the material, which affects the response of the spandrels and can produce significant deviations with respect to the simplified criteria now adopted by the NTC08.

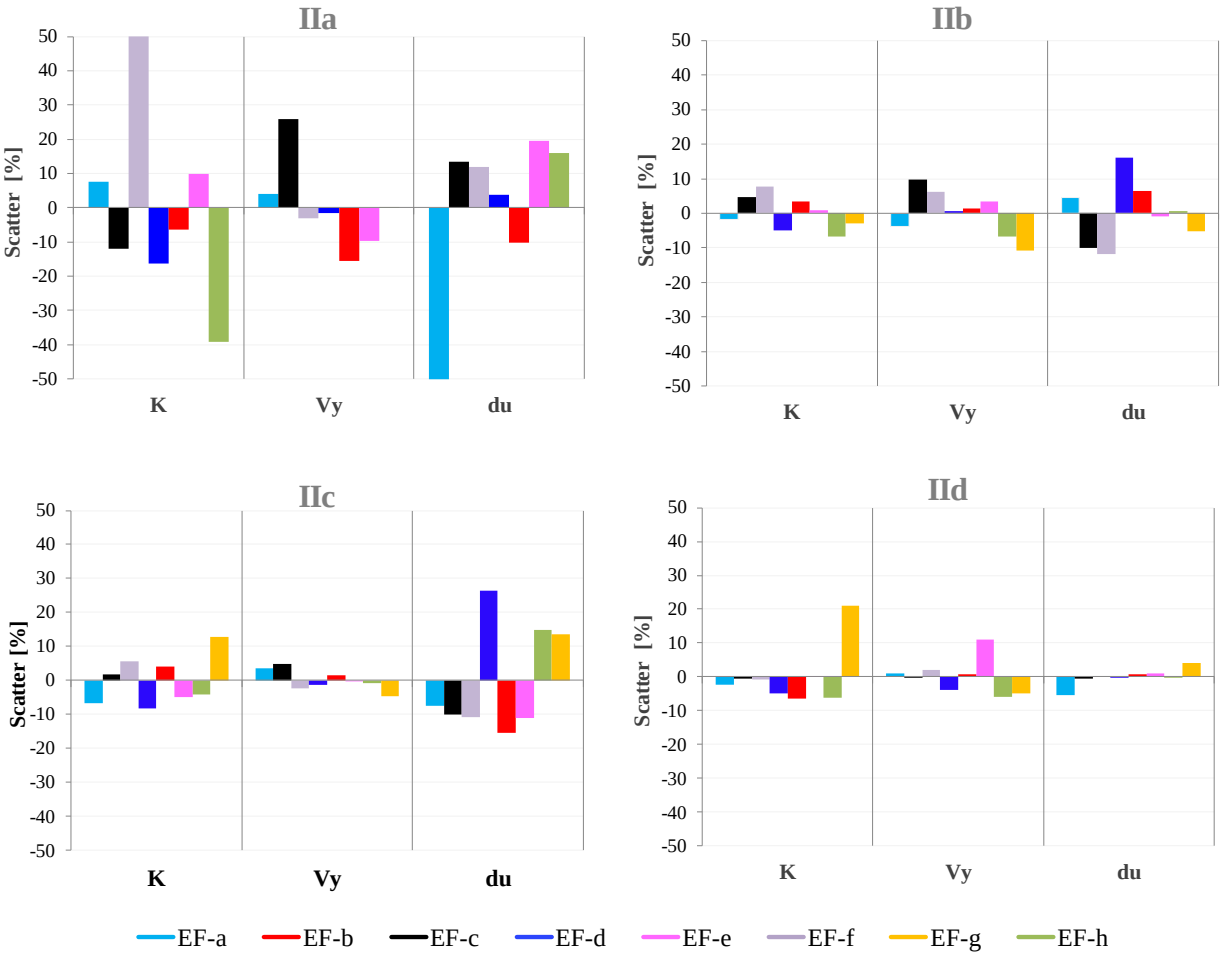

Figure 2.11 - Scatter on the SRPs associated to the equivalent bilinear curves (K_s, $V_{y,s}$ and $d_{u,s}$) for all the examined configurations of structure II.

Except for the configuration IIa, where the possible sources of difference among the predictions of the software have already been discussed, in case of configurations IIc and IId the scatter on $V_{y,s}$ is in general

lower than 10% ,while it is higher (in general within 20%, except few software for which it is even higher) in case of K_s and $d_{u,s}$.

Regarding $K_{s,}$ it has to be noted that in some of the considered models (those where the flexural response is described by means of springs and those using fiber approaches) the stiffness decay is gradual, while in other software it is managed through the adoption, from the beginning of the analysis, of conventionally reduced elastic moduli representative of the cracked condition.

As far as $d_{u,s}$ is concerned, the scatter of the results is ascribable to the adoption of different formulations for the calculation of the drift value and to some discrepancies regarding the modes of failure predicted by the software for specific masonry panels (as better explained in the following).

Comparison in terms of predicted damage pattern

The following figures (Figure 2.12 and Figure 2.13) illustrate the damage pattern predicted by the considered software according to the graphic representation introduced in the previous section (Figure 2.6); in particular, it is recalled that on the *y* axis the number of software predicting a certain type of damage (each failure type is identified through specific colours – see the legend in Figure 2.6) for each structural element is reported. The damage pattern represented in the graphs refers to the step corresponding to a strength degradation of 20% with respect to the maximum one (that represents, according to what is indicated in NTC08, the displacement capacity of the structure associated to the life-safety limit state).

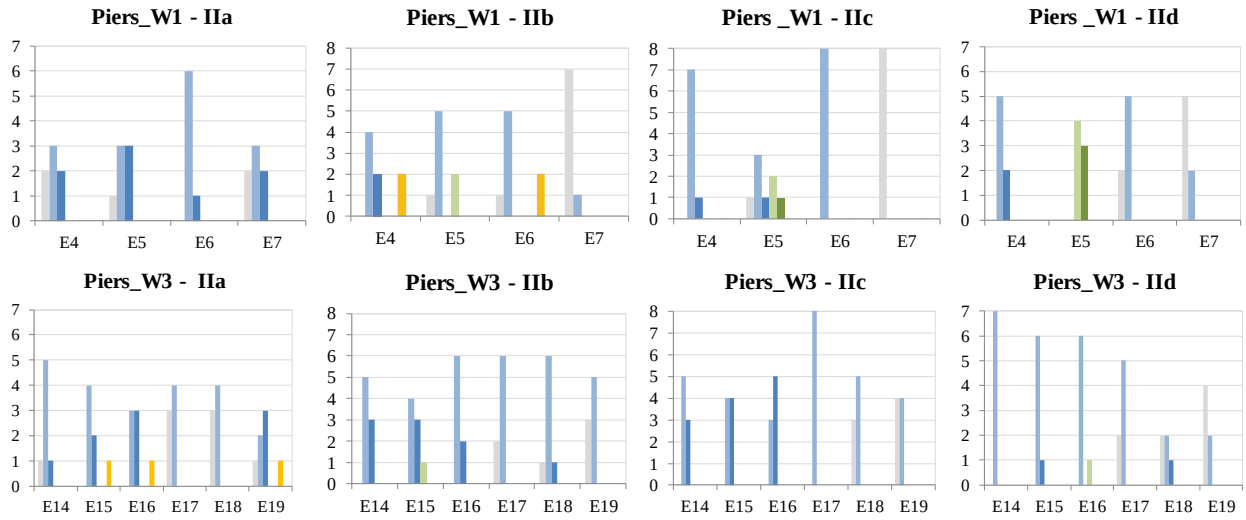

Figure 2.12 - Damage pattern (at the attainment of the life-safety limit state) referring to the piers belonging to Wall 1 and 3 in structure II; the different colours correspond to different occurred failure types, as indicated in Figure 2.6.

By looking at the damage detected in pier elements (Figure 2.12), it is observed that all the software show a substantially good agreement in the case of configuration IIa and IId. Moreover, in these cases the activated failure modes are consistent with what expected: prevailing flexural response in configuration IIa and prevailing diagonal shear cracking in configuration IId, according to the different extreme static schemes characterizing the masonry piers in the two configurations, that are related to the higher or lower constraint provided by the spandrels. Indeed, in case of configuration IIa, with weak spandrels, the piers

are almost uncoupled and their static scheme is close to the cantilever one; on the other hand, in configuration IId the spandrels provide a more significant coupling between the piers and, since the rotations are fixed at each floor level, their static scheme can be assumed as the fixed-fixed one.

On the contrary, higher discrepancies are detected in case of configurations IIb (with tie rods) and IIc (with r.c. tie beams). More in detail, the most significant differences are observed in case of pier E5. However, they can be exhaustively explained by deepening the response of this panel through the definition of its strength domain. This, indeed, has allowed to observe that, considering the range of variation of the normal stress acting on the panel, the predictions about its strength provided by the diagonal shear cracking failure and the flexural failure are similar when the boundary conditions of the panel are representative of the fixed-fixed condition (or close to this situation, as in the case of a spandrel coupled with a tie beam). Small differences between the software in the prediction of the evolution of the normal force acting on the panel can therefore justify the activation of different prevailing failure modes. Moving to the damage in the spandrel elements, also in this case what obtained is consistent with the features of each configurations: prevailing flexural damage in structure IIa, of elastic behavior in case of structure IId, while in structure IIb and IIc (tensile element coupled to the spandrels) also shear failure appears.

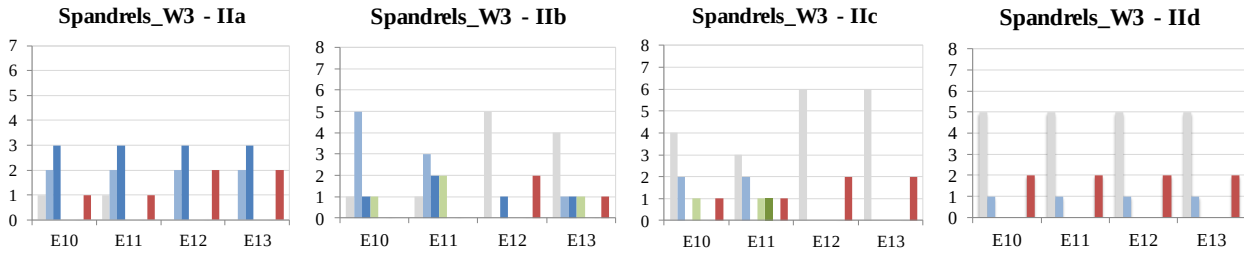

Figure 2.13- Damage pattern (at the attainment of the life-safety limit state) referring to the spandrels belonging to Wall 3 in structure II; the different colors correspond to different occurred failure types, as indicated in Figure 2.6.

It is stressed that in some cases the spandrels present a failure due to crushing (red color). It is caused by the eccentricity of the masonry beams, which leads to the development of an additional bending moment, whose effect has to be summed up with the pre-compression effect given by the presence of the diaphragm.

2.1.3.2 Results from one specific software: sensitivity to the adopted EF idealization

The sensitivity analyses here described were realized within the specific scopes of this PhD thesis through nonlinear static analyses performed both in the positive and in the negative verse by means of 3Muri program. The results refer to configuration IIc, which is the one provided by r.c. tie beams at each level. It is stressed that this kind of configuration is also the most pertaining, among those here introduced, to the walls analysed further on in this study (see section 3.3 and Chapter 4), that are actually characterized by the presence of r.c. tie beams.

Global pushover curves and SRPs related to the bilinear curves

In the following figures the results in terms of pushover curves obtained with the different numerical models are reported, considering both the positive and the negative (Figure 2.14) verse of the analysis. It is possible to observe that the choice of the geometry for the structural elements actually influences the

obtained global response, producing differences in terms of stiffness, strength and displacement capacity which are definitely not negligible.

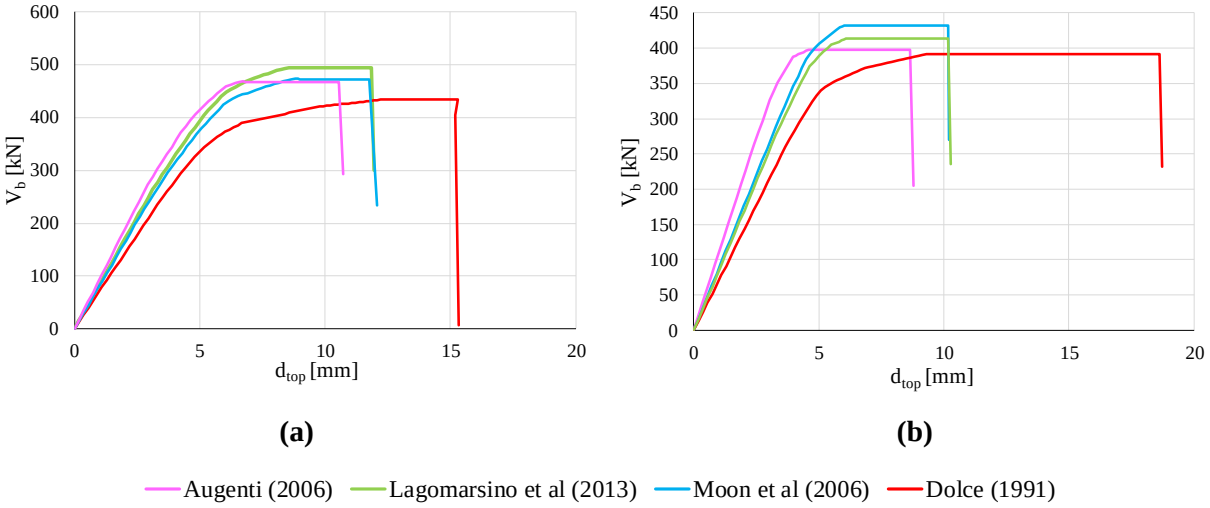

Figure 2.14 – Configuration IIc, analysis in the positive (a) and in the negative (b) verse: global pushover curves according to the different considered criteria for the EF idealization.

As in the analyses described in the previous section, in order to have a quantification of the dispersion associated to the obtained results, for each one of the examined cases the scatter of the SRPs characterizing the equivalent bilinear curve with respect to a reference value was computed.

Regarding this aspect, two different choices were made:

1) the first choice is to assume as reference the results obtained with the selected software;
2) the second choice is to assume as reference, for each parameter, the average value between the results provided by the different considered software in the analyses previously performed, characterized by the same assumptions on the EF idealization (hereinafter referred to as “benchmark solution”).

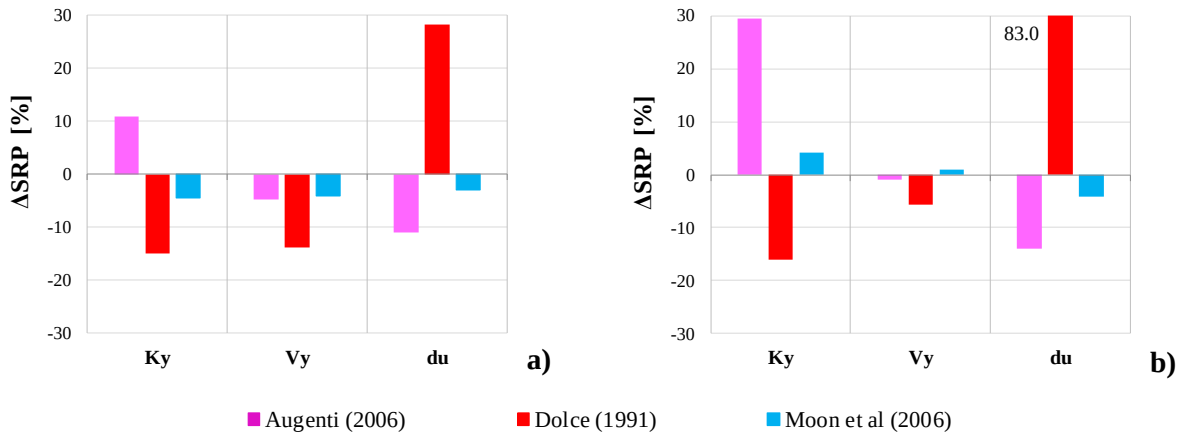

Figure 2.15 – Configuration IIc: scatter with respect to the EF model according to Lagomarsino et al (2013) of the SRPs associated to the equivalent bilinear curves (K_s, $V_{y,s}$, $d_{u,s}$); nonlinear static analyses in the (a) positive and (b) negative verse.

Concerning point 1), the EF model defined on the basis of the rules for the EF schematization proposed in Lagomarsino et al (2013) was adopted as reference, being this idealization exactly the one adopted in the first set of analyses, performed with the different software codes. In this way, it is possible to take into account only the scatter produced by the different choices about the geometry of the structural elements; the results are reported in

Figure 2.15 for the analyses in the positive and in the negative verse.

Moving to point 2), the obtained scatter on the SRPs includes two different contributions: the model uncertainty (related to the choice of the model to use) and the uncertainty due to the adopted geometry for the structural elements. Indeed, with respect to the previous case, the final dispersion is here affected also by the initial scatter characterizing the adopted software with respect to the "benchmark solution". The results obtained in this case are illustrated in Figure 2.16, considering in particular the analysis in the positive verse.

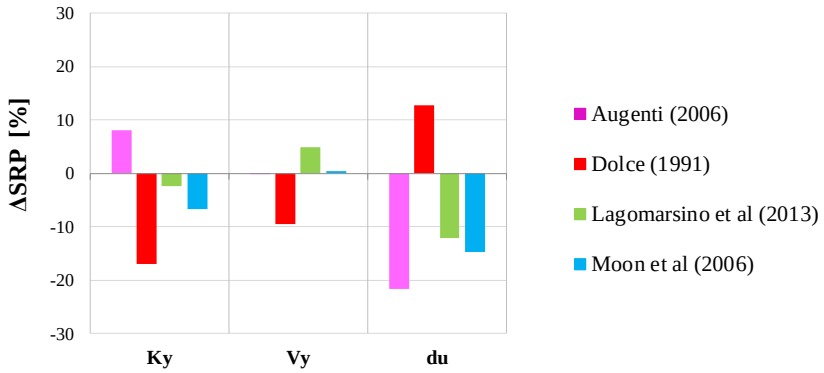

Figure 2.16 – Configuration IIc: scatter with respect to the "benchmark solution" of the SRPs associated to the equivalent bilinear curves (K_s, $V_{y,s}$ and $d_{u,s}$); nonlinear static analyses in the positive verse.

The results represented in Figure 2.15 and in Figure 2.16 confirm that the scatter on the key parameters associated to the seismic response of the structure is not negligible, especially in terms of stiffness and ultimate displacement. By looking at Figure 2.15 and focusing the attention, as for example, on the analysis in the negative verse, it is observed that the criterion proposed by Augenti (2006) tends to predict a stiffness which is much higher than the one of the model adopted as reference (scatter of about 30%); this can be explained by considering that this rule leads in general to the formation of almost squat piers and, consequently, extended rigid nodes, especially in the case of Wall 1 (see Figure 2.5, Table 2.2). However, when considering the analysis in the positive verse, since the big pier elements in Wall 1 (E5 and E7) are characterized by a higher effective height, less extended rigid nodes are introduced in the model and the overestimation of the global stiffness with respect to the reference solution is lower (about 10%). On the other hand, the criterion proposed by Dolce (1991) leads in general to quite slender piers (higher effective heights, see Table 2.2) and so to a higher deformability of the considered walls; this actually results in an underestimation of the global stiffness with respect to the criterion adopted as reference on when considering both the verses of the analysis.

Concerning displacement capacity, again the criteria proposed by Augenti (2006) and by Dolce (1991) are the ones characterized by the highest scatter with respect to the adopted reference solution, and also in this case they are associated to opposite trends. Indeed, the EF model according to Augenti (2006) provides

in general an underestimation of the displacement capacity with respect to the reference solution, while the opposite is for the EF model according to Dolce (1991), where a displacement capacity higher than the one observed in the EF model according to Lagomarsino et al (2013) is observed in both the verses of the analysis. This can be explained by considering again that the rule according to Augenti (2006) tends to produce rather squat piers, which are characterized by a lower displacement capacity with respect to the slenderer ones defined on the basis of the Dolce's criterion. This is motivated by the fact that the failure of masonry panels is governed by the reaching of fixed values of drift, so that the lower is the effective height of the panel the lower is its displacement capacity; moreover, while rather slender panels are usually interested by ductile flexural failures, squat panels tend to undergo shear failure, which is associated to lower drift thresholds (more fragile behavior).

Moving to the results provided by the model according to Moon et al (2006), a quite good agreement with the solution adopted as reference is observed for both the verses of the analysis (scatter on GRPs lower than 10%); in this case, indeed, the geometry of the structural elements is more similar to the one adopted in the EF model according to Lagomarsino et al (2013), both in case of Wall 1 and Wall 3 (Table 2.2). By looking at these results it is important to stress that, according to the current codes (NTC08, EC8), the seismic verifications in case of masonry buildings are performed on the global pushover curves; it is therefore evident that the adoption of different assumptions regarding the geometry of the structural elements can actually affect the outcomes of these verifications.

In Figure 2.17 and in Figure 2.18 the results in terms of global base shear-top displacement curves obtained for the two bearing walls of structure II (Wall 1, which is the B-type wall and Wall 3, which is the A-type wall) are illustrated in case of the analysis in the positive and in the negative verse.

It is possible to observe that the different choices about the EF idealization mainly affect the results obtained for Wall 1. In this wall, indeed, the response is governed by pier E5 (which governs in general the response of the whole structure), that is characterized by very different geometries depending on the applied criterion for the pier effective height, especially in the analysis in the negative verse (see Figure 2.5).

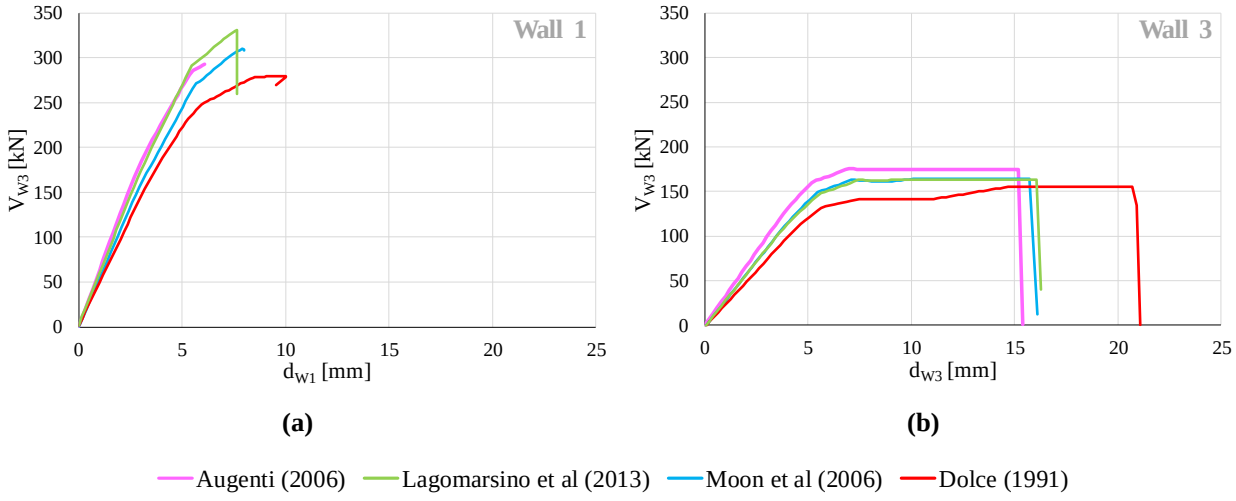

Figure 2.17 – Configuration IIc, analysis in the positive verse: base shear – top displacement curves of the two bearing walls ((a) Wall 1 and (b) Wall 3) according to the different considered criteria for the EF idealization.

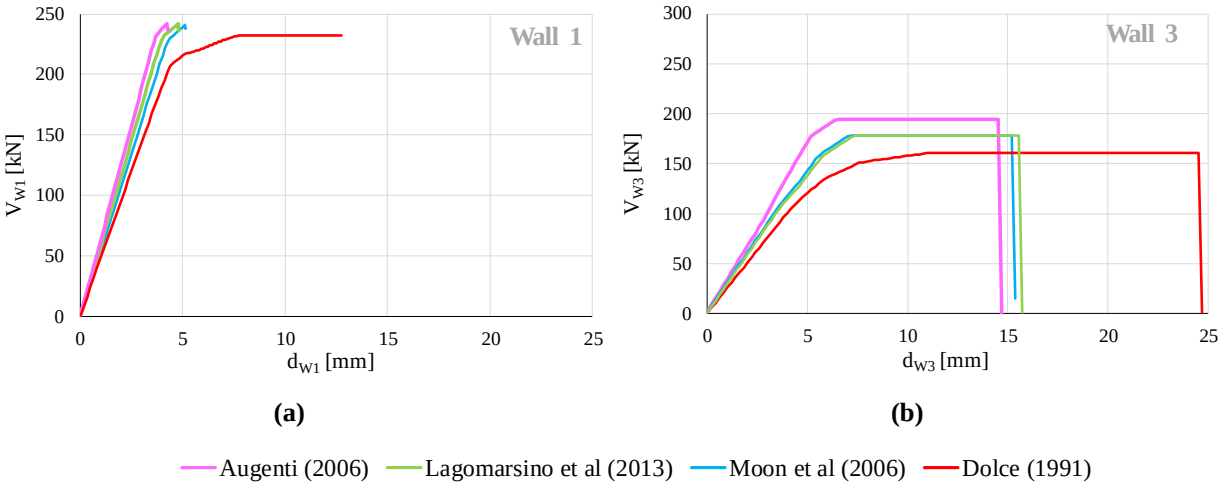

Figure 2.18 – Configuration IIc, analysis in the negative verse: base shear – top displacement curves of the two bearing walls ((a) Wall 1 and (b) Wall 3) according to the different considered criteria for the EF idealization.

Moving to Wall 3, the scatter between the results, although still not negligible, is in general lower with respect to the one observed in case of Wall 1; indeed, in Wall 3 the geometry characterizing the structural elements is almost similar in the different considered EF models, apart few discrepancies mainly regarding the height of the external piers. Moreover, the structural response of the wall is mainly governed by the central pier at the ground floor (E15, carrying almost 60% of the base shear of the whole wall), that is characterized by the same geometry in all the considered EF models, with the only exception of the model according to Dolce (1991), where its effective height is slightly higher.

Comparison in terms of predicted damage pattern

The different effective heights assumed for the pier elements clearly affect also the damage pattern occurred in the walls of the analysed building. In Figure 2.19 the damage pattern associated to the maximum top displacement occurred in the analysis is shown in case of both Wall 1 and Wall 3, considering the 4 EF models obtained according to the different criteria for the EF idealization. By way of example, the analysis in the negative verse, where the most significant differences depending on the choice of the criterion for the identification of the structural elements geometry are detected, is considered.

In the masonry piers of both the walls the flexural failure mode is clearly predominant in almost all the cases, being explained by the fact that the piers in this structure are subjected, in general, to low compression rates; moreover, in all the considered models the spandrels are still elastic, due to the presence of the coupled r.c. tie beams. Also, in almost all the cases the collapse of the building happens due to the failure of the piers at the ground floor in Wall 3, except for the case of the model according to Moon et al (2006), where the reaching of the ultimate condition is governed by the failure of pier E5 in Wall 1.

The most significant differences on predicted type of failure among the different models are actually about pier E5. In particular, in two of the considered EF models pier E5 presents a flexural failure (Lagomarsino et al (2013) and Dolce (1991)), in one case it is still in the elastic phase (Augenti (2006)) and according to the last model (Moon et al (2006)) a shear failure occurs.

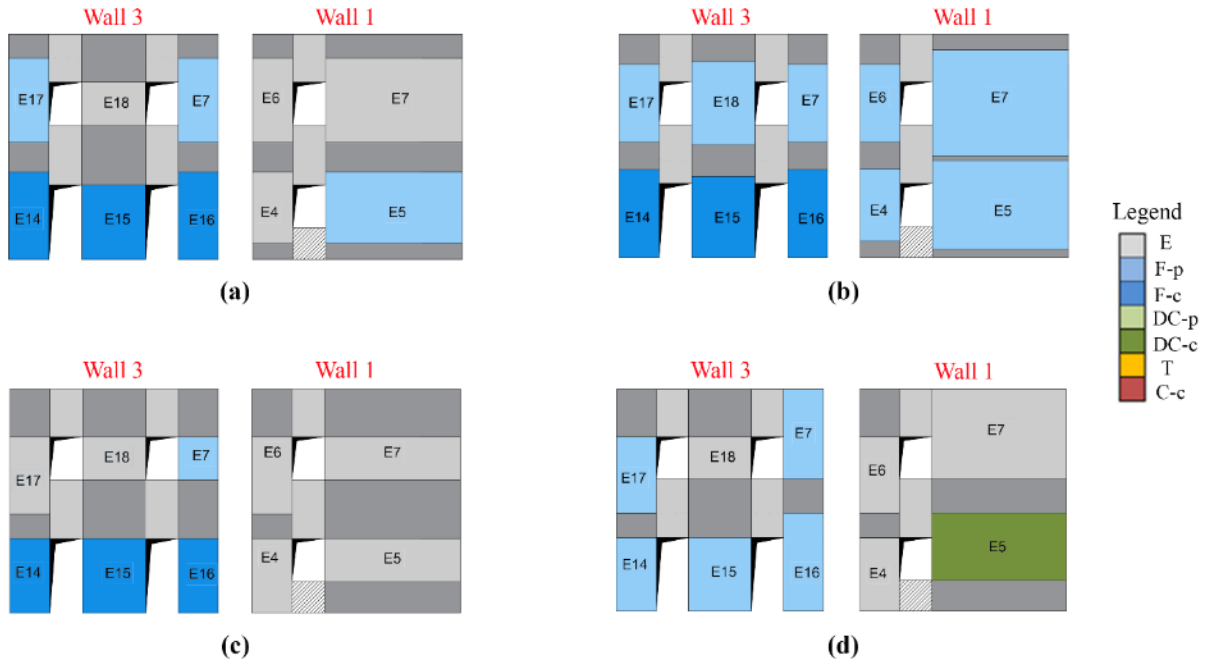

Figure 2.19 – Configuration IIc: damage pattern detected in Wall 1 and in Wall 3 at the end of the pushover analysis (negative verse); EF models according to: a) Lagomarsino et al (2013); (b) Dolce (1991); (c) Augenti (2006); (d) Moon et al (2006). Legend of failure mechanisms: E: Elastic; F-p: Flexural-plastic; F-c: Flexural-collapse; DC-p: Diagonal Cracking-plastic; Diagonal Cracking-collapse; T: Tension; C-c: Compression-collapse.

This can be explained by considering that:

i) by changing the geometry of the pier its strength domain changes;

ii) the range of variation of the normal stress acting on this pier during the analysis is such that we are in the portion of the strength domain close to the intersection between the flexural and shear strength criteria; for this reason, small variations in the value of the axial load predicted by the different models can actually produce different failure modes.

In order to deepen these aspects, in Figure 2.20 the strength domains associated to pier E5 considering the four different hypotheses about its geometry are represented. For the definition of the domain associated to the flexural failure the fixed-fixed condition is considered, being the examined building provided by r.c. tie beams at each level, so that the boundary conditions of the piers should be close to this situation. It is stressed that while significant differences depending on the geometry of the pier can be detected in the predictions of the criterion associated to the flexural failure (i.e. the higher is the effective height, the lower is the flexural strength), on the contrary the predictions of the criterion associated to the shear failure are the same in all the considered cases: indeed, the curves associated to the failure for diagonal cracking (DC) represented in Figure 2.20 are all coincident. This is due to the fact that in the criterion for diagonal shear failure the geometry of the element comes into play only through a coefficient related to the aspect-ratio of the panel (*b* coefficient, see equation 3.7 in section 3.2.1). Since in this case, despite of the variations in its height, the aspect ratio of the panel always remains below 1, the value associated to this coefficient is always the same (in particular it is equal to 1).

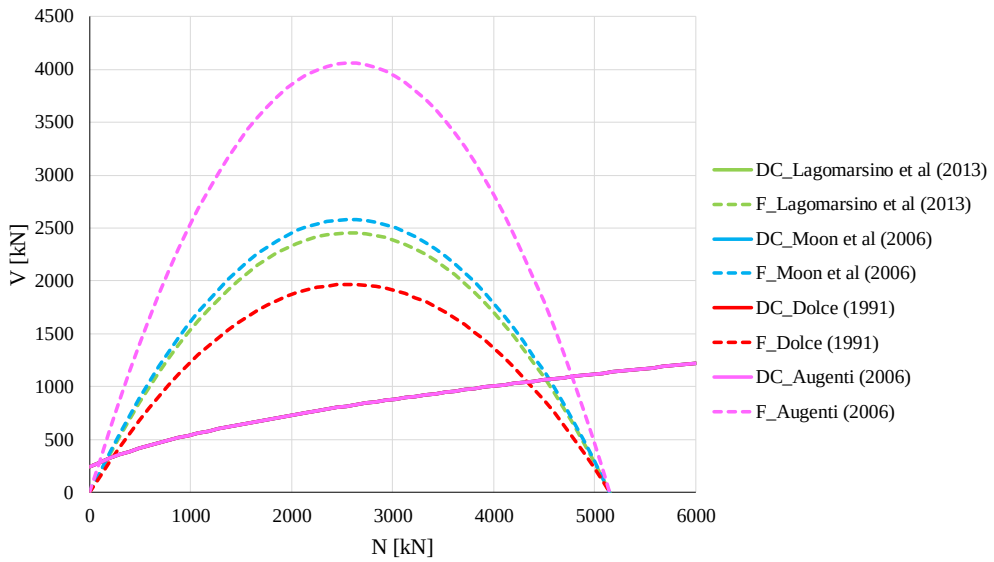

Figure 2.20 – Failure domain of pier E5 for different effective heights attributed to the element (analysis in the negative verse); F: flexural; DC: diagonal cracking. The curves associated to diagonal cracking failure are all coincident, as explained in the text.

In Figure 2.21 for each one of the considered EF models the range of variation of the axial load acting on pier E5 during the analysis is represented on the corresponding failure domain through vertical lines. In particular, since the analysis in the negative verse is here considered, starting from the axial load associated to the application of the dead loads (N_{dl}) the examined pier is subjected to a progressive reduction of normal force, so that in the graphs the minimum value reached in the analysis is represented (N_{min}) In each graph of Figure 2.21, in addition to the diagonal cracking (DC, solid line) and to the flexural (F, dashed line) strength criteria referring to the actual geometry of pier E5 in the four EF models, also the flexural domains associated to the other possible geometries considered for this pier are represented with a dashed-dotted line.

It is stressed that, since the boundary conditions characterizing the piers in the models cannot be considered as a perfect fixed-fixed condition, even if quite close to this situation due to the presence of r.c. tie beams, it should be taken into account that the actual flexural strength may be slightly lower than the one emerging from the represented domain. By comparing the strength predictions associated to the two possible failure modes in correspondence of the highlighted values of axial load, it is possible to observe that, due to the variation of the flexural domain, different failure modes can occur in the examined pier.

In particular:

- in the case of the Dolce's criterion the flexural strength associated to the acting axial load results to be lower than the corresponding shear strength, thus explaining the predictions of this criterion (plasticization associated to a flexural failure);
- in the models according to Lagomarsino et al (2013) and Moon et al (2006) the predictions in terms of flexural strength for the examined values of axial load are quite similar, even if slightly higher in the case of Moon et al (2006), where also the compression level acting on the pier is slightly higher. Adding to these considerations the fact that, as aforementioned, the flexural strength indicated in Figure 2.21 is probably an overestimation of the actual one and the fact that

the axial load of our interest falls in the region of the domain where the predictions of shear and flexural strength are almost similar, it is possible to explain why in the case of Moon et al (2006) a shear failure appears and in the case of Lagomarsino et al (2013) a flexural one is predicted (or, better, a plastic condition associated to a flexural failure);

- in the model according to Augenti (2006) the flexural strength is particularly high, so that a shear failure is highly likely; however, with respect to what happens in the other models, this pier appears to be subjected to a slightly higher compression level, so that its strength is higher. This can explain why it is still in an elastic phase at the end of the analysis.

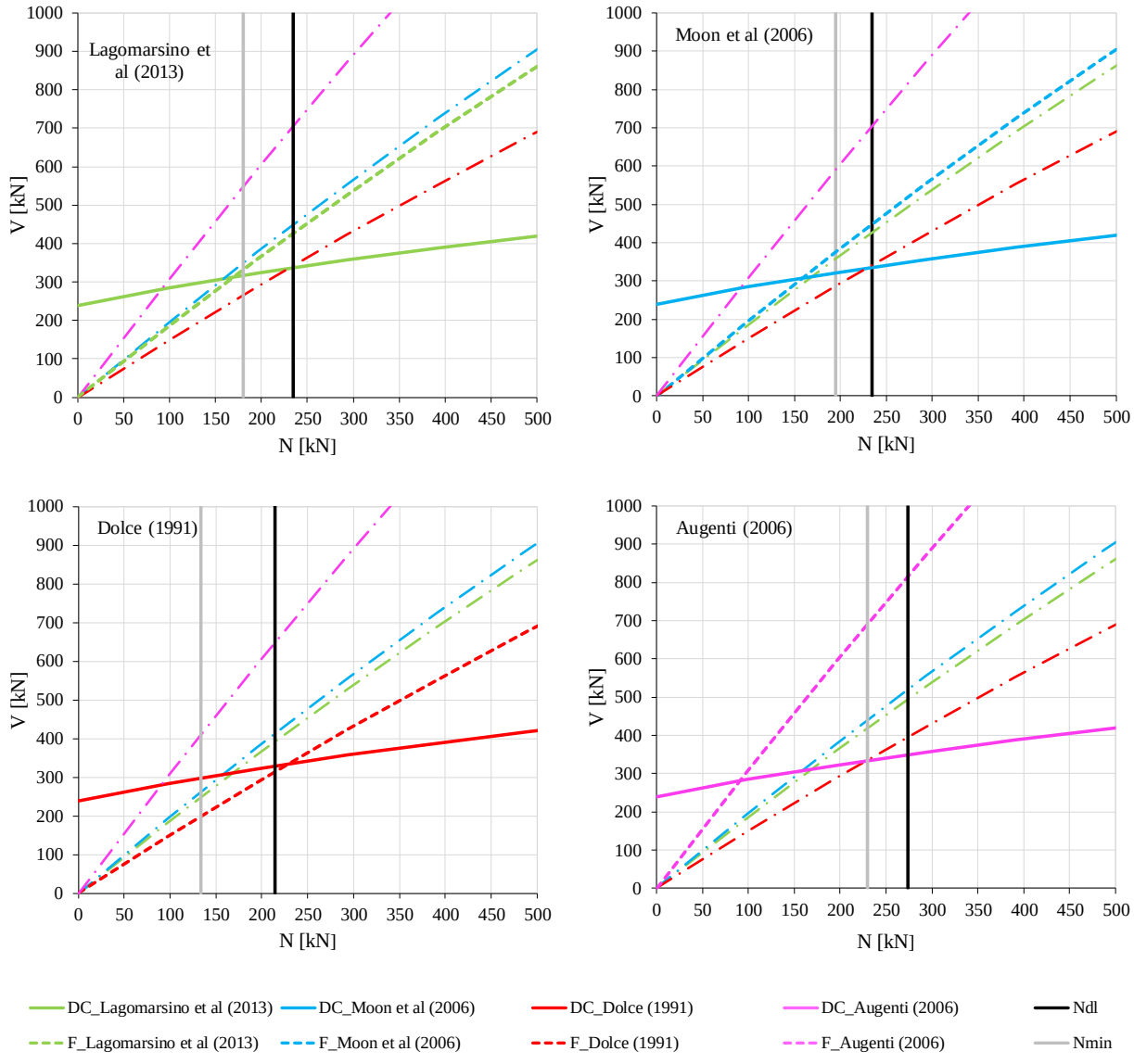

Figure 2.21- Failure domain of pier E5 considering different criteria for its effective height; the vertical lines represent the range of variation of the axial load occurring in this element during the analysis (N_{dl} = axial load after the application of the gravity loads; N_{min}: minimum axial load acting on the pier during the analysis).

2.1.3.3 Results from one specific software: sensitivity to the modelling of the connection between the orthogonal walls

The sensitivity analyses here described were realized on structure IIc by using 3Muri software, considering both the analyses in the positive and in the negative verse; moreover, since the aim in this case is to investigate the role of the flange effect on the structural response, the geometry adopted for the structural elements was fixed (the same adopted in the first set of analyses, i.e. the one according to Lagomarsino et al (2013)).

Two different hypotheses about the modelling of the connection between the walls were considered, namely: i) perfect coupling between the orthogonal walls (named "Coupled"), which was the assumption adopted in the first set of analyses; ii) decoupling between the orthogonal walls, obtained by still considering the contribution to the coupling given by the stiffness of the r.c. tie beams of the side walls (named "Decoupled"). It is stressed that the plan configuration of structure II makes this building particularly suitable for the study of different assumptions about the modelling of the flange effect. Indeed, as it can be seen from the previous Figure 2.3, the piers in the two bearing walls (especially E14, E16, E4) are connected, in the orthogonal walls, to panels that are much more stiff, being the side walls not provided with openings.

The results in terms of global pushover curves are illustrated in Figure 2.22. Moving from the situation of perfect coupling to the hypothesis of decoupling it is possible to observe a progressive reduction of global stiffness and an increase in the displacement capacity; in addition, when decoupling the walls the maximum strength is higher with respect to the case of perfect coupling between them. Similar considerations apply also when considering the pushover curves obtained for the two bearing walls (reported in Figure 2.23 in the case of the analysis in the negative verse).

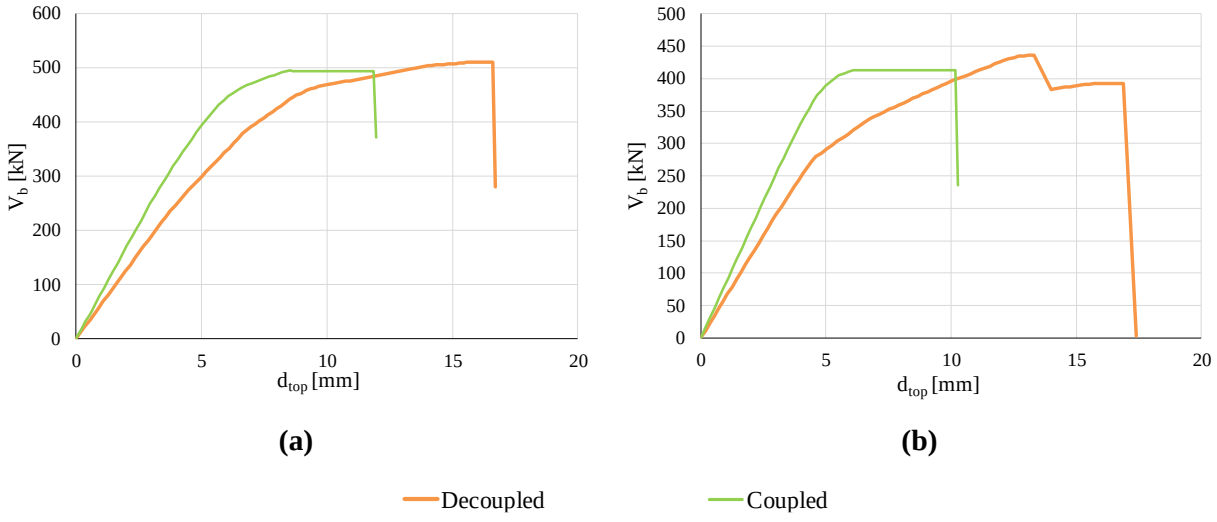

Figure 2.22 - Configuration IIc, analysis in the positive (a) and in the negative (b) verse: global pushover curves according to the different considered assumptions about the connection between the orthogonal walls.

These differences in the global response are mainly ascribable to a different redistribution of the vertical loads between the masonry piers. In Figure 2 24 the comparison in terms of evolution of the axial load in

the piers at the ground floor of Wall 1 and Wall 3 when considering the two modelling hypotheses about the flange effect is shown.

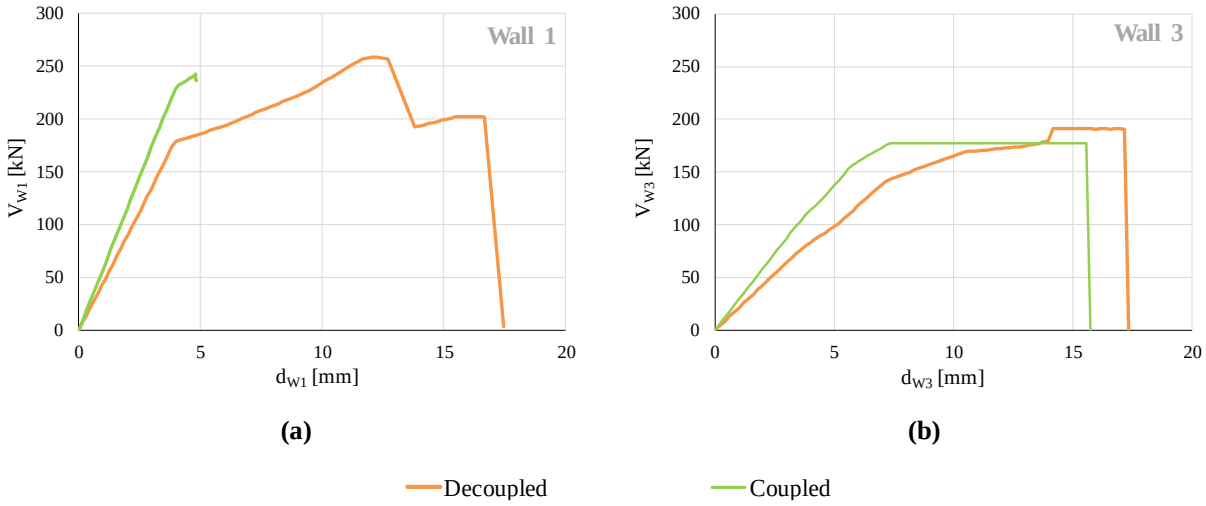

Figure 2.23 - Configuration IIc, analysis in the negative verse: pushover curves of (a) Wall 1 and (b) Wall 3 according to the different considered assumptions about the connection between the orthogonal walls.

Significant differences are observed between the two examined cases, and in particular:

- *after the application of the dead loads*: indeed, when the walls are perfectly coupled the masonry piers of the two bearing walls (Wall 1 and Wall 3) present a lower compression rate, since the perfect connection with the flanges causes the axial load to "move" from the in-plane loaded piers to the panels in the orthogonal direction, which are much more stiff; conversely, this does not happen when the walls are decoupled, so that in this case the piers of the bearing walls all present a higher compression rate;
- *during the analysis*: indeed, the redistribution of the vertical loads between the masonry elements of the two bearing walls is in general more significant when the walls are decoupled, since in this case the overturning of the wall (caused by the applied horizontal actions) is more pronounced than in the other case, where the coupling with the two stiff side walls tends to reduce this phenomenon.

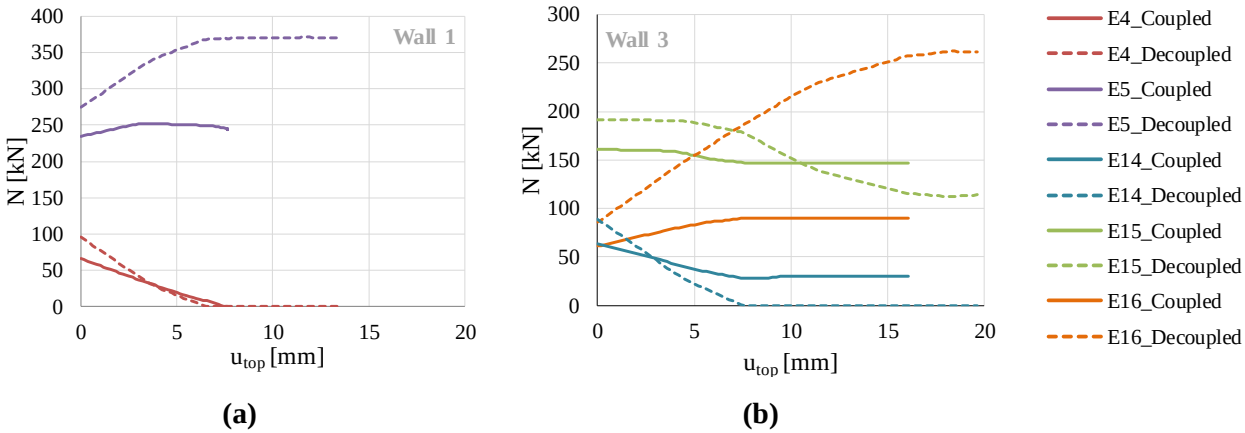

Figure 2 24- Configuration IIc, negative analysis: evolution of the axial load in the piers at the ground floor of: (a) Wall 1 and (b) Wall 3 according to the considered assumptions about the connection between the orthogonal walls.

These considerations can therefore explain the differences detected at the global scale in terms of strength: indeed, since the strength verification is performed always by considering (even in presence of a perfect coupling between the walls) the in-plane pier as a rectangular cross section, a lower compression rate of the in-plane piers (observed in the case of the "Coupled" situation) means a reduced maximum strength, also because in this case the redistribution of the vertical loads during the analysis is limited.

These results show that the modelling of the connection between the walls can significantly affect the redistribution of the axial load among the masonry piers and, therefore, the global response in terms of stiffness, strength and displacement capacity.

It is important to stress that the outcomes here presented refer to analyses performed with one of the software codes considered in this study. However, within the research activities of Task 4.3 group, other sensitivity analyses have been conducted about this aspect by using also other software that work in the field of the EF approach, obtaining substantially similar results.

2.2 RINTC PROJECT: ANALYSIS OF CODE-CONFORMING URM BUILDINGS

The RINTC project (Iervolino et al (2018)) is a joint project of ReLUIS (Network of University Laboratories of Earthquake Engineering) and EUCENTRE, two centres of competence for seismic risk assessment of the Italian Department of Civil Protection (DPC); it has involved during the years several Research Units (RU) belonging to different Italian universities, each one working on specific aspects of the research.

The main goal of this project is the evaluation of the level of seismic risk implicit in buildings designed according to the Italian building Code (NTC08 (2008)), in order to check whether code provisions are able to produce buildings with a uniform seismic risk, both considering sites characterized by a different earthquake hazard and adopting different structural materials and technologies. In particular, five different sites (L'Aquila, Naples, Rome, Caltanissetta and Milan) and two soil conditions (soil type A and soil type C, defined according to NTC08) were considered, while several new buildings typologies were analysed, including masonry, reinforced concrete, pre-cast reinforced concrete, steel, and seismically isolated buildings.

More specifically, the first step of the project consisted in the design, for each structural typology, of a set of building configurations according to the rules and the prescriptions provided by the Italian building code. After that, the second phase was related to the assessment of these structures, with the aim to actually evaluate the implicit risk level characterizing them. It is worth noting that, according to the aim of the project, while for the design phase the most common assumptions and tools adopted in engineering practice and imposed by the Italian code were used, in the assessment phase the structural models were analysed by adopting the most accurate tools now available in the literature in order to capture, as much as possible, the actual seismic behaviour of the structures. To this aim, Nonlinear Dynamic Analyses (NLDA) were performed and more refined constitutive laws were employed for each structural typology.

Within this context, the RU of the University of Genoa (coordinated by Prof. Sergio Lagomarsino) has worked on the aspects related to masonry structures, and I had the possibility to participate to the developed activity as a member of this research group (Manzini et al (2018), Cattari et al (2018b)).

The studies carried out in this project cover a wide range of interesting aspects which helped me to improve my knowledge on many different issues related to masonry buildings. Here the attention is focused only on those results which contributed to motivate some of the choices adopted in the work which this thesis is focused on. In particular, one of the most relevant and interesting aspects that emerged is the role of the different types of uncertainties involved both in the design and in the assessment of masonry buildings. Indeed, the developed activities gave the possibility to investigate the effect of: i) the adopted design method (design phase), ii) the epistemic modelling uncertainty (both in the design and assessment phases), iii) the aleatory uncertainty on the mechanical material properties (assessment phase) and iv) the record-to-record variability (assessment phase). Moreover, these issues were investigated within the framework of the Equivalent Frame modelling technique, which represents the central theme of this thesis; in fact, both in the design and in the assessment phase, the structural models of the analysed building configurations were defined by using this approach. All these aspects are discussed in detail in the following sections.

For the sake of brevity, only the results referring to a subset of building configurations and few sites are presented. A more comprehensive description of the work carried out within the context of masonry buildings can be found in Manzini et al (2018) and in Cattari et al (2018b), while the results obtained within the whole project, including also the other structural typologies, are described in detail in the RINTC Workgroup report (2018).

2.2.1 Design

The work described in the following sections refers to the prescriptions of the Italian building code (NTC08 (2008)); it should be mentioned that an updated version of this code has been released in 2018 (NTC18 (2018)), however with minor differences in terms of seismic design prescriptions for URM structures.

NTC08 allows the use of different methods for the design of masonry buildings; empirical rules applicable to the so-called simple masonry buildings (SB), Linear Static Analysis (LSA), Linear Dynamic Analysis (LDA), NonLinear Static Analysis (NLSA) and NonLinear Dynamic Analysis (NLDA).

Among them, dynamic analyses (LDA and NLDA) are not frequently used for the design of masonry buildings due to different critical issues: LDA (i.e. modal analysis with response spectrum) is not very significant for low-rise structures with a short fundamental period while NLDA can be problematic at engineering practice for the high computational burden, the difficulties in the selection of the seismic input and the choice of proper cyclic hysteretic constitutive laws for masonry elements. On the basis of these considerations, the design methods most commonly adopted in engineering practice are represented by the rules for simple buildings (SB), which are the most simplified method allowed by the code, the NonLinear Static Analysis (NLSA) and the Linear Static Analysis (LSA).

In general, the choice of one method rather than the others on behalf of the professional engineers may be influenced by several factors, first of all the seismicity level of the site under examination. Indeed,

differently from other structural typologies, the NLSA is often used for the design, and not only for the assessment of existing buildings: this is due to the drawbacks of linear methods in case of a highly nonlinear material such as masonry, particularly in areas with high seismicity (e.g. Magenes 2006). Another influencing factor that tends to favour the use of the NLSA is represented by the availability of commercial software-packages specifically dedicated to the seismic analysis of URM buildings in which this method is implemented.

It is briefly recalled that, when applying LSA, the structure is subjected to the application of a static force distribution equivalent to the inertial forces induced by the seismic action; then, the verification is performed, at the individual structural element level, in terms of strength. LSA assumes a linear behaviour of the structure by implicitly considering the material nonlinearity through the behaviour factor q, which reduces the acceleration response spectrum. Furthermore, the code allows the application of LSA also with force redistribution, even if with specific rules depending on diaphragms deformability.

In case of NLSA the nonlinear behaviour of the building is directly included in the analysis and the structural capacity is expressed in terms of the so-called *pushover* curve. Different force distributions must be adopted (e.g. mass proportional and modal distribution), with and without consideration of the effect of accidental eccentricity due to irregular mass distribution. The verification is then performed at a global scale in terms of displacement, using the N2 method (Fajfar 2000). In particular, the ultimate displacement, defined on the pushover curve as the one corresponding to a post-peak strength drop of 20% of the maximum total base shear, is assumed to correspond to the life-safety limit state. The displacement capacity associated to the damage limitation limit state is defined as the minimum between the displacement corresponding to the maximum base shear and the one corresponding to an inter-story drift of 0.3%. For both limit states, the verification consists in checking if the displacement demand induced by the seismic action is lower than the corresponding capacity, represented by these displacement thresholds.

While both LSA and NLSA require the definition of a structural model, the design according to the rules for simple masonry buildings is based on compliance with code provisions related to structural aspects in terms of geometry, materials, structural details, minimum transversal spacing and minimum area of structural walls in two main directions as well as maximum average compressive stress at each story. In addition, simple masonry buildings must be regular in plan and elevation and should be no more than three stories high. A further prescription concerns the necessity to respect minimum ratios between the area of shear walls and the total floor area in both orthogonal directions: these minimum values are provided in the code as a function of the number of stories and the seismic intensity expressed in terms of $a_g S$, being a_g the reference design Peak Ground Acceleration (PGA) on soil type A and S the soil amplification factor.

For the analysis methods that need a structural model (LSA and NLSA) NTC08 allows the use of both Equivalent Frame (EF) and cantilever models (WSSP models, see Figure 1.4), these last ones only in presence of infinitely rigid diaphragms. The main differences between these two kinds of models, as already discussed in section 1.2.2, are briefly recalled in the following section. However, even if the Equivalent Frame (EF) model is explicitly suggested, the code does not provide specific indications about all the possible modelling choices (most of them discussed in the previous section 1.3), thus leaving room for the

assumptions of the engineer. It is evident that different modelling assumptions can lead to different structural models, thus potentially affecting the outcomes of the seismic analyses.

Moreover, also the choice of the design method to consider can be regarded as a source of uncertainty, since the professional engineer can actually choose, among the methods allowed by the code, the one which best fits his needs. However, it is observed that the results of the design may change depending on the adopted method.

In order to quantify the influence of both the choice of the design method and the adoption of different modelling assumptions on the outcomes of the seismic design of new masonry buildings, some case-study buildings were introduced and analysed. In particular, they were designed according to different methods allowed by the code and by considering the possibility of different modelling choices in the corresponding structural models; the design was carried out by respecting the provisions of NTC08 and ensuring compliance with the safety checks at the life-safety and damage limitation limit states.

In the following the introduced case-study structures (section 2.2.1.1), the strategies adopted in the analyses (section 2.2.1.2) and some of the main outcomes of the design phase (section 2.2.1.3) are discussed.

2.2.1.1 Case study buildings

Among all the case-study masonry structures analysed within the RINTC project, here only the so called "C" buildings, which have been analysed by the RU of University of Genoa, are considered.

The starting architectural configuration is represented in Figure 2.25, where a plan and a 3D view of the building are shown.

his configuration, similarly to all the other buildings studied in this project, was meant to be representative of typical Italian residential URM buildings, and it was designed considering both the two- and the three-story solution. Furthermore, the roof was assumed as plane and the inter-story height was set equal to 3.1 m for each floor. It is underlined that this configuration represents an example of *regular* building, both in plan and in elevation, since it complies with the regularity rules provided by the code (see NTC08, §7.2.2).

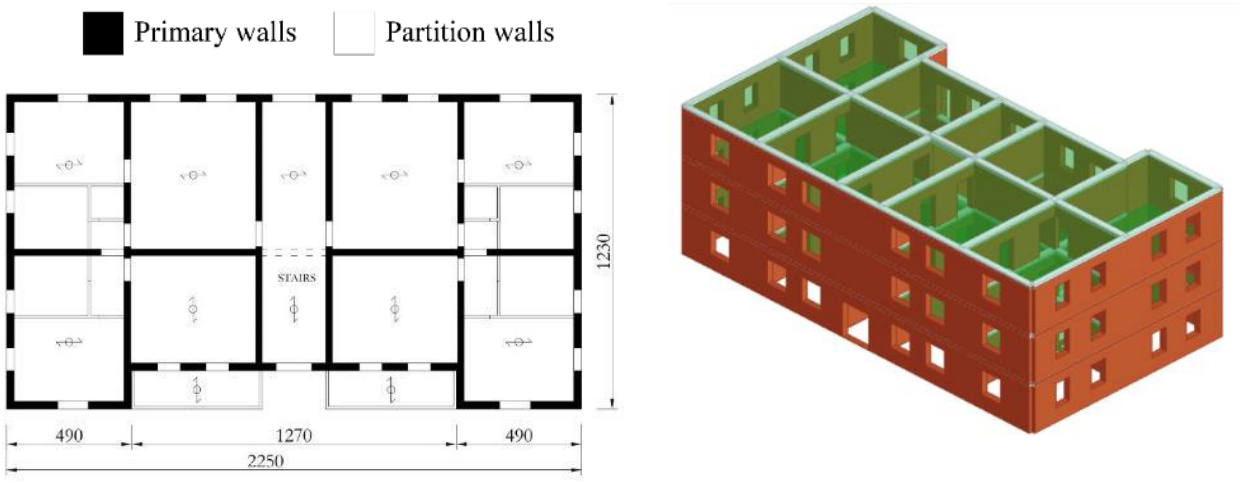

(a) (b)

Figure 2.25 - Plan view (a) and 3D view (b) of the analyzed "C" configuration.

Moving to the structural details, all the requirements imposed by NTC08 for the design of new masonry buildings were respected. In particular, the presence of continuous r.c. tie beams at each level, at the intersection of floors and walls, was considered; moreover, the reinforcement of the tie beams was set equal to the minimum allowed by the code, both in case of longitudinal reinforcements (4 ϕ16) and stirrups (ϕ8 every 25 cm). Regarding diaphragms, one-way spanning mixed r.c. - hollow clay tile floor slabs were employed (total thickness of 25 cm, with top 5 cm of r.c. slab), being the most common practice in new residential masonry buildings in Italy. The spanning direction considered for the diaphragms is indicated in Figure 2.25. Furthermore, attention was paid to satisfy the minimum dimensions of seismically resistant walls and the presence of at least 1 m long masonry wall portions at each corner intersection of external walls.

The materials of the masonry characterizing the buildings were selected as well among those typically used for the construction of new masonry buildings in Italy. In particular, they are represented by vertically perforated clay units with head and bed-joints filled with cement mortar. The values of the material mechanical properties were assumed consistently with the selected construction techniques, making sure that they would respect the minimum code requirements, in terms of mortar and unit strength, for new buildings in seismic areas.

More in detail, a mortar with a mean compressive strength equal to 10 MPa was used, while the characteristic compressive strength of the perforated clay units (f_{bk}) was assumed equal to 8 MPa. From interpolation of values reported in NTC08, they correspond to a characteristic value of masonry compressive strength f_k = 4.66 MPa and a characteristic value of initial shear strength f_{vk0} = 0.20 MPa. A realistic characteristic horizontal compressive strength f'_{bk} =1.5 MPa was adopted for this type of units. As suggested in NTC08, the Young and the shear moduli were estimated as $E = 1000 \cdot f_k$ = 4660 MPa and $G = 0.4 \cdot E$ = 1864 MPa. A specific weight of 9 kN/m^3 was also assumed for masonry.

For reinforced concrete elements, a characteristic concrete compressive strength f_{ck} = 20 MPa was adopted and steel bars with a characteristic yielding strength f_{yk} = 450 MPa were used.

The assumed dead and permanent loads consisted of 5.5 kN/m^2 at intermediate floors, 4.1 kN/m^2 at the roof level (flat terrace roof) and 5.5 kN/m^2 at stairs and balconies. Since the analysed configurations are residential buildings, imposed loads consisted of 2.0 kN/m^2 at all levels and 4.0 kN/m^2 on stairs and balconies, with combination coefficients equal to 0.3 and 0.6 respectively.

Starting from the architectural scheme sketched in Figure 2.25, seven different hypotheses were considered for what concerns the thickness of the shear walls. This lead to seven structural configurations, denoted as “C1” to “C7”, characterized by increasing areas of shear walls as percentage of the total floor area. Furthermore, in C1 and C2, some of the internal walls were replaced by r.c. beams and columns, to further reduce the area of the shear walls (Figure 2.26).

This expedient was useful in order to investigate if the same architectural configuration can lead to different structural solutions, conceived to comply with different analysis methods without being excessively over-designed, as better discussed in the following section.

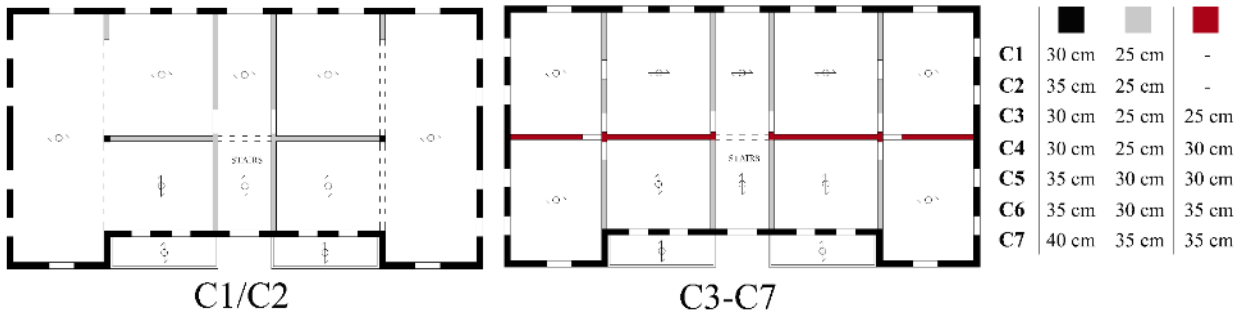

Figure 2.26- Structural configurations derived from the "C" type architectural configuration: (a) C1/C2 with internal r.c. beams and columns; (b) C3 to C7 with internal masonry walls.

2.2.1.2 Adopted tools and strategies

The two- and three- story "C" buildings were designed, as introduced before, by considering both the use of different design methods and, for the methods requiring a structural model, different assumptions about some modelling issues not explicitly addressed by the code.

For what concerns the design methods, those selected in this study were: the rules for simple masonry buildings (SB), the LSA (with and without force redistribution) and the NLSA.

They were chosen since, as mentioned before, they represent the most commonly adopted design strategies in engineering practice.

It is stressed that the configurations under examination can be designed as simple masonry buildings since they are regular both in plan and in elevation. Concerning LSA and NLSA, which require a structural model, the design of the building configurations was carried out by using two different computer programs, both of them based on the Equivalent Frame modelling approach: 3Muri (Lagomarsino et al (2013), STA Data (2017)) and ANDILWall (Magenes et al (2006)). Moreover, while for NLSA only EF models were used, for LSA also cantilever models were considered. When adopting cantilever models the structural model only includes the masonry piers, which are continuous from the foundations to the top of the building, while spandrels are not explicitly modelled and their effect is only to couple the horizontal displacements of the piers at each level (Figure 1.4, WSSP-a). On the other hand, in the Equivalent Frame approach, both piers and spandrels are introduced in the structural model and consequently included in the verification procedure. It is stressed that the force redistribution was applied only in the case of cantilever models; indeed, the absence of horizontal elements connecting masonry piers guarantees a constant level of axial compression in the elements, which does not affect the strength redistribution, facilitating the application of the procedure. Both in case of LSA and NLSA cracked section properties were employed, obtained by applying a reduction coefficient (equal to 0.5) to the lateral stiffness of the structural members.

As prescribed by the code, in the case of NLSA a bilinear elastic-perfectly plastic constitutive law was adopted for masonry panels and for the r.c. structural members. The lateral strength of each masonry panel was determined as the minimum between the values associated with shear and flexural failure modes, computed with the simplified criteria proposed in the code, different for piers and spandrels (Table 2.4).

More specifically, the strength associated to shear failure was computed as the minimum between the shear strength corresponding to a Coulomb-type sliding on the bed-joints and the one associated with unit

failure applied to the compressed portion of the cross section. The strength associated to the flexural failure mode was calculated neglecting the tensile strength of the material and assuming a stress block normal stress distribution at the compressed toe. In case of spandrels similar formulas, modified to account for the different orientation of these structural members, were adopted; in particular, the considered strength criteria assume that the spandrel behaves like a strut, thanks to the presence of the coupled tensile resisting element (r.c. tie beam).

Table 2.4– Strength criteria assumed for piers and spandrels in the analyses.

Failure mode	Piers	Spandrels
Flexure	$M_R = \frac{\sigma_0 t l^2}{2}\left(1 + \frac{\sigma_0}{0.85 f_c}\right)$	$M_R = H_p \frac{h}{2}\left(1 - \frac{H_p}{0.85 f_{c,hd} h t}\right)$
Shear	$V_R = l' t f_v$	$V_R = h t f_{v0}$

l: length of the cross section of the masonry panel;
t: width of the cross section of the masonry panel
h: height of the cross section of the masonry panel
l': length of the compressed portion of the cross section
f_c: masonry compressive strength
$f_{c,hd}$: masonry compressive strength in the horizontal direction;
$f_v = f_{v0} + 0.4\sigma_0 \leq f_{vlt}$, with f_{vlt} limit shear strength associated with unit failure, f_{v0} initial shear strength
σ_0: mean normal stress acting on the gross section of the panel;
H_p: minimum between the strength of the tensile-resistant element coupled to the spandrel and $0.4 f_{c,hd} h t$.

The attainment of the ultimate condition for the panels is determined by assuming a drift threshold equal to 0.4% and 0.8% in case of a prevailing shear and flexural failure modes, respectively.

Regarding the modelling assumptions, those which were considered as epistemic uncertainties in this study are the following:

1) spanning direction of the floor and roof diaphragms;

2) effective length of r.c. tie beams;

3) degree of connection between orthogonal walls.

For each one of these aspects, different plausible assumptions were analyzed.

More in detail, referring to point 1), two modelling options were considered, i.e. unidirectional behavior, with 100% of load transferred in the principal direction of the diaphragm and partially bidirectional behavior, with 80% of the load transferred in the principal direction and 20% in the orthogonal one. This is because mixed r.c. – hollow clay tile rigid diaphragms, typically used in new masonry buildings, have a prevalent unidirectional behavior; however, a partially slab-like behavior can be generated, hence transferring part of the load in the secondary direction.

Referring to point 2), since the choice of the effective length of the r.c. tie beams is again arbitrary (see section 1.3), in this study an effective length equal to the total length of the wall (long tie beams, "L-tb") or, alternatively, equal to the net width of the corresponding opening (short tie beams, "S-tb") has been

assumed. The differences between these two hypotheses about the length of the r.c. tie beams are shown in Figure 2.27 in the case of the EF model of one of the examined building configurations.

Regarding the degree of connection between orthogonal walls, two extreme modelling options were considered, i.e. perfect connection and limited connection.

For all the other modelling issues which are not explicitly addressed by the code, the solutions that were adopted in the structural models reflect what is most currently used in the engineering practice. In particular, the diaphragms are modelled as infinitely rigid in their plane and the out-of-plane stiffness contribution is neglected. Moreover, the effective height of piers is computed according to the criterion proposed in Lagomarsino et al. (2013).

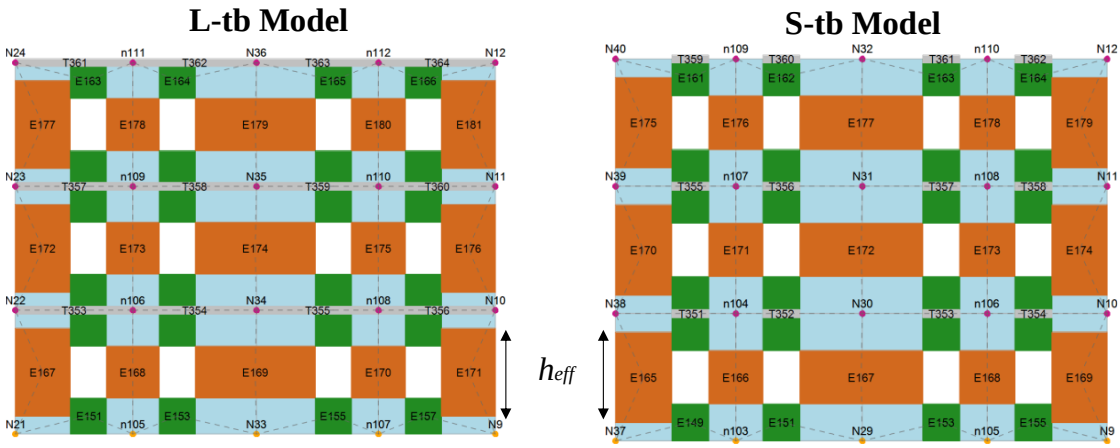

Figure 2.27– One of the walls of C3 3-story building according to the two different hypotheses for the length of the r.c. tie beams (Equivalent Frame model); in both cases, the pier effective height h_{eff} is computed according to Lagomarsino et al (2013).

By combining the uncertainties due to the adopted design method and the modelling uncertainties now introduced, the logic tree represented in Figure 2.28 was obtained.

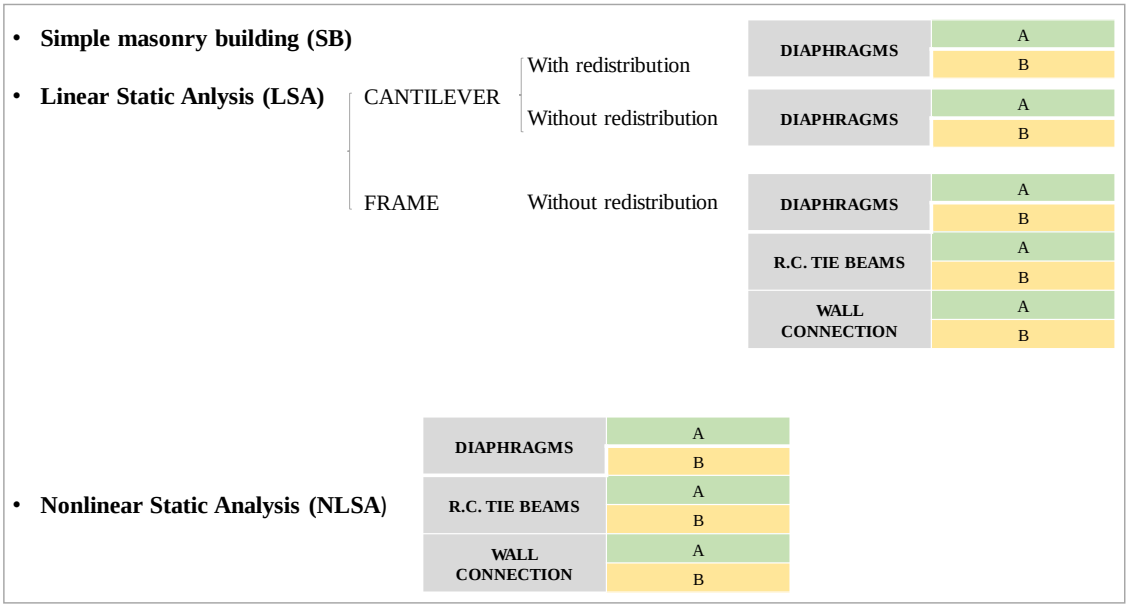

Figure 2.28 - Logic tree obtained by combining the uncertainties due to the selected design method and the considered epistemic modelling uncertainties.

It is worth noting that, depending on the adopted design method, only the uncertainties that may affect the structural response were examined. In particular, regarding the design with LSA, for the cantilever models only the two different hypotheses about the behaviour of the diaphragms were considered. In this kind of models, indeed, both the effective length of the r.c. tie beams and the quality of the connection between the orthogonal walls do not significantly affect the structural response. On the contrary, in the case of frame models (used for NLSA and LSA without force redistribution) all the introduced epistemic uncertainties and the related modelling options were considered.

Obviously, in the case of simple masonry buildings the consideration of different possible modelling choices has no meaning, since the structural model in this case is not required.

Each branch of the logic tree represents, for a fixed site and a fixed number of stories of the building, a possible outcome of the design. It comes out that, considering all the possible combinations, for a fixed site and a fixed number of stories twenty-one possible choices have to be considered, and each one of them may theoretically lead to a different structural configuration that can be designed at that site.

As already anticipated, in the RINTC project five sites were considered for the design (L'Aquila, Naples, Rome, Caltanissetta and Milan), and for each one of them two different soil type conditions were studied (soil type A and soil type C).

For a given site and soil type condition, the possibility of design the introduced structural configurations by using the different design methods under examination was explored. The aim was to identify, for each building-site combination, "meaningful" designs, consisting in cases in which the building barely complies with code requirements, i.e. it satisfies the different safety checks and conditions imposed by the code without however being excessively over-designed.

Considering the design according to the SB rules, it is observed that all the introduced structural configurations satisfy the geometrical and structural requirements prescribed by the code for simple masonry buildings in terms of number, total length and transversal spacing of seismically resistant walls in each orthogonal direction, number of stories and average compressive stress at each story. Therefore, the final building-site combinations according to this design method were obtained by considering the requirements in terms of minimum percentage of shear wall area to the total floor area, which, as abovementioned, are provided in the code as a function of number of stories and level of seismic input. According to the introduced rationale, among the seven structural configurations previously defined only the one having the minimum requirements for each site and number of stories was considered as a "meaningful" design, while all the other configurations having a higher shear wall area were not taken into consideration (being considered as over-designed for that site and number of stories).

Moving to the design methods requiring a seismic analysis, it was necessary to check the performances of the introduced structural models in correspondence of the limit states indicated by the code: life-safety and damage limitation. Regarding this aspect, it is worth noting that, given the typically high stiffness of URM buildings and the relatively high displacement thresholds at the damage limitation limit state, the assessment according to NTC08 is usually driven by the life-safety conditions. This was the case also for the selected building configurations, and hence the results presented in the following will be discussed referring to the ultimate limit state (life-safety) only.

In order to obtain code-conforming buildings not excessively over-dimensioned, in these cases a global safety factor ω was defined as the ratio between the Peak Ground Acceleration (PGA) corresponding to the attainment of the life-safety limit state and the design PGA for a return period of 475 years. Buildings barely complying with code requirements correspond to values of ω not significantly larger than unity: this was the criterion employed for the identification of the "meaningful" design in case of LSA and NLSA.

Concerning NLSA, for each configuration pushover analyses were carried out considering both X and Y directions and using two load patterns, i.e. mass proportional and inverted triangular. The latter was assumed as an approximation of the modal load pattern, as allowed by NTC08.

Figure 2.29 shows some of the pushover curves of the "C" configurations, in terms of overall base shear (V_b) versus top displacement (d_{top}), computed as the average of all nodes weighted on their tributary mass. For what concerns the modelling choices, all the curves here represented refer to models with: i) perfect connection between orthogonal walls; ii) unidirectional behavior of the diaphragms; iii) long r.c. tie beams.

It may be observed that the curves referring to the C1 and C2 configurations present a lower strength with respect to the curves related to the other ones (C3, C4, C5, C6, C7), due the presence of r.c. beams and columns replacing some internal masonry walls and hence reducing the area of shear walls, especially in the Y direction. The increase in the wall thickness (from C3 to C7) corresponds to a relatively limited increase of the overall base shear, being the increase in the resistant area only relevant for shear failure modes and not for rocking mechanisms. On the other hand, the increase in lateral strength is partly counterbalanced by the increase of inertial forces associated with the incremented mass of structural walls.

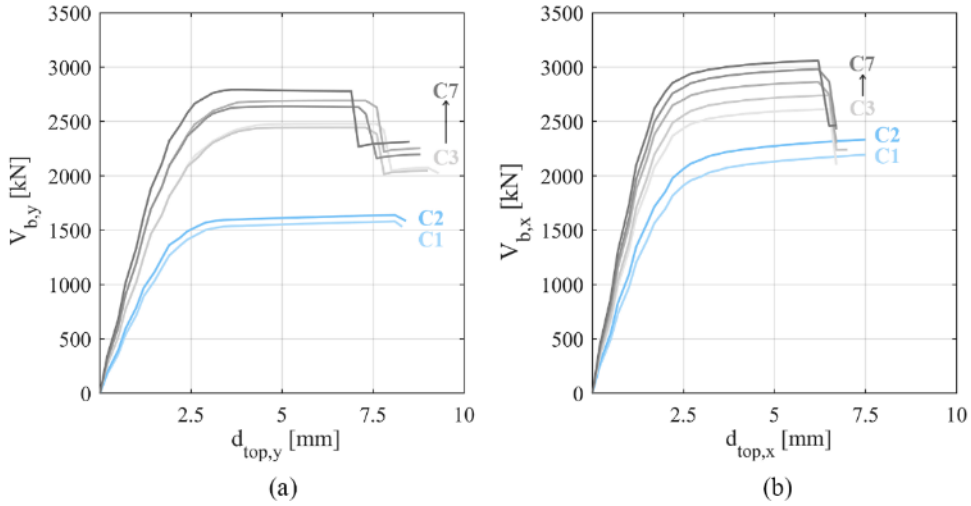

Figure 2.29 - Pushover curves of the 3-story "C" type configurations: (a) inverse triangular distribution and Y positive direction and (b) mass-proportional distribution and X positive direction; Adopted modelling choices: i) perfect connection between orthogonal walls; ii) unidirectional behavior of the diaphragms; iii) long r.c. tie beams.

2.2.1.3 Main results

The meaningful building-site combinations obtained according to the defined rationale are reported in Table 2.5. In particular, the presented results refer to the sites of L'Aquila and Rome, both soil type A (indicated in the table with the acronyms "Aq_A" and "Ro_A", respectively).

The obtained results, as discussed before, depend both on the adopted design method and on the use of different modelling assumptions.

First of all, it may be observed that the influence of the modelling uncertainty is different depending on the considered design method: in case of LSA the different modelling hypotheses do not influence the obtained structural configuration for a fixed site and a fixed number of stories, while they do in the case of NLSA. Indeed, even considering different modelling assumptions, in L'Aquila the design of the "C" configurations with LSA is never possible, neither two nor three-story, while in Rome the final obtained configuration is always the same, both in case of two- and three-story buildings, independently from the adopted modelling choices.

On the contrary, the NLSA resulted to be more sensitive to the considered modelling assumptions. In particular, in the case of the three-story buildings in L'Aquila, if r.c. tie beams are less effective (L-tb) and, at the same time, the connection between the walls is of poor quality, the C1 configuration, that in all the other cases is verified, is no more sufficient, and the C3 one has to be used.

Table 2.5 - Results of the design for the sites of L'Aquila and Rome (soil type A) when both the uncertainties due to the design method adopted and the modelling uncertainties are considered.

Mod	Design method		D	TB	WC	Aq_A 2-story	Aq_A 3-story	Ro_A 2-story	Ro_A 3-story
1	SB RULES		-	-	-	C5	C6	C2	C3
2	LSA	CANT. with red.	A	-	-	-	-	C7	C7+
3			B	-	-	-	-	C7	C7+
4		CANT. w/o red.	A	-	-	-	-	C7	C7+
5			B	-	-	-	-	C7	C7+
6		FRAME w/o red.	A	A	A	-	-	C7	C7+
7			B	A	A	-	-	C7	C7+
8			A	B	A	-	-	C7	C7+
9			A	A	B	-	-	C7	C7+
10			B	B	A	-	-	C7	C7+
11			B	A	B	-	-	C7	C7+
12			A	B	B	-	-	C7	C7+
13			B	B	B	-	-	C7	C7+
14	NLSA		A	A	A	C1	C1	C1	C1
15			B	A	A	C1	C1	C1	C1
16			A	B	A	C1	C1	C1	C1
17			A	A	B	C1	C3	C1	C1
18			B	B	A	C1	C1	C1	C1
19			B	A	B	C1	C3	C1	C1
20			A	B	B	C1	C1	C1	C1
21			B	B	B	C1	C1	C1	C1

LEGEND

D - Diaphragm		TB - Tie Beams		WC - Wall Connection	
A	Unidirectional (100%)	A	Long tie beams (L-tb)	A	Perfect
B	Bidirectional (80%-20%)	B	Short tie beams (S-tb)	B	Not coupled

Concerning the influence of the design method, it comes out that the adoption of different methods actually leads, for a fixed site and a fixed number of stories, to different structural configurations. Indeed, by looking, as an example, at the results of the design of the three-story buildings in Rome, it is possible to see that according to NLSA the C1 configuration is sufficient, while the rules for SB lead to configuration

C3 and with LSA the first structural configuration which satisfies the safety checks is the C7+. This last configuration was obtained starting from the C7 (the most resistant) and improving the mechanical material properties; moreover, also the spanning direction of some of the diaphragms was changed. Only with these expedients it was possible to obtain a three-story configuration verified with LSA in that site.

Similar considerations can be applied to the two-story buildings designed in L'Aquila, where the choice of different design methods produces again a heterogeneous framework: the NLSA leads to configuration C1, the rules for SB to configuration C5 and with LSA, even applying force redistribution, no one of the defined structural configurations satisfied the required safety checks.

From these observations it is possible to evidence the different degree of conservativeness of the examined design methods: in particular, it emerges that LSA is much more conservative with respect to the application of SB rules and NLSA, being not applicable in sites characterized by high seismicity (in L'Aquila no one of the available configurations, either two- or three-story, is verified with LSA). In these cases, when the design according to the SB rules is not possible, an alternative is represented by the use of NLSA.

The effect of the adopted method on the outcomes of the seismic design is discussed more in detail, and by considering also other case-study structures, in Manzini et al (2018).

2.2.2 Assessment

The building-site combinations identified in the design phase were then assessed by means of the most advanced tools available in the literature, in order to reproduce as accurately as possible their actual structural response. In particular, the assessment was carried out by performing NonLinear Dynamic Analyses (NLDA), which represent the most accurate method currently available for the evaluation of the seismic response of masonry buildings, and by adopting advanced models for reproducing the structural behavior of the analysed configurations. Moreover, two main performance conditions, Global Collapse (GC) and Usability-Preventing Damage (UPD), whose definition is better explained in the following section, were considered.

It is underlined that also in this phase different types of uncertainties were investigated. Indeed, a first set of NLDA was carried out by considering only the uncertainties related to the seismic action (record-to-record variability), assuming the use of deterministic models for the assessed buildings, while in a second set of analyses also the uncertainties related to the capacity were introduced. In particular, structural modelling uncertainty was considered by introducing a set of random variables describing the aleatory variability of material parameters and their correlation structure (Franchin et al (2018)); moreover, also the epistemic uncertainty related to some specific modelling choices was taken into account, by proposing a weight to combine the results obtained with the different options (logic tree approach).

Therefore, by comparing the results of the two sets of analyses it was possible to evaluate also the effects of the structural modelling uncertainty on the seismic assessment of the analysed buildings, and some of the obtained results were useful in order to guide specific choices made in this thesis.

According to the same logic that guided the previous section, in the following only the aspects which are more relevant within the context of this thesis are presented, while a more comprehensive overview of the

results about the assessment of the "C" buildings as well as of further types of building configurations can be found in Cattari et al (2018b).

2.2.2.1 Adopted tools and strategies

The nonlinear dynamic analyses were performed following a multi-stripe approach (MSA) framework (Jalayer and Cornell (2002)), which consists in computing the distribution of one (or more) Engineering Demand Parameters (EDPs), for different levels of the seismic action experienced by the structure under consideration. To this aim, 10 values of the return period of the seismic action (ranging from 10 to 100000 years) were identified and, for each of them, 20 two-components real accelerograms were selected, as discussed in detail in Iervolino et al. (2018). For each site and for each soil condition, all the records of each stripe were scaled to provide the value of spectral acceleration resulting from the probabilistic seismic hazard study for the corresponding return period of the seismic action, at a fixed structural period. This period was set equal to 0.15 s, which is compatible with the range of variation of the fundamental periods of the examined URM buildings (0.083 – 0.104 s for two-story buildings and 0.129 – 0.153 s for the three-story ones).

A Rayleigh viscous damping model was adopted, and the coefficients multiplying the mass and damping matrices were determined by assuming a viscous damping equal to 0.03 in a significant range of periods around the fundamental ones.

The analyses were performed with Tremuri program (Lagomarsino et al (2013)), that is the research version of the commercial software 3Muri (STA Data (2017)), and by considering Equivalent Frame models in which both piers and spandrels are included, with the same geometry adopted in the design phase. More in detail, the masonry panels were modelled as nonlinear beams with lumped plasticity and the constitutive model adopted for the description of their behaviour is the piecewise-linear constitutive law presented in Cattari and Lagomarsino (2013). It allows the description of the nonlinear response until very severe damage levels (DL, from 1 to 5), through progressive strength degradation in correspondence of assigned values of drift (see Figure 3.4 in Chapter 3). In addition, it is also possible to simulate a hysteretic response, formulated through a phenomenological approach. A detailed description of this constitutive law is provided in Chapter 3 (3.1.2), having this model been used also for the analyses carried out in this thesis.

For the evaluation of the peak strength of panels, in case of shear failure the criterion proposed by Mann and Müller (1980) was adopted for describing both the failure along the mortar joints and the failure across the units; indeed, it was judged as the most appropriate for the analysed type of masonry. The strength associated with the flexural failure mode was evaluated with the same approach used in the design phase and proposed in NTC08 and in EC8-3(CEN (2005)).

The mechanical parameters adopted in the dynamic analyses are consistent with those employed in the design phase. However, the constitutive law adopted for the assessment is more refined with respect to the models used in the design in terms of stiffness degradation, strength deterioration and cyclic hysteretic behavior. This required a review of the experimental data available in the literature for clay block masonry, to calibrate the constitutive law and, in particular, drift limits and strength degradation parameters. More specifically, the values of drift thresholds used as reference for the determination of the parameters characterizing the adopted constitutive law were obtained from processing of data derived from Magenes et al (2008), Morandi et al (2016) and Petry and Beyer (2014) and refer to the case of URM panels composed

by hollow clay blocks and cement mortar. The final values adopted for the parameters of the piecewise-linear model are reported in Table 2.6; the values of drift thresholds here indicated are those used in the first set of dynamic analyses, where deterministic models were considered, thus accounting only for the uncertainty related to the seismic action.

Table 2.6 - Parameters adopted for piers and spandrels in the piecewise-linear constitutive law; see section 3.1.2 and Figure 3.4 for the detailed meaning of each parameter.

Pier/Spandrel	SHEAR				FLEXURAL			
	Backbone curve		Hysteretic response		Backbone curve		Hysteretic response	
	$\theta_{S,i}$ [%]	$\beta_{E,i}$ [%]	c_1	0.8/0.2	$\theta_{F,i}$ [%]	$\beta_{E,i}$ [%]	c_1	0.9/0.2
DL3	0.24/(*)	0.6/0.7	c_2	0.8/0	0.6/0.6	1	c_2	0.8/0
DL4	0.54/0.4	0.2/0.7	c_3	0/0.3	1.22/0.8	0.85/0.7	c_3	0.6/0.3
DL5	0.7/0.7	0/0			1.6/1.2	0/0	c_4	0.5/0.8

Notes: $\theta_{S,i}$ ($\theta_{F,i}$) : drift value at the attainment of the i^{th} DL and associated to a shear (flexural) failure; β_{Ei}: fraction of the residual strength (with respect to the maximum one) corresponding to $\theta_{S,i}$ ($\theta_{F,i}$).

(*) in case of spandrels, θ_3 has been defined starting from the value of drift corresponding to the yielding point of the element and assuming then a ductility equal to 4, similarly to what suggested in Beyer and Mangalathu (2014)

Regarding the structure-related uncertainties, as introduced before, both uncertainties on the material properties and modelling uncertainties concerning different possible modelling choices were examined.

As far as the latter are concerned, since in the assessment the buildings were modelled trying to reproduce as accurately as possible their actual structural response, only some of the modelling uncertainties introduced in the design phase (and discussed in the previous section) were considered. More in detail, at this stage an unidirectional behavior of the diaphragms was assumed, because preliminary analyses showed a limited influence of this parameter on the structural response of these building configurations. A perfect connection between orthogonal walls was also assumed, because, for newly designed masonry buildings, the code requires the adoption of specific structural details guaranteeing a box-like behavior, with perfect coupling between orthogonal walls.

The only relevant modelling choice considered also in the analysis phase was related to the effective length of r.c. tie beams, for which both options were considered: long r.c. tie beams (L-tb) and short ones (S-tb). This epistemic uncertainty was treated according to the logic tree approach, so that, for each examined building, two different structural models (one with L-tb and the other with S-tb) were analysed. In the first group of dynamic analyses (the ones carried out on deterministic models) the solution with long r.c. tie beams was adopted.

Concerning the uncertainty in material mechanical parameters, both the variability in terms of stiffness and strength properties and the variability of the ultimate displacement capacity characterizing the masonry panels (as consequence of the uncertainty on the drift thresholds) were considered.

To account for these uncertainties, several random variables were introduced, as well as a multivariate statistical model describing the correlation structure among different parameters. The adopted sampling

procedure, which was common for all the building typologies involved in the RINTC project, is discussed in detail in Franchin et al (2018).

Six random variables were considered to take into account aleatory variability in masonry material properties: the Young's modulus (E), the masonry compressive strength (f_c), the initial shear strength (f_{v0}) and the three incremental drift thresholds ($\Delta\theta$) necessary to identify the attainment of different damage conditions in the structural elements. In particular, three meaningful damage conditions were identified by the corresponding drift thresholds: the attainment of a post-peak 20% drop in lateral resistance for failure in shear (indicated by $\theta_{S,3}$) or flexure ($\theta_{F,3}$), the attainment of a 50% drop in lateral resistance for failure in shear (indicated by $\theta_{S,4}$) or flexure ($\theta_{F,4}$) and the attainment of zero residual strength ($\theta_{S,5}$ or $\theta_{F,5}$). The corresponding values of drift were defined by introducing some incremental drift aleatory variables, $\Delta\theta_{S,3}$, $\Delta\theta_{S,4}$ and $\Delta\theta_{F,5}$, defined as:

- $\Delta\theta_{3,S} = \theta_{3,S} - 0.001$
- $\Delta\theta_{4,S} = \theta_{4,S} - \theta_{3,S}$
- $\Delta\theta_{5,F} = \theta_{5,F} - 0.002$

The lognormal functional form was selected for representing the aleatory variables describing the constitutive laws adopted for masonry. The distribution is identified by two parameters, i.e. median and dispersion, whose values for each random variable are summarized in Table 2.7.
The median value of E was derived by fitting a lognormal distribution to the experimental values available in the literature from tests on vertically perforated clay block masonry walls with filled head- and bed-joints (Morandi et al (2016), Franchin et al (2018)); the value of dispersion was derived from the data. The mean value of E is the same assumed in the design phase. Similarly, for the masonry compressive strength the value of dispersion was derived from experimental data and the median value was calculated by assuming a lognormal distribution and using the same mean value adopted for design.

The dispersion associated with the initial shear strength was instead assumed based on expert judgement, as the available experimental data were not sufficient to reliably identify this value. The mean value was derived starting from the characteristic value used for design (f_{v0} = 0.2 MPa) and assuming a ratio between the characteristic and the mean value equal to 0.7, for consistency with the assumption used for design. The median value of f_{v0} was hence derived under the assumption of lognormal distribution.

The drift thresholds were derived from cyclic shear-compression tests on clay block masonry piers (Morandi et al (2016)). These tests allowed defining the dispersion of the three considered random variables, as well as the median values of the incremental aleatory variables above defined.

Table 2.7 -Values of median and dispersion of each considered random variable, assumed to follow a lognormal distribution function.

Material property	E	f_c	f_{v0}	$\Delta\theta_{3,S}$	$\Delta\theta_{4,S}$	$\Delta\theta_{5,F}$
Median	4517 MPa	6.46 MPa	0.27 MPa	0.14%	0.27%	1.65%
Dispersion	0.25	0.25	0.3	0.3	0.25	0.4

The other material parameters required by the adopted constitutive model were assumed to be deterministically related to the considered random variables; in particular, the shear modulus was assumed equal to 0.4 times the Young's modulus, as adopted in the design phase (see section 2.2.1.1). The correlation structure between the different random variables is discussed in detail in Franchin et al (2018).

Through the sampling procedure, for each examined building twenty models were defined, each one representing one realization of the set of mechanical properties in the structural elements. In this way, it was possible to realize a one-by-one association between the models and the time histories of each stripe. It is underlined that, for each building, the same sampling of the aleatory variables was used for both the L-tb and the S-tb models.

Moving to the post-processing of the data obtained with the NLDA, in order to evaluate the performances of the analysed buildings the reaching of two different performance conditions was considered, namely Usability-Preventing Damage (UPD) and Global Collapse (GC) limit state. In particular, for the definition of the attainment of these limit states it was necessary on one hand, to identify a proper engineering demand parameter (EDP), to monitor the response evolution, and on the other to define proper thresholds, to verify the attainment of the corresponding limit conditions.

The selected EDP is the maximum inter-story drift (Θ_{max}) assessed at the wall scale, that is defined as $\Theta_{max} = \max(\Theta_{w,l})$, where w and l refer to the wall number and level number, respectively. It was computed by accounting for the contribution of both horizontal displacement and rotation (Lagomarsino and Cattari (2015a)), even though the latter has a limited role in the examined structures, due to the presence of rigid slabs and systematic r.c. tie beams. Considering the possible different behavior of the buildings in the two directions, the maximum inter-story drift was evaluated separately for each direction ($\Theta_{max,X}$ and $\Theta_{max,Y}$), since all walls were parallel to the main building axes.

The selection of this EDP, commonly adopted in codes and in the literature, is motivated by the presence of rigid diaphragms and r.c. tie beams promoting a global behavior, governed by the in-plane response of walls, with the development of story mechanisms. This expected behavior limits the significance of checks performed on single structural elements (piers), for the identification of global failure modes, which may be instead identified with direct reference to the inter-story drift. Moreover, considering the maximum value among all the walls – instead of an average value at the floor level – allows to identify local concentration of damage induced, for example, by torsional effects due to irregularity in plan.

The reference thresholds of $\Theta_{max,X(Y)}$ for both the considered limit states were defined by means of pushover analyses carried out in the two perpendicular directions (X and Y), considering different load patterns (mass-proportional and inverse triangular) in both positive and negative verse. More specifically, in the case of the UPD limit state only the inverse triangular load pattern was adopted, since it is the one able to well represent the response until the reaching of the maximum strength. For each analysis, the attainment of both the GC and the UPD condition was identified on the pushover curves and the corresponding value of Θ_{max} was recorded.

The specific criteria adopted for the identification of the GC and the UPD conditions on the pushover curves are described in detail in Cattari et al (2018b).

Then, for each examined building and for each limit state, two thresholds, one associated to the X direction ($\Theta_{GC,X}$ and $\Theta_{UPD,X}$) and the other to the Y direction ($\Theta_{GC,Y}$ and $\Theta_{UPD,Y}$), were obtained, computed as the minimum among all the analyses in each direction.

In this way, the limit state functions associated to the two performance conditions (Y_{LS}, i.e. Y_{GC} or Y_{UPD}) can be evaluated according to the following equation (equation 2.1):

$$Y_{LS} = \max\left(\frac{\Theta_{max,X}}{\Theta_{LS,X}}; \frac{\Theta_{max,Y}}{\Theta_{LS,Y}}\right), \tag{2.1}$$

When the capacity-related uncertainties are considered, the values of the thresholds corresponding to the attainment of each limit state were evaluated separately for each one of the twenty models obtained through the sampling of the aleatory variables.

2.2.2.2 Main results

The results of NLDA are shown in terms of IM-Y_{LS} curves, reporting on the vertical axis the value of the Intensity Measure (IM), in this case the spectral acceleration at T_1 = 0.15 s, and on the horizontal axis the value of the limit state variable Y_{LS} (i.e. Y_{GC} or Y_{UPD}), corresponding to given fractiles of the probability density function of the Y_{LS} values obtained from the nonlinear dynamic analysis performed for each stripe. In particular, the median and the 16th and 84th percentiles of the results of each stripe are indicated by the solid and dashed lines, respectively.

In the case of Y_{UPD} the lognormal distribution was assumed, while for the global collapse the procedure herein adopted to define the IM-Y_{GC} curves is illustrated in Figure 2.30. For the stripes characterized by the higher values of IM, among the twenty Y_{GC} values associated to each record, some of them could be obtained from an analysis which cannot be considered still representative of the actual physical behavior of the building. In particular, in the considered analyses this condition was identified with the situations where the residual total base shear is close to zero.

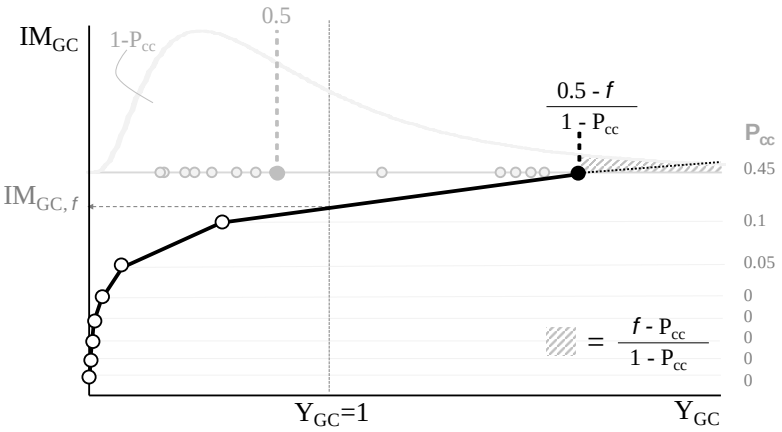

Figure 2.30 - Exemplification of the calculation adopted for including the "Collapse Cases" condition in the definition of the IM-Y_{GC} curves.

These cases are conventionally named "Collapse Cases" (CC) and the corresponding contribution to the probability of global collapse is $P_{CC} = N_{CC}/20$, where N_{CC} is the number of CC. The remaining values of Y_{GC} are assumed distributed according to a lognormal distribution, and the obtained probability density function is multiplied by $(1-P_{CC})$, in order to combine the two contributions to the total probability. When a certain probability of overcoming P, given IM, is considered (namely 0.16, 0.5 and 0.84), the corresponding value $Y_{GC,P}$ is obtained by selecting the fractile $(1-P)/(1-P_{CC})$ in the lognormal probability density function of Y_{GC} obtained from the $(1-N_{CC})$ analyses without CC. It is worth noting that each IM-$Y_{GC,P}$ curve becomes flat when $P_{CC} = P$; therefore, the point cannot be evaluated if $P_{CC} > P$. Considering for example the median IM-Y_{GC} curve (IM-$Y_{GC,0.5}$), Figure 2.30 shows the derivation of $Y_{GC,50}$ (black dot) for one stripe in which 9 CCs occurred (P_{CC}=0.45): the fractile of the lognormal distribution obtained from the other 11 analyses is then 0.909.

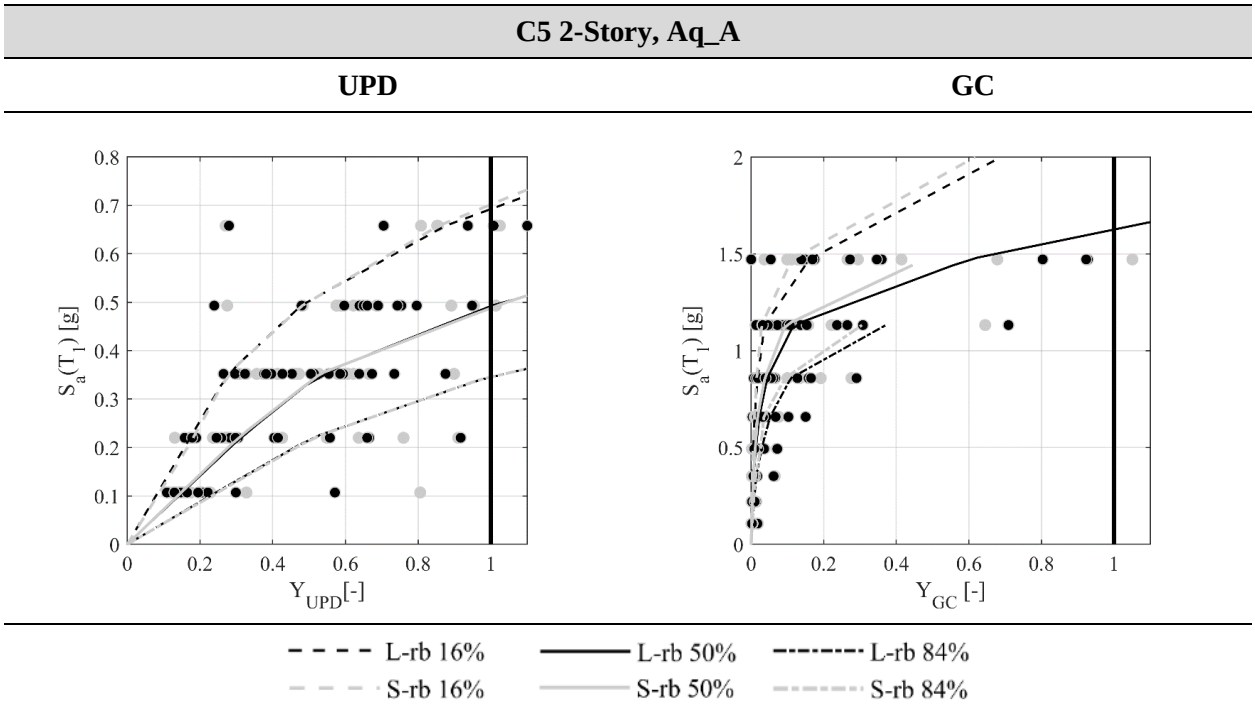

Figure 2.31 - Curves highlighting the effect of the espistemic modelling uncertainty related to the effective length of the r.c. tie beams. The vertical line indicates the attainment of the limit state (Y=1).

The final IM-$Y_{GC,P}$ curve is the piecewise-linear interpolation of the different stripes processed in that way. The value of the IM associated to the GC ($IM_{GC,P}$) is then obtained from the intersection with Y_{GC}=1.

In the following, some of the results of the NLDA analyses performed on the models including the structure-related uncertainties are presented, comparing them with those deriving from the analyses on the corresponding deterministic models. This is useful to highlight the effect of the introduced sources of uncertainty on the seismic response of the investigated buildings.

In Figure 2.31 a first comparison showing the effect of the epistemic modelling uncertainty related to the effective length of the r.c. tie beams is reported. In particular, as an example, the *IM*-Y_{LS} curves associated

to the C5 two-story building located in L'Aquila soil type A and referring to both the L-tb model and the S-tb model are represented.

Since for each examined building the same sampling of the aleatory variables was used for both the L-tb and the S-tb models, the modelling assumption about the effective length of the r.c. tie beams is actually the only difference between the two models. In the light of this consideration, it is possible to observe that, for both the limit states, the influence of this epistemic uncertainty is very limited: indeed, almost the same results are obtained, independently from the effective length adopted for the r.c. tie beams.

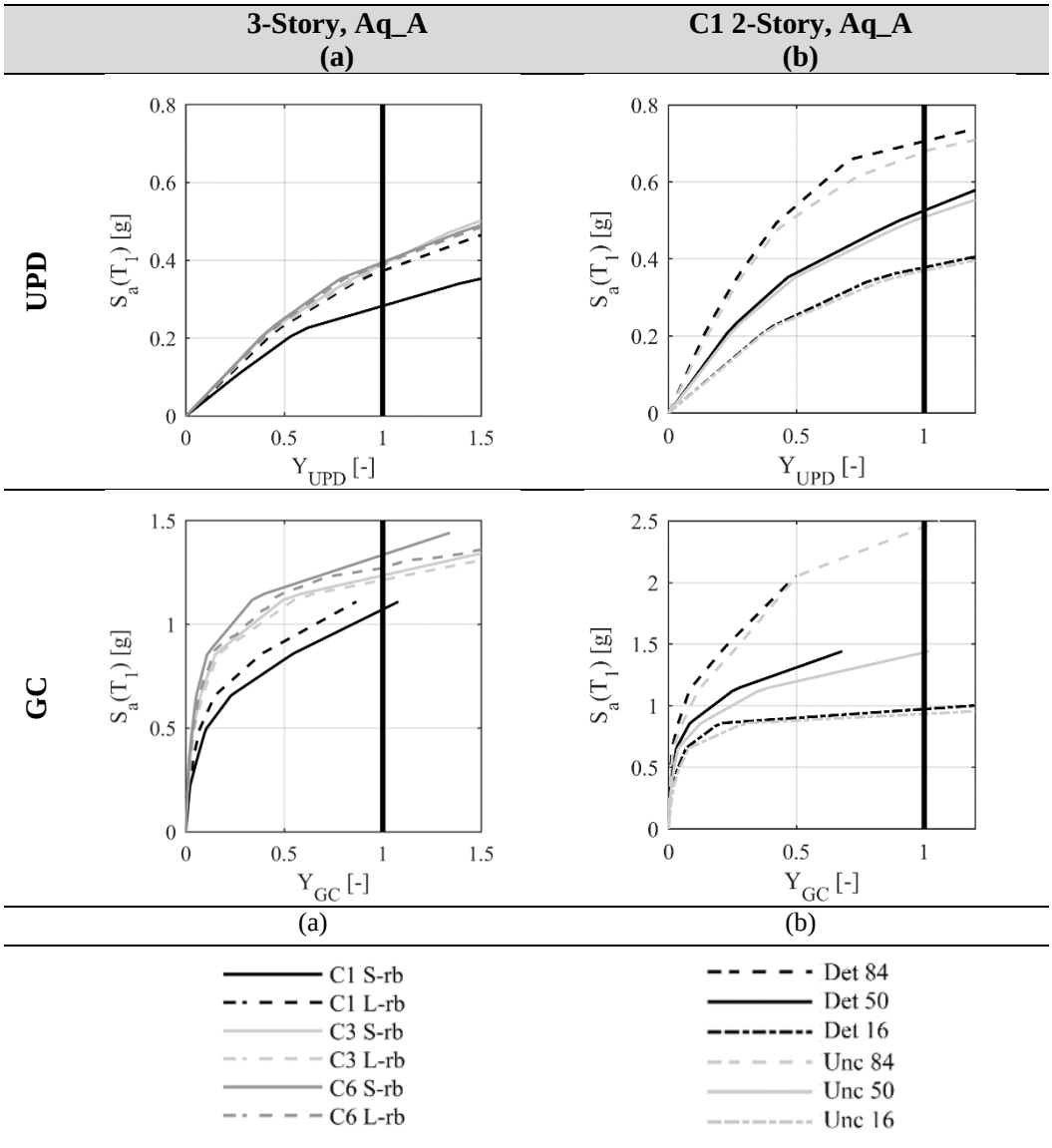

Notes:
Det: referring to the curves associated to the deterministic models (provided with L-tb);
Unc: referring to the curves associated to the models including the uncertainty on the material parameters.

Figure 2.32 - Curves highlighting the role played by (a) the uncertainties in the design procedure (involving the adopted method and the modelling choices used in the design) and the epistemic uncertainty due to the different possible modelling assumptions; (b) the effect of aleatory uncertainty in material parameters. The vertical line indicates the attainment of the limit state (Y=1).

The comparisons shown in Figure 2.32 highlight, for both the considered limit states, the influence of:

- the uncertainties which come into play during the design phase: adopted design method and different possible modelling choices (Figure 2.32a);
- the effect of the structural modelling uncertainty related to the effective length of the r.c. tie beams (Figure 2.32a);
- the uncertainty on the aleatory variables (Figure 2.32b).

More in detail, Figure 2.32a represents the median IM-Y_{LS} curves associated to all the three-story configurations which, according to the performed design procedure (Table 2.5), can be located in L'Aquila, soil type A. The observed results confirm the different level of conservativeness guaranteed by the design carried out applying the SB rules (adopted for building C6) or the NLSA (building C1 and C3). It is recalled that C1 configuration derives from the design of an analyst who adopted S-tb and perfect connection among walls, while C3 configuration from the design of an analyst who adopted L-tb and limited connection among walls.

From the same figure it is also possible to observe the role of the structural modelling uncertainty associated with the effective length of the r.c. tie beams, confirming what previously observed in the case of C5 two-story building (Figure 2.31).

Furthermore, Figure 2.32b shows, as for example considering the C1 two-story configuration in L'Aquila A (L-tb models), the comparison between the IM-Y_{LS} curves associated to the deterministic model and those associated to the models including the aleatory uncertainties. This comparison is useful in order to highlight that, for both the limit states, the effect of uncertainty in material parameters is not very significant, although the case including this uncertainty tends to be slightly more vulnerable than the deterministic case.

These observations can be also illustrated in a more complete and systematic way through Table 2.8, which reports the values of $IM_{LS,50}$ referring to the C1 configuration (two- and three-story) for the two considered definitions of the r.c. tie beams (L-tb and S-tb).

Table 2.8- Values of $IM_{LS,50}$ for the two alternative models (S-tb and L-tb) and for the deterministic model (L-tb) in the case of C1 configuration.

		Det	**Unc**	**Unc**
	L-tb/S-tb	**L-tb**	**L-tb**	**S-tb**
2-story	**$IM_{UPD,50}$**	0.54	0.52	0.51
	$IM_{GC,50}$	1.44	1.44	1.11
	$IM_{GC,50}/IM_{UPD,50}$	2.98	2.77	2.17
3-story	**$IM_{UPD,50}$**	0.43	0.38	0.29
	$IM_{GC,50}$	1.22	1.17	1.07
	$IM_{GC,50}/IM_{UPD,50}$	2.84	3.08	3.69

Further considerations are possible by considering the dispersion of the IM_{LS} values ($\beta_{IM,LS}$), which was computed for the two limit states (LS) from the IM-Y_{LS} curves.

In particular, it was obtained by considering the values corresponding to the attainment of the limit state (Y_{LS}=1) from the curves associated to the 16th and the 84th percentiles, according to the following equation (equation 2.2):

$$\beta_{IM,LS} = \frac{1}{2}\left[\ln\left(IM_{LS,84}\right) - \ln\left(IM_{LS,16}\right)\right] \quad (2.2)$$

The calculation of these values of dispersion was performed both on the curves accounting only for the record-to-record variability (β_{rec}) and on the curves that also include the effect of the element parameters variability (β_{elem} – materials and drift limits), thus obtaining the total uncertainty (β_{tot}). By assuming the two sources of uncertainty as statistically independent, it is possible to obtain an approximate estimate of the contribution of the element variability, as $\beta_{elem} = \sqrt{\beta_{tot}^2 - \beta_{rec}^2}$. By looking at the results collected in Table 2.9 it is possible to observe that, for both the limit states, the values of β_{rec} are always higher than the values of β_{elem}, thus confirming that the contribution of the record-to-record variability on the dispersion is in general more significant with respect to the contribution of the uncertainty on material parameters and element drift limits.

Table 2.9 - Values of the dispersion in IM_{LS} obtained for the two limit states (GC and UPD), considering only the record-to-record variability ($\beta_{rec.}$), only the element variability (β_{elem}), or both of them (β_{tot}).

	GC			UPD		
C1	**$\beta_{rec.}$**	**β_{tot}**	**β_{elem}**	**$\beta_{rec.}$**	**β_{tot}**	**β_{elem}**
2-Story	0.37	0.48	0.30	0.31	0.30	-
3-Story	0.45	0.51	0.24	0.18	0.24	0.16

It is stressed that the achieved results are limited to the case of residential buildings and refer only to masonry buildings made of vertically perforated clay units, that represent the commonly adopted typology for load-bearing masonry in Italy. However, similar conclusions are expected for other masonry types, because buildings were designed to barely comply with code requirements, even if different drift values should be considered for the assessment of different masonry typologies.

2.3 SUMMARY OF THE MAIN OBSERVATIONS

In general, both the experiences described in the previous sections helped to better define, contextualize and motivate the field of investigation here explored, contributing on one hand to identify and directly experience the most critical aspects involved in the use of the EF modelling approach, and on the other to guide the decision about the hypotheses to assume and the aspects on which to focus the attention in this work.

The experience related to the project working on benchmark structures, described in section 2.1, was mainly focused on the study of the EF models, which represent today the most diffused modelling approach at the engineering practice level; the results obtained from the comparison between different software codes confirmed the importance of deepening some modelling aspects involved in the adoption of this modelling technique.

In particular, the analyses performed on the single-unit two-story masonry building show that:

- under the same hypotheses and by guiding some specific modelling choices (same geometry for piers and spandrels, exclusion of the out-of-plane contribution of the walls) it is possible to reduce the scatter between the results provided by the different software codes within acceptable margins, explaining the remaining discrepancies case by case on the basis of specific modelling aspects and assumptions adopted by the different computer programs;
- some configurations more critical than others were detected, depending in particular on the structural details characterizing the spandrels. In particular, increasing scattered results arise in case of configurations with weak spandrels. In these cases, indeed, being the behaviour of the structure mainly governed by these elements, the use of different assumptions in their modelling resulted to have a strong impact on the obtained global response. This result, that was found in the case-study here presented, was confirmed also by the analyses of other benchmark structures performed within the project (here omitted for the sake of brevity); it clearly indicates that the modelling of spandrels represents one of the most critical issues in the EF models (as discussed, from a theoretical point of view, in Chapter 1, section 1.3);
- when removing the constraint of using the same modelling hypotheses the scatter of the results even increases; indeed, other factors that are not explicitly addressed by the codes and are left to the engineer's discretion can come into the play. In particular, the role of the pier effective height and of the adopted degree of connection between the orthogonal walls were explored, showing that the sensitivity of the obtained results to these modelling options is actually high.

Regarding in particular this last point, it was observed that the use of different geometries for the structural elements produces in the examined structure not negligible differences in terms of global and local response as well as in terms of detected damage pattern. In addition, the analyses devoted to deepen the role of the flange effect showed that the way to model the connection between the orthogonal walls influences the axial load distribution acting on the masonry panels after the application of the dead loads and during the analysis, especially when considering slender piers located at the corners of the building and connected in the orthogonal direction to much squatter (and so much stiffer) panels, thus affecting also the global response.

These results confirm the importance of deepening both these aspects, and contribute to motivate the choice to face these problems in the work developed within this thesis. Moreover, in the light of the abovementioned considerations about the critical issues on the modelling of spandrels, it was decided in this work to concentrate the attention on models characterized by a *strong-spandrel* behaviour type, where the response is mainly governed by the masonry piers. These types of configurations are indeed less affected by the uncertainties on the modelling of the spandrels, having these elements a secondary role in the activated response. In this way, it is possible to focus the attention on the specific critical issues previously mentioned and, in a certain amount, to decouple these issues from the uncertainty that is still present in literature about the modelling of spandrels, being the latter a possible future development of the work.

The experience associated to the RINTC Project (presented in section 2.2) was useful to show the consequences that different types of uncertainties which come into play in the structural modelling may have on the results of the design and the assessment of masonry buildings.

Focusing the attention on the role of the uncertainty on the capacity, the most important aspects emerged from the performed analyses are:

- the scarcely significant influence of the aleatory uncertainty on the material parameters, which resulted to have a role of secondary importance with respect to the record-to-record variability, even at the global collapse limit state;
- the adoption of different modelling choices, which represents the other source of capacity-related uncertainty, has a not negligible role in determining the final seismic vulnerability of the examined structures.

On the basis of these results, it was decided not to consider the uncertainty on the material parameters in the parametric analyses carried out in this thesis, assuming them as deterministic, and preferring to focus the attention on the modelling issues involved in the use of the EF models. Indeed, during the design phase (section 2.2.1) it emerged that some modelling options involved in the application of the EF approach for which the Italian building code does not provide specific indications may significantly affect the results of the seismic analyses, even leading to different outcomes of the design for fixed sites (i.e. for fixed levels of seismic hazard). This happens, in particular, when NLSA is adopted as design method. It is stressed that this method actually represents one of the most used analysis tool in practice engineering for the seismic design of masonry buildings, as confirmed also by the results presented in section 2.2.1.3, which showed that in sites with high seismicity it represents the only possibility for designing buildings that cannot be classified as “simple buildings”, due to the difficulties to use linear methods in these cases.

The modelling choices that were found to be the most important in determining the results of the design in the case of the considered buildings are the effective length of the r.c. tie beams (which influences the coupling between the masonry panels) and the degree of connection between the orthogonal walls (i.e. to consider a perfect wall-to-wall connection or a complete decoupling between the orthogonal walls). These two aspects, when combined, have led to the design of different structural solutions for the same architectural configuration in the same site (see Table 2.5). These observations underline the necessity to deepen the aspects related to the flange effect and the study of how it is modelled in the Equivalent Frame models, thus motivating the importance to investigate such theme in this thesis.

Concerning the effective length of the r.c. tie beams, moving to the assessment phase it was possible to observe that the role of this epistemic uncertainty is actually marginal when the seismic behaviour of the examined structures is evaluated through more accurate analysis methods (NonLinear Dynamic Analyses). Therefore, since the structural configurations examined in the parametric analyses performed later on in this thesis (section 3.3 and Chapter 4) are provided with r.c. tie beams, the modelling uncertainty about their effective length was not considered as an actual epistemic uncertainty. However, some preliminary sensitivity analyses on an initial configuration and considering different effective lengths for them were realized, in order to assess the influence of this modelling assumptions on the final structural response (as better explained in section 3.3).

CHAPTER 3

3 REFERENCE MODEL FOR THE VALIDATION OF THE EQUIVALENT FRAME APPROACH

To validate the EF approach with regard to the identification of the effective geometry of the structural elements (piers and spandrels) in presence of an irregular opening pattern, a specific methodological approach was defined. It is based on the execution of numerical nonlinear analyses and considers as reference solution the results of a Finite Element (FE) model in which masonry is modelled as a continuum equivalent material.

In particular, the adopted procedure can be summarized in the following steps:

1. definition of several case-study structures to analyse, consisting in 2D masonry walls with different irregular opening layouts;

then, for each defined wall configuration:

2. individuation of the possible EF idealizations on the basis of the criteria available in the literature and definition of the corresponding reference FE model;
3. execution of nonlinear static analyses (NLSA) on the defined numerical models;
4. comparisons, in terms of global response, damage pattern and local response, of the results obtained with the different models, considering those derived from the FE model as the reference solution.

The introduced methodological approach is totally numerical. This choice is motivated by the fact that the direct comparison with experimental results is rather difficult for many reasons. In the field of masonry structures, some first experimental campaigns performed at the scale of whole buildings are, as for example, the shaking table test described in Costley and Abrams (1996) and the quasi-static cyclic tests described in Cappi et al (1975) and in Calvi and Magenes (1994). More recently, other experimental campaigns, in most cases performed on one- or two- story buildings have been realized: some of them are quasi-static tests (e.g. Yi et al (2006), Esposito et al (2018)) while others are carried out on shaking tables (e.g. Paquette and Bruneau (2003), Bothara et al (2010), Magenes et al (2014), Graziotti et al (2017)). However, the geometry of the tested configurations does not present all the irregularity types that is intention to investigate in this work. It is also stressed that many of the cited experimental campaigns are represented by shaking table tests, where the interpretation of the results is often not simple; furthermore, in general the experimental results are provided only in terms of overall base shear and detected damage pattern, and no detailed information at the single element scale are provided (in terms of generalized forces and displacements), which are instead of interest for the comparisons in terms of local response that is intention to realize in this work. Regarding this aspect, it is worth noting that in the most recent experimental campaigns the use of 3D optical acquisition systems has been introduced (Graziotti et al (2017)) for monitoring the displacements of some points on the walls of the tested prototypes; however, the available data are still limited and not sufficient for conclusive considerations.

On the other hand, the FE models, where masonry is modelled as a continuum equivalent material, represent a more refined modelling technique with respect to the EF approach and a good compromise in terms of computational effort with respect to other modelling strategies that work at micro scale (i.e. the Discrete Element Models). FE models allow in fact to evaluate the seismic response of a structure without making any simplification on the localization of the masonry damage pattern and on the structure geometry.

The nonlinear constitutive laws adopted for the modelling of the material in the FE model and for the modelling of the masonry panels in the EF model are discussed in detail in section 3.1. It is evident that for ensuring consistency to the comparison it is necessary to realize a preliminary calibration between the parameters the two models are based on; the procedure adopted to this aim is described in section 3.2.

As far as the definition of the case-studies is concerned (point 1), it was decided to consider rather simple structures, represented by two-storey masonry walls with openings. In this way, the response is governed by few structural elements, so that it is possible to realize an in-depth analysis of the structural behavior. Moreover, by varying the position of the openings it is possible to consider different types of irregularities representative of the most common ones recurring in the existing masonry buildings.

Furthermore, the attention is focused on walls with a *strong spandrel-weak pier* behavior type, where the response is mainly governed by the masonry piers. In case of spandrels, indeed, in addition to the problem of their geometric identification, there are several critical issues about their modelling that still represent open problems in the literature, even concerning the definition of proper strength criteria (as discussed in Chapter 1, section 1.3). As highlighted also by the results discussed in section 2.1, these modelling uncertainties can lead to significant differences in the obtained structural response, depending on the adopted assumptions and especially when considering walls with weak spandrels, where these elements play a more significant role.

It is evident that all these aspects would not have allowed to achieve conclusive results even in the case of masonry piers. Conversely, the adoption of wall configurations with strong spandrels allows to decouple the problems and to focus the attention especially on piers. Anyhow, the spandrels, even if resistant, come into play as deformable elements, so that it is possible to make some considerations about their identification, providing indications which may be useful for these specific cases.

The NLS analyses were chosen (point 3) since they represent the most used tool for both the design and the assessment of masonry buildings, even at the engineering practice level (as widely discussed in Chapter 2), due to the strong nonlinearity exhibited by masonry. Moreover, the adoption of nonlinear analysis procedures is crucial in the framework of the modern performance based design/assessment. Therefore, it is definitely useful to explore the potentialities and the limits of the EF approach within this field.

The types of comparisons realized between the two modelling strategies (point 4) involve different aspects of the structural response, which range from the global scale response and predicted damage pattern to checks at local scale in terms of generalized forces. Checks at both scales (global and local) are important since the seismic verifications are in general performed on the basis of global pushover analyses, but it is necessary to guarantee the reliability of the obtained results also in terms of local verifications.

In this work the aspect of the seismic verification, which involves further and specific critical issues (as for example highlighted, in the case of the nonlinear static procedures, in Marino (2018)), is not directly faced, being the attention focused on the modelling in all its aspects. However, it is stressed that the

availability of a numerical model able to provide accurate results in terms of both local and global response represents the essential preliminary step for the execution of the seismic verifications needed for the assessment and the design of the masonry buildings.

In section 3.3 the application of the defined methodological approach to a regular wall configuration, which represents the starting point for the parametric analyses performed on the irregular walls, is discussed, moving finally in Chapter 4 to irregular configurations.

3.1 ADOPTED CONSTITUTIVE LAWS

The analyses on the EF models were carried out by using Tremuri program (Lagomarsino et al. (2013)), which is the research version of the software code (3Muri program) used for the analyses discussed in Chapter 2 (sections 2.1.3.2, 2.1.3.3 and 2.2.1). In particular, Tremuri program is a software specifically oriented towards the seismic assessment of masonry buildings and allows to model masonry panels with more refined constitutive laws than the bilinear formulations proposed by Codes. On the other hand, in the case of the FE analyses, masonry was modelled as a continuum equivalent material through the *concrete damaged plasticity* model implemented in ABAQUS v.6.14. In the following sections the constitutive laws adopted in the two numerical models are presented and discussed in detail.

3.1.1 Plastic-damage constitutive model adopted for masonry material

The concrete damaged plasticity (CDP) model, presented by Lubliner et al (1989) and then modified by Lee and Fenves (1998), is an isotropic model that uses concepts of damaged elasticity in combination with tensile and compressive plasticity. Although originally conceived to describe the nonlinear behaviour of concrete, the model can be used for masonry through a proper adaptation of the main parameters (Milani and Valente (2015), Valente and Milani (2016)). Moreover, it has been used in several previous studies for the modelling of masonry buildings, including particularly complex historical structures (Casolo et al (2016), D'Altri et al (2017), Milani et al (2017), Castellazzi et al (2018), Degli Abbati et al (2019)).

The model allows to describe the effects of irreversible damage associated to two main failure mechanisms of the material: tensile cracking and compressive crushing. Moreover, it can be used for describing the behaviour of the material under both monotonic and cyclic loads; however, since in this work it will be used only for performing monotonic analyses, in the following the attention is focused only on the description of this type of behaviour.

As illustrated in Figure 3.1 and in Figure 3.2, where the main input data of the model are reported, a different uniaxial behaviour in tension and compression can be taken into account, both characterized by damaged plasticity. In particular, under uniaxial tension the stress-strain response follows a linear elastic relationship until the value of the peak stress, f_t, is reached. Then, a softening stress-strain response is assumed, in order to macroscopically describe the phenomenon associated to the formation and propagation of micro-cracks in the material. In compression the response is linear until the value of initial yield, f_{ch}. After the yield stress, the response is typically characterized by stress hardening followed by a softening behaviour beyond the reaching of the peak compressive stress, f_c, in order to describe the crushing phenomenon.

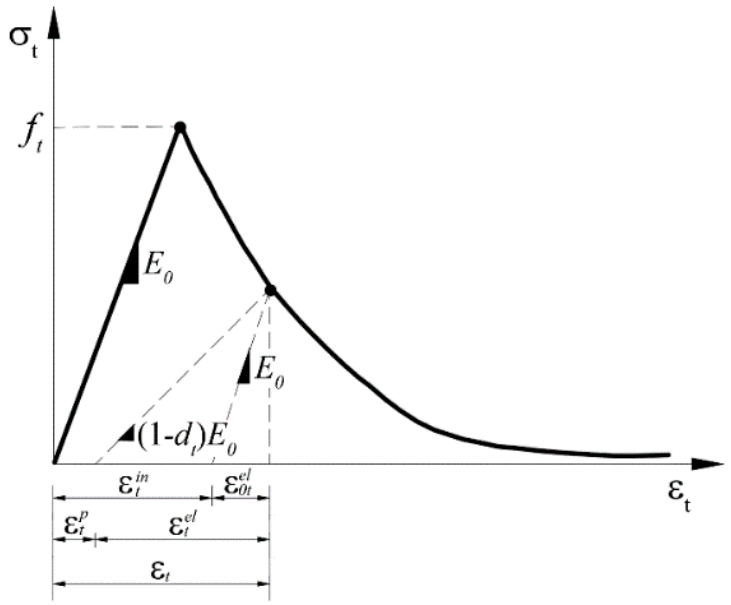

Figure 3.1 – Plastic-damage constitutive law for masonry: tensile uniaxial stress-strain relationship.

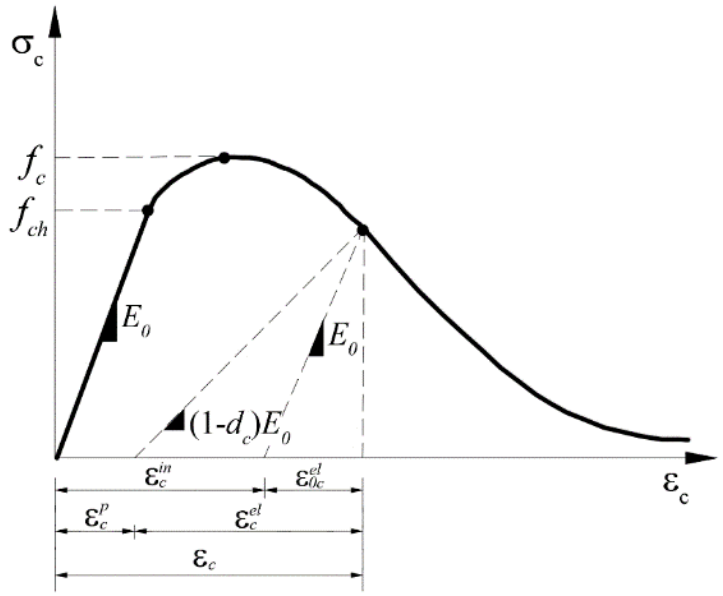

Figure 3.2 – Plastic-damage constitutive law for masonry: compressive uniaxial stress-strain relationship.

It is underlined that the model is based on the assumption of a scalar isotropic damage, which is taken into account through two distinct damage variables in tension (d_t) and compression (d_c).

According to the concepts of scalar damaged elasticity and strain decomposition, the stress-strain relations under uniaxial compression and tension are described by the following equations:

$$\sigma_c = (1 - d_c)E_0\left(\varepsilon_c - \varepsilon_c^p\right) \tag{3.1}$$

$$\sigma_t = (1 - d_t)E_0\left(\varepsilon_t - \varepsilon_t^p\right) \tag{3.2}$$

where E_0 is the initial (undamaged) Young's modulus of the material, σ_c (σ_t) is the mono-axial compressive (tensile) stress, ε_c (ε_t) is the uniaxial compressive (tensile) total strain and ε_c^p (ε_t^p) is the uniaxial compressive (tensile) plastic strain. The two damage variables d_t and d_c can vary from 0 (undamaged material) to 1 (completely damaged material). In this way, as shown in Figure 3.1 and in Figure 3.2, when considering any point on the strain softening branch of the stress-strain curves, the unloading response is weakened, since the elastic stiffness of the material is degraded.

It is underlined that for the definition of the stress-strain uniaxial behaviour of the material outside the elastic range ABAQUS requires to provide the compressive (σ_c) and tensile (σ_t) stress data as tabular functions of the corresponding inelastic strain (ε_c^{in} and ε_t^{in}, respectively). As illustrated in Figure 3.1 and in Figure 3.2, the compressive and tensile inelastic strain are defined as the total strain minus the elastic strain corresponding to the undamaged material. Considering the compressive behaviour, in particular, the inelastic compressive strain is given by $\varepsilon_c^{in} = \varepsilon_c - \varepsilon_{0c}^{el}$, where $\varepsilon_{0c}^{el} = \sigma_c \backslash E_0$; analogous equations define the tensile inelastic strain. Moreover, the unloading data have to be provided in terms of compressive and tensile damage curves (i.e.: $d_c - \varepsilon_c^{in}$ and $d_t - \varepsilon_t^{in}$). In this way, ABAQUS automatically converts the inelastic strain values to plastic strain values using the following relationships:

$$\varepsilon_c^p = \varepsilon_c^{in} - \frac{d_c}{1 - d_c} \cdot \frac{\sigma_c}{E_0} \tag{3.3}$$

$$\varepsilon_t^p = \varepsilon_t^{in} - \frac{d_t}{1 - d_t} \cdot \frac{\sigma_t}{E_0} \tag{3.4}$$

In order to describe the multi-dimensional behaviour in the inelastic range, a Drucker-Prager type surface is assumed as yield surface. This function is specified by the ratio f_{b0}/f_{c0} between the biaxial (f_{b0}) and uniaxial (f_{c0}) initial compressive strengths and a constant K_c, which represents the ratio of the second stress invariant on the tensile meridian to that on the compressive meridian at initial yield. The parameter K_c, applied to the analytical expression of the Drucker-Prager surface in the principal stress space, allows distorting the surface, making it more similar to that of the Mohr –Coulomb criterion. In particular, typical yield surfaces are shown in Figure 3.3-b in the deviatoric plane and in Figure 3.3-a for plane stress conditions.

Additionally, to control the dilatancy in the quasi-brittle material response, a non-associative flow rule is considered to define the plastic strain rate. It is obtained by a flow rule generated by a Drucker-Prager type plastic potential (Drucker-Prager hyperbolic function). In particular, it is defined by the dilatancy angle ψ and a smoothing constant ϵ, referred to as eccentricity parameter, that defines the rate at which the function approaches the asymptote (the flow potential tends to a straight line as the eccentricity tends to 0).

When using material models exhibiting softening behavior and stiffness degradation several convergence difficulties may arise during the numerical analyses. In order to overcome some of these convergence problems, the concrete damaged plasticity model allows to use a viscoplastic regularization of the constitutive equations, which is made through the use of a viscosity parameter η. In particular, small values of the viscosity parameter help to improve the rate of convergence in the softening branch without significantly compromising the results.

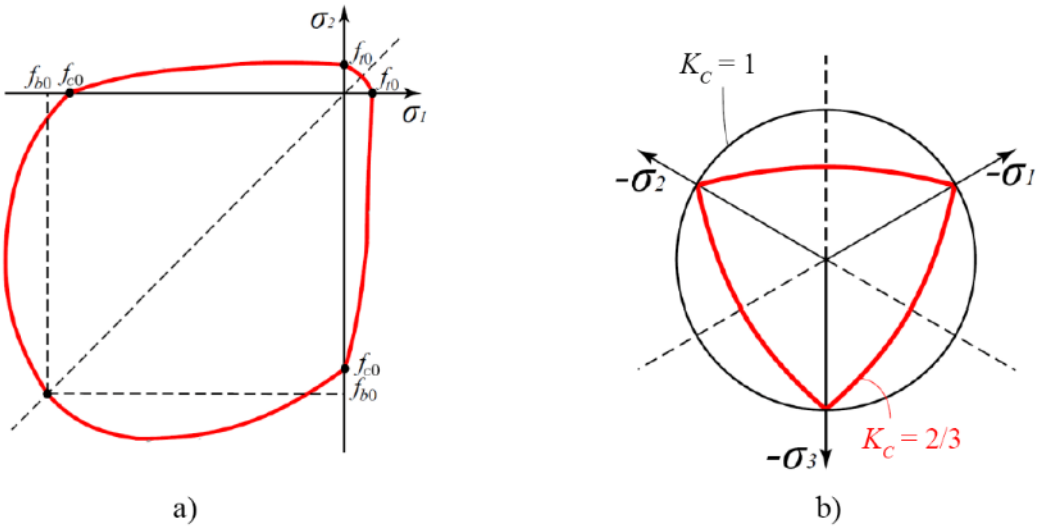

Figure 3.3 – Plastic damage model yielding surface in: a) plane stress and b) the deviatoric plane.

Finally, a fracture energy-based regularization is used to describe the softening in tension and compression; in particular, both tensile and compressive fracture energies are scaled in relation to a representative finite element size (equivalent length l_{eq}). More in detail, this last can be calculated as: $l_{eq} = \alpha_h \sqrt{V_e} = \alpha_h \sum_{\rho}^{n_\rho} \sum_{\xi}^{n_\xi} \sum_{\eta}^{n_\eta} detJ w_\rho w_\xi w_\eta$, where w are the weight factors of the Gaussian integration scheme, J is the Jacobian of the transformation, V_e is the element area and α_h a modification factor that depends on the typology of the element used. In this way, the mesh size does not significantly influence the analysis response.

The specific values adopted for the parameters of the CDP model in the analyses performed in this thesis are presented and discussed in detail in section 3.2.

3.1.2 Piecewise-linear constitutive model adopted for masonry panels

The nonlinear beam model with lumped inelasticity idealization and a piecewise-linear behavior formulated by Cattari and Lagomarsino (2013a) was here adopted for the description of the behavior of the structural elements in the EF models. This constitutive law, which is implemented in Tremuri program (Lagomarsino et al (2013)) allows the description of the nonlinear response until very severe Damage Levels (DLs, from 1 to 5), that can be associated to different performance conditions, through progressive strength degradation in correspondence of assigned values of drift (Figure 3.4). In particular, it is possible to describe both the monotonic and the cyclic behavior of the panels; even if the parametric analyses performed in this thesis (at first on single masonry panels (section 3.2) and then on masonry walls with openings (section 3.3, Chapter 4) are monotonic, in this section also the way the model describes the hysteretic response of the panels is presented, having this been used for the nonlinear dynamic analyses discussed in Chapter 2 (section 2.2).

More specifically, the hysteretic response (Figure 3.4) is formulated through a phenomenological approach to capture the differences among the various possible failure modes (flexural type, shear type or even hybrid) and the different response of piers and spandrels.

The model requires the definition of a first set of parameters aimed to describe the initial stiffness of the panel and its progressive degradation, the maximum strength of the panel (V_y) and the progressing of nonlinear response for increasing damage levels (θ_{Ei} - drift value at the attainment of the i^{th} DL, β_{Ei} - corresponding fraction of the residual shear strength, with respect to V_y).

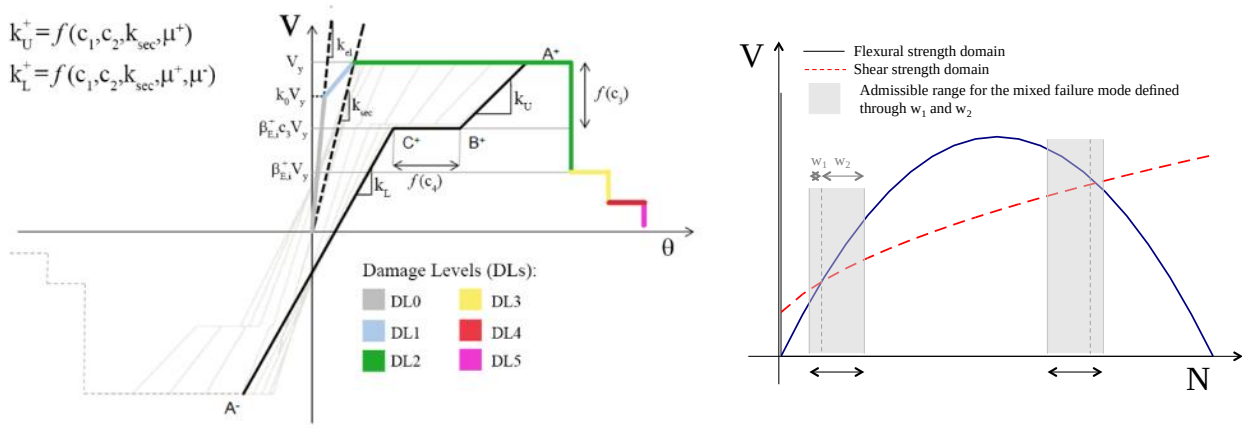

(a) (b)

Figure 3.4 - a) Piecewise-linear constitutive law and associated hysteretic response; b) schematic representation of the criteria assumed to define the occurrence of a hybrid failure.

The elastic phase is described according to the beam theory by defining the elastic Young (E) and shear (G) moduli; then the progressive degradation is computed in an approximate way by a secant stiffness by assigning a proper ratio (k_r) between the initial (k_{el}) and secant (k_{sec}) stiffness, at the point in which the maximum strength is reached, and a ratio (k_0) between the shear at the end of the elastic phase and the shear strength (Figure 3.4-a).

The maximum strength of the panel is computed according to the simplified criteria proposed in literature to interpret the failure modes that may occur (crushing, bed joint sliding, shear diagonal cracking) which are based on the choice of a reference point or section for calculation, as discussed in (Calderini et al (2009a)). The strength V_y is computed as the minimum between the predictions provided by the strength domains associated to the failure criteria evaluated on the basis of the current axial stress acting on the element; in this way, the current prevailing behavior ruling the hysteretic response of the element is also determined.

Finally, different values of $\theta_{E,i}$ and $\beta_{E,i}$ are assigned for describing a prevailing flexural or shear response of the panel. Moreover, they may be differentiated in the case of spandrel and pier elements. For the hybrid failure mode, average values for $\theta_{E,i}$ and $\beta_{E,i}$ are computed by the program starting from those assigned by the user in the case of the basic flexural or shear failure modes. The occurrence of a hybrid mode is then established by assigning in input a given admissible range in the $V - N$ domain (close to the points in which the flexural and shear domains intersect with one another, as illustrated in Figure 3.4-b).

Then, a second set of parameters describes the hysteretic response, by defining the slope of unloading and loading branches of the hysteresis loops. In particular, the unloading branch from A+ to C+ is ruled by the stiffness k_U (Figure 3.4-a). It is computed as follows (in the case of the positive quadrant):

$$k_U^+ = k_{sec}(\mu^+)^{c_1}\left[1 - c_2\left(1 - \beta_{E,i}^+\right)\right] \tag{3.5}$$

where: μ^+ is the maximum value of ductility reached in the backbone of positive quadrant; c_1 is a parameter aimed to degrade the value of k_U with respect to the secant stiffness k_{sec} (it may assume values from 0 - elasto-plastic law- to 1 -secant stiffness); c_2 aims to further degrade the value of k_U by taking into account the progressing strength decay reached on the backbone, described by the maximum damage level reached which corresponds to a specific value of strength decay β_{Ei} (it may assume values from 0 to 1). An analogous expression may be defined for the negative quadrant.

After a first branch (A+ B+) ruled by k_U, the unloading branch may also exhibit a horizontal branch (B+ C+) where: the point B^+ is determined by the c_3 coefficient that varies from 0 (A^+ B^+ branch until the abscissa axis) to 1 (elastic nonlinear condition). The extension of B^+ C^+ branch is determined by the c_4 coefficient: although it may vary from 0 to ∞, suggested values range from 0 to 1. Finally, the loading branch from C+ to A- is ruled by the stiffness k_L. It is computed by taking into account k_u and the maximum ductility value reached in both positive and negative quadrant (μ+,μ-).

Some numerical validations of the model are illustrated in (Cattari and Lagomarsino (2013b), CNR DT 212 (2014), Cattari et al. (2014a), Cattari et al (2014b), Marino et al (2016)) through the comparison with experimental campaigns on shaking table or with the actual response of URM buildings affected by seismic events.

3.2 CALIBRATION OF THE ADOPTED CONSTITUTIVE LAWS

Since the adopted models work at different scales (material and panel) and consequently are based on different mechanical parameters, once fixed the masonry typology to consider in the simulation, it is necessary to realize a preliminary calibration between the parameters used in the two models, in order to ensure consistency between them. This represents the fundamental prelude for the parametric analyses that will be carried out on the irregular walls (Chapter 4).

Mechanical properties to be assumed as reference for a specific masonry type may be found in codes (MIT (2009)) or in the literature, as result of experimental tests. However, such parameters (e.g. shear strength, drift thresholds and strength decays associated to different damage conditions) are usually referred to the scale of masonry panels rather than the scale of the material, as contemplated instead in continuum FE formulations.

That implies, in case of the EF model, the possibility to directly adopt as input data the mechanical parameters representative of the considered masonry type, referred to the structural element scale and derived from the codes or from the literature, without needing any specific calibration of the panel. On the contrary, in case of the FE model a preliminary phase aimed to the definition of a correlation between the parameters of the adopted constitutive law, which is defined in the stress-strain domain, at the scale of the material, and those referring to the structural element scale employed in the EF models is necessary, in order to reproduce the behavior at the panel scale in terms of both strength and post-peak response.

In the following, the process that was used for the calibration (section 3.2.1) and the obtained results (section 3.2.2) are discussed in detail.

3.2.1 Procedure adopted for the calibration

The procedure adopted for the calibration between the two models can be schematized in the following steps:

i. choice of the mechanical parameters representative of the masonry typology of interest (i.e. strength and stiffness properties as well as drift thresholds and corresponding drops of strength associated to different damage conditions for the description of the post-peak behaviour of panels);
ii. definition of a set of representative pier geometries, in terms of in-plane aspect ratios;
iii. definition of the strength criteria to use in the EF model and of the parameters characterizing the multilinear constitutive law on the basis of the assigned material properties;
iv. modelling of the introduced panels in ABAQUS and execution of lateral load monotonic analyses aimed at the evaluation of i) the maximum lateral strength for increasing values of the applied axial load and ii) the associated base shear –top displacement ($V_b - d_{top}$) curves;
v. execution of parametric analyses on step iv), aimed to optimize the calibration of the parameters the FE model is based on.

More in detail, point v) has been carried out by varying specific parameters of the constitutive law characterizing the continuum material in order to find the best solution for the calibration in terms of:

- *strength*: i.e. to reproduce the failure domain of the considered panels, defined according to the strength criteria adopted in the EF models, within the range of variation of the normal stress of interest;
- *displacement capacity*: i.e. to simulate, for different values of the applied axial load, the post-peak behaviour of the panels described through the assigned drift thresholds and corresponding drops of strength.

This last operation, in particular, can be made through the direct comparison between the base shear-top displacement curves obtained with the FE model (point iv)) and the corresponding curves that can be obtained through the execution of the same analyses on the panels modelled in Tremuri program. As aforementioned, indeed, the drift limits and strength degradation parameters assigned as reference can be directly assumed as input data for the multilinear constitutive law, thus representing the target for the calibration of the FE model. Regarding this aspect, it is underlined that, when the masonry panel is modelled at the material scale, it typically exhibits a softening behavior characterized by a gradual strength and stiffness degradation, due to the progressively occurred damage; thereby, the aim of the calibration in this case is to capture the envelope represented by the simplified piecewise-linear behavior assumed at the panel scale.

It is worth noting that the calibration process here performed is carried out by considering only monotonic loading acting on the panels, while cyclic loading has not been investigated in this thesis. Indeed,

it was decided to focus the attention on analysis methods based on the execution of monotonic analyses (the analyses performed at the wall scale described in section 3.3 and in the following Chapter 4 are nonlinear static analyses), which represent, as extensively discussed in section 2.2, the analysis methods most adopted by the professional engineers among those allowed by the codes.

However, it is evident that the simulation of the seismic action through monotonic analyses represents an approximation, since in reality the structures during an earthquake are subjected to cyclic loading. As observed in experimental tests, performed as for example at the scale of single panels subjected to lateral loads, cyclic actions produce a progressive degradation of the mechanical parameters of the material, thus affecting the maximum strength achievable, which results in general to be lower in case of cyclic loads than in case of monotonic analyses.

Since in the adopted constitutive laws (both in case of the FE model and in case of the EF model) there are no parameters accounting for the degradation of the mechanical parameters caused by cyclic actions when applying monotonic loading, it is important to underline that the analyses here carried out are characterized by this approximation. Therefore, the base shear – top displacement curves obtained for the masonry panels through both the FE models and the EF approach are expected to be associated to an overestimation of the maximum strength with respect to the actual behavior of the panels, being the effects of strength degradation due to cyclic loading not included.

Potentially, the adopted constitutive models could be able to include these effects, even in a simplified way, when performing cyclic analyses. As for example, the piecewise-linear constitutive law used for the structural elements in the EF models (and employed in the nonlinear dynamic analyses discussed in section 2.2) includes the formulation of a hysteretic response for the elements, and the slope of the unloading branch (k_U in Figure 3.4-a) is function of a set of parameters, including the maximum ductility achieved in the positive (or negative) quadrant and the occurred strength degradation (see eq. 3.5).

However, in general there are very few proposals and models available in literature or codes aimed to take into account these effects. Only recently, in the commentary of the new Italian building Code (MIT (2019)), a specific formulation for the shear strength in presence of cyclic loads is introduced in case of r.c. beams (§C8.7.2.3.5); more specifically, it takes into account the reduction in shear strength due to cyclic loading as a function of the ductility demand on the element.

In the following each step of the above introduced calibration procedure is described in detail.

Definition of the reference material properties

The methodological approach now introduced for the calibration between the EF model and the FE model is totally general and can therefore be applied to each masonry type, once established the mechanical properties. Indeed, the objective is, starting from assigned mechanical properties, to calibrate the parameters of the continuum constitutive law in order to reproduce the behaviour at the scale of the panel, as simulated through the EF model.

For this reason, the mechanical parameters that were adopted as reference in this study (reported in Table 3.1) are deliberately conventional and not related to a specific masonry typology, although “realistic” for typical existing masonry (e.g. as suggested in MIT (2009) §Tab. C8A.2.1).

Regarding the stiffness parameters, it is underlined that the values reported in Table 3.1 refer to the initial elastic condition. Moreover, for existing masonry buildings the shear modulus *G* is usually defined as 1/3 of the Young modulus *E*, as suggested in MIT (2009). However, in this case the correlation between the Young modulus and the shear modulus proposed in NTC08 (§11.10.3.4) for new masonry buildings, i.e. *G=0.4E* was adopted as reference. In this way, it was possible to use in the FE model (where the stiffness parameters are the Young modulus *E* and the Poisson coefficient *v*, being the material isotropic) a Poisson coefficient equal to 0.2, that is a reasonable value often used for masonry.

Table 3.1 - Mechanical parameters assumed for the masonry panels.

E_m [MPa]	G_m [MPa]	f_c [MPa]	τ_0 [MPa]	w [kN/m^3]
1800	750	6.2	0.147	17.50

Notes: E_m masonry Young modulus; G_m masonry shear modulus; f_c masonry compressive strength; τ_0 masonry shear strength; w masonry specific weight.

As aforementioned, the post-peak behavior of the masonry panels can be described through specific drift thresholds (θ_E) and corresponding strength decays (β_E) associated to different damage conditions (or Damage Levels, DLs). It is evident that these parameters can assume different values depending on the masonry type under study. The values that were adopted in this work, differentiated depending on the failure mode (flexural or shear), are reported in Table 3.2. They are consistent with values proposed in literature (Kržan et al (2015), Vanin et al (2017), Morandi et al (2018), Messali and Rots (2018)).

Table 3.2 - Parameters describing the post-peak behavior assumed for the masonry panels.

	SHEAR		FLEXURAL	
	$\theta_{E,i}$ [%]	$\beta_{E,i}$ [%]	$\theta_{E,i}$ [%]	$\beta_{E,i}$ [%]
DL3	0.3	0.7	0.6	1.0
DL4	0.5	0.4	1.0	0.85
DL5	0.7	0.0	1.5	0.0

$\theta_{E,i}$: drift value at the attainment of the ith DL;

$\beta_{E,i}$: fraction of the residual strength with respect to the maximum strength in correspondence of the ith DL

Definition of the geometry for the pier panels

Three masonry panels were considered for the calibration process, characterized by different geometries and in-plane aspect ratios (λ =H/B), as reported in Table 3.3. It is underlined that the geometry assumed for these panels is the same of those tested by Anthoine et al (1995) at the research centre located in Ispra; as declared by the Authors, these aspect ratios are representative of those characterizing the masonry panels in the "Door Wall", that is one of the walls characterizing the building prototype tested at the University of Pavia by Calvi and Magenes (1994). Such a choice is motivated by the fact that the geometry adopted in this study for the regular wall (see section 3.3) is inspired to the geometry of the Door wall.

Table 3.3 - Geometry and aspect ratios characterizing the three panels considered in the calibration process.

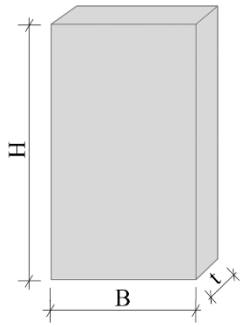

	***B* [m]**	***H* [m]**	***t* [m]**	**λ [-]**
Panel 1	1.30	0.85	0.21	0.65
Panel 2	1.00	1.35	0.25	1.35
Panel 3	1.00	2.00	0.25	2.00

EF model: strength criteria and parameters of the multilinear constitutive law

Considering the calibration in terms of strength, first of all it is necessary to define the strength criteria to adopt in the EF model. They are differentiated depending on the failure mode of the panel (flexural or shear). In particular, the strength associated with the flexural failure mode is evaluated by neglecting the tensile strength of the material and assuming a stress block normal distribution at the compressed toe (as proposed in NTC08 and EC8-3). In this way, the flexural strength V_f can be calculated according to the following equation:

$$V_f = \frac{\sigma B^2 t}{2}\left(1 - \frac{\sigma}{0.85 f_c}\right)\frac{1}{H_0} \tag{3.6}$$

where B and t are the width and the thickness of the panel, respectively (see the figure in Table 3.3), σ is the mean normal stress acting on the cross section of the panel, f_c is the masonry compressive strength and H_0 depends on the static scheme of the panels, being the height of the point of contraflexure ($H_0 = H$ for the cantilever scheme and $H_0 = H/2$ for the fixed-fixed static scheme, being H the length of the panel).

For the computation of the strength associated to the shear failure mode, the criterion proposed by Turnšek and Cačovic (1971), that describes the diagonal shear failure, with the modification introduced in Turnšek and Sheppard (1980), aimed to take into account the different shear stress distribution in the central cross section of the panel depending on its geometry, is assumed as reference. This criterion is based on the assumption that masonry is an equivalent isotropic material and on the hypothesis that diagonal cracking occurs when the maximum principal stress acting at the center of the panel reaches the limit value f_{ds}, assumed as a "reference" tensile strength of masonry. The ultimate shear strength V_s according to this criterion can be calculated through to the following equation:

$$V_s = \frac{f_{ds} B t}{b}\sqrt{1 + \frac{\sigma}{f_{ds}}} \tag{3.7}$$

where B, t and σ have the same meaning discussed above, while b depends on the aspect ratio $\lambda = H/B$ characterizing the panel; in particular, b is assumed equal to 1.5 for $\lambda \geq 1.5$, equal to 1 for $\lambda \leq 1$ and directly equal to λ in the other cases, as suggested in MIT (2009).

The criterion proposed by Turnšek and Cačovic (1971), which is explicitly suggested in MIT (2009) in case of irregular existing masonry, was chosen in this context since it is based on the assumption of an isotropic behaviour for masonry, thus being consistent with the isotropic FE continuum model here adopted; moreover, it is one of most commonly used in the case of existing masonry buildings.

However, other models for describing the shear failure of masonry panels are available in literature. An in-depth review of the most widespread strength criteria present in the literature and codes to interpret the failure modes of piers can be found in Magenes and Calvi (1997) and in Calderini et al (2009a). In general, the choice of the failure criteria to adopt for the masonry panels in EF models depends on the features of the masonry type under examination. Indeed, while the criterion by Turnšek and Cačovic (1971) is particularly suitable, as afore mentioned, for the description of the behavior of irregular masonry (almost isotropic), when dealing with regular masonries (such as brick masonry) other strength criteria should be chosen, capable to take into account the effects of anisotropy, that are significant in these cases. As for example, a possibility may be to adopt, for representing shear failure in regular masonries, the criterion proposed by Mann and Müller (1980), which is suitable for describing both the failure along the mortar joints (considering the so called "stair-stepped" failure modes) and the failure across the units (see Figure 1.5-c). It is worth underlining that the description of masonry typologies with a strong anisotropic behavior, as for example regular brick masonry, would imply the necessity to adopt a different constitutive law also in the case of the continuum FE model. In this case, indeed, the model should be able to account for the orthotropy inherent to this masonry type (with its typical pattern of regular bed and head joints) through proper elastic, strength and softening parameters, thus being able to simulate the inelastic mechanisms typically occurring in these types of masonries (local bed joint shear sliding as well as the opening and closing of the head joints).

However, the objective of the thesis is to provide a general methodology (and an example of its application) for the calibration between the constitutive laws adopted in the FE model and in the EF model (which have both to be consistent with the masonry typology to simulate), with the aim to lay the foundations for a rigorous and robust comparison between the two models. In this case, in particular, the chosen constitutive models (described in section 3.1) are both suitable for describing an isotropic masonry.

The final strength of the panel V_y as well as the predicted mode of failure are then computed, for each value of the applied axial load, as the minimum between the shear strength associated to the flexural failure mode V_f and the strength associated to the shear failure V_s.

It is underlined that all the parameters required by the adopted strength criteria can be immediately derived from the mechanical parameters assumed as reference and reported in Table 3.1 as well as from the geometry and the static scheme characterizing each panel. Considering the criterion adopted for the shear failure, the value of f_{ds} was obtained through the simple relationship suggested in MIT (2009) (eq. 8.7.1.1), where the masonry tensile strength is expressed as a function of the masonry shear strength τ_0, i.e. $f_{ds} = 1.5\tau_0$.

Concerning the stiffness parameters, the initial values of the Young and shear moduli were set equal to those reported in Table 3.1 (which refer to the initial elastic condition). Then, in order to describe the stiffness degradation, also the ratio between the initial and secant stiffness k_r and the ratio between the shear at the end of the elastic phase and the shear strength k_0 has to be defined (see section 3.1.2, Figure 3.4-a). In particular, k_0 was set equal to 0.5, while k_r was assumed equal to 1.54, thus implying that in the cracked

condition the elastic moduli are equal to 65% of their initial values. It is recalled that the Italian building code suggests a reduction of 50% of the initial elastic moduli; however, on the basis of the low rate of compression characterizing the panels of the masonry walls investigated in the parametric analyses here performed (section 3.3, Chapter 4), a lower stiffness reduction was considered more representative for the behaviour of the panels.

Moving to the parameters describing the softening phase, the values of drift thresholds θ_E and the corresponding drops of peak strength β_E were directly assumed equal to those reported in Table 3.2.

Lateral load analyses on the FE models of the panels

The masonry panels were modelled in ABAQUS v.6.14 by means of fully integrated (2x2x2 integration points) 8-node linear brick elements (Figure 3.5) and by using the Concrete Damaged Plasticity (CDP) model discussed in section 3.1.1.

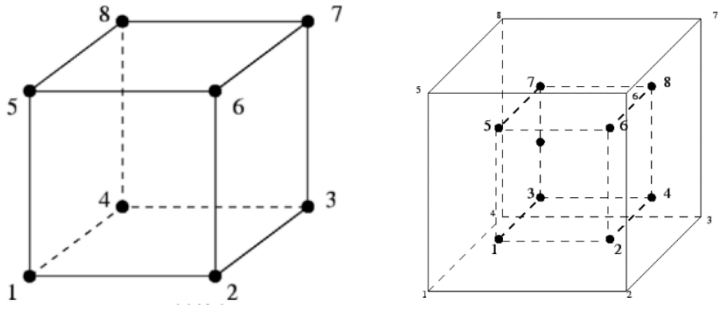

Figure 3.5 - 8-node brick element (CRD8) used in the FE analyses: (a) geometry and node numbering; (b) associated integration point scheme.

Some parameters were assumed as fixed, while others were varied through the calibration process in order to determine the values ensuring the best fitting with the predictions of the EF model.

First of all, it was decided to adopt a simplified behaviour for describing the uniaxial response of the material, as illustrated in Figure 3.6; in particular, for the tensile behaviour, a linear softening was assumed after the reaching of the maximum strength, while in compression the presence of a hardening branch followed by a linear softening was considered. This simplified behaviour can be considered as a schematization of the one represented in Figure 3.1 and Figure 3.2 and was adopted also in other studies available in literature (Degli Abbati et al (2019)).

On the basis of these assumptions it was possible to individuate the parameters to vary in the calibration process, which are marked in red in Figure 3.6: the tensile strength of the material (f_t), which mainly affects the reaching of failure, and the parameters characterizing the slope of the hardening branch in compression and the slope of the softening branches in tension and in compression, which mostly influence the post-peak response.

More specifically, these last are represented by:

- the tensile and the compressive uniaxial strain corresponding to the end of the softening branches ε_{tu} and ε_{cu};
- the uniaxial compressive stress corresponding to the point of initial yield f_{ch};
- the value of the uniaxial compressive strain ε_{cm} corresponding to the reaching of the maximum compressive strength f_c.

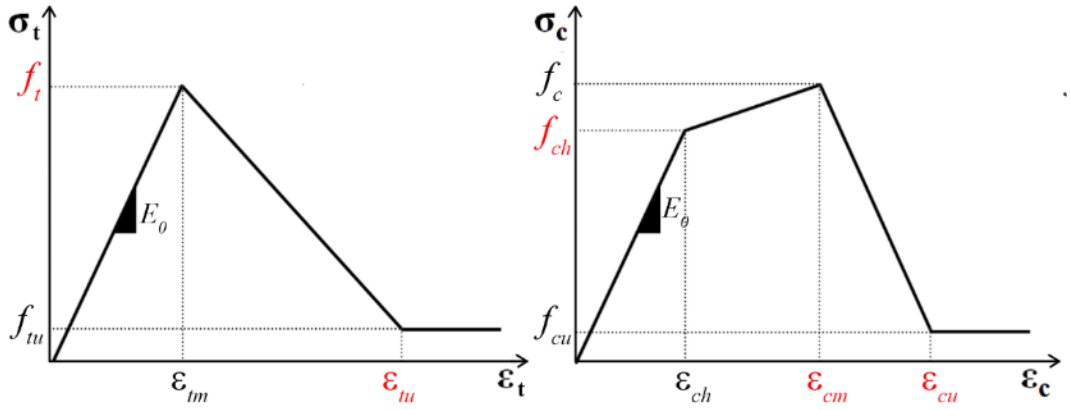

Figure 3.6 - Simplified tensile (a) and compressive (b) uniaxial behaviour assumed for the masonry material in the concrete damaged plasticity model; the parameters subjected to the calibration process are highlighted in red.

As introduced in section 3.1.1, for the definition of the stress-strain curves describing the uniaxial behaviour of the material ABAQUS requires the compressive and tensile stress data as tabular functions of the corresponding inelastic strain. Therefore, in case of the total strain parameters ε_{cm}, ε_{cu} and ε_{tu}, the input data provided in ABAQUS during the calibration process are the corresponding inelastic strain values ε_{cm}^{in}, ε_{cu}^{in}, ε_{tu}^{in}, being these last related to the total strain through the equations 3.3 and 3.4. For this reason, in the following reference will be made to these inelastic strain parameters.

The range of variation considered for each parameter in the calibration process is reported in Table 3.4.

Table 3.4 - Assumed range of variation for the parameters of the uniaxial and tensile behavior of the material subjected to the calibration.

Compressive uniaxial behavior			**Tensile uniaxial behavior**	
f_{ch} **[MPa]**	ε_{cm}^{in} **[-]**	ε_{cu}^{in} **[-]**	f_t **[MPa]**	ε_{tu}^{in} **[-]**
5 – 6.2	0 – 0.003	0.008 – 0.012	0.15 – 0.35	0.0005 – 0.002

By looking at Figure 3.6-a, it is observed that, by varying the parameters f_{ch} and ε_{cm} (or ε_{cm}^{in}), it is possible to obtain different types of compressive behaviour, which in the following are referred to as:

- type A: absence of the hardening branch ($\varepsilon_{cm}^{in} = 0$); the behavior of the material is linear elastic until the reaching of the maximum strength;
- type B: presence of a hardening branch whose slope depends on the adopted values of f_{ch} and ε_{cm}^{in} ($f_{ch} < f_c$, $\varepsilon_{cm}^{in} > 0$);

- type C: presence of a horizontal branch ("plateau"), characterized by increasing plastic strains, which follows the elastic phase and anticipates the softening branch ($f_{ch} = f_c$, $\varepsilon_{cm}^{in} > 0$).

They can be schematized as indicated in Figure 3.7.

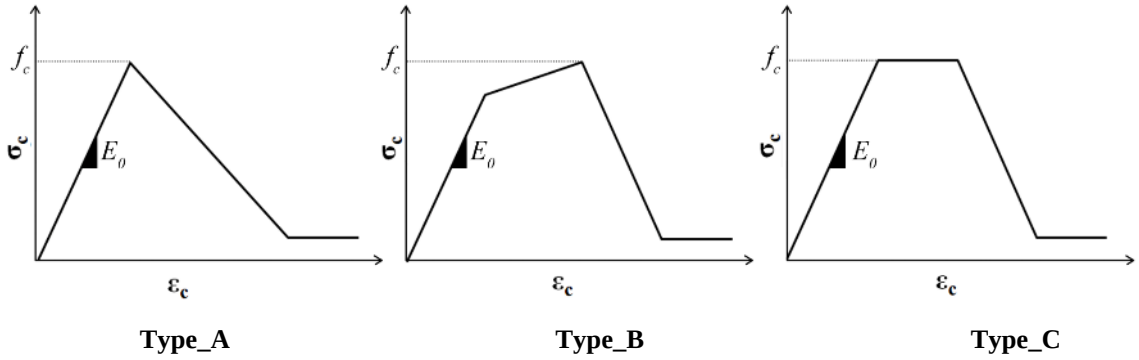

Figure 3.7 – Different types of uniaxial compressive behavior considered in the calibration.

The other parameters describing the concrete damaged plasticity model were assumed as fixed, and are reported in Table 3.5. In particular, the masonry compressive strength f_c was set equal to 6.2 MPa, on the basis of the mechanical properties assumed as reference (Table 3.1) while the values of the residual strength f_{tu} and f_{cu} (corresponding to ε_{tu} and ε_{cu}) were set approximatively equal to 1/10 of the maximum strength in tension and compression respectively, as suggested in the ABAQUS user's guide; indeed, smaller values may lead to convergence problems. In particular, for f_{cu} a value of 0.7 MPa was chosen, while for f_{tu} a value of 0.02 MPa was adopted, on the basis of the values of f_t that were considered in the analyses (see Table 3.4).

Table 3.5. Assumed values for the parameters of the CDP model not subjected to the calibration process.

E [MPa]	ν [-]	f_c [MPa]	f_{cu} [MPa]	f_{tu} [MPa]	ψ [-]	ϵ [-]	f_{b0}/f_{c0} [-]	K_c [-]	η [-]
1800	0.2	6.2	0.7	0.2	20°	0.1	1.2	2/3	0.0001

The evolution of the scalar damage variables d_c and d_t as function of the uniaxial strains was kept substantially proportional to the decay of the uniaxial stresses, as adopted in several numerical campaign of masonry structures (Casolo et al (2016), D'Altri et al (2017), Fortunato et al (2017), Castellazzi et al (2018)). Thereby, the values of the damage variables (both in tension and in compression) were set equal to zero until the reaching of the maximum strength and equal to 0.9 at the strain corresponding to the residual uniaxial stress (ε_{tu} and ε_{cu}), assuming then a linear increment between these values. This implies that damage will occur after the reaching of the maximum strength, both in tension and in compression, and that the elastic stiffness will be progressively reduced with the increment of the plastic strain, assuming a value equal to 10% of the initial one in correspondence of ε_{tu} and ε_{cu}.

The elastic stiffness parameters were defined on the basis of the mechanical properties assumed as reference (Table 3.1): the Young modulus E was set equal to 1800 MPa while the Poisson coefficient ν was assumed equal to 0.2, thus allowing to obtain a shear modulus G equal to 750 MPa, as adopted in the EF model.

Concerning the parameters defining the plastic potential and the failure surface, the assumed values were defined referring to previous studies available in literature. In particular, the dilatancy angle ψ was assumed equal to 20°, as commonly adopted for masonry (Casolo et al (2016), Van der Pluijm (1993)), while the smoothing parameter ϵ was set equal to 0.1 (Milani et al (2017)). Concerning the parameters associated to the failure surface, the ratio between the biaxial f_{b0} and uniaxial f_{c0} initial compressive strengths was set equal to 1.2 and the constant K_c equal to 2/3, as typically adopted for masonry (Milani et al (2017)).

The viscosity parameter η was set equal to 0.0001, after a series of sensitivity analyses aimed to obtain a good compromise between accuracy and good convergence during the analyses. These sensitivity analyses were conducted both on the single panels here introduced and on the regular wall analysed in section 3.3, by checking the effects of the variation of η in terms of response curve (base shear – top displacement curve in case of panels and pushover curve in case of the regular wall) and occurred damage pattern. The obtained results, which are consistent with what emerging also from other studies available in literature on the topic (Degli Abbati et al (2019)), showed that, in general, the adoption of different values of η tend to affect both the global response (with effects on the maximum strength and in the post-peak phase), and the localization of damage. More specifically, lower values of η (which correspond to a less significant effect in terms of viscoplastic regularization) lead to lower values of peak strength and to a more pronounced softening in the response curves as well as to a higher localization of the tensile cracks. The results of the sensitivity analyses carried out on the regular wall are discussed in Appendix A.

The mesh adopted for the analyses is the same for each panel and is shown in Figure 3.8; in particular, the geometry of the brick elements is approximatively equal to 10x10x12.5cm. It was determined through a set of preliminary analyses aimed at assessing the influence of the mesh dimension on the convergence process, as described more in detail in Appendix A.

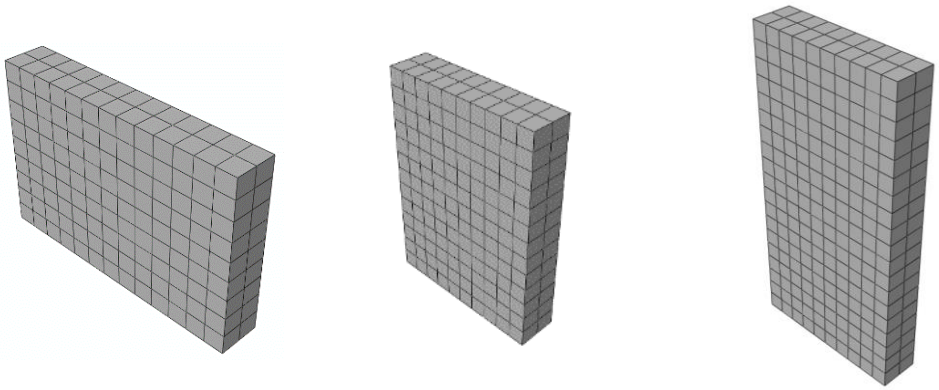

Panel 1 - λ =0.65 **Panel 1 - λ =1.35** **Panel 1 - λ =2.00**

Figure 3.8 - Mesh adopted for the numerical models of the three analysed masonry panels.

For all the panels the fixed-fixed static scheme was adopted; moreover, the panels were subjected to vertical compressive normal stress coupled with shear stress. In order to simulate the fixed-fixed boundary condition, the nodes located at the base section of the panels were fixed, while at the top of each panel an elastic rigid element was modelled by means of 4-node shell elements. Appropriate properties in terms of material elastic stiffness and geometry of the cross section were assigned to this element, such as it was possible to consider it as infinitely rigid. Moreover, the rotations around the Z axis (see Figure 3.9) of the nodes on the top section were fixed.

The definition of the loading conditions was made by steps, separating the application of gravitational and horizontal loads: an initial loading step was defined to apply gravitational loads, while a second loading step was used to perform a displacement control static analysis by applying an incremental horizontal displacement *u* to the node located at the centre of the top section (as highlighted in Figure 3.9).

Several simulations were carried out by considering different values of the vertical normal stress in order to simulate a significant part of the strength domain of each panel and in particular to cover the range of variation of the axial load of our interest. The latter was determined by referring to the maximum variation of normal stress characterizing the panels of the masonry walls analysed with nonlinear static analyses in section 3.3 and in Chapter 4. The compression rates σ/f_c characterizing these panels are in general quite low, and their initial values under the gravity loads may vary during the analysis until, approximatively, a minimum value close to zero (for the panels where the axial load decreases) or a maximum value of 0.2 (for the panels where the axial load increases).

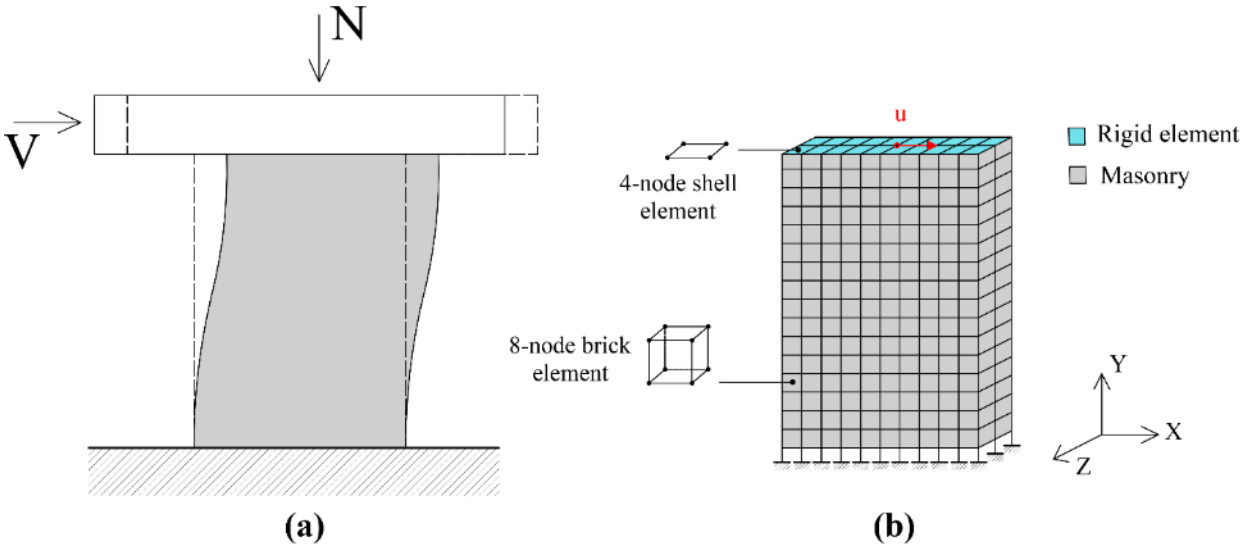

Figure 3.9 - a) Schematization of the static scheme and of the loading conditions characterizing the analysed panels; b) strategy adopted for the modelling of the static scheme and the loading conditions.

The axial load was applied by properly varying the density of the material characterizing the rigid element at the top of each panel; moreover, the density of the masonry material was set close to zero, in order to have the same normal stress acting on each cross section of the panels.

The nonlinear incremental static analyses in control displacement on the panels were performed by means of ABAQUS implicit solver, applying at each increment the full Newton's method for the

equilibrium iterations; furthermore, the definition of the step sizes was made by means of the automatic step control algorithm implemented in the software.

The base shear-top displacement curves associated to each analysis were evaluated by computing, for each step of the analysis, the sum of the horizontal reactions of the nodes at the base section (V_b) and the corresponding horizontal displacement of a node on the top section (d_{top}). Moreover, the maximum strength associated to each analysis (V_{max}) was recorded.

3.2.2 Results of the calibration

In order to properly calibrate the considered parameters of the CDP model, it was necessary to preliminarily investigate their influence on the response of the panels subjected to lateral loads in terms of maximum strength, damage pattern and post-peak behaviour, considering also different values of the applied axial load. The attention is mainly focused on values of axial load falling into the range of variation of our interest (i.e. $\sigma/f_c = 0 \div 0.2$) or slightly higher.

After that, the final outcome of the calibration between the two constitutive laws is presented (section 3.2.2.2). The parameters calibrated in such way are those adopted for the analyses performed at scale of whole URM walls.

3.2.2.1 Sensitivity to the parameters varied in the calibration

First of all, it was observed that the parameters which mainly affect the maximum strength (V_{max}) exhibited by the panels for fixed values of the applied vertical stress are: i) the tensile strength of the material f_t and ii) the assumed type of compressive behaviour (presence or absence of the hardening branch).

Referring to point i), it is useful to show the results of some FE simulations where three increasing values of tensile strength are examined (f_{t1} = 0.15 MPa, f_{t2} = 0.22 MPa and f_{t3} = 0.35 MPa), while the other parameters of the constitutive law are assumed as fixed. In particular, regarding the tensile behaviour ε_{tu}^{in} was set equal to 0.001, while for compression an A-type behaviour (absence of hardening branch, see Figure 3.7-a) was assumed, with ε_{cu}^{in} = 0.009, thus obtaining the stress-strain diagrams illustrated in Figure 3.10.

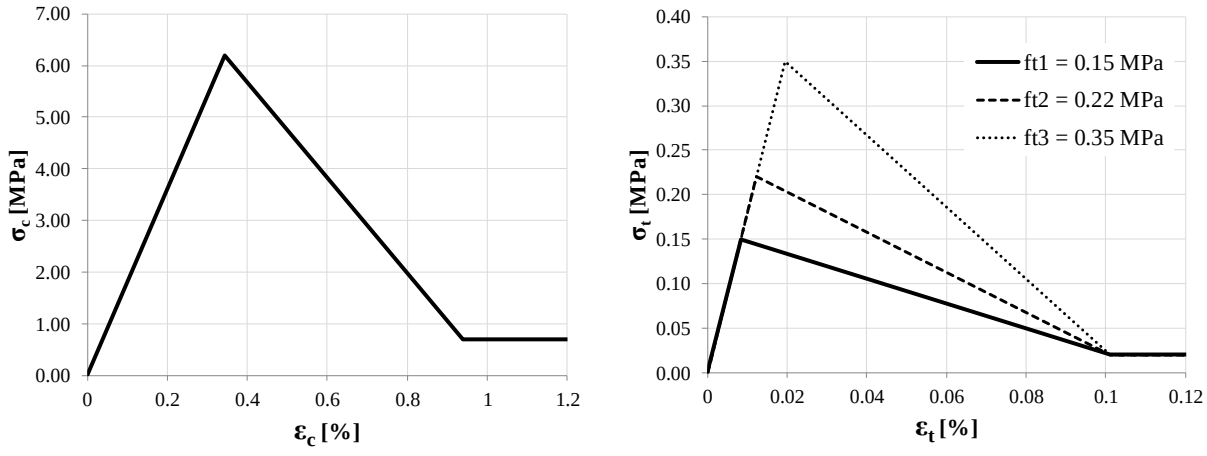

(a) (b)

Figure 3.10 - Uniaxial compressive behaviour (a) and different hypotheses for the tensile uniaxial behaviour (b) of masonry assumed in the sensitivity analyses on the effects of the tensile strength f_t .

In Figure 3.11 the maximum strength V_{max} obtained with the numerical analyses for increasing applied axial loads and by assuming the different above mentioned values of the tensile strength f_t are illustrated, referring, by way of example, to panel 2 (λ = 1.35); they are compared with the strength domain of the panel defined through the failure criteria adopted in the EF model.

As expected, for increasing values of f_t the maximum strength exhibited by the panels increases, for all the considered values of normal stress. More specifically, when considering the lowest tensile strength (f_{t1}) the results associated to small values of axial stress are in good agreement with the predictions of the criterion for flexural failure adopted in the EF model; however, for increasing values of applied axial load the maximum strength exhibited by the panel is too low if compared with the predictions of the criterion associated to shear failure. On the contrary, when adopting the highest value of tensile strength (ft_3), the predictions of the FE model get worst in the initial part of the strength domain (too high values of V_{max} with respect to the EF model), while improve for higher values of axial load.

This can be explained by considering that in the CDP model the shear behaviour is governed by the tensile strength of the material (assumed as isotropic); the value attributed to this last one, however, inevitably influences also the flexural behaviour. It is evident that here it is not possible, differently from the case of the EF model, to decouple the two behaviour types and make that parameter governing only one of them. For this reason, and as testified by the presented results, when adopting too high values of the tensile strength of the material, in order to reach a best fitting in the part associated to shear failure behaviour, the predictions obtained in the initial part of the domain may result higher with respect to the the strength domain assumed in the EF model, where the hypothesis of no tensile strength of the material is made in the criterion ruling the flexural response.

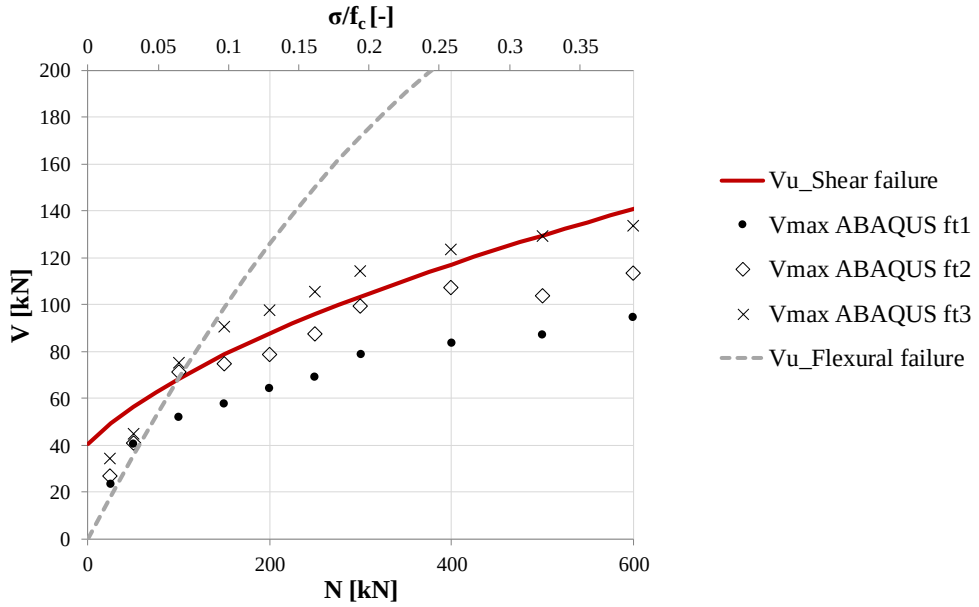

Figure 3.11- Panel 2: sensitivity of the maximum strength exhibited by the panels (V_{max}) in the lateral load analyses to the variation of the adopted tensile strength of the material f_t.

Referring to point ii), further analyses were performed in which the parameters associated to the tensile uniaxial behaviour were fixed, while those ruling the compressive one were varied in order to reproduce

the three behaviour types previously introduced (type A, B and C), for a fixed value of ε_{cu}^{in} = 0.009. The assumed tensile behaviour was defined by considering f_t=0.22 MPa and ε_{tu}^{in} = 0.001, thus resulting the same used in the previous analyses with $f_t = f_{t2}$, as shown in Figure 3.10-b; the parameters adopted for describing the different types of compressive behaviour are reported in Table 3.6, together with the resulting associated stress-total strain (σ_c - ε_c) diaphragms. The three considered combinations of parameters are referred to as *Option A* (compressive behaviour of type A), *Option B* (compressive behaviour of type B) and *Option C* (compressive behaviour of type C).

In Figure 3.12 the results in terms of V_{max} obtained from the lateral load analyses performed with the three different options are illustrated, referring again to panel 2.

It is possible to observe that in presence of low applied axial loads the obtained values for V_{max} are not affected by theadopted type of compressive behavior. In these cases, indeed, the parameter which mainly influence the reaching of the maximum strength is f_t (that is fixed in these analyses) and the compressive behaviour of the material does not come into play. However, for higher values of applied axial load the adoption of a compressive behaviour of type B or C produces a slight increase of the resulting maximum strength. This leads to a better fitting of the strength domain for higher compressive levels with respect to the results obtained in case of adoption of a compressive behaviour of type A (without the hardening branch). Furthermore, it is observed that the compressive behaviour of type B or type C leads to almost similar results.

Table 3.6- Values of the parameters adopted for the definition of the three types of compressive behavior used in the sensitivity analyses and associated stress-strain diagrams.

Option A				**Option B**				**Option C**			
f_{ch} **[Mpa]**	-	ε_{ch}^{in} **[-]**	-	f_{ch} **[Mpa]**	5.2	ε_{ch}^{in}**[-]**	0	f_{ch}**[Mpa]**	6.2	ε_{ch}^{in}**[-]**	0
f_c **[Mpa]**	6.2	ε_{cm}^{in} **[-]**	0	f_c **[Mpa]**	6.2	ε_{cm}^{in}**[-]**	0.003	f_c**[Mpa]**	6.2	ε_{cm}^{in}**[-]**	0.003
f_{cu} **[Mpa]**	0.7	ε_{cu}^{in} **[-]**	0.009	f_{cu} **[Mpa]**	0.7	ε_{cu}^{in}**[-]**	0.009	f_{cu}**[Mpa]**	0.7	ε_{cu}^{in}**[-]**	0.009

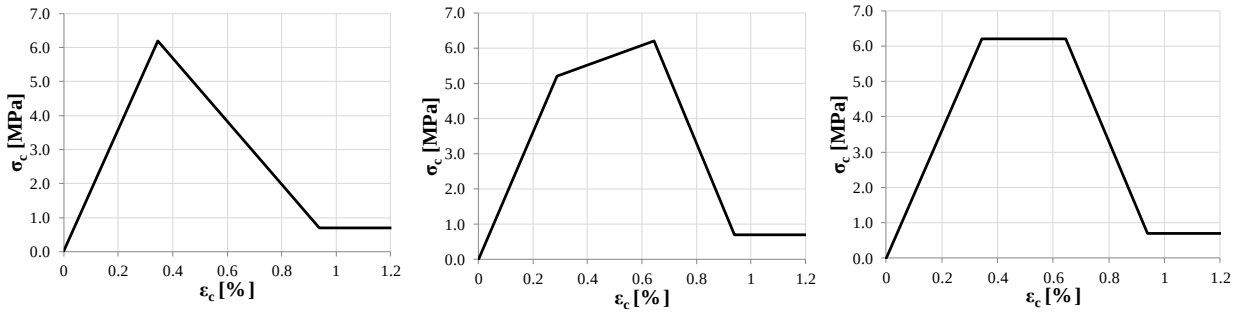

The observed phenomenon is probably due to the fact that the use of a compressive behavior of type B or C includes, with respect to a behavior of type A, the possibility for the material to undergo plastic deformations before the starting of the post-peak phase. This produces, when the applied axial load is higher and so the compressive properties of the material have a more significant role in the response, a less pronounced damage localization, thus resulting in an increased maximum strength.

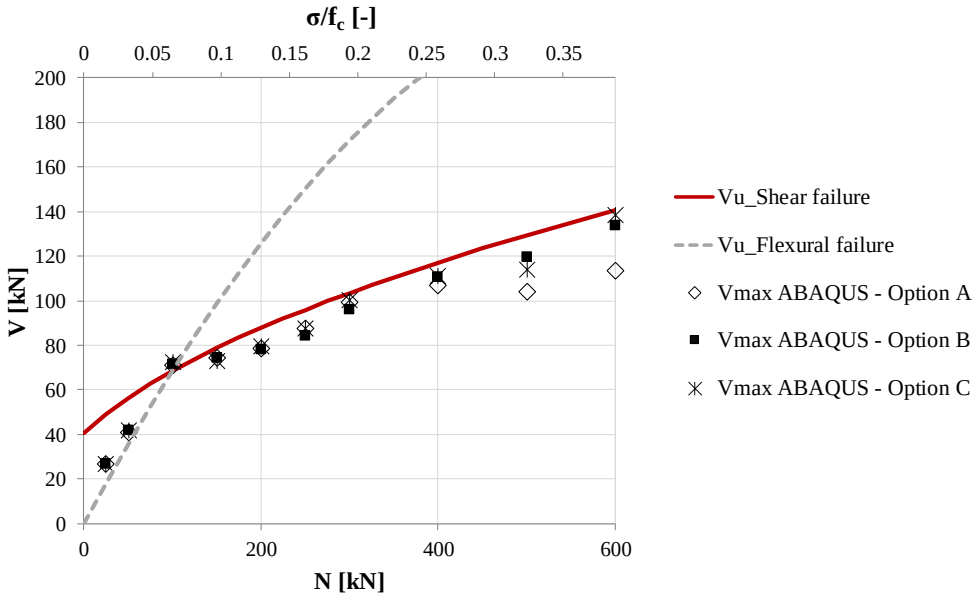

Figure 3.12 - Sensitivity of the resulting values of maximum strength depending on the adopted compressive behaviour of the material in case of panel 2.

In the following the attention is focused on the V_b-d_{top} curves obtained by adopting only *Option A* and *B*, being the results associated to the compressive behaviour of type C (*Option C)* quite similar to the ones obtained through the compressive behaviour of type B.

The comparison between the V_b-d_{top} curves referring to panel 1 (λ=0.65) and panel 3 (λ=2) are reported in Figure 3.13 and in Figure 3.14, respectively, considering in both cases different values of the applied axial load. In general, it may be observed that the adoption of different compressive behaviours for the material actually leads to some differences in the obtained post-peak response. More specifically, the introduction of the hardening branch (*Option B*) tends to produce a more gradual strength degradation in the responses of the panels: the progressive drops of strength, indeed, occur for higher values of top displacement with respect to the curves obtained through the adoption of *Option A*.

Focusing the attention on the squatter panel (panel 1), this phenomenon is present for all the considered values of axial load, even if it is more evident when the compression level increases (Figure 3.13-b and c). In particular, in case of flexural response (Figure 3.13-a and b) the slight differences observed in the curves obtained with *Option A* and *Option B* are ascribable to a different concentration of damage at the compressed toe, which tend to be higher in case of *Option A*.

The other two compression levels correspond to shear failures (Figure 3.13-c and d); here the effect of the introduction of the hardening branch is more significant and affects not only the post-peak response, but also the achieved maximum strength, thus confirming what highlighted by the previously illustrated results in case of panel 2.

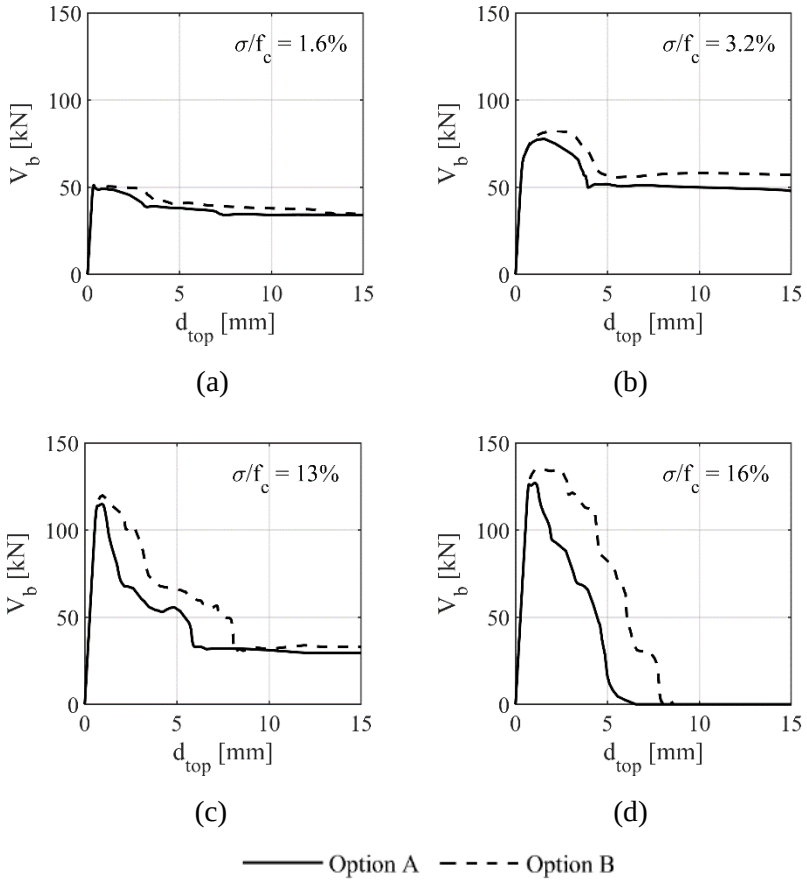

Figure 3.13 - Comparison between the base shear – top displacement (V_b-d_{top}) curves obtained for panel 1 with the adoption of different hypotheses of compressive uniaxial behaviour and for increasing values of applied axial load N (a) N= 27.3 kN (σ/f_c = 1.6%); (b) N= 54.6 kN (σ/f_c = 3.2%) (c) N= 218 kN (σ/f_c = 13%); (d) N=273 kN (σ/f_c = 16%).

Moving to the slender panel, it can be noted that in presence of low axial stress (Figure 3.14-a), which corresponds to a flexural response of the panel, the behaviour is substantially not affected by the compressive behaviour of the material. In this case, indeed, since the element has a high aspect-ratio and is subjected to a low normal stress, crushing does not occur, at least for the considered values of top displacement, so that the response is mainly governed by the tensile behaviour of the material. On the contrary, when the compression level increases, some differences can be observed in the response. In particular, the curves shown in Figure 3.14-b and c, are still associated to a flexural behaviour type, and the observed strength degradation is related to a concentration of damage at the compressed toe. Therefore, similarly to what observed in case of panel 1, when the presence of hardening in compression is assumed, the strength degradation appears to be more gradual.

In presence of a higher axial load (Figure 3.14-d the response is dominated by shear and the curves obtained through *Option A* and *Option B* lead to almost similar results until the reaching of the peak-strength and immediately after peak; however, the panel shows a higher displacement capacity when *Option B* is adopted.

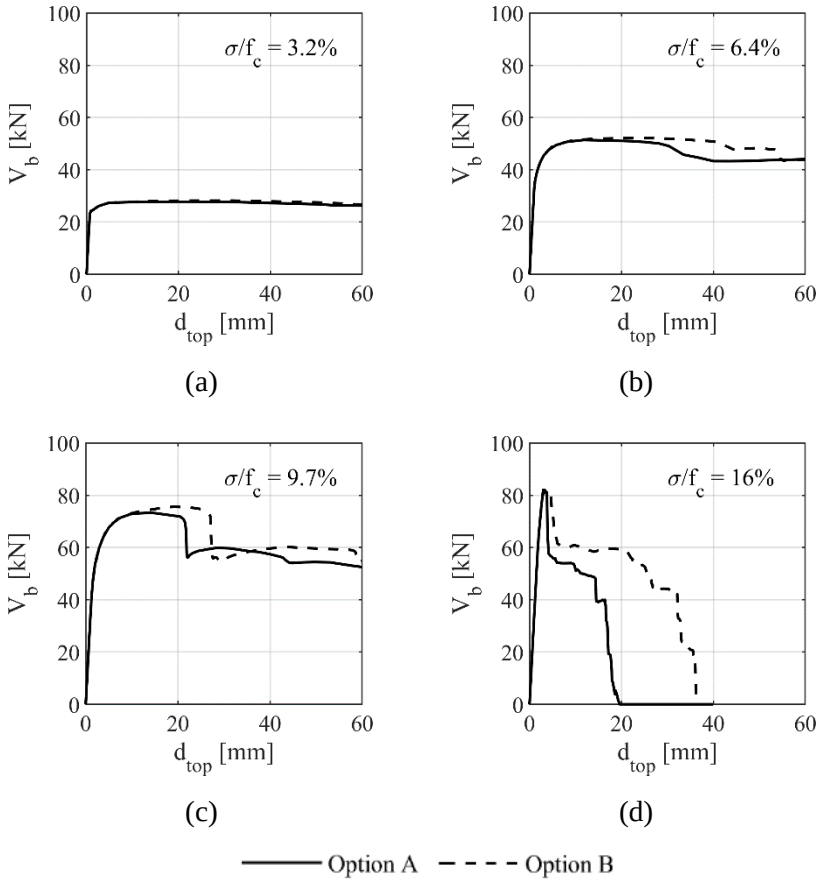

Figure 3.14- Comparison between the base shear – top displacement (V_b-d_{top}) curves obtained for panel 3 with the adoption of different hypotheses of compressive uniaxial behaviour and for increasing values of applied axial load N (a) N= 50 kN (σ/f_c = 3.2%); (b) N= 100 kN (σ/f_c = 6.4%); (c) N= 150 kN (σ/f_c = 9.7%); (d) N=250 kN (σ/f_c = 16%).

The other parameters, among those subjected to the calibration, which affect the post-peak response of the panels are ε_{cu} and ε_{tu}, which represent the strain values corresponding to the residual compressive and tensile strength, respectively; indeed, they govern the slope of the softening branches, which have been assumed as linear both in tension and in compression. Referring to the compressive behaviour, in the following the influence on the response of the panels of the parameter ε_{cu} is illustrated; in particular, some results obtained through the adoption, by fixing the other parameters, of two different values of ε_{cu}^{in} (which are directly related to ε_{cu} through the equations 3.3 and 3.4) are presented. In these analyses the tensile behavior was assumed equal to the one investigated in the previous analyses (f_t=0.22 MPa, ε_{tu}^{in} =0.001), while the compressive behaviour of type B was assumed as reference, varying the value of ε_{cu}^{in}, which was assumed in the first case (referred to as *Option B1*) equal to 0.008 and in the second one (referred to as *Option B2*) equal to 0.012. The values assumed for the parameters ruling the compressive behavior in *Option B1* and *Option B2* are summarized in Table 3.7, as well as the associated stress-strain diagrams.

The curves obtained through the adoption of *Option B1* and *Option B2* for three different values of axial load and referring, by way of example, to panel 1 are reported in Figure 3.15. In particular, the first two compression levels (Figure 3.15-a and b) correspond to a flexural response, while the third one (Figure 3.15-c) refers to a shear failure.

Table 3.7- Parameters adopted for the definition of the two types of compressive behavior (*Option B1* and *Option B2*) used in the sensitivity analyses on the effects of the parameter ε_{cu} and associated stress-strain diagrams.

Option B1			
f_{ch} **[MPa]**	5.2	ε_{ch}^{in} **[-]**	0
f_c **[MPa]**	6.2	ε_{cm}^{in} **[-]**	0.003
f_{cu} **[MPa]**	0.7	ε_{cu}^{in} **[-]**	0.008
Option B2			
f_{ch} **[MPa]**	5.2	ε_{ch}^{in} **[-]**	0
f_c **[MPa]**	6.2	ε_{cm}^{in} **[-]**	0.003
f_{cu} **[MPa]**	0.7	ε_{cu}^{in} **[-]**	0.012

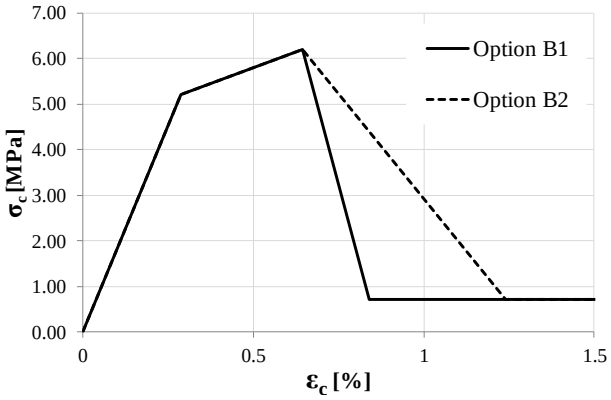

As expected, the results show that a higher value of ε_{cu} corresponds, for all the compression levels, to a more gradual strength degradation in the post-peak response. This is justified by the different slopes of the softening compressive branches associated to *Option B1* and *Option B2*, which assume, once that failure is reached in a point of the material, a more (*Option B1*) or less (*Option B2*) pronounced strength degradation.

The variation of the parameter ε_{tu}, which rules the decay of the tensile strength as a function of the corresponding strain, leads, for all the considered panels, to similar effects.

Finally, concerning the damage pattern, it was observed that, for fixed applied normal stress, the failure mode occurring in the panels is not significantly affected by the variation of the examined parameters, at least in the range of variation that was considered for them. For this reason, the discussion of the failure modes occurring in the panels for different compression levels is presented in the following, referring to the adoption of the mechanical parameters resulting from the calibration.

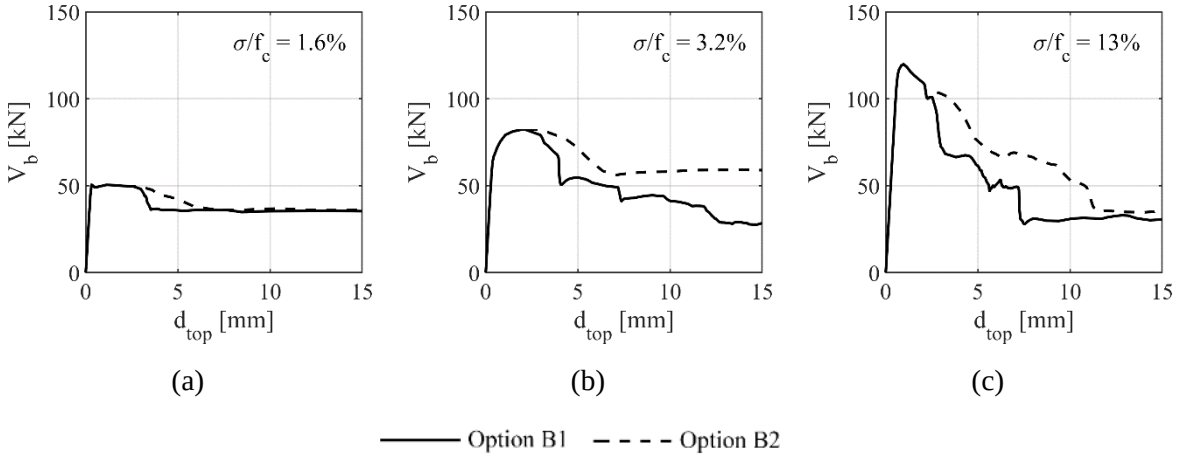

Figure 3.15- Comparison between the base shear – top displacement (V_b-d_{top}) curves obtained for panel 1with the adoption of different hypotheses of compressive uniaxial behaviour (*Option B1* and *Option B2*, see Table 3.7) and for increasing values of applied axial load *N* (a) *N*= 27.3 kN (σ/f_c = 1.6%); (b) *N*= 54.6 kN (σ/f_c = 3.2%) (c) *N*= 218 kN (σ/f_c = 13%).

On the basis of the illustrated results, it is observed that through a proper variation of the parameters which govern the tensile and the compressive behaviour of the material it is possible to modify both the maximum strength obtained for different compression levels and the post-peak response of the panels, in order to capture the behaviour described through the multilinear constitutive law adopted in the EF model.

3.2.2.2 Outcome of the calibration

In Table 3.8 the final values of the parameters adopted for describing the uniaxial and tensile behaviour of the material in the CDP model are reported, indicating in bold those resulting from the calibration; moreover, in Figure 3.16 the associated stress-strain diagrams are illustrated, together with the evolution of the corresponding damage variables. The determined parameters ensure, on average, the best fitting for all the examined panels between the two numerical models, considering both the predictions in terms of strength and displacement capacity, as shown in the following.

Table 3.8 – Values assumed for the parameters describing the uniaxial and tensile behavior of the material in the CDP model. In bold (light blue cells) the parameters determined through the calibration.

Compressive uniaxial behavior					**Tensile uniaxial behavior**				
ε_c^{in} [-]		σ_c [MPa]		d_c [-]	ε_t^{in} [-]		σ_t [MPa]		d_t [-]
ε_{ch}^{in}	0	f_{ch}	**5.5**	0	ε_{tm}^{in}	0	f_t	**0.22**	0
ε_{cm}^{in}	**0.002**	f_c	6.2	0	ε_{tu}^{in}	**0.001**	f_{tu}	0.02	0.9
ε_{cu}^{in}	**0.009**	f_{cu}	0.7	0.9					

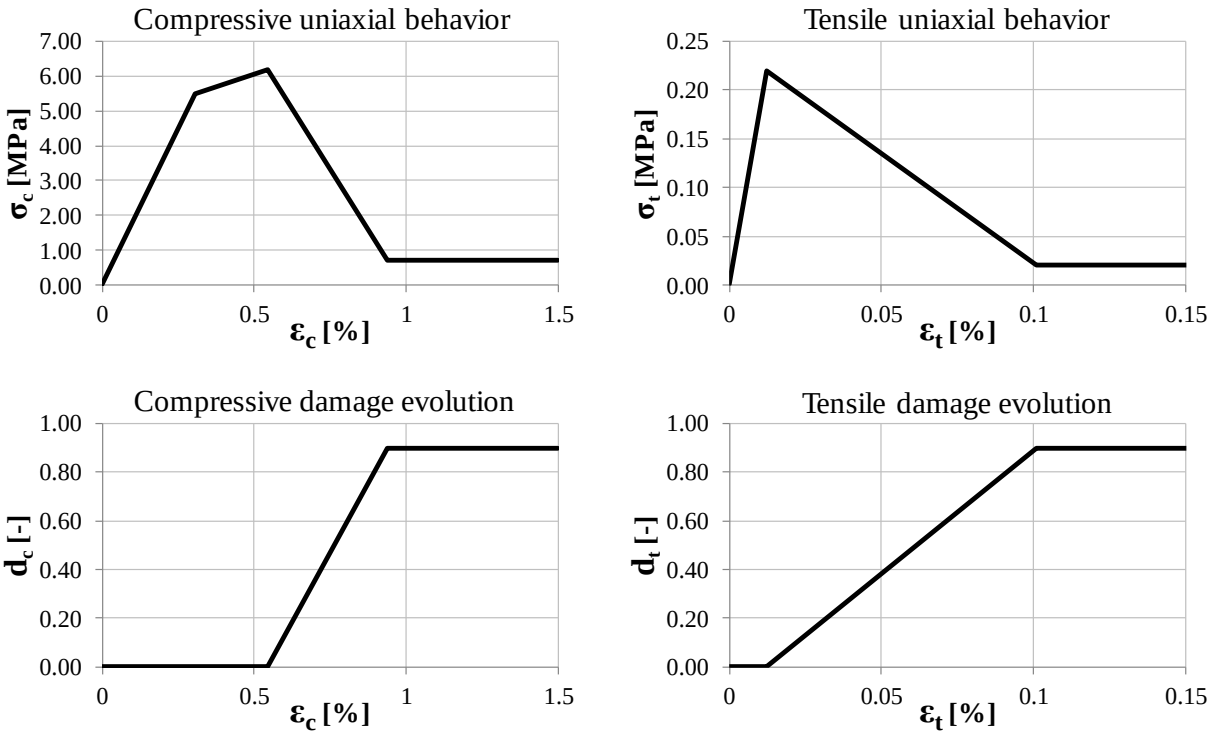

Figure 3.16 - Uniaxial behavior for the compressive and tensile regimes determined through the calibration and associated damage evolution.

The calibration process performed on the three panels, in particular, lead to a value of the tensile strength of masonry equal to 0.22 MPa, respecting the simple relationship $f_t = 1.5\tau_0$ between the masonry tensile strength f_t and the masonry shear strength τ_0, as suggested in MIT (2009), §C8.7.1.5. The same relationship was found also in other studies where a calibration of a FE continuum model at the scale of masonry panels was required (Cattari et al (2016), Degli Abbati et al (2019)).

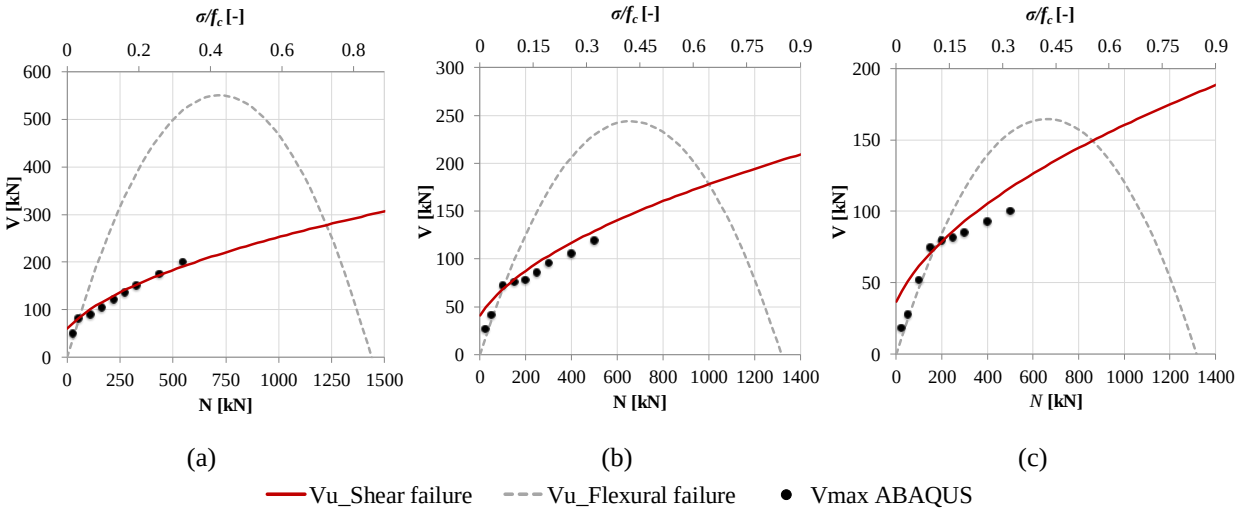

Figure 3.17- Comparison between the results of the numerical simulations performed with ABAQUS and the predictions of the strength criteria adopted in the EF model for the three examined panels: (a) panel 1 - λ =0.65; (b) panel 2 - λ =1.35; (c) panel 3 – λ=2.

In Figure 3.17 the failure domains of the three panels obtained through the strength criteria adopted in the EF model and the results, in terms of maximum strength V_{max}, of the numerical analyses performed in ABAQUS for different compression levels are reported. It is underlined that the maximum value of the ratio σ/f_c (reported in the secondary x-axis) is not equal to 1 due to the adoption, in the flexural strength criterion, of a stress block normal stress distribution with a coefficient equal to 0.85.

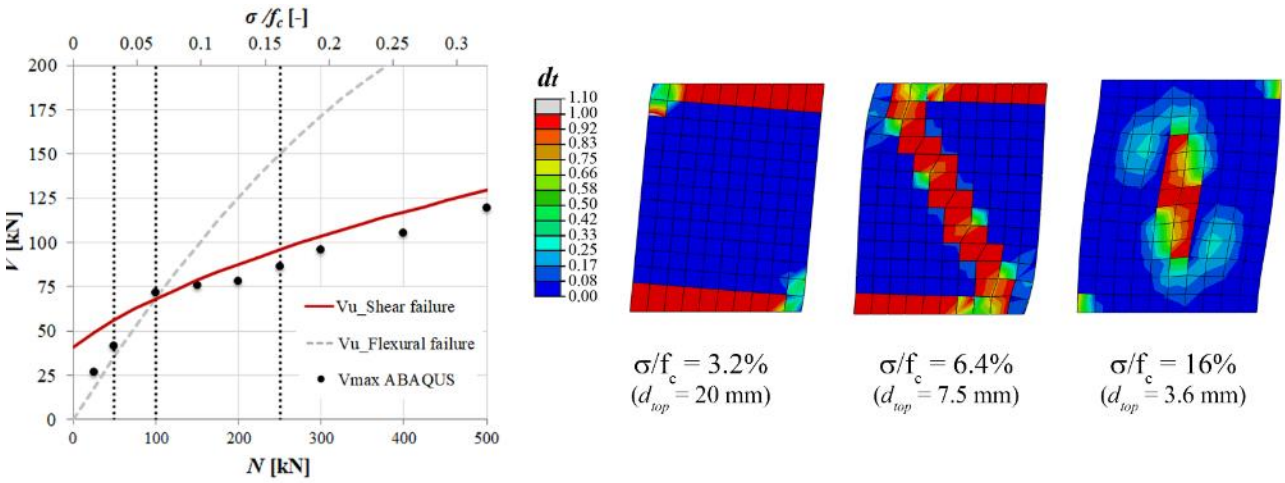

Figure 3.18 - Panel 2: failure modes associated to different values of applied axial load.

It can be seen that the value of f_t here assumed allows to obtain a good reproduction of the failure domain of the three panels when considering the whole range of variation on the normal stress of our interest, that is explicitly indicated in grey in Figure 3.17.

In Figure 3.18 the tensile damage contour plots at failure referring, as for example, to panel 2 are reported, considering different values of the applied axial load.

It is observed that the continuum FE model is actually able to catch the different failure modes predicted by the strength criteria adopted in the EF model. Indeed, when the value of the applied normal stress is low (σ/f_c= 3.2%) the response of the panel is mainly flexural and characterized by rocking, with an evident parzialization of the end sections and a consequent concentration of the stresses at the compressed toe. When considering a higher value of the applied axial load (σ/f_c= 16%) the response of the panel is dominated by shear: the parzialization of the end sections is negligible with respect to the previous case and the failure of the panel is caused by the propagation of a typical shear crack starting from the centre of the panel.

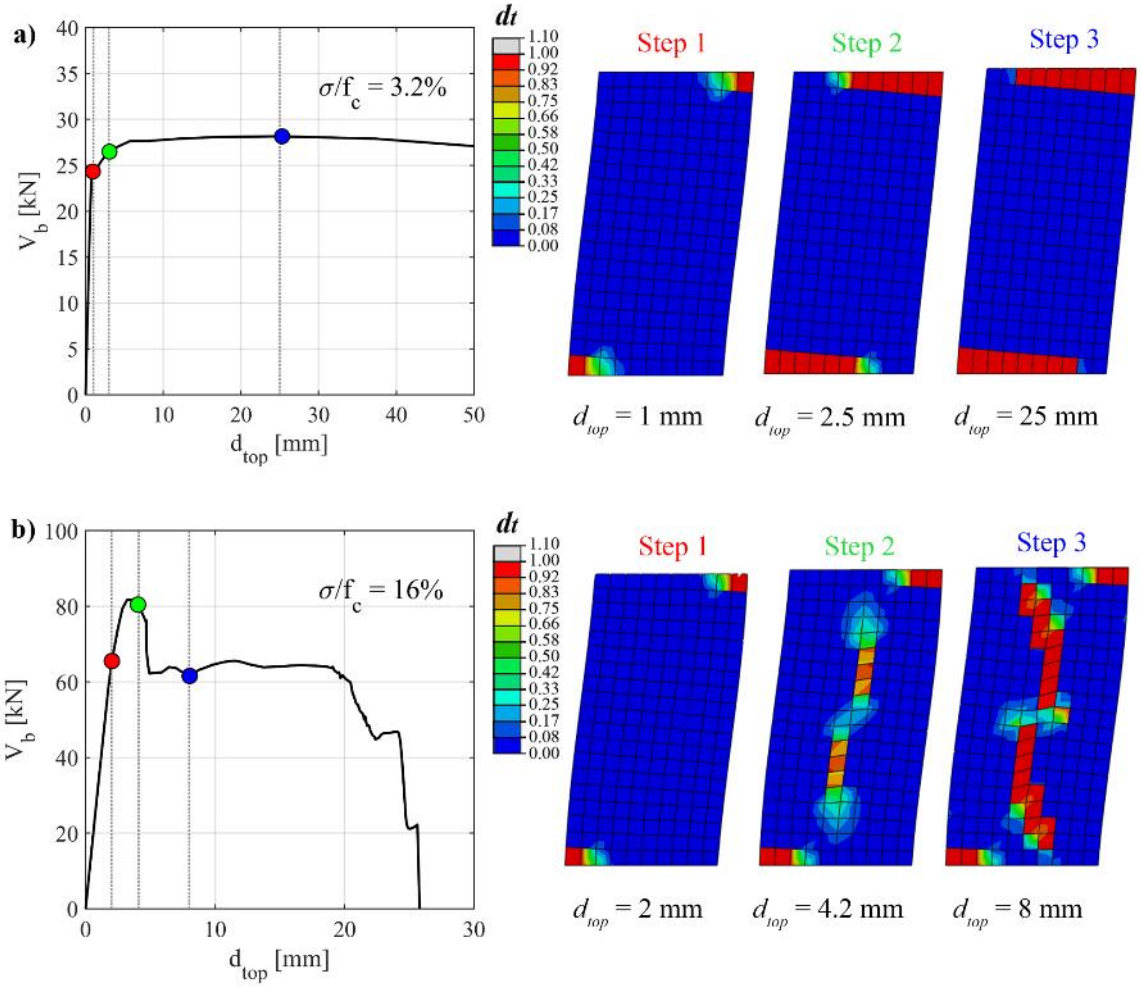

Figure 3.19 - Panel 3: tensile damage evolution for different applied axial loads (a) σ/f_c = 3.2%; b) σ/f_c = 16%).

When in presence of an intermediate value of compression (σ/f_c= 6.4%) the behaviour observed in the FE simulation can be described as a mixed (or hybrid) type, since both the parzialization of the end sections and the development of a diagonal crack are observed at failure. In fact, by looking at the strength domain

of the panel, it can be seen that the applied axial load refers to a transition zone between the prevalence of the flexural failure and the prevalence of the shear one. It is interesting to observe that in this case the shear crack assumes an inclination which is close to 45%, differently from the shear crack observed for the higher compression level, that is almost vertical. This is related to the parzialization of the base section, which causes the progressive inclination of the principal compression stresses and so the formation of the associated inclined strut; on the contrary, when the applied compression is higher the parzialization phenomenon is less significant, so that almost vertical cracks are expected.

In Figure 3.19 the evolution of the tensile damage contour plots associated to 2 different values of compression rate in case of panel 3 are reported. It is possible to observe that while in case of flexural response there is a gradual strength degradation after the reaching of the maximum strength, due to the progressive parzialization of the end sections, on the contrary the shear failure is associated to a sudden drop of strength caused by the formation of the tensile crack.

Moving to the results of the calibration in terms of displacement capacity, in Figure 3.20 the comparison between the V_b-d_{top} curves obtained with the two numerical models for the introduced panels is illustrated, considering increasing compression rates, in order to show different behaviour types that can occur on the panels. In particular, for each panel the considered compression rates vary from 1.6% to 16%. From the comparison of the curves it is possible to observe that the parameters adopted in the CDP model allow to obtain, for all the considered panels and for different values of the applied axial load, a quite good correspondence with the curves resulting from the EF models. Indeed, apart few exceptions, the FE simulations are able to quite well reproduce the softening phase described through the multilinear constitutive law used in the EF model, that actually represents the target of the calibration (Table 3.2).

More specifically, by looking at the curves shown in Figure 3.20 it can be noted that the FE model is able to reproduce the different behaviour types which may occur on the same panel by varying the applied axial load, thus guaranteeing a good agreement with the EF model in the prediction of the displacement capacity in presence of both flexural and shear response.

Indeed, by considering a fixed panel and increasing compression rates (i.e. sliding along each column from a) to d) in Figure 3.20), in addition to the progressive increasing in strength, the behaviour predicted by both the models changes from a ductile behavior type, typical of flexural response, with a high displacement capacity and a slight strength degradation (especially in case of the panels with the highest aspect ratios, i.e. panel 2 and 3), to a more fragile one, typical of shear failure and characterized by a progressive strength degradation that is more significant the higher the applied axial load is. This type of behaviour can be observed, separately for the two numerical models, also through the direct comparison of the curves obtained for each panel by applying increasing values of axial load, as shown in Figure 3.21 in case of panel 3.

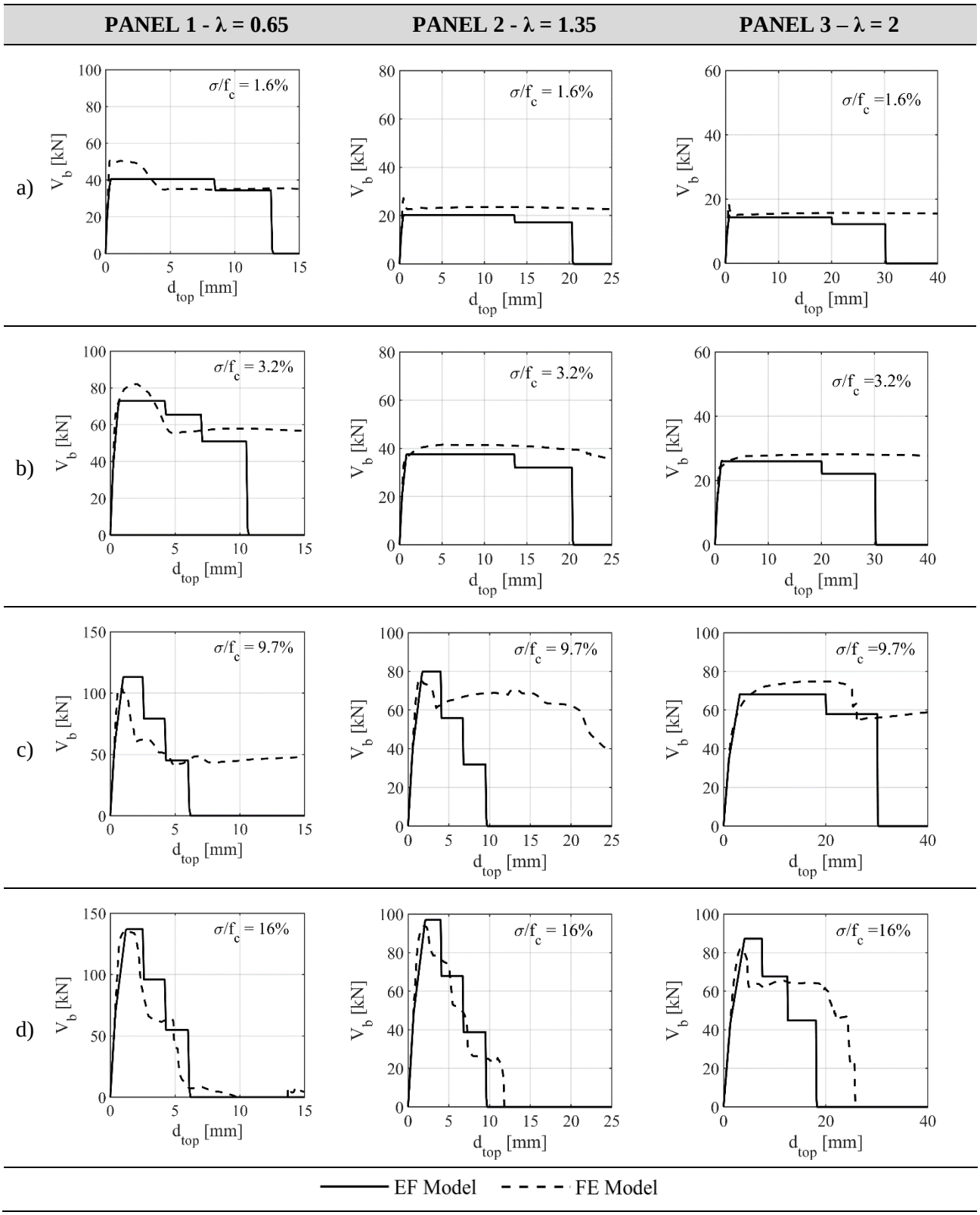

Figure 3.20 - Comparison between the V_b-d_{top} curves obtained for the 3 panels with the FE model and with the EF model considering increasing rates of compression.

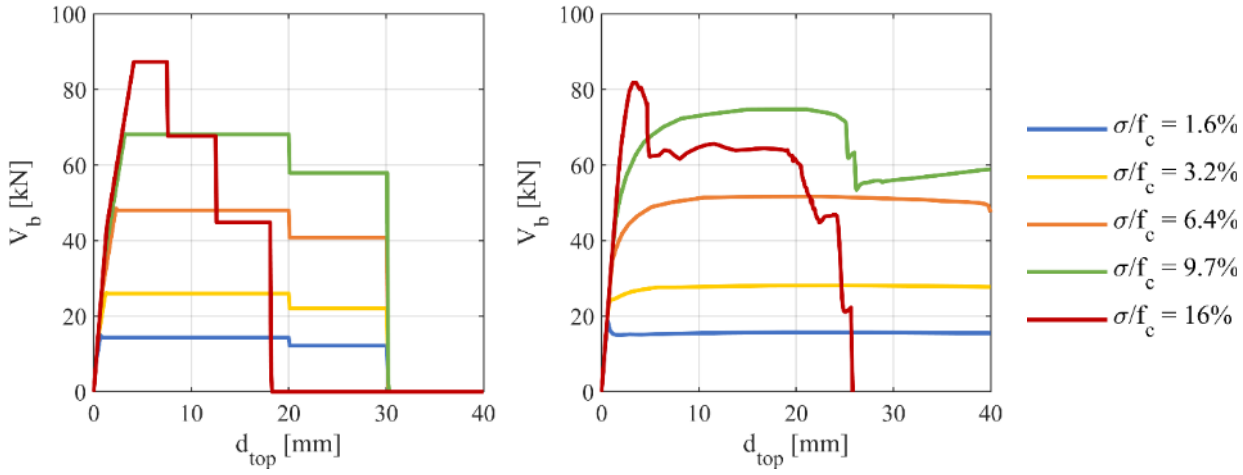

(a) (b)

Figure 3.21 - Panel 3: base shear-top displacement curves obtained for different values of the applied axial load with the EF model (a) and with the FE model (b).

Despite of the general good agreement between the two numerical models in the description of the softening phase of the different panels, some discrepancies on the prediction of the residual strength in the post-peak phase can be noted in presence of flexural response, i.e. when considering low values of applied normal stress, and especially when dealing with the panels characterized by high aspect ratios (panel 2 and 3). Indeed, in these cases the FE model, after the reaching of a value of maximum strength almost consistent with the one predicted by the EF model, initially follows the curve described by the multilinear constitutive law (in correspondence of the plateau of this last one); however, for higher values of top displacement it tends to deviate, showing a strength degradation which is very slight or even approaching zero (as in the case of both panel 2 and 3, σ/f_c = 1.6%), being thus not able to capture the total loss of strength predicted by the EF model (which happens for a drift value equal to 0.15%).

It is underlined that, even varying the parameters of the constitutive law governing the softening behaviour of the material through the calibration process, in these cases it was not possible to obtain a perfect match with the EF model in terms of strength degradation, since a significant strength decay was never observed.

Regarding this aspect, experimental researches on the cyclic behaviour of masonry walls under horizontal loads have shown that the flexural response can be characterized by very large horizontal displacements of the wall top, without a significant reduction of the strength, especially when compressive stresses are low with respect to the masonry compressive strength (ESECMaSE (2005–2007); Fehling et al (2007); Zilch et al (2008)). Moreover, when considering the flexural response of panels with a high aspect ratio it is even possible that crushing does not take place, and the pier exhibits an overturning failure mode, characterized by a progressive reduction of strength due to geometrical effects (Penna and Galasco (2013)). In this failure mode, the wall top section can attain very large horizontal displacements, even greater than one tenth of the wall height (Orlando et al (2016)). In the light of these observations, the response provided by the FE model in the aforementioned cases seems to be in accordance with these experimental evidences, showing that this continuum model is actually able to reproduce the behaviour of masonry panels resulting from experimental tests.

On the contrary, in the case of the EF models it is necessary to define drift thresholds associated to the collapse of the element, in correspondence of which the residual strength is equal to zero; this necessity derives also from the implications in terms of safety verifications.

3.3 ANALYSIS OF A REGULAR URM WALL

Concerning the definition of the case-study structures to analyze, it was decided to start with the study of a regular masonry wall, characterized by the presence of openings of the same size at each storey and perfectly aligned in both the vertical and horizontal direction, moving then to the assessment of walls with different types of irregularities in the opening pattern (described in Chapter 4).

The choice to start with a regular wall is motivated first of all by the necessity to validate the defined methodological approach on a wall configuration where a lower scatter of the obtained results is expected and where their interpretation should be easier. Indeed, the application of the EF model in case of a wall with regularly distributed openings is in general quite well consolidated, since both numerical tests and validation studies based on the comparison with experimental tests showed that it can be successfully applied for the structural analysis in these cases, providing reliable results (as for example in Cattari (2007), Calderini et al (2009b), Marques and Lourenço (2011), Marques and Lourenço (2014), Penna et al (2015)).

However, despite the simplicity of this first case study, the application of the different criteria for the EF idealization may lead to a different geometry for the structural elements, especially in case of external piers (as discussed in section 1.3.1).

3.3.1 Case study description

The geometry of the regular wall configuration here analysed, illustrated in Figure 3.22, is inspired to the one of the masonry wall known in literature as “Door Wall”, which is part of a two-story building prototype tested at the University of Pavia in 1994 (Calvi and Magenes (1994)). Moreover, this geometry was also adopted for the A-type wall of the two-story masonry building, the benchmark configuration discussed in section 2.1.

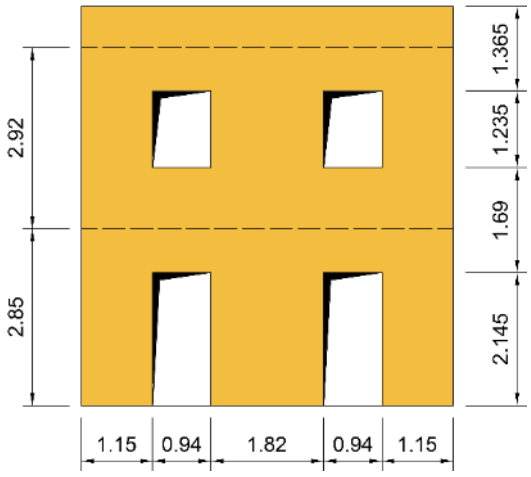

Figure 3.22- Geometry of the regular wall configuration.

As shown in Figure 3.22, the wall is characterized by the presence of two doors at the ground floor and two windows at the upper floor: the openings are of the same size at each story and are perfectly aligned in both the vertical and horizontal direction, thus perfectly corresponding to the definition of a *regular* wall. The thickness of the wall is 0.25 m. and r.c. tie beams are assumed to be present at each level. The latter comply with the aim of promoting a *strong spandrel – weak pier* behaviour type.

The rectangular cross section assumed for the r.c. tie beams is $b_{tb} \times h_{tb}$ = 20 × 25 cm, being h_{tb} the dimension located in the wall plane and b_{tb} the orthogonal one, equal to the thickness of the wall. Moreover, each tie beam is reinforced with 4φ12 longitudinal rebars (two at the extrados and two at the intrados) and φ8 stirrups with 200 mm spacing.

The material properties adopted as reference for masonry are those indicated in the previous section (see section 3.2, Table 3.1 and Table 3.2), while those adopted for the materials of the r.c. tie beams are reported in Table 3.9. The properties assumed for concrete refer to a poor quality material, which is considered as representative of the concrete often present in existing masonry buildings.

Table 3.9- Mechanical properties adopted for the materials of r.c. tie beams.

Concrete				**Steel rebars**		
E_c **[MPa]**	v_c **[-]**	f_{cc} **[MPa]**	f_{tc} **[MPa]**	E_s **[MPa]**	v_s **[MPa]**	f_{ys} **[MPa]**
28600	0.2	24	1.87	210000	0.2	450

Notes:

E_c : elastic modulus of concrete; v_c : Poisson coefficient of concrete; f_{cc} : compressive strength of concrete; f_{tc} *:* tensile strength of concrete; E_s : Young modulus of steel rebars; v_s : Poisson coefficient of steel rebars; f_{ys} : yielding strength of steel rebars.

The vertical loads transferred by the lower and upper floors were assumed to be 20.7 and 19.7 kN/m, respectively. These values are compatible with common r.c. diaphragms.

3.3.2 Numerical models

In the following the FE (adopted as reference solution) and EF models of the wall are described.

Finite Element model

The regular wall was modelled in ABAQUS by using the same element type adopted in the case of the panels previously examined, which is a fully integrated (2×2×2 integration points) 8-node linear brick element. The adopted mesh, illustrated in Figure 3.23, is characterized by elements with an approximate size of 10 × 10 × 12.5 cm, similarly to the one adopted for the masonry panels. This mesh dimension was proved to provide robust results through the convergence analyses discussed in detail in Appendix A.

Masonry was modelled through the CDP model and by adopting the parameters introduced in section 3.2 (Table 3.5 and Table 3.8) ,as resulting from the calibration process; they lead to the uniaxial compressive and tensile behaviour already illustrated in Figure 3.16.

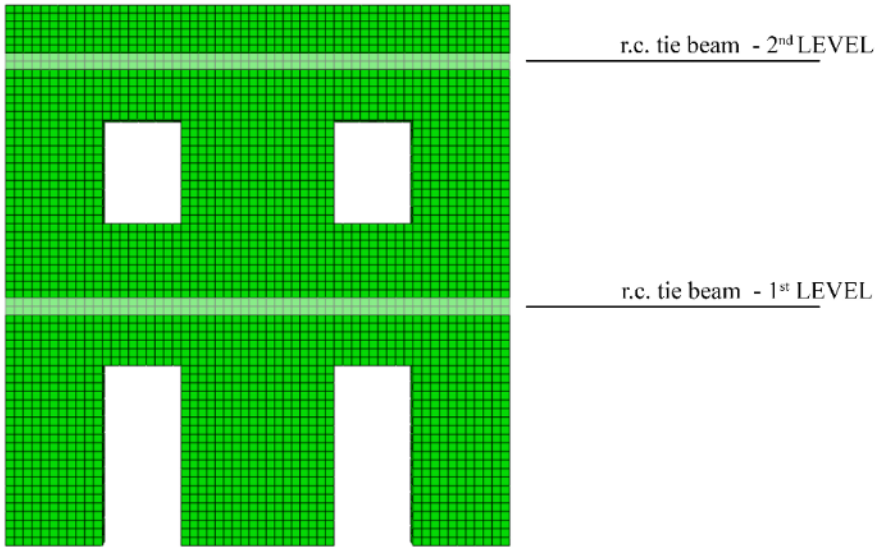

Figure 3.23 – Mesh dimension adopted for the analysis on the regular wall configuration.

The r.c. tie beams were modelled by considering separately the concrete material and the steel rebars. In particular, concrete was modelled as a nonlinear material by using the CDP constitutive model and by adopting, for the tensile and compressive uniaxial behaviour, the parameters collected in Table 3.9. The resulting stress-strain diagrams, as well as the assumed evolution of the associated damage variables are illustrated in Figure 3.24. For the other parameters of the CDP model, the same values used for masonry were adopted as reference (Table 3.5), being acceptable values also in case of concrete: the dilatancy ψ was set equal to 20°, the eccentricity ϵ equal to 0.1, the ratio between the biaxial and uniaxial compressive strength f_{b0}/f_{c0} equal to 1.2, the parameter K_C, ruling the shape of the failure surface, equal to 2/3 and the viscosity parameter η equal to 0.0001. Moreover, also in this case 8-node linear brick elements were adopted, located in correspondence of the diaphragms level, as indicated in Figure 3.23.

Table 3.10 - Parameters adopted for the tensile and uniaxial behavior of concrete.

Compressive uniaxial behavior					**Tensile uniaxial behavior**				
ε_c^{in} [-]		σ_c [MPa]		d_c [-]	ε_t^{in} [-]		σ_t [MPa]		d_t [-]
ε_{ch}^{in}	0	f_{ch}	20.0	0	ε_{tm}^{pl}	0	f_t	1.87	0
ε_{cm}^{in}	0.002	f_c	24.0	0	ε_{tu}^{pl}	0.001	f_{tu}	0.2	0.9
ε_{cu}^{in}	0.009	f_{cu}	2.5	0.9					

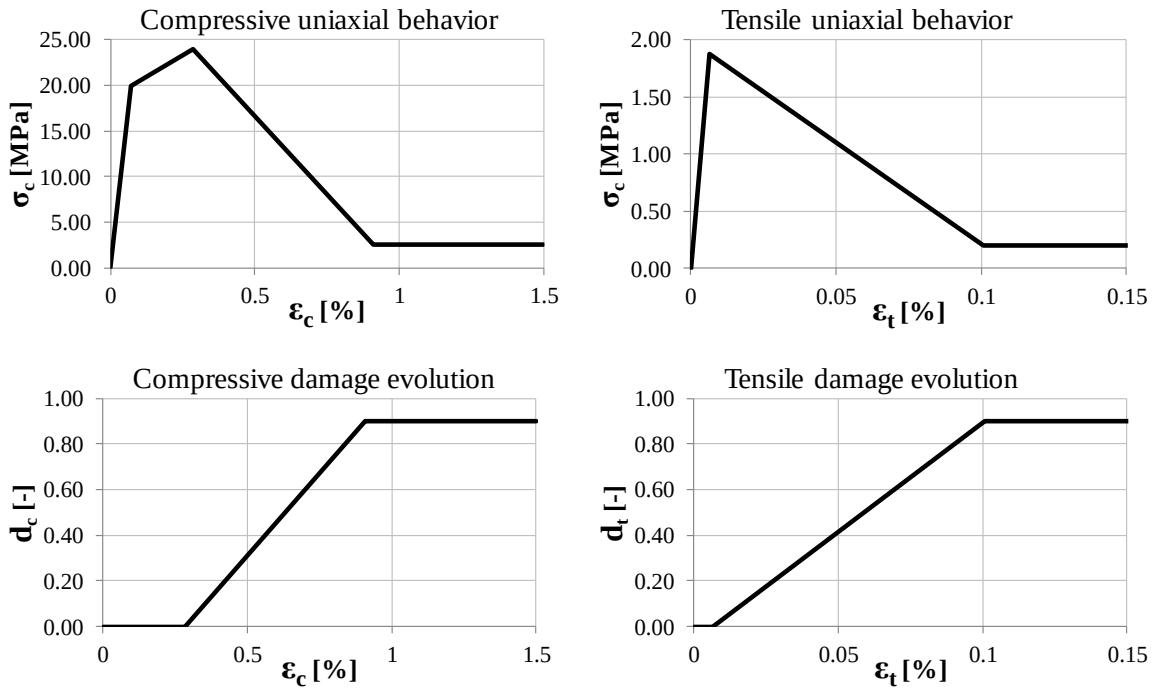

Figure 3.24 - Uniaxial behavior for the compressive and tensile regimes and associated damage evolution assumed for the concrete material used in the r.c. tie beams.

Concerning the steel rebars, they were modelled through the use of 4-nodes linear shell elements located, for each tie beam, at the two interfaces between the masonry and the concrete material, as shown in Figure 3.25; in this way, it is possible to represent the steel rebars located at the intrados and at the extrados of the tie beams. Consequently, the thickness of the shell elements was determined in order to have a cross section equivalent to the area corresponding to the steel rebars (2φ12 at the intrados and 2φ12 at the extrados). An elastic material with stiffness properties (Young modulus and Poisson coefficient) consistent with those reported in Table 3.9 was adopted for the shell elements representing the steel rebars.

The vertical load transferred in correspondence of the two diaphragms was simulated by properly modifying the density attributed to the brick elements representing the concrete material.

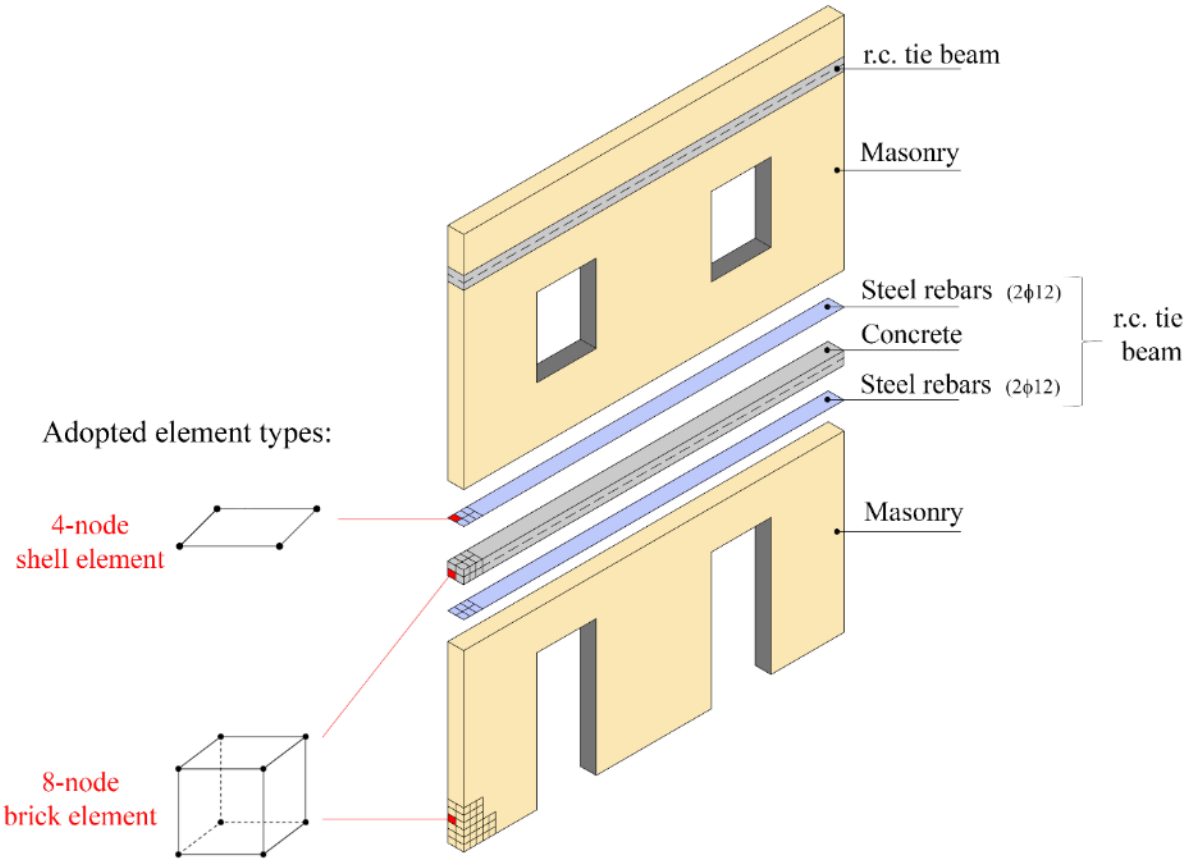

Figure 3.25– Schematization of the modelling adopted for the r.c. tie beams and of the element types used for the different materials composing the wall.

Equivalent Frame model

Different EF models were defined by using the research version of the Tremuri program (Lagomarsino et al 2013) and obtained by varying the geometry of the structural elements according to the rules available in the literature and discussed in section 1.3.1.

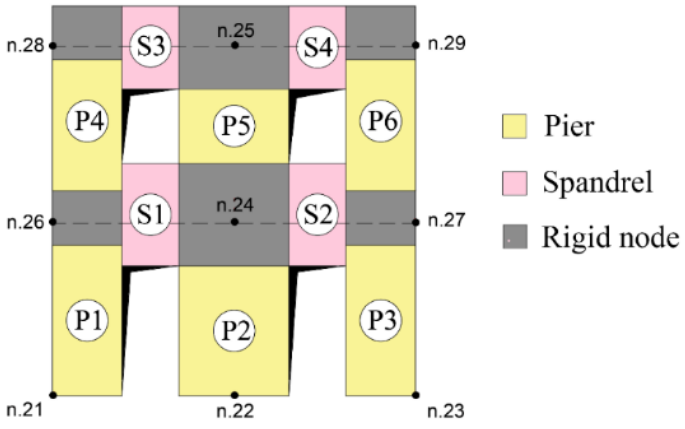

Figure 3.26 – Node numbering and structural element numbering adopted in the EF models of the regular wall.

Each one of the introduced models is characterized by a total of 9 nodes (3 of them, located at the base of the wall, are fixed while the other 6, provided with mass, represent rigid portions), 6 piers (P) and 4 spandrel elements (S). The numbering used in the following for the identification of the nodes and the structural elements is illustrated in Figure 3.26.

Regarding the definition of the geometry for the structural elements, in case of spandrels no specific uncertainties arise in this regular wall, since the openings at the two stories are perfectly aligned, so that the spandrels are simply defined as the masonry portions included between two vertically aligned openings. On the contrary, in case of piers four different criteria, among those presented in section 1.3.1, were adopted. They refer to the proposals formulated by Dolce (1991), Moon et al (2006), Lagomarsino et al (2013) and Augenti (2006). These rules were chosen among the others since they represent the most common criteria adopted today for the discretization of the masonry walls when using the EF approach, both at engineering practice, being already implemented in computers programs specifically oriented to the seismic analysis of masonry buildings (3Muri, Andilwall), and at research level, as testified by the work carried out in Augenti and Romano (2008), Marques and Lourenco (2011), Parisi and Augenti (2013).

The resulting four EF idealizations are shown in Figure 3.27. It is recalled that the criteria suggested by Augenti (2006) and Moon et al (2006) propose a pier effective height which depends on the direction of the seismic action; the models shown in Figure 3.27 refer to the application of the seismic action in the positive verse, coherently with the verse of the numerical analyses performed in this case. In Table 3.11 the effective height h_{eff} of each pier and the associated aspect ratio λ are collected as a function of the different adopted criteria.

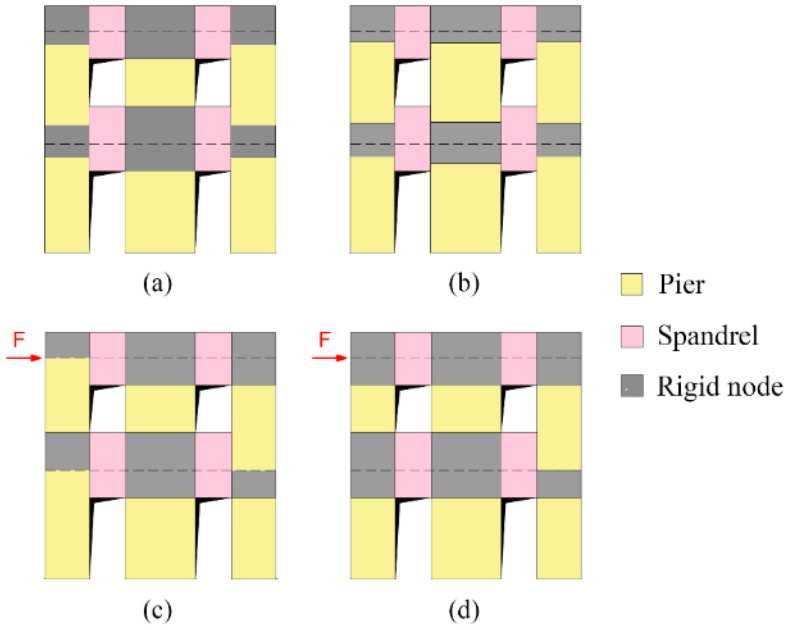

Figure 3.27 - Equivalent Frame idealizations obtained for the regular wall through the application of different criteria for the pier effective height: (a) Lagomarsino et al (2013); (b) Dolce (1991); (c) Moon et al (2006); (d) Augenti (2006).

Table 3.11– Effective height (h_{eff}) and aspect ratios (λ) obtained for the piers of the regular wall according the considered criteria. See Figure 3.26 for element numbering.

			Lagomarsino et al. (2013)	Moon et al. (2006)	Dolce (1991)	Augenti (2006)
1st storey	**P1**	h_{eff} **[m]**	2.498	2.85	2.535	2.145
		λ [-]	2.172	2.478	2.204	1.865
	P2	h_{eff} **[m]**	2.145	2.145	2.344	2.145
		λ [-]	1.179	1.179	1.288	1.179
	P3	h_{eff} **[m]**	2.498	2.145	2.535	2.145
		λ [-]	2.172	1.865	2.204	1.865
2nd storey	**P4**	h_{eff} **[m]**	2.078	1.935	2.105	1.235
		λ [-]	1.807	1.683	1.830	1.074
	P5	h_{eff} **[m]**	1.235	1.235	2.063	1.235
		λ [-]	0.679	0.679	1.134	0.679
	P6	h_{eff} **[m]**	2.078	2.22	2.105	2.22
		λ [-]	1.807	1.930	1.830	1.930

From Figure 3.27 and from the data reported in Table 3.11 it comes out that the main differences among the four criteria are about the effective height of the external piers; on the other hand, when considering the central piers (P2 and P5), the adopted rules lead to the same effective height, with the only exception of the criterion proposed by Dolce (1991), which tends to produce elements with higher aspect ratios.

As already introduced, the masonry panels are modelled as nonlinear beams with lumped plasticity by using the multilinear constitutive law presented in section 3.1.2. The failure criteria and the mechanical parameters adopted in the constitutive law for describing the piers behaviour are those defined in section 3.2 and used for the calibration with the FE model (equations 3.6 and 3.7). Figure 3.28 depicts the assumed shear-drift relationship in case of pier elements.

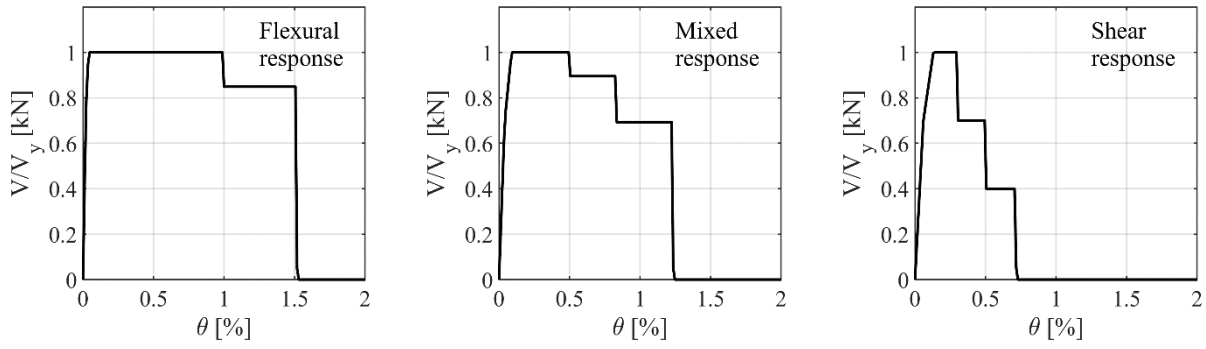

Figure 3.28– Shear-drift (V-θ) relationships assumed for piers (parameters reported in Table 3.2) and associated to different types of response (flexural, mixed, shear).

In case of spandrels the same properties used for piers in terms of stiffness (Young and shear modulus E and G) and strength (shear strength τ_0) were adopted. Moreover, also the parameters used in the multilinear constitutive law for the description of the stiffness degradation are the same adopted for piers: $k_0 = 0.5$ and $k_r = 1.54$. Concerning strength, the assumed criteria are based on the development of a strut mechanism due

to the presence of coupled r.c. tie beams (see Table 2.4, column "spandrel"). This modelling strategy, that is explicitly proposed in the Italian building code (when the horizontal compressive force acting on the spandrel is unknown and tensile resisting elements coupled to it are present), finds confirmation also in the results of several experimental campaigns (Beyer and Dazio (2012), Parisi et al (2014)) which actually showed the development of a strut mechanism, although with an inclination not always consistent with the one adopted by NTC08, that tends to reduce the effective span of the r.c tie beam.

Moving to the description of the post-peak behaviour, the mechanical parameters adopted in the piecewise-linear constitutive law (which are consistent with what suggested in CNR-DT 212 (2014)) are collected in Table 3.12, and the obtained shear-drift relationships are depicted in Figure 3.29. Mixed failures are managed, as in the case of piers, according to what explained in section 3.1.2. It can be noted that both in case of flexural and shear response the ultimate drift (associated to DL5, where the residual strength is zero) is higher with respect to the values adopted for piers (see Table 3.2); indeed, experimental tests performed on spandrels (Beyer and Dazio (2012)) suggest that the deformation capacity of these elements considerably exceeds that of piers.

Table 3.12 - Values of drift thresholds and corresponding residual strength adopted in the multilinear constitutive law for the description of the post-peak behavior of the spandrels.

	SHEAR		**FLEXURAL**	
	$\theta_{E,i}$ [%]	**$\beta_{E,i}$ [%]**	**$\theta_{E,i}$ [%]**	**$\beta_{E,i}$ [%]**
DL3	0.3	0.5	0.3	1.0
DL4	0.6	0.5	0.6	0.5
DL5	2	0.0	2	0.0

$\theta_{E,i}$: drift value at the attainment of the i^{th} DL;

$\beta_{E,i}$: fraction of the residual strength with respect to the maximum strength in correspondence of the i^{th} DL

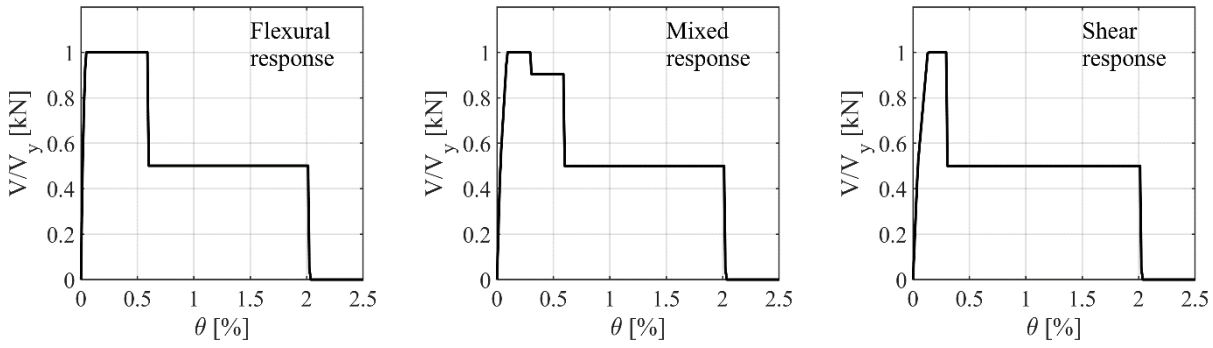

Figure 3.29 – Shear-drift (V-θ) relationships assumed for spandrels and associated to different types of response (flexural, mixed, shear).

The r.c. tie beams are modelled as nonlinear elements with lumped plasticity. They are characterized by a bilinear elastic-perfectly plastic behaviour and the plastic hinges can form at both the end sections of these elements. The considered failure mechanisms are: bending failure, which may occur in both the end sections

of the element and is associated to a ductile behavior with an ultimate rotation, and shear failure, associated to a brittle collapse.

As discussed also in section 1.3, the definition of the effective length of the r.c. tie beams, which should take into account the more or less effective coupling between the masonry panels, actually represents a modelling uncertainty when adopting the EF approach. Although the results of the nonlinear dynamic analyses performed within the RINTC Project (see Chapter 2, section 2.2) showed that this epistemic uncertainty does not significantly affect the final structural response, some deepening has been carried out having at disposal the comparison with the detailed FE model.

Thus, for each one of the four EF idealizations previously introduced three possible effective lengths for the r.c. tie beams were considered:

i) effective length equal to the width of the corresponding opening (referred to as *Short tie beams*, "S-tb");
ii) effective length equal to the distance between the nodes on which the elements are defined, assuming that they are located at the centre of each masonry pier, referred to as *Long tie beams*, "L-tb");
iii) effective length intermediate between the previous two options (referred to as *Intermediate tie beams*, "I-tb").

The structural models obtained by varying the length of the r.c. tie beams, considering as for example one of the introduced EF idealizations (the one according to Lagomarsino et al (2013)), are illustrated in Figure 3.30. Then, several comparisons with the results of the FE simulation of the wall (discussed in detail in section 3.3.5) were realized in order to determine the effective length of the r.c. tie beams which ensures the best agreement in terms of both global and local response with the results of the FE model.

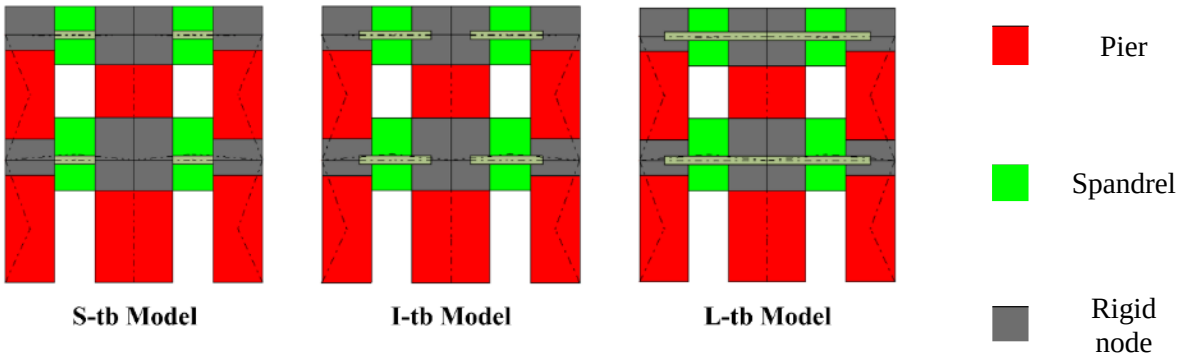

Figure 3.30– Different effective lengths considered for the r.c. tie beams (EF idealization according to Lagomarsino et al (2013)).

Considering both the variation in the geometry of the structural elements (four possible solutions) and the variations in the effective length of the r.c. tie beams (three possible solutions), a total of twelve structural models was obtained.

3.3.3 Execution of the nonlinear static analyses

The nonlinear static analyses were carried out by considering a rightward orientation of the seismic forces (positive verse), as illustrated in Figure 3.31.

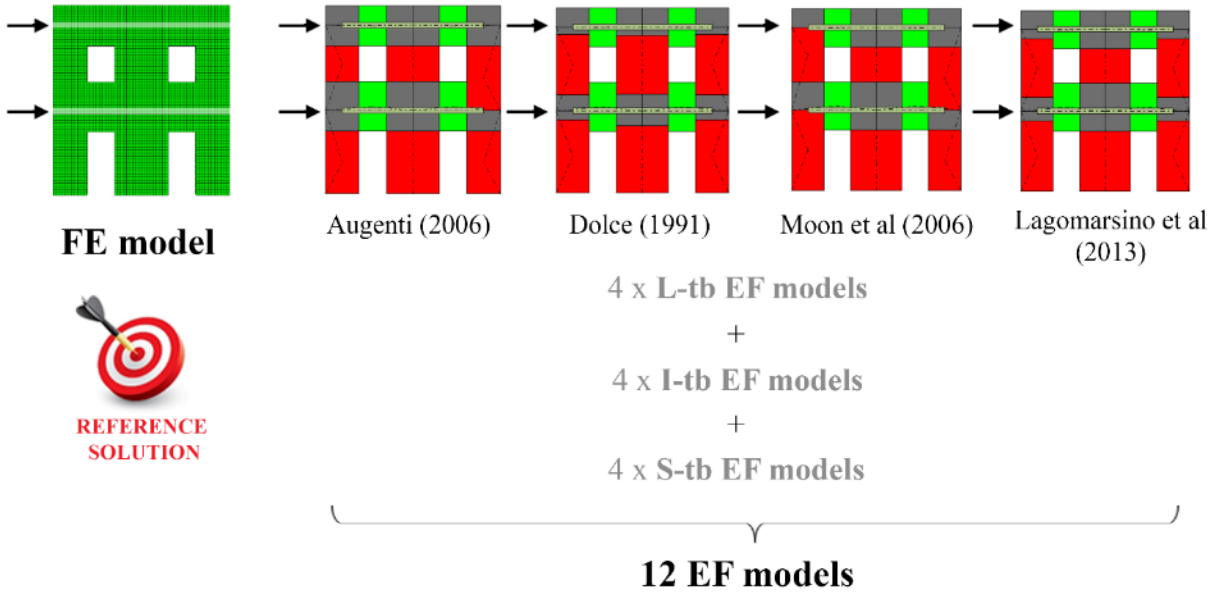

Figure 3.31– Schematization of the nonlinear static analyses performed on the different numerical models of the regular wall configuration.

In order to minimize the differences between the FE and the EF models, the same hypotheses, loading and boundary conditions were used, where possible, in the analyses.

The adopted distribution of horizontal forces is proportional to the seismic masses. In the case of the EF models the application of the horizontal forces was performed through a mixed load and control displacement strategy in correspondence of the rigid nodes. Indeed, through the pushover algorithm implemented in the Tremuri program (and described in detail in Lagomarsino et al (2013)) it is possible to directly assign the chosen load, keeping it constant during the analyses, and at the same time to perform a control displacement analysis by imposing an increasing horizontal displacement to a control node. The control node adopted in these analyses is node 25, located at the upper storey of the wall (see Figure 3.26).

Concerning the analyses carried out on the FE model, in order to capture the softening phase of the response curve, the application of the seismic forces was performed through a control displacement static analysis. To this aim, an external vertical rigid beam was introduced, whose end sections are linked to two nodes of the wall model located at the level of the diaphragms in order to create an isostatic system (see Figure 3.32). The analysis was then performed by increasing the horizontal displacement u_h of a node located along the beam (named “node C” and highlighted in red in Figure 3.32-a). In this way, when this node is moved two horizontal reaction forces generate in correspondence of the level of the two diaphragms (R_A and R_B in Figure 3.32-b). It is underlined that, being the system isostatic, the ratio between these two forces, that through this strategy is kept constant during the analysis, depends on the position of the node C

on the rigid beam. Indeed, by varying the distance of this node from, as an example, the lower end section of the beam (indicated with letter "x" in Figure 3.32-b) it is possible to simulate different force distributions at the two levels, according to the following relation (eq. 3.8), which can be easily obtained through the application of the equilibrium equations and considering the static scheme represented in Figure 3.32-b:

$$\frac{R_A}{R_B} = \frac{L - x}{x} \tag{3.8}$$

where the meaning of each parameter is explained in Figure 3.32-b.

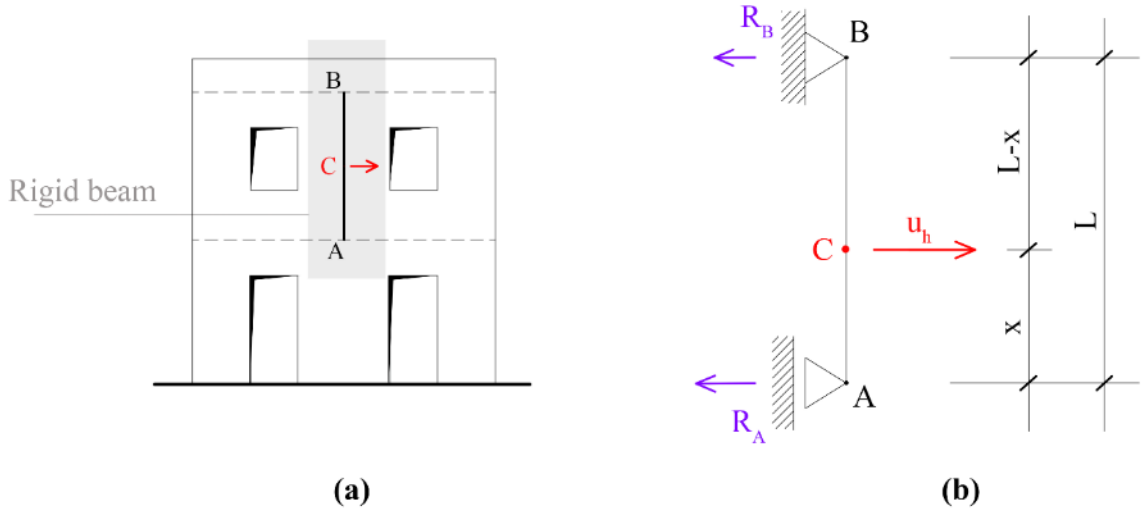

Figure 3.32 – Schematization of the method adopted for the execution of the nonlinear static analyses in control displacement and with a fixed force distribution in the case of the FE model; (b) explanation of the static scheme characterizing the introduced rigid beam.

In this way, once computed the ratio between the forces to apply at the two levels (R_A/R_B) on the basis of the seismic masses characterizing the wall, it is possible to calculate also the position of node C such that to activate the defined force distribution.

Finally, in order to avoid an excessive stress concentration and, consequently, convergence issues, the brick elements located in correspondence of the two end sections of the rigid beam, where the reaction forces are activated, were defined as elastic, with stiffness and density properties equal to the ones of the nonlinear concrete elements they replaced.

As for the single panels described in the previous section 3.2, the nonlinear incremental static analysis on the wall was performed by means of ABAQUS implicit solver, applying at each increment the full Newton's method for the equilibrium iterations and defining the step sizes through the automatic step control algorithm implemented in the software. The same solution procedures were applied also for the nonlinear static analyses conducted on the irregular walls and described in the following Chapter 4.

The hypothesis of concentrating the seismic forces at the floor level, on which the EF approach is based, is reasonable in presence of structures where the masses are actually mainly concentrated in correspondence of the diaphragms, as in the case of r.c. buildings. Conversely, in presence of masonry structures, where often the walls have a significant thickness and the presence of wooden diaphragms is frequent, this

assumption appears to be not always justified and should be properly assessed. On the other hand, even if the use of a distributed load pattern (i.e. characterized by forces distributed along the wall) could be more suitable, however this simplified hypothesis represents the current practice adopted in the codes for the execution of the seismic analyses, also in case of masonry buildings.

Despite the conventionality of such an assumption, in this case it was decided to adopt it for the analyses on the FE models, since for guaranteeing a coherent comparison with the EF approach it is necessary to adopt, as much as possible, the same hypotheses and boundary conditions in the two models. Indeed, the use of a distributed load pattern in the FE model, which clearly cannot be simulated in the EF model, would introduce a further source of difference between the two models, thus making more difficult to focus the attention on the problem here investigated, that is the identification of the structural elements geometry.

3.3.4 Criteria adopted for the comparisons

Once executed the nonlinear static analyses, the comparisons between two models were carried out in terms of:

A. global response;
B. damage pattern;
C. local response.

In the following, each introduced comparison is discussed in detail, as well as the different selected types of representation, which will be adopted also for the results of the analyses on the irregular walls (presented in Chapter 4).

3.3.4.1 Global response

A first type of comparison is about the global pushover curves obtained through the nonlinear static analyses. These curves represent the average horizontal displacement of the upper storey of the wall (named top displacement, d_{top}) as a function of the total base shear V_b.

The nonlinear static analyses were performed until high values of top displacement in both the FE and the EF models, thanks to the adopted constitutive laws which allow to obtain stable results even when the structural response becomes significantly nonlinear. Then, it was decided to represent and to consider the pushover curves only until a top displacement equal to 30 mm, which corresponds to a roof drift Θ_R equal to 5 ‰ ($\Theta_R = d_{top} / h_{top}$, being h_{top} the height of the upper floor, 5.77 m). This decision is motivated by the fact that in correspondence of such value of top displacement the wall has in general already experienced a significant state of damage. Indeed, since the adopted wall configurations are characterized in most of the cases by the activation of a soft storey mechanism at the ground floor, the actual roof drift can be considered as the double of the aforementioned value, thus being equal to 1%. In the case of the EF model, this value of drift corresponds to a high damage level for both the slender and the squat panels: indeed, according to the values adopted in the modelling of masonry panels (Table 3.2), the piers failing in shear reach the ultimate condition (DL5) for a drift equal to 0.7%, while for those where a flexural response prevails a drift equal to 1% leads to the reaching of DL4 (first loss of strength). Moreover, it has to be considered that, due to the presence of the rigid nodes, the roof drift of a wall is usually lower than the drift corresponding to

the masonry panels composing the wall; thereby, the drift values experienced by the single panels may be even higher.

An example of the comparison between the pushover curves obtained with the different numerical models is reported in Figure 3.33.

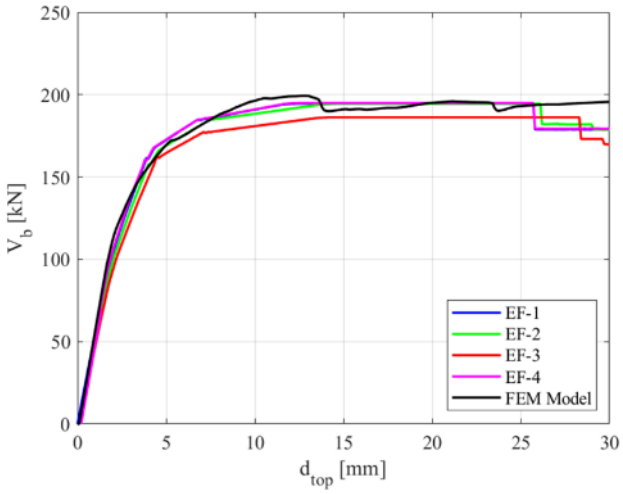

Figure 3.33- Example of the comparison between the pushover curves obtained with the FE model and with the different considered EF models of the wall.

It is worth observing that the plotted pushover curves refer only to points in which the convergence has been properly reached. Indeed, in case of Tremuri program the analysis goes on even if for a displacement increment convergence is not found (that is, the maximum number of iterations assigned in input has been exceeded). Being these points clearly identifiable, it was decided to exclude the points associated to non convergence from the results. In general, the steps characterized by more significant convergence problems are concentrated in the softening phase of the curves, after the reaching of the maximum strength, and are represented by a limited number of steps with respect to the number of steps characterizing the whole analysis.

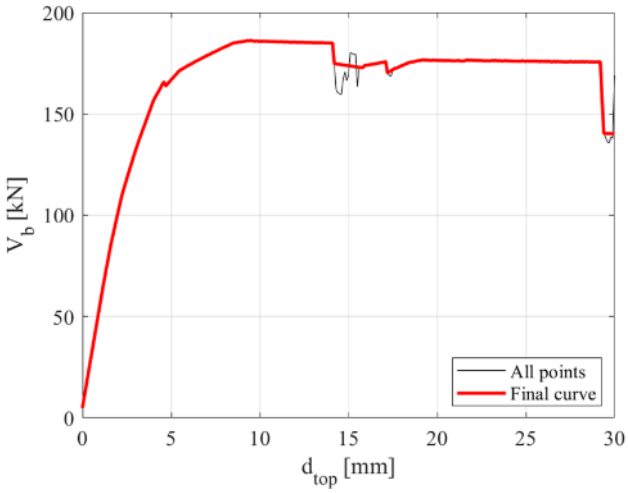

Figure 3.34 - Example of a pushover curve obtained with an EF model: in black the curve provided in output by Tremuri program (including also the non convergence points) and in red the corresponding curve obtained by considering only the equilibrium points.

In Figure 3.34, as an example, it is represented a pushover curve obtained from an analysis on one of the EF models: the black curve is obtained by considering all the points provided by the program (including points where convergence was not found), while the red one is the curve obtained by considering only the equilibrium points (final curve). In this specific case, in particular, the number of steps where convergence was not achieved is 20 on a total of 300 steps characterizing the analyses until the considered value of top displacement.

In addition to the direct comparison between the pushover curves, four additional aspects of the global response were considered: the initial stiffness, the progressive stiffness degradation, the maximum strength and the strength degradation in the post-peak phase. For a quantitative evaluation of each one of these features, four specific parameters, named as GRPs (Global Response Parameters) were defined:

1. the secant stiffness $k_{s,35}$ corresponding to the 35% of maximum strength, which was assumed as representative of the initial stiffness exhibited by the structure;
2. the ratio $R_k = k_{s,70}/k_{s,35}$ between the secant stiffness $k_{s,70}$ corresponding to the 70% of the maximum strength and $k_{s,35}$, which gives a measure of the occurred stiffness degradation;
3. the maximum global strength V_{max} exhibited by the wall;
4. the top displacement $d_{top,n}$ corresponding to a fixed value of global strength, computed as the n% reduction of maximum strength in the pushover curve of the FE model; in particular, two values of strength reduction were considered: 30% and 15% (n=15,30). The corresponding parameters are therefore $d_{top,15}$ and $d_{top,30}$.

It is stressed that the values of secant stiffness k_s were evaluated on the pushover curves removing the eventual contribution given by horizontal displacements occurred after the application of the dead loads.

Furthermore, the comparison between the FE model and the EF models on the parameter $k_{s,35}$ was introduced in order to quantify the effect of the introduction of the rigid nodes on the initial stiffness of the examined structure; the introduction of the rigid nodes, indeed, represents a significant simplification adopted in the EF models, since in the real masonry walls no rigid portions are present.

However, the use in the EF models of the multilinear constitutive law introduced in section 3.1.2 for the description of the behavior of the masonry panels does not allow to obtain a perfect estimate of the initial stiffness characterizing the structure under examination. This constitutive law, indeed, includes the possibility to take into account, even if in a simplified way, the progressive stiffness degradation of the structural elements through the use of a first branch, representative of the initial stiffness, followed by a second branch associated to a secant stiffness and representative of the cracked condition. In particular, the initial stiffness of each element is obtained starting from the values of the elastic moduli (E and G) referring to the cracked condition, which are provided as input data, through the application of a nonlinear correction which operates only on the shear component of the associated stiffness matrix. As a consequence, the value of the parameter $k_{s,35}$ computed on the pushover curves performed by using the multilinear constitutive law with stiffness degradation represents a slight underestimation of the actual initial stiffness of the structure.

With the aim to obtain a correct estimate of such parameter, it was decided to perform, in the examined configurations, also pushover analyses where for the masonry panels the same constitutive law is adopted

but removing the stiffness degradation, thus using only the elastic moduli referring to the uncracked condition. The parameter $k_{s,35}$ was therefore computed on such curves.

On the other hand, it is worth observing that the simplification provided by the multilinear constitutive law with stiffness degradation leads to a quite slight underestimation of the initial stiffness (that in average is lower than 8%); thus, apart those referring to $k_{s,35}$, all the other results presented in the following were carried out by adopting as reference this assumption.

Then, for a fixed GRP and for each considered EF model, the scatter ΔGRP_{EFi} with respect to the value derived from the curve of the FE model (GRP_{FE}) was computed, according to the following relation (eq. 3.9):

$$\Delta GRP_{EFi} = \frac{GRP_{EFi} - GRP_{FE}}{GRP_{FE}} \tag{3.9}$$

where GRP_{EFi} is the value of the given GRP calculated from the pushover curve of the i^{th} EF model (i=1,…,4). In this way, it is possible to have a quantitative measure of the "error" made on the predictions of the GRPs by the different considered EF models with respect to the predictions of the FE model. An example of this type of representation is reported in Figure 3.35.

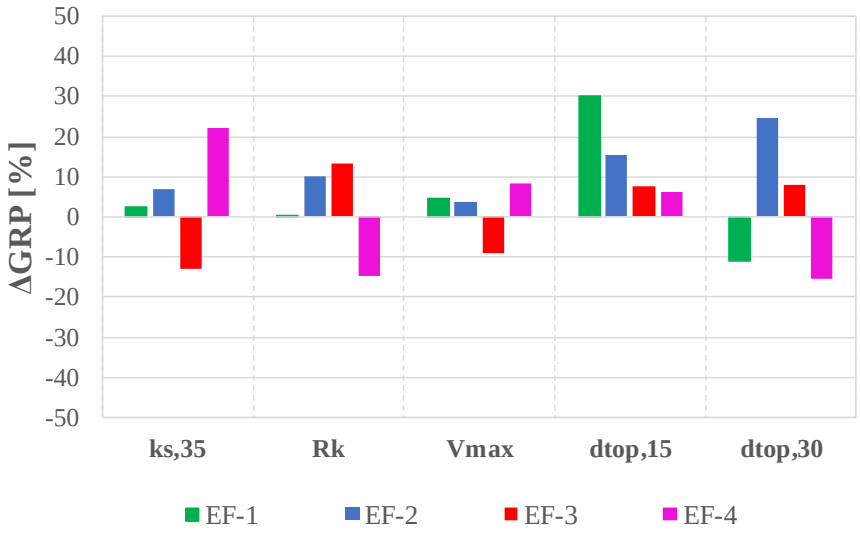

Figure 3.35 - Example of the graph adopted for the representation of the scatter with respect to the FE model (ΔGRP) of the introduced Global Response Parameters ($k_{s,35}$, R_k, V_{max}, $d_{top,15}$ and $d_{top,30}$) obtained with the EF models associated to the different criteria for the EF idealization (EF-i, i=1,…,4).

While the meaning of the scatter with respect to the FE model in case of the parameters $k_{s,35}$, *and* V_{max} is straightforward, further considerations can be made for the parameters R_k and $d_{top,n}$.

Regarding R_k, it is observed that values of $\Delta R_k > 0$ indicate that the EF model is underestimating the stiffness degradation, being the ratio $k_{s,70}/k_{s,35}$ higher with respect to the one computed in the FE pushover curve. The opposite is for values of $\Delta R_k < 0$.

The parameters $d_{top,15}$ and $d_{top,30}$ provide information about the comparison between the post-peak phase of the pushover curves obtained with the two models. In particular, as illustrated in Figure 3.36, values of

$\Delta d_{top,n} > 0$ indicate that the curve associated to the considered EF model reaches the fixed value of strength for a higher value of top displacement with respect to the FE model, thus being characterized by a less significant strength degradation. The calculation of two values of $d_{top,n}$, in correspondence of different levels of strength degradation, helps to realize a more complete comparison of the post-peak response characterizing the pushover curves of the two models, by monitoring both the initial part ($d_{top,15}$) and a more advanced phase ($d_{top,30}$).

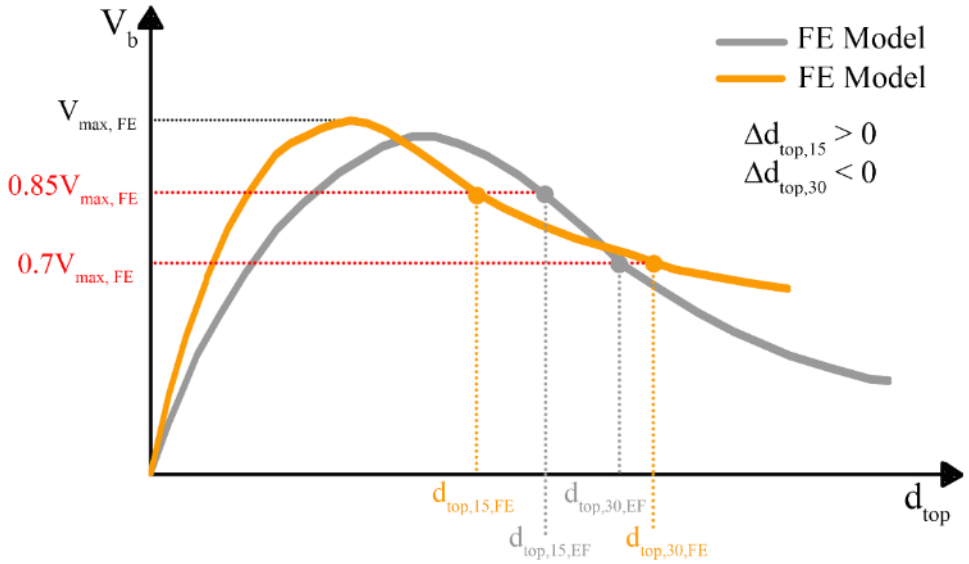

Figure 3.36 – Identification of the GRPs $d_{top,15}$ and $d_{top,30}$ on the global pushover curves of the FE model and of the EF model.

3.3.4.2 Damage pattern

The comparison in terms of damage pattern is realized by considering fixed and increasing values of top displacement, in order to monitor the progressive evolution of the occurred damage in the considered numerical models. An example of the representation of the damage pattern for a fixed step of the analysis is reported in Figure 3.37 and in Figure 3.38, for the two considered modelling approaches. It can be seen that while in the case of the FE model (Figure 3.38) the compressive and tensile damage contour plots are represented referring to the values of the corresponding damage variables d_c and d_t, in the case of the EF model (Figure 3.37) damage is expressed in terms of failure type (shear, flexural or hybrid) and Damage Levels (DLs) which correspond to attained values of drift. It is stressed that, as explained in section 3.1.2, the different Damage Levels which may occur in the masonry panels are associated to different performance conditions. More specifically, in addition to DL0 (grey color in Figure 3.37-b), which corresponds to the initial elastic (undamaged) condition, the considered Damage Levels are in total 5 (DLi, i=1,…,5): DL1 (light blue), associated to the elastic cracked condition (the cracked elastic moduli are adopted), DL2 (green) corresponding to the reaching of the peak strength (yielding point), DL3, DL4 and DL5, referring to the post-peak phase and to the progressive strength degradation occurring in the panels. More in detail, while DL3 (yellow) is associated to a drop of strength only in presence of shear or hybrid failure in case of both piers and spandrels (see Table 3.2 and Table 3.12), DL4 (red) refers to a very severe damage state, always associated to a drop of strength with respect to the peak (in case of piers and spandrels, both flexural and shear failure, see Table 3.2 and Table 3.12); then, the attainment of DL5 (purple) establishes the

reaching of collapse (i.e. the element is no more able to sustain horizontal actions, even if it still bears vertical loads). It is stressed that the word "tension" in the damage legend referring to the EF models (Figure 3.37) indicates that the element under consideration is subjected to tension, so that it does not give any contribution to the global strength, on the basis of the hypothesis assumed in the case of the flexural failure criterion (the tensile strength of the material is neglected).

It is important to underline that, differently from what happens in the EF models, where the type of failure associated to the different masonry panels can be rigorously identified, when using a continuum FE model it is not always simple to univocally classify the damage mode occurred in the different portions of the wall. Thus, this comparison will be mainly examined from a qualitative point of view, trying to recognize, from the tensile and compressive damage contour plots, the typical flexural failures, associated to the propagation of the tensile cracks at the end sections of the elements (parzialization of the cross sections, as in the case of the left piers at the ground floor and at the upper floor in Figure 3.38), the shear failures, associated to the propagation of diagonal cracks, as well as the hybrid failures (which present both the types of cracks, as in the case of the left and central pier at the ground floor in Figure 3.38).

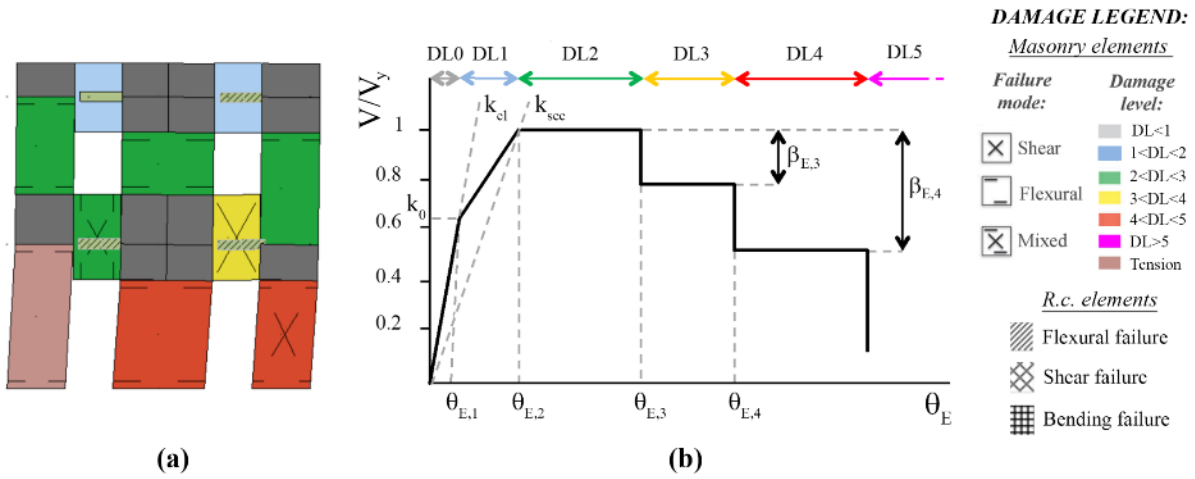

Figure 3.37 – (a) Representation of the damage pattern corresponding to a fixed step of the analysis in the EF model and (b) associated damage legend.

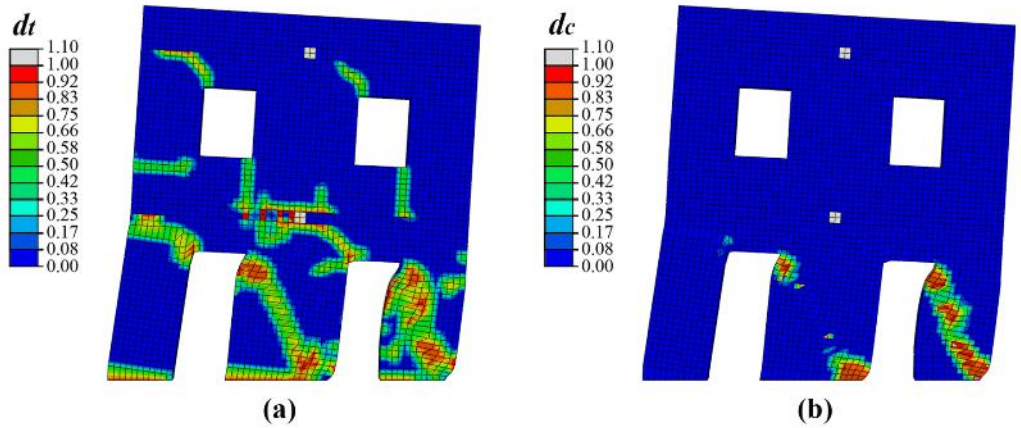

Figure 3.38 - Representation of a tensile (a) and a compressive (b) damage contour plot associated to a fixed step of the analysis in the FE model.

3.3.4.3 Local response

As far as the local response concerns, the attention is focused on the following entities:

i. the evolution, during the analysis, of the generalized forces (normal force *N*, shear force *V*, bending moment *M*) acting at the base sections of the wall;
ii. the generalized forces and displacements associated to specific sections of the structure in correspondence of fixed steps of the analysis;
iii. the values of drift characterizing the pier panels of the wall, again in correspondence of fixed steps of the analysis.

Concerning point i), the aim is to evaluate how the redistribution of the actions acting on pier panels develops in the considered numerical models. The redistribution of the vertical loads among the masonry piers, which is a function of the coupling provided between them by the spandrel elements, is particularly important to be checked, since it affects the compression level acting on the piers and, therefore, their strength and type of failure (which is also associated to the exhibited displacement capacity). The evolution of the generalized forces is represented as a function of the top displacement d_{top}. An example of this type of comparison is illustrated in Figure 3.39.

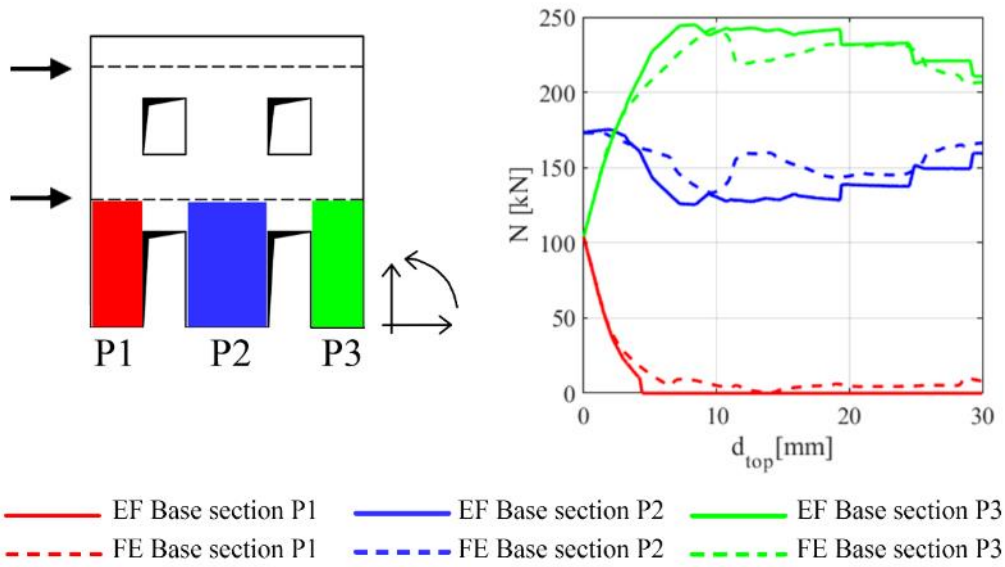

Figure 3.39 - Example of comparison between the FE model and one EF model in terms of the evolution of the normal force at the base sections of the wall.

In case of point ii) the aim is to compare generalized forces and displacements associated to the cross sections of fixed alignments defined on the wall. More in detail, three vertical alignments (C1, C2 and C3) and two horizontal alignments (R1 and R2) were identified in the case of the regular wall here analysed, as illustrated in Figure 3.40. Regarding the displacements, in addition to the rotations of the cross sections φ, the attention is focused on the horizontal displacements (u) in case of the vertical alignments, and on the vertical displacements (v) for the horizontal alignments.

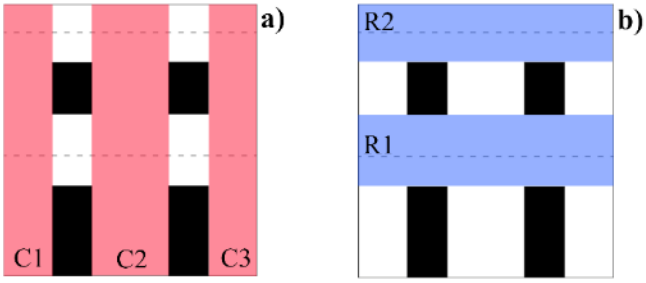

Figure 3.40 - a) Vertical (C1, C2, C3) and b) horizontal (R1, R2) alignments considered for the comparison in terms of generalized forces between the FE model and the EF models in case of the regular configuration.

In the case of the EF model, where the modelling is based on the identification of macroscopic structural elements described from a kinematic point of view through a limited number of variables and from a static point of view through their internal forces, the extrapolation of generalized forces and displacements on the introduced alignments is straightforward. However, these values are available only in correspondence of specific sections: the end sections of the deformable elements and, in case of displacements, also in correspondence of the nodes located at the two floors of the wall.

The final diagrams of the generalized forces can be obtained by assuming a linear interpolation between the values associated to the two end sections of piers and spandrels, in order to describe the behavior inside the deformable elements. In this way, a constant diagram and a linear diagram are obtained for shear and bending moment, respectively; this is consistent with the hypothesis of the absence of distributed loads applied along the elements. Similarly, also the deformed shapes (in terms of vertical and horizontal displacements) associated to the different alignments can be determined through a linear interpolation between the values corresponding to the nodes and to the end sections of the structural elements. Some examples of the obtained results are illustrated in Figure 3.41 and in Figure 3.42 in case of a vertical and a horizontal alignment, respectively. In particular, with regard to the axial load *N* (Figure 3.41-a), which progressively increases from the top to the base of the considered vertical alignment, in addition to the values of *N* through the structural elements, that are linear due to dead loads, also the axial load in the regions corresponding to the rigid nodes is represented (by using a thinner line). In this case, the discontinuity in correspondence of the nodes location is due to the vertical loads transferred at the diaphragms level. Concerning horizontal displacements, it is stressed that for each vertical alignment the value of displacement associated to the top of the wall has been set equal to the one corresponding to the node at the level of the second diaphragm (Figure 3.41-b). Indeed, being the rotations of the rigid nodes quite limited due to the presence of the r.c. tie beams and due to the fact that the steps of the analysis considered for these comparisons refer to a phase in which the structural response is not at the ultimate condition (i.e. the reduction of the maximum base shear is not close to zero), it was considered as acceptable to adopt this approximation.

With regard to the rotations, the representation shown in Figure 3.43 has been adopted, being the linear interpolation not adequate in this case.

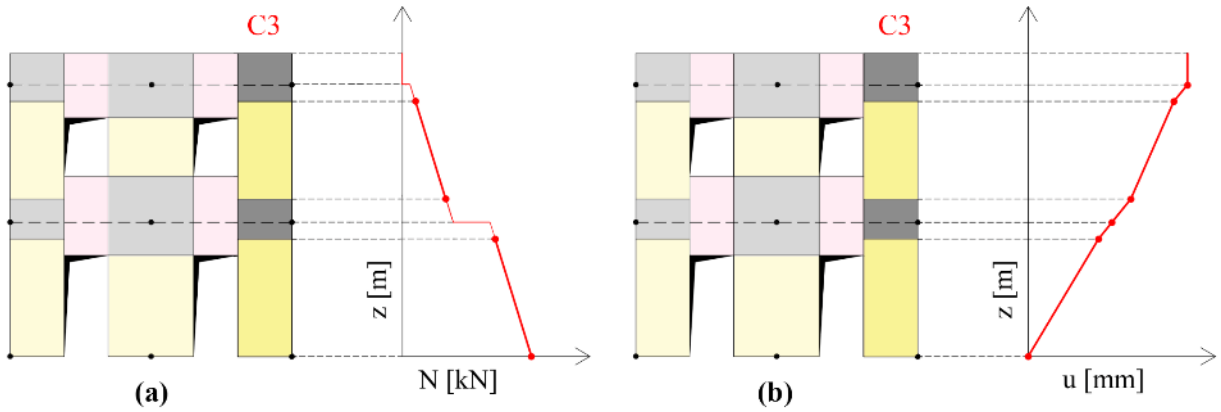

Figure 3.41– Example of the extrapolation for a fixed step of the analysis of: a) a generalized force diagram (normal force *N* – the thicker red line represents the axial load through the effective height of the structural element) and b) a deformed shape (horizontal displacements *u*) associated to the vertical alignment C3 in case of the EF model.

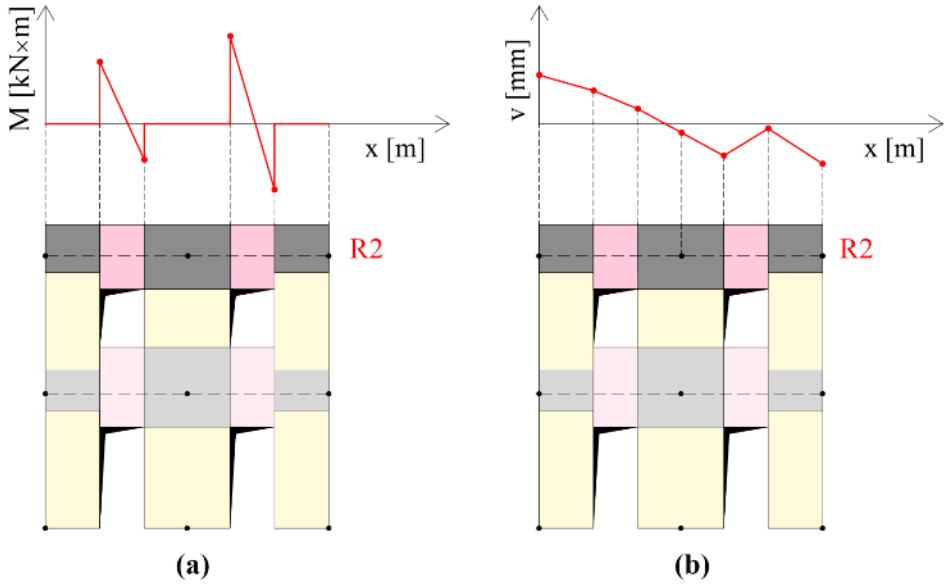

Figure 3.42 – Example of the extrapolation for a fixed step of the analysis of: a) a generalized force diagram (bending moment *M*) and b) deformed shape (vertical displacements *v*) associated to the horizontal alignment R2 in case of the EF model.

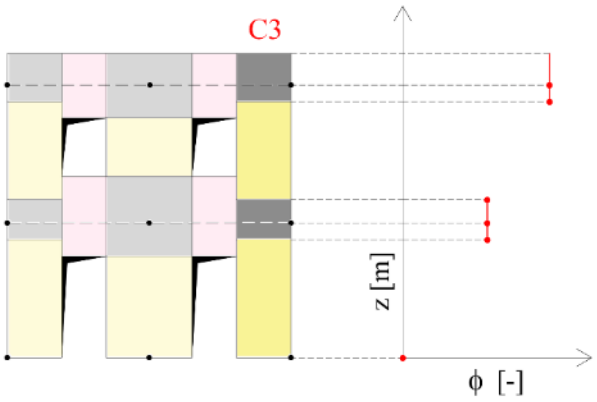

Figure 3.43 – Example of the extrapolation for a fixed step of the analysis of the diagram representing the rotations φ of the rigid nodes in the vertical alignment C3 in case of the EF model.

Moving to the FE model, the output of the analysis is represented by values of stresses, strains and displacements referring to each node of the model. Therefore, in order to make a consistent comparison with the EF model, it is necessary to identify in the introduced alignments specific sections where the integration of the nodal stresses and the choice of representative displacements have to be done.

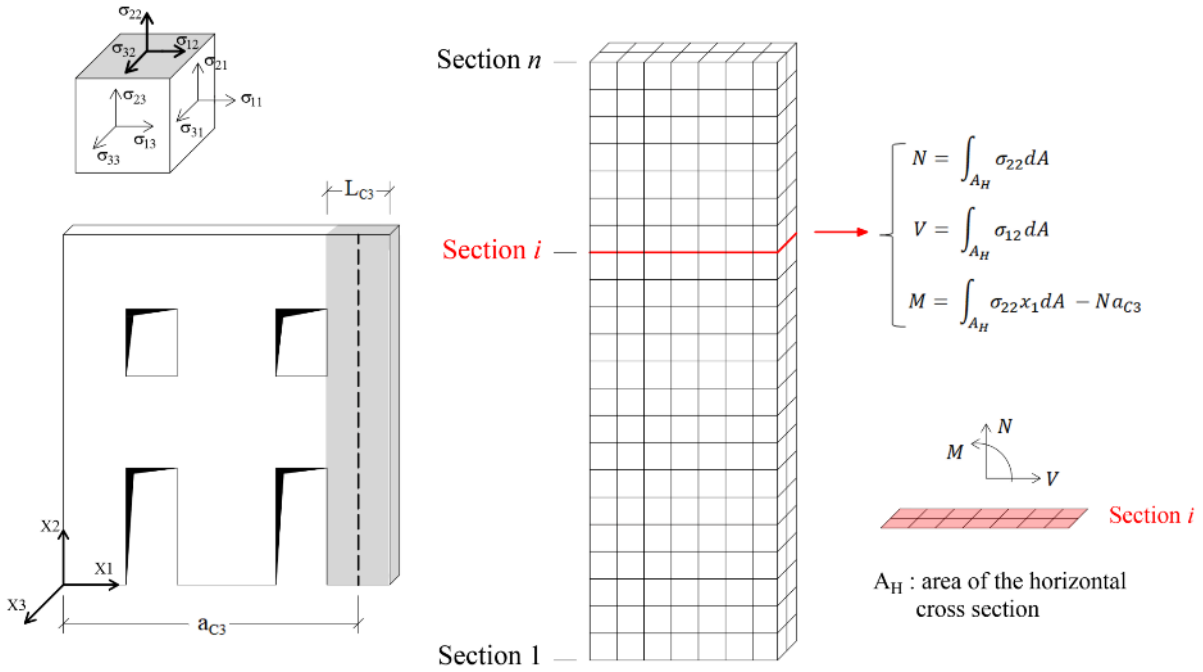

Figure 3.44 – Simplified scheme explaining the integration of the nodal stresses realized in the cross sections of the vertical alignments in the FE model.

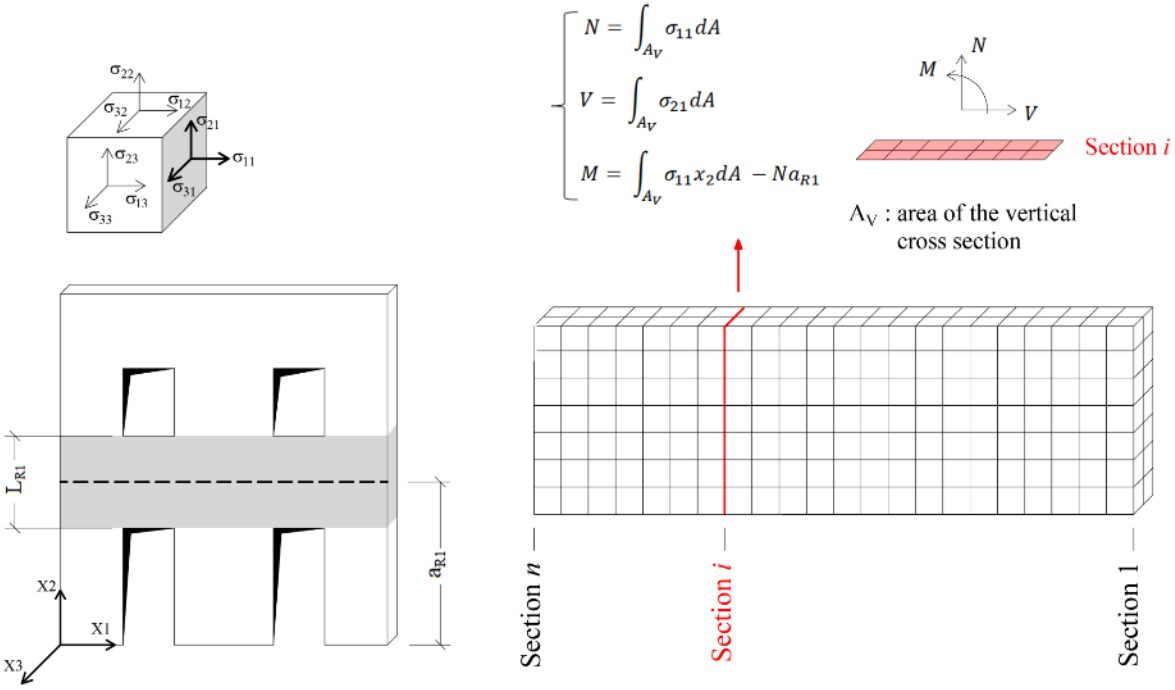

Figure 3.45 – Simplified scheme explaining the integration of the nodal stresses realized in the cross sections of the horizontal alignments in the FE model.

On each alignment it is possible to consider several cross sections, as illustrated in the simplified schemes proposed in Figure 3.44 and in Figure 3.45. For each cross section the integration of the nodal stresses leads to the definition of the corresponding generalized forces; it is stressed that the bending moment was computed by considering as reference point the centroid of each cross section.

Regarding the evaluation of the displacements, it was decided to assume as representative for each cross section the displacement of its central node. Moreover, also the rotations associated to each cross section were evaluated. In case of the vertical alignments they were obtained on the basis of the vertical displacements of the nodes in the mid-plane of the section, computing for each node the rotation with respect to the axis of symmetry of the section and then evaluating the average value between all the nodes. In case of the horizontal alignments the rotations were calculated according to the same method, but on the basis of the horizontal displacements of the nodes of each cross section.

Through these operations it is possible, for each alignment, to evaluate the displacements and the generalized forces acting on the cross sections corresponding to the different lines of nodes. On the basis of the dimension of the adopted mesh, each 10 cm a cross section on which to compute displacements and generalized forces is present. Then, a linear interpolation between the values obtained for each cross section was assumed. An example of the final outcome in terms of generalized forces, is represented in Figure 3.46, where four different steps of the analysis are considered.

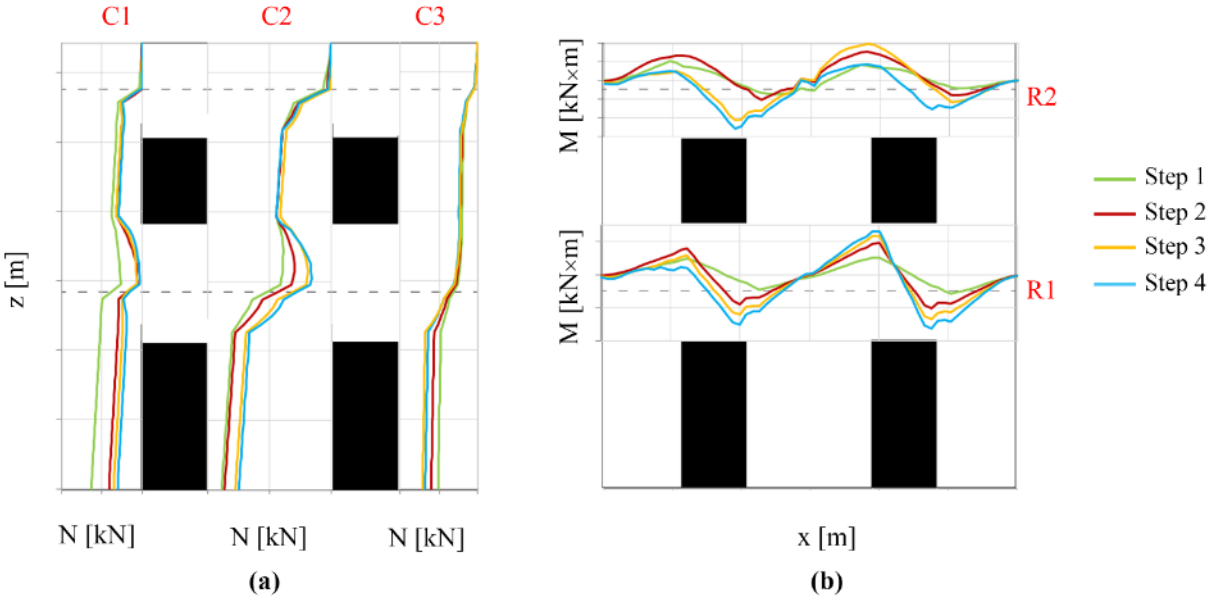

Figure 3.46 - Example of the generalized forces obtained in the FE model for different steps of the analysis (associated to different colors). in case of (a) vertical alignments (axial load *N*) and (b) horizontal alignments (bending moment *M*).

As far the comparison in correspondence of fixed steps of the analysis concerns, it was decided to consider 4 different steps: the first 2 representative of the initial response of the structure, while the other 2 to explore also a more advanced nonlinear phase. In general, by considering all the pushover curves

obtained for the configuration under examination, the first two steps were chosen on the ascending branch of the curves, the third almost in correspondence of the peak strength and the fourth in the descending branch.

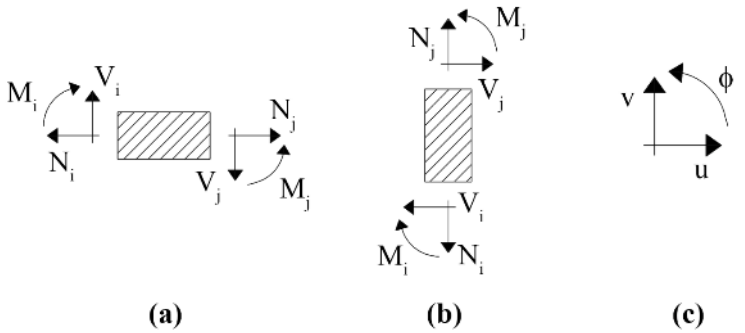

Figure 3.47 – Convention adopted for the definition of the sign characterizing the generalized forces *N*, *V* and *M* acting on the (a) horizontal and (b) vertical alignments and (c) the displacements *u,v, φ*.

The sign of the generalized forces was defined in all the cases according to the classical representation adopted in beams theory, as illustrated in Figure 3.47; regarding displacements and rotations, the sign was defined according to the notation indicated in Figure 3.47-c.

In Figure 3.48 the representation adopted for the comparison in terms of generalized forces is illustrated, referring, as an example, to the vertical alignment C2.

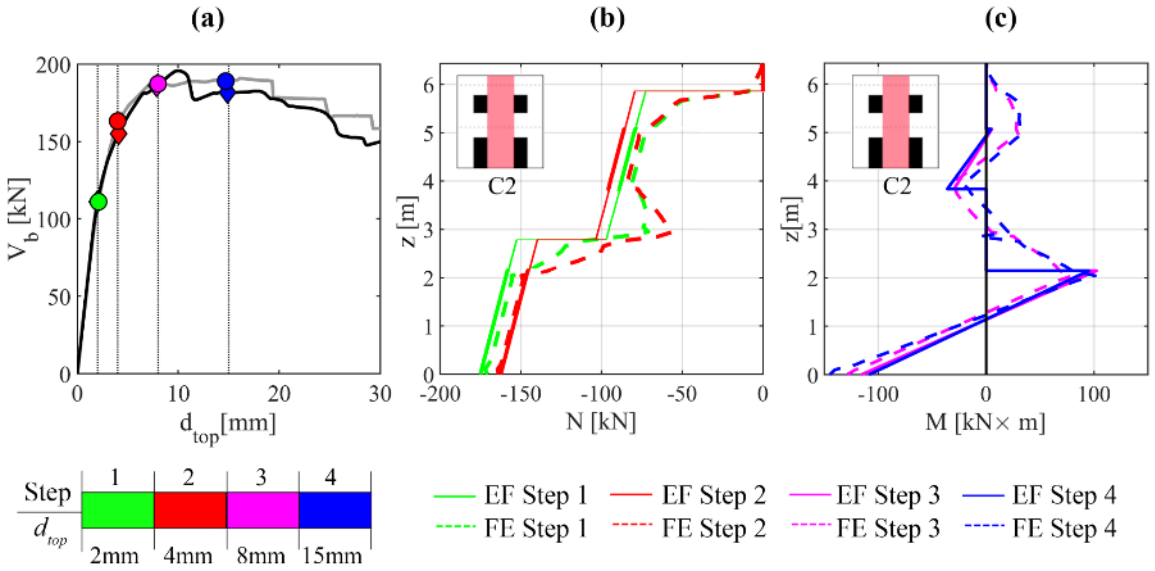

Figure 3.48 - Example of the comparison between the FE model and one EF model in terms of generalized forces: (a) identification on the pushover curves of the 4 considered steps; (b) normal force *N* and (c) bending moment *M* acting on the alignment C2 in correspondence of the 4 steps.

On the basis of the diagrams of the generalized forces obtained from the FE model, it is possible to identify the effective geometry of the structural elements which actually activate during the analysis (by looking, as an example, at the obtained bending moment diagrams) and to compare it with the one predicted by the different criteria for the EF idealization under examination.

In addition, the comparisons of the deformed shapes are useful in order to understand if the hypothesis of the introduction of the rigid nodes in the wall, which represents one of the most critical assumptions within the EF approach, finds or not a confirmation in the results of the FE model.

Finally (point iii), a last type of comparison between the results of the different numerical models refers to the drift values associated to the pier panels of the wall in correspondence of fixed steps of the analysis.

As known, the drift of a masonry panel is a parameter which provides a measure of its deformation under the effect of horizontal loads. It can be evaluated at the two end sections of the panel, by making reference to the inflection point (chord rotation), or as an element property (mean drift of the panel), that is the strategy here adopted. In this last case, the drift represents the lateral displacement of the panel expressed as a percentage of the height. The simplest definition of this parameter considers only the horizontal displacements at the two end sections of the panel; however, in presence of deformable spandrels, which allow the rotations of the nodes, it is more correct to define an element drift that accounts for the effective average angular deformation, by removing the contribution of the rotations at the ends of the panel.

According to this logic, therefore, the drift θ of the pier panels has been computed as follows (eq. 3.10), as suggested in Lagomarsino et al (2013):

$$\theta = \frac{(u_j - u_i)}{h} + \frac{(\varphi_j + \varphi_i)}{2} \tag{3.10}$$

being u_j and φ_j the horizontal displacement and the rotation of the top section of the panel, respectively, and u_i and φ_i the horizontal displacement and the rotation of the bottom section. Since in the FE model the wall is characterized by a continuum equivalent material, it is necessary to *a- posteriori* identify the portions corresponding to masonry panels, in order to have specific sections to consider for the computation of drift. Then, once identified the position of these sections in the wall, the associated values of horizontal displacement u_i and u_j and rotation φ_i and φ_j can be obtained through a linear interpolation between the values calculated for each cross section of the vertical alignments C1, C2 and C3. Indeed, the distance between two subsequent cross sections is limited (approximatively 10 cm) with respect to the whole dimension of the wall, so that a linear interpolation between them for the computation of these quantities can be considered as acceptable.

It is recalled that the EF models considered in the analyses are characterized by a different geometry of the structural elements, which is the result of the application of different criteria for the pier effective height. Therefore, for a given pier the drift predicted for a fixed step of the analysis by each EF model is compared with the value of drift computed in the FE model on the corresponding masonry portion.

As an example, in Figure 3.50 the drift values predicted for piers 1 and 4 by the EF model according to Lagomarsio et al (2013) are compared with the drift values computed in the FE model in correspondence of a masonry portion coincident with the geometry of that pier, as illustrated in Figure 3.49-a.

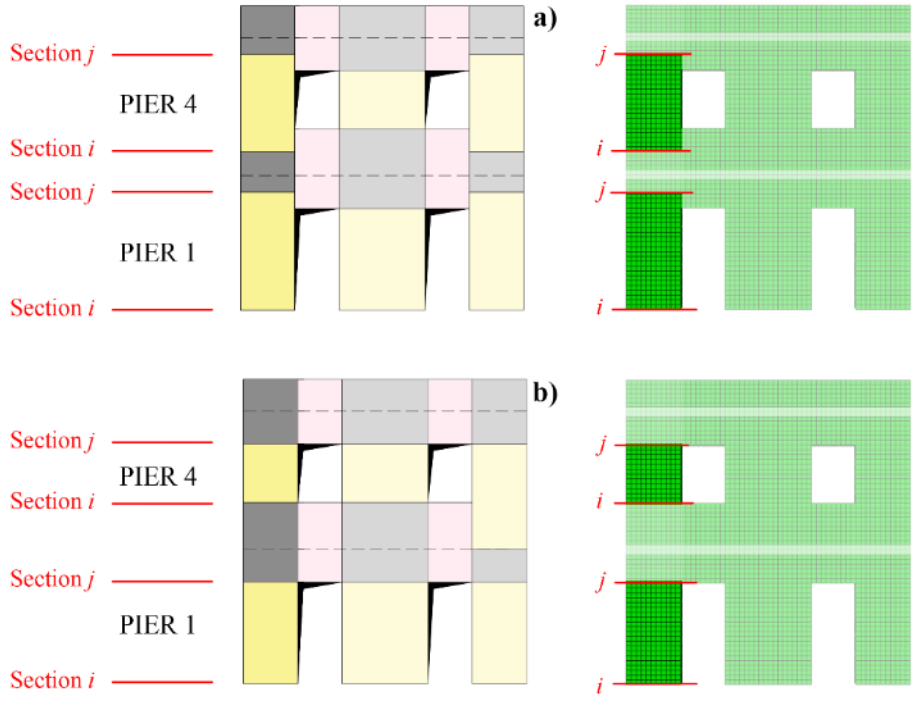

Figure 3.49 – Schematization of the sections considered in the FE model for the computation of the drift values associated to the masonry piers in the alignment C1 (Pier 1 and pier 4) in case of comparison with the EF model according to (a) Lagomarsino et al (2013) and (b) Augenti (2006).

Moving then to the EF model associated to the criterion by Augenti (2006), the geometry of pier 1 and 4 is different; therefore, the drift values predicted by this EF model will be compared with the ones obtained by considering, in the FE model, a different portion of masonry (Figure 3.49-b). An example of the graphical representation adopted for this type of comparison is illustrated in Figure 3.50.

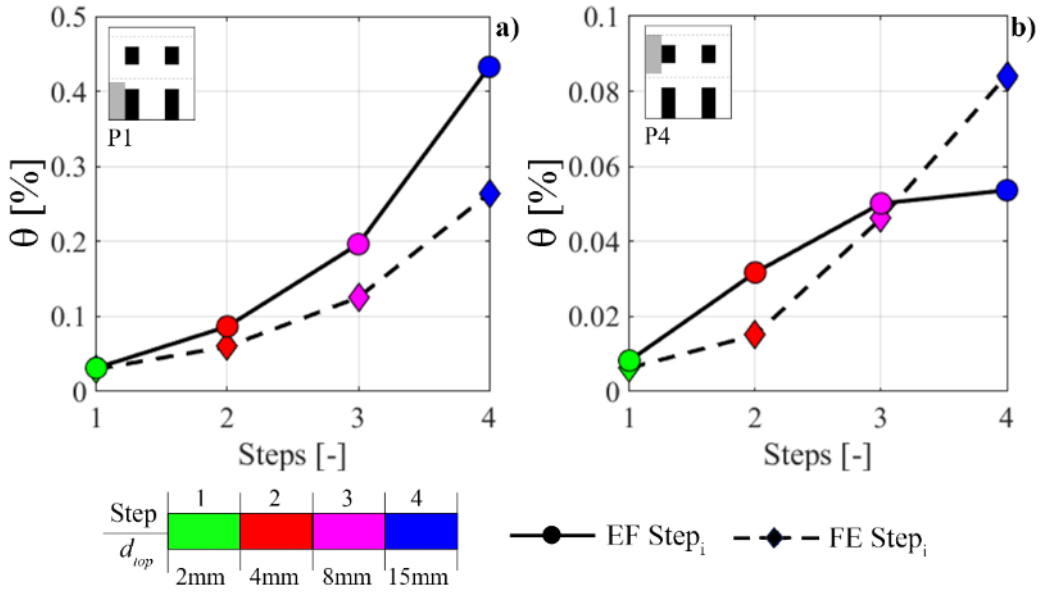

Figure 3.50 – Example of comparison between the FE model and one EF model (according to Lagomarsino et al (2013)) in terms of drift values θ associated to: a) Pier 1 (P1) and b) Pier 4 (P4) for different steps of the analysis.

3.3.5 Results of the nonlinear analyses

In this section the results of the nonlinear static analyses performed on the numerical models of the regular wall are discussed by means of the different types of comparison introduced in the previous section.

3.3.5.1 Results in terms of global response

First of all, the influence of the effective length of the r.c. tie beams on the global response predicted by the EF models is explored. To this aim, in Figure 3.51 the pushover curves associated to the different EF models are reported; in particular, for each criterion adopted for the definition of the pier effective height, the global curves obtained by considering different effective lengths of the r.c. tie beams (L-tb, I-tb, S-tb) are represented.

It can be seen that, in general, the influence of the effective length of the r.c. tie beams on the global response is limited. Indeed, the pushover curves obtained for a fixed criterion for the pier effective height are, in almost all the cases, very similar in terms of stiffness and maximum strength.

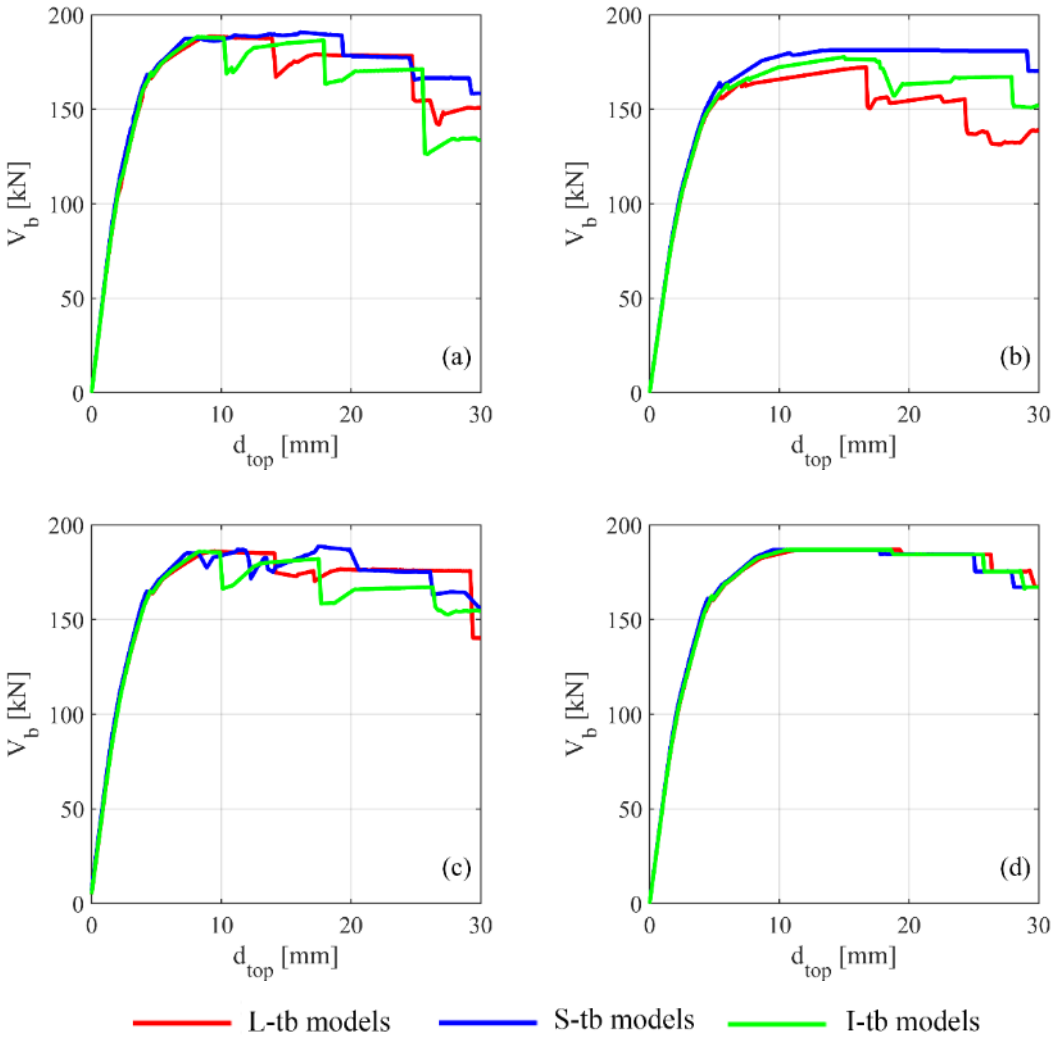

Figure 3.51 - Comparison between the pushover curves obtained by considering different effective lengths for the r.c. tie beams. EF models according to: (a) Augenti (2006); (b) Dolce (1991); (c) Moon et al (2006); (d) Lagomarsino et al (2013).

Slight differences are detected only in the post-peak phase, except for the EF models associated to the proposal by Lagomarsino et al 2013 (Figure 3.51-d), where the three curves are almost coincident. This is consistent with the fact that in this specific wall the effective length of the r.c. tie beams does not significantly change from one model to the other, as illustrated in the previous Figure 3.30. As a consequence, the stiffness of these elements, which affects the coupling between the masonry piers, is quite similar in the models with short, intermediate and long r.c. tie beams.

However, in the case of the EF models associated to the proposal by Dolce (1991) (Figure 3.51-b) a higher sensitivity of the global response as a function of the effective length of the r.c. tie beams is observed: in particular, the pushover curve obtained from the L-tb model is associated to a lower maximum strength with respect to the corresponding I-tb and S-tb models.

In Figure 3.52 the comparisons between the pushover curves obtained with the FE model and the pushover curves derived from the EF models associated to the different criteria for the pier effective height are shown, considering, as an example, the S-tb and the L-tb EF models.

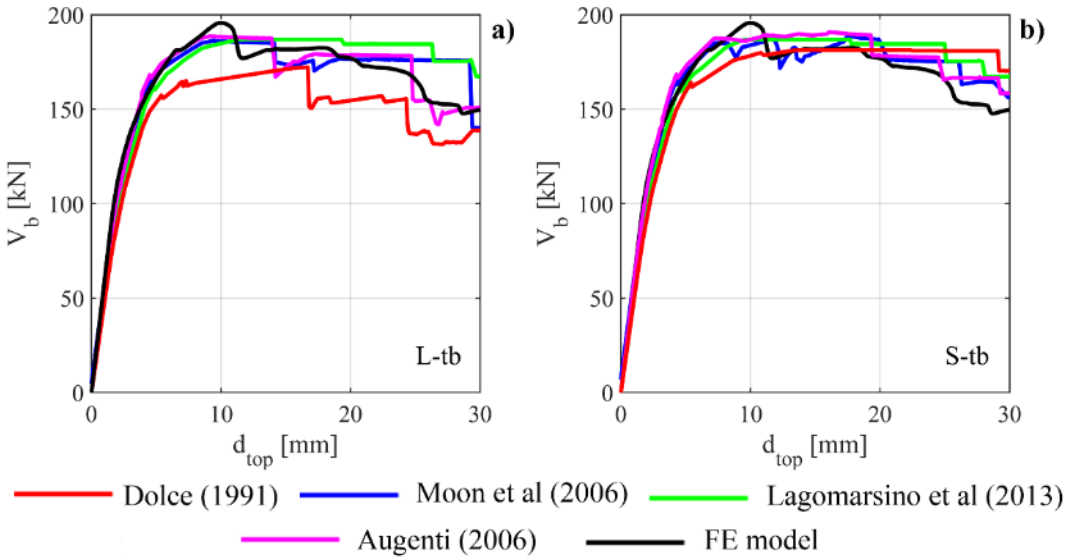

Figure 3.52 - Comparison in terms of global pushover curves between the FE model and the EF models associated to the different criteria for the piers effective height: (a) EF models with long r.c. tie beams (L-tb) and (b) EF models with short r.c. tie beams (S-tb).

By looking at the results associated to the S-tb EF models (Figure 3.52-b), it may be observed that:

- the adoption of different criteria for the pier effective height does not significantly affect the final global response, being the obtained pushover curves substantially similar;
- there is a good agreement between the predictions of the EF models and the pushover curve obtained from the FE analysis; indeed, the pushover curves associated to all the EF models, regardless the adopted criteria for the pier effective height, well capture the initial part of the response and the maximum strength characterizing the curve of the FE model. Moreover, also the subsequent post-peak phase is quite well described, even if the strength degradation appears to be slightly lower in the EF models.

Similar considerations apply also to the case of the L-tb EF models (Figure 3.52-a), with the only exception of the EF model associated to the criterion proposed by Dolce (1991). The pushover curve, in this case, is significantly different not only from the curves associated to the other EF models, but also from the pushover curves obtained with the FE model. This type of behavior, highlighted also in the previous Figure 3.51, is due to the activation of a different collapse mechanism, as discussed more in detail in the following.

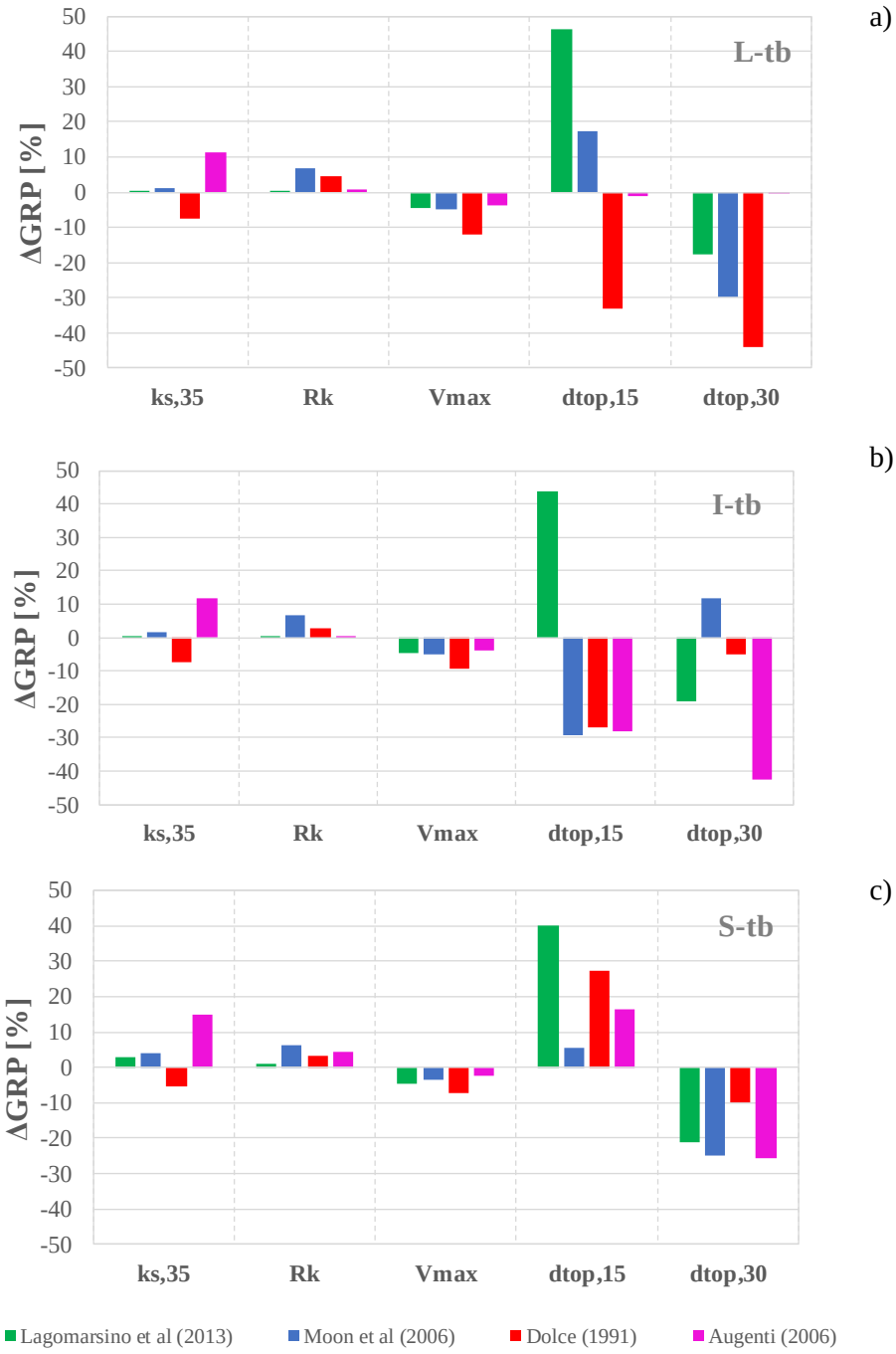

Figure 3.53 - Comparison of the results in terms of ΔGRP (scatter of the Global Response Parameters with respect to the FE model) obtained through the different EF models: a) L-tb EF models; b) I-tb EF models; c) S-tb EF models.

In Figure 3.53 the comparison in terms of the Global Response Parameters introduced in section 3.3.1 is reported. Considering first of all the parameters referring to stiffness and strength ($k_{s,35}$, R_k, V_{max}), it may be observed that, in general, for all the considered EF models the scatter with respect to the FE model is rather low. More specifically, with regard to the parameters R_k and V_{max}, it is lower than 10% in almost all the cases. In particular, a low scatter on parameter R_k indicates that the stiffness degradation characterizing the response of the FE model is well captured by the EF models, even if the latter tend to predict a slightly lower stiffness degradation with respect to the reference solution ($\Delta R_k > 0$). This result demonstrates the efficacy of the multilinear constitutive law adopted in the EF models in describing the stiffness degradation actually occurring in the structure.

Concerning V_{max}, it can be seen that all the EF models tend to slightly underestimate the maximum strength occurred in the FE model.

Moving to the parameter $k_{s,35}$, it is observed that, with the exception of the model obtained through the application of the Dolce's criterion, the EF models have an initial stiffness higher with respect to the FE model, with differences in general within 15%. Moreover, considering a fixed effective length for the r.c. tie beams, it can be seen that the different criteria for the pier effective height lead to different results for $\Delta k_{s,35}$: this is justified by the different dimensions of the rigid nodes in the considered models, as a consequence of the different geometry adopted for the structural elements.

In particular, while the models associated to the proposal by Moon et al (2006) and Lagomarsino et al (2013) are slightly more rigid than the FE model, the contribution of the rigid nodes is much more significant when the Augenti's criterion is applied. The Dolce's criterion, on the contrary, provides an underestimation (however lower than 8%) of the initial stiffness with respect to the FE model. In this case, indeed, the extension of the rigid nodes is lower with respect to the other models, being the masonry piers characterized by a higher effective height (see Table 3.11).

The differences among the EF models with a different effective length of the r.c. tie beams are quite negligible. However, despite of a small overestimation with respect to the FE model of the initial stiffness, the S-tb EF models provide slightly better predictions in terms of maximum strength (scatter within 5%).

Moving to the examination of the post-peak phase of the pushover curves, the attention has to be focused on the parameters $d_{top,15}$ and $d_{top,30}$. In general, by looking at the results reported in Figure 3.53, it is observed that the scatter with respect to the FE model is higher than in the case of the previous discussed parameters; moreover, the predictions of the EF models actually differ depending on both the considered length of the r.c. tie beams and the criterion adopted for the EF idealization.

In this case, the parameters $d_{top,15}$ and $d_{top,30}$ represent the top displacements associated to a lateral strength equal to approximatively 166 kN and 136 kN, respectively. In the light of these observations the high values in terms of $\Delta d_{top,15}$ can be explained by considering that all the pushover curves are characterized by a very gradual strength degradation in the post-peak phase, especially the curves of the EF models, which in some cases are almost horizontal, as it can be seen in Figure 3.52; thereby, the reaching of the fixed value of strength may happen for different values of top displacement even if the curves are substantially similar in the post-peak phase.

The parameter $d_{top,30}$, on the other hand, refers to a value of lateral strength which occurs in almost all the cases for top displacements higher than 30 mm, when the structural response is in advanced nonlinear

phase and the damage occurred in the wall is significant. In this case, the EF models tend to predict a higher strength degradation with respect to the FE model ($\Delta d_{top,30} < 0$). This can be explained by considering that in the EF models the masonry panels, once that specific drift thresholds are attained, are subjected to sudden drops of strength (see Figure 3.28); on the contrary, when the modelling is made at the material scale, as in the FE model, the strength degradation is typically more gradual, due to the progressive damage occurred.

In general, the S-tb EF models allow to obtain better results with respect to the models characterized by the long and intermediate r.c. tie beams, being associated to a lower scatter (within 25%, except few cases) on both the parameters $d_{top,15}$ and $d_{top,30}$.

3.3.5.2 Results in terms of damage pattern

The comparison in terms of damage pattern was realized in correspondence of fixed steps of the analyses, associated to increasing values of top displacement identified on the pushover curves: Step1: d_{top} = 2 mm, Step 2: d_{top} = 4 mm, Step3: d_{top} = 8 mm and Step 4: d_{top} = 15 mm.

The analysis of the occurred damage showed that the predictions of the EF models with short r.c. tie beams (S-tb) provide the best match with the results of the FE model for all the adopted criteria for the EF schematization (Figure 3.54).

First of all, it can be observed that in the FE model damage actually concentrates in the portions of masonry corresponding to piers and spandrels, while the remaining parts, which in the EF models are idealised as rigid nodes, are almost undamaged. The only exception is represented by the portion of masonry located in the central part of the wall, between the door openings at the ground floor and the windows at the upper floor, in particular in case of step 4 where some concentration of damage here occurred. This is probably due to the method adopted for the execution of the nonlinear static analysis: indeed, the lower end of the rigid beam used for the application of the lateral loads (see Figure 3.32) is linked to the masonry material in correspondence of a node exactly located in this part of the wall potentially producing a concentration of stresses in this area. Despite this difference, globally the damage pattern of the wall is not significantly affected by this issue.

In general, by looking at the progressive evolution of damage, it is possible to observe that the predictions of all the EF models represented in Figure 3.54 are in good agreement with the results of the FE model.

The first elements where damage occurs are the spandrels at the first storey, followed by the piers located in the left part of the wall (where the compression decreases due to the overturning phenomenon); then, damage involves also the other portions of the wall.

More specifically, considering the piers at the ground floor in the FE model damage occurs at first in the portions of the wall corresponding to P1 and P2; then, at step 3 also P3 starts to have a concentration of tensile damage at the base section, failing then with a hybrid failure mode (step 4). All the EF models provide predictions which agree with the FE model: indeed, in all the cases P1 and P2 are interested by a flexural failure; moreover, in P3 a hybrid failure occurs, which is reached in some cases at step 3 (Figure 3.54-a, Figure 3.54- c) and in the others at step 4. In all the cases, from step 3 P1 is subjected to tension (and thus gives no contribution to the global strength), due to the overturning phenomenon characterizing the wall under the horizontal forces.

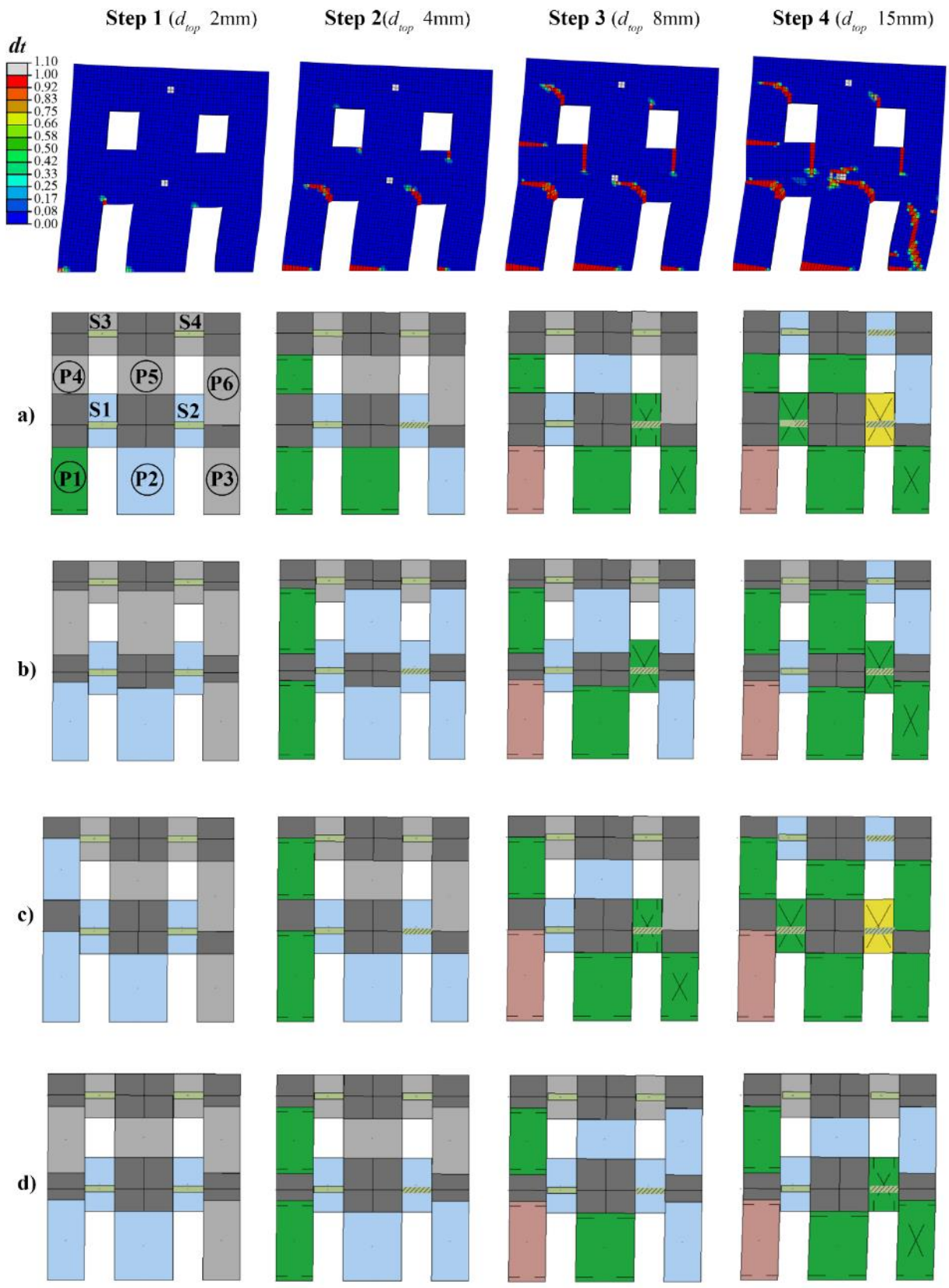

Figure 3.54 - Damage pattern associated to 4 fixed values of top displacement for the FE model and the S-tb EF models: a) Augenti (2006); b) Dolce (1991); c) Moon et al (2006); d) Lagomarsino et al (2013). See Figure 3.37 for the meaning of colours and symbols in case of the EF models.

Moving to the piers located at the top floor, in the FE model damage is mainly concentrated in the portion corresponding to P4, while the parts corresponding to P5 and P6 are almost undamaged. The EF model associated to the proposal by Lagomarsino et al (2013) accurately reproduces the state of damage characterizing the piers at the top floor (see Figure 3.54-d, step 4); the other EF models at step 4 predict the reaching of the maximum strength (DL2) also for P5 and in one case (Figure 3.54-c) for P6.

Concerning spandrels, it is observed that in all the EF models damage is concentrated on the spandrels at the first floor, while those at the top floor are almost undamaged (elastic phase with initial or cracked stiffness), and this is consistent with what detected in the FE analysis. However, the EF models tend to predict shear failures (or hybrid in some cases) for spandrels, while in the FE model, in the considered steps of the analysis, spandrels are characterized by cracks that are typical of a flexural failure.

It is worth noting that, at Step 4 (d_{top} = 15 mm), the structural elements of the considered EF models have reached, at maximum, Damage Level 2 (peak strength, see Figure 3.37) in case of piers and Damage Level 3 in case of spandrels (first drop of strength in case of shear failure). In order to make a comparison of the damage pattern also in a more advanced phase, in Figure 3.55 and Figure 3.56 the deformed shapes detected by the above considered numerical models in correspondence of a top displacement equal to 30 mm are illustrated; in this way it is possible to compare the collapse mechanisms predicted for the wall under examination.

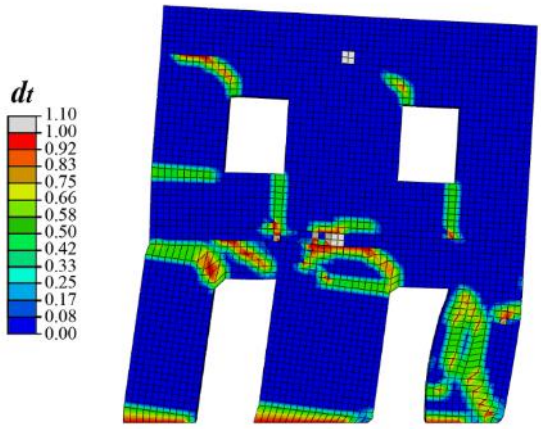

Figure 3.55 - Damage pattern associated to a top displacement of 30 mm in the FE model of the regular wall.

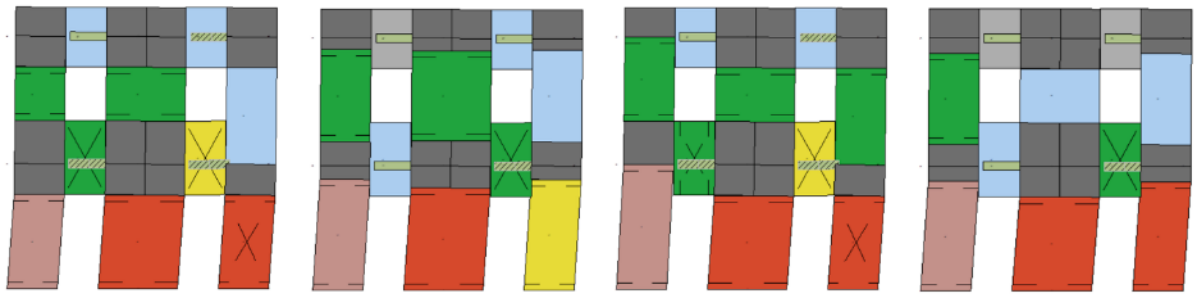

Figure 3.56 - Damage pattern associated to a top displacement of 30 mm in the S-tb EF models of the regular wall: (a) Augenti (2006); (b) Dolce (1991); (c) Moon et al (2006); (d) Lagomarsino et al (2013). See Figure 3.37 for the meaning of colours and symbols.

All the considered EF models predict a collapse mechanism characterized by a significant concentration of damage in the piers at the ground floor (soft storey mechanism), in agreement with the predictions of the FE model. This type of mechanism, indeed, is favoured by both the presence of strong spandrels and the adoption of a uniform load pattern. Moreover, also the types of failure predicted for the masonry piers are almost consistent with the ones occurring in the FE model; the different predictions of the EF models on the failure mode associated to pier P3 (hybrid or flexural) can be explained by small variations in the axial load acting in the element (see the following comparisons in terms of local response). Furthermore, in the FE model spandrel S4 is actually interested by a hybrid failure, which is correctly predicted by the EF model according to Moon et al (2006) (Figure 3.56-c).

In Figure 3.57 the damage pattern obtained with the L-tb EF model associated to the Dolce's proposal in correspondence of different values of top displacement is reported. It can be seen that in this case the predicted collapse mechanism is not a soft story at the ground floor, and that the occurred damage pattern is different from the one predicted by both the FE model and the S-tb EF models. This motivates the discrepancies in the associated pushover curve already detected in terms of global response (Figure 3.52).

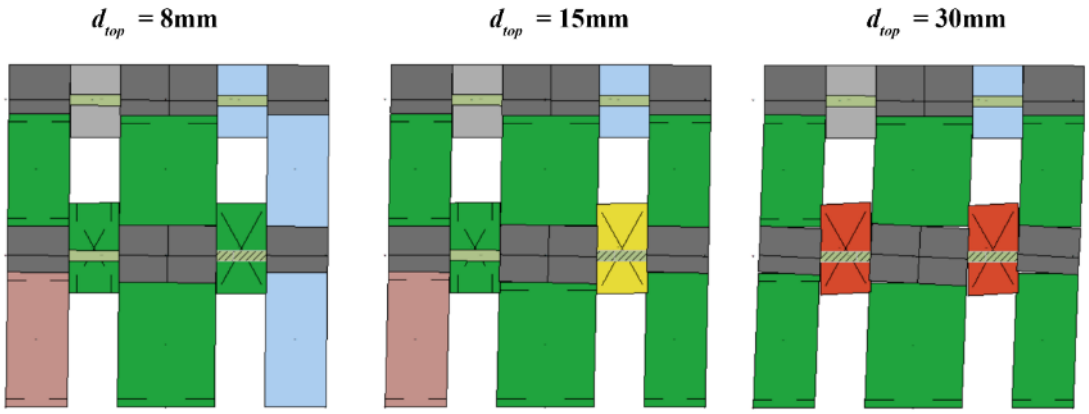

Figure 3.57 - Damage pattern in the L-tb EF model associated to the proposal by Dolce (1991) for different values of top displacement d_{top}. See Figure 3.37 for the meaning of colors and symbols.

3.3.5.3 Results in terms of local response

Concerning the comparison in terms of evolution of the reaction forces at the base sections of the wall, no significant differences between the predictions of the different EF models were detected. Some results are illustrated in Figure 3.58 and in Figure 3.59, considering, by way of example, the S-tb EF models associated, respectively, to the proposals by Augenti (2006) and Lagomarsino et al (2013).

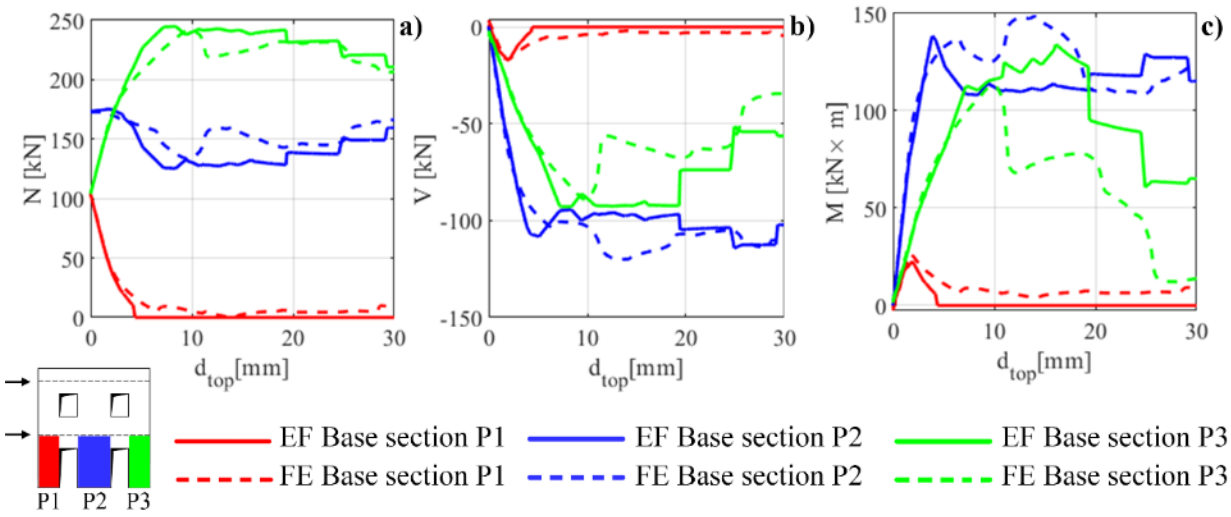

Figure 3.58. Comparison between the FE model and the S-tb EF model associated to the proposal by Augenti (2006): evolution of the a) normal force; b) shear force and c) bending moment at the base sections of the wall.

In both cases a good correspondence with the results of the FE model is observed. In particular, the redistribution of the vertical loads (Figure 3.58-a and Figure 3.59-a) among the three piers at the ground floor predicted by the two EF models provides a quite perfect match with the predictions of the FE model both in the initial response and in a more advanced nonlinear phase. With regard to shear forces and bending moments, a good agreement with the FE results is observed in the initial phase (until approximatively d_{top} = 10 mm, which corresponds for all the models to the reaching of the maximum strength, see Figure 3.52); then, more differences are detected for higher values of top displacement.

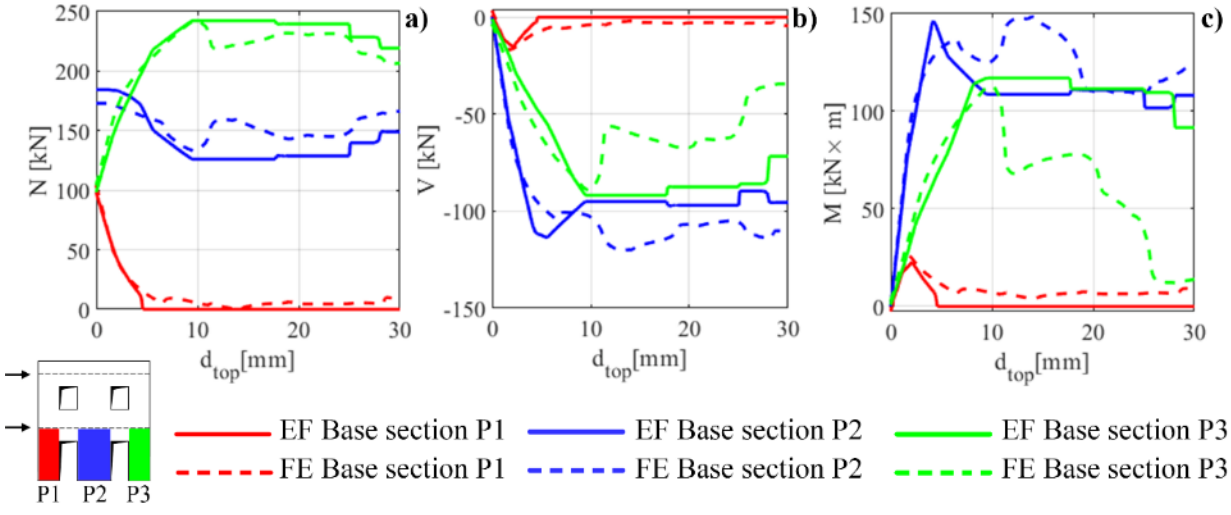

Figure 3.59 - Comparison between the FE model and the S-tb EF model associated to the proposal by Lagomarsino et al (2013): evolution of the a) normal force, b) shear force and c) bending moment at the base sections of the wall.

Regarding the comparisons in terms of generalized forces and displacements acting on the vertical and horizontal alignments identified in the wall, the same four steps introduced in the comparisons in terms of damage have been considered as reference.

In Figure 3.60 some results associated to different vertical alignments are shown, considering, as an example, the comparison between the FE model and the S-tb EF model associated to the proposal by Moon et al (2006). Moreover, in Figure 3.62 some generalized force diagrams referring to the horizontal alignments R1 and R2 are illustrated, considering this time the comparison between the FE model and the S-tb EF model associated to the proposal by Lagomarsino et al (2013).

From these results it is possible to observe a very good correspondence between the FE model and the examined EF models for all steps and especially in the case of the masonry piers (vertical alignments).

Moreover, by looking at the results of the FE model, it emerges that the wall actually behaves like a frame, allowing to distinguish the parts corresponding to the rigid nodes and those representing the pillars and the beams of the equivalent frame. Indeed, in the case of the vertical alignments (Figure 3.60) the normal force, shear force and bending moment diagrams obtained by the FE model match well with the ones derived from the EF model, which are the typical force diagrams associated to a frame structure, with a linear normal force (due to the dead loads), a constant shear force and a linear bending moment in the portions of the wall corresponding to the pillars of the frame.

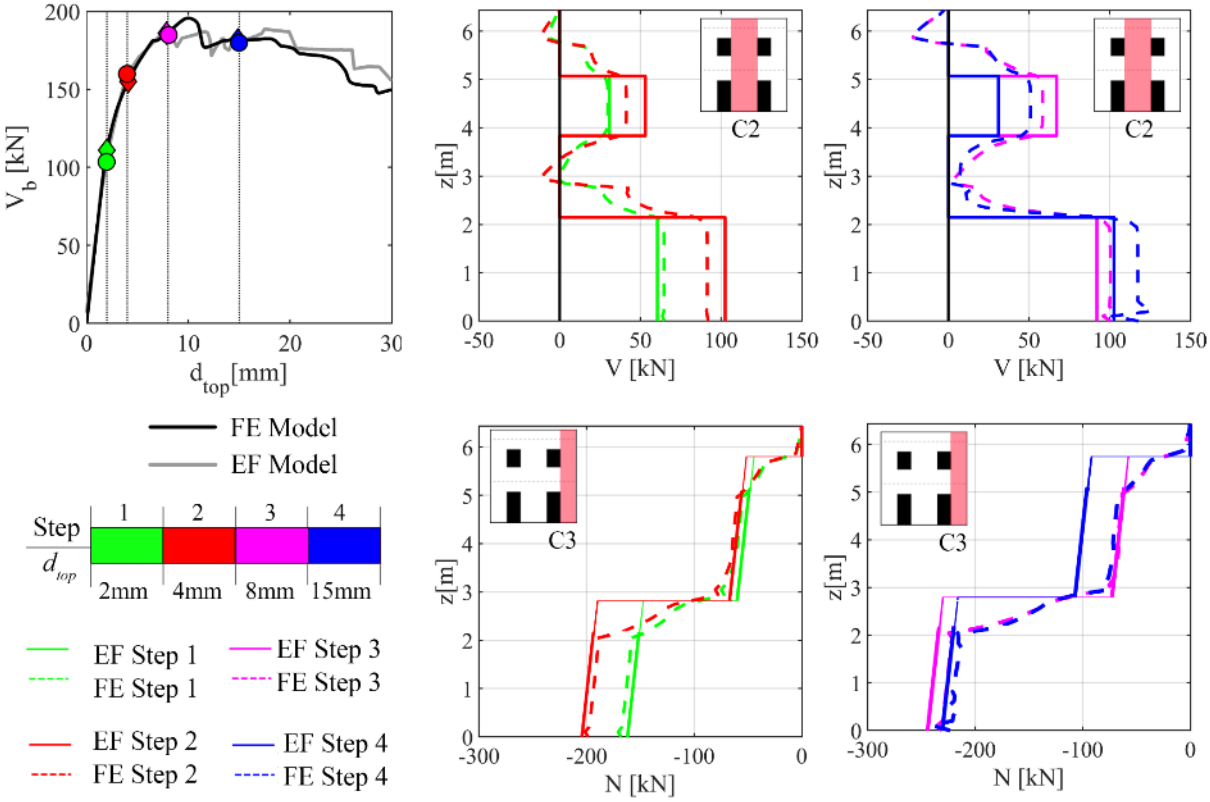

Figure 3.60 Comparison between the FE model and the S-tb EF model associated to the proposal by Moon et al (2006): normal force acting on the vertical alignment C3 and shear force acting on the vertical alignment C2 in correspondence of four fixed values of top displacement identified on the pushover curves

Moving to the generalized forces acting in the horizontal alignments, it is worth reminding that, as discussed in Chapter 1 (section 1.3), in the EF models it is in general difficult to obtain a reliable estimation of the axial load acting in the spandrels. Moreover, in the strength criteria here adopted for these elements, based on the development of a strut mechanism due to the presence of a coupled r.c. tie beam, the value of

the axial load computed during the analysis actually does not come into play (see the equation in column "spandrels" in Table 2.4).

On the other hand, it is underlined that in the FE model the axial load estimated in the cross sections of the horizontal alignments may vary depending on how the horizontal forces are applied to the wall. As an example, in Figure 3.61 it is reported a comparison between the generalized forces diagrams obtained from the FE model for alignment R1 when considering two different ways for applying the horizontal forces:

- Strategy A: the horizontal forces are "distributed" at the level of each diaphragm (i.e. they are applied on each node located at the floor level), by executing a force control analysis;
- Strategy B: the horizontal forces are applied through the introduction of a rigid isostatic beam and by progressively increasing the horizontal displacement of a node located on it (as described in section 3.3.3), in order to perform the analysis in control displacement.

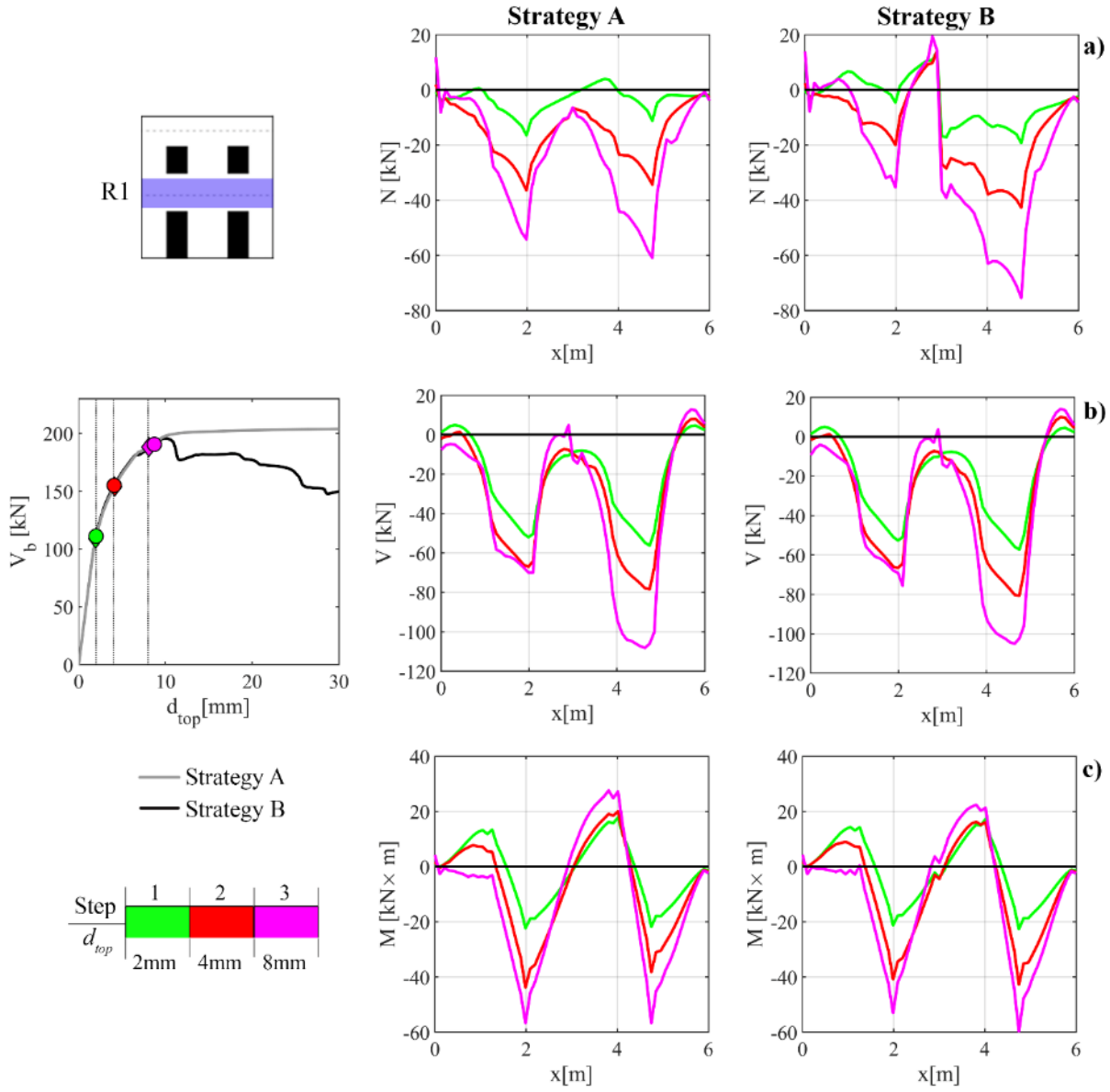

Figure 3.61- Comparison between the generalized forces diagrams (a) normal force *N*, 2) shear force *V* and 3) bending moment *M*) referring to the alignment R1 and obtained from FE models where different strategies are adopted for applying the horizontal forces (Strategy A and Strategy B).

From Figure 3.61 it is possible to observe that the distribution of the axial load is influenced by the way adopted for applying the seismic loads; nevertheless, the shear force and bending moment diagrams do not show significant differences in the two situations. This results, therefore, underlines that in this case the axial load acting on the spandrels does not substantially affect the strength of these elements.

For all the now discussed reasons, it was decided not to monitor the axial load associated to the cross sections of the horizontal alignments; therefore, in the following only the comparisons in terms of shear force and bending moment diagrams are shown.

In particular, also when considering the horizontal alignments (Figure 3.62) the generalized forces obtained from the FE model allow to identify the portions of masonry corresponding to the beams of the frame (i.e. the spandrels in the EF model). Furthermore, the differences observed between the FE model and the EF model in the shear force diagrams can be explained by considering that in the EF model the uniformly distributed vertical loads are transformed into concentrated forces acting on the nodes at the end sections of each spandrel element, thus producing a constant shear diagram. On the contrary, in the FE model this simplification is not introduced, so that the shear force diagram resulting for the horizontal alignments is linear in the portions of the wall corresponding to the spandrels.

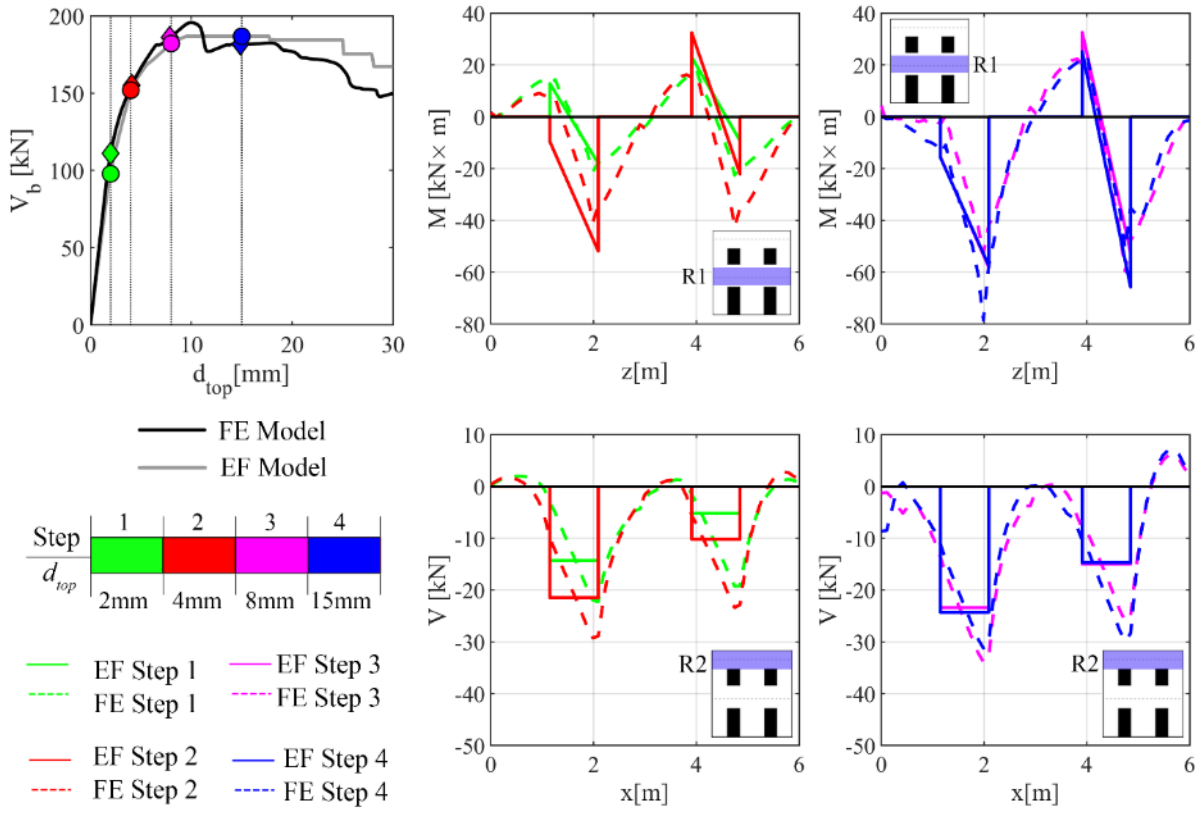

Figure 3.62. Comparison between the FE model and the S-tb EF model according to the proposal by Lagomarsino et al (2013): bending moment acting on the horizontal alignment R1 and shear force acting on the horizontal alignment R2 in correspondence of four fixed values of top displacement identified on the pushover curves.

This interpretation of the diagrams of the generalized forces resulting from the FE model allows the identification of the effective geometry of the structural elements and its comparison with that suggested by the different criteria available in the literature.

As introduced in Section 3.3.1 and confirmed by the results from FE model herein presented, in the regular wall here analysed no significant uncertainties about the identification of the spandrels are present, being the openings vertically aligned.

More interesting is the determination of the effective height of piers, on which several uncertainties may arise even in this case of a regular wall. Regarding this aspect, in the following figures the bending moment diagrams resulting from the FE model for the two vertical alignments C1 and C3 (C1-Figure 3.63; C3-Figure 3.64) are compared with the predictions of the various considered EF models. These two alignments, indeed, are the ones including the external piers, and so the most interesting, in this case of a regular wall, with regard to the determination of the effective height of the elements. The S-tb EF models are considered, being the results associated to the I-tb and L-tb EF models almost similar.

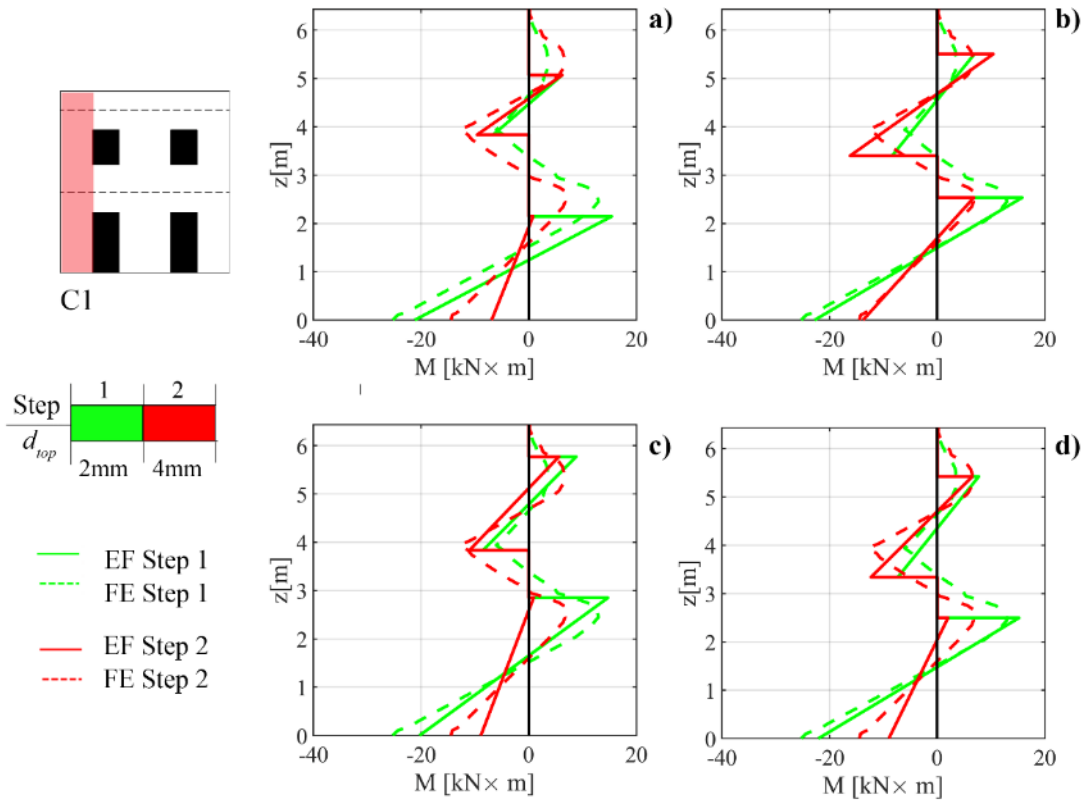

Figure 3.63- Comparison between the FE model and the S-tb EF models in terms of bending moment diagram acting on the vertical alignment C1 in correspondence of two different steps of the analysis (Step 1 – d_{top} = 2mm, and 2 – d_{top} = 4mm). EF models according to: a) Augenti (2006); b) Dolce (1991); c) Moon et al (2006); d) Lagomarsino et al (2013)

First of all, it is observed that all the examined EF models provide, in correspondence of both the alignments, bending moment diagrams which are substantially consistent with the ones computed from the FE model for all steps. However, slight differences depending on the adopted criterion for the pier effective height can be detected.

More specifically, in case of alignment C1 (Figure 3.63), the EF model associated to the criterion proposed by Dolce (1991) provides the best match with the results of the FE model when considering the pier at the ground level (P1): indeed, the predicted effective height for this pier is coincident with the one which emerges from the FE model, and also the values of bending moment acting along the pier are almost equal to the ones predicted by the FE model in case of both step 1 and step 2. All the other EF models tend to underestimate the bending moment acting in P1 in correspondence of step 2. However, they provide quite good estimates for the effective height of this pier, especially the criterion proposed in Lagomarsino et al (2013). This last, indeed, similarly to the Dolce's rule, leads to an effective height which is higher than the height of the adjacent opening. In this way it is possible to take into account the propagation of an inclined crack starting from the corner of the opening, which actually appears in the FE model, already for a top displacement equal to 2mm (Step1, see Figure 3.54 in the paragraph on the discussion of the damage pattern). On the contrary, the criterion by Augenti (2006), which does not consider this aspect, produces a slight underestimation of the effective height of the examined pier. Moving to the pier at the upper floor (P4), the predictions of all the EF models are in general almost in agreement with the results of the FE model.

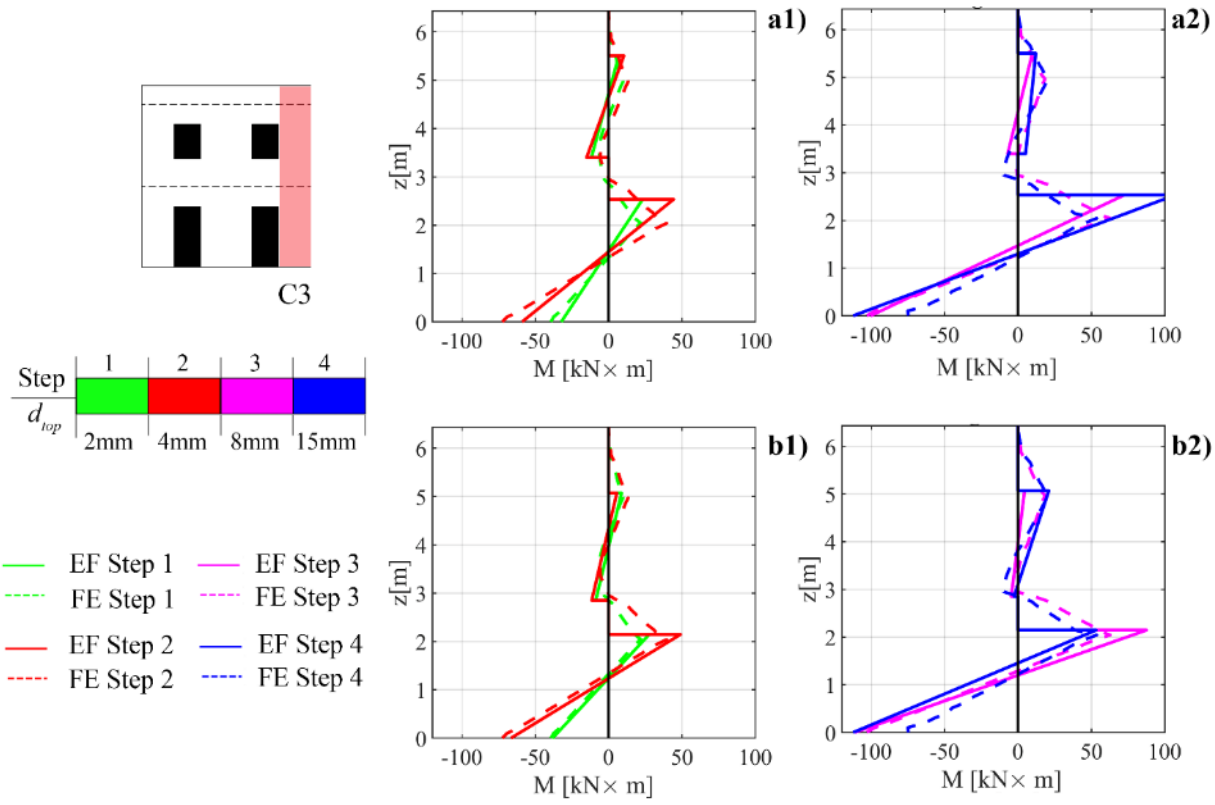

Figure 3.64 - Comparison in terms of bending moment diagram acting on the vertical alignment C3 in correspondence of 4 different steps of the analysis (1): Step 1 and 2; 2) Step 3 and 4). S-tb EF models according to: a) Dolce (1991); b) Moon et al (2006)

Focusing now the attention on the alignment C3, in Figure 3.64 the results provided by the S-tb EF models according to Moon et al (2006) and Dolce (1991) are illustrated, for all the four considered steps of the analysis. It is observed that the model according to Moon et al (2006) provides a very good match with

the predictions of the FE model in case of all the examined steps, well describing the effective height of both the pier at the ground floor (P3) and the one at the upper floor (P6). However, also the EF model by Dolce (1991) allows to obtain predictions in terms of bending moment values close to the reference solution, even if it tends to slightly overestimate the effective height of the pier at the ground floor. This can be explained by considering the damage occurred in the FE model in correspondence of this pier (P3): indeed, in this case there are no tensile cracks developing from the corners of the adjacent openings (see Figure 3.54).

The S-tb EF model by Augenti (2006) provides results similar to the one according to Moon et al (2006), while the S-tb model by Lagomarsino et al (2013) gives predictions similar to those obtained through the application of the Dolce's criterion.

Moving to the comparisons in terms of displacements, in Figure 3.65 the deformed shapes (horizontal displacements) and the rotations obtained for the vertical alignment C3 through the FE model are compared with the corresponding ones derived by considering, as an example, the EF model associated to the Dolce's criterion, both in case of short r.c. tie beams and in case of intermediate r.c. tie beams.

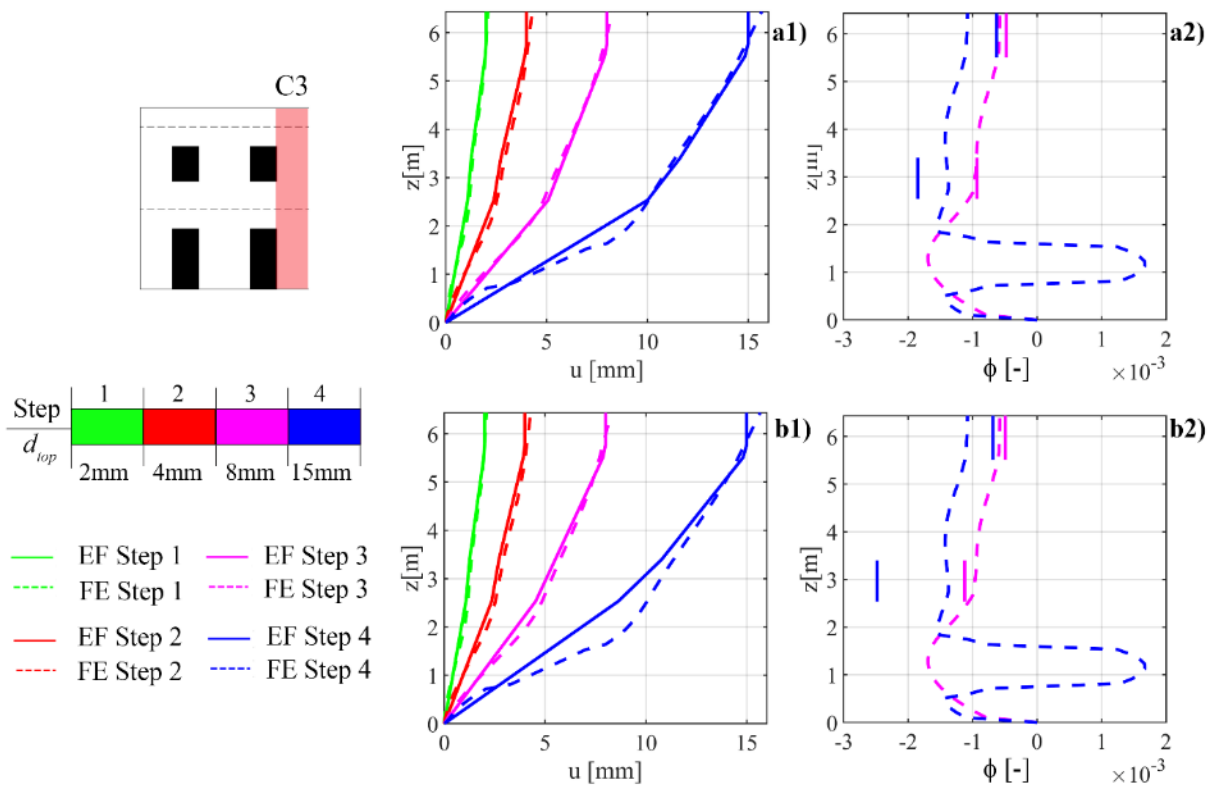

Figure 3.65 – Comparison in terms of horizontal displacements (1) and rotations (2) associated to the vertical alignment C3 in correspondence of different steps of the analysis. EF models according to Dolce (1991): a) S-tb model and b) I-tb model

It is observed that both the EF models allow to obtain a good agreement with the results of the FE model for almost all the considered steps; however, the S-tb EF model provides slightly better results in terms of horizontal displacements and also rotations, especially when considering steps 3 and 4.

Moreover, by looking at the graphs representing the rotations along the vertical alignment (Figure 3.65 – a2 and b2) it is possible to see the presence, in the FE model, of some cross sections with higher rotations with respect to the others. The comparison with the EF model, where only the results associated to the rotation of the rigid nodes are available, allows to understand that the sections with more significant rotations actually correspond to the piers in the EF model, while lower rotations are associated to the portions corresponding to rigid nodes.

Furthermore, when considering step 4, the results of the FE model show a very high concentration of deformation in the lower part of the alignment C3: this clearly indicates the formation of a plastic hinge in this portion of masonry, which corresponds to the pier at the ground floor (P3). Indeed, as it can be observed in the comparisons in terms of damage pattern (see Figure 3.54), when step 4 is reached that portion of masonry is interested by a shear failure. In the EF models the results in terms of plastic rotations along the element are not available; however, the values of rotations computed in correspondence of the rigid nodes well match the results deriving from the FE simulation.

In Figure 3.66 the vertical displacements of the alignment R1 and the rotations of the alignment R2 associated to the four considered steps are illustrated. In particular, the results of the FE model are compared, by way of example, with the S-tb EF model according to Augenti (2006).

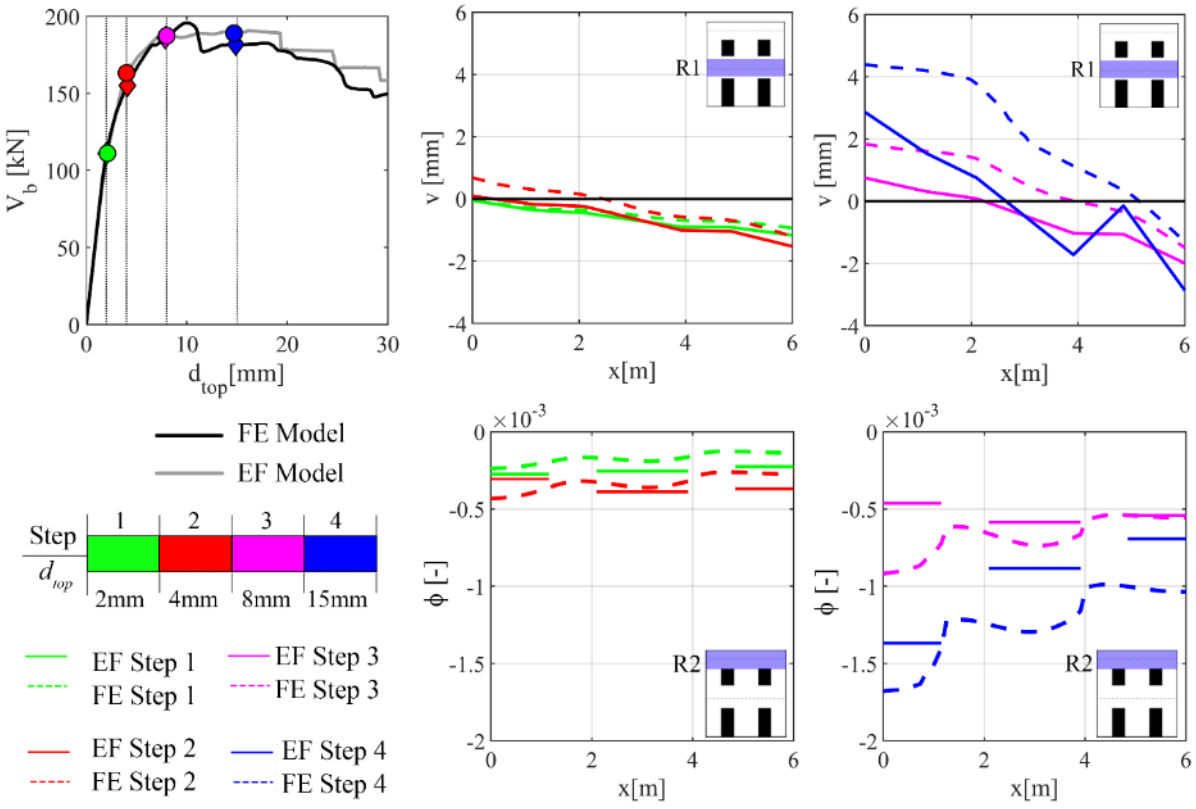

Figure 3.66 - Comparison between the FE model and the S-tb EF model according to Augenti (2006): vertical displacement of the horizontal alignment R1 and rotations associated to the horizontal alignment R2 in correspondence of different values of top displacement identified on the pushover curves.

With regard to the vertical displacements of the alignment R1, it is observed that the examined EF model is able to provide predictions which well reproduce the behavior detected by the FE model, at least for the first three steps. In correspondence of step 4 higher differences can be found, which are ascribable to a different damage condition characterizing, in the two models, the portion of masonry including the spandrels, as highlighted in the comparison in terms of damage pattern (see Figure 3.54). Similar considerations can be made about the comparisons in terms of rotations.

In general, this type of comparison confirms that in the FE model there are some portions of masonry working like rigid nodes and others which are more deformable, thus providing deformed shapes which are similar in the two models. This can be clearly seen, especially when considering the response of the model in advanced nonlinear phase (step 3 and 4).

In order to conclude the analysis about the local response, in the following some results of the comparisons in terms of drift values associated to the pier panels of the wall are reported. In particular, it is underlined that also in this case all the examined EF models were able to provide results close to the FE model, and no significant differences emerged depending on the considered effective length for the r.c. tie beams.

In Figure 3.67, as an example, the comparisons between the FE model and the S-tb EF models associated to the different criteria for the pier effective height are reported; the illustrated comparisons refer to the three piers at the ground floor (P1, P2 and P3), which in these analyses are those characterized by the most significant state of damage.

The results illustrated in Figure 3.67 clearly show a good agreement between the results of all the considered EF models and those obtained from the FE model. More specifically, it is observed that, in general, the EF models provide drift values slightly higher than the FE model, thus being on the safe side. This result can be explained by considering that in the FE model the deformation is more diffused in the wall, which is modelled as a continuum deformable material; on the contrary, in the EF models the presence of the rigid nodes inevitably produces a higher concentration of deformations in the portions of the wall were the nonlinear response is concentrated.

In addition, it emerges that, in this case of a regular wall, all the examined criteria for the definition of the pier effective height lead to similar results. In particular, the adoption of the Dolce's criterion (Figure 3.67-b) allows to obtain results very close to the ones of the FE model for all the three considered piers.

Focusing the attention on the external pier P1, the use of the criterion suggested by Augenti (2006) leads to an overestimation, with respect to the FE model, of the drift values, especially when considering steps 3 and 4: indeed, this criterion provides, when compared to the others, the shortest effective height for this pier. On the contrary, the results derived from the FE model indicates that the actual deformation associated to that masonry portion is lower, being distributed on a bigger portion of the wall. When considering the other criteria, which all take into account the possibility of the development of inclined cracks from the opening corners in case of external piers, a higher effective height is obtained, and the predictions of the associated EF models are closer to the actual deformations occurring in the corresponding masonry portion (represented by the results provided by the FE model).

Moving to the other external pier, that is P3, the criteria proposed by Dolce and by Lagomarsino et al (2013) provide results which are slightly better than the ones associated to the other two criteria. Finally,

in case of the central pier (P2), all the EF models lead to similar results, being the effective heights of this element according to the different criteria the same (the only difference is in the case of the Dolce's criterion, where a slightly higher effective height is predicted for this pier).

It is stressed that, when considering the piers at the upper floor, which are characterized in this case by lower deformations with respect to those at the ground floor, the results now discussed are in general confirmed, included the tendency on behalf of the EF models to slightly overestimate the drift values.

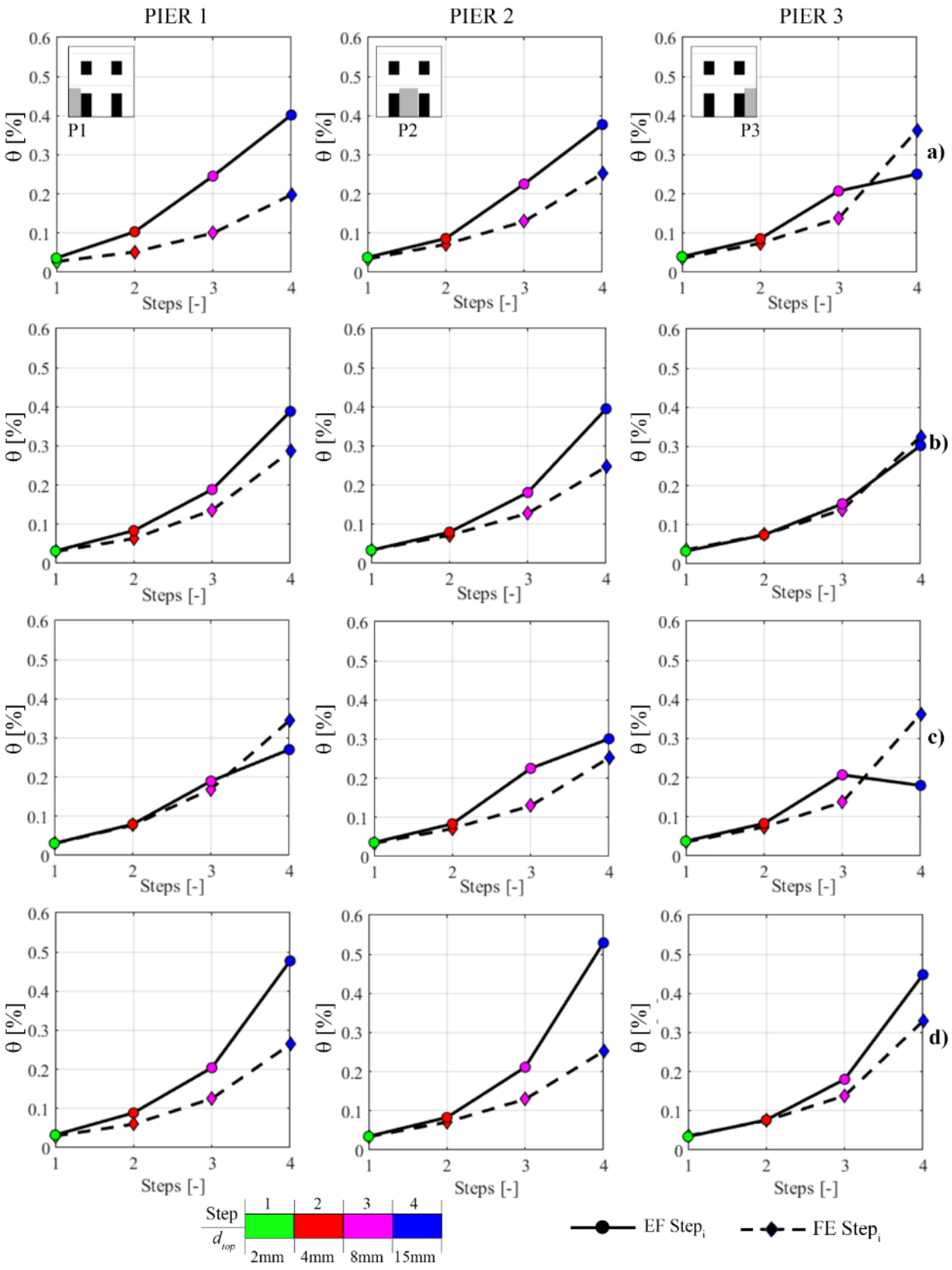

Figure 3.67 Comparisons between the FE model and the S-tb EF models in terms of drift values associated to different steps of the analysis for the 3 piers at the ground floor: a): Augenti (2006); b) Dolce (1991); c) Moon et al (2006); d) Lagomarsino et al. (2013).

3.3.6 Summary of the main outcomes

The different types of comparisons between the FE model and the examined EF models discussed in the previous section were aimed to:

i) define the effective length of the r.c. tie beams which ensures the best match with the results of the FE model. The same, then, will be used in the parametric analyses on the irregular walls (Chapter 4);
ii) evaluate the differences in the predictions of the EF models associated to the four considered criteria for the EF schematization, as well as their consistency with the results of the FE model.

With regard to point i) the illustrated results showed that the influence of the effective length of the r.c. tie beams on the predictions of the EF models is in this case quite limited, confirming the results already discussed in Chapter 2 (section 2.2.2.2). However, it was observed that the L-tb EF models are characterized by a high sensitivity of the obtained response to the criterion adopted for the pier effective height: the L-tb EF model according to Dolce (1991), in particular, leads to results which are not consistent with the ones of the FE model in terms of global pushover curve and damage pattern. Conversely, the S-tb EF models on one hand provide more stable results when varying the criterion for the effective height of piers and, on the other, lead to a slightly better description of the global response with respect to I-tb and L-tb EF models in terms of both maximum strength and post-peak phase (as confirmed by the lower scatter on the GRPs V_{max}, $d_{top,15}$ and $d_{top,30}$), well capturing the evolution of damage in the structural elements and also the final collapse mechanism. Moreover, the adoption of short r.c. tie beams in the EF models guarantees slightly better results with respect to the corresponding I-tb and L-tb EF models even in terms of local response, and in particular on the predictions about displacements and rotations, especially when considering an advanced nonlinear phase of the structural response.

For these reasons, it was decided to adopt in the following analyses an effective length of the r.c. tie beams equal to the width of the openings.

Concerning point ii), it was observed that the EF models obtained through the adoption of the different criteria for the definition of the pier effective height provide almost similar results in the case of the regular wall in terms of both global and local response; moreover, these results are close to the reference solution.

More specifically, the illustrated results showed that all the EF models, regardless the criterion adopted for the pier effective height, are able to correctly reproduce the pushover curve derived from the FE analysis in terms of progressive stiffness degradation, maximum strength and post-peak response and also the associated damage pattern, well capturing the final collapse mechanism.

Furthermore, it was observed that in the FE model the wall subjected to the horizontal forces actually behaves like a frame, allowing to distinguish the portions corresponding to the rigid nodes and those representing the pillars and the beams of the corresponding equivalent frame. As a consequence, in the case of the vertical alignments the bending moment diagram is linear in the portions of the wall corresponding to the pillars of the frame (the piers in the EF model), thus allowing the identification of the effective height of piers and its comparison with that suggested by the different adopted criteria. This comparison, in particular, showed that all the adopted criteria for the pier effective height allow to obtain predictions in terms of generalized forces substantially consistent with the results of the FE model; however, when

considering the external piers, the criteria proposed by Lagomarsino et al (2013) and by Dolce (1991), which take into account the possibility of the development of inclined cracks starting from the opening corners, provide in general a better match with the FE model, especially when considering the structural response in advanced nonlinear phase, as confirmed also by the comparisons in terms of damage pattern and drift values associated to the masonry panels.

Finally, the comparisons in terms of displacements was useful to see that in the FE models there are some portions of masonry working like rigid nodes and others more deformable, thus providing deformed shapes which are similar, both qualitatively and quantitatively, to the ones described through the EF models.

Concluding, all the discussed results confirm the capability of the EF model to correctly predict the seismic response of a regular masonry wall, even in presence of slight uncertainties in the identification of the effective height of masonry piers. Moreover, the application of the introduced methodological approach to this first configuration actually demonstrated the effectiveness of the method in realizing an in-depth investigation of all the aspects characterizing the response of the analysed structure.

CHAPTER 4

4 ANALYSIS OF IRREGULAR URM WALLS

In this chapter the analyses carried out on the wall configurations with an irregular opening pattern are discussed. Firstly, (sections 4.1 and 4.2) the case studies and the associated numerical models are presented, and then (section 4.3) some specifications about the criteria adopted for the comparisons are provided. Finally, the results of the nonlinear analyses are illustrated (section 4.4).

4.1 CASE STUDIES DESCRIPTION

The irregular wall configurations were defined starting from the geometry of the regular wall (described in section 3.3.1) and introducing different types of irregularities in the opening pattern. As highlighted in figure 4.1, this was realized by varying the dimensions and the position of two openings: one of the doors at the ground floor (indicated as "OP-1_R" in Figure 4.1) and the corresponding window at the upper floor (indicated as "OP-1_R" in Figure 4.1).

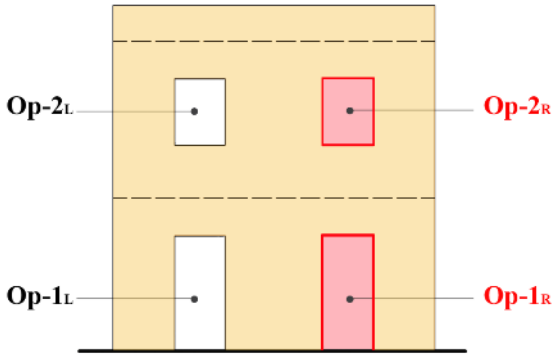

Figure 4.1 – Indication of the openings of the regular wall whose position and dimensions are varied in order to obtain different irregular opening layout.

In this way, nine different case study structures were obtained, as illustrated in Figure 4.2.

According to the classification proposed in Parisi and Augenti (2013) (discussed in section 1.3.2 – see Figure 1.18), the obtained types of irregularity can be summarized as follows (each one denoted with a specific letter):

- *offset irregularity*, indicated with letter A in case of offset irregularity in the horizontal direction (i.e. vertically misaligned openings) and with letter C in case of offset irregularity in the vertical direction (i.e. horizontally misaligned openings);
- *horizontal irregularity*, indicated with letter B;
- *vertical irregularity*, indicated with letter D;
- *different number of openings per storey*, indicated with letter E.

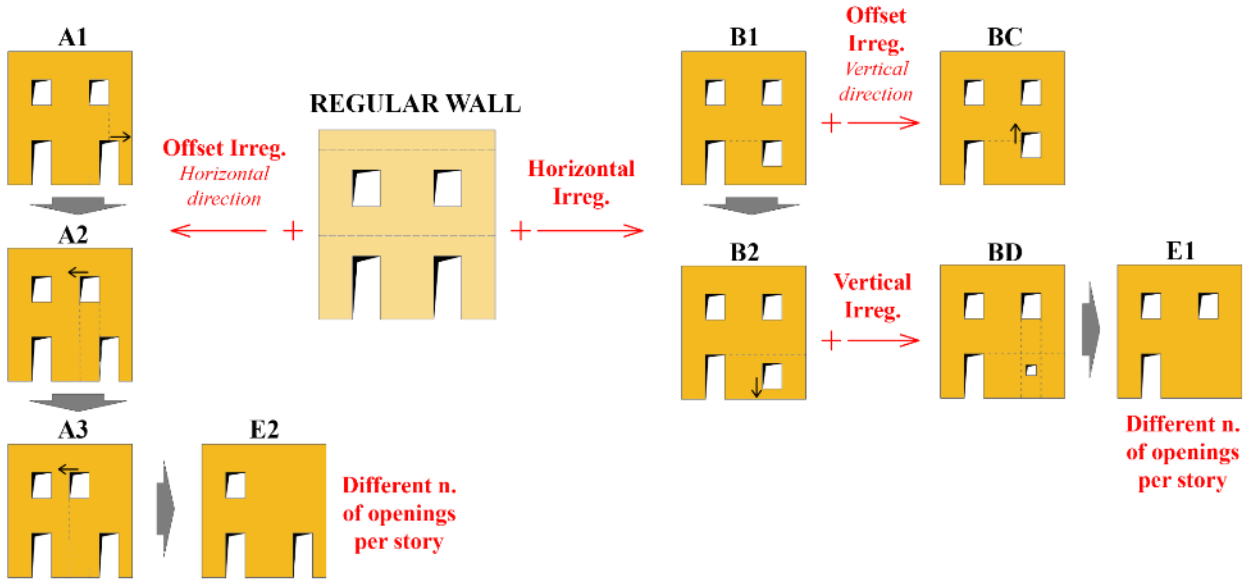

Figure 4.2 - Analysed irregular wall configurations (types of irregularity according to Parisi and Augenti (2013)).

In such way, the name of each configuration (indicated in bold in Figure 4.2) reflects the types of irregularity that characterize it. It is underlined that in some configurations different types of irregularity are present together. Furthermore, when more than one configuration presents the same type of irregularity, a number is added to the names of the corresponding case studies (e.g. A1, A2, A3).

The problems the identified configurations were meant to explore are (Figure 4.3):

- **Problem 1** - identification of the pier geometry in presence of openings with different heights at the same storey (horizontal irregularity, see Figure 4.3-a);
- **Problem 2** - presence of very little openings (Figure 4.3-b);
- **Problem 3** - identification of the spandrels in presence of vertically misaligned openings or a different number of openings per storey (Figure 4.3-c).

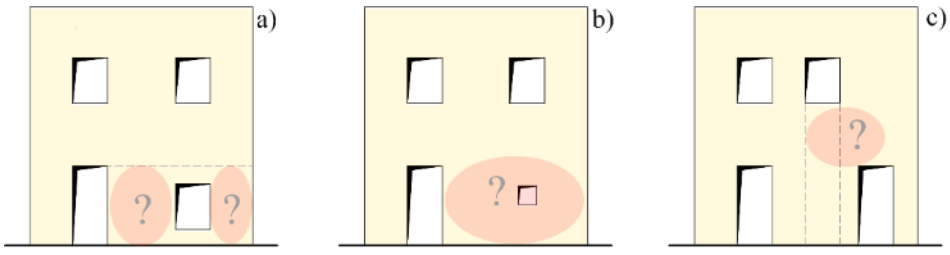

Figure 4.3 – Critical issues for the EF idealization associated to different types of irregularities in the opening pattern: a) effective height of piers in presence of horizontal irregularity; b) presence of little openings; c) identification of spandrels in presence of vertically misaligned openings.

More in detail, the configurations of type “B” (B1, B2, BC) are aimed to deepen Problem 1 (Figure 4.3-a). Configuration B1 is produced by transforming the door at the ground floor of the regular wall (indicated

as OP-1_R in Figure 4.1) into a window; then, by moving down this window configuration B2 is obtained, while by moving it up (i.e. adding *offset irregularity* in the vertical direction) configuration BC is produced.

Furthermore, by introducing vertical irregularity, it is possible to obtain configuration BD, which is interesting in order to deepen Problem 2 (Figure 4.3-b), that is very common in the existing buildings. The crucial aspect in these situations is if it may be more correct, when the opening is very little, to neglect it in the structural model; indeed, the observation of masonry buildings damaged by past earthquakes often shows that the inclination of the cracks seems to ignore the presence of the very little openings (Figure Figure 4.4).

Figure 4.4 – Damage detected in a masonry wall with a little opening after the earthquake in central Italy (2016, Preci, PG); the cracks, which seem to neglect the little opening, are highlight in red.

The configurations of type "A" (A1, A2, A3) were introduced in order to explore the modelling of the portion of masonry between two vertically misaligned openings (Problem 3 – Figure 4.3-c). In these situations, indeed, due to the vertical misalignment between the openings at the two levels, the definition of the spandrel between them represents the most critical issue for the EF idealization. Thereby, in this case the idea is to understand if the spandrel has or not to be considered in the EF model, as a function of the entity of the misalignment between the two openings. To this aim, different irregularity levels are considered, by progressively shifting the openings at the two stories (*offset irregularity* in the horizontal direction): in configuration A1 there is still an overlapping part between the two openings, in A3 there is no overlapping at all and A2 represents the transition situation between the presence and the absence of an overlapping between the two openings, which are aligned only in correspondence of one edge. Moreover, also the two configuration of type "E" (E1, E2) are useful in order to investigate the above mentioned issue. Indeed, they present a different number of openings per storey, and can therefore be considered as extreme cases of vertical misalignment between the openings at two consecutive levels, in which the opening at one

of the stories is missing. This type of irregularity is usually treated in the EF idealization with the introduction of a unique rigid node above/below the pier where the opening is missing, but studies confirming such an approximation are still lacking.

Specifications on the geometry of the introduced wall configurations are provided in Figure 4.5.

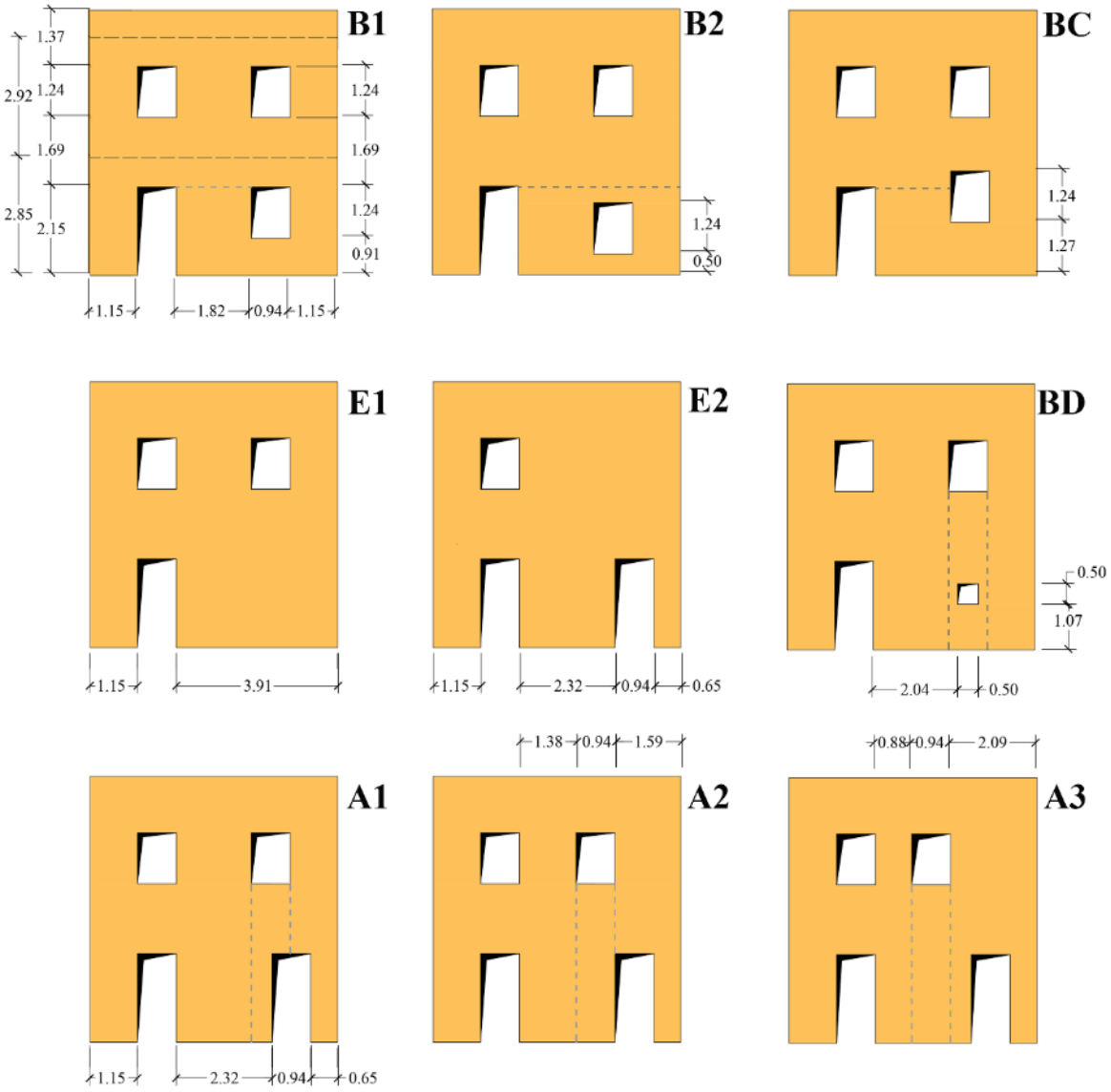

Figure 4.5- Geometry of the irregular wall configurations (measures in meters).

Regarding the structural details, like the regular wall these configurations are provided with r.c. tie beams at each level, thus promoting a *strong spandrel – weak pier* behavior type, where the response is mainly governed by piers. This hypothesis allows to better deepen Problems 1 and 2, which are connected to the identification of the geometry of these elements. Moreover the spandrels, even if resistant, in these configurations come into play as deformable elements, so that it is possible to make some considerations

about their identification in these terms, with the aim to provide indications which may be useful for the specific cases here analysed.

The mechanical properties of the materials (in case of both masonry and r.c. tie beams) as well as the vertical loads transferred by the lower and upper floors are the same adopted for the regular wall.

4.2 NUMERICAL MODELS

According to the adopted methodological approach (described in Chapter 3), for each introduced case study structure a FE model and different EF models (characterized by different geometries for the structural elements) were defined.

In particular, the FE models of the irregular walls were realized exactly in the same way as in the case of the regular wall, by simply changing the position and the dimensions of the openings. As far as the modelling of the r.c. tie beams is concerned, on the basis of the results of the preliminary analyses performed on the regular wall, in all the EF models the effective length of these elements is assumed equal to the net width of the corresponding opening (short r.c. tie beams – S-tb).

Moreover, with regard to the mesh characterizing the models, for the brick elements the same reference dimensions used in the regular wall were adopted: in particular, the 8-node elements have, in all the configurations, an approximate size of 10x10x12.5 cm, compatibly with the geometry of each wall and with the necessity to have nodes located on fixed alignments (i.e. at the level of the two diaphragms and also in correspondence of the alignments identified in each wall for the computation of the generalized forces through the integration of the nodal stresses, as illustrated in the following section). This mesh dimension, indeed, was proved to provide robust results in the analyses carried out on the regular wall (Appendix A).

The different EF models associated to each irregular configuration were obtained through the application of the same criteria for the identification of the structural elements adopted for the regular wall; in particular:

- the proposals by Augenti (2006), Dolce (1991), Moon et al (2006) and Lagomarsino et al (2013) for the definition of the effective height of piers;
- the empirical criterion proposed in Lagomarsino et al (2013) for the identification of spandrels.

Concerning the issue related to the identification of spandrels, the most significant uncertainties arise when considering the configurations of type "A". In this case, in fact, the above mentioned empirical rule predicts the presence of the spandrel in case of configuration A1 and the absence of this element in case of A3, while A2 actually represents the transition between these two options, being the openings at the two levels aligned only in correspondence of one edge. For this reason, being configurations A2 and A3 characterized by more uncertainties in the identification of the effective geometry of the spandrel, in these two cases two different modelling options were considered:

i) absence of the spandrel, substituted by a unique rigid node (EF models $A2_{NS}$ and $A3_{NS}$, where "NS" means "No Spandrel");

ii) presence of a spandrel with an effective length equal to the average width of the openings at the two levels and symmetrically located with respect to them (EF models $A2_{WS}$ and $A3_{WS}$, where "WS" stays for "With Spandrel").

The different EF idealizations obtained according to the above illustrated logic for each wall configuration are illustrated in the following, together with the information about the associated geometry of the structural elements (from Table 4.1 to Table 4.9). In particular, the data collected in the following tables refer only to piers, which are the elements whose geometry is subjected to the most significant modifications from one configuration to the other and according to the four considered criteria; conversely, spandrels geometry is almost the same in all the examined configurations. The numbering adopted for the identification of the structural elements is illustrated in Figure 4.6.

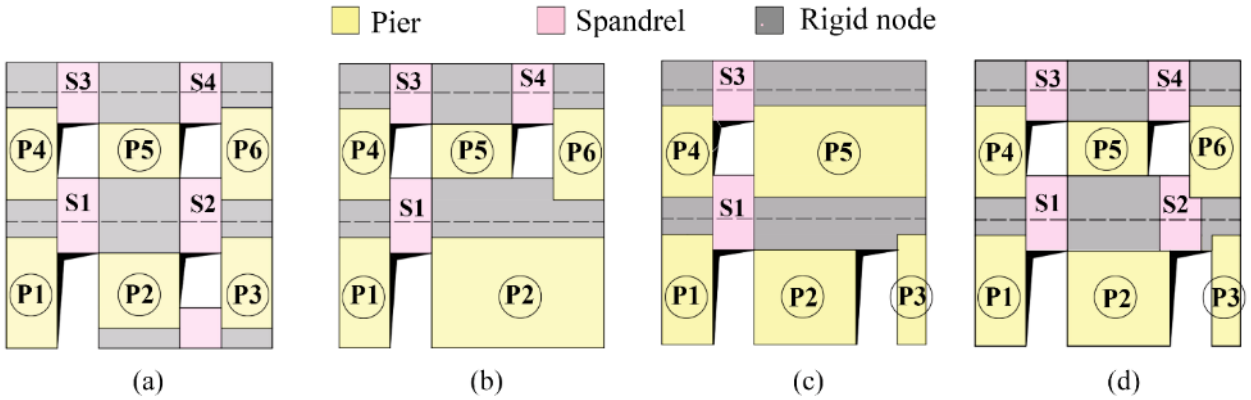

Figure 4.6 – Element numbering adopted for the structural elements of the introduced configurations: (a) walls of type "B"; (b) configuration E1; (c) configuration E2; (d) walls of type "A".

Table 4.1 – Adopted EF idealizations and data of the piers geometry in configuration B1.

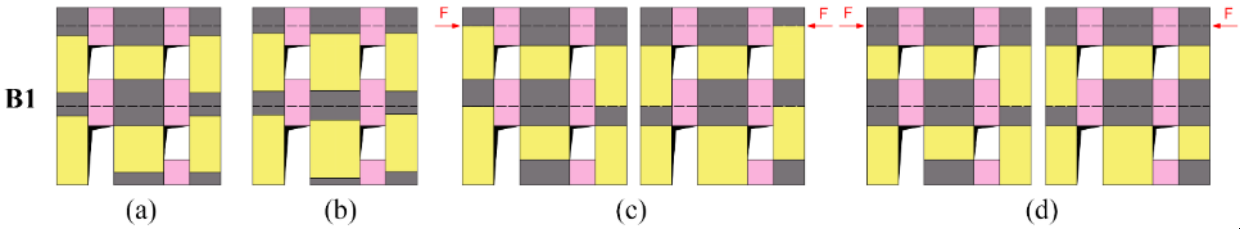

B1			(a) Lagomarsino et al. (2013)	(b) Dolce (1991)	(c) Moon et al (2006)		(d) Augenti (2006)	
					Pos	Neg	Pos	Neg
1st storey	P1	h_{eff} [m]	2.50	2.54	2.85	2.15	2.15	2.15
		λ [-]	2.17	2.20	2.48	1.87	1.87	1.87
	P2	h_{eff} [m]	1.69	2.11	1.24	2.15	1.24	2.15
		λ [-]	0.93	1.16	0.68	1.18	0.68	1.18
	P3	h_{eff} [m]	2.04	2.09	2.15	1.94	2.15	1.24
		λ [-]	1.78	1.82	1.87	1.69	1.87	1.07
2nd storey	P4	h_{eff} [m]	2.08	2.11	1.94	2.22	1.24	2.22
		λ [-]	1.81	1.83	1.68	1.93	1.07	1.93
	P5	h_{eff} [m]	1.24	2.06	1.24	1.24	1.24	1.24
		λ [-]	0.68	1.13	0.68	0.68	0.68	0.68
	P6	h_{eff} [m]	2.08	2.11	2.22	1.94	2.22	1.24
		λ [-]	1.81	1.83	1.93	1.68	1.93	1.07

Table 4. 2 – Adopted EF idealizations and data of the piers geometry in configuration B2.

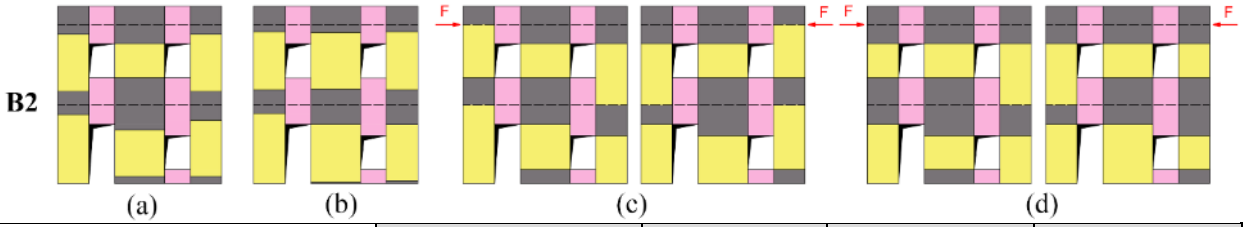

B2			(a) Lagomarsino et al. (2013)	(b) Dolce (1991)	(c) Moon et al. (2006)		(d) Augenti (2006)	
					Pos	Neg	Pos	Neg
1st storey	P1	h_{eff} [m]	2.50	2.54	2.15	2.15	2.15	2.15
		λ [-]	2.17	2.20	1.87	1.87	1.87	1.87
	P2	h_{eff} [m]	1.69	2.10	1.65	1.74	1.24	2.15
		λ [-]	0.93	1.16	0.90	0.95	0.68	1.18
	P3	h_{eff} [m]	2.04	2.04	1.74	2.35	1.74	1.24
		λ [-]	1.78	1.77	1.51	2.04	1.51	1.07
Notes: the geometry of P4, P5 and P6 is the same as in configuration B1								

Table 4.3 – Adopted EF idealizations and data of the piers geometry in configuration BC.

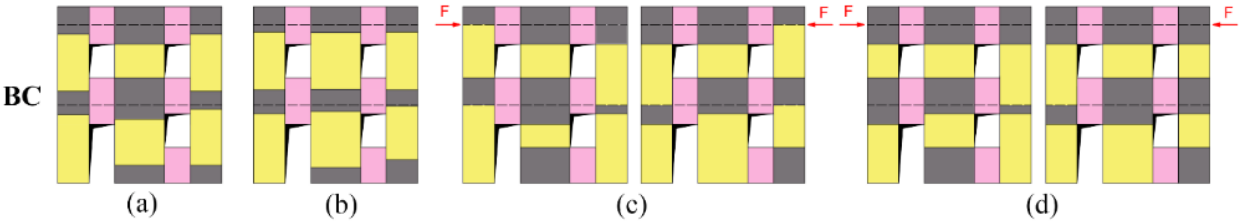

BC			(a) Lagomarsino et al. (2013)	(b) Dolce (1991)	(c) Moon et al. (2006)		(d) Augenti (2006)	
					Pos	Neg	Pos	Neg
1st storey	P1	h_{eff} [m]	2.50	2.54	2.85	2.15	2.15	2.15
		λ [-]	2.17	2.20	2.48	1.87	1.87	1.87
	P2	h_{eff} [m]	1.69	2.04	0.85	2.54	1.24	2.15
		λ [-]	0.93	1.12	0.46	1.39	0.68	1.18
	P3	h_{eff} [m]	2.04	1.95	2.54	1.55	2.54	1.24
		λ [-]	1.78	1.70	2.20	1.35	2.20	1.07
Notes: the geometry of P4, P5 and P6 is the same as in configuration B1								

Table 4.4– Adopted EF idealizations and data of the piers geometry in configuration BD.

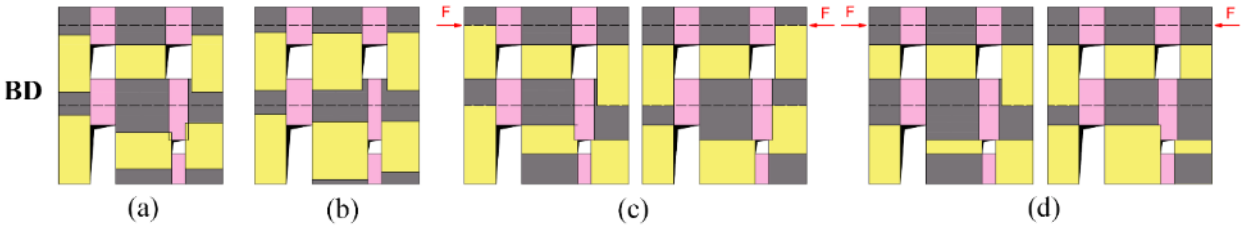

BD			(a) Lagomarsino et al. (2013)	(b) Dolce (1991)	(c) Moon et al (2006)		(d) Augenti (2006)	
					Pos	Neg	Pos	Neg
1st storey	P1	h_{eff} [m]	2.50	2.54	2.85	2.15	2.15	2.15
		λ [-]	2.17	2.20	2.48	1.87	1.87	1.87
	P2	h_{eff} [m]	1.32	2.11	1.05	1.60	0.50	2.15
		λ [-]	0.65	1.03	0.51	0.78	0.25	1.05
	P3	h_{eff} [m]	1.68	1.84	1.60	1.75	1.60	0.50
		λ [-]	1.22	1.35	1.17	1.28	1.17	0.37
Notes: the geometry of P4, P5 and P6 is the same as in configuration B1								

Table 4.5– Adopted EF idealizations and data of the piers geometry in configuration E1.

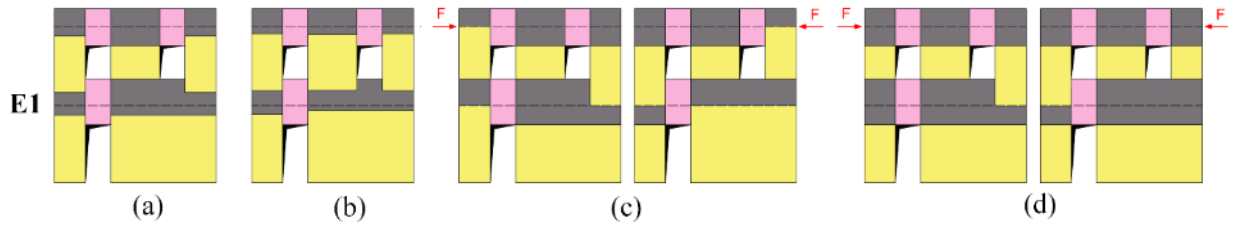

E1			(a) Lagomarsino et al. (2013)	(b) Dolce (1991)	(c) Moon et al (2006)		(d) Augenti (2006)	
					Pos	Neg	Pos	Neg
1st storey	P1	h_{eff} [m]	2.50	2.54	2.15	2.15	2.15	2.15
		λ [-]	2.17	2.20	1.87	1.87	1.87	1.87
	P2	h_{eff} [m]	2.50	2.68	2.15	2.85	2.15	2.15
		λ [-]	0.64	0.69	0.55	0.73	0.55	0.55
Notes: the geometry of P4, P5 and P6 is the same as in configuration B1								

Table 4.6 – Adopted EF idealizations and data of the piers geometry in configuration E2.

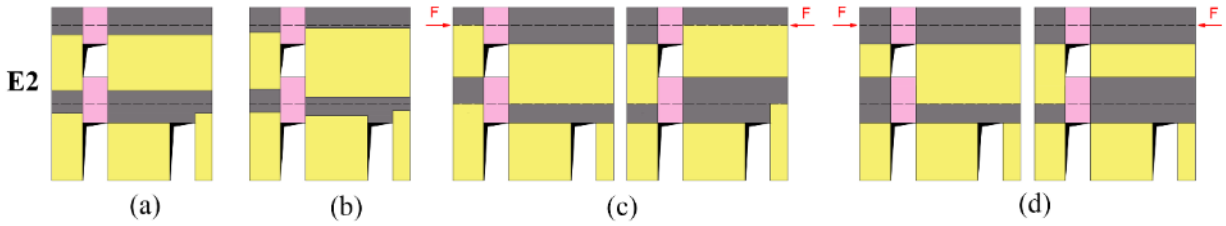

E2			(a) Lagomarsino et al. (2013)	(b) Dolce (1991)	(c) Moon et al (2006)		(d) Augenti (2006)	
					Pos	Neg	Pos	Neg
1st storey	P1	h_{eff} [m]	2.50	2.54	2.85	2.15	2.15	2.15
		λ [-]	2.17	2.20	2.48	1.87	1.87	1.87
	P2	h_{eff} [m]	2.15	2.40	2.15	2.15	2.15	2.15
		λ [-]	0.92	1.03	0.92	0.92	0.92	0.92
	P3	h_{eff} [m]	2.50	2.59	2.15	2.85	2.15	2.15
		λ [-]	3.84	3.99	3.30	4.38	3.30	3.30
2nd storey	P4	h_{eff} [m]	2.08	2.11	1.94	2.22	1.24	2.22
		λ [-]	1.81	1.83	1.68	1.93	1.07	1.93
	P5	h_{eff} [m]	2.08	2.56	2.22	1.94	2.22	1.24
		λ [-]	0.53	0.66	0.57	0.49	0.57	0.32

Table 4.7 – Adopted EF idealizations and data of the piers geometry in configuration A1.

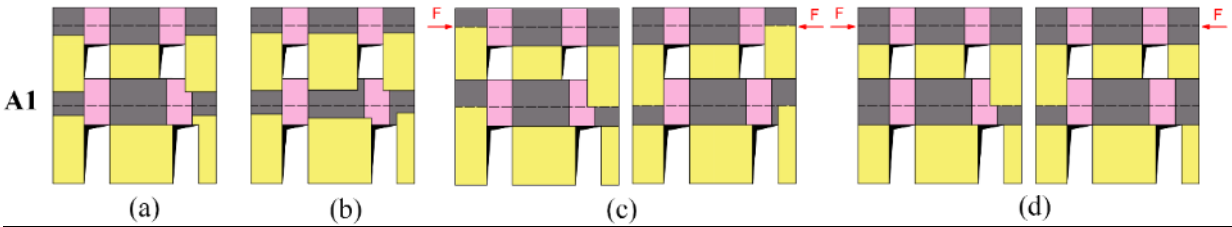

A1			(a) Lagomarsino et al. (2013)	(b) Dolce (1991)	(c) Moon et al (2006)		(d) Augenti (2006)	
					Pos	Neg	Pos	Neg
1st storey	P1	h_{eff} [m]	2.50	2.54	2.15	2.15	2.15	2.15
		λ [-]	2.17	2.20	1.87	1.87	1.87	1.87
	P2	h_{eff} [m]	2.15	2.40	2.15	2.15	2.15	2.15
		λ [-]	0.92	1.03	0.92	0.92	0.92	0.92
	P3	h_{eff} [m]	2.50	2.59	2.15	2.85	2.15	2.15
		λ [-]	3.84	3.99	3.30	4.38	3.30	3.30
Notes: the geometry of P4, P5 and P6 is the same as in configuration B1.								

Table 4.8– Adopted EF idealizations and data of the piers geometry in configuration A2.

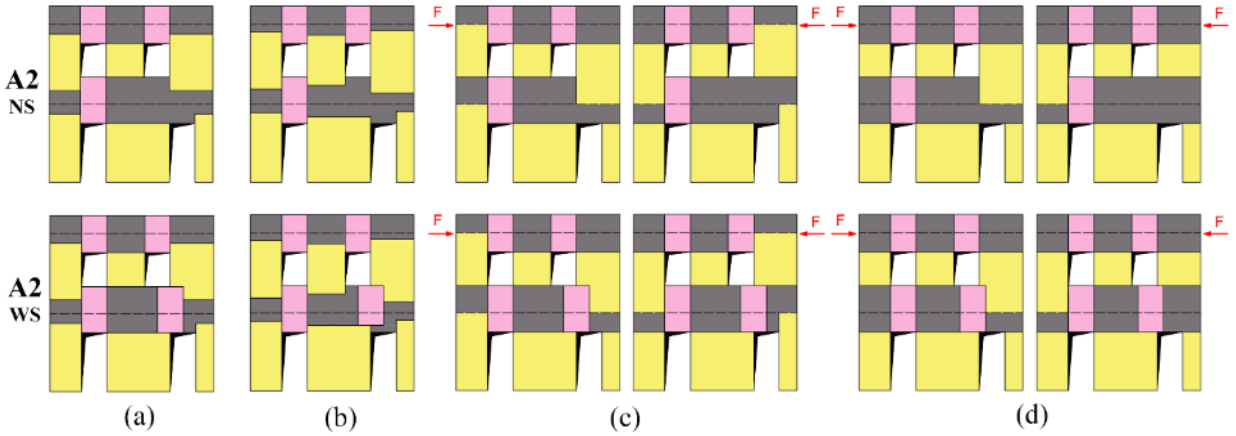

A2			(a) Lagomarsino et al (2013)	(b) Dolce (1991)	(c) Moon et al (2006)		(d) Augenti (2006)	
					Pos	Neg	Pos	Neg
2nd storey	P4	h_{eff} [m]	2.08	2.11	1.94	2.22	1.24	2.22
		λ [-]	1.81	1.83	1.68	1.93	1.07	1.93
	P5	h_{eff} [m]	1.24	1.84	1.24	1.24	1.24	1.24
		λ [-]	0.89	1.33	0.89	0.89	0.89	0.89
	P6	h_{eff} [m]	2.08	2.28	2.22	1.94	2.22	1.24
		λ [-]	1.31	1.44	1.40	1.22	1.40	0.78
Notes: the geometry of P1, P2 and P3 is the same as in configuration A1.								

Table 4.9– Adopted EF idealizations and data of the piers geometry in configuration A3.

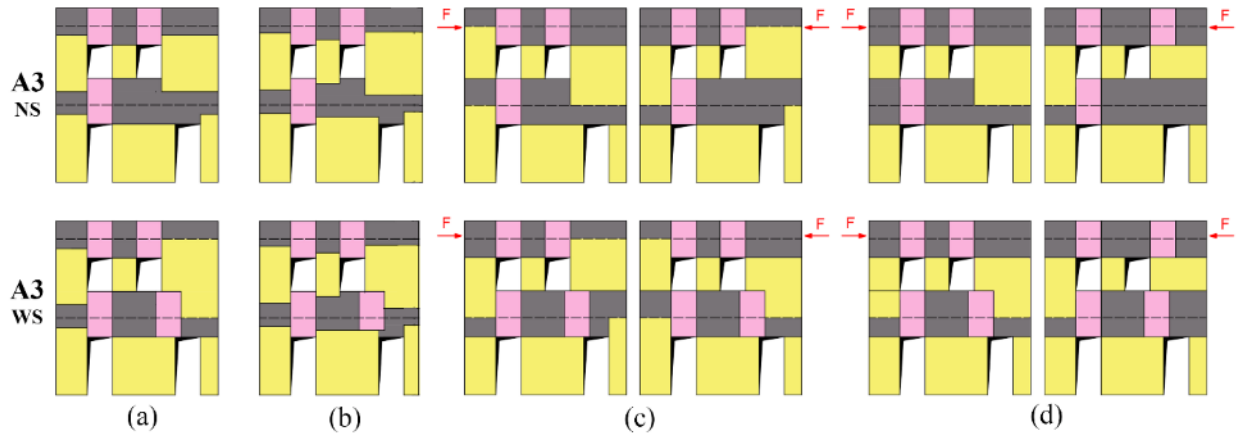

A3			(a) Lagomarsino et al. (2013)	(b) Dolce (1991)	(c) Moon et al (2006)		(d) Augenti (2006)	
					Pos	Neg	Pos	Neg
2nd storey	P4	h_{eff} [m]	2.08	2.11	1.94	2.22	1.24	2.22
		λ [-]	1.81	1.83	1.68	1.93	1.07	1.93
	P5	h_{eff} [m]	1.24	1.62	1.24	1.24	1.24	1.24
		λ [-]	1.40	1.84	1.40	1.40	1.40	1.40
	P6	h_{eff} [m]	2.08	2.33	2.22	1.94	2.22	1.24
		λ [-]	0.99	1.12	1.06	0.93	1.06	0.59
Notes: the geometry of P1, P2 and P3 is the same as in configuration A1.								

The data reported in Figure 4.7, which represent the ratios between the pier effective height h_{eff} and the interstorey height h_w are useful to give an idea of the variations which may occur in the geometry of these elements when adopting different rules for the EF idealization. In particular, it comes out that in the configurations of type "A" (see as for example the data referring to A3 in Figure 4.7) the differences in the piers geometry are mainly about those at the upper storey, while for the elements at the ground floor less differences are detected. Conversely, in case of the configurations of type "B" (see as for example configuration B1 and BC in Figure 4.7), the presence of the horizontal irregularity at the ground floor causes not negligible differences in the resulting effective height for piers when applying the considered rules for their identification. These discrepancies, in particular, are even more evident when moving to configuration BD, especially in case of P2, and are associated also to very different values of aspect ratio λ (which range from a minimum of 0.25 to a maximum of 1.05, see Table 4.4). As a consequence, these elements are expected to show different types of responses in terms of stiffness, strength and also displacement capacity when subjected to horizontal forces.

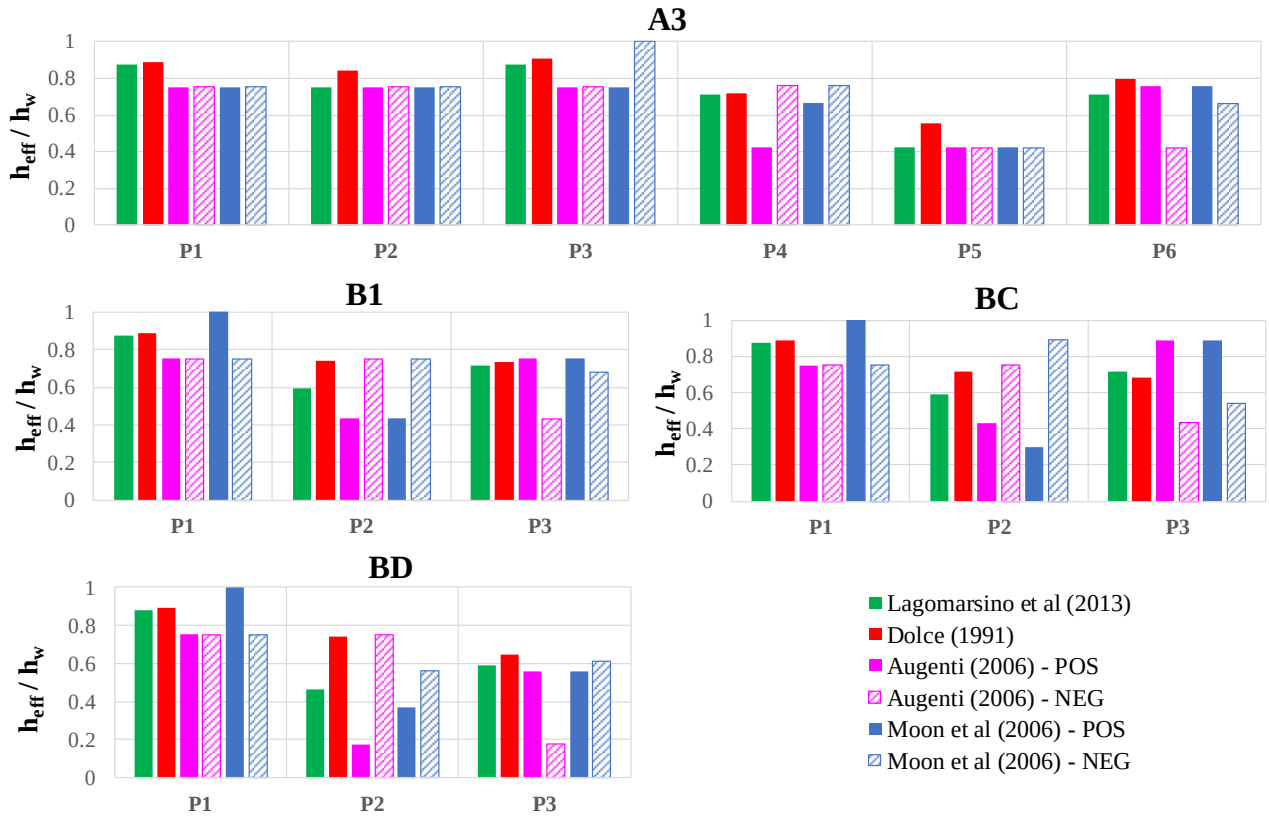

Figure 4.7 – Ratio between the effective height of piers (h_{eff}) defined according to the different considered criteria and the interstorey height (h_w) in some of the analysed wall configurations.

The nonlinear static analyses were performed, for each configuration, on the different introduced structural models, according to the same procedure followed in the case of the regular wall. In particular, a uniform load pattern was adopted. As already discussed in section 3.3.3, in the FE models the application of the defined load pattern was realized through the introduction of a rigid beam with the end sections located at the level of the diaphragms and linked to the nodes of the wall mesh in order to obtain an isostatic system (see Figure 3.32); moreover, for each configuration it was necessary to properly define the position

on this beam of the node to which apply the incremental horizontal displacement, depending on the seismic masses located at each story and according to equation 3.8.

Differently from the regular case, here the nonlinear static analyses were performed by considering, for each configuration, both the positive and the negative verse. It is stressed that in the case of the criteria suggested by Moon et al (2006) and by Augenti (2006) the geometry of the pier elements changes depending on the direction of the analyses, so that different structural models have to be used, depending on the direction of the applied seismic forces (as illustrated also in the previous Tables from 4.1 to 4.9).

4.3 CRITERIA ADOPTED FOR THE COMPARISONS

In general, the same types of comparisons introduced in the case of the regular wall (see section 3.3.4) were performed between the results of the FE and of the EF models.

Regarding the comparison in terms of generalized forces and displacements acting on specific sections of the walls, due to the irregularity characterizing these configurations it is necessary to identify, for each one of them, specific horizontal and vertical alignments whose cross sections will be considered for the computation of such forces and displacements. The alignments identified to this aim in the examined walls are illustrated in Figure 4.8, Figure 4.9 and Figure 4.10. In these figures, in particular, the bold lines associated to each alignment indicate the position of the reference point that was considered, in the corresponding cross sections, for the computation of the bending moment; the chosen reference points are represented by the centroid of each cross section.

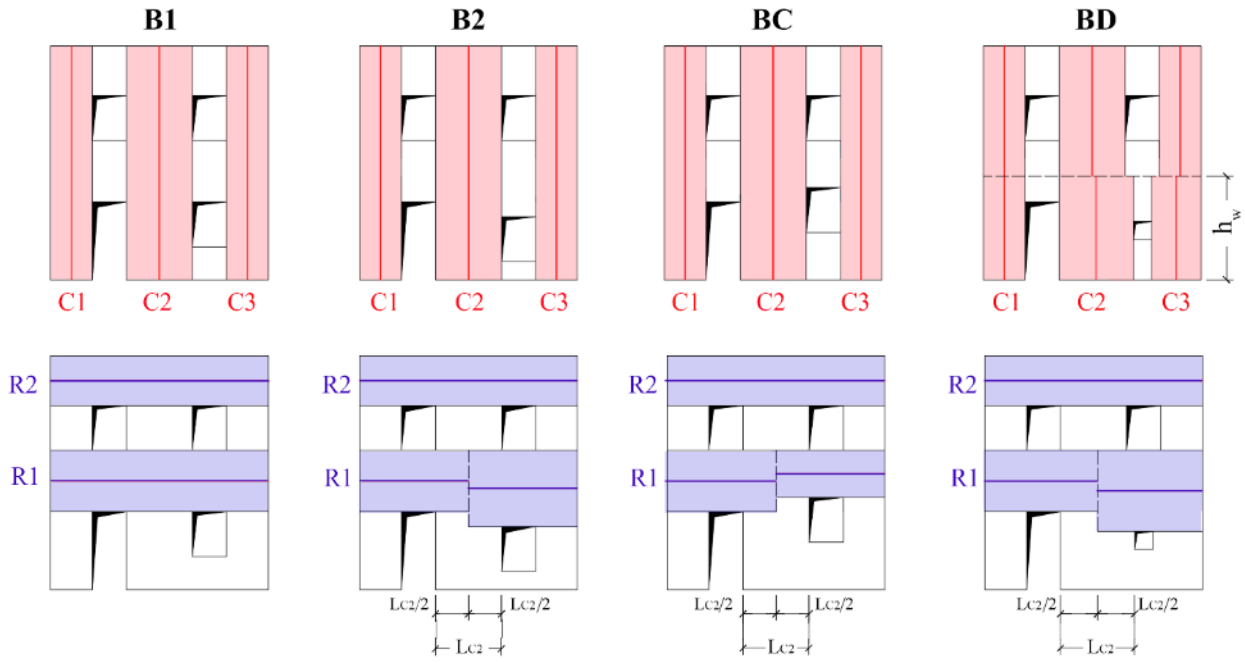

Figure 4.8 – Vertical (C1, C2 and C3) and horizontal (R1 and R2) alignments considered for each one of the configurations of type "B" for the comparisons in terms of generalized forces and displacements between the FE and the EF models (L_{C2} = width of alignment C2; h_w = interstorey height).

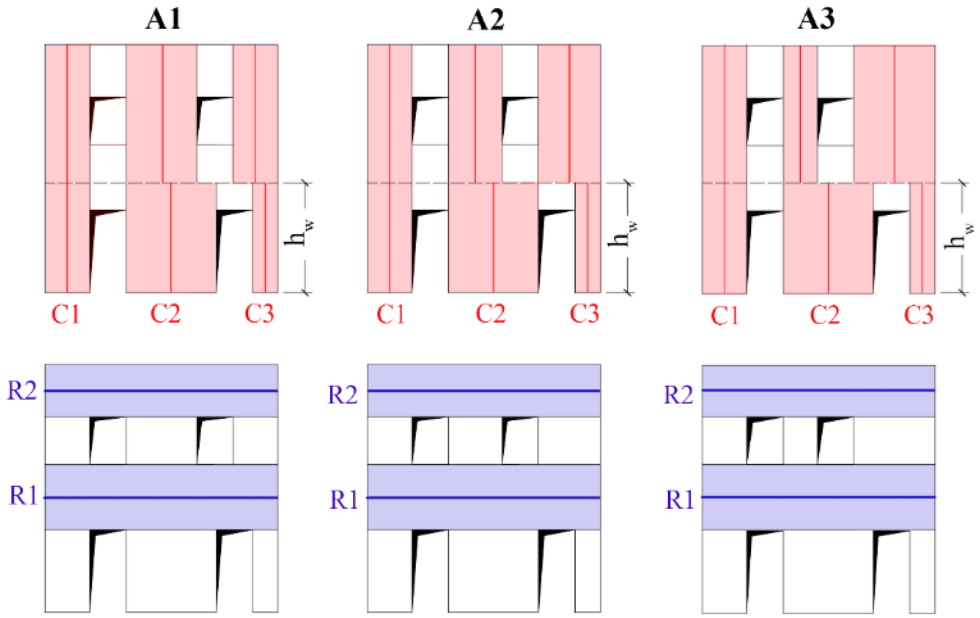

Figure 4.9 - Vertical (C1, C2 and C3) and horizontal (R1 and R2) alignments considered for each one of the configurations of type "A" for the comparisons in terms of generalized forces and displacements between the FE and the EF models (h_w = interstorey height).

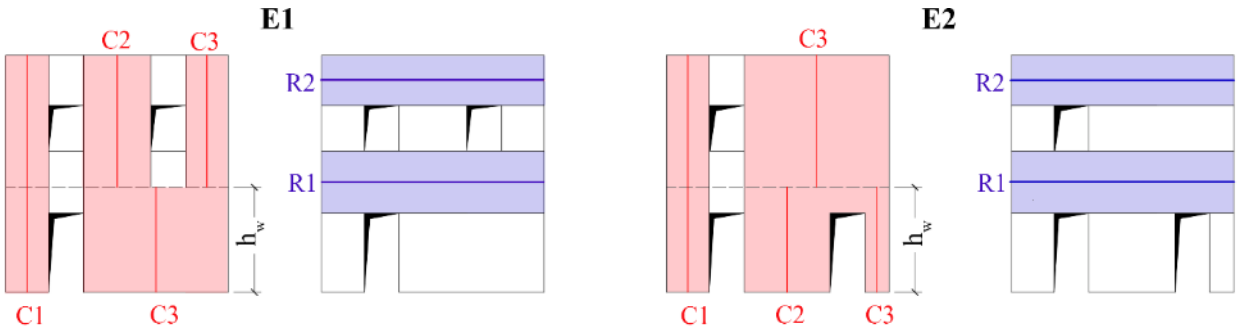

Figure 4.10 - Vertical (C1, C2 and C3) and horizontal (R1 and R2) alignments considered for each one of the "E" type configurations for the comparisons in terms of generalized forces and displacements between the FE and the EF models (h_w = interstorey height).

4.4 RESULTS OF THE NONLINEAR ANALYSES

The results of the nonlinear analyses performed on the irregular walls are discussed in the following by grouping the analysed configurations depending on the problems they were meant to investigate and on the basis of the types of comparisons previously introduced.

4.4.1 Problem 1: identification of pier effective height

In this section the results associated to configurations B1, B2 and BC are discussed. These configurations, indeed, are all characterized by horizontal irregularity and are therefore critical with regard to the problem of the correct identification of the pier effective height.

A. *Results of the comparisons in terms of global response*

In the following figures (Figure 4.11, Figure 4.12 and Figure 4.13) the comparison between the pushover curves obtained with the different numerical models is presented for each analysed configuration and for each considered verse of the analysis (positive and negative verse).

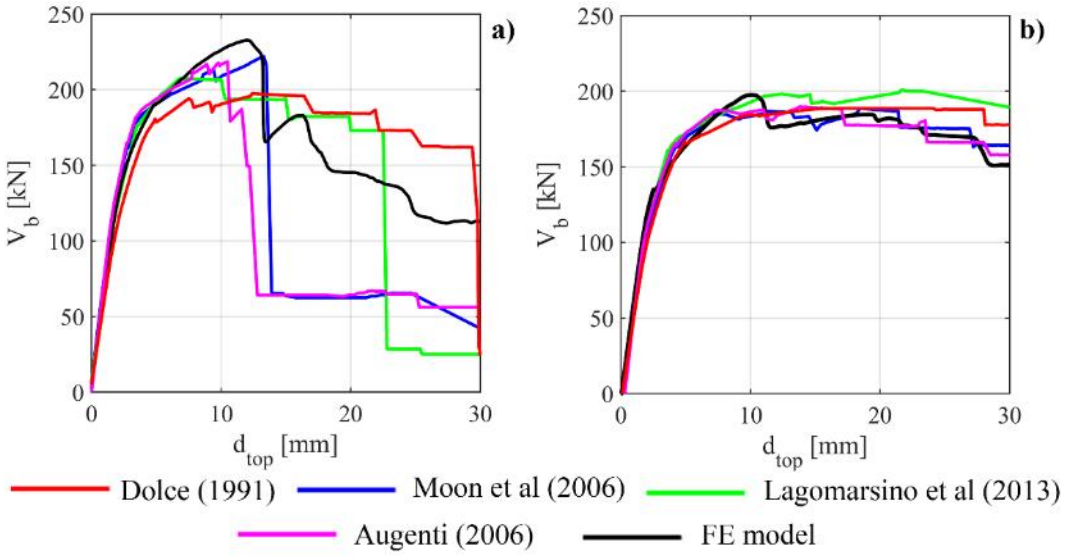

Figure 4.11 - Comparison in terms of pushover curves for configuration B1: a) analysis in the positive verse; b) analysis in the negative verse

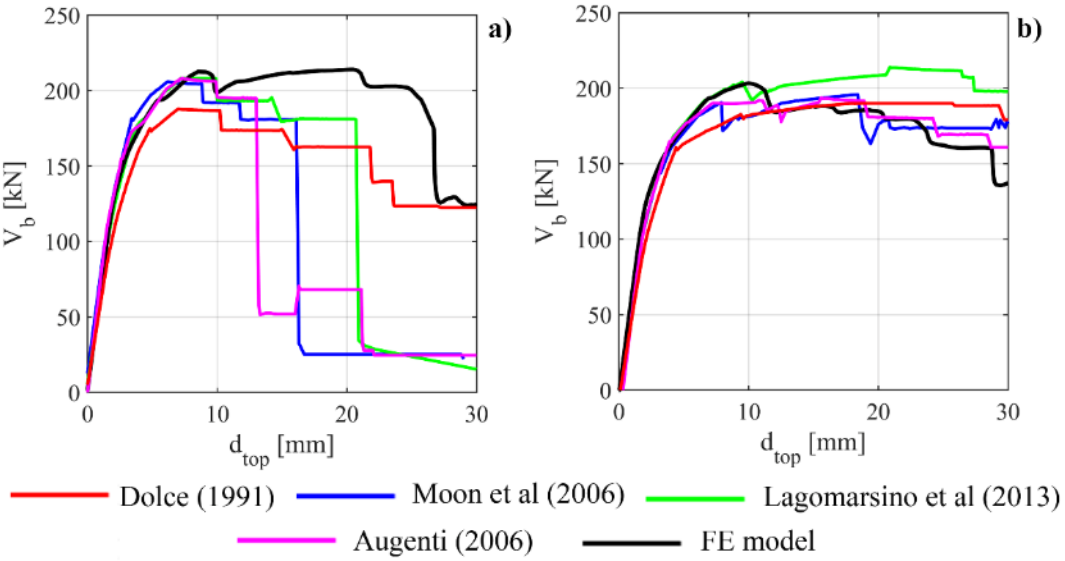

Figure 4.12 - Comparison in terms of pushover curves for configuration B2: a) analysis in the positive verse; b) analysis in the negative verse

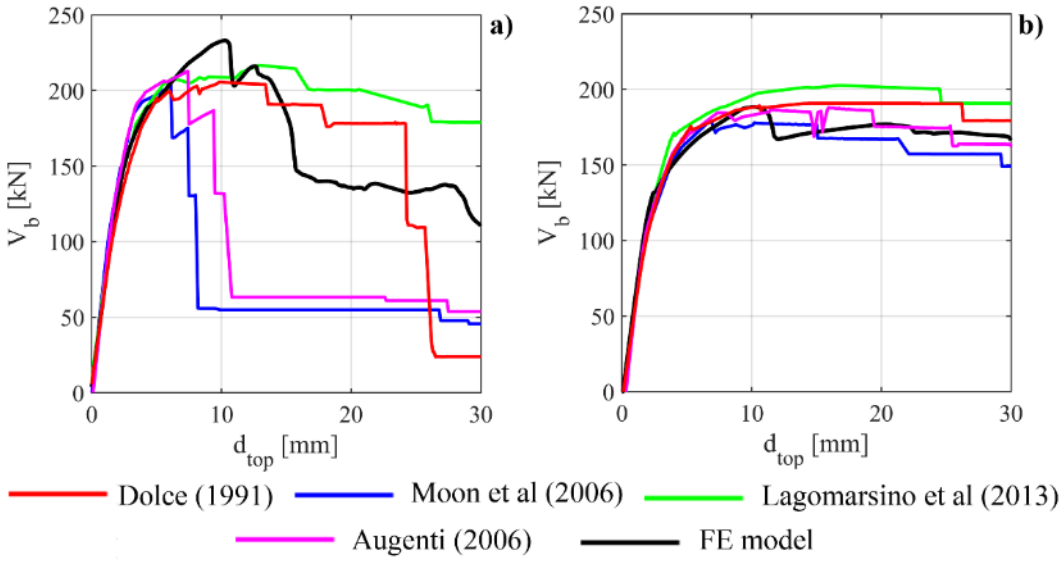

Figure 4.13 - Comparison in terms of pushover curves for configuration BC: a) analysis in the positive verse; b) analysis in the negative verse.

By looking at the results of the analyses in the negative verse, it is observed that, for all the examined configurations, the different EF models provide quite similar results in terms of global response, with only slight discrepancies in terms of stiffness and maximum strength; moreover, these results are close to the reference solution, represented by the curve associated to the FE model.

However, when examining the results of the analyses in the positive direction more significant differences can be detected, being the scatter of the results provided by the EF models really significant, especially in the post-peak phase.

This difference on the EF models depending on the verse of the analysis can be explained by considering that when pushing the wall in the positive direction, due to the overturning phenomenon, the part of the wall that gives the higher contribution to the structural response (i.e. the part where the compression stresses increase) is actually the one where the irregularity is present, and where the different criteria for the pier effective height lead to more significant differences in the geometry of the structural elements.

By looking, as an example, at the pushover curves provided by the EF models in case of configuration B1 (Figure 4.11-a), it can be seen that there are slight differences in terms of initial stiffness and more significant discrepancies in terms of maximum strength and post-peak response. Regarding this last aspect, in particular, it may be noted that the models associated to the proposals by Moon et al (2006) and by Augenti (2006) predict a sudden drop of strength in correspondence of a top displacement approximatively equal to 13 mm, while the response obtained through the other two EF models (pier effective height according to Dolce (1991) and Lagomarsino et al (2013)) is characterized by a more gradual strength degradation, with the reaching of the ultimate condition for higher values of top displacement. The comparison of these results with the FE curve shows that the EF model associated to the proposal by Moon et al (2006) provides a good description of the behavior until the maximum strength and is also able to capture the first drop of strength (which in the FE model occurs for almost the same value of top displacement); however, the strength degradation in the curve of the FE model is more gradual, and tends

to be more in accordance with the one described by the models associated to the criteria suggested by Dolce (1991) and by Lagomarsino et al (2013).

Similar considerations can be made when looking at the pushover curves (positive analysis) obtained for configurations B2 and BC (Figure 4.12 and Figure 4.13): indeed, in general the EF models obtained through the application of the proposals by Augenti (2006) and Moon et al (2006) predict sudden drops of strength for low values of top displacement which do not find a correspondence in the results of the FE model, despite of the calibration of the adopted constitutive models in terms of strength degradation performed at the scale of single panels (presented in Chapter 3). On the contrary, the other two models are associated to a more gradual strength degradation, and provide a better match with the FE curve in the post-peak phase.

The results in terms of GRPs referring to stiffness and strength ($k_{s,35}$, R_k and V_{max}) are illustrated in Figure 4.14.

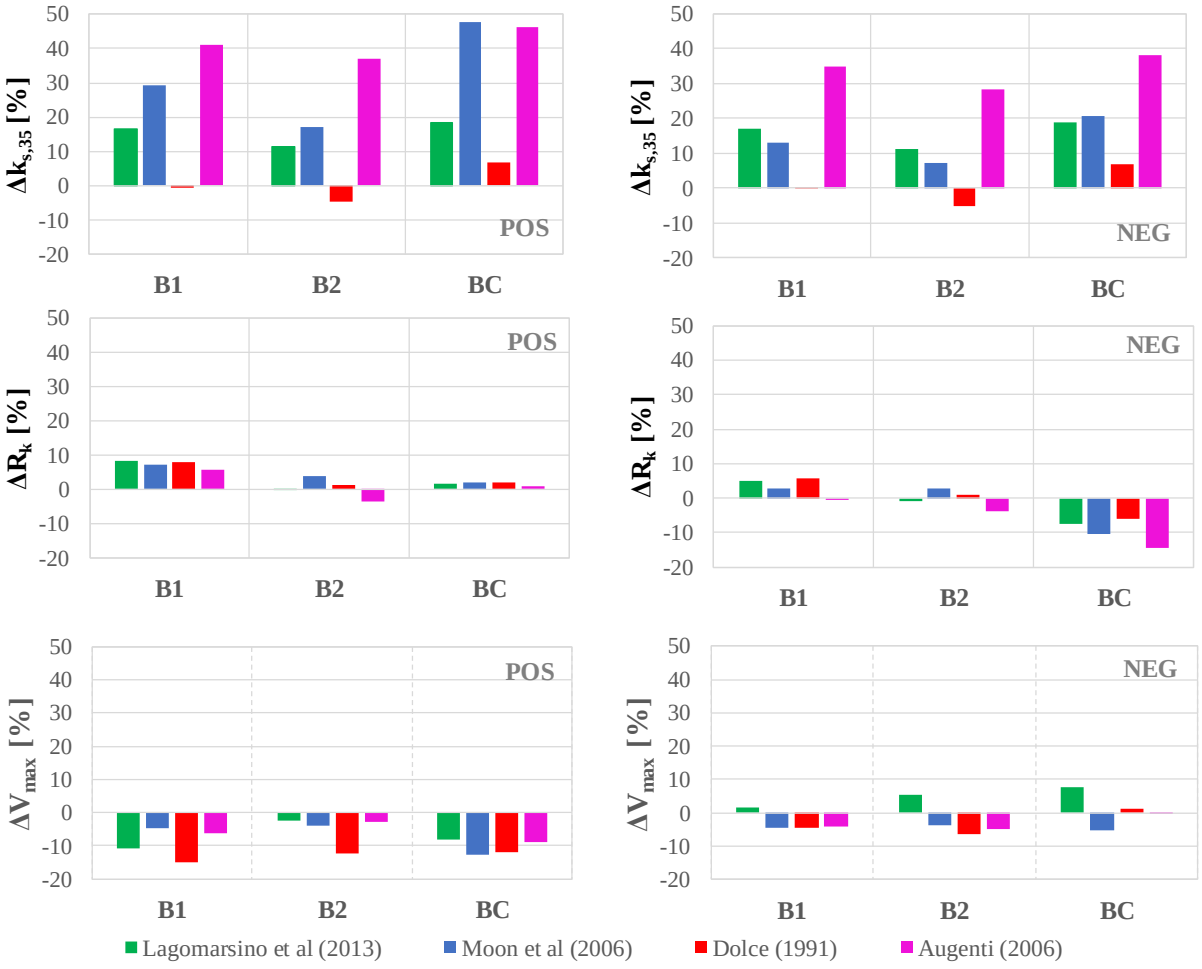

Figure 4.14 - Comparison of the results in terms of ΔGRP (scatter of the Global Response Parameters $k_{s,35}$, R_k and V_{max} with respect to the FE model) obtained through the EF models defined according to the different criteria for the EF idealization and for configurations B1, B2 and BC; positive (left) and negative (right) verse of the analysis.

Concerning $k_{s,35}$, it is possible to observe that the adoption of the criterion suggested by Dolce (1991) leads to the lowest scatter with respect to the FE model ($\Delta k_{s,35}$ almost equal to 0) in all the considered configurations; moreover, also the proposal by Lagomarsino et al (2013) allows to obtain good results, with

an overestimation of the initial stiffness which is in general lower than 15%. On the contrary, the criteria proposed by Moon et al (2006) and by Augenti (2006) produce values of $\Delta k_{s,35}$ considerably higher, especially in the positive verse, with values in some cases close to 50% (configuration BC). This clearly indicates that according to these two criteria the extension of the parts of the wall modelled as rigid nodes is significant; as a consequence, rather squat piers are introduced in the model. In the case of negative verse, the overestimation of the initial stiffness on behalf of these two criteria is slightly lower; however, the criterion by Augenti (2006) provides also in this case values of $\Delta k_{s,35}$ quite high (close to 30%).

The scatter with respect to the parameter R_k is lower than 10% in almost all the cases, thus indicating the capability of the EF models to well capture the stiffness degradation phenomenon occurring in the FE model. In this case, no significant differences among the models are detected.

Similar considerations can be made when looking at the results in terms of maximum strength. The values of ΔV_{max} are in almost all the cases lower than 10%; moreover, in general the EF models tend to underestimate the maximum strength with respect to the FE model (ΔV_{max} <0).

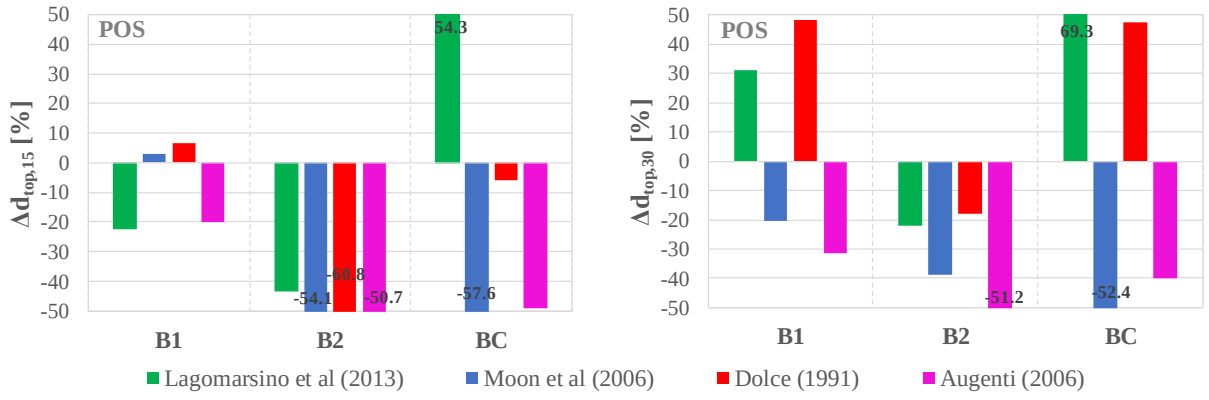

Figure 4.15- Comparison of the results in terms of ΔGRP (scatter of the Global Response Parameters $d_{top,15}$ and $d_{top,30}$ with respect to the FE model) obtained through the EF models according to the different criteria for the EF idealization and for configurations B1, B2 and BC; positive verse of the analysis.

In Figure 4.15 the results in terms of the parameters $d_{top,15}$ and $d_{top,30}$ are illustrated for the analyses in the positive verse, which are the most interesting to be discussed, due to the very different post-peak responses provided by the different EF models. These results substantially confirm what observed in the global pushover curves: indeed, a high scatter with respect to the FE model can be observed in almost all the configurations and when considering all the examined criteria adopted for the pier effective height. However, some differences depending on the adopted rule can be highlighted.

More specifically, the results referring to configuration B1 have already been discussed in detail, and the values of $\Delta d_{top,15}$ and $\Delta d_{top,30}$ help to quantify the considerations previously made on the comparison between the pushover curves in terms of post-peak phase.

In case of configuration BC, the criteria proposed by Moon et al (2006) and by Augenti (2006) lead to a very high underestimation of the displacement capacity with respect to the FE model (scatter on $\Delta d_{top,15}$ and $\Delta d_{top,30}$ in general higher than 50%), which is related to the premature drop of strength observed in the pushover curves associated to these models. Also the EF model according to Lagomarsino et al (2013) is

associated to a not negligible scatter on $\Delta d_{top,15}$ and $\Delta d_{top,30}$, which in this case is due to an opposite situation (i.e. underestimation of the strength degradation with respect to the FE model). On the contrary, the criterion proposed by Dolce (1991) provides in general better results, especially when considering $d_{top,15}$.

Moving to configuration B2, similar observations apply to the case of the criteria proposed by Moon et al (2006) and by Augenti (2006). Conversely, the criterion suggested by Lagomarsino et al (2013) leads to a scatter with respect to the FE model lower than the other criteria when considering both $d_{top,15}$ and $d_{top,30}$, while Dolce's rule works well when considering a high level of strength degradation ($\Delta d_{top,30}$ within 15%).

B. Results of the comparisons in terms of damage pattern

The analysis of the damage pattern associated to the different EF models helps to better understand the discrepancies observed in the global pushover curves.

In Figure 4.16 the comparison between the damage pattern resulting from the FE model and from the four different EF models for three increasing values of top displacement in case of configuration B1, positive analysis, is illustrated. Similar results are obtained also in the case of the positive analyses on configurations BC and B2.

Focusing the attention on the element P2, which in this configuration significantly affects the global response predicted by the EF models (carrying almost 60% of the total base shear), it is possible to observe that the application of the different frame idealisation criteria leads to very different geometries for this structural element. In correspondence of a top displacement equal to 15 mm both the EF models according to Moon et al (2006) and Augenti (2006) predict the actual collapse (DL5), and so the total loss of strength, for P2. On the other hand, according to the other two EF models this pier is characterized by a lower state of damage (DL2 in case of the model according to Dolce (1991) and DL3 in case of the model according to Lagomarsino et al (2013)), so that it still has some residual strength with respect to the horizontal actions.

This explains the different strength degradation observed in the pushover curves associated to the different EF models. Regarding this aspect, it is stressed that in the EF models the failure of masonry panels is governed by the reaching of fixed values of drift; as a consequence, it is evident that rather squat panels will fail for very low values of the horizontal displacement, thus potentially affecting the global ductility of the system. Moreover, under the same hypotheses and boundary conditions, when the aspect ratio of a panel reduces, a shear failure is more likely to occur than a flexural failure, and the shear failure is associated to lower values of drift thresholds with respect to flexural one, being characterized by a more fragile response. This is exactly what happens in case of the EF models according to the criteria proposed by Moon et al (2006) and by Augenti (2006), where the geometry characterizing P2 is particularly squat ($\lambda = 0.67$). Conversely, in the other EF models (Dolce (1991) and Lagomarsino et al (2013)), where P2 is not so squat (having $\lambda = 1.16$ and $\lambda = 0.93$, respectively), the sudden drop of strength observed in the other two models does not occur.

By comparing the damage pattern obtained in the FE model with those predicted by the four EF models, (Figure 4.16) a quite good agreement is in general observed.

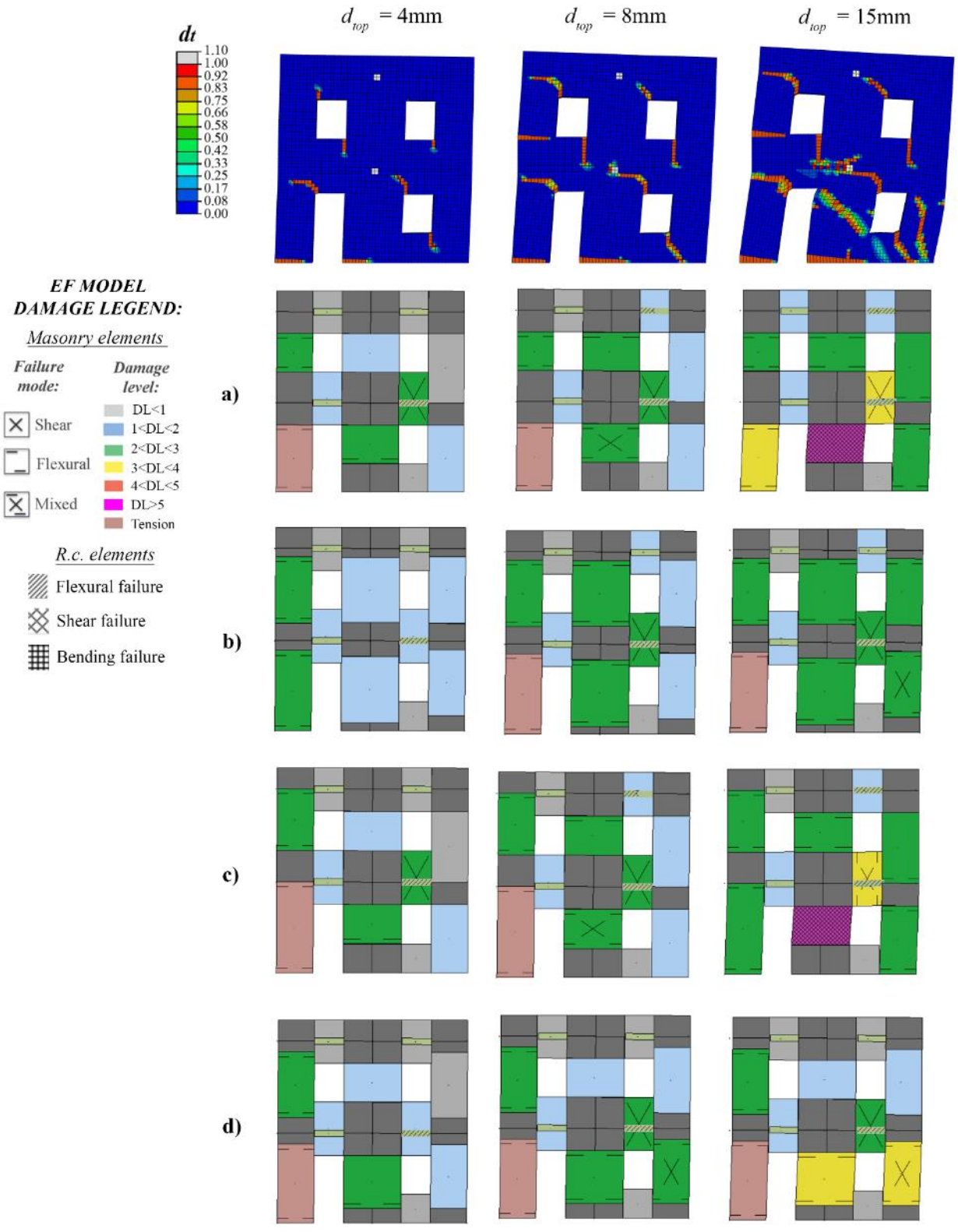

Figure 4.16 - Configuration B1, analysis in the positive verse: comparison between the damage pattern resulting from the FE model and the EF models associated to the different criteria for the pier effective height: a) Augenti (2006); b) Dolce (1991); c) Moon et al (2006); d) Lagomarsino et al (2013).

In particular, regarding the piers at the upper storey, all the considered EF models predict flexural failures for these elements, being thus consistent with the damage detected in the FE model, where the propagation of the tensile cracks clearly indicates the parzialization of the end sections of the corresponding masonry portions. However, while in the models according to Dolce (1991), Moon et al (2006) and Augenti (2006) for a top displacement equal to 15 mm all the piers of the second storey have already reached their peak strength (DL2), in the model associated to Lagomarsino et al (2013) P5 and P6 are still in the elastic phase, and this seems to be more in accordance with the results of the FE model, where the damage occurred in these two elements is lower than the one occurred in the portion of masonry corresponding to P4.

Moving to the piers located at the ground floor, which have in this configuration a more significant role in the structural response, for a top displacement equal to 15 mm all the EF models predict a flexural failure in case of P1, which is consistent with what emerges also from the FE model.

More differences come out when considering P2 and P3:

- in case of P3 the EF models according to Lagomarsino et al (2013) and Dolce (1991) predict, as in the FE model, a hybrid failure, while the application of the other two criteria leads to a flexural failure;
- in case of P2 the EF models according to Moon et al (2006) and Augenti (2006) both predict a hybrid failure, which is consistent with the tensile cracks observed in the FE model in the corresponding portion of masonry, interested by the propagation of a diagonal crack but also by the parzialization of the end sections. On the other hand, in the other two EF models this pier, being characterized by a higher aspect ratio, presents a prevailing flexural failure. This can explain the higher displacement capacity characterizing the structural response in these cases and also why the maximum global strength predicted by these two models is slightly lower than the one obtained with the other two models (see the pushover curves in (Figure 4.11-a).

From these considerations it emerges that the EF models according to Lagomarsino et al (2013) and Dolce (1991) lead to a better description of the global response of the wall, avoiding a premature drop of strength.

Considering the analyses in the negative verse, less differences in the damage pattern predicted by the four EF models are detected; moreover, the evolution of damage and the types of failure occurring in the panels are substantially consistent with the predictions of the FE model. This is coherent with the similar global responses provided by the considered numerical models.

As an example, in Figure 4.17 the comparison between the damage pattern resulting from the FE model and from two EF models (Lagomarsino et al (2013) and Moon et al (2006)) for different values of top displacement in case of configuration B1, negative analysis, is illustrated.

It is possible to see that in the FE model damage first appears in the pier elements at the ground floor, and especially in P3, located in the right part of the wall (where the compression decreases due to the overturning phenomenon of the structure), involving then also P1, which presents a hybrid failure (d_{top} =15 mm), the spandrels at the first floor and the piers at the upper storey (particularly P6), characterized by a flexural failure.

The considered EF models are able to quite well reproduce this damage pattern, both in terms of damage evolution and in terms of failure types characterizing the different structural elements. In particular, the piers at the upper storey are characterized by a prevailing flexural response, while those at the ground floor present, in correspondence of a d_{top} equal to 30 mm, the same failure type detected in the FE model: hybrid failure in P1 and flexural failure in P2 and P3. With regard to the spandrels, as in the FE model those at the upper storey remain almost undamaged, while significant damage occurs, for a top displacement equal to 30 mm, in those located at the first floor. Moreover, spandrel S2 in both the EF models is interested by a hybrid failure, and this is almost consistent with the damage emerging from the FE model.

Similar considerations can be made also when moving to the results of the negative analyses performed on the other two configurations (B2 and BC); indeed, also in these cases a substantial agreement between the predictions of the different EF models and between these last and the results of the FE analysis is observed.

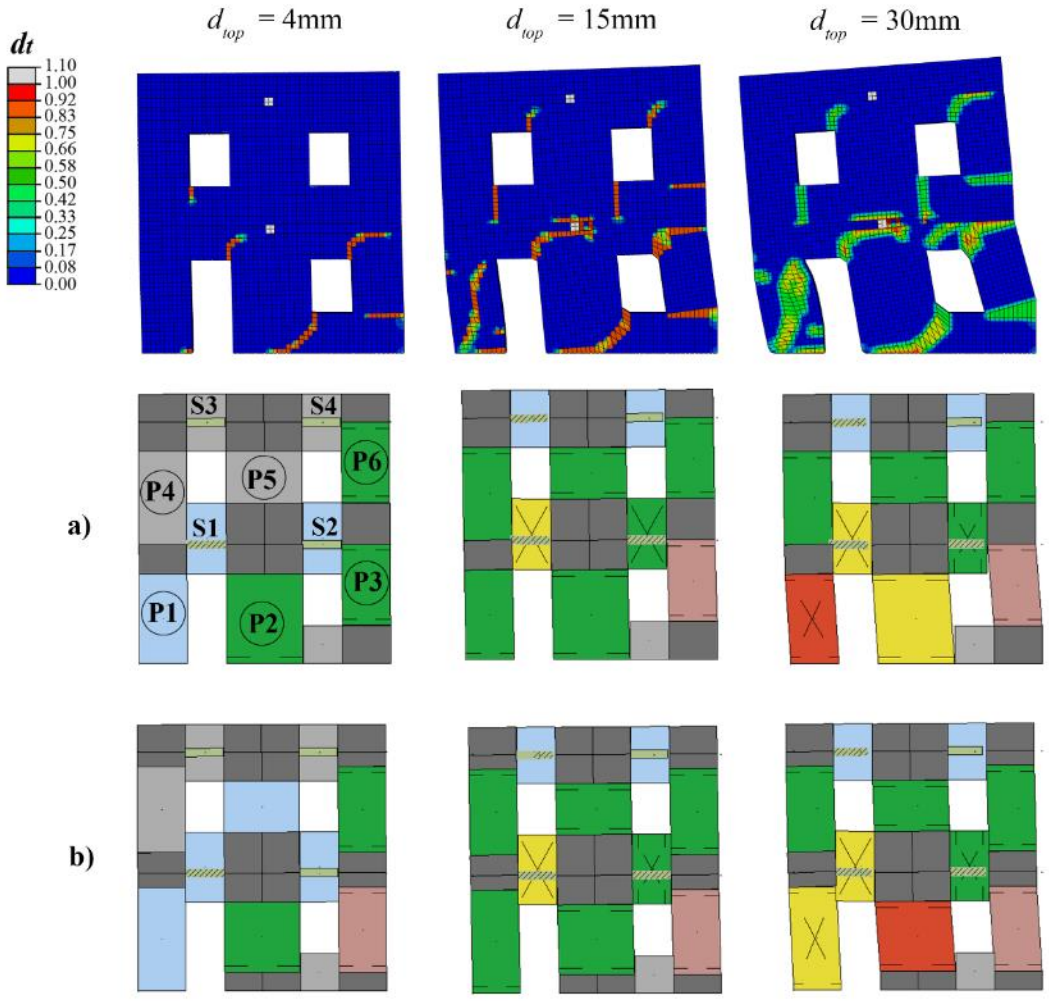

Figure 4.17 - Configuration B1, analysis in the negative verse: comparison between the damage pattern resulting from the FE model and the EF models associated to the different criteria for the pier effective height: a) Moon et al (2006); b) Lagomarsino et al (2013) for different values of top displacement. See Figure 4.16 for the meanings of colors and symbols in case of the EF models.

The observation of the tensile crack propagation in the FE model is useful in order to identify the portions of masonry where damage is concentrated, that should correspond to the structural elements composing the EF models. To this aim, in the following figures the damage pattern predicted by the FE model associated to the positive and negative analysis on configuration B2 (Figure 4.18) and BC (Figure 4.19) is reported, considering a top displacement equal to 30 mm. The damage pattern obtained in case of configuration B1 has already been illustrated in the previous figures (Figure 4.16 and Figure 4.17).

For the comparison with the geometry of the structural elements defined according to the 4 examined criteria, see the pictures in Table 4. 2 in case of configuration B2 and in Table 4.3 for configuration BC.

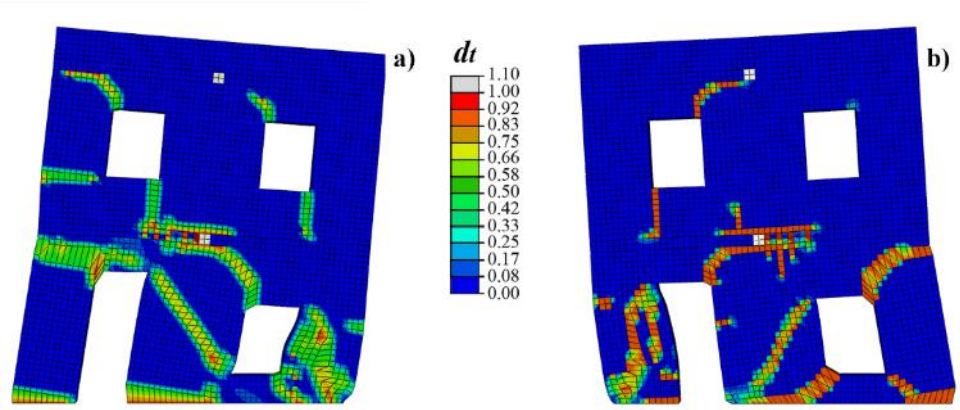

Figure 4.18 Configuration B2 - damage pattern predicted by the FE model in correspondence of a top displacement equal to 30 mm: (a) analysis in the positive verse; (b) analysis in the negative verse.

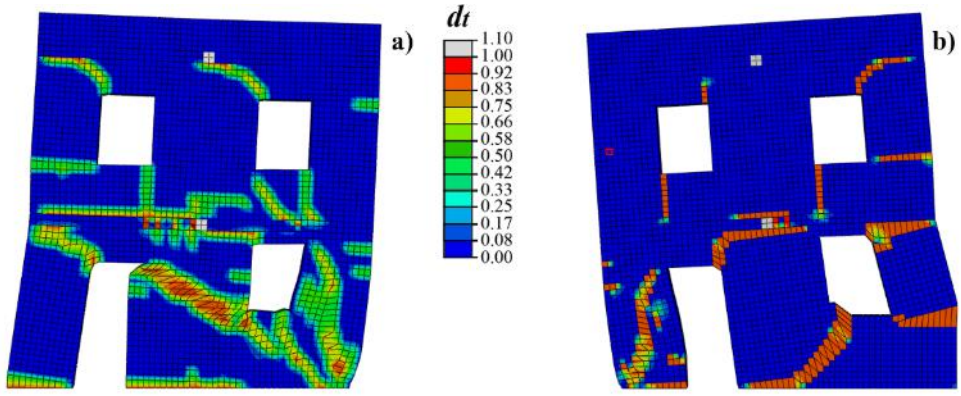

Figure 4.19 - Configuration BC - damage pattern predicted by the FE model in correspondence of a top displacement equal to 30 mm: (a) analysis in the positive verse; (b) analysis in the negative verse.

As already observed in the case of the regular configuration, it is stressed that the damage concentration in the central part of the wall at the first storey, which would correspond to a rigid node in the EF models, is associated to the introduction of the rigid beam adopted for performing the nonlinear analyses. Except for this aspect, in general damage concentrates in the portions which correspond to piers and spandrels in the EF models. With regard to the spandrel elements, in these configurations their identification is not an issue, and the concentration of damage in the FE analyses confirms that, in all the configurations, they seem to be actually located in the portions of masonry included between two vertically aligned openings.

More interesting is the examination of the damage occurred in the portions of masonry corresponding to the piers, which may help the identification of their effective height. It is possible to note that, in all the examined configurations, the different positions of the right window at the ground floor actually lead to a different propagation of the cracks, thus confirming that the opening pattern actually influences the effective height of the piers activated during the analysis. Moreover, for a fixed configuration the inclination of the tensile crack changes depending on the direction of the analysis, and seems to follow the rule of the compression strut, which coincides with the criterion proposed by Moon et al (2006). This is particularly evident in the case of the piers at the ground floor, where damage is mainly concentrated.

C. Results of the comparisons in terms of local response

For the computation of the reaction forces in the "B" configurations, three base sections were considered, as indicated in Figure 4.20. It is stressed that while in the EF models the three sections are associated to three different nodes, in the FE model the portion of masonry corresponding to sections 2 and 3 is actually a unique section; however, for the aim of comparison with the EF models, it was decided to split it into two different sections, defined on the basis of the respective influence areas.

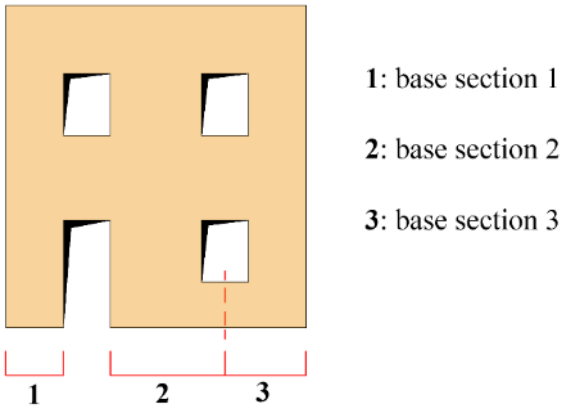

Figure 4.20 - Base sections considered for the computation of the evolution of the reaction forces in case of the "B" configurations.

When considering the analyses in the negative verse the comparisons on the evolution of the reaction forces in the examined base sections show that, in general, a good agreement between all the EF models and the corresponding FE model is present. Nevertheless, the Dolce's criterion allows to obtain in almost all the cases slightly better predictions with respect to the other criteria in terms of axial load acting in the considered base sections after the application of the dead loads ($d_{top} = 0$).

On the contrary, when considering the results of the analyses in the positive verse more significant differences with respect to the predictions of the FE model can be detected.

As an example, in the following figures the normal force, shear force and bending moment acting at the base sections of the wall in case of configuration B2, negative (Figure 4.21) and positive (Figure 4.22 and Figure 4.23) analyses, are reported, comparing the results of the FE model with the ones deriving from the EF models according to Dolce (1991) (Figure 4.21 and Figure 4.22) and Moon et al (2006) (Figure 4.23).

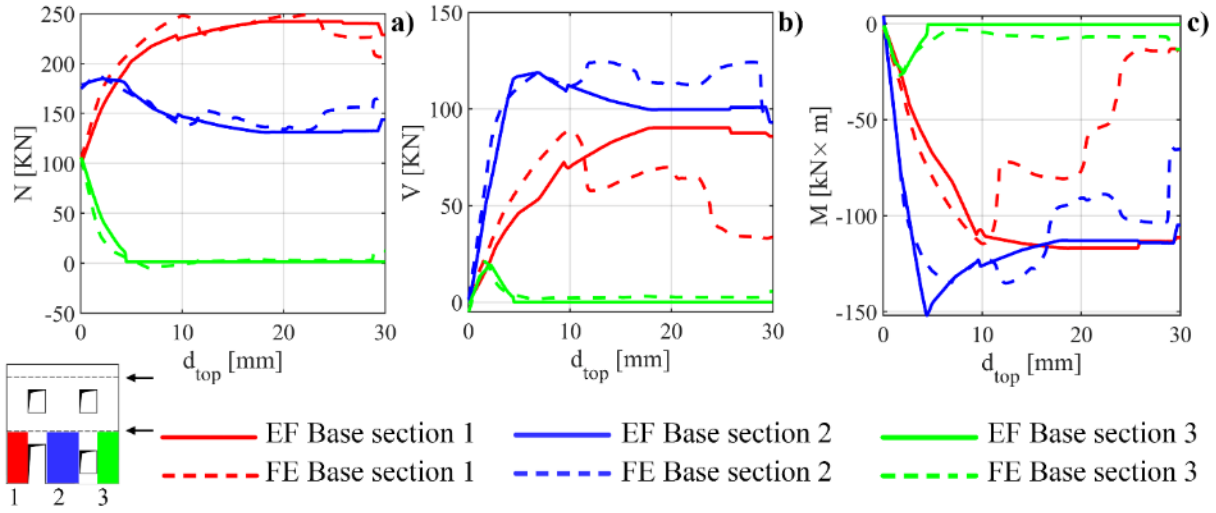

Figure 4.21 - B2, negative analysis - comparison on generalized forces at the base sections of the wall (a)normal force; b) shear force; c) bending moment) between the FE model and the EF model according to Dolce (1991).

In particular, by looking at the Figures referring to the analysis in the positive verse (Figure 4.22 and 4.23), it can be observed that also in this case the criterion suggested by Dolce allows to obtain a very good estimate of the redistribution of the vertical loads after the application of the dead loads ($d_{top} = 0$), providing a better result than the EF model according to Moon et al (2006). Moreover, in both cases there is a quite good agreement with the FE model in the initial phase of the response, while more differences arise when the structural response becomes strongly nonlinear, especially considering the reaction forces associated to sections 2 and 3 (in section 1 for high values of d_{top} the reaction forces are almost equal to zero according to all the considered models, due to the overturning of the wall). This is consistent with what observed also in terms of global response (see Figure 4.12-a).

The fact that in the configurations here examined the predictions of the EF models and the corresponding FE model present more significant differences in the case of the analyses in the positive verse than those in the negative verse can be explained by considering what follows. When pushing the wall in the negative verse the redistribution of the stresses mainly occurs between section 1 and 2, which are two separate sections in both the FE and the EF models. On the other hand, when pushing the wall in the positive direction the redistribution mainly occurs between section 2 and 3, that indeed have been artificially introduced in the FE model.

Furthermore, the discrepancies between the predictions of the EF models and the FE model in case of the positive analyses increase moving from configuration B2 to configuration BC (Figure 4.24). In this case, even if the axial load acting after the application of the dead loads in the three considered base sections is quite perfectly coincident in the FE model and in the EF model, the redistribution of the vertical loads occurring during the analysis between section 2 and 3 is considerably different in the two models. In particular, in the FE model the axial load acting in section 2 rapidly decreases due to the progressive parzialization of the section (as observed in Figure 4.19), becoming almost zero for d_{top} equal to 10 mm; conversely, the compression in section 3 significantly increases. On the contrary, in the EF model the redistribution of the vertical load between the base sections of the corresponding piers is less pronounced. Similar considerations apply also to the redistribution of the shear force V.

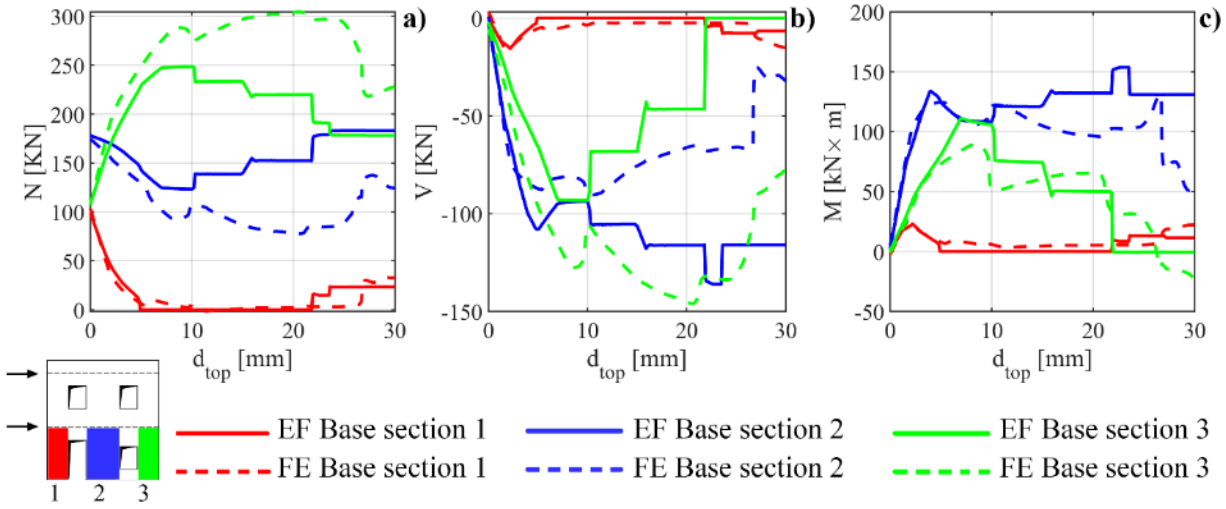

Figure 4.22 - B2, positive analysis - comparison on generalized forces at the base sections of the wall (a)normal force; b) shear force; c) bending moment) between the FE model and the EF model according to Dolce (1991).

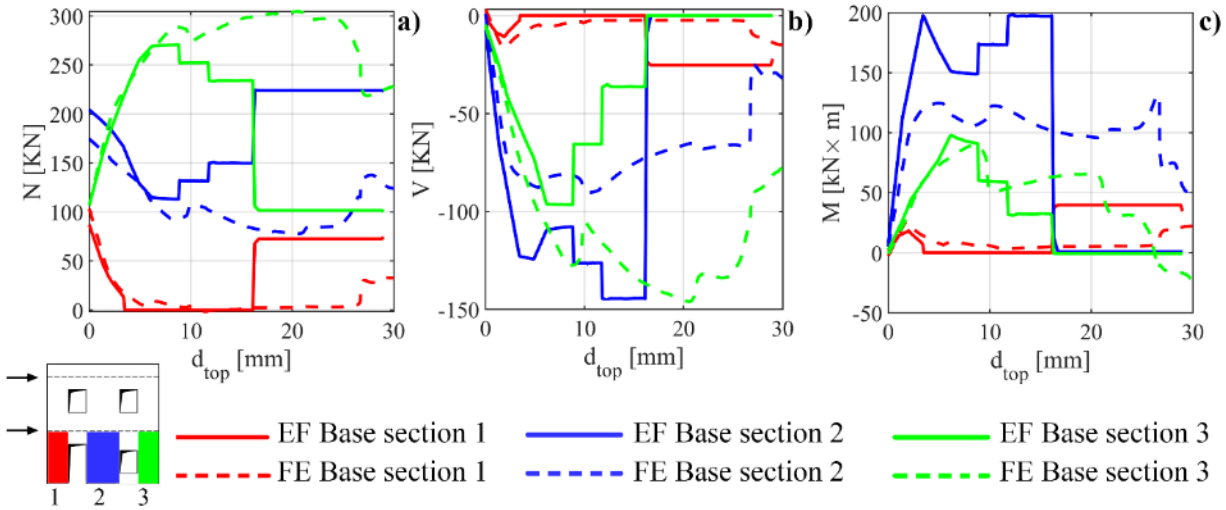

Figure 4.23 - B2, positive analysis – comparison on generalized forces at the base sections of the wall (a)normal force; b) shear force; c) bending moment) between the FE model and the EF model according to Moon et al (2006).

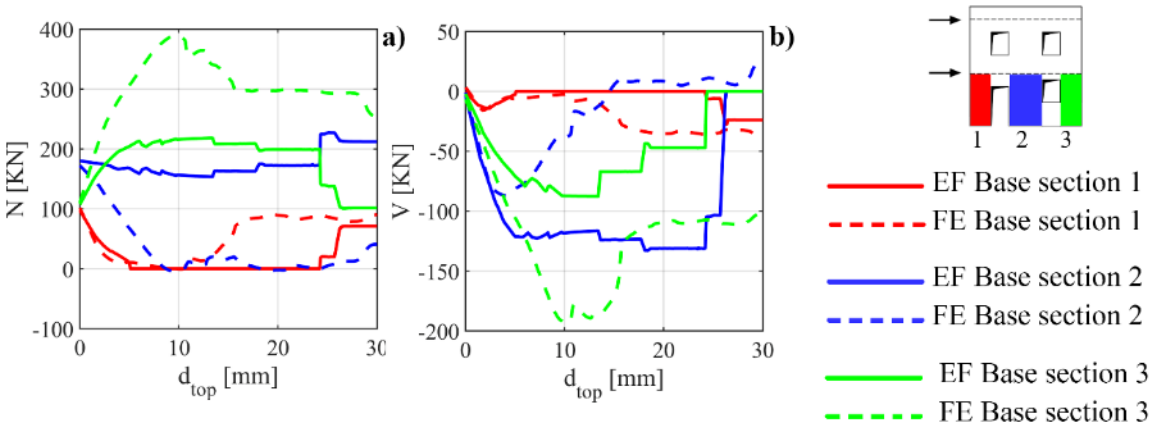

Figure 4.24 - BC, analysis in the positive verse - comparison on generalized forces acting at the base sections of the wall (a) normal force; b) shear force) between the FE model and the EF model according to Dolce (1991).

The above mentioned observations highlight some critical issues which may come out when adopting a FE model for the seismic design/assessment of masonry buildings, and in particular the problem of the identification of the sections to consider in the walls for the evaluation of the generalized forces when local verifications are required.

Concerning the comparison in terms of generalized forces acting on the alignments identified in the walls, the attention is here focused on the vertical alignments, where the most significant differences in the predictions of the EF models were detected. In fact, in case of the horizontal alignments all the considered EF models provided similar results, substantially consistent with the ones emerging from the corresponding FE model.

The comparisons illustrated in the following refer in particular to alignment C2. Indeed, the results associated to this alignment are of particular interest, since it includes at the ground floor the pier P2, which, as introduced before, is characterized by significantly different geometries according to the considered criteria and, furthermore, it is the structural element that mostly affects the global response of the analysed configurations.

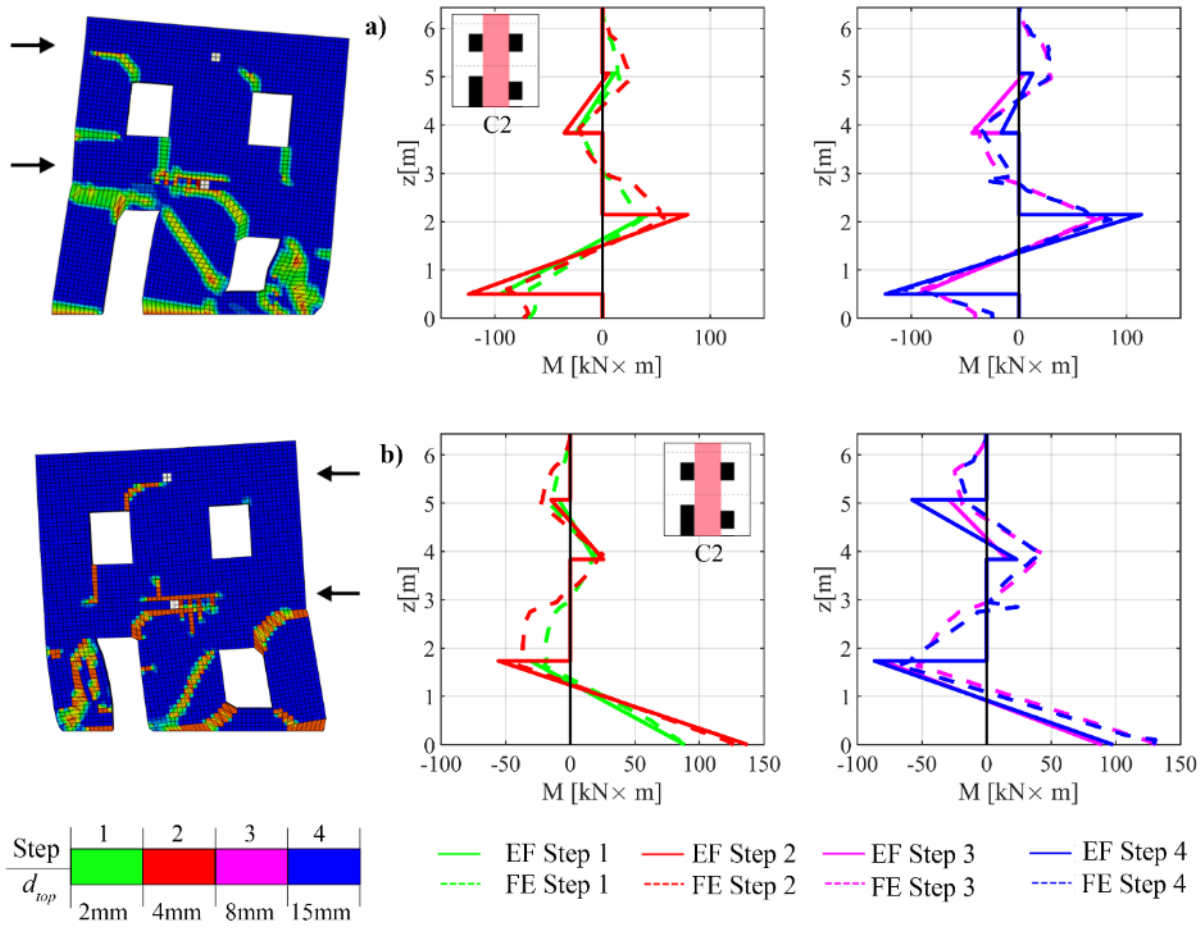

Figure 4.25 – Configuration B2, analysis in the positive verse (a) and in the negative verse (b): on the left tensile damage deriving from the FE analysis (d_{top} = 30 mm) and on the right comparison between the FE model and the EF models according to Moon et al (2006) in terms of bending moment *M* acting on the vertical alignment C2.

In Figure 4.25, in particular, some results referring to configuration B2 are shown, comparing the bending moment diagrams resulting for different steps of the analysis from the FE model and from the EF models according to Moon et al (2006). As previously introduced, and here recalled through the images of the damage pattern resulting from the FE analyses (referring to a d_{top} = 30 mm) the propagation of the tensile cracks in the FE model actually changes depending on the verse of the analysis and is consistent with the rule of the compression strut, on which the proposal by Moon et al (2006) is based. The analysis of the local response in terms of bending moment diagram shown in Figure 4.25 confirms that the effective height predicted for pier elements by this criterion is in good agreement with what emerges from the FE model.

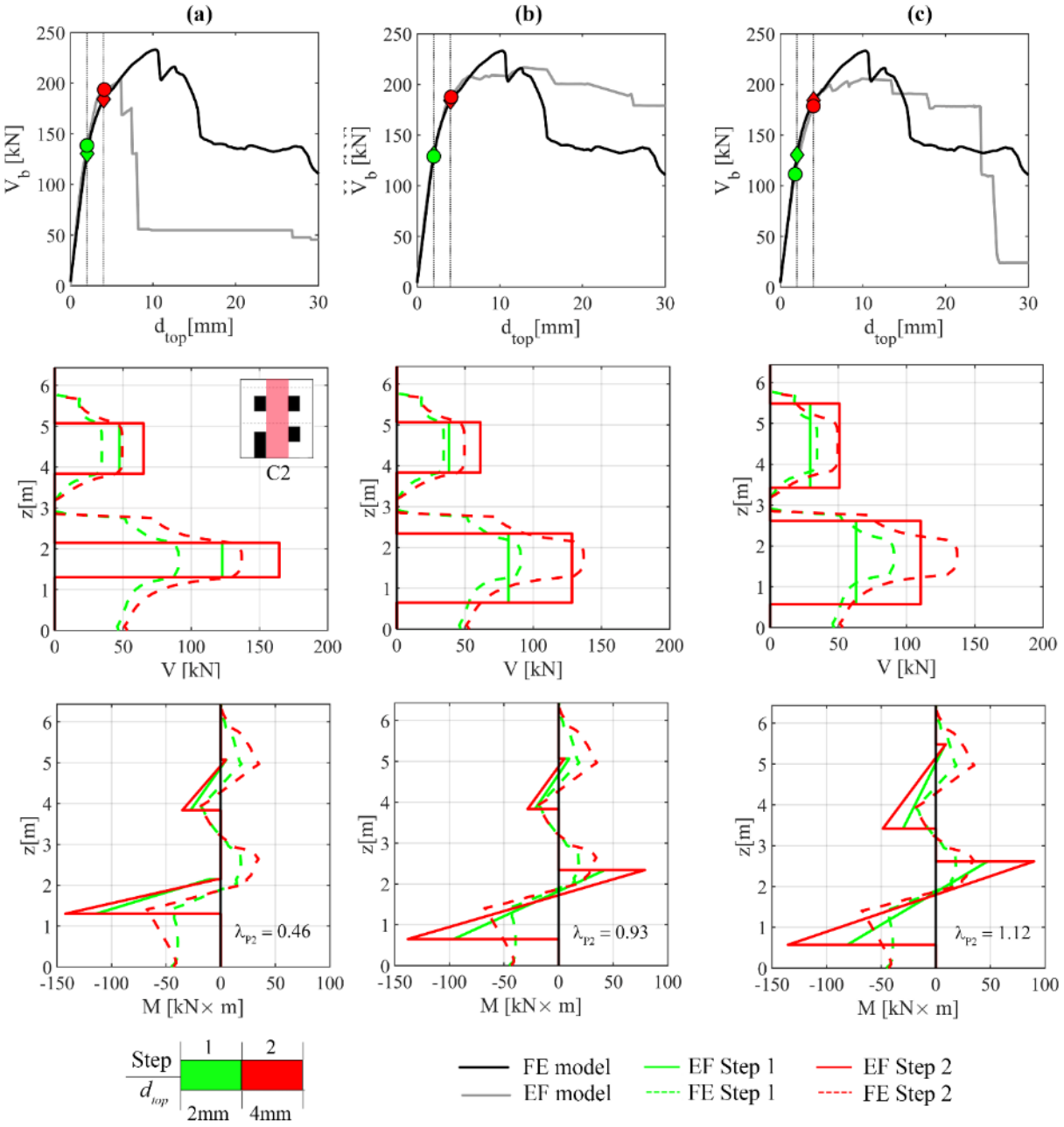

Figure 4.26 - Configuration BC, analysis in the positive verse: comparison between the FE model and different EF models ((a) Moon et al (2006), (b) Lagomarsino et al (2013), (c) Dolce (1991)) in terms of shear force *V* and bending moment *M* acting on the vertical alignment C2 for two different steps of the analysis; λ_{P2} is the aspect-ratio of pier P2.

Moving to the positive analysis on configuration BC, Figure 4.26 shows the comparison of the results on alignment C2 deriving from the models according to Moon et al (2006), Lagomarsino et al (2013) and Dolce (1991). The results of the EF model according to the Augenti's criterion are not shown, being substantially similar to the ones obtained with the model according to Moon et al (2006).

By looking at what obtained in case of step 1 (d_{top} = 2 mm) and 2 (d_{top} = 4 mm), it is possible to observe that, also in this case, the EF model associated to the criterion proposed by Moon et al (2006) is capable to well capture the effective height predicted by the FE analysis in case of both the pier at the ground floor and the one at the upper floor. However, if we look at the shear force diagrams in Figure 4.26, it is worthy observing that the model which provides the best match with the results of the FE model is the one associated to the criterion proposed by Lagomarsino et al (2013). Indeed, the model according to Moon et al (2006) overestimates the shear force, especially in case of the pier at the ground floor; on the contrary, the model associated to the Dolce's criterion tends to underestimate the shear force acting in P2.

These different results are related to the fact that the effective height predicted by the criterion suggested in Lagomarsino et al (2013) for the pier at the ground floor (P2) is intermediate between the ones predicted by the other two criteria. Since the shear force is, for definition, the derivative of the bending moment, the EF model according to Lagomarsino et al (2013) actually provides a better description, with respect to the other models, also in terms of bending moment diagram.

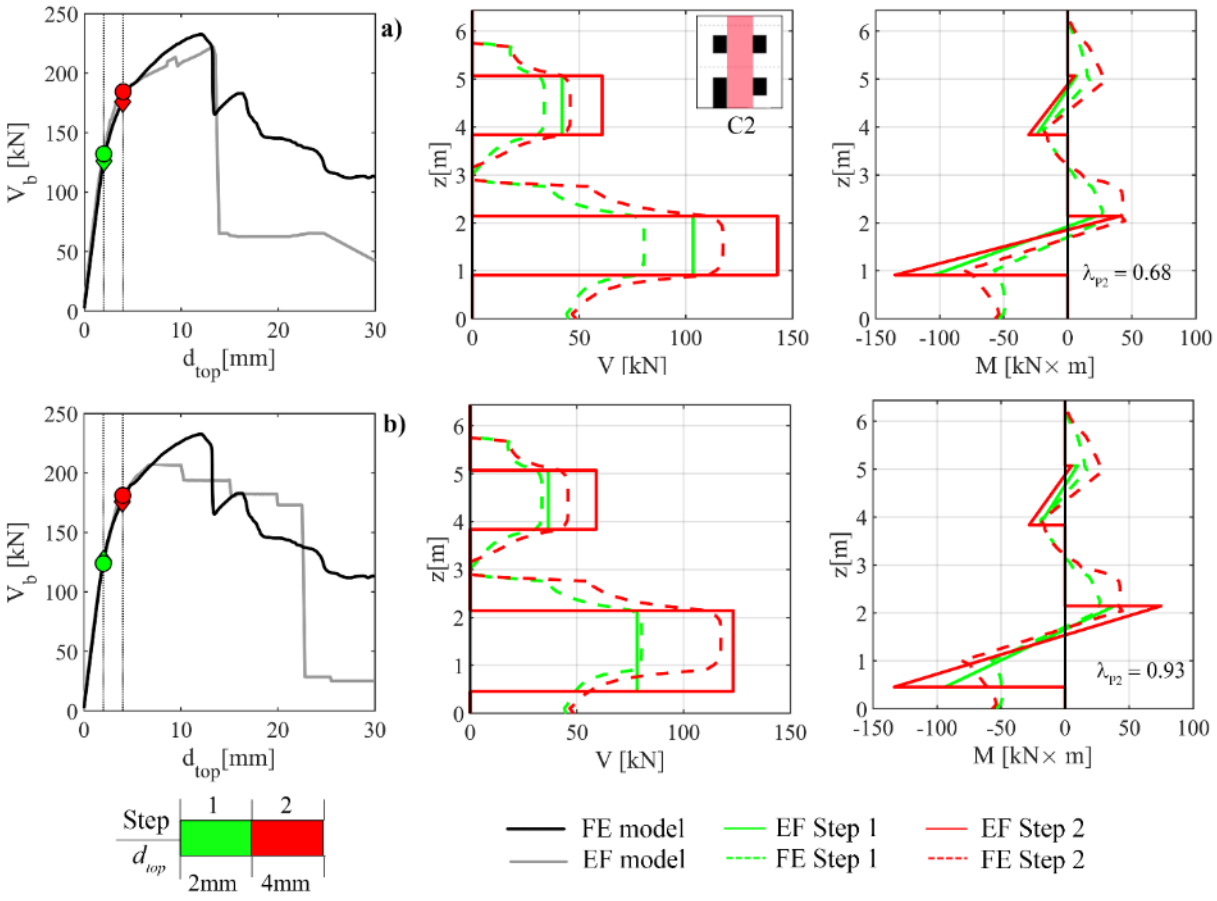

Figure 4.27 - Configuration B1, analysis in the positive verse: comparison between the FE model and different EF models (a) Moon et al (2006), b) Lagomarsino et al (2013)) in terms of shear force *V* and bending moment *M* acting on the vertical alignment C2 for different steps of the analysis.

Results substantially similar to the ones above discussed are obtained also when considering the positive analyses on the configurations B1 and B2.

As an example, in Figure 4.27 the results of the comparison in terms of shear force and bending moment diagrams between two different EF models (Moon et al (2006), Lagomarsino et al (2013)) and the FE model in case of configuration B1 (positive analysis) are illustrated. These results (referring to step 1 and 2) confirm what previously observed in case of configuration BC: also in this case the EF model according to Lagomarsino et al (2013) provides a very good match with the FE model considering both the shear force and the bending moment diagrams, especially when looking at the pier at the ground floor (P2). Conversely, the EF model according to Moon et al (2006) overestimates the shear force acting in P2, thus providing also worse estimates of the bending moment values acting in this element.

Moving to a more advanced nonlinear response (step 3 and 4, Figure 4.28), it can be seen that the EF model associated to the proposal by Lagomarsino et al (2013) still provides good results in terms of both shear force and bending moment, considering the piers at the two floors. It is highlighted that in the model according to the Moon's criterion the shear force and bending moment acting in P2 at step 4 are equal to zero, having this element already reached the actual collapse for the considered value of top displacement (d_{top} = 15 mm, see Figure 4.16). This clearly indicates that this criterion does not provide a well description of the actual local response.

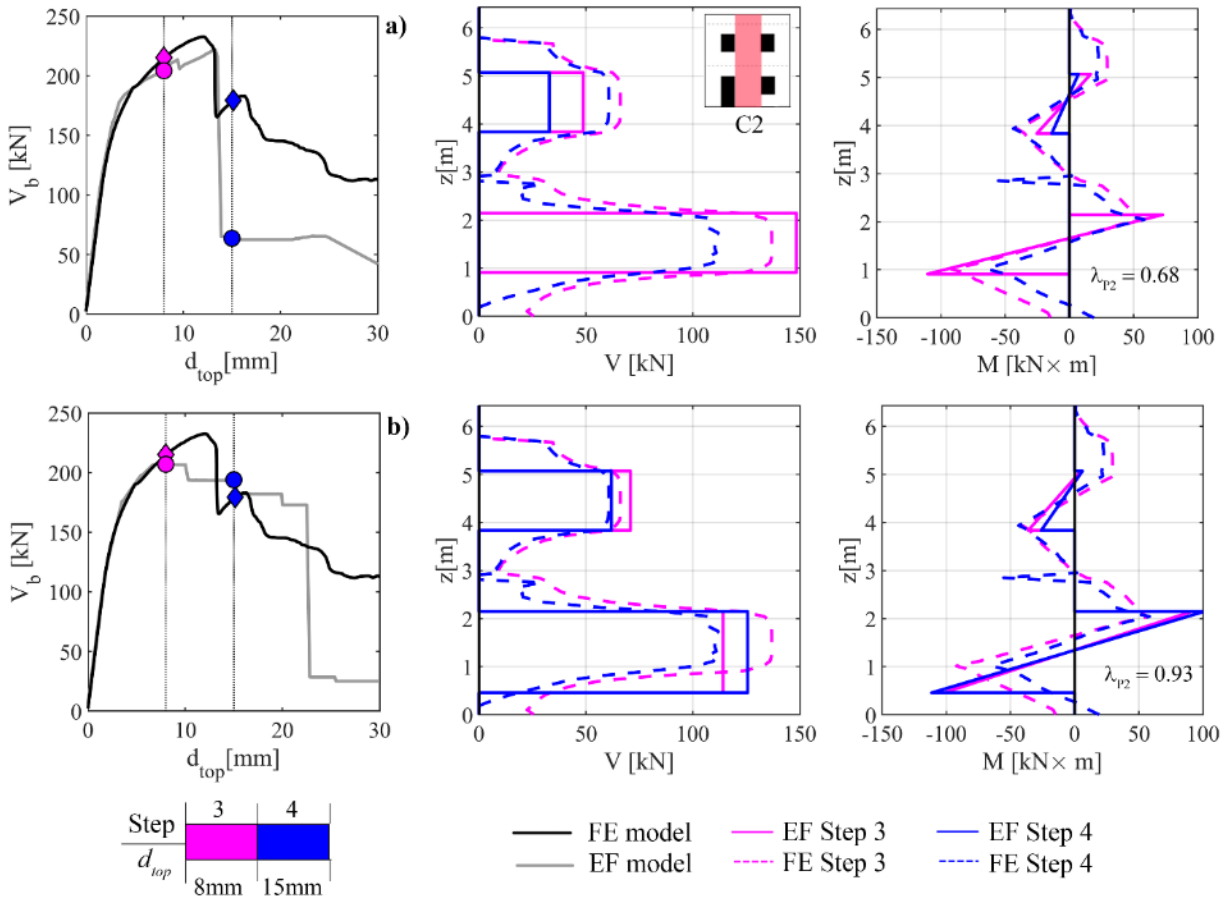

Figure 4.28 - Configuration B1, analysis in the positive verse: comparison between the FE model and different EF models (a) Moon et al (2006), b) Lagomarsino et al (2013)) in terms of shear force *V* and bending moment *M* acting on the vertical alignment C2 for different steps of the analysis.

Moving to the analyses in the negative direction, the geometry of P2 according to the different criteria is almost similar. Therefore, in these cases all the considered EF models provide similar predictions in terms of generalized forces acting in this pier and substantially consistent with the ones representing the reference solution. As an example, in Figure 4.29, the results of the FE model are compared with those of the EF models associated to the proposals by Moon et al (2006), Lagomarsino et al (2013) and Dolce (1991) in terms of shear force and bending moment diagrams acting on the alignment C2 (negative analysis).

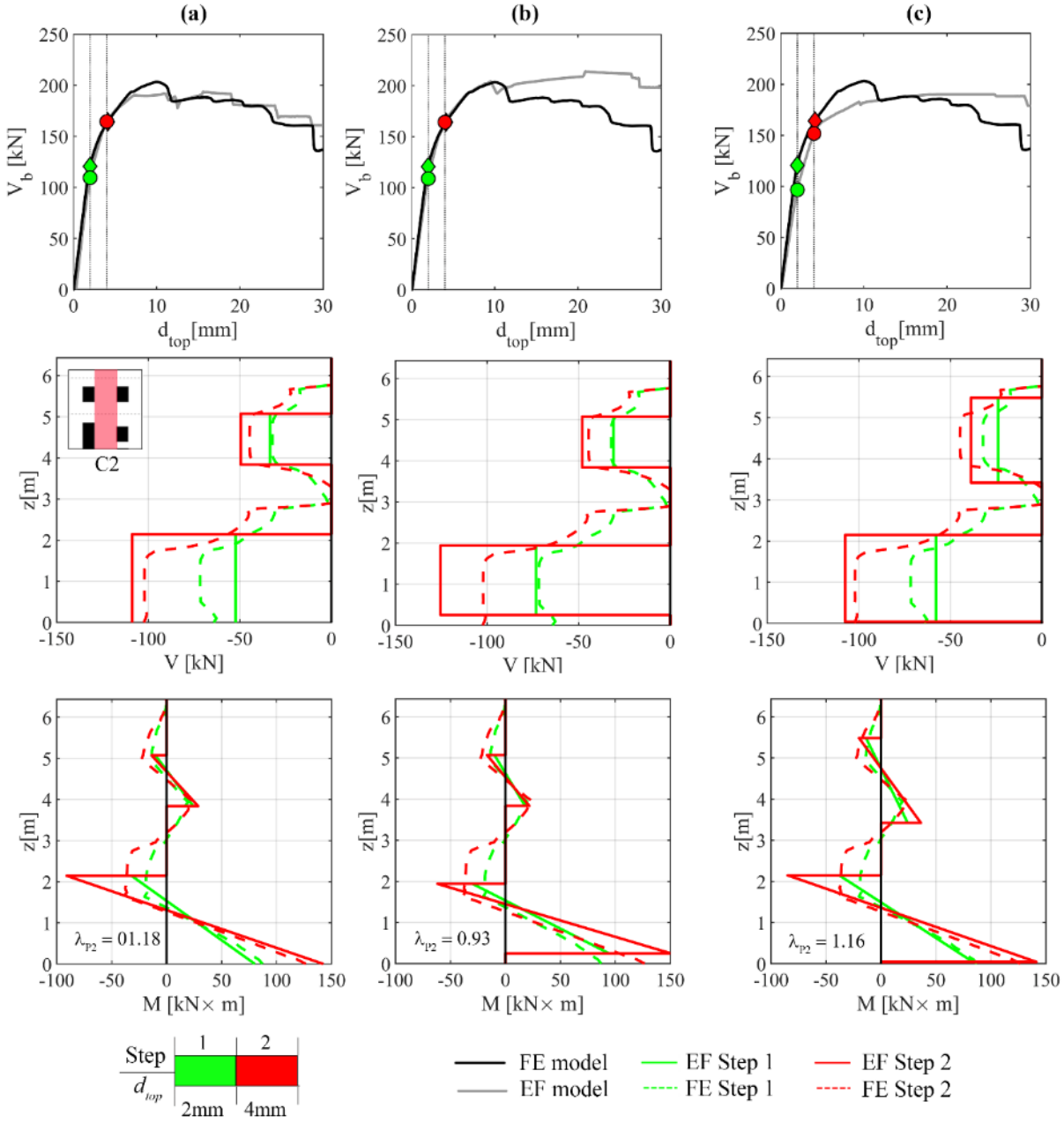

Figure 4.29 - Configuration B2, analysis in the negative verse: comparison between the FE model and different EF models (a) Augenti (2006), b) Lagomarsino et al (2013), c) Dolce (1991)) in terms of shear force *V* and bending moment *M* acting on the vertical alignment C2 for different steps of the analysis.

The comparisons in terms of deformed shapes associated to the vertical alignments identified in the walls show that in some cases the EF models associated to the criteria suggested by Dolce (1991) and Lagomarsino et al (2013) provide results closer to the FE model with respect to the other two EF models, especially when considering a more advanced nonlinear response. In particular, in Figure 4.30-a/b, the results of the FE model are compared with the ones derived from the EF models according to Augenti (2006) and Dolce (1991), respectively.

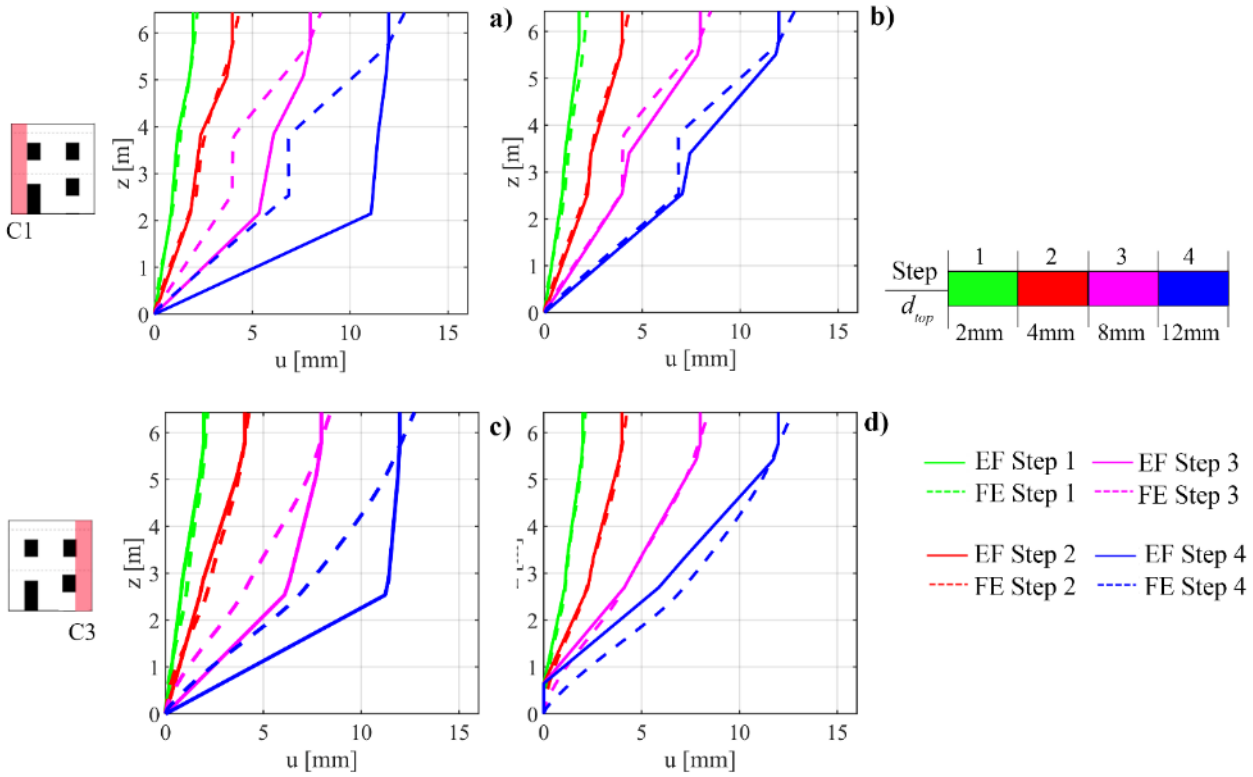

Figure 4.30 - Configuration BC, analysis in the positive verse: comparison between the FE model and different EF models (a) Augenti (2006) b) Dolce (1991); c) Moon et al (2006); d) Lagomarsino et al (2013)) in terms of deformed shapes associated to the vertical alignments C1 and C3 for different steps of the analysis.

In the same figure also the comparison referring to the vertical alignment C3 is proposed (Figure 4.30-c and d), comparing this time the results of the FE model with the ones deriving from the EF models according to Moon et al (2006) and to Lagomarsino et al (2013).

Finally, in the following the comparisons in terms of drift values associated to the masonry piers are discussed.

In general, for all the examined configurations a good agreement between the predictions of the EF models and those of the corresponding FE models was observed for all the considered steps. However, as already observed for the regular wall, due to the presence of the rigid nodes the EF models tend to slightly overestimate the drift characterizing the masonry panels, especially in case of the steps associated to the higher values of top displacement, when significant deformations are involved. The attention is here focused on the three piers at the ground floor where the damage is mainly concentrated. Figure 4.31 shows the comparison in terms of drift in the case of positive analysis on configuration B1.

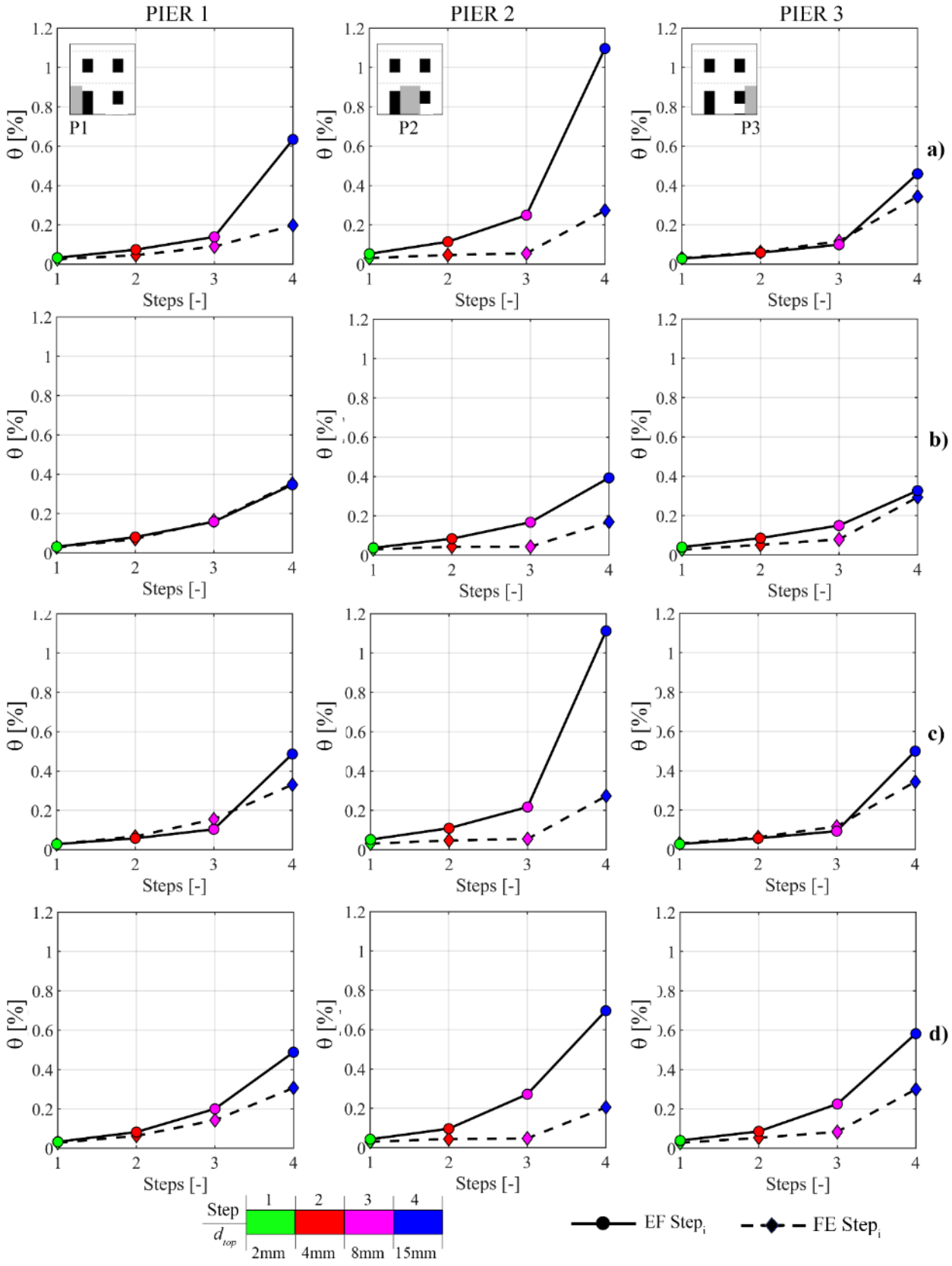

Figure 4.31 - Configuration B1, analysis in the positive verse: comparison in terms of drift values associated to the three piers at the ground floor between the FE model and different EF models (a) Augenti (2006); b) Dolce (1991) c) Moon et al (2006); d) Lagomarsino et al (2013)) for different steps of the analysis.

It is observed that while in the case of the external piers (P1 and P3) the predictions of the EF models and the FE model are, apart few exceptions (as in the case of P1, Figure 4.31-a) almost similar, more differences are detected on the central pier. In this case, in particular, the EF models according to Moon et al (2006) and to Augenti (2006) significantly overestimate the value of drift in correspondence of step 4 with respect to the results derived from the FE model. This result indicates that the adoption of these criteria leads, in this case, to an incorrect description of the deformations occurring in the corresponding masonry portion of the wall. Indeed, the introduction of significantly squat piers (and consequently big rigid nodes) in the structural models, as in these cases, produces a high concentration of damage in a limited portion of the wall: this is rather unrealistic since in the real masonry structures, where no rigid nodes are present, the deformations are distributed in bigger portions of masonry, as actually emerges from the FE analysis. Therefore, when considering the results provided by the EF models associated to the other two criteria (Lagomarsino et al (2013)) and Dolce (1991), which predict for P2 a higher effective height, a more accurate description of the state of deformation characterizing the corresponding masonry portions is obtained for all the examined steps.

The different predictions in terms of drift values provided for P2 by the 4 EF models help to explain what previously observed in the post-peak phase of the global pushover curves and in terms of occurred damage.

Similar results are obtained also when considering the other two configurations, as confirmed, by way of example, in Figure 4.32 for pier P2 associated to BC configuration (positive analysis).

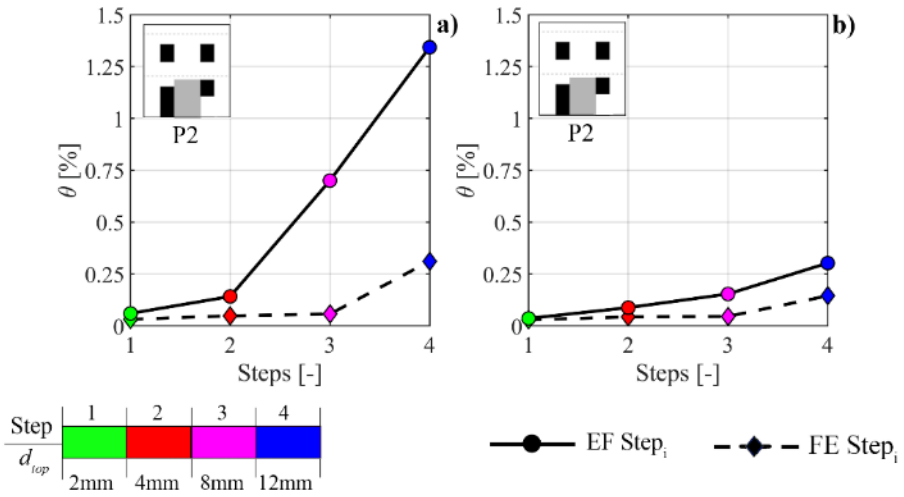

Figure 4.32 - Configuration BC, analysis in the positive verse: comparison in terms of drift values associated to pier P2 between the FE model and different EF models (a) Moon et al (2006) and b) Dolce (1991) for different steps of the analysis.

When considering the analyses in the negative verse, since in this case the rules for the EF idealization lead to a similar effective height for P2, the predictions of the four EF models in terms of drift are almost the same for all the 4 considered steps. Moreover, they are substantially consistent with the results provided by the FE model (Figure 4.33).

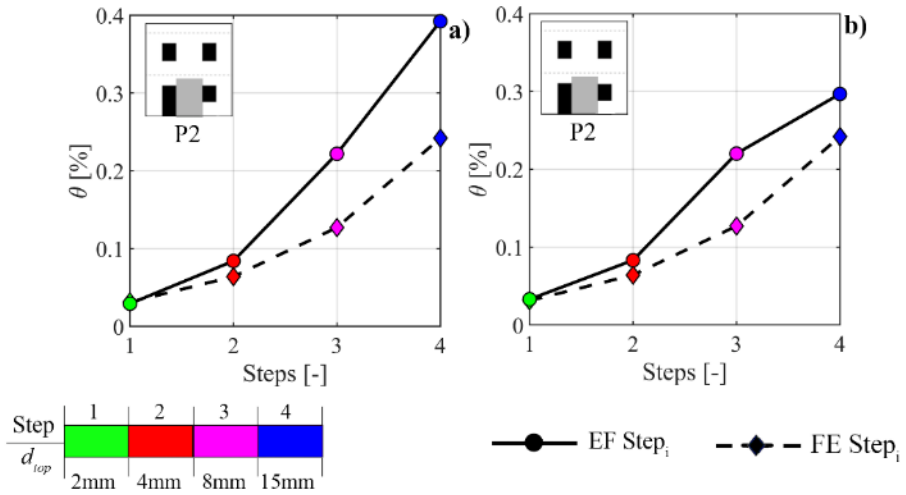

Figure 4.33 Configuration B1, analysis in the negative verse: comparison in terms of drift values associated to pier P2 between the FE model and different EF models (a) Augenti (2006) and b) Moon et al (2006)) for different steps of the analysis.

4.4.1.1 Main recommendations on the basis of the achieved results

The results obtained from the above discussed comparisons are summarized in Table 4.11, according to the criteria explained in the following.

Table 4.10 –Attribution of the labels (judgment and associated color) to the results obtained with the four EF models in terms of global response, local response (generalized forces and drift) and damage pattern.

A - Global response			
$0 \leq \mu_{\Delta GRP} \leq 15\%$	**$15\% < \mu_{\Delta GRP} \leq 35\%$**	**$35\% < \mu_{\Delta GRP} \leq 50\%$**	**$\mu_{\Delta GRP} > 50\%$**
LOW difference (L)	MODERATE difference (M)	HIGH difference (H)	VERY HIGH difference (VH)
B - Generalized forces, drift, damage pattern (global failure)			
Well captured	Moderate difference	Not good	
C- Damage pattern (damage in piers)			
f – Flexural failure in FE	**h** – Flexural failure in FE	**s** – Flexural failure in FE	
f – Flexural failure in EF	h – Flexural failure in FE	s – Flexural failure in EF	

Global response: for each criterion for the pier effective height, the average of the absolute values of ΔGRPs (named $\mu_{\Delta GRP}$) obtained by considering all the wall configurations analysed for the examined problem (B1, B2, BC) has been computed. The GRPs assumed as reference are: $k_{s,35}$, V_{max} and $d_{top,n}$; in this last case, the average between the absolute values of $\Delta d_{top,15}$ and $\Delta d_{,top30}$ has been considered. In this way, for each criterion and for each considered GRP, a unique value of $\mu_{\Delta GRP}$ is obtained, and then associated to a label (composed by judgment and an associated colour), according to the rules illustrated in Table 4.10-A.

Generalized forces and drift: the results obtained with the EF models are associated to the labels (judgment and associated colour) indicated in Table 4.10-B, considering again an average (in this case from a qualitative point of view and based on the above discussed considerations) between the examined configurations (B1, B2, BC). The reported results refer in particular to pier P2, which is the element carrying almost 60% of the total base shear and most affecting the response of the walls under consideration.

Damage pattern: the results in terms of damage pattern are summarized by taking into account the capability of the model to well capture both the global failure mode (global failure) and the local damage in single pier elements (damage in piers); in particular:

- "Global failure": by considering again an average (from a qualitative point of view) between the examined configurations, the labels (judgment and associated colour) indicated in Table 4.10-B are assigned, depending on if the examined EF model has been able or not to catch the global failure mode detected in the FE analysis;
- "Damage in piers": by considering the piers at the ground floor (P1, P2, P3, where damage mainly concentrates), the failure mode predicted in the FE model (indicated in bold and underlined), is compared with the one predicted in the EF models, as indicated in Table 4.10-C; this comparison is provided separately for all the examined configurations (B1, B2, BC).

Table 4.11– Summary of the main outcomes obtained in case of the B configurations (B1, B2, BC)

		Moon et al (2006)			**Augenti (2006)**			**Lagomarsino et al (2013)**			**Dolce (1991)**		
Global response	V_{max}	L			L			L			L		
	$d_{top,n}$	H			H			M			M		
	$k_{s,35}$	H			H			L			L		
Damage pattern	**Global failure**	Well captured			Well captured			Well captured			Well captured		
	Damage in Piers	**B1**	**B2**	**BC**	**B1**	**B2**	**BC**	**B1**	**B2**	**BC**	**B1**	**B2**	**BC**
	P1	**f**/f	**f**/f	**f**/f	**f**/f	**f**/f	**f**/f	**f**/f	**f**/f	**f**/f	**f**/f	**f**/f	**f**/f
	P2	**h**/h	**h**/f	**h**/h	**h**/h	**h**/f	**h/s**	**h**/f	**h**/f	**h**/f	**h**/f	**h**/h	**h**/f
	P3	**h**/f	**h/s**	**h**/f	**h**/f	**h/s**	**h**/f	**h**/h	**h**/h	**h**/h	**h**/h	**h**/h	**h**/h
Generalized forces	**Shear force**	Not good (Overestimated)			Not good (Overestimated)			Well captured			Moderate Diff.		
	Bending moment	Not good			Not good			Well captured			Well captured		
Drift		Not good (Overestimated)			Not good (Overestimated)			Well captured			Well captured		

Furthermore, in all the cases the data reported in Table 4.11 refer to the most punitive between the analyses performed in the two verses (i.e. the one associated to the highest scatter of the results with respect to the FE model), that in this case is always the one in the positive verse. Indeed, the concept is that the adoption of the given criterion should produce good results for both the verses of the analyses, being this necessary for verification purposes.

In general, the configurations with horizontal irregularity turned out to be quite critical, since the considered rules for the EF idealization of the walls lead to significant differences in the geometry of the structural elements and consequently to considerably different responses.

The inclination of the tensile cracks which develop in the FE models in the portions corresponding to masonry piers seems to vary depending on the direction of the seismic action, following the rule of the compression strut suggested in Moon et al (2006). Nevertheless, the adoption of this criterion and, even more, of the one proposed by Augenti (2006) leads to very squat piers and consequently big rigid nodes, thus strongly affecting also the initial stiffness of the structure. Furthermore, since in the EF models the failure of masonry panels is governed by the reaching of fixed values of drift, it is evident that rather squat panels will fail for very low values of the horizontal displacement, thus potentially affecting the global ductility of the system. This is exactly what happens in these cases, where in terms of global response premature drops of strength (with respect to what observed in the FE model), mainly ascribable to shear or hybrid failures, are observed. It is important to stress that this happens despite of the calibration in terms of both strength and displacement capacity performed at the scale of single panels between the adopted constitutive models (especially in terms of shear response); therefore, this indicates a response which is not consistent with the reference solution. Moreover, in these cases the comparisons in terms of local response showed a high concentration of deformation in small portions of the wall, which is rather unrealistic, as well as very high values of the associated shear force, which do not find a correspondence in the results of the FE model.

In the light of these considerations, the criteria by Augenti (2006) and Moon et al (2006) are not recommended in presence of horizontal irregularity. Conversely, the criteria indicated in Lagomarsino et al (1991) and in Dolce (1991), which provide a unique geometry for the piers regardless of the direction of the seismic forces, propose a higher effective height obtaining a better description of the behaviour, not only at the global level (lower overestimation of the initial stiffness, more gradual strength degradation) but also in terms of local response. In particular, the application of the rule proposed by Dolce (1991) allowed to obtain the best observed results in terms of deformed shapes in almost all the examined cases. Therefore, the obtained results (as it is possible to see from Table 4.11) support the idea that the rules for the identification of the pier effective height suggested in Lagomarsino et al (2013) and in Dolce (1991) can be applied without specific corrective measures.

4.4.2 Problem 2: presence of little openings

In this section the results associated to configuration BD are discussed. This irregular wall is characterized, as explained in section 4.1, by horizontal and vertical irregularity; it was introduced, in particular, in order to study the problem of the presence of very little openings in the masonry walls, which can lead to several uncertainties when the EF idealization of the wall has to be realized.

A. Results of the comparisons in terms of global response

In Figure 4.34 the results in terms of global pushover curves (positive verse and negative verse) are shown. It is stressed that, in addition to the EF models obtained with the application of the four considered criteria for the pier effective height, a further model where the presence of the little opening is neglected was considered, being this latter one of the possible modelling choice in such situations. In particular, this model (named in the following "No window") coincides with configuration E1, which is actually characterized by the same geometry of configuration BD, except for the presence of the window at the ground floor. In this model, the pier effective height is determined according to Lagomarsino et al (2013). It is stressed that in this case the pushover curves are represented until a top displacement equal to 50 mm, so that it is possible to appreciate the strength degradation occurred in the post-peak phase of the curve associated to the FE model.

First of all, by looking at the responses provided by the EF models a significant scatter between the obtained results is observed, especially when considering the analyses in the positive verse.

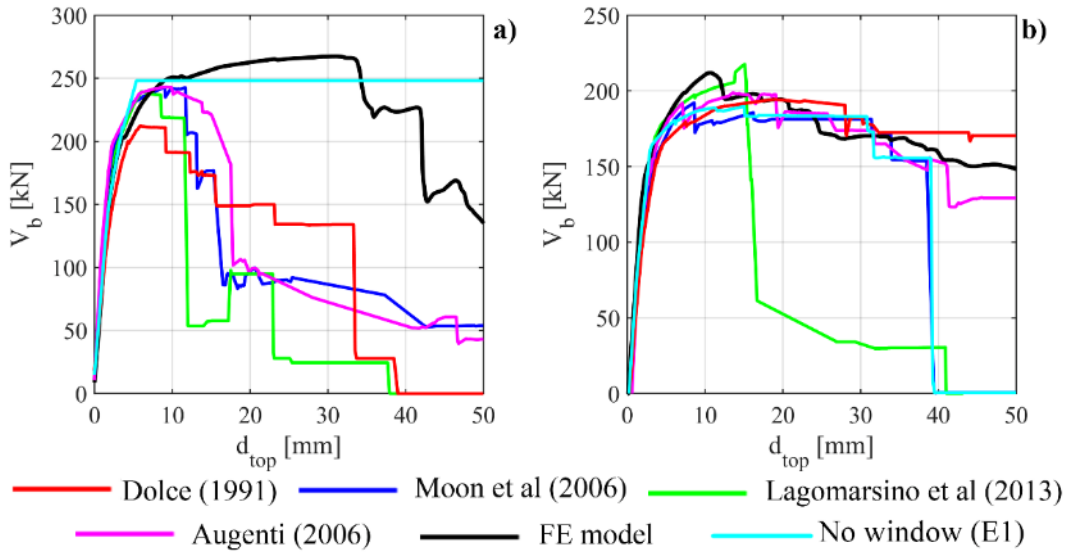

Figure 4.34 - Comparison in terms of pushover curves for configuration BD: a) analysis in the positive verse; b) analysis in the negative verse.

In this case, indeed, (Figure 4.34-a) considerable differences can be noted in the predictions of the different EF models, both in the ascending branch of the curves, in terms of stiffness and strength, and in the post-peak response. Moreover, all the curves obtained with the EF models including the little opening provide global responses which are substantially different from the pushover curve associated to the FE

model. On the contrary, the model without the opening seems to provide a better match with the considered reference solution.

The scatter of the GRPs with respect to the values resulting from the FE model (Figure 4.35) confirms these observations, helping also to quantify the detected differences.

In particular, from the data represented in Figure 4.35 it emerges that all the EF models which include the little opening, with the only exception of the one associated to the Dolce's proposal, tend to overestimate the actual initial stiffness ($k_{s,35}$), especially the EF model according to Augenti's criterion, where the difference with respect to the FE model is higher than 80%. The model associated to the Dolce's proposal, on the contrary, being characterized by piers with an effective height higher than that of Augenti's criterion (see Table 4.4), presents an initial stiffness closer to the FE model ($\Delta k_{s,35}$ close to 0). However, also the EF model without the opening provides a quite good estimate of the initial stiffness, with a scatter of only 10% with respect to the FE model.

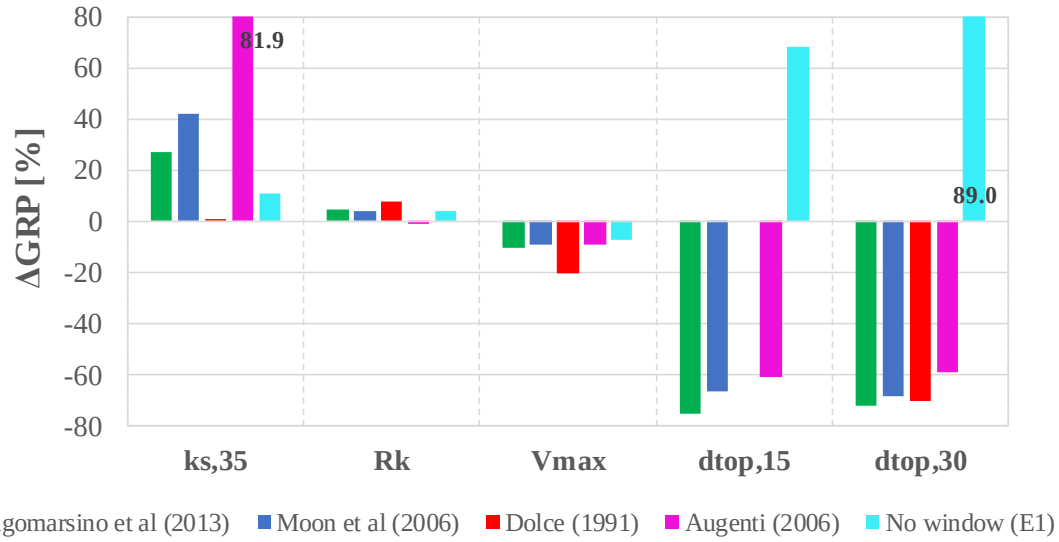

Figure 4.35 - Comparison of the results in terms of ΔGRP (scatter of the Global Response Parameters with respect to the FE model) obtained through the different EF models in case of configuration BD, analysis in the positive verse.

The stiffness degradation, expressed through the parameter R_k, is similar for all the considered models and it is substantially consistent with the one characterizing the FE model ($\Delta R_k < 10\%$).

With regard to the maximum strength V_{max}, all the EF models slightly underestimate, of about 10%, the maximum strength recorded by the FE model; in the case of the EF model associated to the Dolce's criterion this underestimation is even higher, and approximatively equal to 20%. On the contrary, the EF model without the opening provides a result closer to the one of the reference solution.

The analysis of the post-peak response characterizing the pushover curves represented in Figure 4.34-a shows that, apart the Dolce's configuration, the EF models including the little opening predict a significant strength degradation which occurs for values of top displacement ranging from 12 mm to 18 mm. This type of behavior is considerably different with respect to the one detected by the FE model, and leads therefore to very high values of the scatter on the parameters $d_{top,15}$ and $d_{top,30}$: indeed, all the EF models are associated to an underestimation of these parameters which is on average about 65%. It is also stressed that in the case

of the model according to Dolce (1991), since the scatter with respect to V_{max} is higher than 15%, it is not possible to compute $\Delta d_{top,15.}$ On the contrary, in the curve obtained through the EF model without the little opening no strength degradation is observed for the examined values of top displacement, thus providing a better match with the considered reference solution, at least until a top displacement of 35 mm. Nevertheless, this EF model does not well capture the strength decay observed in the FE model for higher values of top displacement, as evidenced by the not negligible values of $\Delta d_{top,15}$ and $\Delta d_{top,30}$ observed in Figure 4.35.

Moving to the analyses in the negative verse, a better agreement between the predictions of the different EF models can be observed ((Figure 4.34-b); moreover, these predictions are substantially consistent with the assumed reference solution, in terms of both maximum strength and post-peak response. This is demonstrated, from a quantitative point of view, by the results in terms of ΔV_{max} (for the maximum strength) and $\Delta d_{top,n}$ (for the softening behavior) reported in Figure 4.36.

However, the EF model according to Lagomarsino et al (2013) exhibits a considerable strength reduction in correspondence of a top displacement equal to 16 mm, differently from the pushover curves obtained with the other EF models, which present a more gradual strength degradation, thus being more consistent with the behavior described by the FE model. This is caused by the failure of the central pier at the ground floor, as better explained in the following comparisons in terms of damage pattern.

The scatter of the other GRPs (Figure 4.36) shows also that by using the EF model without the window it is possible to obtain results which are closer to the FE solution, especially in terms of stiffness degradation (ΔR_k almost equal to zero) and initial stiffness: indeed, $\Delta k_{S,35}$ in this case is equal to 10%.

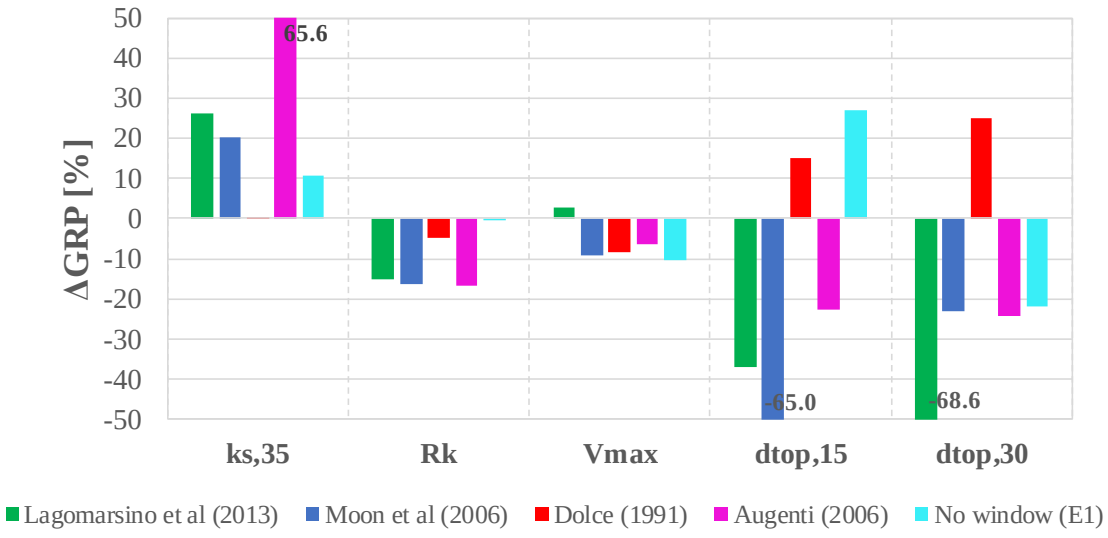

Figure 4.36 - Comparison of the results in terms of ΔGRP (scatter of the Global Response Parameters with respect to the FE model) obtained through the different EF models in case of configuration BD, analysis in the negative verse.

Regarding the post-peak response, the scatter with respect to $d_{top,15}$ and $d_{top,30}$ shows that also in this case the EF model without the window provides in general quite good results: they are comparable to the ones obtained with the models associated to the proposals by Dolce (1991) and Augenti (2006) and at the same

time substantially better than those derived from the EF models according to Moon et al (2006) and Lagomarsino et al (2013) (in this last case the premature drop of strength previously observed leads to high values of $\Delta d_{top,15}$ and especially of $\Delta d_{top,30}$).

B. *Results of the comparisons in terms of damage pattern*

In the following the attention is mainly concentrated on the damage occurring in pier P2, that carries more than 60% of the total base shear of the analysed wall.

Figure 4.37 shows the damage pattern in correspondence of increasing values of top displacement, considering the analysis in the positive verse. The observation of the damage evolution in the EF models allows to explain the drops of strength observed in the associated global pushover curves.

In particular, in most of the cases the drops of strength are caused by the reaching of a high state of damage in element P2, that, due to the presence of the little opening, tends to assume a very squat geometry, except for the case of the Dolce's proposal (from Table 4.4: λ=0.25 according to Augenti (2006), λ=0.65 according to Lagomarsino et al (2013), λ=0.51 according to Moon et al (2006), λ=1.03 according to Dolce (1991)).

Indeed, in all the considered EF models this pier has already reached DL2 (peak of strength) for a top displacement equal to 4 mm. Moreover, in correspondence of a higher top displacement (d_{top} =15 mm), a significant state of damage (DL4) is predicted by the models associated to the proposals by Moon et al (2006) and by Augenti (2006), while in case of the model according to Lagomarsino et al (2013) even the actual collapse (DL5) has occurred. Only in the EF model according to the Dolce's proposal this pier presents a lower state of damage, being in this case the damage concentrated in the right pier at the ground floor (P3), where DL4 has been reached.

On the basis of these results it is observed that no one of the considered EF models provides a satisfactory description of the actual state of damage characterizing, according to the FE model, the portion of masonry with the little opening. Indeeed, as illustrated in Figure 4.37 by the FE model, in this case the tensile cracks propagate starting from the corners of the little opening, and affect portions of masonry which does not exactly correspond to the piers identified in the EF models according to the different criteria.

The fact that the considered EF models are not able to correctly predict the actual state of damage characterizing the portion of wall with the little opening is even more relevant when looking at the damage pattern emerging from the analyses in the negative verse, even if in this case the global responses provided by the EF models are all quite similar to the curve considered as the reference solution. As an example, in the following figure (Figure 4.38) the comparison between the damage occurred for a top displacement equal to 20 mm in the FE model and in the EF models according to Lagomarsino et al (2013) and Moon et al (2006), which are associated to different types of global response (see Figure 4.34-b), is illustrated.

In the FE model the inclination of the tensile crack which develops at the ground floor seems to neglect the presence of the little opening. This suggests that the big masonry portion at the ground floor behaves as a unique pier. On the contrary, when in the EF models the presence of the opening is considered, two different piers are introduced in that part of the wall, so that this type of damage propagation cannot be captured.

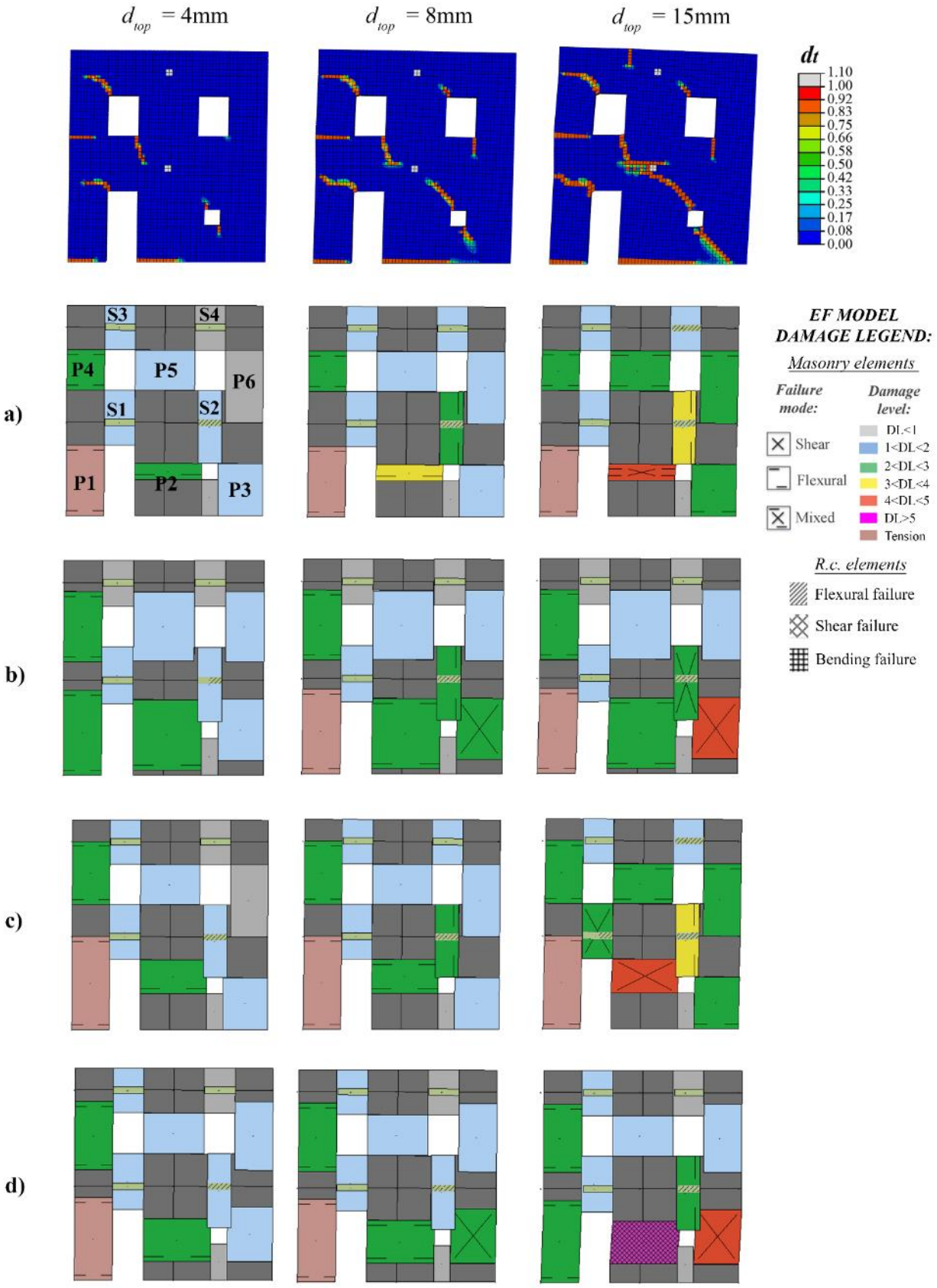

Figure 4.37 - Configuration BD, analysis in the positive verse: comparison between the damage pattern resulting from the FE model and the EF models associated to the different criteria for the pier effective height: (a) Augenti (2006); b) Dolce (1991); c) Moon et al (2006) and d) Lagomarsino et al (2013).

In particular, in the model according to Lagomarsino et al (2013) the central pier at the ground floor, which has the same geometry as in the positive analysis (λ=0.65), for a top displacement equal to 20 mm has already reached the actual collapse (DL5, as illustrated in Figure 4.38), thus explaining the significant reduction of global strength observed in the corresponding pushover curve.

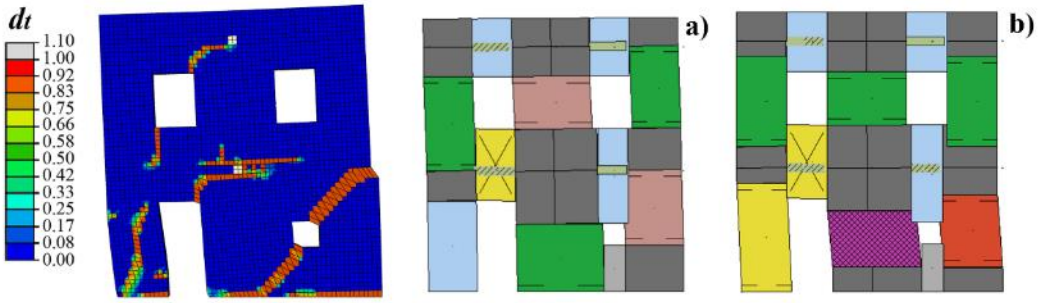

Figure 4.38 – Configuration BD, analysis in the negative verse: comparison between the damage pattern resulting (d_{top} = 20 mm) from the FE model and the EF models according to: a) Moon et al (2006); b) Lagomarsino et al (2013). See Figure 4.37 for the meanings of colors and symbols in case of the EF models.

On the contrary, according to the criterion proposed by Moon et al (2006), this pier results to be less squat than in the positive analysis (λ=0.78), and in correspondence of d_{top} =20 mm it is characterized by a damage level (DL2) which is not yet associated to a strength degradation. Indeed, in the corresponding pushover curve no significant strength degradation occurs within the considered values of top displacement.

It is observed that the aspect ratios characterizing P2 in the two considered EF models are quite similar, so that for a given horizontal displacement the corresponding values of drift are almost similar as well. In this case, the different behavior exhibited by the panel is ascribable to slight differences in the evolution of the normal stress acting on the element in the two models. Indeed, the range of variation of the normal stress refers to situations in which the flexural and the shear strength are close, so that small variations in the acting axial load may lead to different failure modes as well as to hybrid failures.

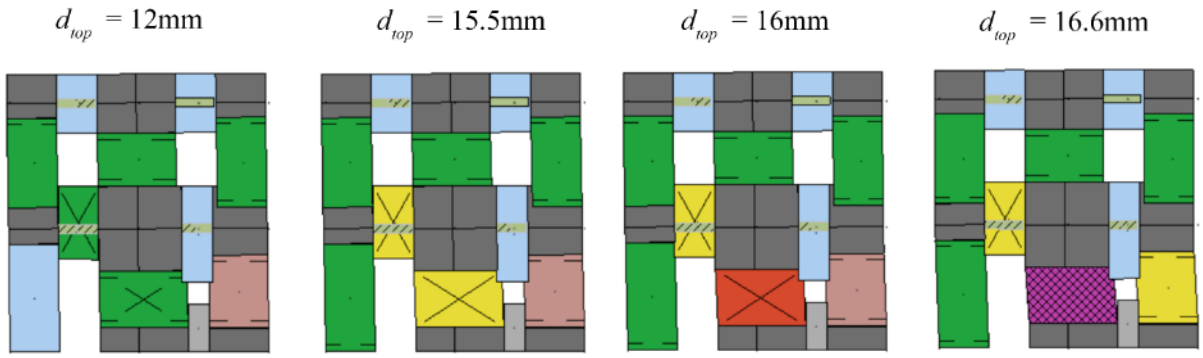

Figure 4.39 - Configuration BD, analysis in the negative verse: damage pattern resulting from the EF model according to Lagomarsino et al (2013) for different values of top displacement. See Figure 4.37 for the meanings of colors and symbols.

Actually, in the model according to Moon et al (2006) the considered pier undergoes flexural failure, which is associated to a quite high displacement capacity without significant loss of strength, being the drift

limits associated to this type of failure higher than in the case of shear failure. Conversely, the evolution of damage occurring in the EF model according to Lagomarsino et al (2013), which is illustrated in Figure 4.39, shows that in P2 at first a hybrid failure occurs, which is associated to drift limits that are intermediate between the ones adopted in case of shear failure and flexural failure (see section 3.1.2); moreover, immediately after the pier is interested by a shear failure, governed by values of drift limits even lower. This can explain why the damage level characterizing P2 rapidly passes from DL2 to DL5 for a little increase in the horizontal displacement.

C. Results of the comparisons in terms of local response

The same three base sections already explained in case of the "B" type walls have been assumed as reference for the computation of the evolution of the generalized forces (see Figure 4.20).

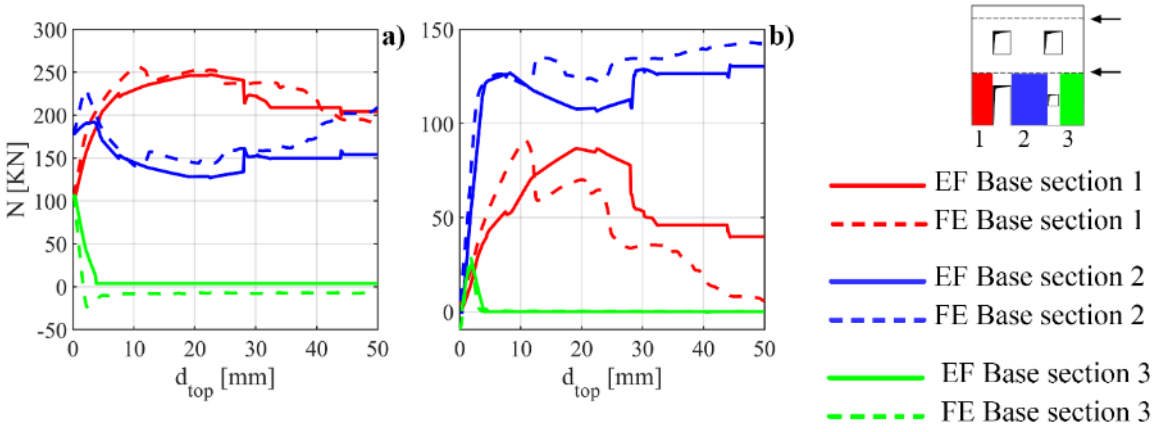

Figure 4.40 Configuration BD, analysis in the negative verse: comparison in terms of generalized forces acting at the three base sections of the wall (a) normal force; b) shear force) between the FE model and the EF model according to Dolce (1991)

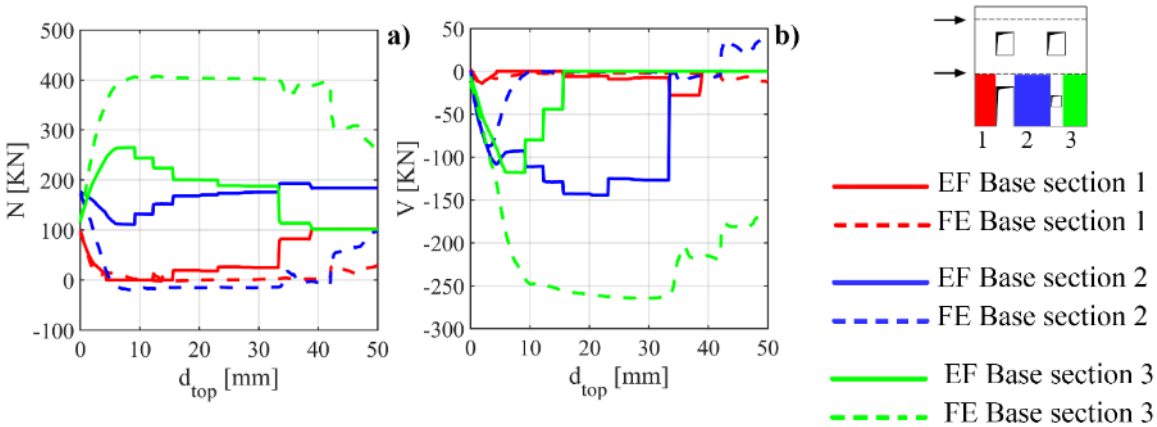

Figure 4.41 - Configuration BD, analysis in the positive verse: comparison in terms of generalized forces acting at the three base sections of the wall (a) normal force, b) shear force) between the FE model and the EF model according to Dolce (1991)

These comparisons substantially reflect the differences observed in the global pushover curves. In particular, the obtained results confirm what observed in the case of the configurations B1, B2 and BC, i.e. a quite good agreement with the FE model in the redistribution of the vertical and horizontal loads in case of the analysis in the negative verse (Figure 4.40) and higher differences when considering the analysis in the opposite verse (Figure 4.41), mainly regarding sections 2 and 3, due to the fact that in the FE model the diffusion of the stresses involves also the part of masonry below the little window at the ground floor.

Moving to the comparisons in terms of generalized forces acting on the alignments identified in the wall, the results discussed in the previous section in case of configurations B1, B2 and BC are substantially confirmed and even amplified, due to the presence of two adjacent openings with considerably different heights at the ground floor of the wall.

In the following figures the comparison in terms of shear force and bending moment diagrams acting on the alignment C2, which include P2, is illustrated.

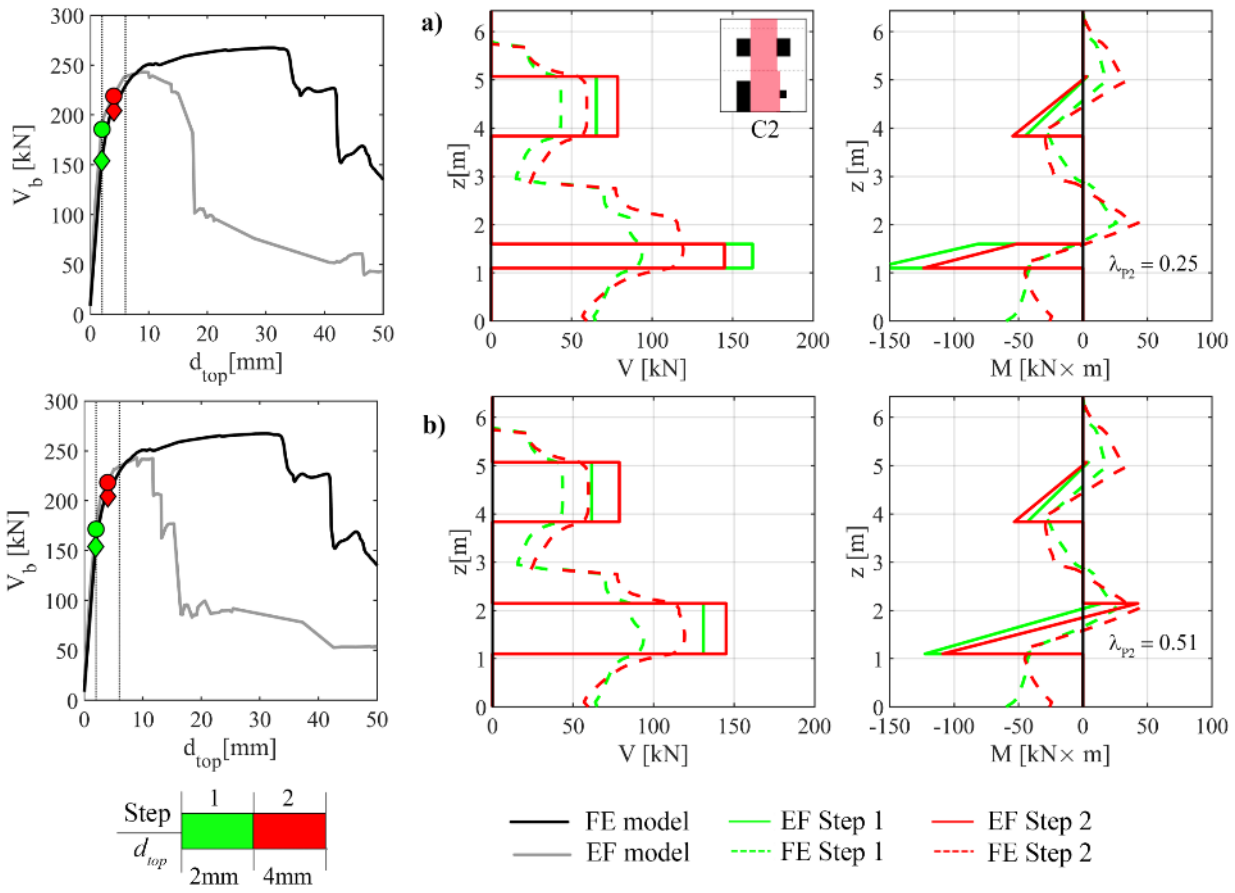

Figure 4.42 - Configuration BD, analysis in the positive verse: comparison between the FE model and different EF models (a) Augenti (2006), b) Moon et al (2006)) in terms of shear force *V* and bending moment *M* acting on the vertical alignment C2.

From Figure 4.42 it is possible to observe that the criterion proposed by Augenti (2006) does not provide good predictions in terms of effective height of the pier at the ground floor, being it too short when

compared with the bending moment diagram derived from the FE model. This is associated to a strong overestimation of the shear force acting in this portion of masonry; the same occurs also for the predicted values of bending moment, especially in the case of the pier at the lower storey. Conversely, the criterion suggested by Moon et al (2006) provides a good estimate of the effective height for both piers; however, as already observed in the configurations B1, B2 and BC, also in this case an overestimation of the corresponding shear forces is detected, even if lower than in case of Augenti's model.

On the other hand, considering the EF model according to Lagomarsino et al (2013) (Figure 4.43), better results in terms of generalized forces are obtained in the initial phase, until the failure of P2, which causes the strong drop of strength observed in the pushover curve. By looking at Figure 4.43, indeed, rather good predictions in terms of shear force are obtained in correspondence of steps 1 and 2. Nevertheless, when moving to a more advanced nonlinear response, also the predictions of this model are no more consistent with the results of the FE model. This happens in terms of both generalized forces (Figure 4.43) and displacements (Figure 4.44-a).

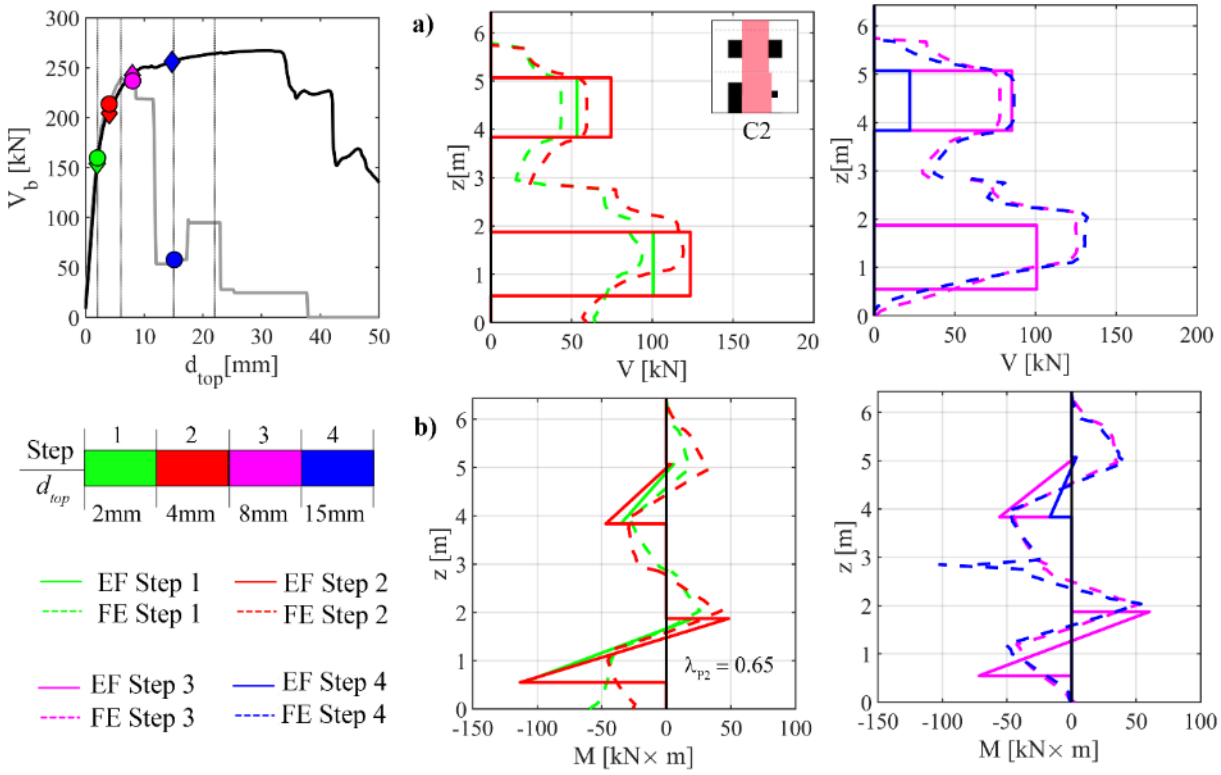

Figure 4.43 - Configuration BD, analysis in the positive verse: comparison between the FE model and the EF model according to Lagomarsino et al (2013) in terms of a) shear force *V* and b) bending moment *M* associated to the vertical alignment C2 for different steps of the analysis.

When examining the model according to Dolce (1991), where P2 is characterized by the highest aspect ratio, the predictions in terms of horizontal displacements (Figure 4.44-b) are slightly closer to the FE model results, even if they are still not satisfactory, especially when considering an advanced nonlinear response.

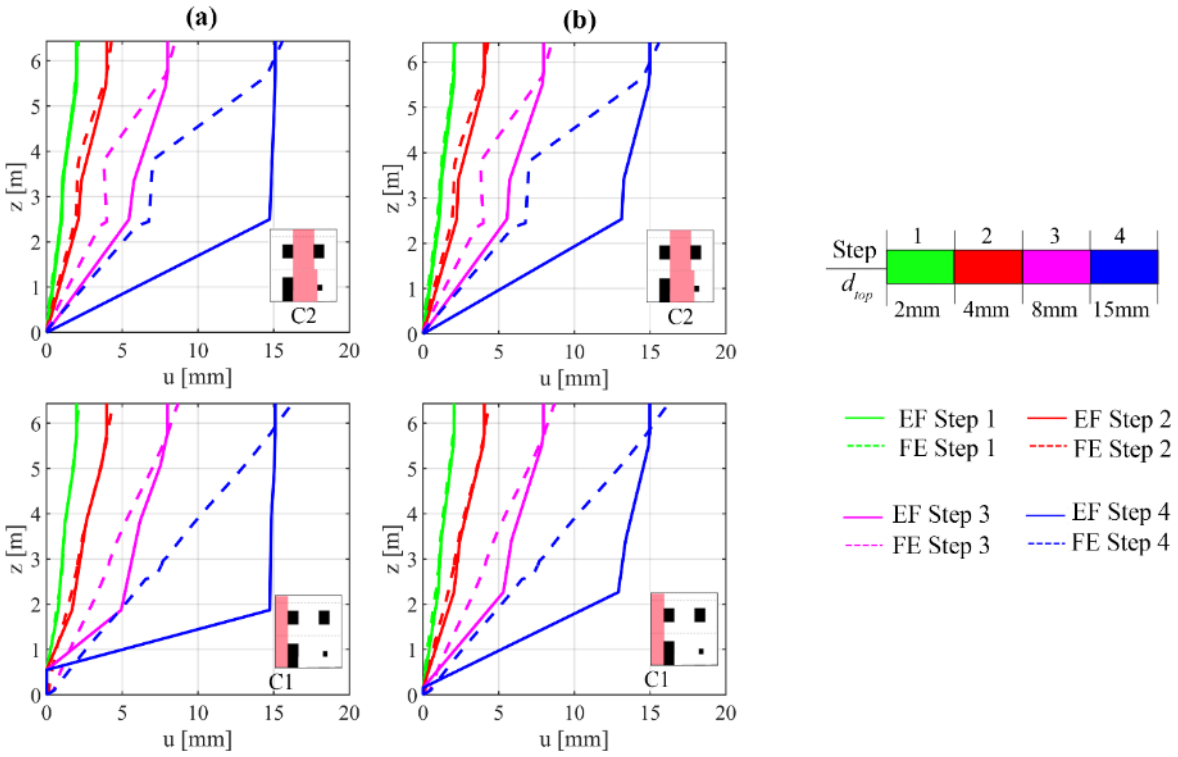

Figure 4.44 - BD, positive analysis: comparison between the FE model and the EF models according to: a) Lagomarsino et al (2013); b) Dolce (1991) in terms of horizontal displacements *u* on alignments C1 and C2.

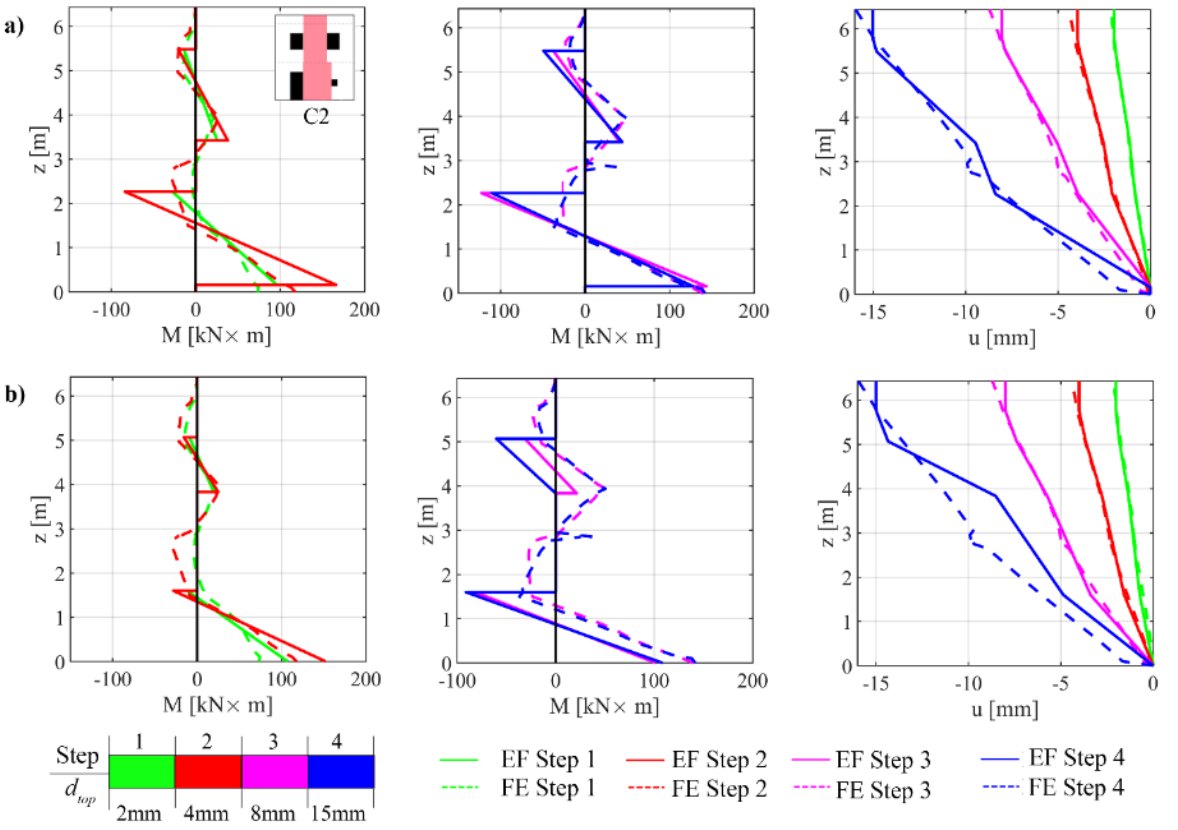

Figure 4.45 - BD, negative analysis: comparison between the FE model and the EF model according to: a) Dolce (1991); b) Moon et al (2006) in terms of bending moment *M* and horizontal displacements *u* on alignment C2.

Moving to the analyses in the negative verse, in general the comparison between the numerical models provides better results than those associated to the previous case. The only exception is represented by the EF model according to Lagomarsino et al (2013), where even if a good agreement with the FE model is detected in the first steps of the analysis, strong differences arise when moving to steps associated to higher values of top displacement, due to the premature drop of global strength observed on the corresponding pushover curve. Among the other EF models, the one according to Dolce (1991) provides a quite good match with the reference solution, in terms of both generalized forces and especially displacements. As an example, in Figure 4.45 the comparisons of the bending moment diagrams and the deformed shapes resulting for alignment C2 in the FE model and in the EF models according to Dolce (1991) and Moon et al (2006) are represented for different steps of the analysis.

From this figure it is possible to see that even if the effective height of the piers included in the considered alignment is better captured by the model according to Moon et al (2006), however the model defined on the basis of the Dolce's proposal allows to obtain good results in terms of bending moment values in case of both the piers of the alignment (P2 and P5) as well as a quite good reproduction of the horizontal displacements occurring in the alignment, even when considering an advanced nonlinear phase (step 4). However, when looking at the results obtained for alignment C3, as for example in terms of deformed shapes (Figure 4.46), despite of a good match with the reference solution in the first steps of the analysis (step 1 and 2), no one of the considered EF models, including the one according to Dolce's rule, is capable to capture the actual collapse mechanism activated in the FE analysis (as a confirmation of what observed in terms of damage pattern in Figure 4.38).

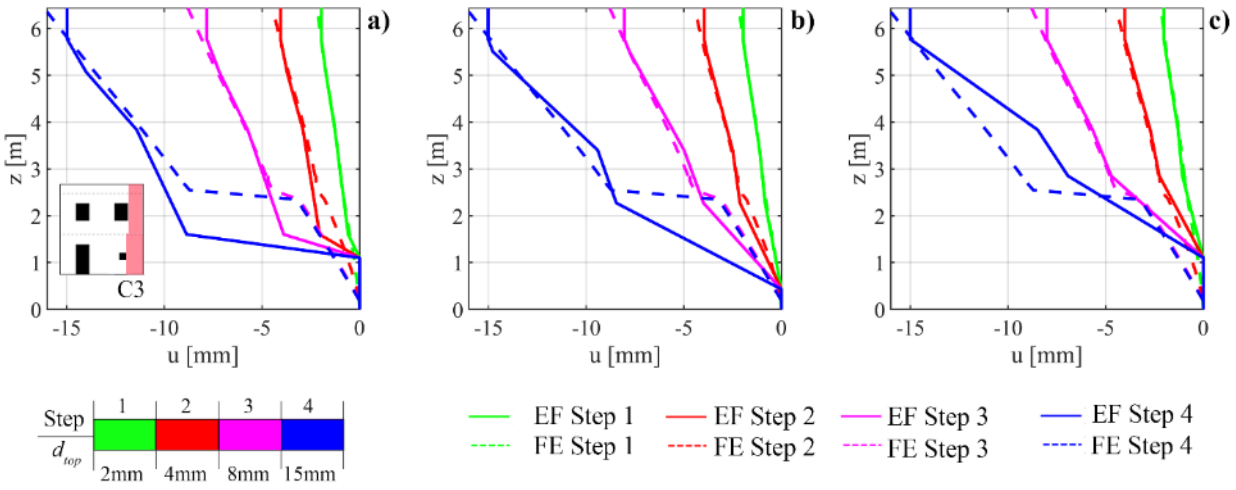

Figure 4.46 - Configuration BD, analysis in the negative verse: comparison between the FE model and the EF model according to: a) Augenti (2006); b) Moon et al (2006); c) Dolce (1991) in terms of horizontal displacements *u* associated to the vertical alignment C3.

The comparisons in terms of drift values associated to the masonry piers uphold the considerations above expressed. Considering the analyses in the positive verse, indeed, all the examined EF models overestimate the drift associated to P2 with respect to the value computed in the corresponding masonry portion in the FE model, as illustrated in Figure 4.47. Only the EF model according to Dolce (1991), where the effective

height considered for this pier is not so squat, provides better predictions in terms of drift, even if still overestimated.

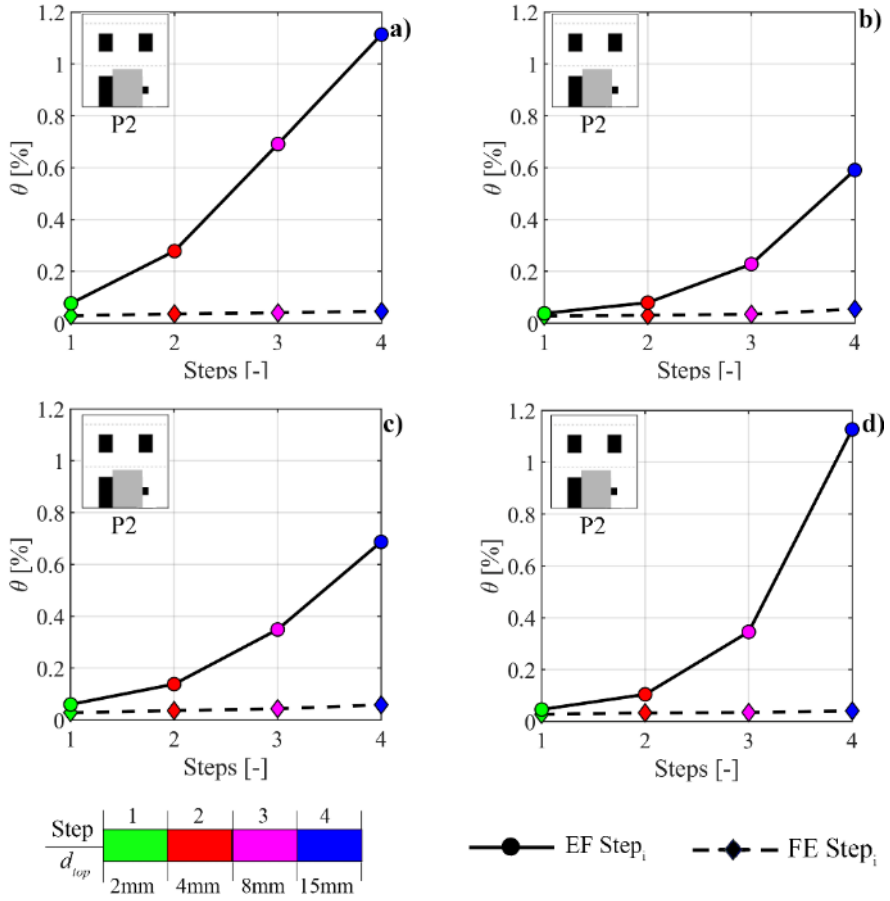

Figure 4.47 - Configuration BD, analysis in the positive verse: comparison in terms of drift values associated to pier P2 between the FE model and different EF models (a) Augenti (2006); b) Dolce (1991) c) Moon et al (2006) and d) Lagomarsino et al (2013)) for different steps of the analysis.

When considering the results of the analysis in the opposite verse, there is, in general, a better agreement about the different EF models and also between these and the reference solution in case of the predictions of drift values for P2, with the only exception of the EF model according to Lagomarsino et al (2013), due to the observed premature failure of this element. With regard to the other piers at the ground floor, the obtained results are represented in Figure 4.48. In particular, it can be noted that in case of P1, that is over compressed during the analysis, both the models according to Dolce (1991) and Augenti (2006) provide very satisfactory results, which well match the reference solution. Conversely, when looking at P3, more differences are detected. In particular, both the models according to Dolce (1991) and to Moon et al (2006) still provide good results, while a very high overestimation of the actual values of drift associated to the corresponding masonry portion is observed in case of the model according to Augenti (2006). In this model, indeed, this pier is particularly squat ($\lambda = 0.37$). However, no significant repercussions are present on the associated global pushover curve, since during the analysis this pier is subjected to a progressive reduction of the compression level, due to the overturning of the wall under the horizontal forces; therefore, it does not have a significant role in the structural response. This underlines that even if the global response, in this

analysis, is quite well caught, however by applying this rule it is not possible to obtain also a good description in terms of local response (deformations and displacements).

In the light of what emerged also in the case of the analysis in the positive verse, this consideration may be generalized in case of rules leading to very squat piers in presence of specific opening patterns.

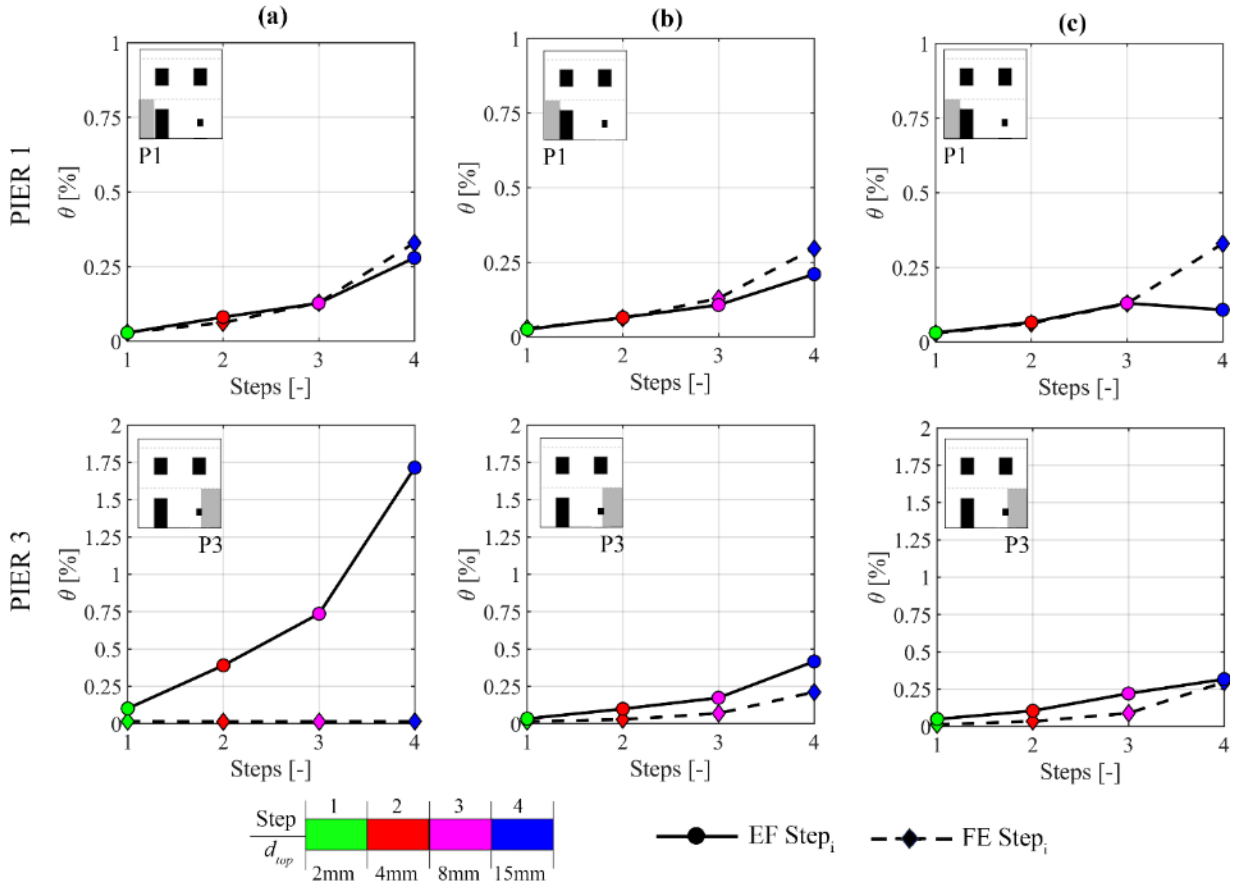

Figure 4.48 - Configuration BD, analysis in the negative verse: comparison in terms of drift values associated to pier P1 and P3 between the FE model and different EF models (a) Augenti (2006); b) Dolce (1991) c) Moon et al (2006) for different steps of the analysis.

4.4.2.1 Main recommendations on the basis of the achieved results

For what concerns configuration BD, no one of the considered criteria resulted to be able to well capture the actual response activated in the structure both at global and local scale. Indeed, in most of the cases the adopted rules lead to particularly stocky piers adjacent to the little opening, strongly affecting the capability of the EF models to reproduce the actual global ductility. This happens in particular when considering the analysis in the positive verse, which is associated to the highest scatter of the results with respect to the FE model.

In this case, the EF model according to Lagomarsino et al (2013) provides quite good results in terms of generalized forces but only in the initial phase of the analysis, being then the response conditioned by the premature failure of the central pier at the ground floor (P2). The Dolce's criterion, which predicts a higher effective height for the piers adjacent to the little opening, leads to results in terms of generalized forces and drift closer to the reference solution but still not satisfactory in terms of global response. Moreover,

even if all the considered EF models are able to capture the global activated failure mode, characterized by a concentration of damage at the ground floor, however the propagation of the tensile cracks observed in the FE model seems to neglect the presence of the opening, and when a structural model without the opening is considered it is possible to obtain a better global response. In this case this solution is therefore recommended. Further investigations on the issue related to the presence of little openings in masonry walls aimed to generalize the considerations here emerged are described in Chapter 5 (Section 5.2).

The above discussed results are summarized in Table 4.12, according to the same criteria introduced at section 4.4.4.1 (Table 4.10). Therefore, also in this case the data collected in the table are derived from the most punitive between the analyses in the two verses and, for what concerns the drift and the generalized forces, these data refer to pier P2 and to the alignment including it (C2). However, in the case of the local damage ("Damage in piers"), the comparison for each pier element is substituted with the attribution of a label as well as in the case of the global failure mode ("Global failure"). This because, as aforementioned, in the FE model the detected damage pattern at the ground floor seems to be better described by a unique element, and therefore cannot be captured when considering two distinct piers, as it happens in all the EF models including the little opening.

Table 4.12 – Summary of the main outcomes obtained in case of configuration BD.

		Moon et al (2006)	**Augenti (2006)**	**Lagomarsino et al (2013)**	**Dolce (1991)**
Global response	V_{max}	L	L	L	M
	$d_{top,n}$	VH	VH	VH	VH
	$k_{s,35}$	H	VH	M	L
Damage pattern	**Global failure**	Well captured	Well captured	Well captured	Well captured
	Damage in Piers	Not Good	Not Good	Not Good	Not Good
Generalized forces	**Shear force**	Not Good (Overestimated)	Not Good (Overestimated)	Moderate difference	Moderate difference
	Bending moment	Not Good	Not Good	Moderate difference	Moderate difference
Drift		Not Good (Overestimated)	Not Good (Overestimated)	Not Good (Overestimated)	Not Good (Overestimated)

4.4.3 Problem 3: identification of spandrels

In this section the results referring to the wall configurations aimed to study the problem of the identification of spandrel elements are discussed. In particular, two groups of walls were analysed:

- configurations of type "A", characterized by the presence of vertically misaligned openings at the two levels but still having the same number of openings per storey;
- configurations of type "E", characterized by the presence of a different number of openings per storey.

In these configurations, in addition to the problem of the identification of the spandrels, which actually represents the main uncertainty in presence of these types of irregularity, also the influence on the structural response of the adoption of different effective heights for piers was investigated.

4.4.3.1 Configurations of type "A": vertically misaligned openings

A. Comparisons in terms of global response

In Figure 4.49 the pushover curves obtained for configuration A1 (where there is still an overlapping part between the vertically misaligned openings), positive and negative verse of the analysis, are shown. In general, it is possible to observe a good agreement between the predictions of the four EF models) and the results provided by the FE model, considering both the positive and the negative verse of the analysis. It is useful to observe that the EF models differ only for the geometry of piers, being the spandrel between the vertically misaligned openings always included in the structural models (see the pictures in Table 4.7). However, while in the positive verse the results are almost coincident in terms of stiffness, maximum strength and post-peak response, in the negative verse the scatter of the results slightly increases, in particular regarding the post-peak phase of the curves.

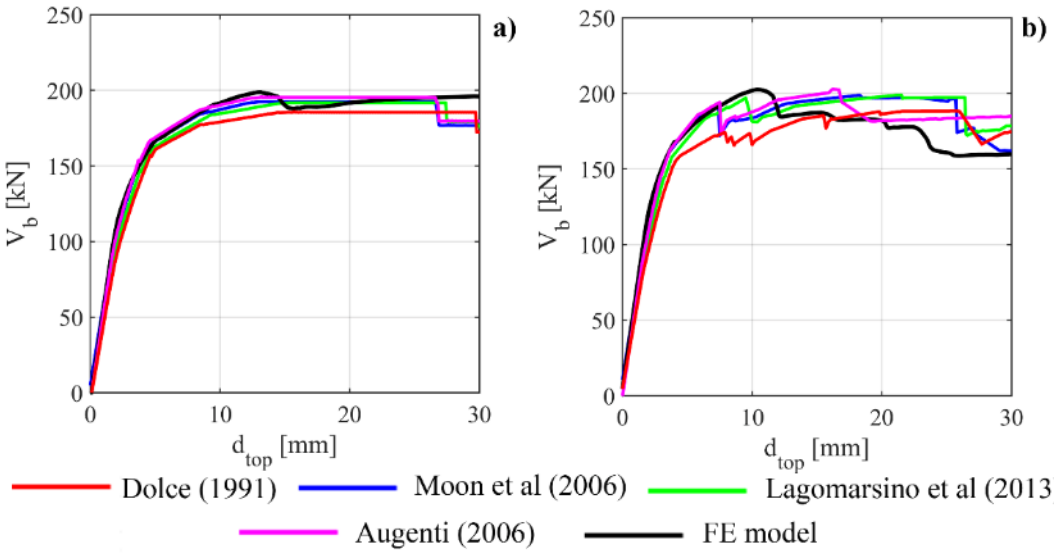

Figure 4.49 - Comparison in terms of pushover curves for configuration A1: a) analysis in the positive verse; b) analysis in the negative verse.

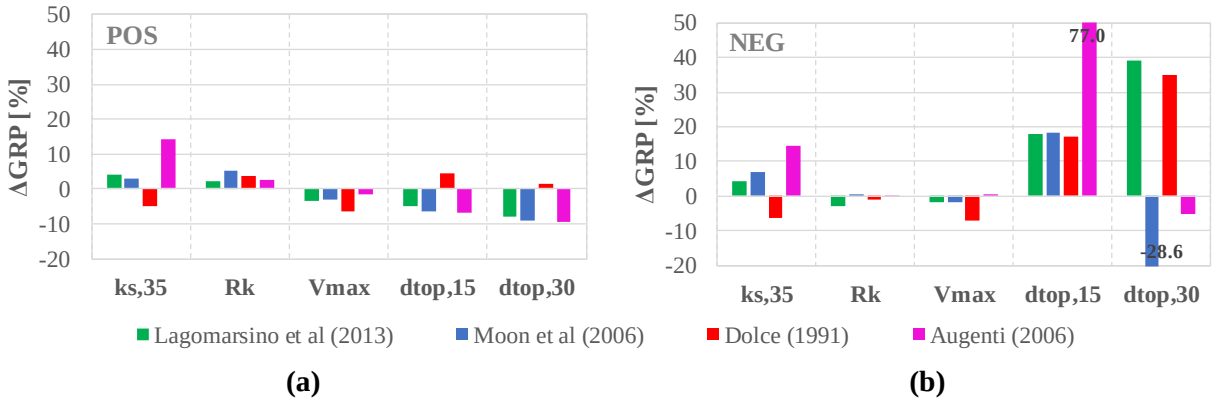

Figure 4.50 - Comparison of the results in terms of ΔGRP (scatter of the Global Response Parameters with respect to the FE model) obtained through the different EF models in case of configuration A1, analysis in the positive verse (a) and in the negative verse (b).

The results in terms of scatter of the GRPs (illustrated in Figure 4.50) testify values in general lower than 10% with respect to the reference solution (except for the case of the model according to Augenti (2006), which leads also in this case to a more significant overestimation of the initial stiffness with respect to the other models, being $k_{s,35}$ > 10%), thus indicating a quite perfect agreement on all the parameters characterizing the global response. The only case in which scatters higher than 10% are observed is represented by the parameters $d_{top,15}$ and especially $d_{top,30}$ referring to the analysis in the negative verse; this result is mainly due to a less pronounced strenght degradation predicted in the post-peak phase of the curves by the EF models.

These results on configuration A1 highlight that:

- in presence of vertically misaligned openings the determination of the pier effective height is not an issue, since the different examined rules lead to similar geometries for the pier elements and, therefore, the corresponding EF models provide global responses which are substantially similar. This consideration applies also to configurations A2 and A3, since they differ only about the vertical misalignement between the openings at the two levels, which does not significantly changes the geometry of the pier elements involved in these configurations;
- the inclusion of the spandrel in the EF model in presence of openings vertically misaligned but still overlapping, as in case of the configuration here examined, seems to be correct, since it allows to obtain a good match with the considered reference solution in terms of global response.

In the case of configuration A2 (where the misaligned openings overlap only in correspondence of one edge), in addition to the application of the different criteria for the pier effective height, also the influence of the presence (named as “WS”) or the absence of the spandrel (named as “NS”) in the structural model has been considered. The results of the pushover analyses obtained with the different numerical models are compared in terms of GRPs referring to stiffness and strength in Figure 4.51.

By looking at these data, a general good agreement between the predictions provided by the examined numerical models is observed, despite the configurations “WS” or “NS”. This clearly indicates that including or not the spandrel in the EF models does not significantly change the final result in terms of

global response. This result can be explained by considering that in the analysed configurations, which are two-storey masonry walls with r.c. tie beams, the role played by the spandrels in the structural response is not so significant: thus, such a result cannot be considered as conclusive. Between the two options ("WS" or "NS") it seems preferable to introduce the spandrel, since its introduction contributes to slightly reduce the scatter with respect to the FE model in terms of predictions about initial stiffness and stiffness degradation.

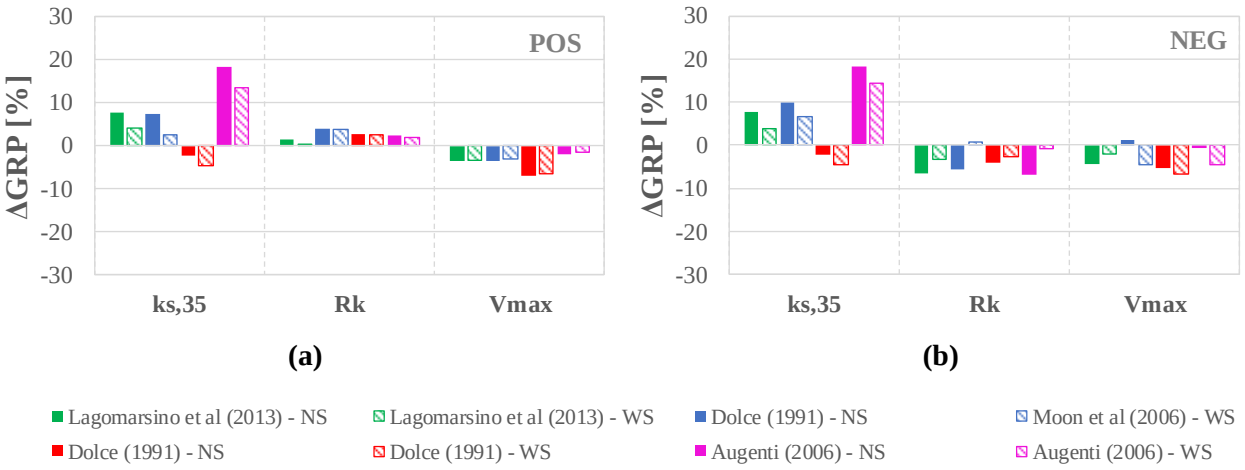

Figure 4.51 - Comparison of the results in terms of ΔGRP (scatter of the Global Response Parameters with respect to the FE model) obtained through the different EF models in case of configuration A2, analysis in the positive verse (a) and in the negative verse (b).

Moving to configuration A3 (where the openings at the two storeys do not overlap at all), in Figure 4. 52 and in Figure 4. 53 the comparison between the global pushover curves obtained with the numerical models under examination is shown, for both the verses of the analysis, while in Figure 4.54 the results referring to the analysis in the negative verse, which is the most interesting in this case, are summarized in terms of scatter of the associated GRPs.

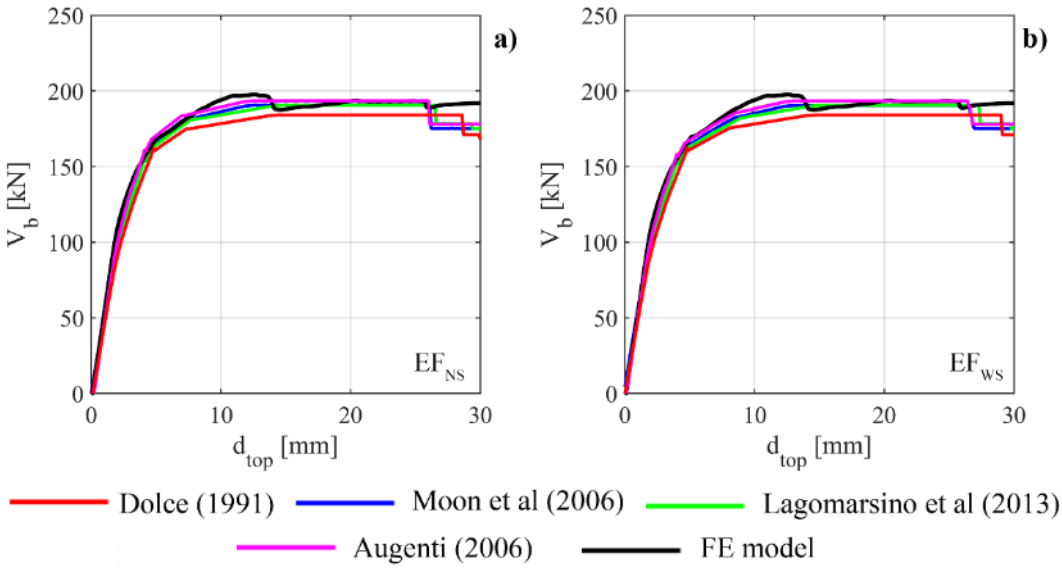

Figure 4. 52 - Comparison in terms of pushover curves for configuration A3, analysis in the positive verse: (a) EF models without the spandrel (EF_{NS}); (b) EF models including the spandrel (EF_{WS}).

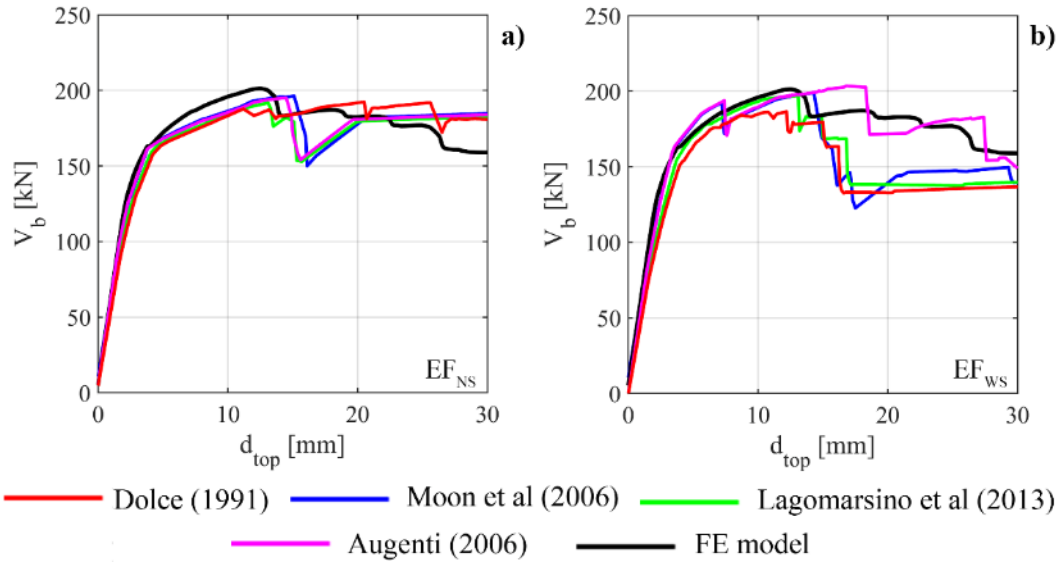

Figure 4. 53 Comparison in terms of pushover curves for configuration A3, analysis in the negative verse: (a) EF models without the spandrel (EF_{NS}); (b) EF models including the spandrel (EF_{WS}).

When looking at the analysis in the positive verse, the results obtained for configurations A2 are substantially confirmed: a very good agreement between the predictions of all the considered EF models and those of the corresponding FE model as well as the fact that the presence or the absence of the spandrel does not affect the final result.

Nevertheless, when examining the results obtained for the analysis in the negative verse, a higher sensitivity to the presence or not of the spandrel in the structural model is observed. Indeed, the introduction of the spandrel in the EF models leads to a strength decay in correspondence of a top displacement approximatively equal to 15 mm (caused by the failure of this elements, as illustrated in the following comparison in terms of damage pattern) which does not find a correspondence in the results of the FE analysis, where a more gradual strength degradation is observed.

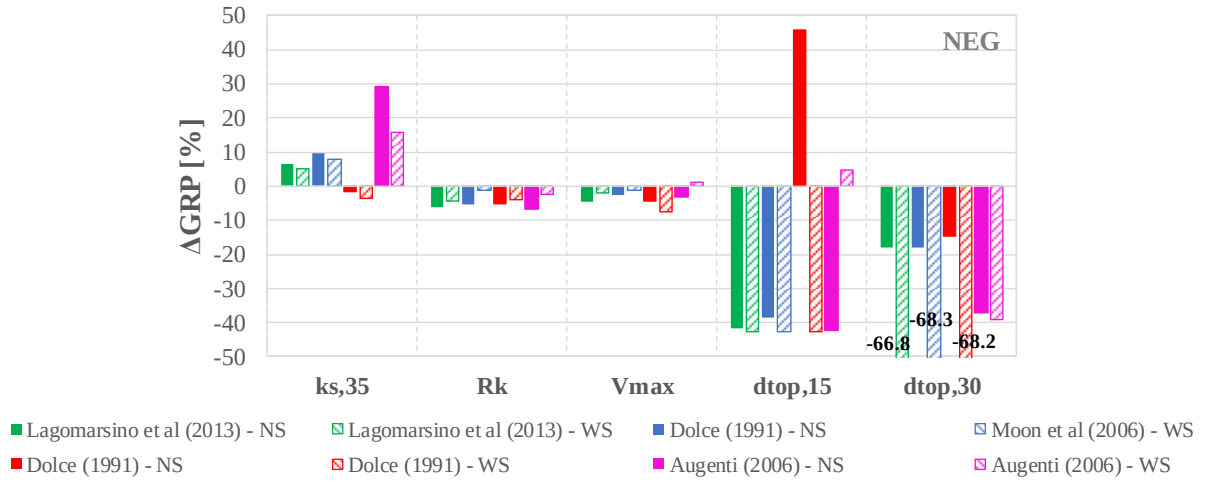

Figure 4.54 - A3, analysis in the negative verse: comparison of the results in terms of ΔGRP (scatter of the Global Response Parameters with respect to the FE model) obtained through the different examined EF models.

On the contrary, the EF models where the spandrel is not present, being substituted by a unique rigid node, provide a better match with the reference solution.

The results in terms of GRPs referring to this analysis (Figure 4.54) highlight that even if, as in the case of configuration A2, the inclusion of the spandrel slightly improves the obtained global response in terms of initial stiffness and stiffness degradation, however it leads to worse predictions in terms of post-peak response, as testified by the higher values of $\Delta d_{top,30}$ obtained from the EF models including this element.

B. Comparisons in terms of damage pattern

The results in terms of damage pattern substantially confirm that the EF models obtained with the different criteria for the pier effective height lead to almost the same results, close to the reference solution. Moreover, the analysis of the damage pattern emerging from the FE model is useful in order to check if the portion of masonry between the two vertically misaligned openings at the two levels undergoes or not damage during the analysis. This can provide indications about if it is correct or not to model that portion as a rigid node or as a deformable element in the EF model of the wall.

As an example, in Figure 4.55 the comparison in terms of evolution of the damage pattern derived from the FE model and the EF model according to Dolce (1991) for configuration A1 (positive analysis) is illustrated.

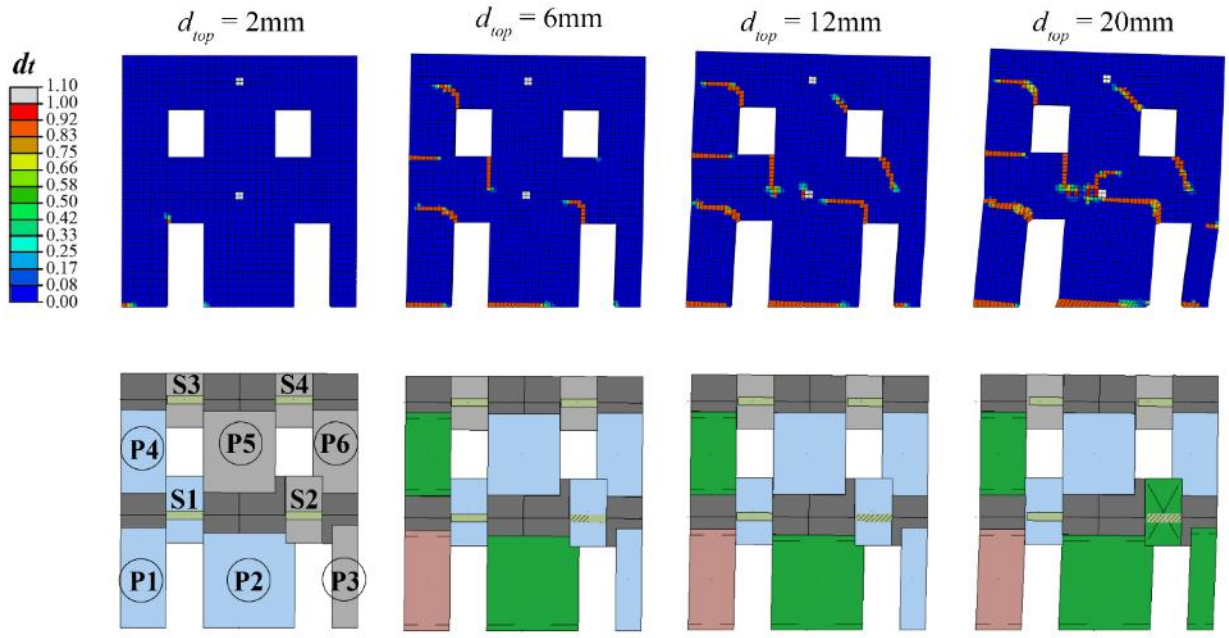

Figure 4.55 - Configuration A1, analysis in the positive verse: comparison between the damage pattern resulting from the FE model and the one emerging from the EF model according to Dolce (1991) for different steps of the analysis. See Figure 4.37 for the meanings of colors and symbols in case of the EF models.

It is noted that the EF model is able to correctly reproduce the evolution of damage detected by the FE model as well as the type of failure occurring in the different portions of the wall, especially those corresponding to masonry piers: in particular, for a top displacement equal to 20 mm piers P1, P2 and P3 at the ground floor and P4 at the upper floor present a prevailing flexural failure, while P5 and P6 are still

undamaged. With reference to spandrels, it is observed that, as predicted by the FE model, damage is mainly concentrated in the spandrels at the first storey, while no damage occurs in those located at the top floor. It is stressed that, according to the FE model, in the portion of masonry located between the vertically misaligned openings there is actually a concentration of damage (tensile cracks indicating the parzialization of the cross sections in this portion); this seems to indicate that it is correct to model that part of the wall as a deformable and nonlinear element. This observation is supported by the fact that the considered EF model, where the presence of the spandrel is included, actually predicts a concentration of damage (reaching of failure, DL2) in this element, consistently with what observed in the FE model.

A good correspondence with the predictions in terms of damage pattern on configuration A1 is observed also when considering the analysis in the negative verse, as evidenced in Figure 4.56, where the results representing the reference solution are compared, this time, with the EF model according to Moon et al (2006). Indeed, the damage occurring in piers is well captured; regarding spandrels, in the FE model damage mainly occurs spandrel S1, while the portion of masonry which would correspond to the spandrel under consideration (spandrel S2) remains substantially undamaged; the same happens also in the examined EF model.

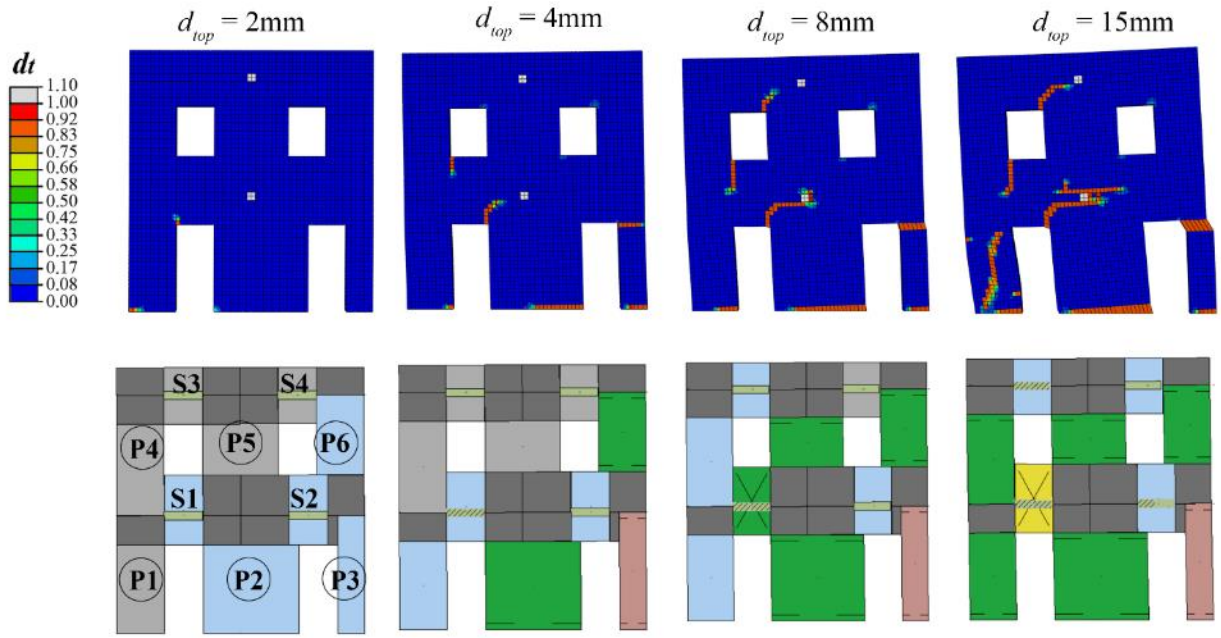

Figure 4.56 - Configuration A1, analysis in the negative verse: comparison between the damage pattern resulting from the FE model and the EF model according to Moon et al (2006) for different steps of the analysis. See Figure 4.37 for the meaning of colours and symbols in case of the EF models.

Moving to the results referring to configuration A3, in which no overlapping is present between the two openings, the comparison of the damage scenario resulting for different steps of the analysis from the FE model and the EF model according to Dolce (1991) is reported in Figure 4.57 in case of the analysis in the positive verse and in Figure 4.58 in case of the analysis in the negative verse, for both options "WS" or "NS". By looking at the pictures collected in Figure 4.57 it is observed that according to the FE model the portion of masonry included between the vertically misaligned openings is interested by the propagation of tensile cracks (d_{top} = 20 mm, d_{top} = 30 mm). However, the EF model with the spandrel and the EF model

without the spandrel predict exactly the same damage pattern for the different considered steps of the analysis; moreover, the spandrel, when present, is actually not interested by damage. These considerations explain why the global responses observed in Figure 4. 52 are not affected by the incorporation or not of the spandrel in the model. Concerning piers, results are substantially in agreement.

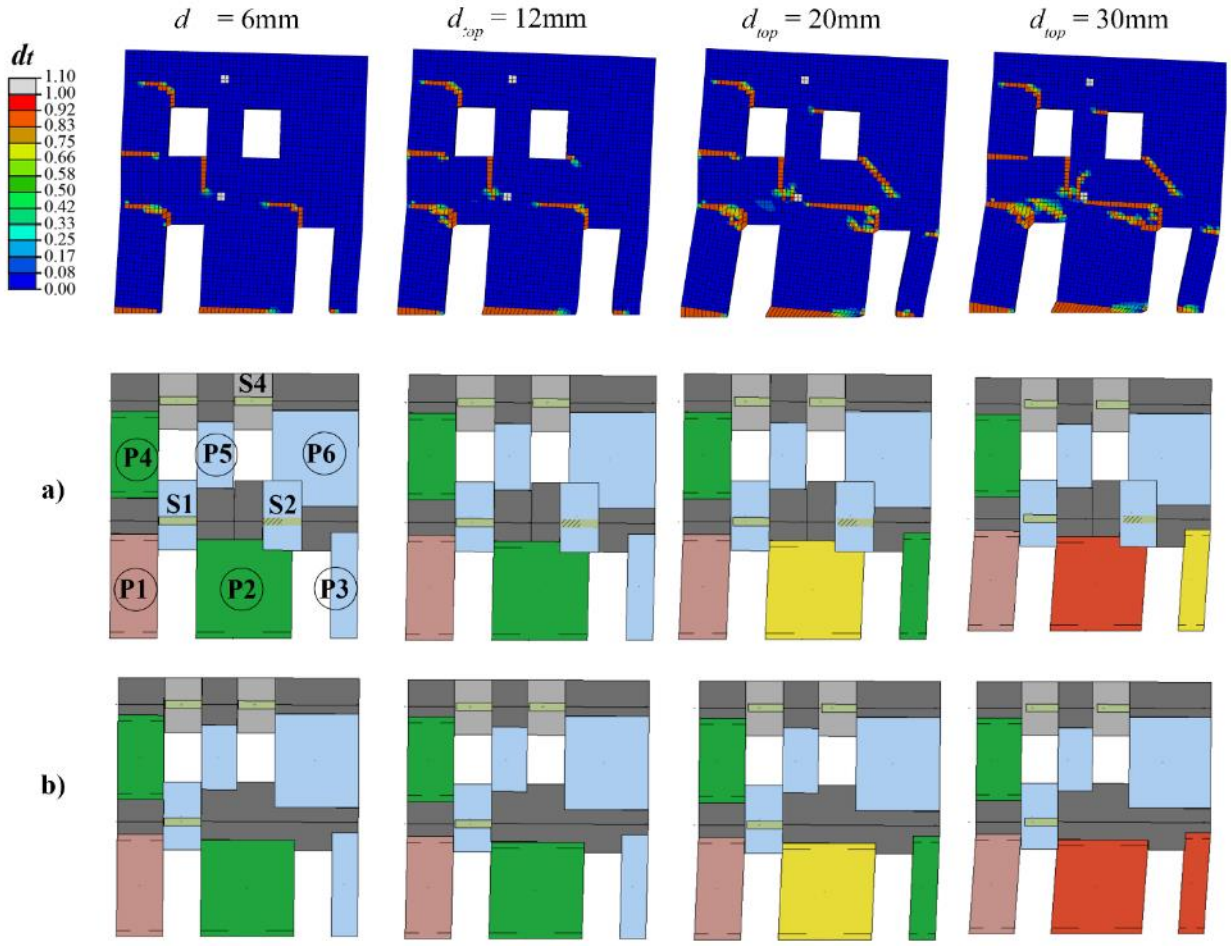

Figure 4.57 - Configuration A3, analysis in the positive verse: comparison between the evolution of damage pattern resulting from the FE model and the EF model according to Dolce (1991) with(a) and without (b) spandrel S2. See Figure 4.37 for the meaning of colors and symbols in case of the EF models.

Moving to the analysis in the opposite verse (Figure 4.58), differently from the previous case the adoption of an EF model with or without the spandrel actually affects the obtained damage pattern. When including the spandrel in the structural model this element undergoes significant damage, thus producing the strength decay observed in the corresponding global pushover curves (the spandrel S2, indeed, reaches DL3 for d_{top} = 15mm, which is associated, in case of shear failure, to the first reduction of the maximum strength). This results is not consistent with the FE model predictions. Indeed, in the FE model the portion of masonry included between the two misaligned openings does not exhibit tensile cracks that may suggest the presence of a spandrel (neither parzialization of the cross sections nor diagonal shear failures).Furthermore, it is worth underlining that the cracks which start from the centre of the wall and propagate in correspondence of the interfaces between masonry and the r.c. tie beams (d_{top}=15mm, d_{top}=30mm), which were observed

also in the other configurations, may be attributed, as discussed before, to the concentration of stresses here occurring due to the presence of the rigid beam used for performing the nonlinear analysis.

These considerations suggest that it would be better to adopt the solution of a unique rigid node.

Nevertheless, it is worth noting that in this way, due to the rotation of this big rigid portion, element P5 undergoes tension stresses, which is quite unrealistic. All these issues suggest the need of some refinements as discussed in the following (see section 4.4.3.3).

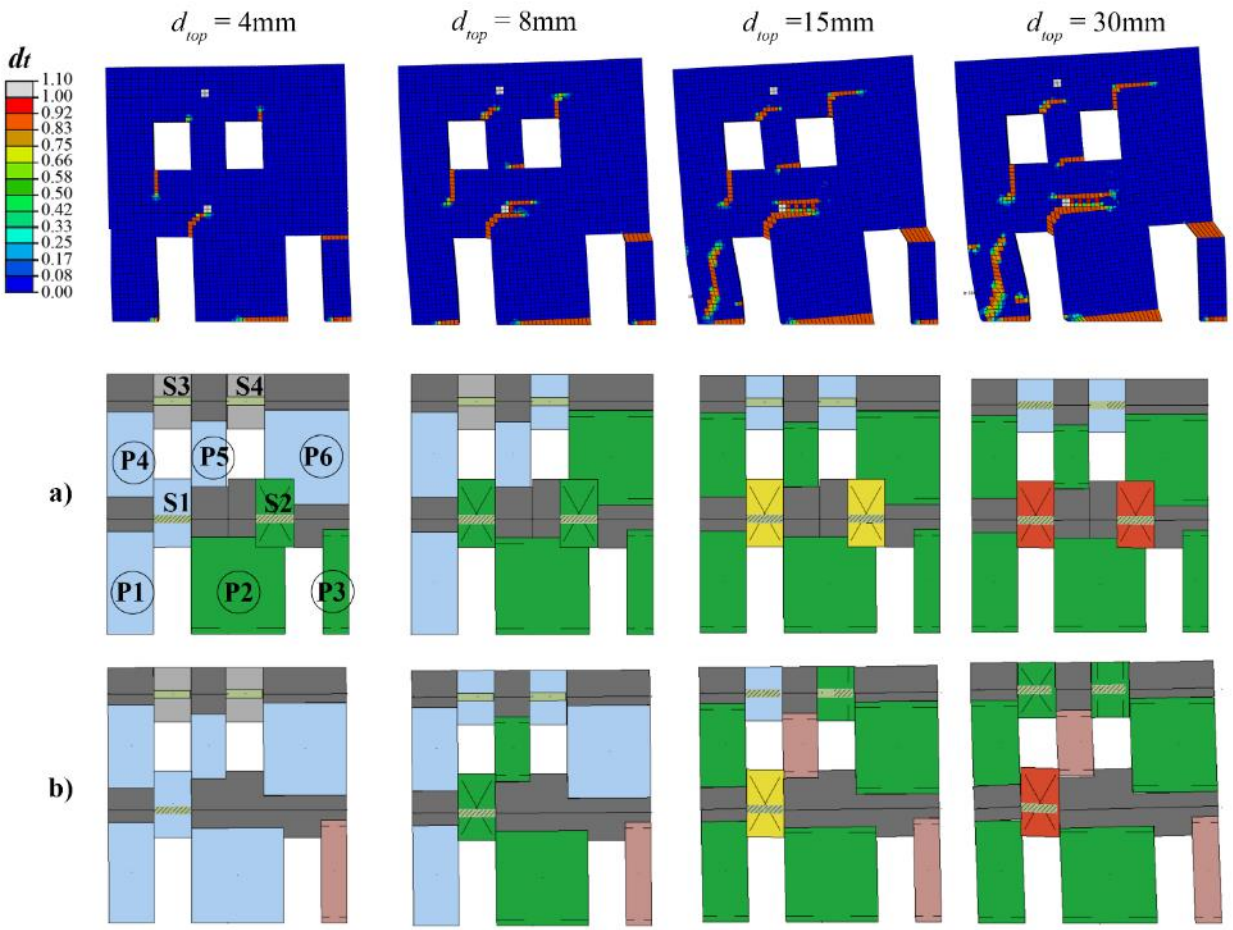

Figure 4.58 - Configuration A3, analysis in the negative verse: comparison between the evolution of damage pattern resulting from the FE model and the EF model according to Dolce (1991) with (a) and without (b) the spandrel S2. See Figure 4.37 for the meanings of colours and symbols in case of the EF models.

C. Comparisons in terms of local response

The comparison between the generalized forces diagrams illustrated in the following mainly refer to the horizontal alignment R1, due to the nature of the problem here investigated, which mainly involves the modelling of the spandrels at the first floor. In the case of the vertical alignments, the comparisons on the shear force and bending moment diagrams as well as displacement showed that all the considered EF models provide similar results, close to the reference solution. This confirms that in these types of wall the modelling of pier elements is not an issue and the adoption of one or the other criteria for their effective height does not affect the final results, even in terms of local response.

In Figure 4.59 the comparison in terms of shear force and bending moment diagrams referring to alignment R1 in configuration A1(positive verse) is shown (EF model with pier effective height according to Dolce (1991)); moreover, also the comparisons in terms of generalized displacements are illustrated.

From the analysis of the results deriving from the FE model (dashed lines) it is possible to observe that in the portion of masonry between the two vertically misaligned openings, which is highlighted in grey in the graph, the shear force and the bending moment diagrams actually indicate the presence of the spandrel; indeed, they are similar to the ones associated to the portion of masonry in the left part of the wall, where no uncertainties on the presence of the spandrel arise, being the openings at the two stories perfectly aligned. This observation confirms the fact that the spandrel has to be included in the model when the openings at the two levels are still overlapping, as suggested by the criterion expressed in Lagomarsino et al (2013). Actually, the inclusion of the spandrel in the EF model allows to obtain a good description of the generalized forces occurring in the examined part of the wall, when considering not only the initial response but also a more advanced nonlinear phase.

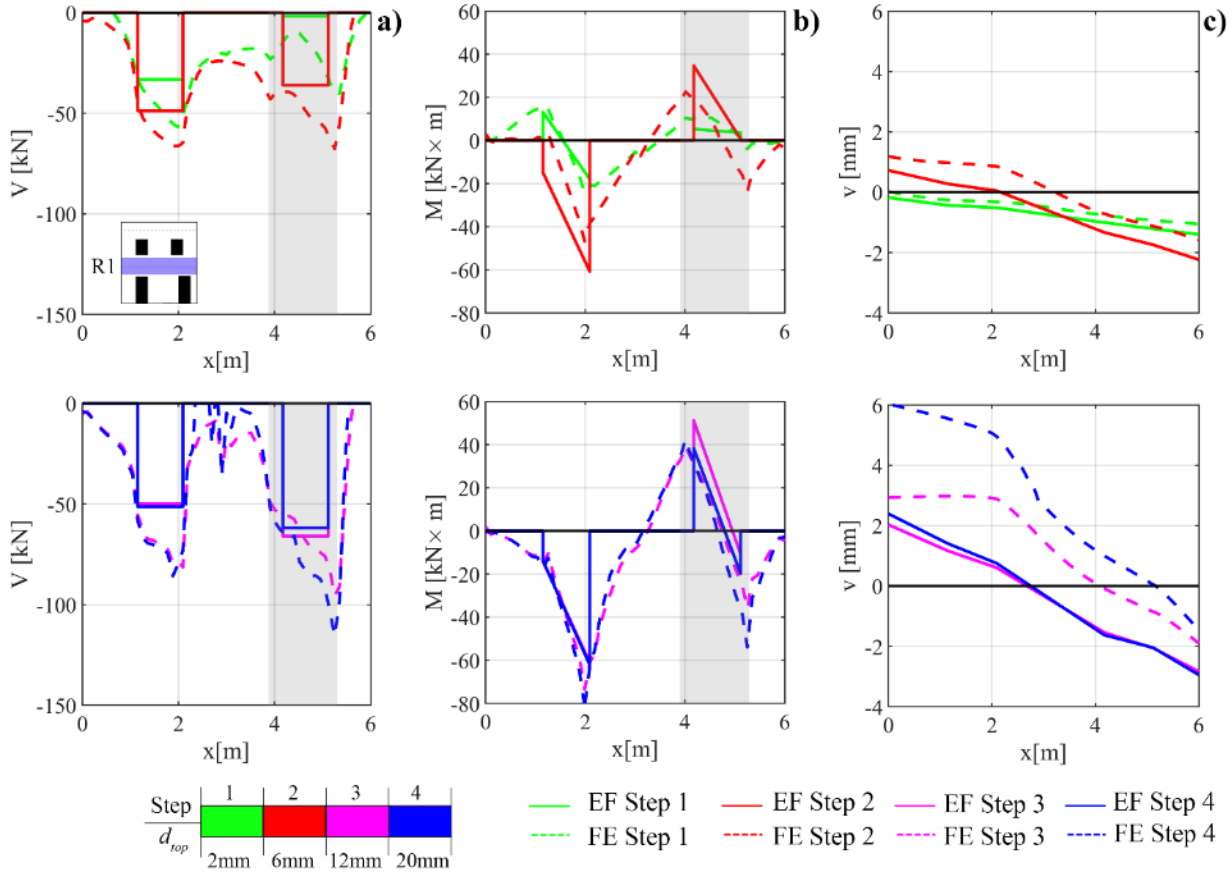

Figure 4.59 - Configuration A1, analysis in the positive verse: comparison between the FE model and the EF model according to Dolce (1991)) in terms of: a) shear force *V*; b) bending moment *M;* and c) vertical displacements *v* associated to the horizontal alignment R1 for different steps of the analysis. In grey the abscissae corresponding to the part of the wall included between the vertically misaligned openings.

The comparisons in terms of vertical displacements (Figure 4.59-c) help to confirm that the inclusion of the spandrel in the model is correct; indeed, it allows to obtain a good representation of the deformed shape

of the considered alignment, from both a qualitative and a quantitative point of view, especially when considering the first steps (from step 1 to step 3). Regarding step 4, the EF model tends to underestimate the vertical displacement occurring in the right part of the wall (i.e. the part that is subjected to uplift due to the rocking mechanism which involves the wall under the application of the horizontal forces).

This result is confirmed also when considering the analysis in the opposite verse, even if from the observation of damage deriving from the FE model the examined part of the wall was not evidently characterized by the occurrence of tensile cracks. As a confirmation of that, in Figure 4.60 the comparison in terms of bending moment diagrams, displacements and rotations obtained in this analysis for alignment R1 are shown, considering two steps (3 and 4).

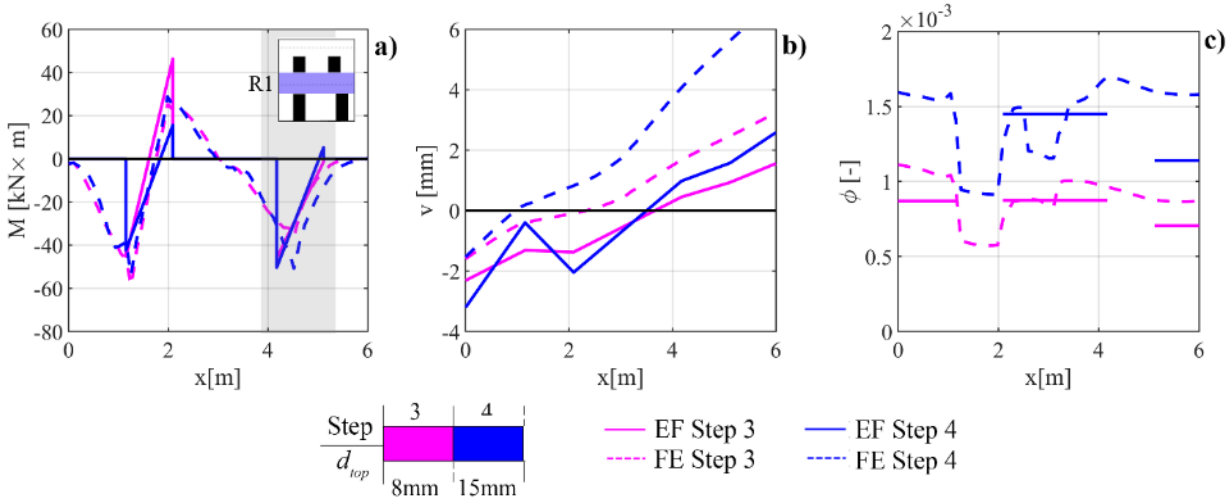

Figure 4.60 - Configuration A1, analysis in the negative verse: comparison between the FE model and the EF model according to Lagomarsino et al (2013)) in terms of a) bending moment M, b) vertical displacements *v* and c) rotations φ associated to the horizontal alignment R1 for different steps of the analysis. In grey the abscissae corresponding to the part of the wall included between the vertically misaligned openings.

Moving to the analysis of the results referring to configuration A3, in Figure 4.61 and in Figure 4.62 the bending moment diagrams obtained for different steps of the analysis in the positive and in the negative verse, respectively, are reported, comparing the predictions of the EF model without the spandrel (as an example the one with the pier effective height according to Dolce (1991)) and the FE model.

First of all, it is worth noting that the predictions of the EF model about the bending moment acting in spandrel S1 (the left one) quite perfectly agree with the FE results. In addition, for what concern the right part of the alignment, which is of more interest, also in this case the results of the FE analysis indicate that in the portion of masonry included between the vertically misaligned openings (and in particular above the right door opening, highlighted in grey in the graph) there is some deformability. Indeed, the bending moment values associated to the cross sections in this part of the wall seem to resemble a linear path, even if not so evidently as in the previous case of configuration A1. These results show that it would be more correct to model that part of the wall by taking into account that it actually presents a certain deformability than modelling it as a totally rigid portion.

When the spandrel is introduced in the EF model (Figure 4.63), even if in spandrel S1 the predictions in terms of bending moment are still consistent with those of the reference solution, however in the left part of the wall also in this case the bending moment deriving from the FE model is not perfectly captured.

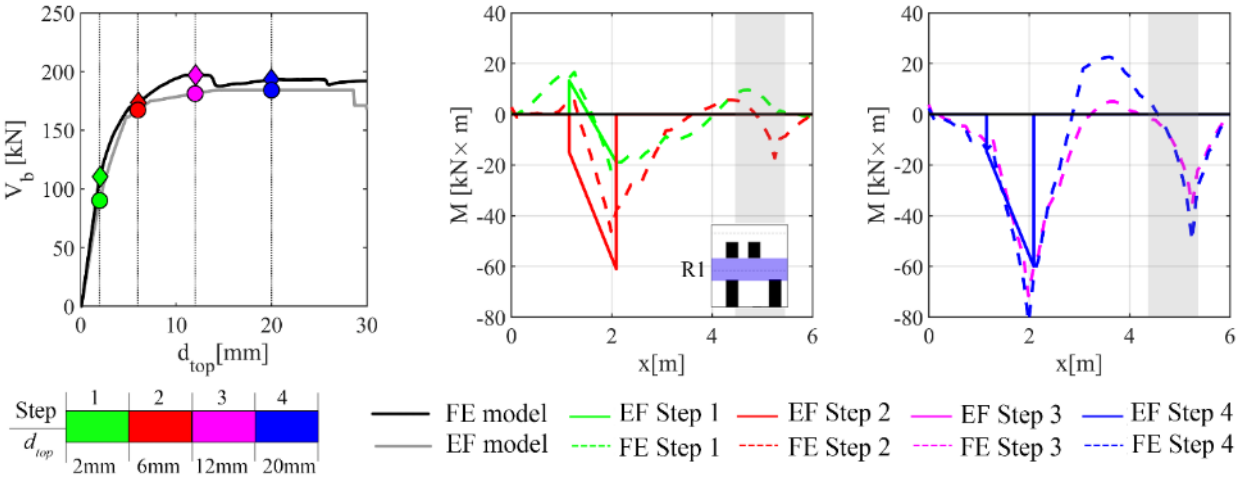

Figure 4.61 - Configuration A3, analysis in the positive verse: comparison between the FE model and the EF model according to Dolce (1991) – NS (without spandrel) in terms of bending moment *M* acting on the horizontal alignment R1 for different steps of the analysis. In grey the abscissae corresponding to the part above the right door opening.

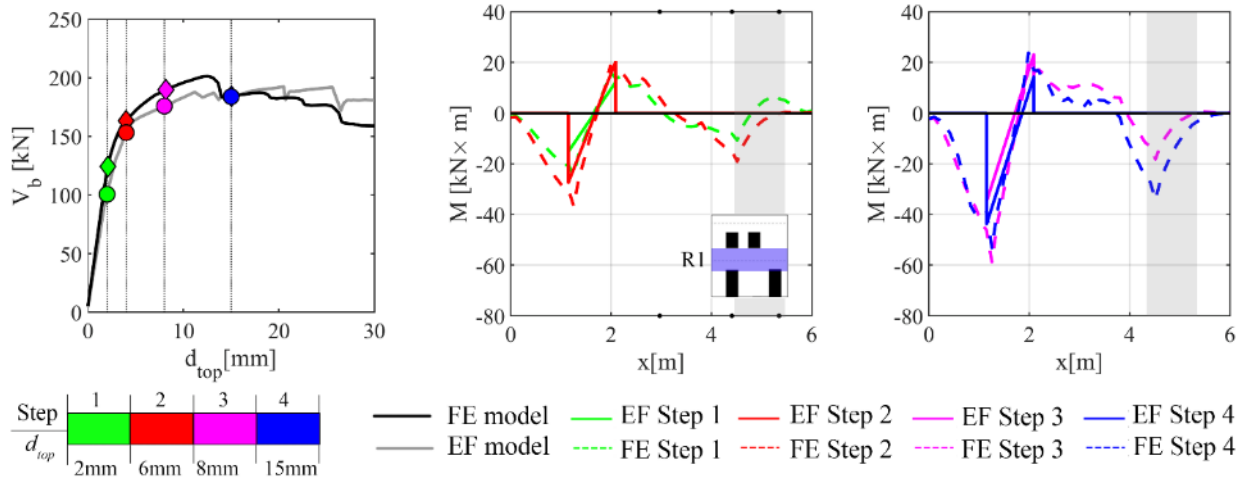

Figure 4.62 - Configuration A3, analysis in the negative verse: comparison between the FE model and the EF model according to Dolce (1991) – NS (without spandrel) in terms of bending moment *M* acting on the horizontal alignment R1 for different steps of the analysis. In grey the abscissae corresponding to the part above the right door opening

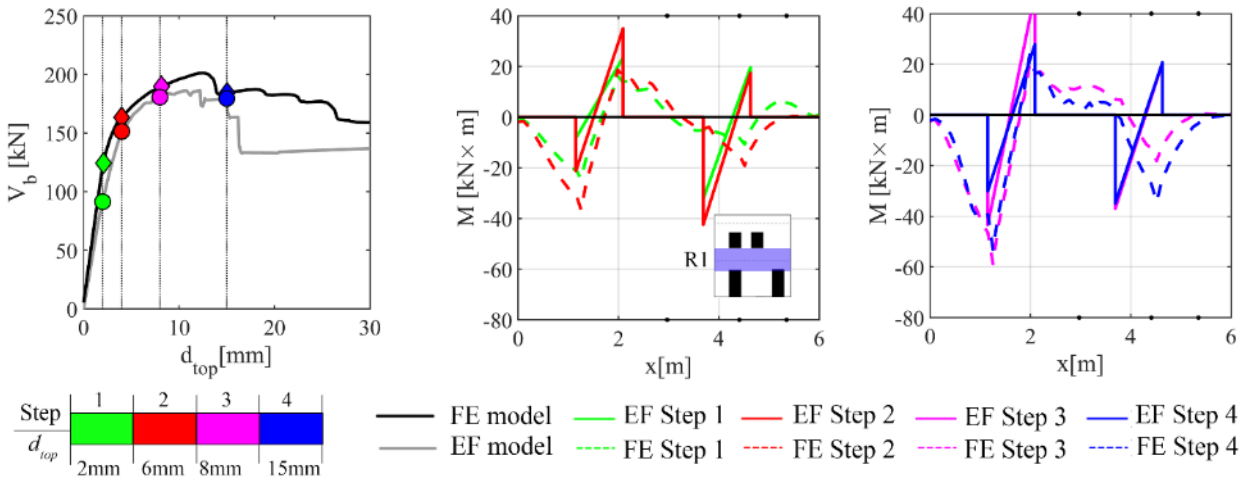

Figure 4.63 - Configuration A3, analysis in the negative verse: comparison between the FE model and the EF model according to Dolce (1991) – WS (with spandrel) in terms of bending moment *M* acting on the horizontal alignment R1 for different steps of the analysis.

Concluding, the results shown in this section referring to the walls of type "A" indicate that:

- in presence of walls with openings vertically misaligned but still overlapping (A1), even in correspondence of a single edge (A2), it turned out to be correct to include the spandrel in the structural model;
- in presence of openings vertically misaligned and no more overlapping (A3) the inclusion of the spandrel in the model leads to results not completely consistent with the reference solution, especially in terms of global response (due to the concentration of damage in the introduced spandrel, which produces a drop of strength not detected in the FE model); however, the comparisons in terms of local response indicate that it would be more correct to consider a deformable part rather than a completely rigid portion in the model, thus allowing also a better description of the global stiffness (in terms of both initial stiffness and stiffness degradation).

4.4.3.2 Configurations of type "E": different number of openings per storey

A. Results of the comparisons in terms of global response

The irregularity related to the presence of a different number of openings per storey was explored through configurations E2 (absence of one opening at the second storey) and E1 (absence of an opening at the ground floor). In Figure 4.64 and in Figure 4.65 the pushover curves obtained (positive and negative verse) for configuration E1 and E2, respectively, are compared.

More in detail, in case of the analysis in the positive verse on configuration E1 (Figure 4.64-a), all the EF models provide global curves that are almost coincident. Moving to the comparison with the FE curve, some differences in the predictions of maximum strength and also in the post peak response can be observed. Regarding the first aspect, in particular, the FE model predicts a higher strength with respect to the EF models; however, this difference is not so significant, being lower than 10%. Considering the post-

peak response, the FE model predicts a drop of strength in correspondence of a top displacement equal to approximatively 26 mm, while in all the EF models no strength degradation is present for the considered values of top displacement. This difference can be explained by considering the state of damage characterizing the wall in the different numerical models, as discussed in the following.

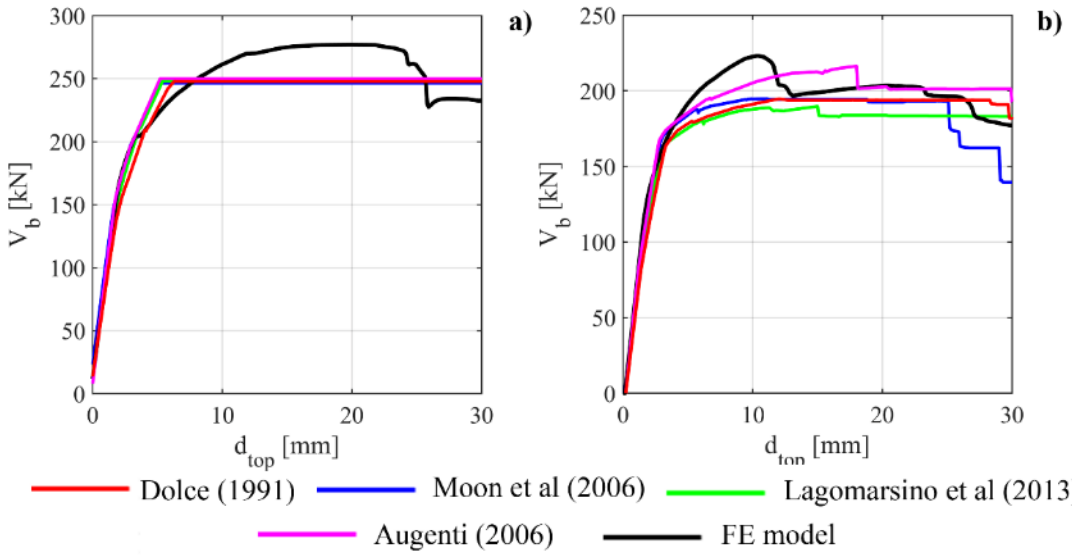

Figure 4.64 - Comparison in terms of pushover curves for configuration E1: a) analysis in the positive verse; b) analysis in the negative verse.

With reference to the analyses in the negative verse (Figure 4.64-b), it can be seen that the choice of the criterion to use for the pier effective height in the EF models actually produces a slightly higher scatter in the obtained results, especially in terms of maximum strength; nevertheless, all the EF models are able to provide a good prediction of the actual response of the wall, even with regard to the post-peak phase.

A good agreement between all the EF models and the FE model is observed also in the case of configuration E2, considering both the analyses in the negative and in the positive verse (Figure 4.65). Indeed, all the numerical models lead to substantially similar predictions in terms of stiffness, maximum strength and post-peak response. Regarding in particular this last one, even if a higher scatter between the obtained results can be observed when considering the analysis in the negative verse, however all the EF models are able to well capture the different behavior of the wall activated when pushing it in the two opposite directions and evidenced in the results of the FE analysis. More specifically, almost no softening is present for the examined values of top displacement in the case of the positive analysis, while a more significant strength degradation occurs when pushing the wall in the negative verse.

The results in terms of global response here discussed show that, as in the case of the configurations of type "A", the choice of the criterion for the pier effective height is not an issue for this type of configuration, since the possible different choices about this aspect actually lead to almost similar results.

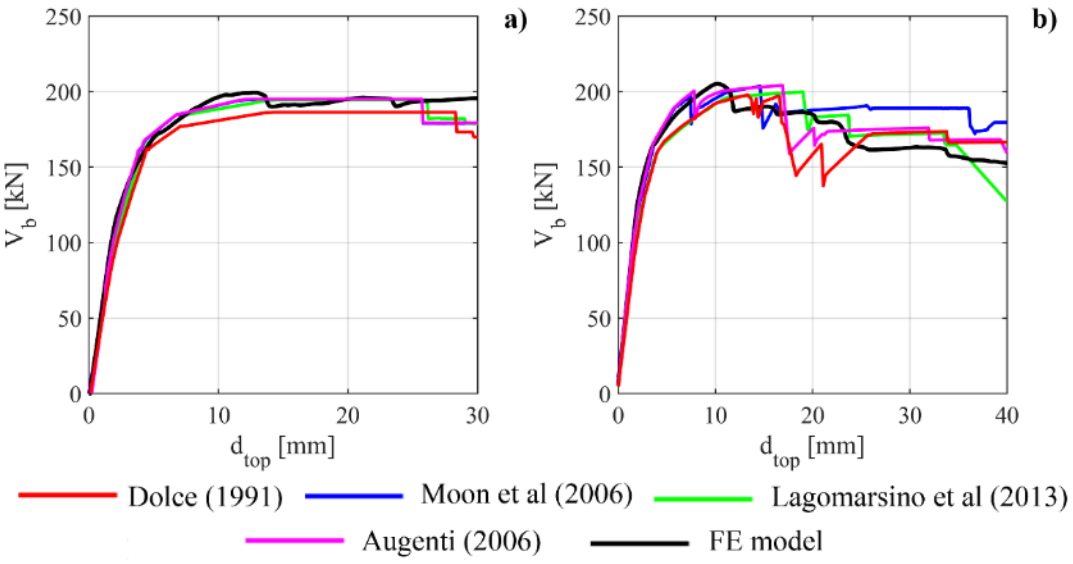

Figure 4.65 - Comparison in terms of pushover curves for E2 configuration: a) analysis in the positive verse; b) analysis in the negative verse.

B. Results of the comparisons in terms of damage pattern

The comparison in terms of damage pattern confirms, for both the configurations, the good agreement observed on the global pushover curves. As an example, in Figure 4.66 the comparison between the damage pattern resulting from the FE model and one of the EF models (Lagomarsino et al (2013)) for different values of top displacement in case of configuration E2, positive analysis, is illustrated.

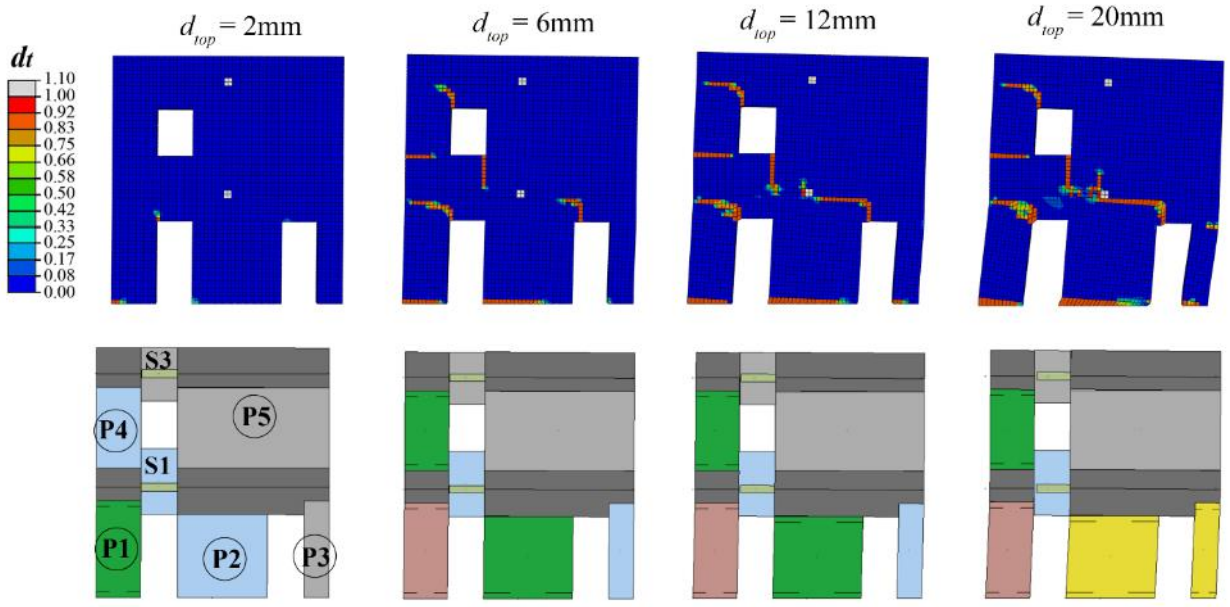

Figure 4.66 - Configuration E2, analysis in the positive verse: comparison between the evolution of damage pattern resulting from the FE model and from the EF model according to Lagomarsino et al (2013). See Figure 4.37 for the meanings of colours and symbols in case of the EF models.

It can be seen that the EF model is able to quite well capture the evolution of damage occurring in the FE model, especially with regard to masonry piers. In particular, it correctly describes the flexural failure of the piers at the ground floor as well as the damage in the pier P4 at the upper floor; moreover, as in the FE model, pier P5 remains undamaged (elastic). The examination of the damage occurred in the FE model shows that, for top displacements higher than 6 mm, a tensile crack propagates in the portion of masonry above the right door opening at the ground floor; this indicates the presence of a deformable portion above this opening. In the EF model, since the portion above the right door opening at the ground floor is modelled as a unique rigid node, this type of damage cannot be captured.

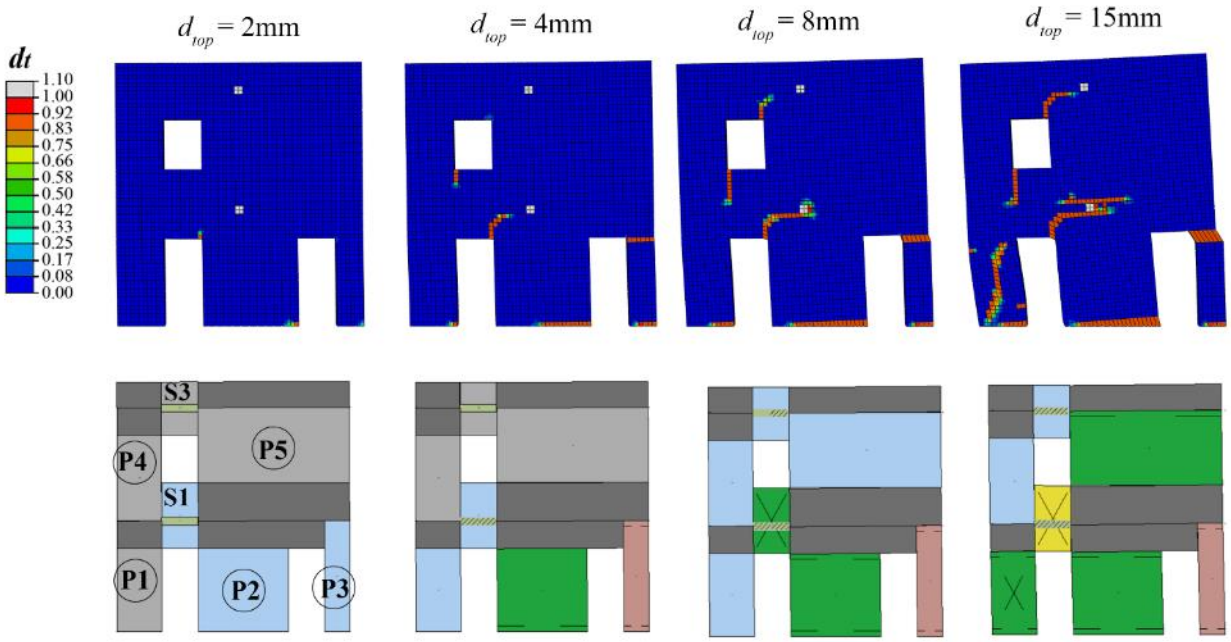

Figure 4.67 - Configuration E2, analysis in the negative verse: comparison between the evolution of damage pattern resulting from the FE model and the EF model according to Moon et al (2006). See Figure 4.37 for the meaning of colours and symbols in case of the EF models.

In Figure 4.67 the same type of comparison in case of configuration E2, analysis in the negative verse, is illustrated, considering this time the EF model obtained through the rule suggested by Moon et al (2006).

It may be noted that in the FE model no tensile damage appears in the portion of masonry which is modelled as a unique rigid node in the EF models, except for some cracks (clearly visible for d_{top} = 15 mm) which start from the centre of the wall and propagate in correspondence of the interfaces between masonry and the r.c. tie beams. However, as discussed before, they are favoured by the concentration of stresses in this position due to the presence of the rigid beam used for performing the nonlinear analysis.

Moving to configuration E1, in case of the positive analysis the observation of the damage occurred in the numerical models is useful to explain the differences in the strength degradation previously observed in the pushover curves. To this aim, in Figure 4.68 the comparison in terms of damage pattern (d_{top} = 30 mm) between the FE model (compressive and tensile damage) and one of the EF models (Moon et al (2006)) is reported.

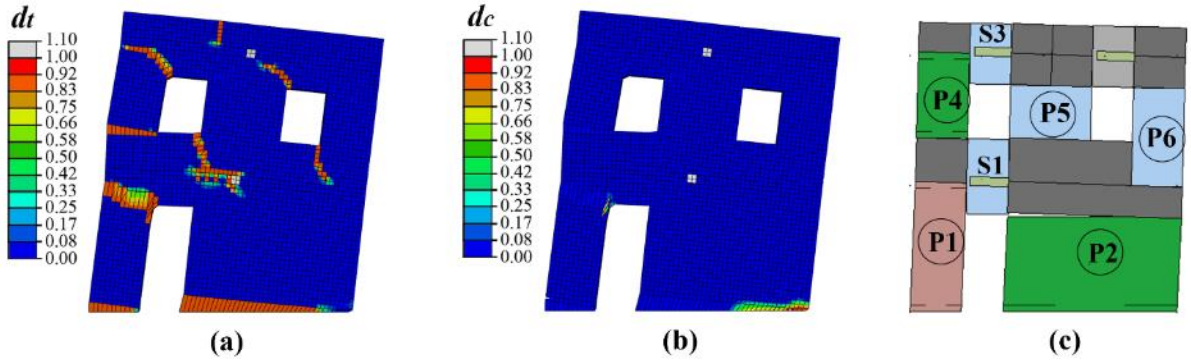

Figure 4.68 - Configuration E1, analysis in the positive verse: comparison in terms of damage pattern corresponding to d_{top} = 30mm between the FE model ((a) tensile damage and (b) compressive damage) and (c) the EF model according to Moon et al (2006). See Figure 4.37 for the meaning of colors and symbols in the EF model.

It is possible to see that in the FE model there is a significant concentration of compression damage in correspondence of the compressed toe of the big masonry portion at the ground floor; this can explain the drop of strength observed in the pushover curve in correspondence of a d_{top} approximatively equal to 26 mm. In the EF model, on the other hand, the response is governed by the big pier at the ground floor (P2), which is subjected to rocking. For the considered value of top displacement, in particular, this pier is characterized by the reaching of DL2 (peak of strength), which is not yet associated to a drop of strength; this last, indeed, for flexural failure occurs only when the masonry panel reaches a state of damage corresponding to DL4, and so for higher values of horizontal displacement. Therefore, no strength degradation is visible in the corresponding global pushover curve for the values of top displacement of our interest. The fact that P2, even if during the analysis increases its compression level due to the overturning of the wall, presents a flexural failure can be explained by considering that its static scheme is actually that of a cantilever beam, as it comes out from its bending moment diagram, shown in Figure 4.69 for different steps of the analysis. It is possible to see that also in the FE model the examined pier actually presents the same static scheme.

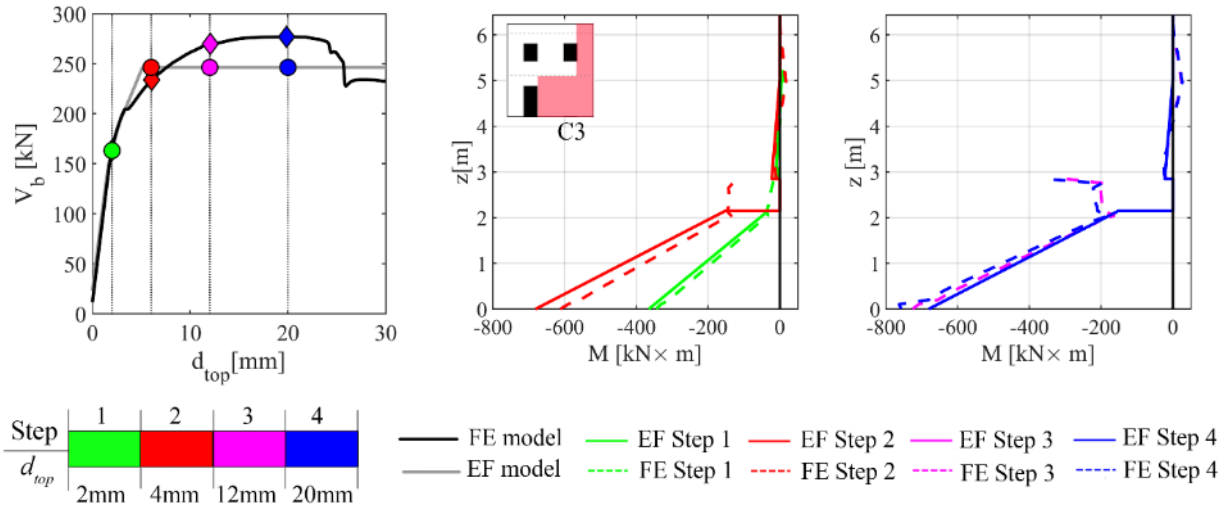

Figure 4.69 Configuration E1, analysis in the positive verse: comparison between the FE model and the EF model according to Moon et al (2006) in terms of bending moment *M* acting on the vertical alignment C3 for different steps of the analysis.

This happens even if the wall is provided with r.c. tie beams and, also, the spandrel at the first storey in the EF model is not interested by damage. Indeed, the boundary conditions of this pier do not depend only on the stiffness of the adjacent spandrel but also on the stiffness of the adjacent part of the wall, that in this case is characterized by very slender piers (P1 and P4) when compared to the squat and stiff P2; therefore, they cannot provide an effective constrain for P2 (i.e. the fixed-fixed condition for this pier is not activated).

C. Results of the comparisons in terms of local response

In general, all the considered EF models provide a satisfactory agreement with the corresponding FE model in terms of redistribution of vertical and horizontal loads among the base sections of the examined walls (both E1 and E2). However, when looking at the analysis in the negative verse on configuration E1, some differences with respect to the FE model can be highlighted, as illustrated in Figure 4.70. In this case, indeed, the axial load redistribution occurring between the two base sections of the wall in the EF models is less pronounced than what happens in the FE model, so that P1 results to be less compressed, while the opposite is for P2. This can explain the differences in terms of maximum strength observed at the global scale, where most of the EF models resulted in a lower maximum strength with respect to the FE model (see previous Figure 4.64-b).

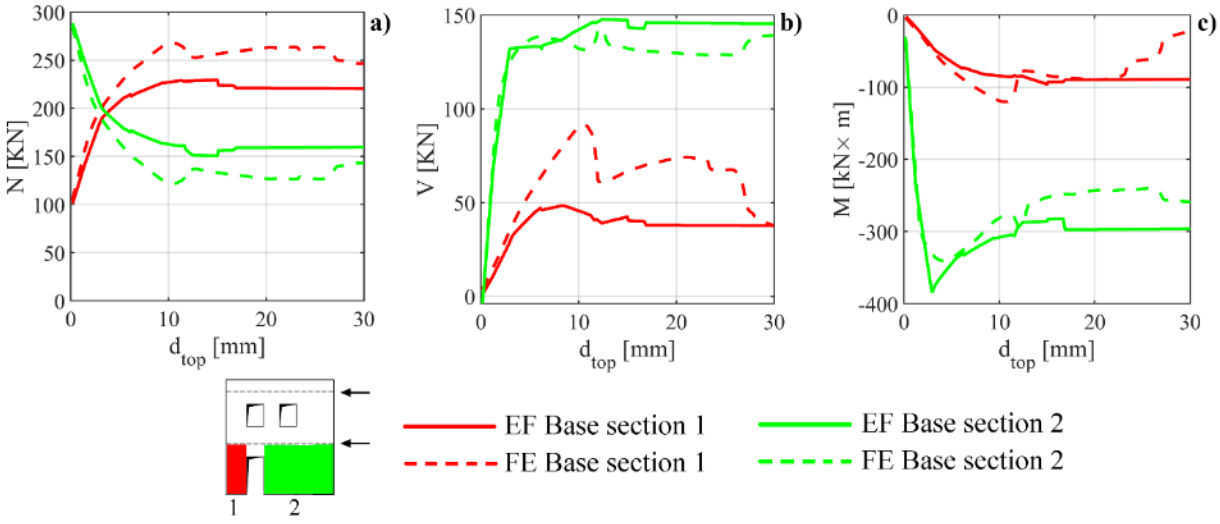

Figure 4.70 - Configuration E1, analysis in the negative verse: comparison in terms of generalized forces acting at the two base sections of the wall (a) normal force; b) shear force c) bending moment) between the FE model and the EF model according to Lagomarsino et al (2013)).

Regarding the comparisons in terms of generalized forces and displacements, as in the case of the configurations of type "A", also here the attention is focused on the horizontal alignments, since the main problem under investigation deals with the modelling of the masonry portion above (in case of E1 configuration) or below (in case of E2 configuration) the panel without the opening. However, as far as the vertical alignments are concerned, all the EF models are able to give reliable results when compared to the considered reference solution.

In Figure 4.71 the comparisons of bending moment diagrams acting on horizontal alignments R1 and R2 during the analysis in the positive verse on configuration E2 are illustrated; the part highlighted in grey refers to the position of the door opening at the ground floor. First of all, by looking at the results of the FE

analysis (dashed lines) it is evident that in case of alignment R2 the stresses acting in the cross sections of the right part of the wall are negligible, and it seems to be correct to consider that portion as a rigid node, as adopted in the EF models due to the absence of the opening. On the contrary, in case of alignment R1 the bending moment diagram indicates the presence of some deformability in that part of the wall, being the bending moment diagrams in this portion resembling a linear path. This is confirmed also when looking at the results referring to the analysis on configuration E1 (positive verse), illustrated in Figure 4.72; in this case the part highlighted in grey in the graphs corresponds to the position of the right opening at the second storey.

In any case, the results provided by the EF models for the bending moment acting on the left spandrel are always very good when compared to the reference solution.

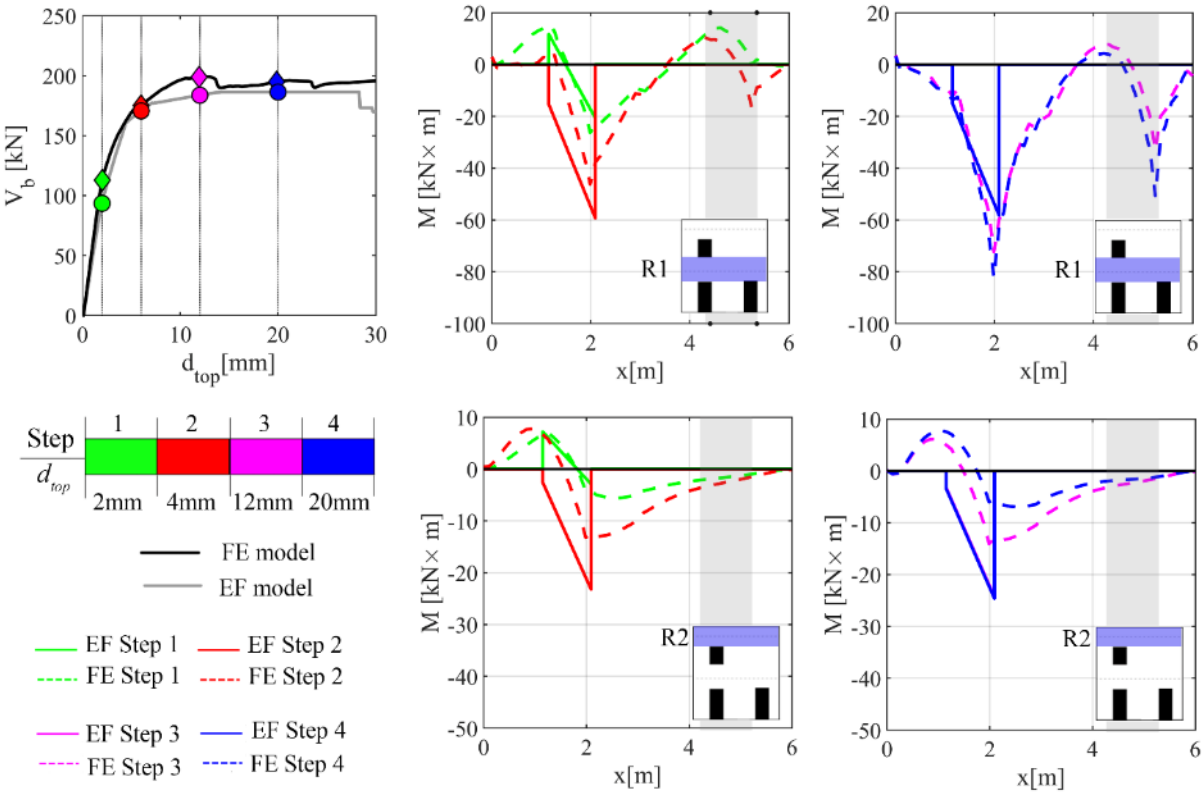

Figure 4.71 - Configuration E2, analysis in the positive verse: comparison between the FE model and the EF model according to Dolce (1991) in terms of bending moment *M* acting on the horizontal alignments R1 and R2 for different steps of the analyses. In grey the abscissae corresponding to the position of the left door opening at the ground floor.

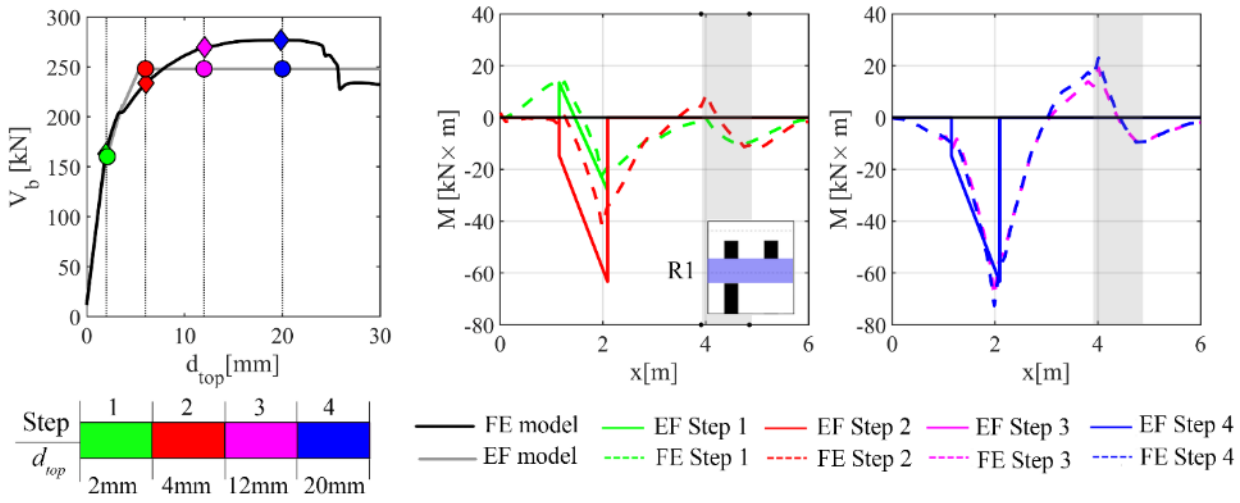

Figure 4.72 - Configuration E1, analysis in the positive verse: comparison between the FE model and the EF model according to Lagomarsino et al (2013) in terms of bending moment *M* acting on alignment R1 for different steps of the analyses. In grey the abscissae corresponding to the position of the right opening at the second storey.

4.4.3.3 Investigation of alternative modelling strategies

In this section, with the aim to improve, in the light of the above mentioned considerations, the results obtained with the EF models on configuration A3, E1 and E2, the investigation of some alternative modelling strategies is discussed.

Configuration A3

In case of configuration A3 two further modelling strategies were investigated:

1) the introduction in the EF model of an elastic beam with a proper stiffness, aimed to substitute the spandrel under examination;
2) the modelling of the spandrels of the EF model as elastic-plastic elements.

The solution indicated at point 1) has been thought in order to: i) introduce a deformable element to take into account the deformability observed in the FE model and, at the same time, ii) avoid the drop of strength at the global scale. The adoption of this solution implies to split the rigid node between the openings at the two levels into two parts and to introduce the elastic element between the two nodes created in such way, as illustrated in Figure 4.73-a. The stiffness of this element is the same (shear and flexural) of the spandrel element the beam is meant to substitute. The EF model obtained in such way is indicated in the following as “EB-Model”.

With reference to the solution indicated at point 2), the idea is to avoid the strength degradation of the spandrel modelled as a nonlinear element; this is assumed to be reasonable thanks to the presence of the r.c. tie beams. The EF model obtained in such way is identified in the following as “EPS-Model”.

Regarding this aspect, it is worth underlining that the calibration of the constitutive models adopted for the nonlinear analyses (described in Chapter 3) has been carried out only on pier elements. In case of spandrels such an accurate calibration was omitted due to the lack of a consolidated literature as in the case of masonry piers. The multilinear constitutive laws adopted for these elements in the EF models have been

defined on the basis of values of drift thresholds and strength degradation which are reasonable and representative of the behavior of these elements according to the experimental tests; however, many uncertainties and open issues are still present on this topic, also regarding the definition of proper strength criteria (as highlighted in Chapter 1), and even more regarding their constitutive behavior. In the light of these considerations, the modelling option now proposed for spandrel elements represents as well a plausible choice; furthermore, it has been verified that the assumption of an elastic-plastic behavior for these elements is consistent with what comes out from the analysis of the local response in the FE model.

Since the results previously discussed underlined that the choice of the criterion to use for the pier effective height in this case is not an issue, these further investigations were performed on the EF model obtained by applying, by way of example, only the criterion proposed in Lagomarsino et al (2013).

Figure 4.73-b shows the results achieved in terms of global pushover curves (negative verse). The results show that both the proposed solutions work very well, allowing to obtain a very good reproduction of the global response considered as reference. In particular, the EPS-Model provides the best results, even if also the EB-Model produces a very good prediction of the actual global response. Therefore, both these modelling strategies represent an improvement with respect to the solutions previously explored.

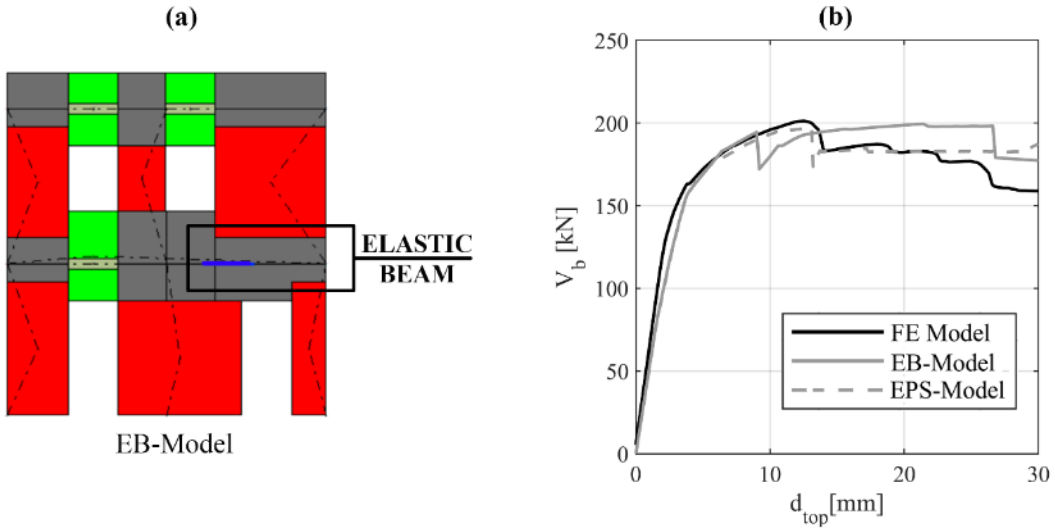

Figure 4.73- Configuration A3: (a) EF model obtained through the introduction of the elastic beam; (b) comparison between the pushover curves (negative verse) resulting from the FE analysis and from EF models associated to different modelling assumptions.

In Figure 4.74 the comparison in terms of damage pattern occurred when considering different modelling assumptions (namely, the presence of a unique rigid node, referred to as RN-Model, the EB-Model and the EPS-Model) is reported.

The EB-Model actually provides the damage pattern most similar to the one detected by the FE model: indeed, a hybrid failure is predicted in case of P1, and spandrel S1 is interested by hybrid failure as well, which is more consistent than the pure shear failure detected by the other EF models. Furthermore, it is worth noting that while the presence of a unique rigid node in the model, due to the rotation of this big rigid portion, may produce anomalous stresses in the adjacent elements (as in the case of P5, which is subjected to tension), when considering the EB-Model, thanks to the fact that the rigid node is split into two parts which are free to rotate, this does not happen, and a more realistic damage pattern is obtained. Also the

EPS-Model allows to avoid this situation; however, the resulting damage scenario is less consistent with the tensile damage emerging from the FE model.

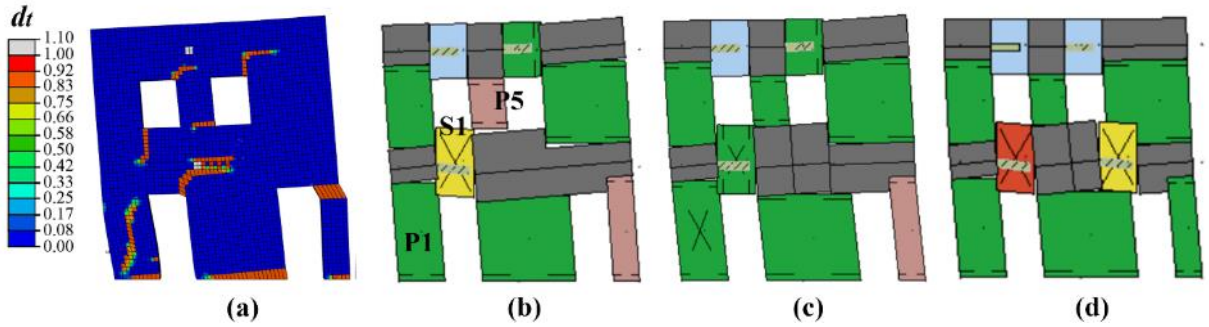

Figure 4.74 - A3, negative analysis: damage scenarios for d_{top} = 15 mm deriving from the FE model and from EF models with different modelling assumptions: (b) RN-Model; (c) EB-Model (c) EPS-Model.

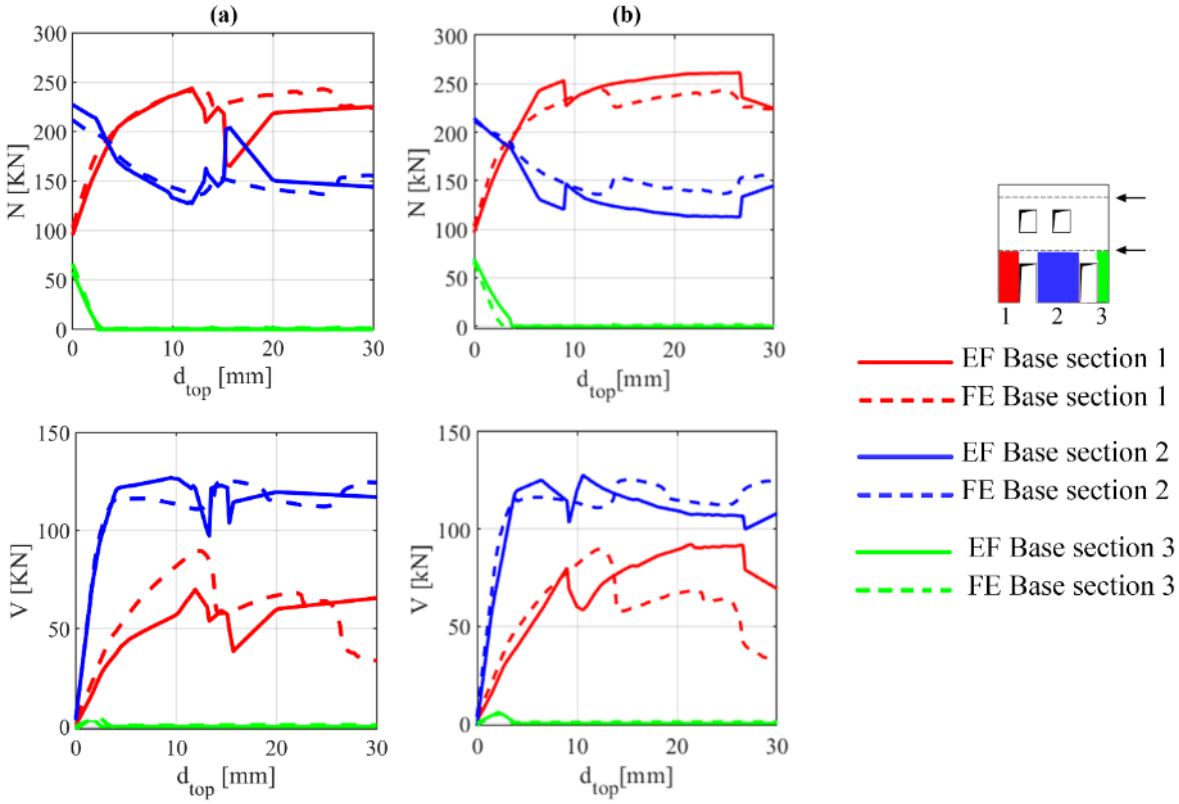

Figure 4.75 - A3, negative analysis: comparison on generalized forces acting at the base sections of the wall (normal force *N*; shear force *V*) between the FE model and the following EF models: (a) RN-Model; (b) EB-Model.

Moreover, the comparison on the evolution of the generalized forces acting at the base sections of the wall shows that the EB-Model provides a slightly better description of the redistribution of the axial and shear loads between these sections with respect to the solution characterized by the presence of a unique rigid node, as illustrated in Figure 4.75.

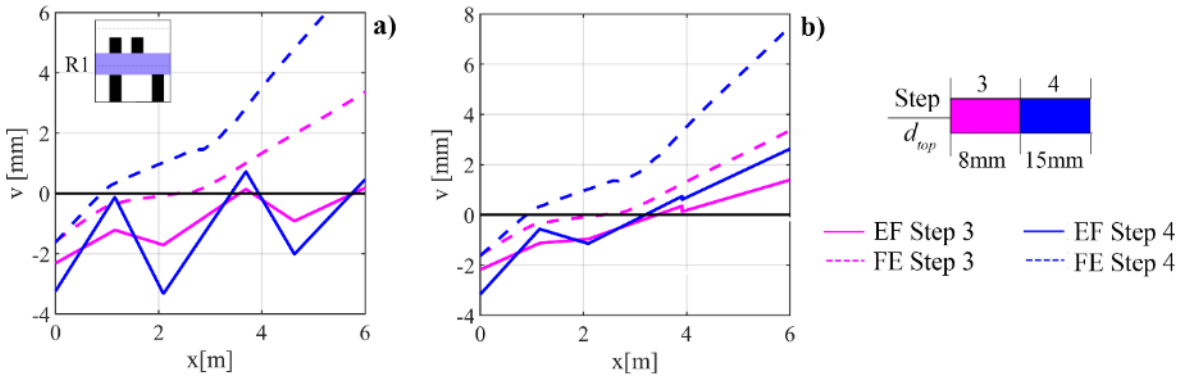

Figure 4.76 - A3, negative analysis: comparison between the FE model and the EF model with (a) elastic-plastic spandrels and (b) elastic beam in terms of vertical displacements associated to alignment R1 for different steps of the analyses.

The comparison with the FE model results in terms of vertical displacements associated to the alignment R1, which is reported in Figure 4.76 in case of both the EB-Model and the EPS-Model, shows that it is more correct to adopt the solution of the elastic beam, which actually allows to obtain a better reproduction of the deformed shape along this alignment in case of both the considered steps. Indeed, the introduction of a nonlinear element (EPS-Model), produces a concentration of deformation (associated to high values of drift in the spandrel itself) which is actually not detected by the FE model.

Concluding, even if in terms of predicted global response the solution associated to the modelling of the spandrels as elastic-plastic elements provides the best result among the considered modelling strategies for the configuration A3, when considering also the results in terms of local response it gives place to less accurate predictions with respect to the EF model where the elastic beam is adopted; this last, therefore, represents the recommended choice when modelling masonry walls presenting the type of irregularity here examined.

Configurations E1 and E2

In order to take into account the deformability observed in the FE model in the portion of masonry below the window in case of configuration E1 and above the door opening in case of the configuration E2, which emerged from the previously discussed examination of the local response, the modelling strategy involving the introduction of an elastic beam with a proper stiffness was explored; indeed, it resulted to be effective in the case of configuration A3. The EF models obtained for E1 and E2 are shown in Figure 4.77; also in this case, the stiffness attributed to the elastic beam has been defined as the stiffness of a spandrel element of the wall model.

Considering, as an example, the analysis on configuration E1 (negative verse), in Figure 4.78-a the results obtained with the two different solutions considered in the EF model (presence of the elastic beam or of the unique rigid node) are compared with the assumed reference solution; in both cases the rule adopted for the pier effective height is the one according to Lagomarsino et al (2013).

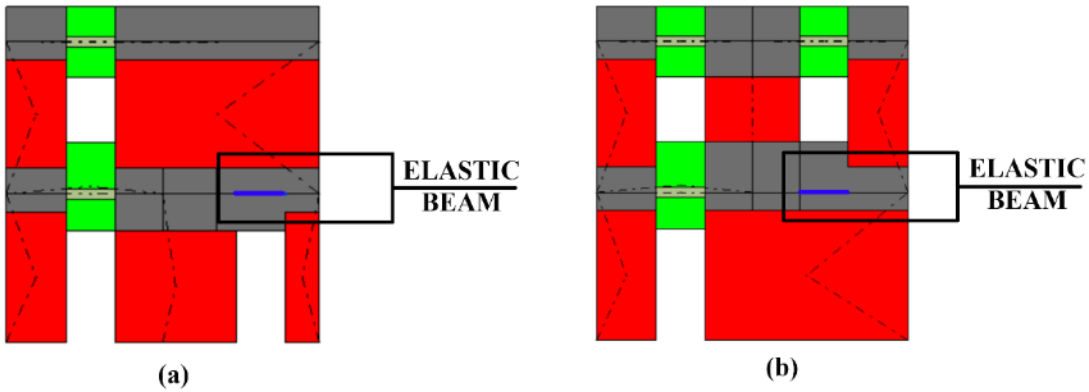

Figure 4.77 - EF models obtained through the introduction of the elastic beam in case of: (a) configuration E2; (b) configuration E1.

It is observed that the EB-Model allows to obtain a global response which is more consistent with what emerges from the FE model in terms of predicted maximum strength; indeed, as illustrated in Figure 4.78-b and c, the introduction of the elastic beam gives place to a better description of the redistribution of the vertical and horizontal stresses among the base sections of the wall. In particular, since the big rigid node at the first storey has been split into two parts which are free to rotate, when pushing the wall in the negative verse it happens that the left part of the wall (that includes P1) is less restrained by the right part of the wall (that is much more stiff since it includes P2). This allows to obtain a more pronounced redistribution of the stresses between the two base sections, which is actually closer to what happens in the FE model.

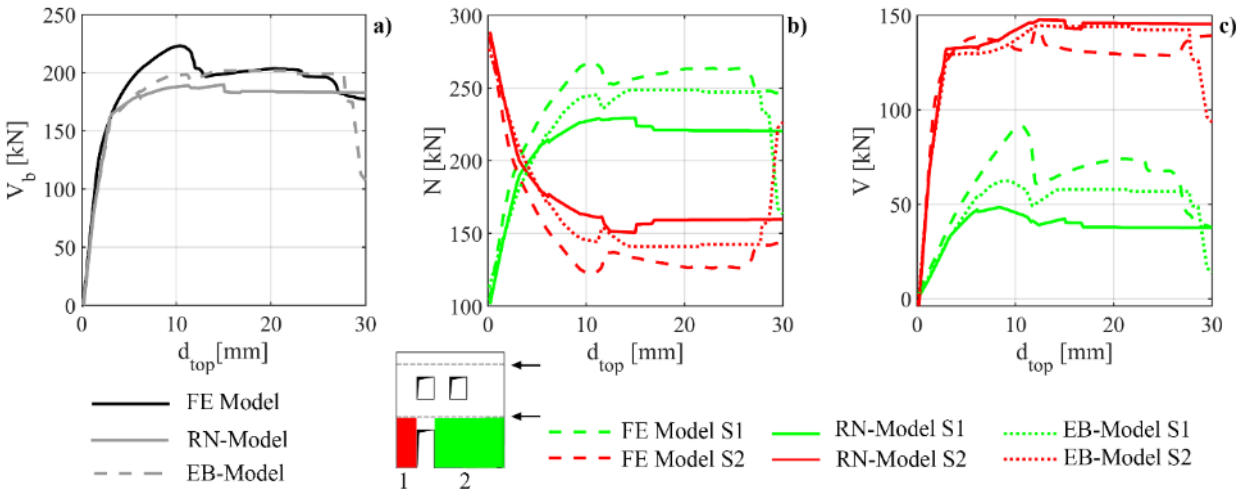

Figure 4.78– Configuration E1, analysis in the negative verse: comparison between the FE model and EF models associated to different modelling assumptions (RN-Model and EB-Model) in terms of (a) pushover curves and evolution of generalized forces (b) normal force *N* and c) bending moment *M*) at the base section of the wall.

Furthermore, also in terms of generalized forces the results obtained with the EB-Model are more consistent with the reference solution than those achievable with the traditional solution of the unique rigid node (RN-Model), as shown in Figure 4.79, where a comparison in terms of bending moment acting on alignment C1 is presented for different steps of the analysis.

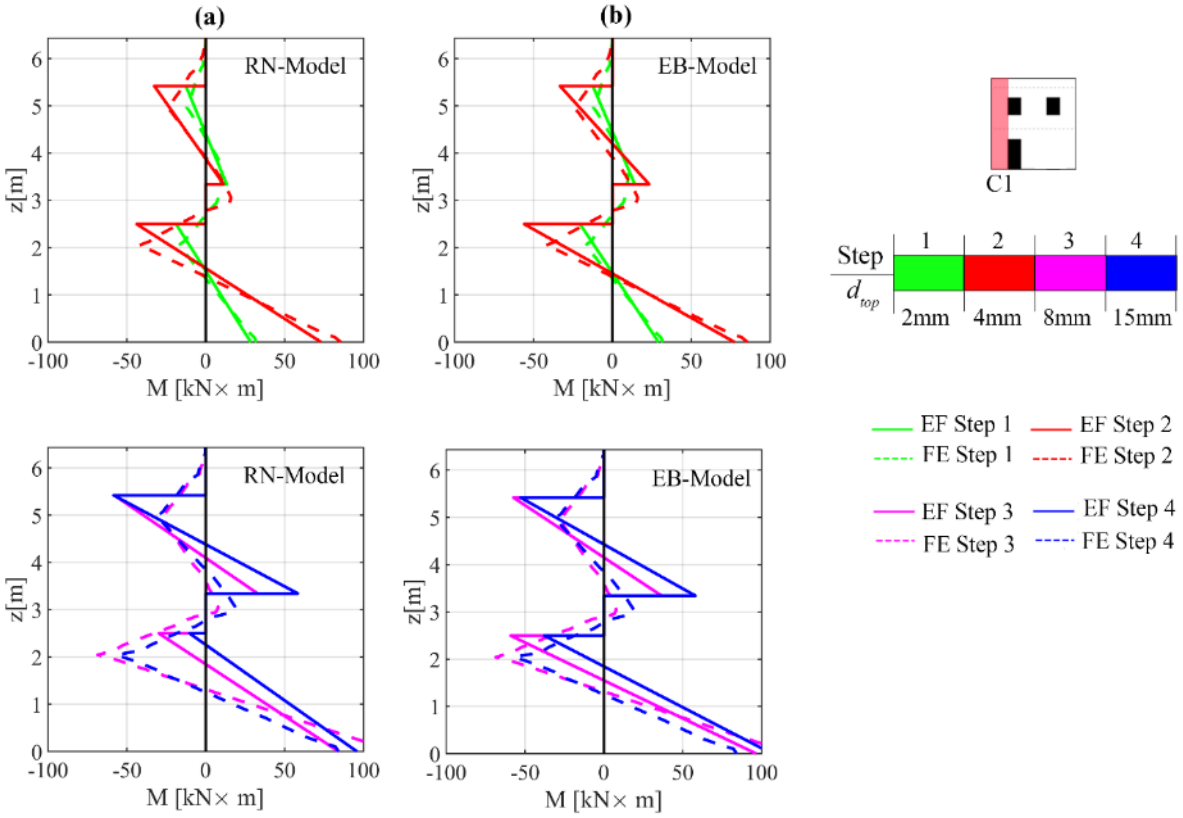

Figure 4.79 – Configuration E1, analysis in the negative verse: comparison between the FE model and (a) the RN-Model and (b) the EB-Model (effective height according to Lagomarsino et al (2013)) in terms of bending moment *M* acting on the vertical alignment C1 for different steps of the analysis.

In addition, as it may be seen from Figure 4.80, where a comparison in terms of the damage pattern occurred for a top displacement equal to 15 mm is shown, the solution adopted in the EB-Model allows to avoid in pier P4 the development of tension stresses, that in the EF model with the unique rigid node is caused by the rotation of the big rigid portion below this element.

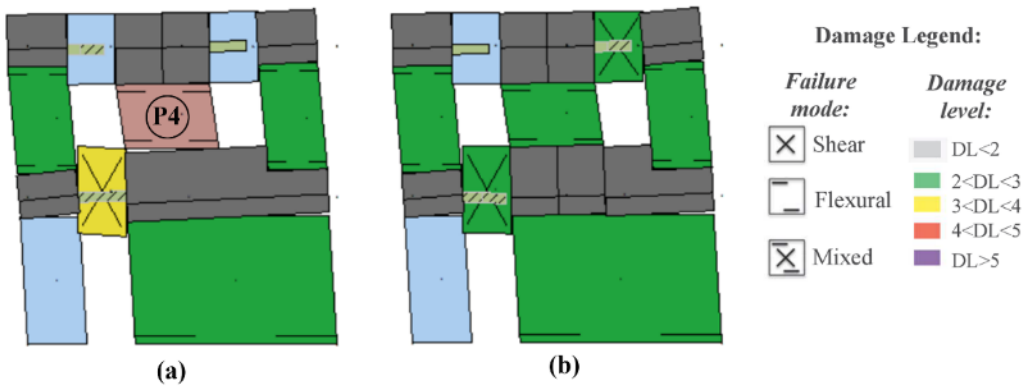

Figure 4.80 – Configuration E1, analysis in the negative verse: damage pattern corresponding to d_{top} = 15 mm according to the (a) RN-Model and (b) EB-Model (effective height according to Lagomarsino et al (2013).

Moving to configuration E2, the results provided by the EF model in terms of global response, which were already close to the reference solution, turned out to be not significantly affected by the introduction

of the elastic beam; however, the EB-Model allows to obtain a slightly better description of the vertical displacements and rotations associated to the horizontal alignment R1, as it may be seen in Figure 4.81.

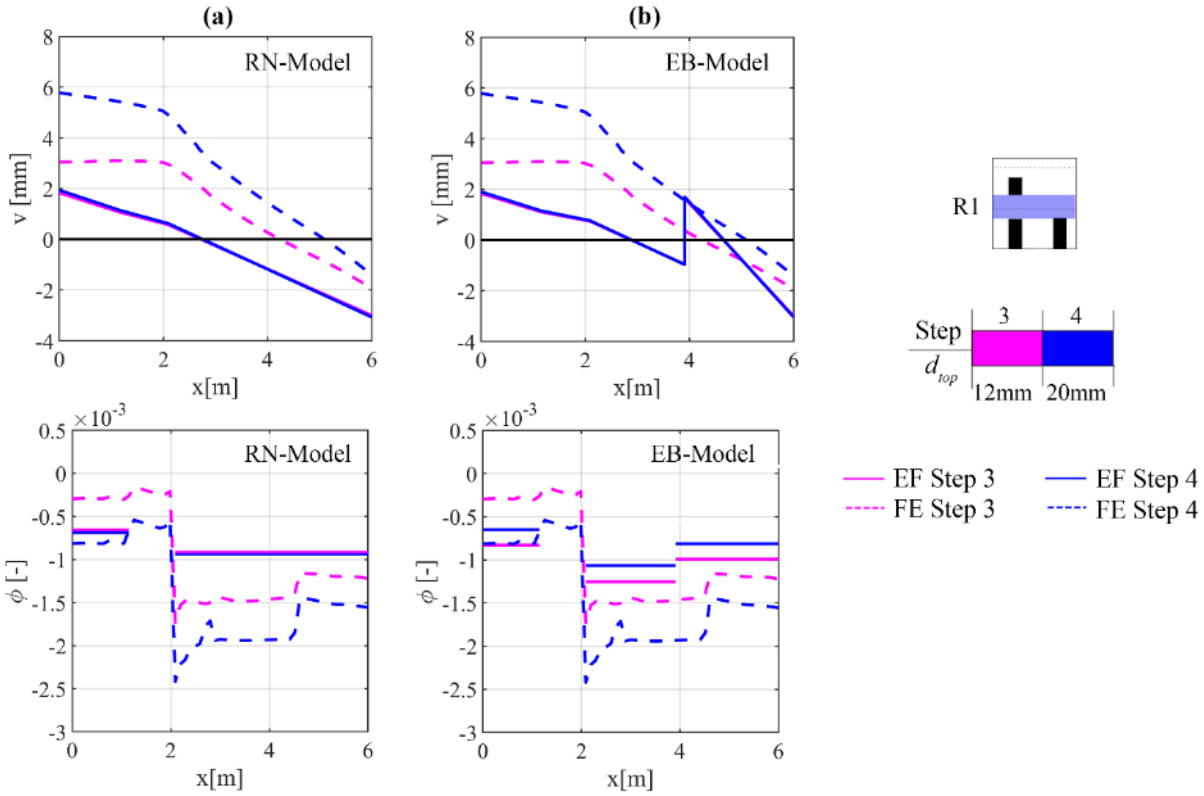

Figure 4.81 Configuration E2, analysis in the positive verse: comparison in terms of global pushover curves as well as vertical displacements *v* and rotations φ associated to alignment R1 for different steps of the analyses between the FE model and the EF models with: (a) the unique rigid node (RN-Model) and (b) the elastic beam (EB-Model).

4.4.3.4 Main recommendations on the basis of the achieved results

First of all, the performed analyses demonstrated that in presence of walls with openings misaligned at two consecutive stories or with a different number of openings per story the choice of the criterion for the determination of the pier effective height is not an issue; indeed, the different possible rules provide substantially similar geometries for pier elements in these cases and, therefore, almost similar global responses.

Moving to the problem of the identification of the spandrel, the obtained results showed that, when there is still an overlapping part between the vertically misaligned openings, even in correspondence of a single edge, it is correct to consider the spandrel in the structural model, as predicted by the empirical criterion suggested in Lagomarsino et al (2013).

When the two openings are not aligned at all, in addition to this criterion (which predicts the presence of a unique rigid node) also EF models including the spandrel were considered; however, in general no significant differences were detected in the obtained response, which is substantially consistent with the reference solution in both cases. This happens since in the analysed configurations, which are two-storey masonry walls with r.c. tie beams, the role played by the spandrels in the structural response is not so

significant. Nevertheless, the introduction of the spandrel leads to a concentration of damage (due to its failure) and a consequent drop of strength in the pushover curve which is not consistent with what emerges from the FE model, where the portion which would correspond to the spandrel is not always damaged and, in any case, no significant drops of strength are observed in the curve.

The criterion according to Lagomarsino et al (2013) seems therefore to be appropriate also in these cases, even if it may be improved. Indeed, the analysis of the local response in terms of generalized forces acting in the FE model highlights the presence of a part with a slight deformability between the two vertically misaligned openings; moreover, the same outcome was found even in presence of walls with a different number of openings per storey, this time regarding the portion of masonry below (or above, depending on at which storey the irregularity is located) the panel characterized by the missing opening. These results, therefore, indicate that, in order to have a better description of the local response in these cases, it is better to include in the model a deformable element rather than a completely rigid portion, as would be predicted by the empirical rule presented in Lagomarsino et al (2013).

It was found that an effective modelling strategy in presence of vertically misaligned openings at two consecutive stories is to introduce, instead of a spandrel, an elastic beam with an equivalent stiffness, which allows to obtain better results also in terms of damage pattern. This strategy, which was found to be effective also in presence of walls with a different number of openings per storey, represents an improvement of the criterion for the identification of spandrels proposed in Lagomarsino et al (2013).

It is stressed, however, that regarding the problem of the identification of the spandrel geometry the results found with the introduced configurations, even if useful to give specific indications in these cases, cannot be conclusive; indeed, other structural typologies where the spandrels have a more important role in the response (multi-story walls or walls with weak spandrels) should be considered in order to gain more exhaustive results.

The above discussed results are summarised in Table 4. 13, according to the criteria introduced at section 4.4.4.1 (Table 4.10). However, since in this case the obtained outcomes are almost not affected by the criterion adopted for determining the pier effective height, in substitution of that each column collects the results referring to the problems here examined and, more specifically, to the configurations adopted for exploring that specific problems. Furthermore, for each configuration the illustrated results refer to the different investigated modelling strategies and to the analysis (between those performed in the two verses) giving the worst results with respect to the FE model. The results in terms of generalized forces and displacements refer to the horizontal alignment R1, being the most interesting for the problems here analysed. Finally, for what concerns the configurations with a different number of openings per storey, the results associated to configuration E1 are taken as reference, being these last almost similar to the ones achieved in the case of configuration E2.

Table 4. 13 – Summary of the main outcomes obtained in case of configurations A1, A3, E1.

		Still overlapping (A1)	No overlapping (A3)			Different n. of openings per storey (E1)	
		With Spandrel	With Spandrel	Rigid Node	Elastic Beam	Rigid Node	Elastic Beam
Global	V_{max}	L	L	L	L	M	L
	$d_{top,n}$	L	VH	M	L	M	L
	$k_{s,35}$	L	L	L	L	L	L
Damage	Global failure	Well captured	Well captured	Well captured	Well captured	Well captured	Well captured
	Damage in Piers	Well captured	Well captured	Moderate difference (tension)	Well captured	Moderate difference (tension)	Well captured
Gen. forces	Shear force	Well captured	Moderate difference	Moderate difference	Moderate difference	Moderate difference	Moderate difference
	Bending moment	Well captured	Moderate difference	Moderate difference	Moderate difference	Moderate difference	Moderate difference
Def. shape	Deformed shapes	Well captured	Not Good	Well captured	Well captured	Well captured	Well captured

CHAPTER 5

5 FURTHER CRITICAL ISSUES ON THE APPLICATION OF THE EQUIVALENT FRAME APPROACH

This Chapter deals with some additional critical issues on the modelling of URM piers in the framework of the EF modelling approach.

In particular, the first two sections (section 5.1 and 5.2) are aimed to deepen some issues emerged from the analysis on the irregular walls discussed in Chapter 4, by considering further case studies and different possible geometries, with the aim to generalize modelling rules related to:

- the modelling of URM piers without openings (section 5.1);
- the modelling of URM piers with openings of different size and positions, with particular attention to the problem of the presence of little openings (section 5.2), in order to solve some criticalities emerged in section 4.4.2.

Finally, the last section (section 5.3) faces the problem of the modelling of URM piers with flanges, which is of great concern when dealing with the analysis of 3D EF models, where the connections between the orthogonal walls come into play. Regarding this aspect, the potentialities of the modelling strategies commonly adopted in the EF models for the description of the flange effect are investigated, highlighting also some of their limits. Even if the study carried out has to be intended as preliminary and for the moment no specific modelling rules are proposed, on the basis of the obtained results some possible improvements to be adopted in the EF models are outlined.

In all the cases, analogously to what presented in the previous chapters, the adopted approach is numerical and based on comparisons with results of FE analyses, considered as the "exact" reference solution.

5.1 ANALYSIS OF URM PIERS WITHOUT OPENINGS

One of the problems which may arise when adopting an EF modelling of a masonry building is related to the presence of particularly squat panels, which correspond to large portions of masonry without openings. In these cases, a possible modelling choice (Di Ludovico et al (2011), Quagliarini et al (2017)) is to subdivide the single panel into two or more elements.

The objective of the analyses described in this section is to explore the reliability and actual need of this modelling option, considering in particular the influence of two aspects: the aspect ratio of the pier and the compression level which it is subjected to.

In order to reach this objective, the following approach was adopted:

1. definition of a series of panels characterized by different aspect ratios;
2. modelling of the panels in ABAQUS and execution, for different values of applied axial load, of lateral load monotonic analyses, aimed to obtain: i) the associated base shear –top displacement (V_b – d_{top}) curves, and in particular the maximum exhibited strength V_y; ii) the occurred damage pattern

(which is of help in order to understand, on the basis of the examination of the tensile cracks propagation, if the activated behavior is representative of that of a single panel or of more coupled elements). Such results are considered as the reference solution;

3. analytical calculation of the maximum strength predicted when adopting the failure criteria associated to both flexural and shear failure proposed in literature (that is representative of what would come out when adopting an EF modelling approach). Both the strategies, that is to model each panel as a single element and to split it into two equal panels, have been considered;
4. comparison between the results in terms of maximum strength obtained through the FE analyses and the predictions of the analytical calculations.

5.1.1 Case studies description

Starting from the panel without openings located at the ground floor in the wall configuration E1 (see Chapter 4 and Figure 5.1), whose dimensions are 3.91x2.85x0.25 m (λ = 0.73), further panels with higher and lower aspect ratios were defined. In particular, by fixing the height of the panel and by varying its width, other 7 panels with increasing aspect ratios (ranging from 0.63 to 1.78) were obtained, as illustrated in Figure 5.1.

As far as the material characterizing the panels is concerned, it was decided to use, for continuity with the previously developed work, the same mechanical properties adopted for the single panels analysed in Chapter 3 and also for the irregular walls introduced in Chapter 4 (see Table 3.1).

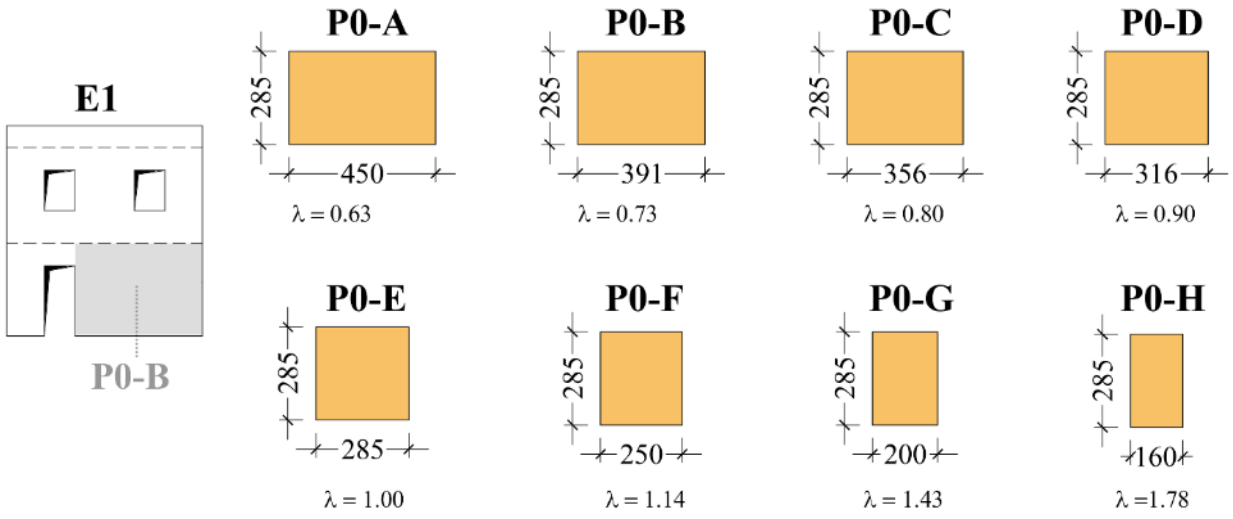

Figure 5.1 – Geometry and aspect ratios λ of the introduced panels (dimensions in cm); on the left, the irregular wall E1, from which panel P0-B is derived.

The introduced panels were modelled in ABAQUS according to the same strategy adopted for the pier panels analysed in Chapter 3. In particular, the behavior of the masonry material was described through the CDP model, by adopting the parameters representing the outcome of the calibration between this constitutive model and the piecewise-linear one used in the EF models (see Table 3.5 and Table 3.8).

Moreover, 8-node brick elements with dimensions approximatively equal to 10x10x12.5 cm were employed, as resulting from the convergence analyses described in Appendix A.

The panels were tested by considering the fixed –fixed condition, which was simulated through the same strategy used in the case of the panels previously analysed (see Figure 3.9).

The failure criteria employed for the analytical calculation of the strength are the same adopted as reference for performing the calibration between the constitutive models and for describing the behavior of the pier panels in the wall configurations analysed in Chapter 4. It is briefly recalled that these criteria are: in case of shear failure the criterion proposed by Turnšek and Cačovic (1971), that describes the diagonal shear failure, with the modification introduced in Turnšek and Sheppard (1980), and in the case of flexural failure the approach proposed in NTC08.

As afore introduced, the final strength V_y of each panel was computed according to two hypotheses, corresponding to two different modelling strategies:

1) the panel is modelled as a single element; in this case the maximum strength V_y is simply the minimum between the strength associated to the flexural failure V_f and the strength associated to the shear failure V_s of the examined pier panel: $V_y = \min(V_s, V_f)$;
2) the panel is split into two equal panels; in this case V_y is evaluated as: $V_y = V_{y,P1} + V_{y,P2}$, being $V_{y,P1}$ and $V_{y,P2}$ the maximum strength of the two panels (P1 and P2) in which the initial panel has been divided; they are computed again as the minimum between the flexural and the shear failure associated to each panel (i.e.: $V_{y,Pi} = \min(V_{s,Pi}, V_{f,Pi})$, i=1,2).

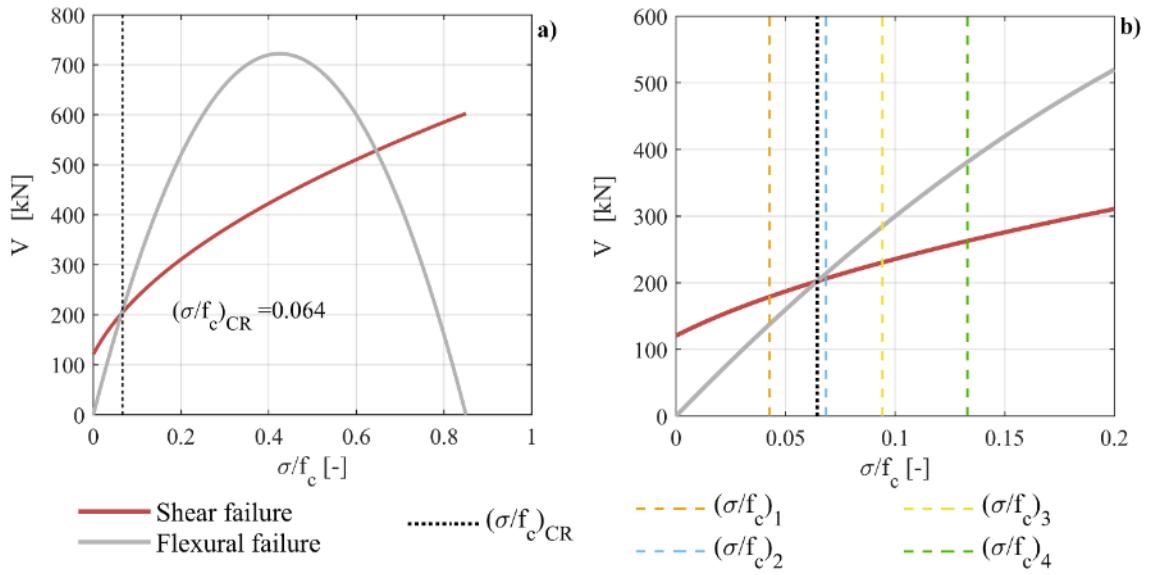

Figure 5.2 – Panel P0-F (λ=1.14): a) failure domain of the panel with the identification of $(\sigma/f_c)_{CR}$; b) representation on the failure domain of the four applied compression levels $(\sigma/f_c)_i$, i=1,..,4.

Each panel was tested by considering four increasing axial load ratios σ/f_c (being σ the mean normal stress acting on the cross section of the panel and f_c the masonry compressive strength). In particular, for each panel the value of the "critical axial load ratio" $(\sigma/f_c)_{CR}$, which is the compression level corresponding to the first intersection between the shear and the flexural strength according to the adopted criteria (Figure

5.2-a), was determined (its analytical derivation is discussed in detail in Appendix B); then, the axial load ratios to apply to each panel were established in order to be both lower and higher to this value, with the aim to activate different failure modes on the examined panels. The compression levels were in general kept within 12-13% with the main scope to consider values representative of the actual compression rates acting in the pier panels of real masonry buildings.

As an example, in Figure 5.2 the strength domain of panel P0-F is represented, with the identification of $(\sigma/f_c)_{CR}$ (Figure 5.2-a) and of the four compression levels (Figure 5.2-b) considered for this panel.

The specific values of the axial load ratios applied to each panel are reported in Table 5.1, as well as the associated values of $(\sigma/f_c)_{CR}$. Once defined the FE model of each panel, lateral load monotonic analyses in control displacement were carried out, whose results are discussed in the following section.

Table 5.1– Value of the critical axial load ratio $(\sigma/f_c)_{CR}$ and values of the compression levels $(\sigma/f_c)_i$ (i = 1,…,4) adopted for each introduced panel (values referring to the mid-section of each panel).

	P0-A	**P0-B**	**P0-C**	**P0-D**	**P0-E**	**P0-F**	**P0-G**	**P0-H**
	λ=0.63	λ=0.73	λ=0.80	λ=0.90	λ=1.0	λ=1.14	λ=1.43	λ=1.78
$(\sigma/f_c)_{CR}$ **[%]**	3.23	3.94	4.54	5.44	6.44	6.44	6.44	8.74
$(\sigma/f_c)_1$ **[%]**	2.09	2.39	3.19	3.49	2.69	4.26	3.61	4.39
$(\sigma/f_c)_2$ **[%]**	3.49	5.39	4.59	5.19	4.89	6.84	6.84	7.39
$(\sigma/f_c)_3$ **[%]**	6.79	8.59	7.59	8.49	8.29	9.42	10.1	9.99
$(\sigma/f_c)_4$ **[%]**	11.8	11.8	12.19	12.6	11.7	13.2	13.2	12.4

5.1.2 Discussion of the results

In Figure 5.3 and in Figure 5.4 the results of the FE analyses performed on panels P0-C and P0-G, respectively, are reported. In particular, for each examined compression level the associated base shear – top displacement curve $V_b - d_{top}$ is represented, together with the tensile damage referring to two different steps of the analysis, in order to examine the propagation of the tensile cracks.

It is possible to see that for both the panels the first applied compression level $(\sigma/f_c)_1$ corresponds to a prevailing flexural behavior, characterized by the progressive parzialization of the end sections and by a ductile response in terms of V_b - d_{top} curve (Figure 5.3-a and Figure 5.4-a). When moving to higher compression levels, also shear cracks appear, whose formation and propagation cause a more significant drop of strength in the corresponding response curves. In particular, at first the activation of a hybrid behavior occurs, with the presence of both the parzialization of the end sections and of a diagonal shear crack ($(\sigma/f_c)_2$ for both the panels – Figure 5.3-b and Figure 5.4-b). By further increasing the applied axial load ratio, in case of both the examined panels (Figure 5.3-c and Figure 5.4-c) the parzialization progressively reduces and more vertical shear cracks appear.

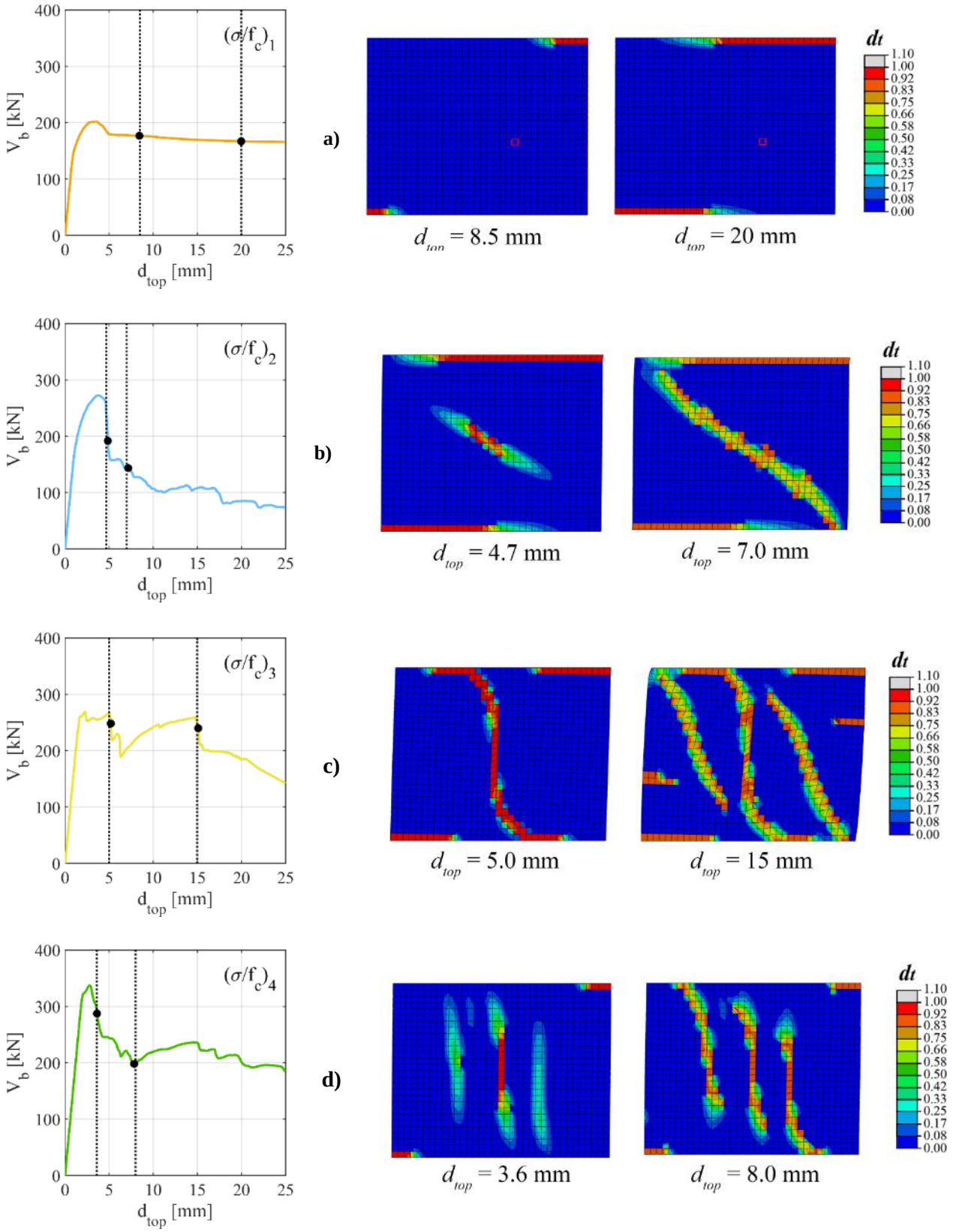

Figure 5.3 - Panel P0-C (λ=0.8): base shear – top displacement (V_b – d_{top}) curves associated to different applied axial loads and damage patterns corresponding to different values of top displacement.

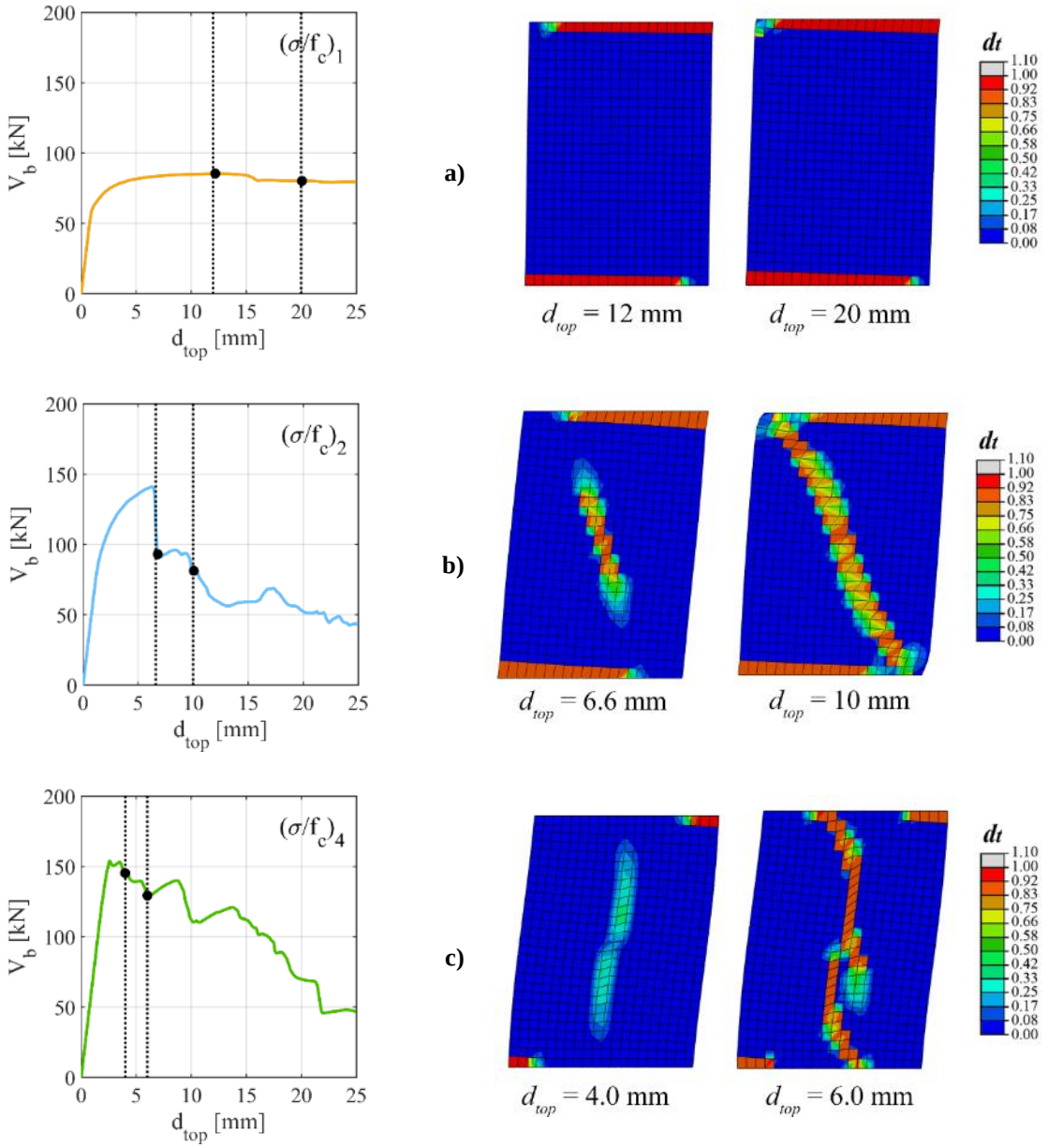

Figure 5.4 - Panel P0-G (λ=1.43): base shear – top displacement ($V_b - d_{top}$) curves associated to different applied axial loads and damage patterns corresponding to different values of top displacement.

This phenomenon depends on the different inclination of the compression strut which activates. Indeed, it is evident that when the parzialization phenomenon is more pronounced (i.e. when the compression level is not so high), the principal compression stresses assume a higher inclination (Figure 5.3-b and Figure 5.4-b); conversely, when the parzialization is limited, the principal compression stresses tend to remain almost vertical, thus leading to the formation of almost vertical tensile cracks. This phenomenon can be appreciated by looking at the pictures reported in Figure 5.5, where, as for example referring to panel P0-C (λ=0.8), the maximum principal stresses developing in the panel for different steps of the analysis, associated to two different compression levels, are illustrated.

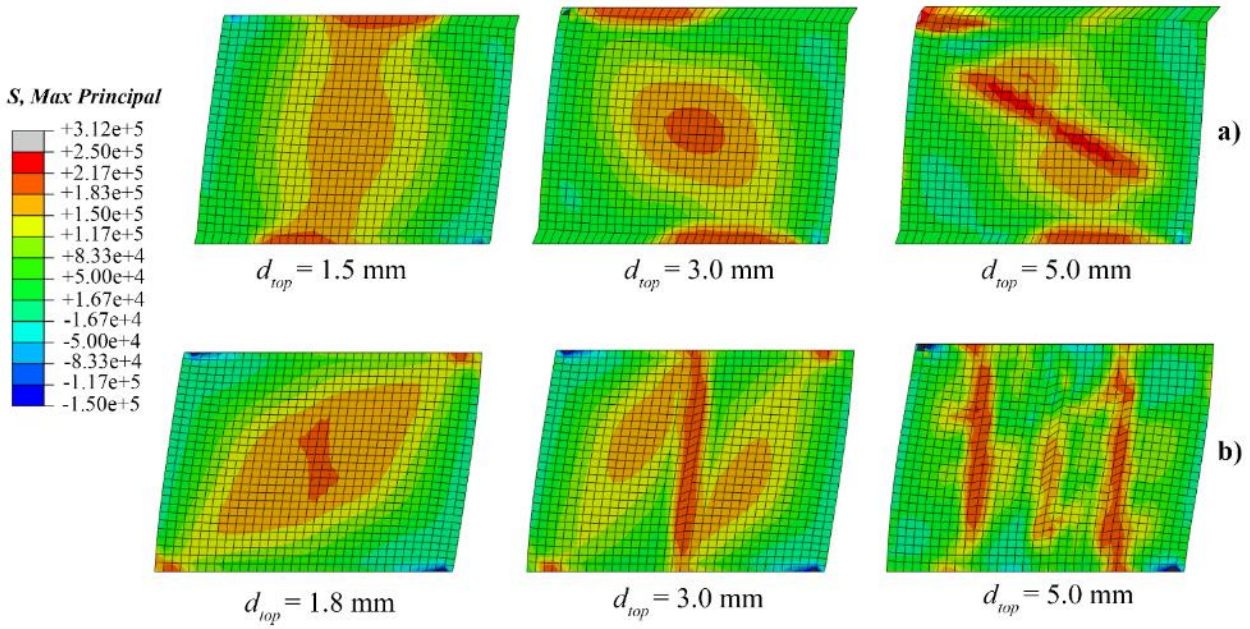

Figure 5.5– Panel P0-C (λ=0.8): maximum principal stresses associated to different steps of the analysis in case of two different values of applied axial load: a) $(\sigma/f_c)_2$ and b) $(\sigma/f_c)_4$.

However, some differences between panel P0-G and P0-C can be detected when considering the activation of a prevailing shear behavior. In particular, in case of the squatter panel (P0-C) it is evident that for both $(\sigma/f_c)_3$ and $(\sigma/f_c)_4$ (Figure 5.3-c, Figure 5.3-d) the development of the shear cracks is associated to the formation of more adjacent compressive struts (three in total, as it possible to see also from Figure 5.5-b).

More specifically, when looking at the results referring to the compression level $(\sigma/f_c)_3$, the occurred damage pattern indicates that the first shear crack, which develops almost in correspondence of the centre of the panel, leads to the activation of a behaviour determined by the presence of two panels, where at first a flexural response occurs, then followed by the development of two further diagonal shear cracks. This motivates the ductile response detected in the associated V_b - d_{top} curve (Figure 5.3-c) after the first drop of strength. In the case of the curve associated to the compression level $(\sigma/f_c)_4$, even if a similar damage pattern is detected, the effect in terms of displacement capacity in the associated response curve is less significant, being the compression level higher, so that the two panels rapidly undergo shear failure.

It is worth noting that in the case of the slenderer panel P0-G this type of failure does not appear, since even for the higher examined compression level ($(\sigma/f_c)_4$) the tensile damage occurs in the form of a unique (almost vertical) shear crack (Figure 5.4-c).

These observations are confirmed when looking at the tensile damage contour plots emerging from the analyses of the other examined panels, some of them reported in Figure 5.5 and in Figure 5.6. In particular, in these figures the tensile damage occurred in panels P0-B, P0-D (Figure 5.5), P0-E and P0-H (Figure 5.6) for each one of the four examined values of axial load ratio is represented. It is stressed that these pictures were taken by considering a top displacement after the one corresponding to the reaching of the peak strength, in order to capture the development of all the tensile cracks.

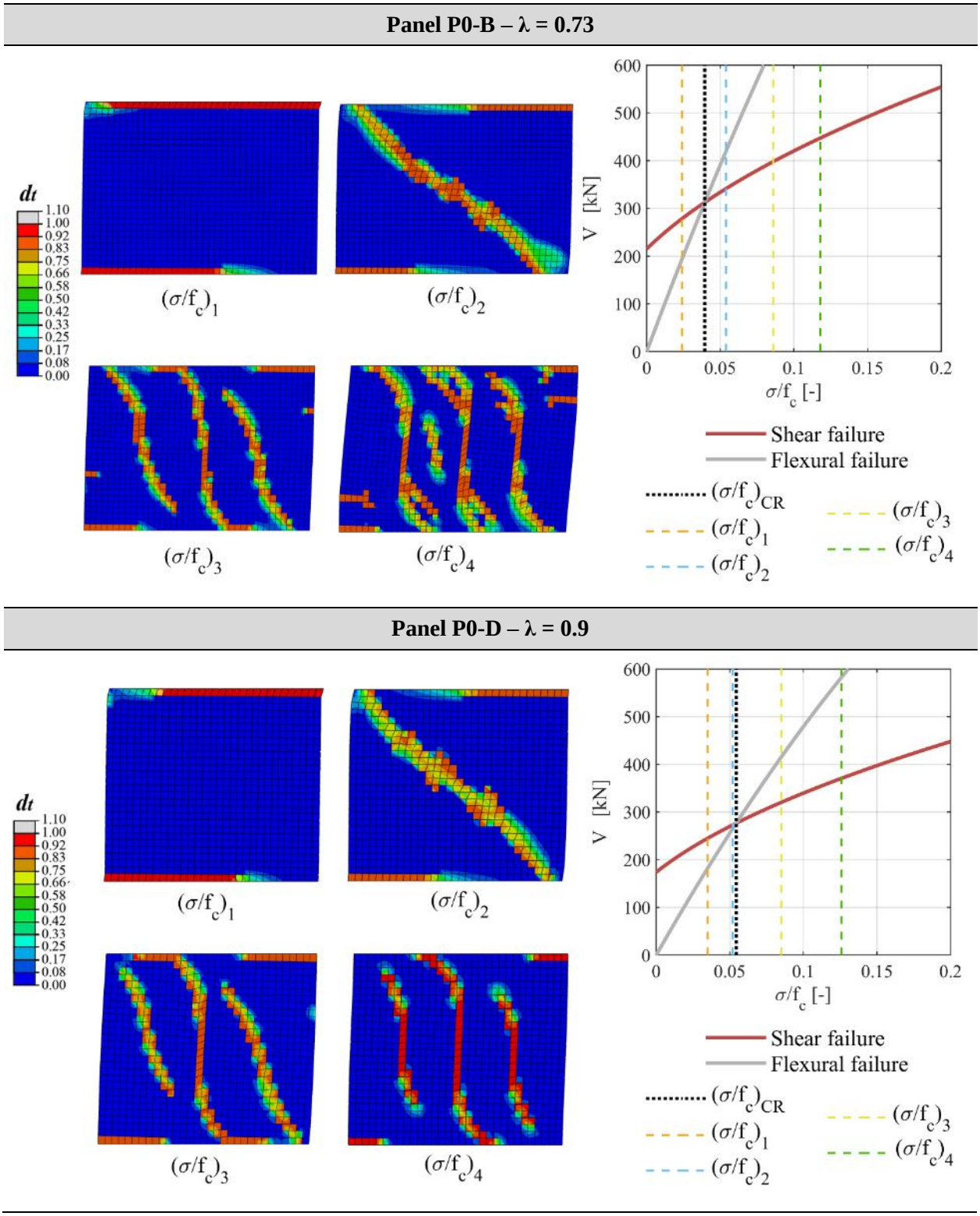

Figure 5.6 - Panel P0-B and P0-D: tensile damage contour plots at failure for each one of the applied compression levels σ/f_c and identification of these last on the associated failure domains.

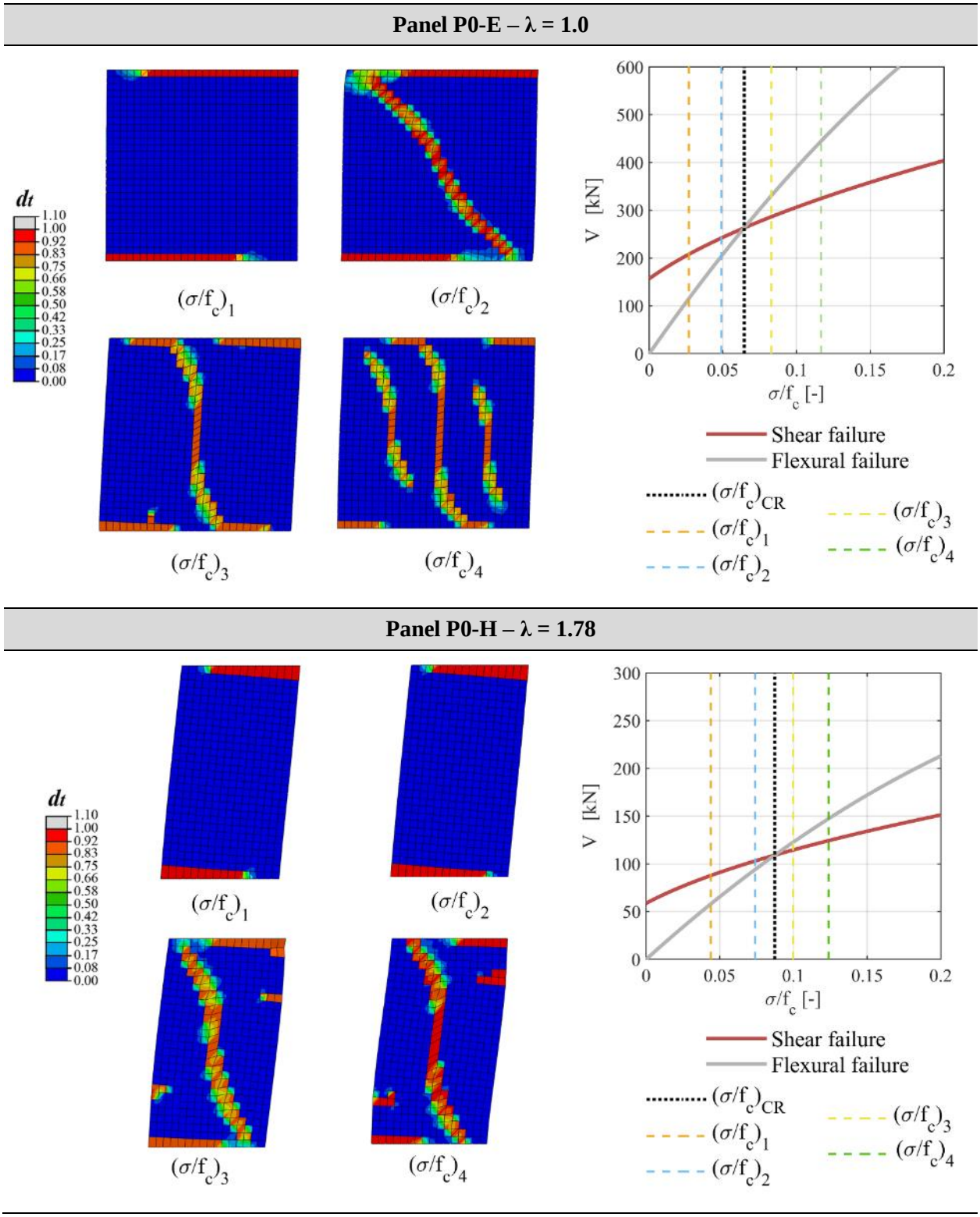

Figure 5.7 - Panel P0-E and P0-H: tensile damage contour plots at failure for each one of the applied compression levels σ/f_c and identification of these last on the associated failure domains.

Moreover, the failure domain of each panel, together with the identification of the four examined compression levels and of the critical axial load ratio $(\sigma/f_c)_{CR}$ are illustrated as well.

By examining these results, it comes out that in the case of all the squatter panels, and in particular when $\lambda \leq 1$, the high compression levels correspond to the propagation of more than one diagonal (or almost vertical) shear crack. In particular, for panels P0-B and P0-D this happens when applying $(\sigma/f_c)_4$ and also $(\sigma/f_c)_3$, which are both much higher than $(\sigma/f_c)_{CR}$, while for panel P0-E it happens only when applying $(\sigma/f_c)_4$, which is again much higher than $(\sigma/f_c)_{CR}$. Conversely, when considering the panel P0-H (Figure 5.6), with an aspect ratio higher than 1 ($\lambda = 1.78$), the occurred damage changes from the development of more sub-parallel shear cracks to the activation of only one crack; a similar behavior was detected also in presence of the panels P0-G ($\lambda = 1.43$, as seen in the previous Figure 5.4-c) and P0-F ($\lambda = 1.14$).

The analysis of the damage pattern of the examined piers, therefore, indicates that while the slenderer panels actually behave as a unique element, independently from the applied axial load, conversely the squatter panels ($\lambda \leq 1$), when considering a rather high compression level (in general, much higher than $(\sigma/f_c)_{CR}$), present a damage pattern which suggests the idea that the panel behaves as two coupled elements.

The comparison between the predictions of the FE models and of the performed analytical calculations in terms of maximum strength for each examined panel are reported in Figure 5.8; in particular, in the case of the analytical calculations both the above mentioned hypotheses (EF Single Panel and EF Two Panels) are taken into account. More specifically, the graphs represent the maximum strength V_y obtained according to the different considered hypotheses as well as the values of V_y emerging from the FE analyses as a function of the corresponding compression level σ/f_c; furthermore, for each panel also the critical axial load ratio $(\sigma/f_c)_{CR}$ is represented with a black dashed vertical line.

By looking at these graphs it is possible to observe that:

1) for the panels with $\lambda > 1$ the predictions of the analytical calculations in which the panel is modelled as unique element quite perfectly agree with the results of the FE analyses for all the considered compression levels; conversely, the idea to split the panel into two parts does not work well, since it always provides an underestimation of the actual maximum strength;
2) for the panels with $\lambda \leq 1$:
   - when the applied axial load ratio is lower than the critical one ($\sigma/f_c < (\sigma/f_c)_{CR}$, i.e. when flexural failures prevail) the estimates of the maximum strength according to the strategy that considers a unique panel provide a good match with the reference solution , while the strategy to split the panel again does not work well, leading to an underestimation of the final strength. Indeed, when splitting the initial panel into two elements these last are slenderer and this may result in an increased vulnerability to flexural failure, especially when the acting axial load is low;
   - when the applied compression level is higher with respect to the critical value ($\sigma/f_c > (\sigma/f_c)_{CR}$, i.e. when shear failures prevail), the strategy to split the panel provides better results with respect to the consideration of a unique element, which conversely leads to a quite significant overestimation of the values of strength assumed as reference solution.

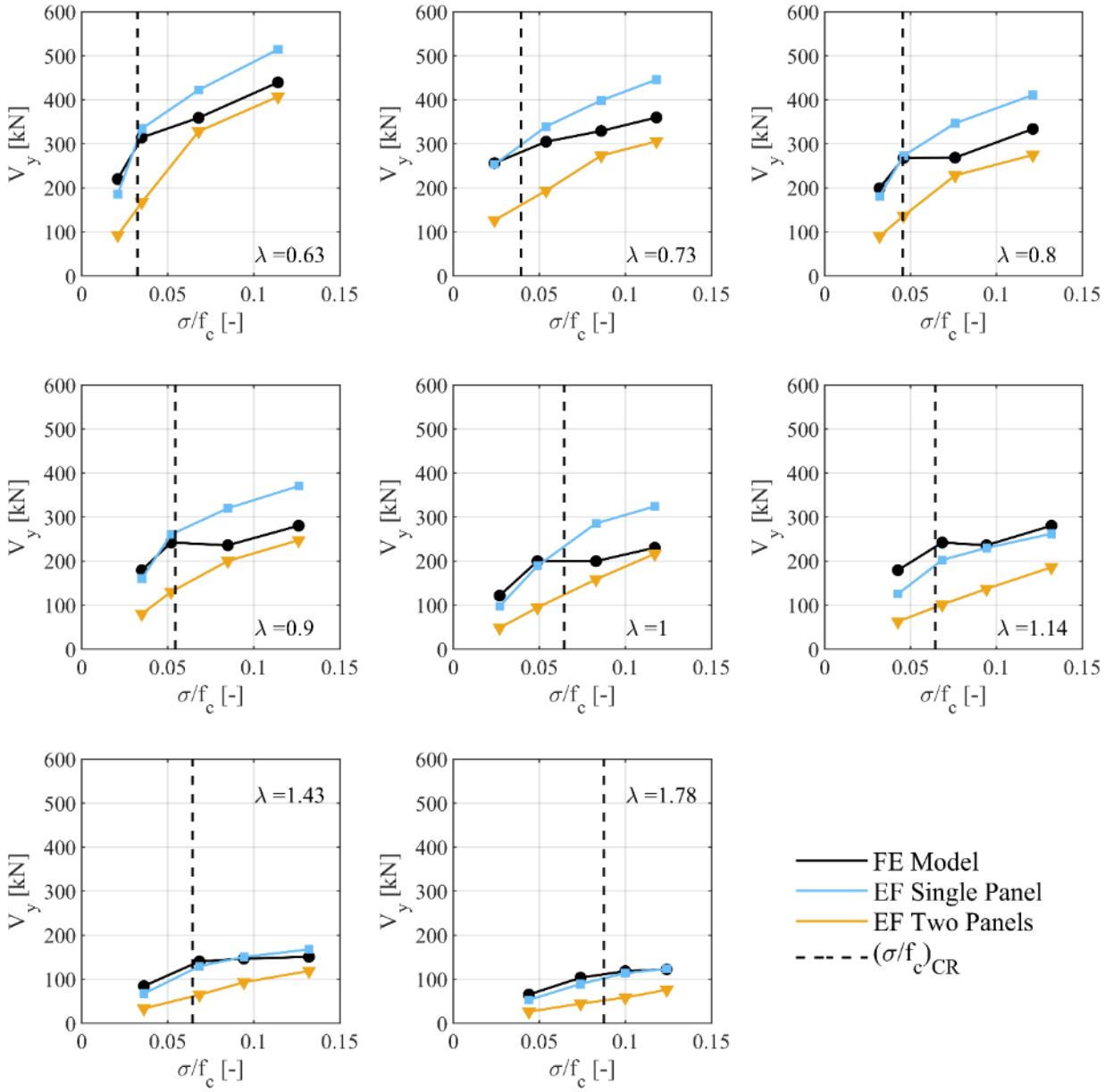

Figure 5.8 – Comparison in terms of maximum strength V_y between the results of the FE analyses and the predictions of the analytical calculations performed according to the panel-scale strength criteria for each examined panel.

This overestimation can be partly ascribed to the approximate evaluation, in the shear failure criterion, of the shape coefficient *b*, which is related to the tangential stresses distribution in the mid-section of the panel. Indeed, on the basis of what indicated in the commentary of the Italian building code (MIT (2009)), which is here considered as reference, *b* is assumed as a function of the aspect ratio of the panel: in particular, it is assumed equal to 1 for panels with $\lambda \leq 1$.

With the aim to deepen this aspect, some investigations on the distribution of the tangential stresses acting in the mid cross section of the examined panels were performed, and the obtained results showed that also in case of panels with $\lambda \leq 1$ values of *b* higher than 1 should be adopted. This would therefore

lead to a reduction of the maximum shear strength predicted by the criterion for shear failure in case of these panels, thus mitigating the differences with respect to the FE models observed in Figure 5.8.

This result contributes to further confirm what already found through specific studies available in the literature and based on results of linear and nonlinear FE analyses (Magenes and Calvi (1997), Cattari (2007), Calderini et al (2009), Betti et al (2015)). However, the objective of the deepenings here performed was simply to better explain the differences emerged in the obtained results between the predictions of the FE and the EF models (Figure 5.8), and not to provide a specific proposal for the evaluation of the coefficient *b*. Indeed, a comprehensive study on this topic should take into account, in addition to the aspect ratio of the panels, also other factors which may affect the evaluation of this coefficient, such as the type of the constitutive model adopted in the FE analyses and the boundary conditions characterizing the panels. Regarding this last aspect, in particular, recently it has been observed that also other structural parameters, such as the drift capapcity of the masonry panels, can be affected by the boundary conditions, as shown for example in the experimental campaigns described in Petry and Beyer (2014).

In the light of what now discussed, the execution of a series of specifically dedicated sensitivity analyses, aimed to systematically evaluate the effect of each one of the above mentioned factors on the evaluation of the tangential stresses distribution is deemed necessary in the view of the formulation of a new proposal for the determination of the coefficient *b*. However, up to now there are no exhaustive and robust studies on the topic available in the literature.

Moving back to the results shown in Figure 5.8, concluding, it is possible to highlight that the strategy to model the panel as split into two elements provides results closer to the ones deriving from the corresponding FE model only when the applied compression level is higher than the critical one (almost pure shear failure) and only when considering the squattest panels. This is consistent with what has come out from the analysis of the damage pattern detected in the FE analyses, as previously discussed.

5.1.3 Proposed modelling strategy

The above discussed results underline that the panel, in the view of the application of an EF approach, can be described as a unique element or as two coupled elements depending on both its aspect ratio and the applied compression level. In the light of these observations, the proposed modelling strategy can be summarized through the following expression (5.1):

$$\begin{cases} \lambda > 1: & \forall\ {}^{\sigma}/_{f_c} \quad single\ panel \\ \lambda \leq 1: & \\ \begin{cases} {}^{\sigma}/_{f_c} < \alpha \left({}^{\sigma}/_{f_c}\right)_{CR} & single\ panel \\ {}^{\sigma}/_{f_c} > \alpha \left({}^{\sigma}/_{f_c}\right)_{CR} & split\ panel \end{cases} \end{cases} \tag{5.1}$$

where α is a parameter > 1, such as to correspond to a situation of almost pure shear failure (σ/f_c largely higher than $(\sigma/f_c)_{CR}$). On the basis of the results obtained from the analyses here performed, a reasonable value for α seems to be 1.5.

According to this modelling strategy the panel has not to be split, whatever is the applied axial load, when its aspect ratio is higher than 1. Conversely, if the aspect ratio is lower or equal to 1 a differentiation is made on the basis of the acting compression level, if higher or lower than $\alpha(\sigma/f_c)_{CR}$: in the first case it is recommended to split the panel, while in the second case it is recommended to model it again as a single element.

It is important to stress that the application of the suggested modelling rule should be limited to the cases of adoption, for the interpretation of the shear failure, of strength criteria associated to the diagonal cracking (e.g., the one proposed by Turnšek and Cačovic (1971) or the one proposed in Mann and Müller (1980)).

Furthermore, it is worth underlining that according to some authors (Di Ludovico et al (2011)) the solution to split the panel may be erroneous under horizontal loads, since the elements underestimate the overall flexural stiffness of the masonry portion that they are intended to represent, influencing both the generalized forces and the structure's period of vibration. Regarding this aspect, the following considerations can be made.

First of all, in a squat panel the contribution of the shear stiffness is prevalent, while the one associated to the flexural behavior is negligible; this last becomes more significant when the aspect ratio of the panel increases. Moreover, when splitting a panel into two elements the shear stiffness contribution is not affected, and only the flexural one changes. Therefore, the aforementioned shortcoming could be significant only when the panels to be split are many with respect to those composing the structure under examination and, at the same time, if the obtained panels are particularly slender (i.e. with an aspect ratio such that the flexural contribution starts to be significant). Since on the basis of the proposed modelling rule the necessity to split the panel depends on both the aspect ratio and the acting compression level, in general it is expected that this operation has to be performed only for a limited number of panels with respect to the total panels of the structure; furthermore, it has to be realized only in the case of very squat panels. Therefore, the aforementioned issue should be very mitigated.

The employment in practice of the proposed rule presupposes to assess both the aspect ratio and the applied axial load ratio associated to the panel under examination.

While the aspect ratio of a pier panel can be immediately evaluated, for what concerns the considerations about the acting compression level more difficulties arise. Indeed, on one hand the compression level acting in a masonry panel inside a building can be *a-priori* estimated only with reference to the effect of the vertical loads; however, when the horizontal forces are applied, the axial load changes due to the redistribution of the vertical loads, and its variation can be correctly determined only after the execution of the analysis. On the other hand, the identification of the critical compression level is not immediate as well; indeed, if, as for example, the strength criteria suggested in NTC08 are adopted, it depends on parameters known a priori (geometry of the panel and mechanical parameters of masonry) but also on the boundary conditions characterizing the panel ($H_{0,}$ which is the shear span).

It is worth underlining that, for the determination of the boundary conditions of the pier panels under examination, it is possible to make some *a-priori* considerations based on the structural details of the building in which they are put in: if r.c. tie beams are present, the boundary conditions are close to the fixed-fixed scheme, while if no tensile resisting elements are available, the cantilever scheme is more likely.

However, these are hypothetical considerations which may turn out to be not correct and more in general may change progressing the nonlinear response (e.g. due to the failure mode activated in spandrels).

What now discussed highlights the necessity, for the application of the proposed rule, of performing preliminary analyses on the structure under examination.

In the light of these considerations a specific procedure for applying the introduced modelling rule is here outlined; it can be schematized in the following four steps:

1. individuation, in the structure under examination, of the panels with $\lambda \leq 1$, which are liable to be split;

if there are any,

2. execution of a preliminary analysis, in the form of pushover analysis;
3. at this point, the results of the analysis have to be examined; to this aim, two possible approaches may be adopted, namely a "practical approach" and an "analytical approach":
   - PRACTICAL APPROACH: after the execution of the analysis the type of failure occurred in each one of the identified panels have to be examined; if the panel has undergone flexural (or hybrid, if the adopted model allows the evaluation of these types of failures) failure, it means that, according to the proposed modelling rule, the panel should not be split, while if the panel has undergone shear failure, it means that the panel should be split;
   - ANALYTICAL APPROACH: after the execution of the analysis, it is necessary: i) to monitor the variation of the axial load occurred during the analysis in the panels under consideration and ii) to evaluate the bending moment diagrams of such panels, in order to be able to compute the corresponding shear span H_0. In this way, it is possible on one hand to correctly define the strength domain of the panels and to evaluate the critical axial load ratio, and on the other to compare it with the axial load acting on the element, taking into consideration its variation during the whole analysis;
4. if, from the previous evaluations, it emerges that some of the panels under consideration should have been split, the analysis is performed again after having split these elements.

Example of application to the analysis of a masonry wall

A practical example of application of the proposed procedure is presented in the following, by making reference to one of the irregular wall configurations described and analysed in the previous Chapter 4.

In particular, the examined wall is the configuration E1, which is characterized by the presence of a different number of openings per storey. As shown in Chapter 4 – section 4.2 (Table 4.5), the application of the different criteria for the pier effective height in this case leads to almost similar geometry for the pier elements, so that in the following only one of them, as for example the one according to Dolce (1991), is considered.

The application of the four steps of the procedure previously introduced is described in the following.

1. First, of all, the panels with $\lambda \leq 1$ have to be individuated; in this case, only the pier P2 is considered (as shown in Figure 5.9-a), which presents an aspect ratio equal to 0.69 (B= 3.91m, h_{eff} = 2.69m, see Table 4.5).
2. A pushover analysis with a uniform load pattern has already been performed on this wall (whose outcomes have been discussed in section 4.4), so that its results are used for the following steps; in particular, for the sake of brevity, only the analysis in the positive verse is here considered.
3. As an example, both the analytical and the practical approach are tried in the following.
   - PRACTICAL APPROACH

     By looking at the damage scenario referring to the end of the analysis (Figure 5.9-b), it is possible to see that the pier under consideration has undergone flexural failure; this indicates that the compression level acting on the element is quite low and it is not so significant to activate a shear failure. Therefore, by adopting the practical approach, the conclusion would be not to split the panel.

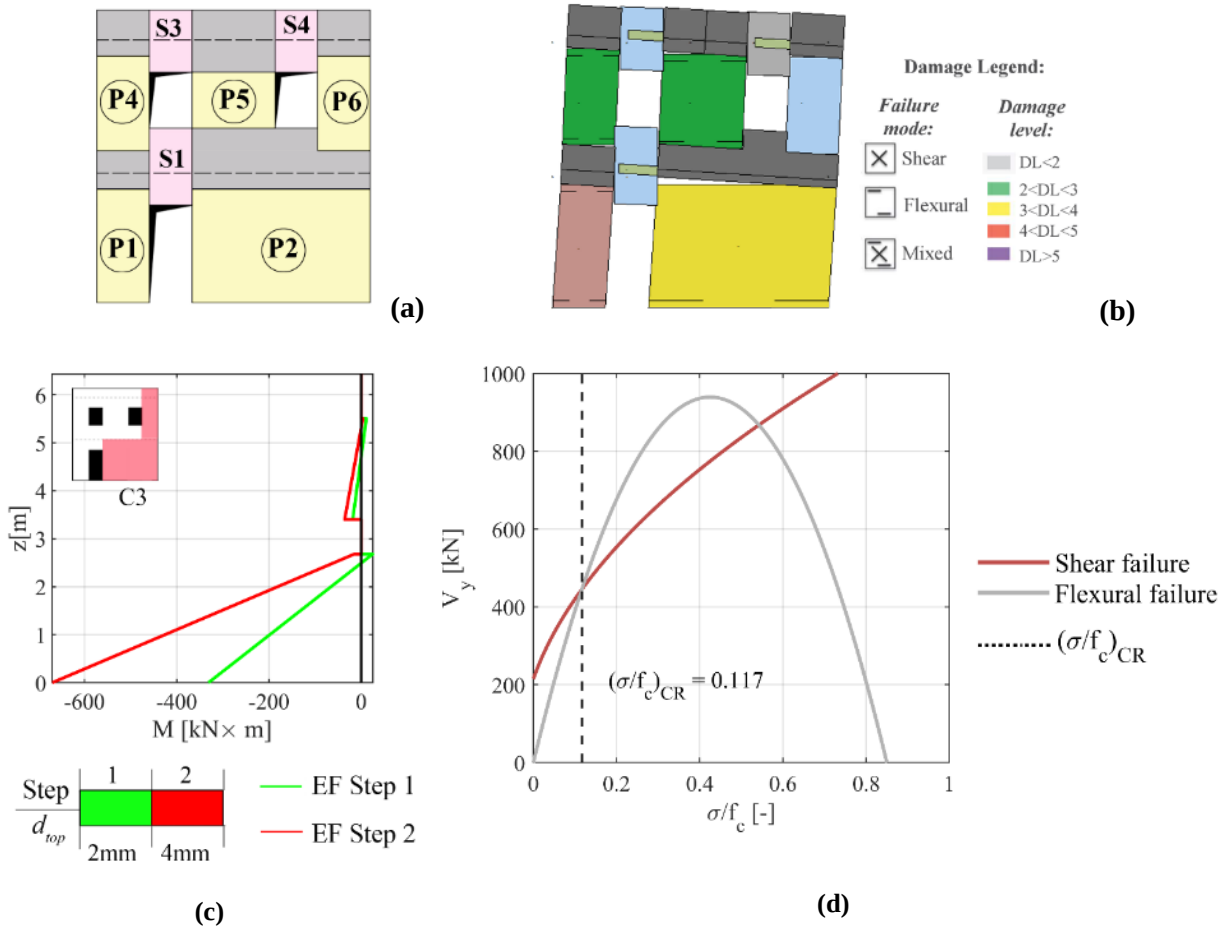

Figure 5.9 – (a) Wall configuration E1; (b) damage pattern (d_{top} = 50 mm) occurred during the analysis in the positive verse on configuration E1; (c) bending moment diagram referring to alignment C3, which includes pier P2 at the ground floor for two different steps of the analysis; (d) strength domain of pier P2 with the identification of $(\sigma/f_c)_{CR}$.

Table 5.2 – Configuration E1, analysis in the positive verse – element P2: values of the critical axial load ratio ($(\sigma/f_c)_{CR}$), of the compression level acting after the application of the dead loads ($(\sigma/f_c)_{dl}$) and taking into account the axial load variation occurring in the analysis ($(\sigma/f_c)_{dl}+\Delta(\sigma/f_c)$). Graphical representation of the strength domain and of the compression levels under consideration.

$(\sigma/f_c)_{CR}$ [%]	$\alpha(\sigma/f_c)_{CR}$ [%]	$(\sigma/f_c)_{dl}$ [%]	$(\sigma/f_c)_{dl}+\Delta(\sigma/f_c)$ [%]
11.7	17.6	4.4	5.9

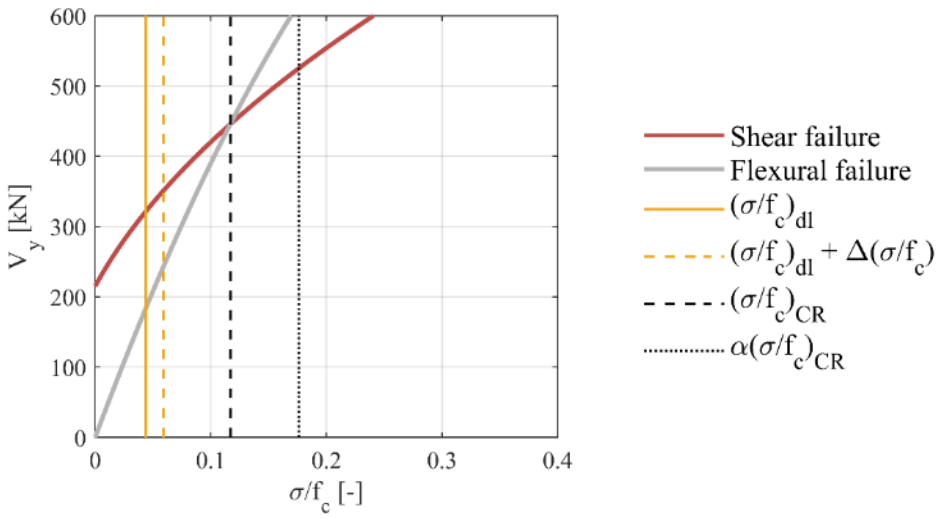

- ANALYTICAL APPROACH
  - i) The bending moment diagram derived from the results of the analysis (see Figure 5.9-c) clearly shows that the boundary condition associated to the pier under examination is that of a cantilever beam (H_0=H=2.68m); in this way, the failure domain of the panel can be univocally determined (see Figure 5.9-d), as well as the associated critical axial load ratio, which is equal to 11.7%, as reported in Table 5.2.
  - ii) The examination of the axial force acting during the analysis on pier P2, which is subjected to a progressive increase in compression (analysis in the positive verse), leads to the axial load ratios σ/f_c reported in Table 5.2; in particular, these values are associated to the mid-section of the panel and refer to both the application of the vertical loads only ($(\sigma/f_c)_{dl}$) and to the variation occurring during the analysis ($((\sigma/f_c)_{dl}+\Delta(\sigma/f_c)$).

  By comparing the obtained values with the critical one multiplied for the coefficient α (which can be posed, as previously suggested, equal to 1.5), it is observed that the actual compression rate, even if when the variation of the axial load is taken into account, is far from $(\sigma/f_c)_{CR}$ and even more from $\alpha(\sigma/fc)_{CR,}$ as it is possible to see from the graph represented in Table 5.2. Therefore, also by following this approach the result previously obtained is confirmed.

4. In the light of what obtained by applying both the analytical and the practical approach, the modelling strategy adopted for the panel under examination has not to be changed (i.e. the panel should not be split, being the acting compression level too low for producing a pure shear failure), so that the analysis already performed can be considered as correct and consistent with the rule

herein discussed. Actually, the obtained results were in good agreement with what emerging from the FE model, as widely discussed in Chapter 4.

5.1.3.1 Sensitivity analyses on the critical axial load ratio

The "critical" axial load ratio associated to a given masonry panel represents, as discussed before, the compression rate associated to the transition between a prevailing shear failure and a prevailing flexural failure. The exact value of σ_{CR} (which normalized to f_c leads to $(\sigma/f_c)_{CR}$) can be analytically evaluated by equating the strength criteria referring to the flexural and shear failures here adopted as reference (as indicated in the following equation 5.2):

$$\frac{\sigma_{CR}B^2t}{2}\left(1-\frac{\sigma_{CR}}{0.85f_c}\right)\frac{1}{H_0}=\frac{1.5\tau_0Bt}{b}\sqrt{1+\frac{\sigma_{CR}}{1.5\tau_0}} \qquad (5.2)$$

The analytical resolution of this equation is discussed in Appendix B.

According to the proposed modelling rule, the parameter $(\sigma/f_c)_{CR}$ represents, in case of the panels with $\lambda \leq 1$, the discriminatory element for the decision to split or not the panel; therefore, the determination of its exact value as a function of the different parameters on which it depends may lead to useful considerations about real cases the professional engineer may have to deal with.

As it is possible to see from equation 5.2, σ_{CR} depends on:

- the boundary conditions (H_0);
- the mechanical parameters characterizing the masonry under examination (f_c, τ_0);
- the geometry of the panel (H, B, b).

In order to study how these parameters affect the final value of σ_{CR} for a given panel, some sensitivity analyses were carried out making specific assumptions about plausible values they may assume in real cases. In particular, the following assumptions were made:

- <u>BOUNDARY CONDITIONS</u>: three different boundary conditions were explored, corresponding to different values of the parameter H_0 (shear span):
  - fixed-fixed condition: $H_0 = H$;
  - cantilever condition: $H_0 = H$;
  - intermediate condition: $H_0 = 0.75H$.

  This last condition has been included since it is actually more representative of the real situations, in which often the boundary conditions characterizing the masonry panels are intermediate between the two "ideal" static schemes previously mentioned.
- <u>GEOMETRY OF THE PANEL</u>: two different aspect ratios were considered:
  - $\lambda = 0.6$ (B = 4.75m, H = 2.85m);
  - $\lambda = 1.0$ (B = 2.85m, H = 2.85m).

  Higher values of λ have not been investigated since the analysis of the value of $(\sigma/f_c)_{CR}$ is interesting mainly in case of the panels with $\lambda \leq 1$.
- <u>MASONRY TYPE</u>: three types of masonry were examined, chosen in order to be representative of masonries with different quality of the associated mechanical parameters:

- Type 1: irregular stone masonry (poor quality)
- Type 2: masonry with regular stone blocks (intermediate quality)
- Type 3: masonry made of clay bricks and cement mortar (good quality):

For each masonry type, specific plausible ranges of the mechanical parameters f_c and τ_0 were defined (reported in Table 5.3), on the basis of what is suggested in the commentary of NTC08 (MIT (2009), Table C8A.2.1).

Table 5.3 – Range of variation and corresponding mean value μ for the masonry compressive strength f_c and the shear strength τ_0 in case of each one of the 3 different types of masonry considered in the sensitivity analyses.

	TYPE 1		**TYPE 2**		**TYPE 3**	
	Range of variation	μ	**Range of variation**	μ	**Range of variation**	μ
f_c [MPa]	1 - 1.8	1.4	2.6 - 3.8	3.2	5.0 - 8.0	6.5
τ_0 [MPa]	0.02 - 0.032	0.026	0.056 - 0.074	0.065	0.24 - 0.32	0.28

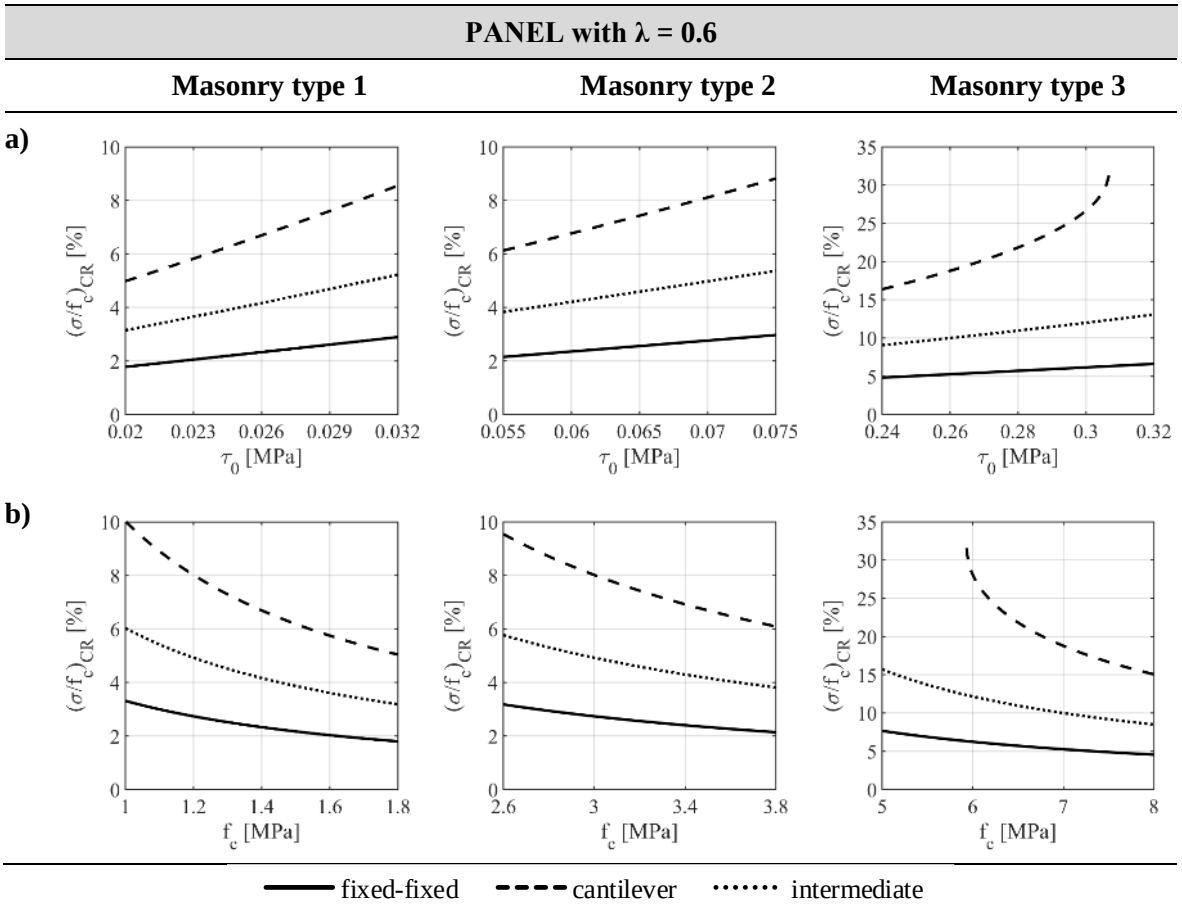

Figure 5.10 – Panel with λ = 0.6: effects on $(\sigma/f_c)_{CR}$ of the variation of: a) the shear strength of masonry τ_0; b) the compression strength of masonry f_c for the three considered masonry types.

The results of the sensitivity analyses are reported in Figure 5.10 in case of the panel with λ=0.6 and in Figure 5.11 in case of the panel with λ=1.0. Each graph refers to a specific masonry type among the three considered and shows $(\sigma/f_c)_{CR}$ as a function of :

- Figure 5.10-a and Figure 5.11-a: the shear strength τ_0 (f_c in this case is assumed as fixed and equal to the mean value of the examined range - μ in Table 5.3)
- Figure 5.10-b and Figure 5.11-b: of the compression strength f_c (τ_0 in this case is assumed as fixed and equal to the mean value of the examined range - μ in Table 5.3).

Moreover, in each graph the results referring to the three considered boundary conditions are shown.

It is stressed that when the curve associated to one of the three boundary condition is not present at all or is not drawn for some of the values of the parameter reported in the x-axis, it means that the intersection point between the two strength criteria in that conditions cannot be determined, since it does not exist (i.e. for each applied compression level the flexural failure always prevails).

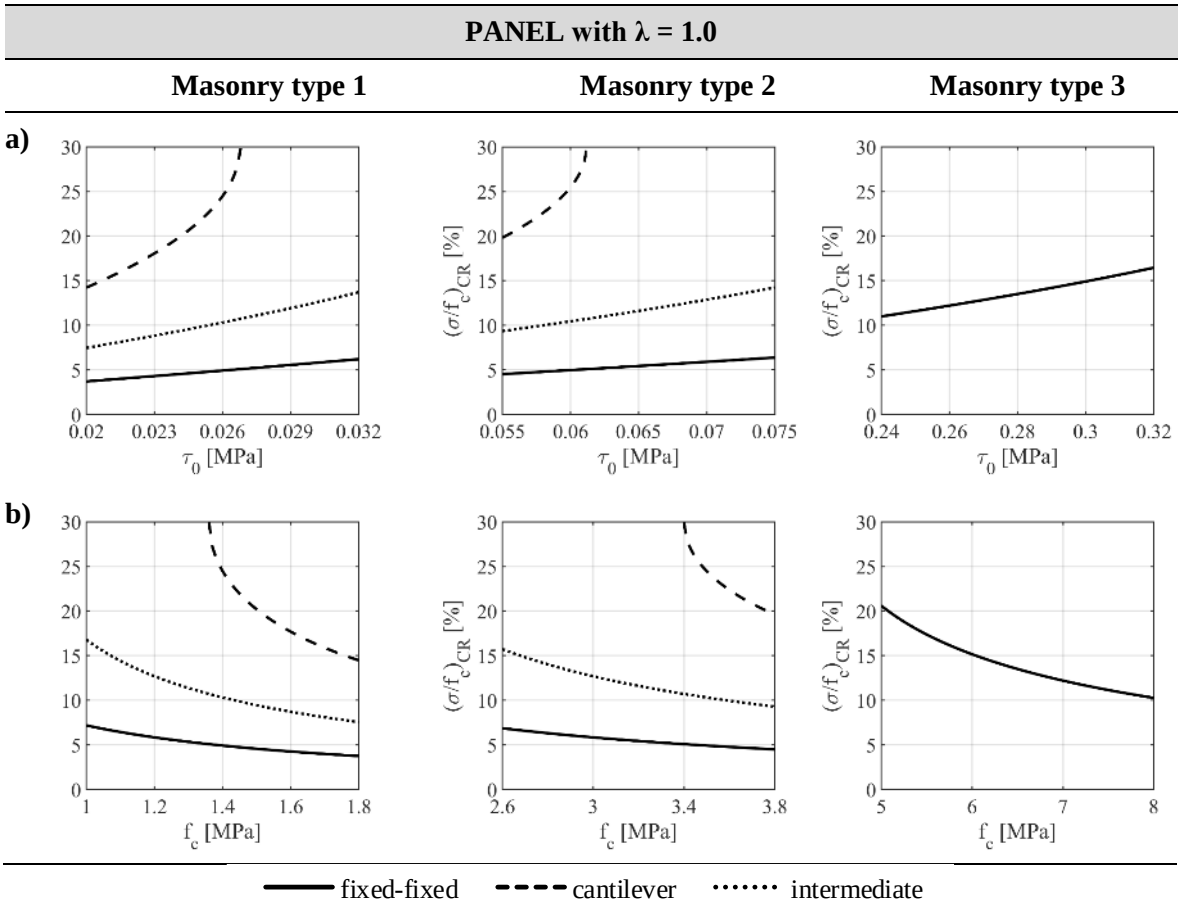

Figure 5.11 – Panel with λ = 1.0: effects on $(\sigma/f_c)_{CR}$ of the variation of: a) the shear strength of masonry τ_0; b) the compression strength of masonry f_c for the three considered masonry types.

From the graphs reported in Figure 5.10 and in Figure 5.11 some useful considerations about how the different examined parameters affect the variable $(\sigma/f_c)_{CR}$ can be made:

1. in general, for all the considered masonry typologies and boundary conditions and for both the examined values of aspect ratio $(\sigma/f_c)_{CR}$ increases when τ_0 increases and decreases when f_c increases;
2. in presence of the cantilever boundary conditions, the values of $(\sigma/f_c)_{CR}$ are always higher with respect to those obtained when assuming the other two boundary conditions; this is because the lower is the degree of constraint of the panel, the higher is its vulnerability with respect to flexural failure, so that in some cases there is even no more intersection between the two strength criteria and $(\sigma/f_c)_{CR}$ can no longer be evaluated. This happens, as an example, for the squat panel ($\lambda = 0.6$) in presence of a masonry of good quality and low values of compression strength (f_c approximately lower than 6.0 MPa) or high values of shear strength (τ_0 approximately higher than 0.3 MPa). Moreover, it happens even more frequently in case of the panel with $\lambda = 1.0$; indeed, being this panel slenderer with respect to the previous one, the vulnerability to flexural failure, fixing all the other parameters, is higher. In this case, therefore, in presence of a masonry of good quality for all the considered values of f_c and τ_0 the critical compression level can be determined only if the boundary condition is fixed-fixed;
3. moving from masonry type 1 (with poor mechanical properties) to masonry type 2, where the mechanical properties are slightly higher, the values of $(\sigma/f_c)_{CR}$ slightly increase, while when moving to masonry type 3 (with good mechanical properties) they significantly increase;
4. when fixing all the other parameters, the higher is the aspect ratio, the higher is the corresponding critical compression level.

This last observation, in particular, is confirmed also by looking at the graphs reported in the following Figure 5.12, where, for each one of the examined masonry typologies (f_c and τ_0 are assumed as fixed and equal to the mean value of the corresponding ranges of variation – see μ in Table 5.3), the value of $(\sigma/f_c)_{CR}$ is represented as a function of the aspect ratio of the panel λ, considering values of λ ranging from 0.5 (very squat panels) to 3 (very slender panels). The flattening of the curves in correspondence of values of λ between 1 and 1.5 are due to the piecewise-linear definition of the coefficient *b* as a function of the aspect ratio λ in the criterion for the diagonal shear failure.

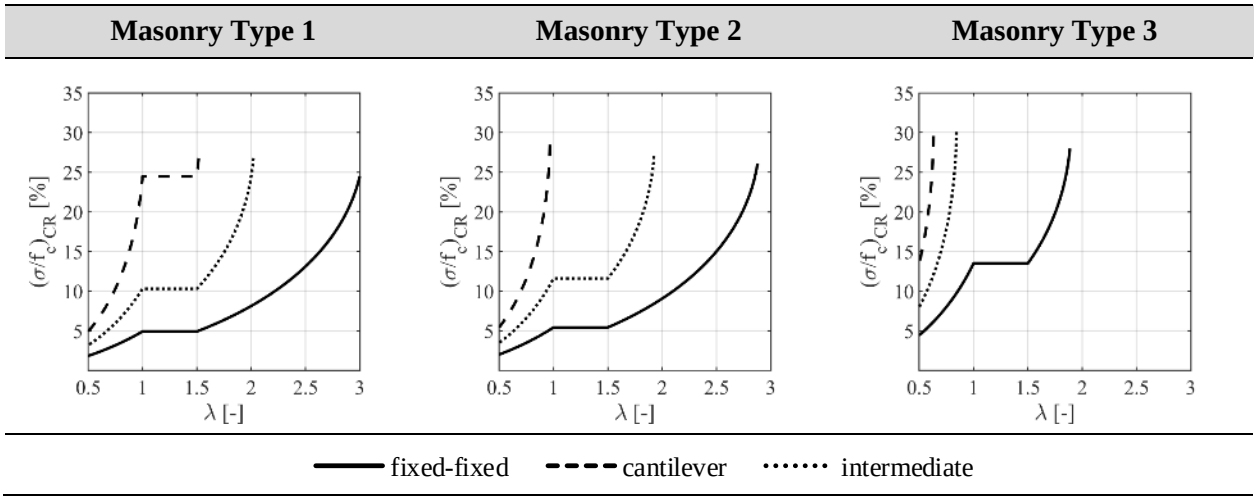

Figure 5.12 – Effect on $(\sigma/f_c)_{CR}$ of the variation of the aspect ratio λ of the panel for each one of the three considered masonry types.

The above discussed considerations on the effect of the different examined parameters on the value of $(\sigma/f_c)_{CR}$ may be useful to support the preliminary evaluations that a professional engineer should make when defining the structural model of a masonry building including pier panels with an aspect ratio $\lambda \leq 1$.

Indeed, it is possible that in particular situations, due to the specific boundary conditions, the values of the mechanical properties of masonry and of the aspect ratio of the panels, the value of $(\sigma/f_c)_{CR}$ corresponds to compression levels much higher than the ones actually characterizing the panels under examination. Moreover, even situations in which this critical value does not exists are possible.

In these situations, even if the aspect ratio of the panel under examination falls into the range of values for which the panel should be potentially split, the boundary conditions are such that $(\sigma/f_c)_{CR}$ is unlikely to be reached. Therefore, in these cases the possibility to split the panel may be *a-priori* excluded.

Some more specific considerations referring to real and practical cases can be made by looking, as for example, at the average compression levels σ/f_c acting on the masonry piers of one of the external walls of building C3 (considering both the 2- and the 3-story solution), which is one of the building prototypes introduced in Chapter 2 (section 2.2) and studied within the RINTC research project before presented. These values, which refer to the axial load acting in the mid-section of the piers after the application of the dead loads, are reported in Table 5.4 and can be assumed as representative of the compression levels characterizing the pier elements in common 2- and 3-story masonry buildings.

Table 5.4 - Compression levels σ/f_c acting due to the vertical loads only in the pier elements of common 2- and 3-story masonry buildings (derived from the buildings C3 2-story and C3-3-story described in Chapter 2, sect. 2.2).

	3-story building	**2-story building**
	σ/f_c [%]	**σ/f_c [%]**
1st story	5.3%	3.3%
2nd story	3.1%	1.5%
3rd story	1.3%	-

Starting from the analysis of the data referring to the 3-story building and examining the piers at the top floor, from the graphs reported in Figure 5.10 and in Figure 5.11 it is possible to see that the compression rate σ/f_c acting in this case after the application of the vertical loads, which is on average equal to 1.3%, is far from the critical condition in almost all the considered cases (i.e. whatever the aspect ratio, the masonry type and the boundary conditions are), also taking into account that in these elements a rather low variation of the axial load is expected during the analysis. Moving to the piers at the intermediate storey (σ/f_c on average equal to 3.1%), the acting axial load is closer to the critical condition, especially in presence of rather squat panels (as for example with $\lambda = 0.6$, see Figure 5.10), masonry with poor or intermediate quality (type 1 or 2) and fixed-fixed boundary condition.

More interesting is the situation of the masonry piers at the ground floor, which usually mainly govern the structural response and are also characterized by the highest compression level; in particular, as indicated in Table 5.4, in a common 3-story building this last may be, on average, equal to 5.3%. In case these elements are represented by rather squat panels (as for example with λ around 0.6) and in presence of

a masonry with poor or intermediate quality of the mechanical properties (masonry type 1 or 2), this value may be, depending on the boundary conditions, already higher (fixed-fixed condition), close (intermediate condition) or still lower (cantilever condition) to the critical compression level (see Figure 5.10). Moreover, by taking into account that, during the analysis, the compression level in these elements may increase (from the numerical analyses carried out a plausible value is represented by a maximum increment of 5%, thus leading in this case to a final σ/f_c equal to approximatively 10%), $(\sigma/f_c)_{CR}$ may be attained also in presence of the cantilever boundary condition. Conversely, if the masonry under consideration is characterized by a better quality (higher compression and shear strength, as in the case of masonry type 3), since the values of $(\sigma/f_c)_{CR}$ are higher, when in presence of a cantilever static scheme the reaching of the critical condition is unlikely to occur, even taking into account the increment of the axial load during the analysis.

If the pier panels under consideration are slenderer (as for example with $\lambda = 1.0$, see Figure 5.11), the attainment of the critical condition is in general less likely, being the values of $(\sigma/f_c)_{CR}$ higher. In particular, when a masonry with mechanical properties similar to those of masonry type 3 is examined, the attainment of the critical axial load ratio is not an issue unless in presence of a fixed-fixed condition; in this case, indeed, $(\sigma/f_c)_{CR}$ may be reached in the piers which undergo an increment of compression during the analysis, especially when the compression strength f_c is rather high (almost 8 MPa, i.e. close to the upper bound of the range of variation here considered) or, alternatively, the shear strength τ_0 is quite low (almost 0.25 MPa, i.e. close to the lower bound of the range of variation here considered).

Similar considerations apply to the piers of the 2-story building, whose average compression levels are perfectly comparable with those of the piers at the second and third storey of the 3-story building above discussed.

In the light of these observations, it emerges that, in general, the piers at the top floor of a building, being subjected to quite low vertical loads and also to a not significant variation of the normal stress during the analysis, are usually far from the reaching of the critical condition; conversely, the piers at the ground floor of a building (especially in case of multi-story structures) are more likely to reach the critical condition, especially if the masonry under consideration has poor mechanical properties and if the boundary condition is close to the fixed-fixed one (i.e. presence of r.c. tie beams or tie rods). Therefore, with the aim to apply the modelling rule here proposed, specific attention should be paid in particular to these elements.

5.2 ANALYSIS OF URM PIERS WITH OPENINGS OF DIFFERENT SIZE AND POSITION

The analyses described in this section are devoted to study the effect of position and size of openings on the performance of masonry panels subjected to in-plane loading. This deepening is motivated by some results emerged from the study of the wall with the little opening (configuration BD) described in Chapter 4. The specific aim is to understand if, by varying these parameters, there are situations in which the response of the panel is no more affected by the presence of the opening. In other words, in these cases the opening could be neglected in the definition of the corresponding EF structural model.

The evaluation of the effects of position and dimensions of the openings on the behavior of the masonry piers is carried out by considering the outcomes of a series of FE analyses performed on case-studies

structures *ad-hoc* defined, analyzing, in particular, the repercussions in terms of response curve and occurred damage.

5.2.1 Conceived case studies

The case studies structures here analysed (in total 19) were defined starting from the geometry of the panel "P0-B" introduced in the previous section. This panel has been chosen since it has the same geometry of the panel located at the ground floor in the wall configurations E1 and BD (see Chapter 4, Figure 4.5) (its dimensions are: 3.91 x 2.85x 0.25 m). In particular, the following case studies were introduced:

- Configurations of Type 1: obtained by introducing an opening, centred in the panel, whose dimensions are homothetically scaled; the configurations obtained in such way are in total 5 (indicated as P1,…,P5 moving from the smallest to the biggest opening, as shown in Figure Figure 5.135.13). Since the objective here pursued is to understand if, when applying an EF modelling approach, it is better to include or not the opening in the model, depending on its dimensions, the most interesting configurations are those where the opening has the smallest size (P1, P2 and P3). In the other cases, the dimensions of the opening are such that there is no doubt about the necessity to include it in the structural model; however, these case studies are useful in order to better capture the progressive change in the response of the panel when varying the opening size.

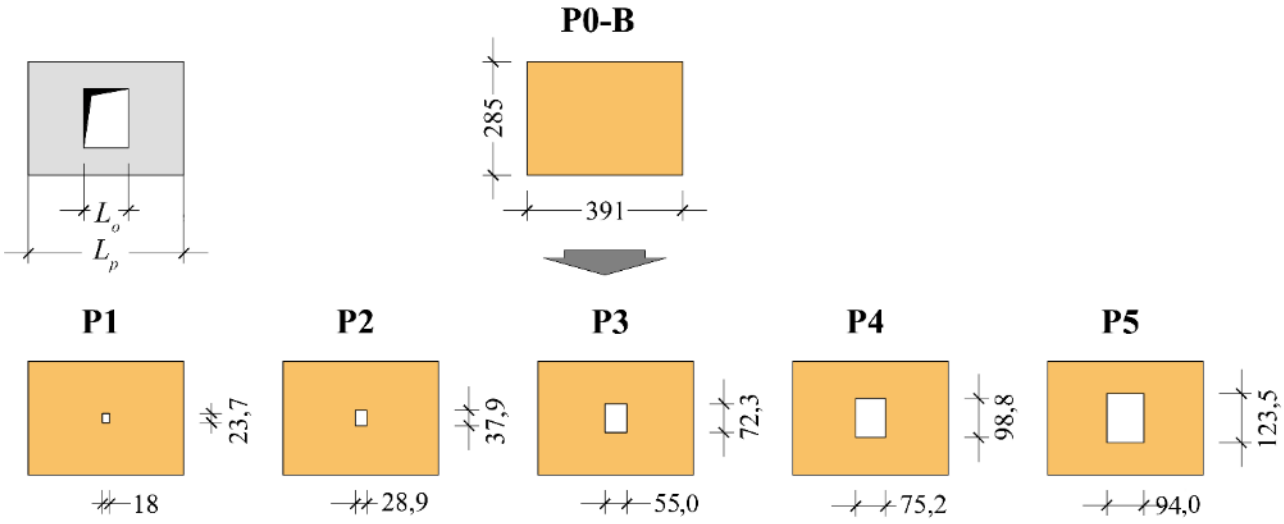

Figure 5.13 – Geometry of the configurations of type 1 (measures in cm).

- Configurations of Type 2: obtained starting from configuration P1 and by varying the height of the opening (while keeping constant its width) and its position along the panel. With regard to the height of the opening, in addition to the initial one (h1) two further heights were considered (h2 and h3); for what concerns the position, in addition to the initial one (centre of the panel), four further possibilities were investigated for each one of the three introduced heights. Each position is identified through the parameter x_o/x_p, where x_o is the position of the centroid of the opening and x_p is the total length of the panel (see Figure 5.14). The considered positions are associated to the following values of x_o/x_p: 1/6, 1/3, 1/2, 2/3 and 5/6; they are indicated in the name of each

configuration through a subscript. As for example, in case of height h2, the names associated to the introduced configurations are: P1-h2$_{1/6}$, P1-h2$_{1/3}$ and so on. The configurations obtained in such a way are illustrated in Figure 5.14.

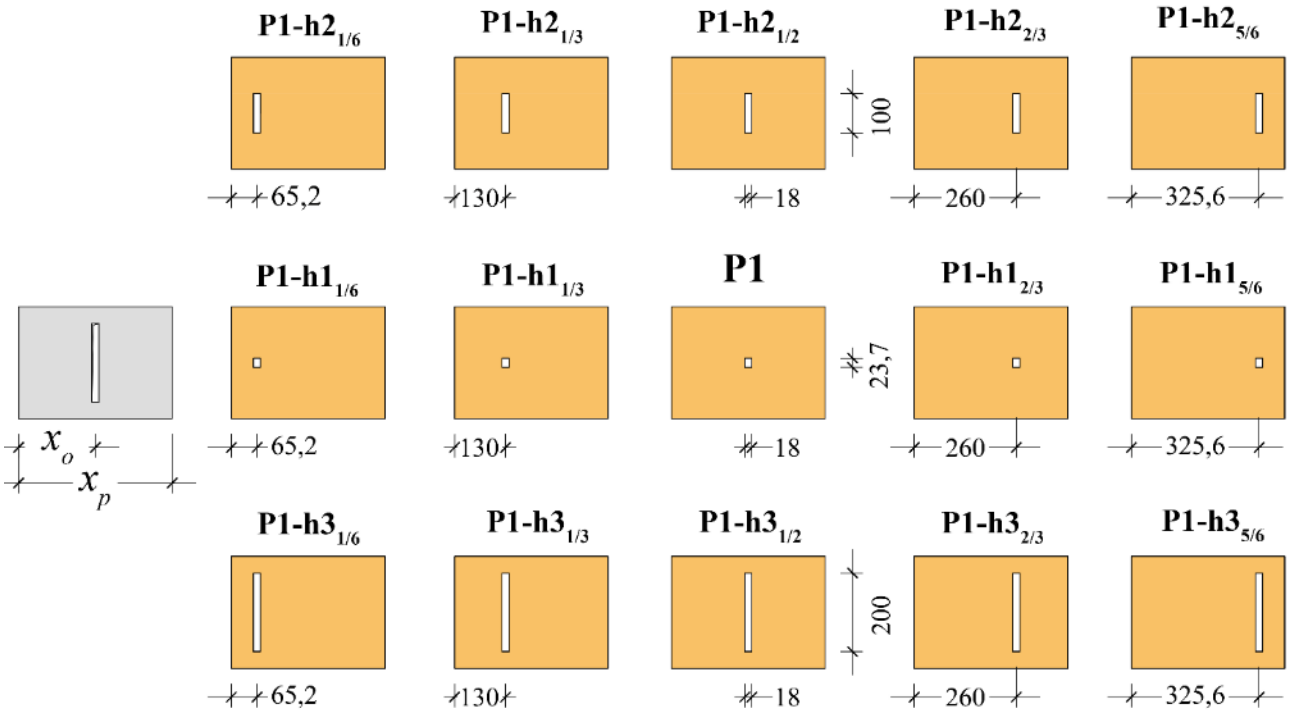

Figure 5.14 – Geometry of the configurations of type 2 (measures in cm).

In Table 5.5 for each configuration two geometric parameters are indicated:

- the ratio between the length of the opening L_o and the total length of the panel L_p (which represents a measure of the reduction of the resisting cross section due to the introduction of the opening);
- the ratio between the height of the opening h_o and the height of the panel h_w, which in this case can be assumed representative of an interstorey height (h_w = 2.85m).

Table 5.5 - Geometric parameters L_o/L_p and h_o/h_w associated to the introduced configurations.

	Configurations of type 1					**Configurations of type 2**	
	P1	**P2**	**P3**	**P4**	**P5**	**P1-h2**	**P1-h3**
L_o/L_p **[-]**	0.05	0.07	0.14	0.19	0.24	0.05	0.05
h_o/h_w **[-]**	0.08	0.13	0.25	0.35	0.43	0.35	0.70

The panels were modelled in ABAQUS by using the CDP model and according to the same strategy adopted for the panels described in the previous section. Moreover, they were analysed by considering both the fixed –fixed and the cantilever static scheme.

With the aim to investigate also the influence of the applied compression level, in the case of the fixed-fixed static scheme two different axial loads were applied on the top section of the introduced structures: the first one equal to 300 kN (identified in the following as Axial Load 1, AL-1) and the second one equal to 500 kN (AL-2); the panels in the cantilever static scheme were analysed only considering AL-1. With reference to the top section of each panel, the compression rates σ/f_c associated to AL-1 and AL-2 are 4.95% and 8.25%, respectively.
On each one of the introduced configurations lateral load monotonic analyses were performed.

5.2.2 Results of panels with openings homothetically scaled (type 1)

In Figure 5.15 the comparison between the base shear – top displacement $V_b - d_{top}$ curves obtained through the FE analyses in case of the configurations of type 1 is reported, with reference to both AL-1 and AL-2 and to the fixed-fixed static scheme. Moreover, in each graph also the curve associated to the corresponding panel without opening (P0-B) is reported (black curve).

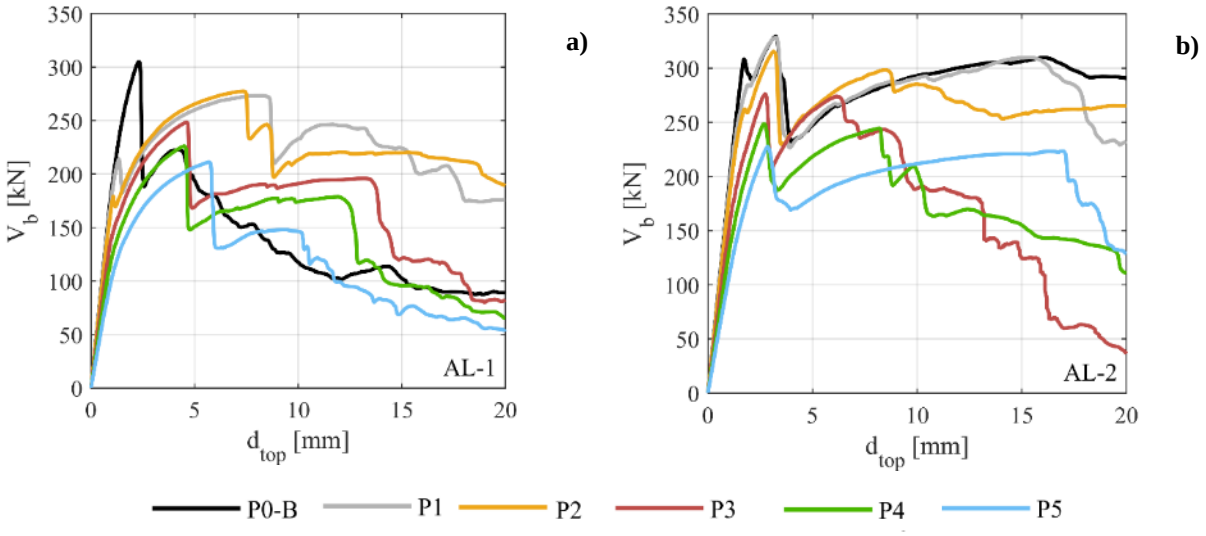

Figure 5.15 – Configurations of type 1: base shear – top displacement ($V_b - d_{top}$) curves associated to: a) Axial Load 1 and b) Axial Load 2.

By examining these results, it is possible:

i) to understand if the introduction of the opening affects or not, depending on its dimensions, the response of the initial panel P0-B and therefore if it is better to model the examined configurations as a unique panel, by neglecting the opening, or as two panels coupled by the spandrel above the opening;
ii) if yes, to study how the dimensions of the opening affect the response.

First of all, by looking at the results obtained for the Axial Load 1 (Figure 5.15-a), with reference to point i) it is observed that the introduction of the opening leads in general to a different response curve with respect to the one of the initial panel P0-B in terms of maximum strength, global stiffness and displacement

capacity. This happens for all the examined configurations, even for the ones with very small openings (P1 and P2). These last, in particular, present almost the same type of response: in the initial phase actually equal to that of panel P0-B and then in correspondence of a $d_{top} \approx 1.8$mm with a first drop of strength, giving place to a different stiffness degradation, to a lower maximum strength and to a higher displacement capacity with respect to panel P0-B. The drop of strength is caused by a different propagation of the tensile damage, as discussed in the following. Moreover, the obtained curve is comparable to the one associated to the other panels (from P3 to P5), supporting the idea that all the examined structures, in this case, behave as two coupled panels rather than as unique elements.

Moving to point ii), it is observed that the maximum strength and the global stiffness of the examined configurations progressively reduce when the dimensions of the opening increase (i.e. from P1 to P5). This is due to the fact that, by varying the width of the opening, the geometrical features of the two adjacent portions of masonry, which govern the structural response of the system, change, in terms of both resistant cross section (thus affecting the peak strength) and aspect ratio (thus affecting the global stiffness).

Moreover, also the post-peak response is affected by the introduction of the opening, which leads in all the cases to a higher displacement capacity with respect to P0-B. This can be explained again by interpreting the behavior of the panel as determined by two coupled elements. Indeed, when moving from a system represented by a single panel to a system made of two slenderer coupled elements, the structural response becomes in general more ductile. This is particularly evident in this case since the initial panel P0-B is characterized by a shear failure, and so by a rather fragile response.

Moving to the results associated to AL-2 (Figure 5.15-b), the abovementioned considerations are substantially confirmed, even if the following has to be highlighted:

- the curves associated to panels P1 and P2 are substantially coincident with the one of panel P0-B in terms of stiffness, strength and post-peak response;
- the post-peak response of all the panels with the opening is substantially similar to the one detected in the case of panel P0-B, characterized by a first drop of strength ($d_{top} \approx 4$mm) followed by a ductile branch.

These aspects may be explained in the light of the modelling rule introduced in the previous section (equation 5.1). Indeed, panel P0-B presents an aspect ratio equal to 0.73 and is characterized by the compression levels σ/f_c reported in Table 5.6, such that the panel should be split in case of AL-2, while it should be considered as a single element in case of AL-1.

Table 5.6 – Compression levels σ/f_c acting on panel P0-B, value of $(\sigma/f_c)_{CR}$ for this panel (fixed-fixed scheme) and application of the modelling rule introduced in eq. 5.1. The compression levels refer to the mid-section of the panel.

	σ/f_c [%]	$(\sigma/f_c)_{CR}$ [%]	Application of eq. 5.1
AL- 1	5.39%	3.94%	$5.39\% < 1.5*(\sigma/f_c)_{CR}$
AL- 2	8.59%		$8.59\% > 1.5*(\sigma/f_c)_{CR}$

Therefore, with reference to AL-2 it is evident that, since the panel already without the opening behaves like two coupled panels, the introduction of the opening, when it is sufficiently little with respect to the

overall dimensions of the panel (i.e. in case of P1 and P2), does not produce a significant variation in its response and may therefore be neglected. Obviously, when the dimensions of the opening increase, it is no more correct to neglect it, since the resistant cross section changes and both the global stiffness and the maximum strength significantly reduce.

On the other hand, regarding AL-1, the obtained results indicate that the presence of the little opening extends the necessity to split the panel, also in correspondence of a compression level for which the panel should not have been split according to the proposed modelling rule, which has been meant for panels that are from the beginning without openings.

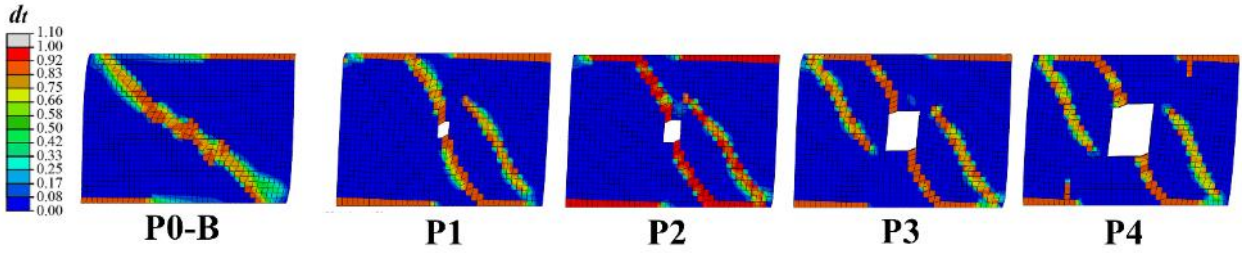

Figure 5.16 – Tensile damage occurred in the FE analyses of the configurations of type 1 and on P0-B (AL-1, fixed-fixed static scheme).

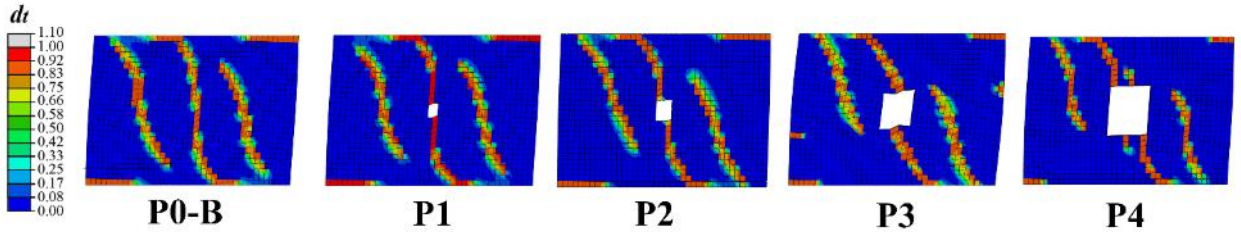

Figure 5.17 – Tensile damage occurred in the FE analyses of the configurations of type 1 and on P0-B (AL-2, fixed-fixed static scheme).

The results in terms of damage pattern substantially confirm the observations afore discussed.

In particular, in Figure 5.16 (AL-1) and in Figure 5.17 (AL-2) the pictures representing the tensile cracks propagation detected in the FE analyses performed on the configurations from P1 to P4 are reported, compared to the damage pattern resulting from the corresponding panel without opening P0-B. It is stressed that these damage scenarios refer, for each configuration, to a step of the analysis subsequent to the first significant drop of strength, in order to catch the associated failure mode.

By looking at these results it may be observed what follows:

- in the configurations P3 and P4 the propagation of the tensile cracks clearly indicates that, for both AL-1 and AL-2, the behavior of the panel can be described through two coupled elements individuated by the opening. Indeed, the tensile cracks tend to follow (as already observed in the analyses on the irregular walls in Chapter 4) the rule of the compression strut: the diagonal crack on the left ends in correspondence of the bottom left corner of the opening, while the diagonal crack on the right starts from the top right corner of the opening. This indicates that the presence of the opening actually affects the obtained damage pattern;

- moving to the more interesting configurations P1 and P2, the observations that come out from the analysis of the damage pattern support what previously observed from the examination of the response curves. In particular, by comparing the damage detected in P1 with the one obtained for P0-B it emerges what follows:
  a) ***Axial Load 2 (AL-2):*** the presence of the opening does not affect the propagation of the cracks; indeed, the damage scenario resulting from configuration P1 is almost the same obtained in the case of P0-B. More specifically, a first tensile crack propagates starting from the centre of the panel, followed by the development of shear diagonal cracks in both the portions of masonry adjacent to the opening. This can be again explained by considering that, as afore discussed, in this case panel P0-B should be split into two elements; therefore, if a little opening is introduced, this does not modify the activated behavior, which is already describable as that of two coupled elements;
  b) ***Axial Load 2 (AL-2)***: the propagation of the tensile cracks differs from the damage pattern detected in panel P0-B; indeed, while in panel P0-B a unique diagonal shear crack develops through the whole panel, in P1 the damage scenario is more similar to the one emerging from the other configurations where the opening is bigger. More specifically, the first tensile cracks develop starting from the corners of the opening and their propagation causes the first drop of strength observed in the corresponding response curve ($d_{top} \approx 1.8$mm, see Figure 5.15-a); subsequently a shear diagonal crack appears in the portion of masonry on the right side of the opening. The final detected damage, therefore, suggests that, notwithstanding the small dimensions of the opening with respect to the whole panel, its presence leads the panel to behave like two coupled elements rather than a unique element.

Similar considerations apply also to the case of panel P2.

Such results highlight that, going in the direction to neglect the opening in the structural model when it is sufficiently little with respect to the panel, and then to apply the modelling rule introduced in equation 5.1, it is necessary to modify the range of compression levels for which the panel should be split; this can be done by adopting α=1.2 rather than 1.5.

Moving to the panels analyzed with the cantilever boundary conditions, in Figure 5.18 the base shear – top displacement curves and the associated damage pattern at failure obtained for configurations P1, P2 and P3 are illustrated and compared with the corresponding results obtained for panel P0-B analysed under the same hypotheses. It is observed that, in case of configuration P1, both the response curve and the damage pattern at failure are perfectly coincident to what comes out from the analysis of the panel without opening. This clearly indicates that here, in presence of an evident flexural failure, the little opening does not affect the response of the panel in which it is introduced.

Concerning configuration P2, the base shear – top displacement curve is almost similar to the one of P0-B, even if after the peak strength ($d_{top} \approx 10$ mm) the behaviour slightly changes, due to the propagation of tensile cracks starting from the opening corners that do not activate in the case of P1 and P0-B. However, the overall response is almost similar to the one observed in the case of the panel without opening.

Moving to configuration P3, where the opening is characterized by a more significant extension, the behavior substantially changes in terms of both global response (different stiffness degradation and not negligible reduction of the maximum strength) and detected damage pattern, which further differentiates from the one of P0-B due to the development of a shear crack in the portion of masonry subjected to an increase of compression. In this case, therefore, the presence of the opening should not be neglected, since the activated response indicates that the panel actually behaves as two distinct elements.

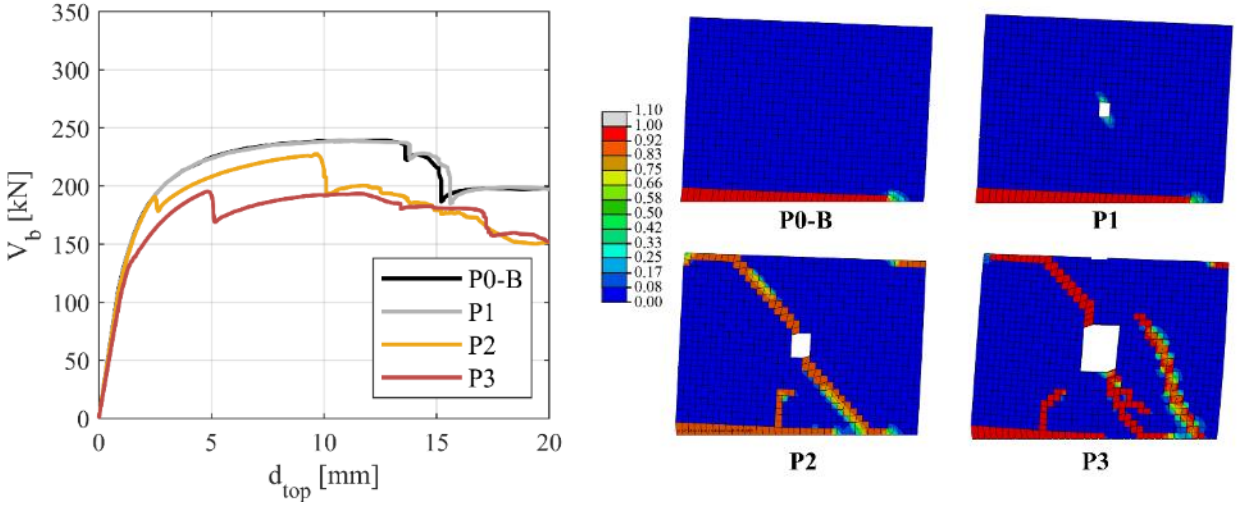

Figure 5.18 – (a) Base shear - top displacement V_b – d_{top} curves obtained through the analysis of configurations P1, P2 and P3 in case of AL-1 and cantilever static scheme; (b) associated tensile damage in correspondence of d_{top} = 10mm.

The results illustrated in Figure 5.18 confirm that, when the opening is "sufficiently small" with respect to the panel, by neglecting it in the structural model and then applying the modelling rule meant for the panel without opening, it is possible to obtain results consistent with the actual response.

Regarding the definition of the limit dimensions of the opening below which it is possible to use this strategy, the analyses here performed allow to give some indications, through the introduced geometrical parameters L_o/L_p and h_o/h_w, about what "sufficiently small" means. Indeed, the possibility to neglect the window has come out only in the case of configurations P1 and P2. Therefore, when the opening presents a height such that $h_o/h_w < 0.25$ and, at the same time, its width is such that $L_o/L_p < 0.14$ (like in the configurations P1 and P2 here examined), it can be considered as "sufficiently small" with respect to the whole panel it is introduced in.

It is worth noting that the results here obtained are consistent with what observed through the analysis of the irregular wall BD (discussed in Chapter 4, section 4.4.2). In this case, indeed, if we look at the dimensions of the little opening at the ground floor with respect to the dimensions of the panel ($h_o/h_w = 0.17$ and L_o/L_p=0.127), it comes out that, according to what above stated, it can be considered as "sufficiently little" and could be neglected in defining the structural model. Moreover, the panel that is obtained when neglecting the presence of the opening is exactly the one without opening located at the ground floor in wall E1 (see also Figure 4.5). As shown in the previous Figure 5.9, from the execution of the pushover analysis on wall E1 it came out that such panel is characterized by a cantilever boundary condition and by

a failure due to a rocking mechanism (which means that $\sigma/f_c << (\sigma/f_c)_{CR}$). Therefore, it should be modelled as a unique panel.

5.2.3 Results of panels with openings of varying height and position (type 2)

The graphs illustrated in Figure 5.19 summarize the results obtained from the analyses performed on the different configurations of type 2. More specifically, in the case of the fixed-fixed static scheme and for both AL-1 and AL-2, these graphs represent the maximum base shear V_y recorded during each analysis as a function of the position of the opening along the panel (see Figure 5.14). Moreover, V_y is normalized with respect to the maximum base shear obtained from the analysis on the corresponding panel without opening (named in the following $V_{y,\,P0\text{-}B}$), in order to quantify the reduction in strength due to the introduction of the opening.

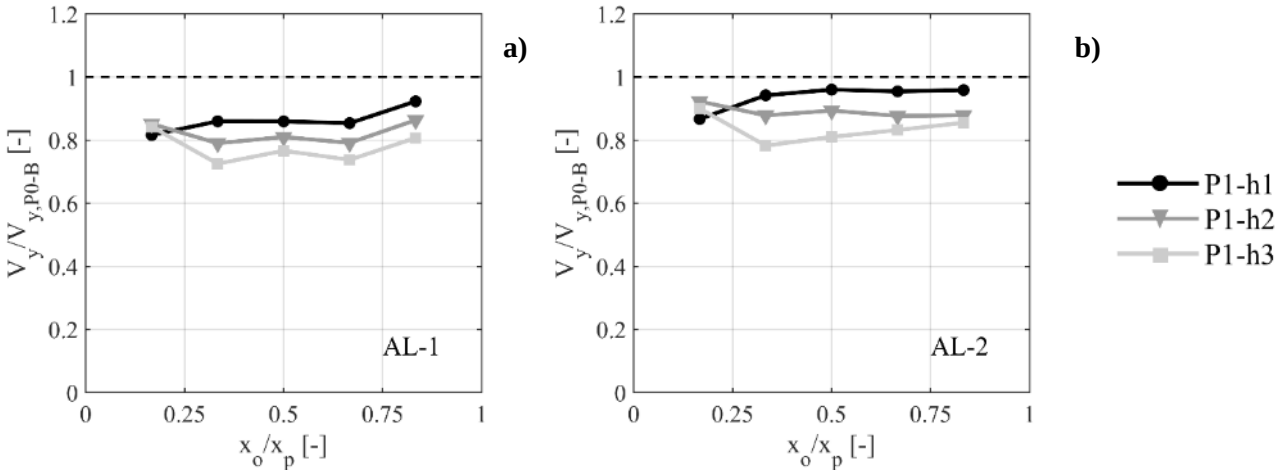

Figure 5.19 – Configuration of type 2 (fixed-fixed static scheme) -maximum base shear V_y obtained from each analysis normalized with respect to the maximum base shear of the corresponding panel without opening $V_{y,\,P0\text{-}B}$: a) AL-1 1; b) AL- 2.

From these graphs, it is possible to observe how the height of the opening (i), the position of the opening (ii) and the applied axial load (iii) affect the maximum strength $V_{y,}$ exhibited by the panels under examination.

i) Effect of the height of the opening

For both the applied axial loads and for a fixed position, when the height of the opening increases the maximum base shear detected by the numerical model decreases, even if the resisting cross section is always the same. In particular, by looking, as for example, at the results obtained for the AL-1(Figure 5.19-a), when considering the panels with the lower height of the opening (h1) the reduction of V_y with respect to P0-B is almost equal to 10%, while in case of the configurations with the highest height of the opening (h3) the penalization in strength with respect to P0-B becomes close to 25%.

In Figure 5.20-a the V_b-d_{top} curves associated to the configurations with the opening in the position x_o/x_p = 1/3 and characterized by the three different examined heights are illustrated; it may be seen that even if the peak strength slightly changes, however the type of response is substantially the same.

The trend observed in the detected values of V_y due to the variation of the height of the opening can be explained by considering that, when the height of the opening increases, the coupling between the two parts in which the opening splits the panel (i.e. that provided by the portion of masonry above the window) is lower, being this portion characterized by a lower stiffness. This effect is clearly visible in Figure 5.20-b, where the redistribution of the vertical loads between the base sections of these two masonry portions is shown for the different considered heights, again for the case of the opening in position x_o/x_p = 1/3.

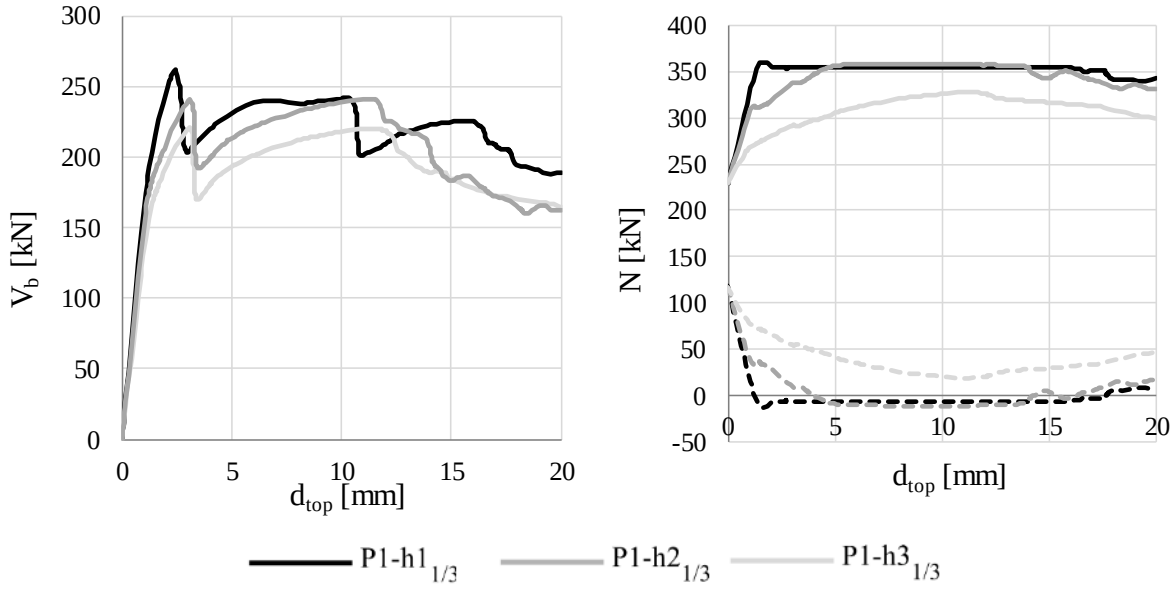

Figure 5.20 – Configurations P1-h1$_{1/3}$, P1-h2$_{1/3}$ and P1-h3$_{1/3}$ (AL-1, fixed-fixed scheme): a) base shear – top displacement V_b-d_{top} curves; b) redistribution of the axial load N between the two base sections corresponding to the two parts in which the opening splits the panel (solid line: right base section, dashed line: left base section).

ii) Effect of the position of the opening

The position of the opening does not significantly affect the obtained values of V_y, which are almost the same for a fixed loading condition and a fixed height. However, it may be noted that in the configurations where x_o/x_p = 1/6 the height of the opening less affects the final value of V_y. This may be explained by considering that in these cases the opening is located in the part of the panel subjected to the reduction of the axial load during the analysis and which, therefore, gives a negligible contribution to the final response.

iii) Effect of the applied axial load

The results in terms of maximum base shear obtained by varying the position of the opening as well as its height are almost the same for both the examined values of applied axial load. However, it may be noted that when the applied vertical load is higher (AL-2), the obtained values of $V_{y,}$ are closer, with respect to what happens in case of AL-1, to the maximum strength of the corresponding panel without opening, especially in the case of panels P1-h1 (where $V_y/V_{y,P0\text{-}B} \approx 1$).

This confirms what previously obtained in the case of the little opening centred in the panel (P1) and extends it also to the other positions that the opening may have: since P0-B, when applying AL-2, already

behaves like two coupled panels (according to the modelling rule proposed in equation 5.1), the introduction of the little opening does not produce a significant variation in its maximum strength. Conversely, it does in the case of panel P0-B in AL-1, since when the opening is not present this panel should be modelled as a unique element. These results in terms of V_y, therefore, indicate that, whatever is the position of the little opening, the panel tends to behave as two coupled elements in both the loading conditions and that, again, the effect of the opening is to extend the range of compression levels for which the panel should be split with respect to the one defined for the panels already without openings.

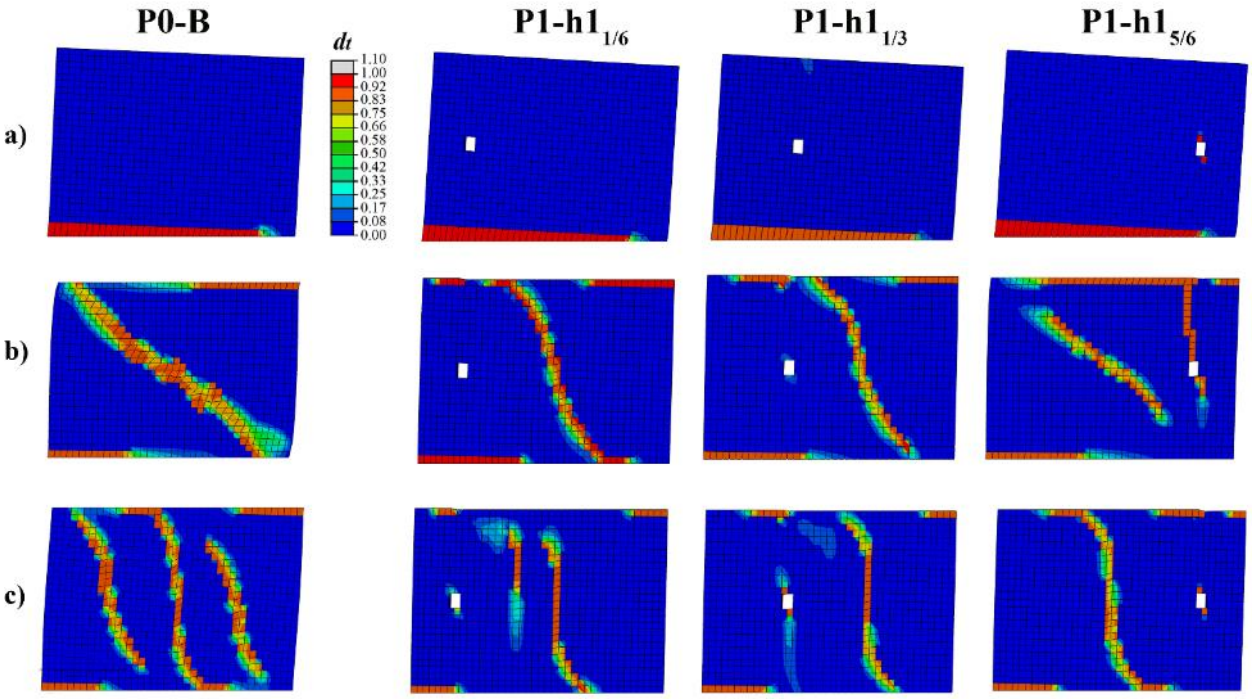

Figure 5.21 – Damage pattern detected from the FE analyses performed on the configurations P1-h1$_{1/6}$, P1-h1$_{1/3}$ and P1-h1$_{5/6}$ compared with the damage pattern of the corresponding panel without opening: a) cantilever, AL-1 (d_{top} = 8mm) b) fixed-fixed, AL-2 (d_{top} = 4mm), c) fixed-fixed, AL-2 (d_{top} = 4mm).

In Figure 5.21 the tensile damage patterns detected in the FE analyses performed on some of the configurations with the little opening (P1-h1$_{1/6}$, P1-h1$_{1/3}$ and P1-h1$_{5/6}$) in case of AL-1 (cantilever and fixed-fixed static scheme) and in case of AL- 2 (fixed-fixed static scheme) are illustrated, compared to the tensile damage deriving from the corresponding panel without opening, analysed under the same hypotheses.

By looking at these pictures it is possible to highlight the following aspects:

- in the case of the cantilever scheme (Figure 5.21-a) the detected damage pattern (flexural failure) is not affected by the position of the opening and is always equal to the one of the corresponding panel without opening;
- moving to the other two situations (Figure 5.21-b and Figure 5.21-c), where also shear cracks appear, it may be noted that the position of the opening affects their propagation; this last indicates, in all the cases, that the panel with the opening behaves as two coupled elements individuated by the position of the opening itself. Regarding this aspect, in particular, when the opening is located in the left part of the panel (x_o/x_p = 1/6 and x_o/x_p = 1/3) the shear crack appears in the right portion

of the panel, which is squatter and, moreover, subjected to an increase of the axial load during the analysis. The opposite happens when the opening is located in the right part of the panel (x_o/x_p = 5/6): the part on the right becomes slenderer and so with a higher vulnerability to flexural failure, which motivates the fact that no more shear cracks appear, while they do in the left portion, that is now rather squat.

Similar observations apply also to the case of the configuration P1-h1$_{2/3}$.

These results suggest that the modelling strategy outlined from the analyses on the configurations of type 1 may be applied whatever is the position of the little opening along the panel. In particular, by applying the defined rule to the case-studies here examined and by recalling that the aspect ratio of the whole panel is $\lambda \leq 1$, it is observed that:

i) cantilever, AL-1 (Figure 5.21-a): the panel should be modelled as a unique element;
ii) fixed-fixed, AL-2 (Figure 5.21-b): the panel should be split; furthermore, the examination of the damage shows that the division should be made in correspondence of the position of the opening;
iii) fixed-fixed, AL-1 (Figure 5.21-c): the panel has to be divided and again the damage pattern suggests that the identification of the two panels should be made in correspondence of the position of the opening.

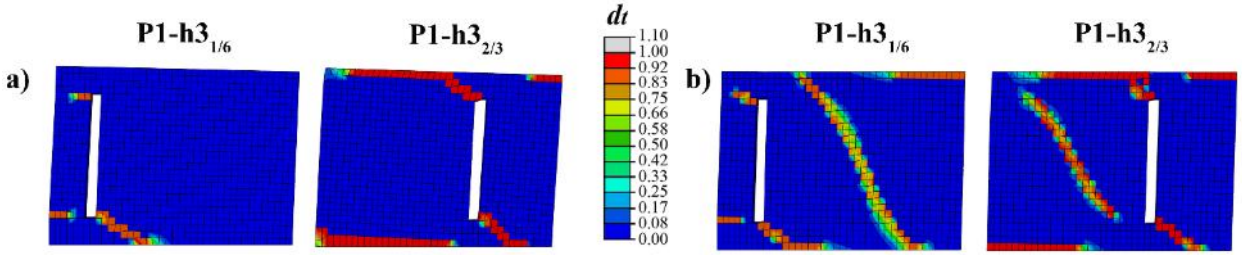

Figure 5.22 – Tensile damage detected in the FE analyses executed on the configurations P1-h3$_{1/6}$ and P1-h3$_{2/3}$, AL-1: a) cantilever static scheme (d_{top} = 7mm); b) fixed-fixed static scheme (d_{top} = 4mm).

In Figure 5.22 the tensile damage patterns resulting for the configurations P1-h3$_{1/6}$ and P1-h3$_{2/3}$ (AL-1 for both the cantilever – Figure 5.22-a, and the fixed-fixed scheme – Figure 5.22-b), are illustrated. In all the cases (and even when considering the cantilever boundary condition) the detected damage clearly indicates that the overall behavior is given by two coupled panels individuated by the position of the opening; indeed, due to the increased height of the opening, this type of behavior is clearly identifiable and even more accentuated than in the configurations P1-h1. It is stressed that, differently from the configurations with the little opening previously presented (Figure 5.21-a), this type of behavior is evident also when considering the cantilever static scheme.

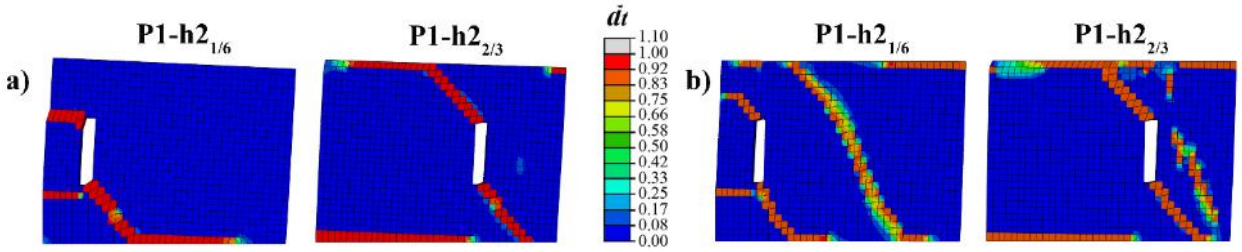

Figure 5.23 – Tensile damage detected in the FE analyses executed on the configurations P1-h2$_{1/6}$ and P1-h2$_{2/3}$, AL.1: a) cantilever static scheme (d_{top} = 7mm); b) fixed-fixed static scheme (d_{top} = 4mm).

Similar considerations apply also to the case of the configurations with the intermediate height of the opening (h_o = h2), as confirmed by the damage patterns illustrated in Figure 5.23, which refer to configurations P1-h2$_{1/6}$ and P1-h2$_{2/3}$, again considering AL-1 and both the fixed-fixed and the cantilever scheme.

The illustrated results, therefore, suggest that both in case of the configurations P1-h1 (h_o/h_w = 0.35) and in the case of the configurations P1-h3 (h_o/h_w = 0.70), independently from the boundary conditions and from the applied axial load ratio, the correct modelling strategy when applying an EF modelling approach would be to consider two distinct elements, individuated by the position of the opening.

With the aim to provide a practical indication about the height of the opening in correspondence to which this necessity arises, on the basis of the results here obtained the value of h_o/h_w previously introduced for the identification of the little openings, i.e. h_o/h_w = 0.25, can be confirmed; indeed, the configurations P1-h2 are associated to a ratio h_o/h_w slightly higher and equal to 0.35.

5.2.4 Summary of the main outcomes

The execution of the parametric FE analyses described in the previous section has allowed to:

i) study the problem of the presence of little openings in the masonry panels;
ii) study the effect of the opening height on the structural response of the panels.

The final outcomes are summarized in Table 5.7, where, for each examined configuration, boundary condition and applied axial load, the most adequate modelling strategy as emerged from the critical examination of the results provided by the FE analyses is reported.

In particular, with reference to point i), it came out that the necessity to include or not an opening in the structural model of a masonry panel substantially depends on the size of the opening, that has to be "sufficiently small" with respect to the panel containing it. On the basis of the achieved results, when the opening presents a height such that $h_o/h_w < 0.25$ and, at the same time, its width L_o is such that $L_o/L_p < 0.14$, it can be considered as "sufficiently small" with respect to the whole panel it is introduced in.

Once verified that the opening satisfies these conditions, it can be neglected in the corresponding structural model, thus obtaining a unique panel without openings, to which apply the modelling rule introduced in section 5.1 (see equation 5.1). At this point, the other parameter which comes into play is the compression level; regarding this, a modification on the coefficient α (in particular, α equal to 1.2 instead of 1.5) is proposed, aimed to take into account that the effect of the opening is to further extend the range of the compression levels in which the panel has to be split. Conversely, if the dimensions of the opening are such that it cannot be considered as "sufficiently small" ($h_o/h_w \geq 0.25$ and $L_o/L_p \geq 0.14$), the opening has to be included in the structural model, which implies the definition of two different piers connected by a spandrel; in these cases, indeed, the obtained results confirmed that the structural response of the system is clearly determined by the presence of two distinct coupled elements.

Furthermore, it emerged that the outlined modelling strategy is effective whatever is the position of the opening along the panel (i.e.: $\forall\ x_o/x_p$), underlining that, if the panel has to be split when removing the opening, the division should be made in correspondence of its position.

Table 5.7 – Summary of the results for conf. of type 1 and 2: modelling strategies to adopt in the different cases.

Configurations of type 1

	L_o/L_p [-]	h_o/h_w [-]	Cantilever (C)	Fixed-fixed (FF)	
			AL-1	AL-1	AL-2
P1	0.05	0.08	SP (ns)	SP (s)	SP (s)
P2	0.07	0.13	SP (ns)	SP (s)	SP (s)
P3-P4-P5	≥ 0.14	≥ 0.25	TP	TP	TP

Configurations of type 2

	h1 (h_o/h_w = 0.08)			h2, h3 ($h_o/h_w \geq 0.25$)
	C	FF		∀ Boundary condition
	AL-1	AL-1	AL-2	∀ Applied axial load
∀ x_o/x_p	SP (ns)	SP (s)	SP (s)	TP

LEGEND

SP (ns)	Single Panel not to be split according to eq. 5.1	SP (s)	Single Panel to be split according to eq. 5.1	TP	Two Panels

With reference to point ii), the illustrated results have shown that when the height of the opening inside the panel increases (by keeping constant its width) the necessity to split the panel becomes more evident and seems to be required independently from the boundary conditions characterizing the panel itself (i.e. the static scheme and the acting compression level). With the aim to provide a practical indication about the height of the opening in correspondence to which this necessity arises, the performed analyses confirm that a reasonable limit value for h_o/h_w may be 0.25.

It was also observed that in the examined configurations the height of the opening (h_o) affects the stiffness of the portion of masonry above the window, which provides the coupling between the two panels adjacent to the opening, with consequences on the maximum strength exhibited by the system, that progressively reduces when h_o increases. This would highlight the necessity to take into account the contribution of the spandrels for the correct reproduction of the behavior detected from the FE analyses. However, regarding this aspect it is stressed that the case studies here analysed are "ideal structures", being represented by isolated panels; in the reality these panels are always included in the context of a more complex wall, where other elements that can affect the coupling provided by the spandrel to the two panels may come into play, such as the stiffness of the diaphragm as well as different possible structural details (tie rods or r.c. tie beams).

Finally, it is worth underlining that the numerical values introduced for the geometrical parameters h_o/h_w and L_o/L_p, aimed to identify the "limit" situations for neglecting or not the opening, should be interpreted as a first attempt to give some suggestions about how to face the modelling of walls containing little openings; indeed, they provide operative indications about what to do in situations for which the modelling choices are for the moment not properly addressed by literature or codes. However, with the aim to refine the calibration of these "limit" values, it should be necessary to perform analyses on further case study structures, by varying with continuity the opening dimensions.

5.3 ANALYSIS OF URM PIERS WITH FLANGES

The modelling of the connection between the orthogonal walls (and so of the flange effect) represents one of the main critical issues in the framework of the Equivalent Frame approach, as already introduced in Chapter 1 (section 1.3), where the analysis of the state of art about this topic has been presented.

Furthermore, in Chapter 2 it was shown that the adoption of different possible choices about the modelling of the orthogonal walls in the EF models (i.e. perfect coupling or total decoupling between them) may lead to significantly different results in terms of global response in a pushover analysis of a 3D building (section 2.1) and even to different outcomes of the design (section 2.2).

In the light of these considerations, in this section the aim is to explore the potentialities and the limits of the strategies commonly adopted in the EF models for modelling URM panels with flanges.

In particular, in determining the behavior of a pier panel with flanges in an EF model two main issues arise: the determination of the redistribution of the axial load between the in-plane loaded panel (the web) and the flanges, on which the maximum strength of the in-plane panel depends, and the correct definition of the associated failure domain.

Within this framework, the objective of the analyses discussed in this section is to give an answer to the following questions:

- starting with the aim to simulate a perfect coupling between the orthogonal walls, the strategies commonly adopted in the EF models for the evaluation of the redistribution of the vertical loads between the connected panels are able to effectively capture the actual redistribution of the stresses?
- the failure criteria adopted in the EF models, which refer only to the in-plane loaded panel, are effective or a different strength domain, specific for a flanged section, should be introduced?

In order to answer these questions and to highlight some eventual critical issues on the EF approach as commonly applied nowadays in engineering practice, the following strategy was defined:

1. definition of the case studies constituted by masonry panels with symmetrical I-shaped cross sections (section 5.3.1);
2. modelling of the structures in ABAQUS and execution of lateral load monotonic analyses for different values of the applied axial load;
3. for each analysis, the maximum base shear is evaluated, in order to be able to define the interaction domain between the applied axial load N and the corresponding maximum shear force V of the examined structures, comparing it with the one that would be adopted in the EF model (associated to the in-plane loaded panel);
4. the vertical load redistribution occurring during the analysis between the flanges and the web is evaluated and compared with the predictions that would derive from the adoption of an EF approach.

The obtained results are discussed in section 5.3.2.

5.3.1 Examined case studies

The examined case studies (illustrated in Figure 5.24) are represented by three I-shaped sections, hereinafter referred to as FS-1, FS-2, FS-3. The dimension of both the flanges is progressively increased

moving from FS-1 to FS-3, while the web panel always presents the same geometry. In this way the obtained sections are characterized by different relative ratios in terms of axial stiffness k_A and flexural stiffness k_F between the flanges and the web ($k_{A,F}/k_{A,W}$ and $k_{F,F}/k_{F,W}$, respectively); the values of $k_{A,F}/k_{A,W}$ and $k_{F,F}/k_{F,W}$ are reported in Table 5.8 for each introduced configuration.

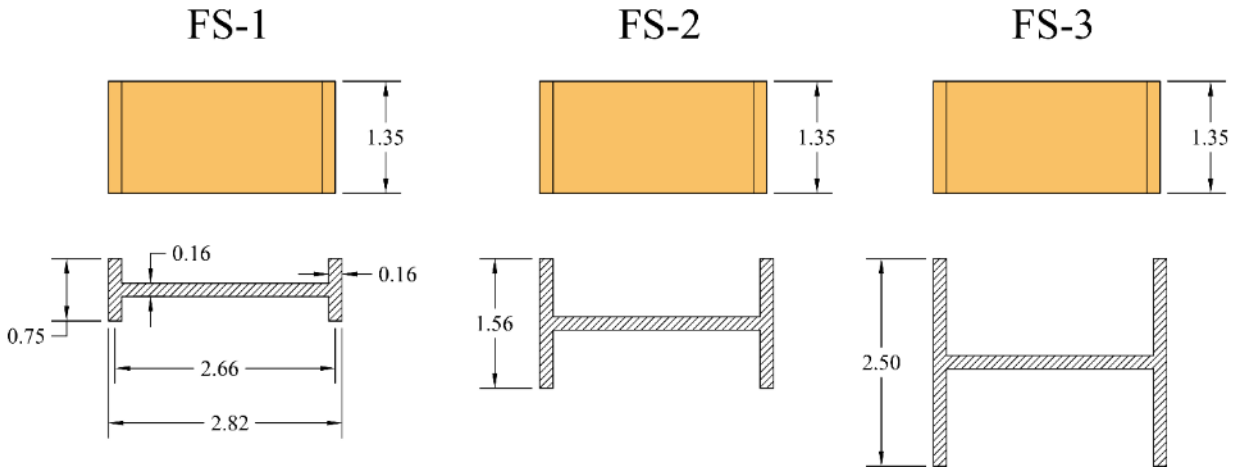

Figure 5.24 – Case study structures: I-shaped flanged sections with varying length of the flange (measures in m).

Table 5.8 - Relative ratios in terms of axial stiffness k_A and flexural stiffness k_F between the flange panel and the web ($k_{A,F}/k_{A,W}$ and $k_{F,F}/k_{F,W}$ respectively) associated to the introduced case studies

	FS-1	**FS-2**	**FS-3**
$k_{,A,F}/k_{A,W}$ **[-]**	0.30	0.62	1.00
$k_{,F,F}/k_{F,W}$ **[-]**	0.03	0.24	1.00

The introduced case studies were modelled in ABAQUS by using the CDP model and according to the same strategy adopted for the panels described in the previous sections.

Then, by considering both the cantilever and the fixed-fixed static scheme, lateral load monotonic analyses were performed in control displacement for different compression levels σ/f_c; it is important to underline that in all the cases the vertical load was applied on the web only, while the flanges bear just their own weight. Furthermore, in the case of the cantilever condition 6 increasing compression levels ($(\sigma/f_c)_i$, i=1,..,6) were explored, and in the case of the cantilever scheme 7 values were investigated (the additional one is aimed to better explore the region of the failure domain associated to flexural failure); the specific values adopted for both cases are reported in Table 5.9.

Table 5.9 – Compression levels σ/f_c applied on the examined case study structures

	$(\sigma/f_c)_1$ [%]	$(\sigma/f_c)_2$ [%]	$(\sigma/f_c)_3$ [%]	$(\sigma/f_c)_4$ [%]	$(\sigma/f_c)_5$ [%]	$(\sigma/f_c)_6$ [%]	$(\sigma/f_c)_7$ [%]
Cantilever	-	1.8	3.4	5.0	8.3	14.7	24.4
Fixed-Fixed	0.9	1.8	3.4	5.0	8.3	14.7	24.4

5.3.2 Discussion of the results

After the execution of the lateral load FE analyses, for a given configuration and for each value of the applied axial load, the following entities were determined:

- the maximum total base shear, computed by considering the reaction forces at the base of the whole section (including flanges), named $V_{y\,tot}$;
- the maximum base shear computed by considering only the reaction forces associated to the web panel, named $V_{y,W}$.

In Figure 5.25, the failure domain of the web panel (defined on the basis of the strength criteria indicated in equations 3.6 and 3.7) is compared with the values of $V_{y,tot}$ (black dots) and $V_{y,W}$ (white dots) obtained from the performed FE analyses. The capability of the constitutive model adopted in the FE analyses to correctly reproduce the failure domain of URM piers without flanges has been already demonstrated in Chapter 3 and, for this reason, it is omitted in the following.

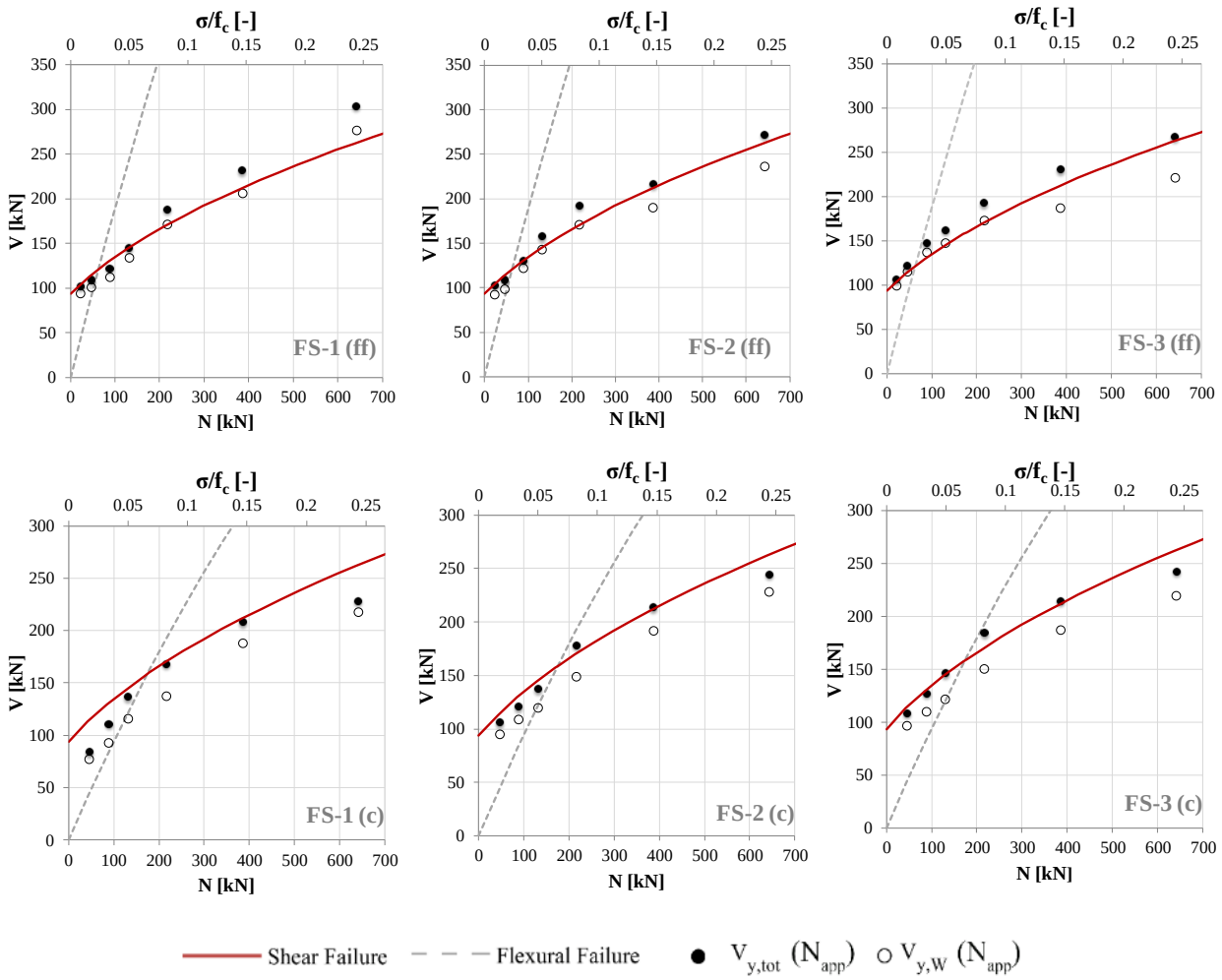

Figure 5.25 - Failure domain of the web panel compared with the results of the numerical FE analyses for each one of the introduced case study structures ("c" = cantilever scheme; "ff" = fixed-fixed scheme); the values of $V_{y,tot}$ and $V_{y,W}$ are represented in correspondence of N_{app}.

. It is stressed that in the graphs reported in Figure 5.25 the values of $V_{y,tot}$ and $V_{y,W}$ are represented in correspondence of a value of axial load (named in the following N_{app}) computed as the sum of the axial load applied at the top section and half the weight of the web. This is consistent with the assumption that the vertical load applied at the top section remains on the web panel and no redistribution occurs between the web and the flanges.

By looking at these graphs it may be highlighted that:

- the distance (in the vertical direction) between the black dot and the white dot associated to a fixed analysis gives a measure of the contribution to the global strength given by the out-of-plane panels (flanges). It is stressed that this contribution is usually not modelled in the EF models, which commonly consider only the strength of the in-plane loaded panel; in this way, therefore, it is possible to quantify the associated error. It comes out that, by taking into account also the contribution of the flanges (which is, in percentage, substantially similar for both the static schemes and the different applied axial loads), the maximum base shear increases, on average, of 15%. However, it should be noted that in presence of flanges with a more significant width (that is plausible as for example in presence of old masonry buildings) this contribution may be more significant;
- if we look at the values of $V_{y,W}$ (white dots), which are those that actually have to be compared with the failure domain represented in the graphs (that refers to the web panel), it is possible to see that in the initial part of the domain they are higher with respect to the predictions of the flexural failure criterion. This happens in particular for configuration FS-2 and FS-3 (where the flange is longer), while it is less significant when the flange is rather short (FS-1). Furthermore, this phenomenon occurs in both the considered static schemes, even if it is more visible in presence of the cantilever boundary condition, being in this case the part of the domain with prevailing flexural response more extended;
- when moving to the part of the domain associated to the prevalence of shear failure, in the case of the fixed-fixed static scheme the values of $V_{y,W}$ are almost in agreement with the predictions of the shear failure criterion, while they are always lower when considering the cantilever boundary condition.

In Figure 5.26, for the case of the cantilever static scheme, a different type of representation is proposed. In particular, this time the values of $V_{y,W}$ (white dots) are represented in correspondence of the actual axial load acting after the application of the vertical loads in the mid-section of the web panel (named in the following $N_{W,eff}$), which was computed from the FE model through the integration of the vertical stresses on the mid cross section of the web. Conversely, the values of $V_{y,tot}$ (black dots) are still represented as in the previous graph and, therefore, in correspondence of N_{app}; this explains the shifting between the black and the white dots referring to the same analysis.

In this way, by looking at the white dots, it is possible to see the actual axial load and the actual maximum base shear referring to the web panel, which is of main concern in the view of an EF approach. Indeed, being the pier panels modelled as in-plane elements, when describing the behavior of a flanged section it is important to correctly estimate the shear and the normal force actually acting on the in-plane loaded panel.

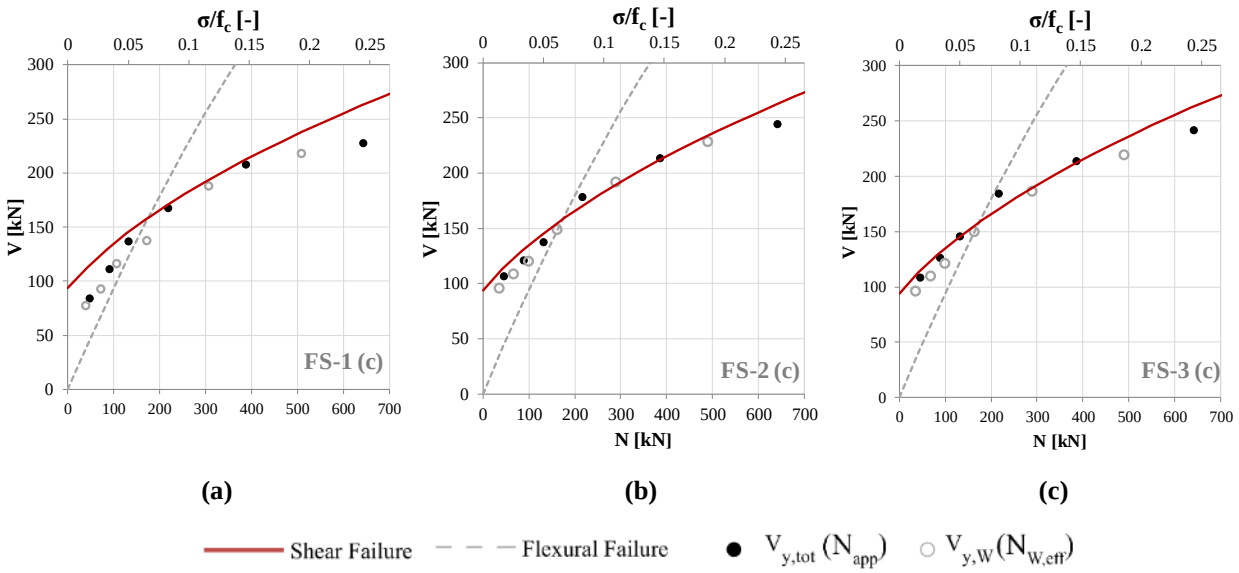

Figure 5.26 - Failure domain of the web panel compared with the results of the numerical FE analyses for each one of the introduced case study structures (cantilever scheme): a) FS-1; b) FS-2; c) FS-3; the values of $V_{y,tot}$ are represented in correspondence of N_{app}, while the values of $V_{y,W}$ are represented in correspondence of $N_{W,eff}$.

From the results reported in the graphs in Figure 5.26 it is possible to observe that:

- the distance (in the horizontal direction) between the white and the black dot for a fixed analysis gives a measure of the difference between the actual axial load acting in the mid-section of the web ($N_{W,eff}$) and the axial load that would act in this section if no redistribution between the web and the flanges occurred ($N_{W,app}$). It may be noted that this difference is not negligible, which indicates that the axial load applied at the top section of the web actually redistributes, moving in part to the two flanges. This effect is visible for all the configurations and so for all the considered length of the flange; however, in general it is slightly higher when considering FS-2 and FS-3 than in the case in which the flange is shorter (FS-1);
- by looking at the dots representing $V_{y,W}$, which are now referred to the correct value of axial load acting on the web panel, it may be seen that they correctly reproduce, in all the three examined configurations, the strength domain of the web panel, especially when considering the highest values of applied vertical load (i.e. where, according to the strength domain, shear failure is expected);
- the discrepancies in the initial part of the domain already observed in the previous graphs are still present and even emphasised; in particular, for low applied axial loads the values of $V_{y,W}$ are higher than what expected, especially in presence of the configurations where the flange is longer (FS-2 and FS-3). In both these cases, they actually follow the shear failure criterion instead of the one of flexural failure.

This last observation can be explained by considering that the presence of the flange inhibits the flexural failure of the web panel, avoiding the associated rocking mechanism; consequently, also when applying low axial loads the web is interested by the development of shear cracks rather than pure flexural failures with the only parzialization of the base section. This happens in particular when the length of the flange is

higher (FS-2, FS-3), since in these cases, thanks to its not negligible weight with respect to the web, the flange provides a more significant contribution to counterbalance the overturning of the web panel. Conversely, when the length of the flange is significantly lower with respect to that of the web (FS-1), the inhibition of the flexural failure does not happen, as it possible to see from Figure 5.26-a, where the values of $V_{y,W}$ (white dots) in the initial part of the domain are substantially closer to the flexural failure criterion, being the slight overestimation explained by considering that the constitutive model employed in the FE analyses includes the tensile strength of the material, while the strength criterion adopted for the flexural failure neglects this contribution.

These observations are confirmed by the pictures representing the damage pattern detected in FS-1, FS-2 and FS-3 (cantilever static scheme) in correspondence of two different values of applied axial load ($(\sigma/f_c)_2$ and $(\sigma/f_c)_4$), which are reported in Figure 5.27. In particular, by looking at the results obtained for FS-1 when applying $(\sigma/f_c)_2$, it is possible to see that a pure flexural failure occurs, with the parzialization of almost all the base section.

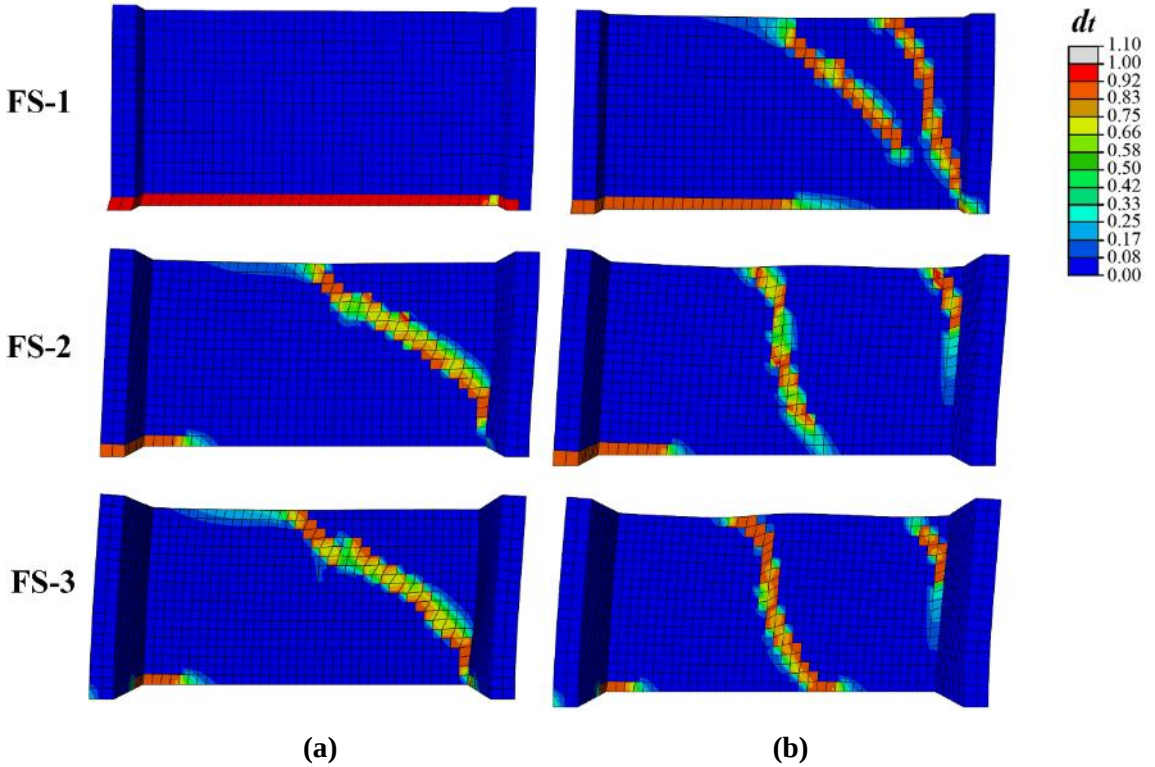

Figure 5.27 – Tensile damage contour plots obtained from the FE analyses performed on the introduced I-shaped panels (cantilever scheme): a) applied axial load $(\sigma/f_c)_2$; b) applied axial load $(\sigma/f_c)_4$.

This is consistent with the fact that, as already observed, the associated value of $V_{y,W}$ is substantially close to the predictions of the flexural strength criterion (Figure 5.26-a). Moving to FS-2 and FS-3, it is worth noting that, even for the lowest applied vertical load ($(\sigma/f_c)_2$), which corresponds to the very beginning of the failure domain, the web panels are already interested by the development of shear cracks, and a pure flexural failure does not occur, due to the presence of the tension flange that minimizes the rocking phenomenon and the parzialization of the base section of the web. When moving to a higher level of applied

axial load ($(\sigma/f_c)_4$), in FS-1 shear cracks start to develop, but the parzialization of the base section is still evident and still interests a quite significant part of the base section; conversely, in FS-2 and FS-3 an almost vertical crack develops starting from the centre of the panel.

The results now discussed highlight that, by assuming to be able to effectively capture the actual axial load acting in the web panel, the strength criteria already adopted in the EF models for the in-plane loaded panel are able to almost correctly predict its maximum strength; moreover, when the flange is sufficiently long with respect to the in-plane loaded panel, the flexural criterion has to be neglected and only the shear failure one can be used, also for the lower values of applied vertical load.

Therefore, it comes out the importance within the EF models to be able to effectively evaluate the actual vertical load acting on the web panel after the redistribution which occurs between it and the flanges, at least after the application of the dead loads and, possibly, also during the analysis.

Regarding this aspect, the representations introduced in the following are aimed to understand if the strategies commonly adopted in the EF models to compute this redistribution are able to provide results consistent with what emerges from the FE model.

In particular, for some of the performed analyses, the evolution of the vertical reaction forces acting at the base sections of the three panels composing the I-shaped cross section was evaluated. In order to compare the results obtained from the FE analyses with what would come out when adopting an EF modelling technique, an analytical approach was adopted, by assuming the hypothesis of perfect coupling between the web and the flanges.

First of all, the axial load acting after the application of the dead loads in the web ($N_{W,dl}$) and in the flanges ($N_{F,dl}$) is computed as a function of the axial stiffness of each panel; this is the strategy often adopted in the EF models when the hypothesis of perfect coupling between the panels is assumed.

Then, by considering that the axial load in the web remains constant and equal to the initial value $N_{W,dl}$, the redistribution of the vertical loads between the two flanges during the incremental analysis was evaluated through an analytical method under the following hypotheses:

- the boundary condition is represented by the cantilever static scheme;
- the applied shear load V_i to which the structure is subjected at the i-th step is derived from the FE analysis: this means to assume that, when using an EF model, it is possible to exactly evaluate this quantity for each incremental step of the analysis.

The adopted analytical method is explained in detail in Appendix C.

The evolution of the axial load N obtained in such way for the three base sections is compared with the one derived from the FE analyses performed on FS-1, FS-2 and FS-3 (cantilever condition) in Figure 5.28, considering as for example two different values of the axial load applied at the top section ($(\sigma/f_c)_3$ and $(\sigma/f_c)_5$).

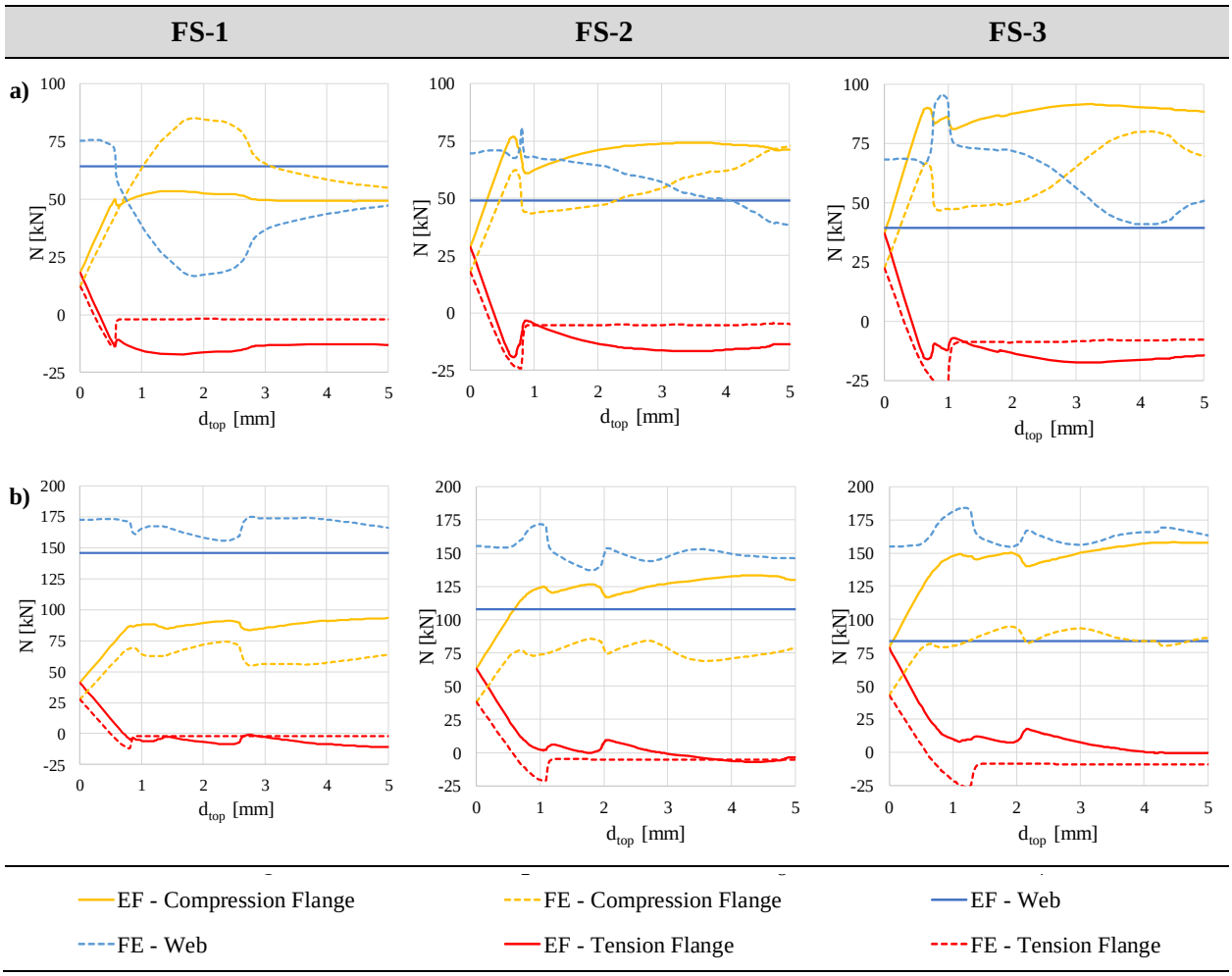

Figure 5.28 – Axial load redistribution between the web and the two flanges at the base section of the examined panels (cantilever scheme): a) compression level $(\sigma/f_c)_3$ and b) compression level$(\sigma/f_c)_5$,

By looking at the results obtained from the FE model (dashed lines), the following observations come out:

- when comparing the values of $N_{F,dl}$ and $N_{W,dl}$ (d_{top} =0) obtained for the examined structures it is possible to see that, moving from FS-1 to FS-2 the axial load acting in the web $N_{W,dl}$ slightly decreases (and consequently the one acting on the flanges slightly increases), while when moving from FS-2 to FS-3 these values are almost equal. This indicates that, beyond a certain limit, the axial load redistribution between the panels is no more affected by the length of the flange;
- when considering the results referring to the compression level $(\sigma/f_c)_3$ (Figure 5.28-a) the redistribution of N between the web and the flange in compression is for all the examined case studies higher than when applying a more significant axial load (Figure 5.28-b). As for example, by examining what happens to FS-1, it may be noted that, when considering the lower compression level ($(\sigma/f_c)_3$), the significant redistribution between the web and the flange (approximatively occurring for d_{top} between 0.7mm and 2.5 mm) is due to the parzialization of the base section of the web panel, which produces a consequent increment of the axial load in the compression flange. After that, due to a significant concentration of compression damage in the flange (crushing), the axial load comes back to the web (d_{top} > 2.5mm). On the contrary, when applying $(\sigma/f_c)_5$, since the

rocking mechanism is no more activated, the axial load acting at the base section of the web is almost constant during the analysis and the main redistribution occurs between the two flanges.

Moving to the comparison with the results representing the predictions of the EF approach, in Table 5.10 the percentage errors of these predictions with respect to those of the FE model on the axial load acting after the application of the dead loads on the web panel ($\Delta N_{W,dl}$) are collected, referring to all the three examined case-studies and to the two compression levels here examined ($(\sigma/f_c)_3$) and ($(\sigma/f_c)_5$).

Table 5.10 – Percentage errors of the predictions according to the EF approach with respect to the FE model on the axial load acting on the web after the application of the vertical loads ($\Delta N_{W,dl}$) in the three case studies (cantilever scheme)

		FS-1	FS-2	FS-3
$\Delta N_{W,dl}$ [%]	$(\sigma/f_c)_3$	-14.6	-29.4	-42.1
	$(\sigma/f_c)_5$	-15.4	-30.7	-45.9

From the analyses of the results reported in Figure 5.28 and in Table 5.10 it comes out that:

- with respect to the values of $N_{F,dl}$ and $N_{W,dl}$, the predictions of the analytical calculations are in reasonable agreement with the values detected from the FE model only in case of FS-1, where the flange is of limited dimensions ($\Delta N_{W,dl} \approx 15\%$ for both ($(\sigma/f_c)_3$ and ($(\sigma/f_c)_5$). When moving to FS-2 and, even more, to FS-3, the percentage error with respect to the predictions of the FE model becomes very high: indeed, the approach followed in the EF model produces a strong underestimation of the axial load acting on the web panel (and consequently an overestimation of the one acting on the flanges), with percentage errors on $N_{W,dl}$ higher than 40%;
- with respect to the redistribution of N during the analysis, it is stressed that, according to the approach followed in the EF model it is not possible to capture the redistribution occurring between the web and the flanges, since, inevitably, the axial load acting during the analysis in the web is constant. Therefore, it is not possible to well capture the evolution of N detected in the FE model when applying $(\sigma/f_c)_3$ (Figure 5.28-b); conversely, when a higher axial load is applied at the top section (($(\sigma/f_c)_3$, Figure 5.28-b), since, as previously observed, also in the FE analysis the vertical load redistribution between the web and the flanges is lower, a better agreement can be obtained. Nevertheless, since the predicted values of $N_{F,dl}$ and $N_{W,dl}$ are not correct in case of FS-2 and FS-3, a reasonable agreement is obtained only in the case of FS-1 (very short flange).

At this point, it is worth reminding that the redistributions of N according to the EF approach have been obtained under the assumption of being able to exactly evaluate the total shear applied to the structure for each incremental step of the analysis (indeed, the values of the shear load V_i to which the structure is subjected at the i-th step of the incremental analysis adopted in the calculations have been derived from the FE analysis). Of course, it is not obvious to always have such a perfect agreement, so that, when performing an analysis on such structures with an EF model, further discrepancies may arise.

5.3.3 Summary of the main outcomes

The results discussed in the previous section lead to the following considerations about the modelling of masonry piers with flanges in the EF models:

- *Vertical load redistribution between the connected panels*

The strategy now adopted in the EF models for modelling a perfectly rigid connection, which often implies to compute the initial redistribution of the axial loads only on the basis of the axial stiffness of the connected panels, is not always effective, even when simulating a perfect connection between orthogonal walls. In particular, it produces results which are still acceptable (percentage error with respect to the exact solution equal to almost 15%) when the dimension of the flange is limited with respect to the dimension of the web (in the configurations here examined it happens in case of FS-1, where $k_{A,F}/k_{A,W}$ =0.30). However, when the dimension of the flange increases with respect to the dimension of the web, this strategy leads to an overestimation of the axial load acting on the flanges and, consequently, to an underestimation of the one acting on the web: the percentage error of the EF approach with respect to the reference solution is almost of 30% in presence of a flange such that $k_{A,F}/k_{A,W}$ = 0.62 and higher than 40% in presence of a flange such that $k_{A,F}/k_{A,W}$ =1.00. This may imply an underestimation of the maximum strength of the in-plane loaded panel as well as a not correct description of its failure mode and post peak behavior (that in the EF Models is determined on the occurred type of failure, flexural or shear). Consequently, the repercussions on the obtained global response, when examining a 3D building, may be significant; regarding this aspect, the sensitivity analyses on the modelling of the flange effect performed on the simple two-storey masonry building discussed in Chapter 2 (section 2.1) may be useful to give an idea of how much this incorrect hypothesis can affect the final result.

- *Failure domain*

By assuming to be able to correctly capture the vertical load redistribution between the web and the flanges and so to correctly estimate the axial load acting on the web panel, the obtained results demonstrate that the failure domains employed for describing the maximum strength of the in-plane loaded panels are actually effective.

Nevertheless, it has come out that, when the dimension of the flange is significant with respect to that of the web, the flexural failure of the web panel is inhibited due to the presence of the tension flange, which tends to reduce the rocking phenomenon in the web panel, anticipating the development of shear cracks (in the cases here examined it already happens when $k_{A,F}/k_{A,W}$ = 0.62). In these cases, when applying low values of axial load, the maximum strength detected in the web panel does not follow the failure criterion referring to the flexural failure in the associated strength domain, but already follows the shear failure criterion. The performed analyses show that this happens for both the examined static schemes (cantilever and fixed – fixed), even if it is more evident in the case of the cantilever condition, being in the other case the region of the domain with the prevalence of flexural failure limited. This indicates that, in order to obtain the correct strength domain, it seems necessary to adopt only the criterion for shear failure (i.e. it is no more necessary to consider the minimum between two failure criteria), otherwise the maximum strength of the panel would be underestimated in presence of a low applied axial load.

On the basis of these results, it may be said that the definition of strength criteria for panels with flanges (which some works present in the literature are addressed to, as highlighted in the state of the art about this topic in Chapter 1 – section 1.3) seems to be not necessary.

Even if for the moment it is not possible to provide specific modelling rules, however the results here obtained allow to provide some indications which could be taken into account in the EF models and towards which the future development of this work will be addressed:

- when modelling a perfect coupling between orthogonal panels, if there are flanges with significant dimension with respect to the in-plane loaded piers to which they are connected, it is necessary to avoid an excessive redistribution of the vertical loads between the web and the flanges. Regarding this aspect, a possible strategy would be to adequately calibrate the stiffness of the connection between the panels (which in most of the EF models can be managed through the introduction of beams or links with a proper stiffness) in order to capture the actual redistribution detected in the FE analyses; this should be done in presence of flanges whose dimensions with respect to the web are higher than a limit value. Further parametric analyses may be useful in order to determine such limit dimension of the flange;
- in order to take into account that the flexural failure of the web may be inhibited, when performing the in-plane strength verification of a URM panel with flanges in a pushover monotonic analysis it would be useful to check if the tension flange is or not in compression. Indeed, if it is compressed it means that the rocking mechanism in the web cannot occur and, therefore, the panel can be verified by using only the shear failure criterion.

It is worth underlining that these considerations derive from parametric analyses performed on pier panels with symmetrical I-shaped cross sections, but the piers included in a real masonry building may have also C-, L-, and also T-shaped cross sections; therefore, also these situations should be investigated in order to further confirm or extend these considerations.

CHAPTER 6

6 CONCLUSIONS AND FURTHER DEVELOPMENTS

The objective of the present research was to investigate some of the critical issues related to the application of the Equivalent Frame (EF) modelling technique for the seismic analysis of masonry buildings, with the aim of improving the reliability of this method.

Indeed, despite of the large use of these models, there are many aspects that should be considered in order to verify their actual reliability and that have not yet been validated in a robust way. On one hand, seismic codes do not provide specific indications about all the possible modelling choices the EF idealization implies, and on the other a dedicated technical literature, available also to practitioners, does not exist. As a consequence, many uncertainties arise, leading to a quite arbitrary application of the method on behalf of the professionals and the analysists who commonly work with it.

In this work, in particular, the investigations were focused on the problem of the correct *a priori* identification of the geometry of the structural elements, since it represents the first step to face in the application of this approach.

As validation tool for the EF modelling technique, a numerical approach was adopted; it was based on the execution of nonlinear static analyses on more accurate Finite Element (FE) models, considered as the "exact" reference solution, and on subsequent comparisons of results. In such a way, a systematic validation of the different rules available in the literature for the EF schematization was carried out, applying them to walls with irregular opening patterns. Specific critical situations in which it was deemed necessary to provide indications about how to proceed for the identification of the structural elements were individuated, as representative of very common and recurrent cases in real masonry buildings. Thus, *ad-hoc* case-study structures were defined in order to explore these problems, which are:

- *Problem 1*: identification of the pier effective height in presence of horizontal irregularity;
- *Problem 2*: presence of little openings;
- *Problem 3*: identification of spandrels in presence of vertically misaligned openings or a different number of openings per storey.

A first important result obtained through the performed analyses is the general effectiveness of the Equivalent Frame approach in predicting the actual response of the examined wall configurations, even in presence of irregularly distributed openings. Indeed, the comparisons with the results provided by the FE models showed that in most of the cases the examined EF models are able to provide good estimates of the maximum base shear detected in the performed pushover analyses and to well capture the activated global failure mode. However, also problematic situations were detected in specific cases. In particular, the configurations with horizontal irregularity were found to be the most critical, being the ones where the considered rules for the EF idealization lead to significant differences in the geometry of the structural elements, and consequently to considerably different responses.

In all the examined cases, the comparison with the results of the FE models allowed to provide specific indications about the criteria for the EF schematization to be used (or avoided), depending on the type of irregularity characterizing the wall under examination.

In general, the obtained results showed that the definition of completely new rules for the identification of the structural elements is not essential, since some of the empirical proposals already available in the literature allow to obtain, when accompanied by the indications here provided, results close to the reference solution; moreover, some possibilities for their improvement were discussed.

The main contributions of the thesis with regard to these aspects are synthetized in Figure 6.1, where the solutions identified for each one of the aforementioned problems are collected.

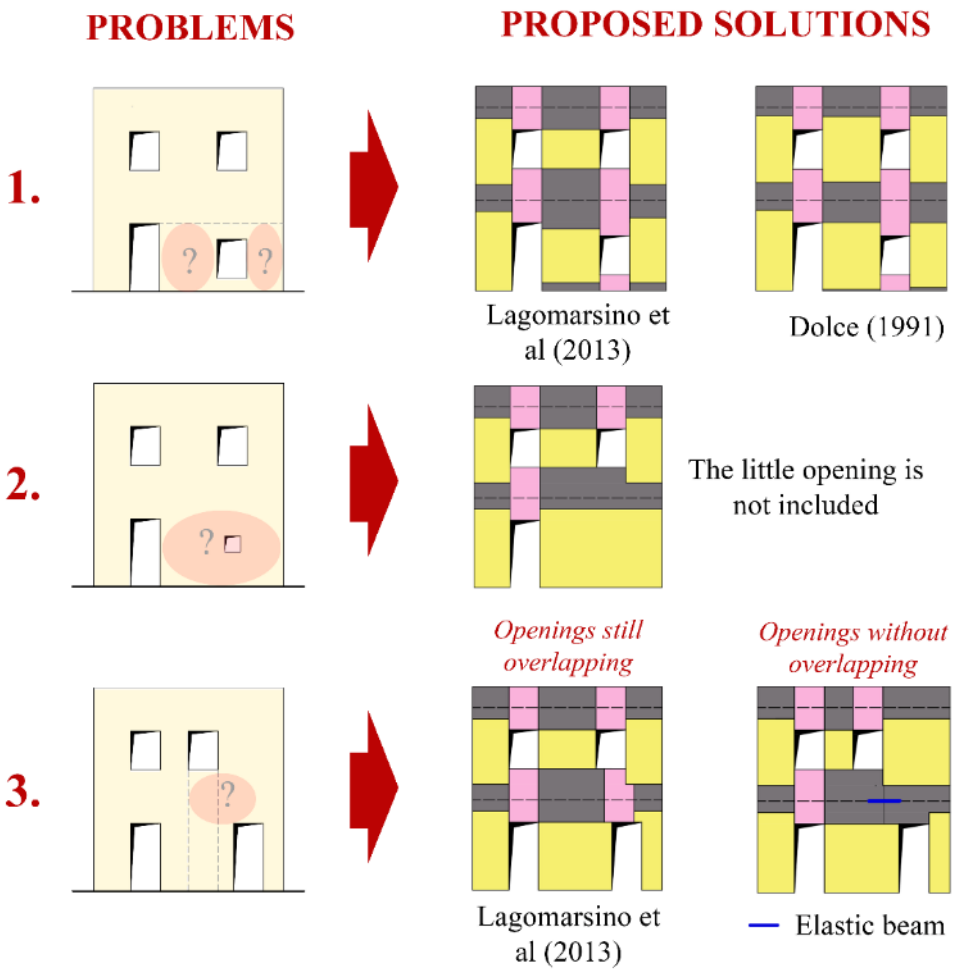

Figure 6.1 – Problems about the EF schematization faced in the thesis and related proposed solutions.

In particular, with reference to *Problem 1*, it was found that it is not necessary to define new rules for determining the pier effective height, but at the same time the obtained results indicated the necessity to avoid the use of the rules proposed by Augenti (2006) and Moon et al (2006). These last, indeed, lead to very squat piers and consequently big rigid nodes, thus strongly affecting the initial stiffness of the structure as well as the global ductility of the system, due to premature drops of strength caused by high

concentrations of deformation in small portions of the wall, which do not find a correspondence in the results of the FE model. Conversely, the rules indicated in Lagomarsino et al (2013) and in Dolce (1991), proposing a higher effective height for pier elements in these cases, allow to have a better description of the behaviour, not only at the global scale but also in terms of local response. This supports the fact that the two rules can be applied without specific corrective measures.

With reference to *Problem 2*, the necessity to define an alternative modelling strategy with respect to those analysed has come out. Indeed, no one of the EF schematizations defined by including the little opening in the model was able to well capture the actual response activated in the structure both at global and local scale. Conversely, the adoption of a structural model without the opening allowed to obtain a better description of the actual global response. In this case, this solution is therefore recommended.

With reference to *Problem 3*, the obtained results contributed on one hand to validate the empirical rule suggested in Lagomarsino et al (2013) for the identification of spandrels in case of walls with openings vertically misaligned but still overlapping, and on the other to improve it with regard to the situation in which the two openings are not aligned at all. In this last case, indeed, it was found that the inclusion in the model of a deformable element rather than a completely rigid portion (as would be predicted by this criterion) allows to obtain a better description of the local response and of the detected damage pattern. On the basis of this consideration, the proposed refinement is to introduce an elastic beam with an equivalent stiffness; this strategy was found to be effective also in presence of walls with a different number of openings per storey.

It is worth recalling that the case studies structures here analysed are provided with strong spandrels (promoted by the presence of r.c. tie beams at each level). Therefore, the results found with the introduced configurations, even if useful to give specific indications in these cases, cannot be conclusive about the problem of the identification of the spandrel geometry. Indeed, other structural typologies where the spandrels have a more important role in the response (multi-story walls or walls with weak spandrels) should be considered in order to gain more exhaustive results. This therefore will represent a future development of the research.

Some critical issues emerged from the analyses on the irregular walls gave the cue for additional deepenings faced in Chapter 5. To this aim, further analyses were performed, this time on single masonry piers. In this way, modelling rules to be applied in presence of pier panels without openings or including little openings were addressed, discussing also possible strategies, based on the execution of preliminary analyses, for the practical application of the proposed rules.

On the basis of the above discussed results, some recommendations to take into account in the definition of the EF schematization of masonry walls can be provided.

In particular, it has come out that the introduction of very squat piers in the models should be avoided. Indeed, it causes on one hand the inclusion of very big rigid nodes, which is rather unrealistic and alters the initial stiffness of the structure, and, on the other, potentially affects the global ductility of the system. In fact, since in the EF models the failure of masonry panels is governed by the reaching of fixed values of drift, it is evident that rather squat panels will fail for very low values of horizontal displacement. Therefore, in presence of walls with horizontal irregularity or little openings, that are the most critical with regard to

this issue, an important recommendation is to pay attention to the definition of the geometry of piers, which is often defined on the basis of automatic algorithms implemented in the adopted software code.

In the wall configurations here examined the above mentioned shortcoming was highlighted in particular in the application of the criteria suggested by Moon et al (2006) and by Augenti (2006). However, it may occur also in case of other rules for the determination of the pier effective height which take into account only the height of the adjacent openings, not relating these last to the global geometry of the wall level under consideration. As for example, a problematic situation in this sense may be the one depicted in Figure 6.2, where two adjacent openings with the same small height are present. In this case, indeed, also the criterion suggested in Lagomarsino et al (2013) (Figure 6.2-a), that is one of the criteria, among those here examined, associated to the best results when considering all the studied configurations, will lead to the definition of a particularly squat pier between the two little openings (highlighted in red in Figure 6.2).

Among the four examined rules for the pier effective height, only the one according to Dolce (1991) gives place to a rather slender element also in this situation. This is due to the fact that the formula proposed by Dolce (1991) for the pier effective height (see the equation in Figure 6.2) takes into account not only the height of the two openings adjacent to the pier (through the parameter h' – for its meaning see Figure 1.14), but also the width of the pier B as well as the height of the wall level under consideration (h_w = interstorey height) with respect to the height of the openings (through the quantity $(h_w\text{-}h')/h'$). In this situation, therefore, the approach on which Dolce's rule is based seems to be the most effective, allowing to avoid the presence of squat piers.

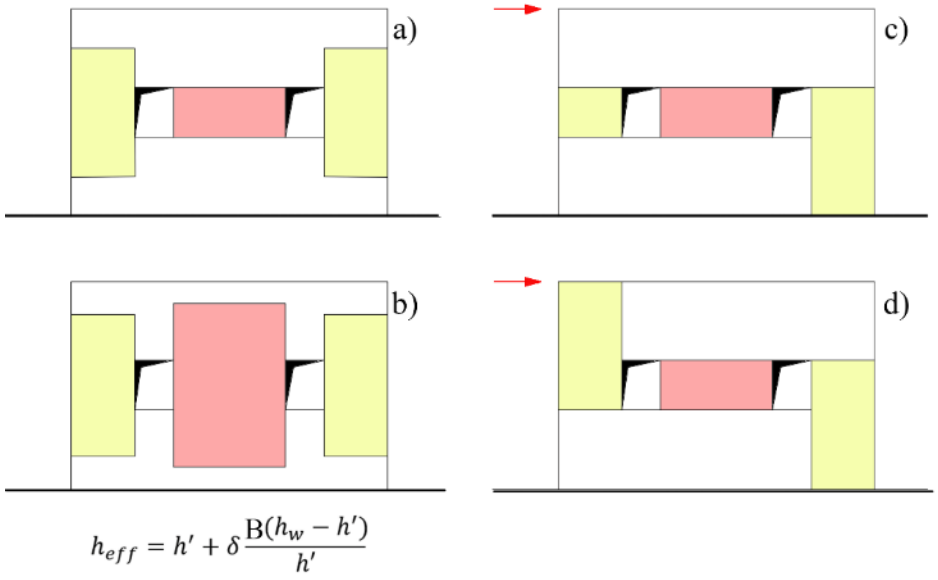

Figure 6.2– Effective height of piers according to different criteria: a) Lagomarsino et al (2013); b) Dolce (1991); c) Augenti (2006); d) Moon et al (2006).

These considerations highlight that, in addition to the examined case-study structures, which have been meant to be representative of recurrent situations of irregular opening patterns in real buildings but of course are not exhaustive of all the possible real cases, it would be necessary to consider further wall

configurations, as for example the one depicted in Figure 6.2. These cases, indeed, could underline the necessity to introduce specific corrective measures in order to avoid the formation of particularly squat piers even in the case of criteria for the pier effective height for which, from the analyses here performed, this necessity has not come out.

Furthermore, also the extension of these investigations to the analysis of whole buildings would be an important and necessary future development of the research. In particular, this will be of crucial importance for further validate the modelling rules and the solutions here proposed through both the analyses on the irregular walls (Figure 6.1) and the analyses on the single panels described in Chapter 5.

Indeed, having here analysed 2D walls where the response is governed by few structural elements, the scatter on the obtained results due to the use of different geometries for piers and spandrels can be emphasized with respect to real structures. When moving to more complex 3D buildings, the effects on the final response here observed are expected to be confirmed or mitigated, depending on the features of the walls which mainly govern the structural response, and in particular if they are walls with irregular opening patterns or not.

Another important observation emerging from the obtained results is that, within the framework of a simplified modelling approach as the EF method, the definition of modelling rules for the EF idealization that can be *a priori* and uncritically applied is in general not always simple. Indeed, many factors come into play, as the performed analyses have contributed to highlight: the dimensions of the opening with respect to the panel, the boundary conditions of the panel, the compression level acting on it as well as the presence of different possible structural details.

From these considerations, the necessity to perform preliminary analyses with the aim to better determine the structural behavior and to estimate such parameters that would be difficult to *a-priori* estimate (actual static scheme, variation of the axial load during the analysis) arises. Actually, the modelling rules suggested in Chapter 5 go in the direction to use this tool in order to orientate the choice of the most adequate modelling strategy to adopt.

Furthermore, for what concerns the analyses on the masonry panels with flanges reported in Chapter 5, even if the study here carried out on this aspect has to be intended as preliminary and for the moment no specific modelling rules are proposed, the obtained results allow to provide some indications which could be already taken into account in the EF models and towards which the future development of this work will be addressed; in particular, they are about:

- the necessity to improve the way to manage the redistribution of the axial load between the connected panels, which turned out to be a critical aspect when in presence of flanges with significant dimensions with respect to the web;
- the fact that, by assuming to be able to correctly describe the normal stress redistribution, the failure domains commonly used in the EF models, which refer to only the in-plane loaded panel, are effective; however, the presence of flanges with significant dimensions with respect to the web may inhibit the flexural failure of the web panel, anticipating shear failures.

It is stressed that these initial results, which refer to piers with I-shaped cross section, should be supported and integrated by further analyses performed, as for example, on pier panels with different types of cross sections (C-, L-, and also T-shaped), in order to further confirm or extend these considerations.

In addition to the modelling of the flange effect, another important aspect which comes into play when moving from the analysis of 2D walls to that of 3D buildings is represented by the modelling of floors. This aspect, which for the moment has not been treated in the thesis, is however of great interest within the framework of the Equivalent Frame approach, where floors are usually modelled by considering strongly simplified hypotheses (floors infinitely rigid in their plane or at least with a linear elastic behavior, including only their in-plane stiffness). Therefore, one of the future developments of this work will be also the deepening of some of the simplified assumptions commonly made in these models for describing the behavior of the diaphragms, as for example regarding the contribution of their out-of-plane stiffness and the inclusion of their nonlinear behavior. This represents a fundamental step in the view of a robust and comprehensive validation of the EF approach, since the seismic design and assessment of masonry buildings require to perform the analyses on 3D models.

Concluding, it is worth highlighting the potential repercussions in practice of the results obtained within this thesis. Indeed, the Equivalent Frame models represent today one of the most used computational tools for the execution of the seismic analyses on masonry buildings, especially at engineering practice level. The absence of codified rules or specific indications about the modelling choices that this approach implies leads to an arbitrary application of the method, with not negligible repercussions on the outcomes of the seismic verifications. Both the preliminary analyses discussed in Chapter 2 and the results obtained through the analyses performed in this thesis, in fact, have demonstrated that the assumption of different (all plausible) modelling hypotheses with regard to the themes here investigated (EF schematization and flange effect) gives place to global responses which may significantly differ, and in the case of masonry buildings the seismic verifications are performed on the global pushover curve.

In the light of these considerations, to provide clear suggestions about modelling choices on which for the moment no specific indications are given may represent an important contribution for reducing the scatter in the achieved results, thus leading to a general improvement within the framework of the seismic safety verifications.

REFERENCES

ABAQUS®, theory manual, version 6.14.

AEDES.PCM (2018) Progettazione di Costruzioni in Muratura, Release 2017.1.4.0, Manuale d'uso (in Italian), www.aedes.it.

Anthoine A, Magonette G, Magenes G (1995) Shear-compression testing and analysis of brick masonry walls. *Proceedings of the 10th European Conference on Earthquake Engineering*, Rotterdam, Netherlands.

ASCE/SEI 41–13 (2014) Seismic evaluation and retrofit of existing buildings. American Society of Civil Engineers, Reston. ISBN 978-0-7844-7791-5.

Augenti N (2006) Seismic behavior of irregular masonry walls. *Proceedings of the 1st European Conference on Earthquake Engineering and Seismology*, Geneva, Switzerland.

Augenti N, Romano A (2008) Assessment of irregular masonry walls, *Proceedings of 6th International Conference on structural analysis of historic construction*, 2-4 July, Bath, UK.

Augenti N, Parisi F (2010) Learning from Construction Failures due to the 2009 L'Aquila, Italy, Earthquake, *Journal of Performance of Constructed Facilities*, 24(6), pp: 536–555.

Belmouden Y, Lestuzzi P (2009) An equivalent frame model for seismic analysis of masonry and reinforced concrete buildings. *Construction and Building Materials*, 23, pp: 40–53.

Berti M, Salvatori L, Orlando M, Spinelli P (2017) Unreinforced masonry walls with irregular opening layouts: reliability of equivalent-frame modelling for seismic vulnerability assessment. *Bulletin of Earthquake Engineering*, 15(3), pp:1213-1239.

Betti M, Galano L, Petracchi M, Vignoli A (2015) Diagonal cracking shear strength of unreinforced masonry panels: a correction proposal of the b shape factor, Bulletin of Earthquake Engineering, 13 (10), pp: 3151 – 3186.

Beyer K (2012) Peak and residual strengths of brick masonry spandrels, *Engineering Structures*, 41, pp: 533-547.

Beyer K., Dazio A (2012) Quasi-static cyclic tests on masonry spandrels, *Earthquake Spectra*, 28(3), pp: 907-929.

Beyer K, Mangalathu S (2014) Numerical study on the peak strength of masonry spandrels with arches, *Journal of Earthquake Engineering*, 18(2), pp: 169-186.

Binda L, Cardani G (2007) Proposta di una metodologia per la valutazione della qualità muraria. In: Reluis, progetto esecutivo 2005–2008, Linee guida per la compilazione della scheda di valutazione della qualita' muraria, Decembre (in Italian).

Borri A (2006) Proposta di una metodologia per la valutazione della qualità muraria. In: Reluis, prog. esecutivo 2006–2008, Prog. di ric. n.1, Valutazione e riduzione della vulnerabilità sismica di edifici in muratura. Rend. Scient. 1◦anno, Nov. (in Italian).

Bosiljkov V, Maierhofer C, Koepp C, Wöstman J (2010) Assessment of structure through non-destructive tests (NDT) and minor destructive tests (MDT) investigation: case study of the Church at Carthusian Monastery at Žiˇce (SLOVENIA), *International Journal of Architectural Heritage*, 4(1), pp:1–15.

Bothara JK, Dhakal RP, Mander JB (2010) Seismic performance of an unreinforced masonry building: an experimental investigation, *Earthquake Engineering and Structural Dynamics*, 39(1), pp:45–68.

Bracchi S, Rota M, Penna A, Magenes G (2015) Consideration of modelling uncertainties in the seismic assessment of masonry buildings by equivalent-frame approach, *Bullettin of Earthquake Engineering*, 13(11), pp: 3423-3448.

Bracchi, S, Galasco A, Penna A, Magenes G (2018) An improved macroelement model for the nonlinear analysis of masonry buildings. *Proceedings of the 10th Australasian Masonry Conference*, 11–14 February, Sydney, Australia.

Braga F, Liberatore D, Spera G. (1998) A computer program for the seismic analysis of complex masonry buildings. In: Pande GN, Middleton J, Kralj B (Eds.), *Computer methods in structural masonry*, vol. 4. London: E & FN Spon; pp: 309–16.

Brandonisio G, Lucibello G, Mele E, De Luca A (2013) Damage and performance evaluation of masonry churches in the 2009 L'Aquila earthquake, *Engineering Failure Analysis*, 34, pp: 693–714.

Brencich A, Lagomarsino S (1997) A macroelement dynamic model for masonry shear walls. In: *Proceedings of the STRUMAS IV—4th Int. Symp. On Computer Methods in Structural Masonry*, Pratolino (Fi), 3-5 Sept., E&FN Spon, London, pp: 67–75.

Brencich A, Gambarotta L, Lagomarsino S (1998) A macroelement approach to the three-dimensional seismic analysis of masonry buildings. *Proc. XI European Conference on Earthquake Engineering*, Paris, A.A. Balkema (Abstract Volume & CD-ROM)

Brignola A, Pampanin S, Podestà S (2012) Experimental evaluation of the in-plane stiffness of timber diaphragms, *Earthquake Spectra*, 28(4), pp. 1687-1709.

Calderini C, Lagomarsino S (2008) Continuum model for in-plane anisotropic inelastic behavior of masonry, *Journal of Structural Engineering*, 134 (2), pp. 209–220.

Calderini C, Cattari S, Lagomarsino S (2009a) In-plane strength of unreinforced masonry piers, *Earthquake Engineering and Structural Dynamics*, 38, pp: 243.267

Calderini C, Cattari S, Lagomarsino S (2009b) In-plane seismic response of unreinforced masonry walls: comparison between detailed and equivalent frame models. *Proceedings of the 2nd COMPDYN Conference*, 22-24 June, Rodhes, Greece.

Calderini C, Cattari S, Lagomarsino S, Rossi M (2010) Review of existing models for global response and local mechanisms. Technical Report, PERPETUATE (EU-FP7 Research Project), Deliverable D7 (www.perpetuate.eu/D7/)

Calderini C, Cattari S, Degli Abbati S, Lagomarsino S, Ottonelli D, Rossi M (2012) Modelling strategies for seismic global response and local mechanims. Technical Report, PERPETUATE (EU-FP7 Research Project), Deliverable D26 (www.perpetuate.eu/D26/).

Calderoni B, Marone P, Pagano M (1987) Modelli per la verifica statica degli edifici in muratura in zona sismica. *Ingegneria sismica*, 3, pp: 19-27 (in Italian).

Calderoni B, Lenza P, Pagano M (1989) Attuali prospettive per l'analisi sismica non lineare di edifici in muratura. *Proceedings of IV Convegno ANIDIS*, Milan, Italy (in Italian).

Calderoni B, Cordasco EA, Lenza P (2007) Analisi teorico sperimentale della fascia di piano delle pareti murarie per azioni sismiche. *Proceedings of XII Convegno ANIDIS*, Pisa, Italy (in Italian).

Calderoni B, Cordasco EA, Sandoli A, Onotri V, Tortoriello G (2015), Problematiche di modellazione strutturale di edifici in muratura esistenti soggetti ad azioni sismiche in relazione all'utilizzo di software commerciali. *Proceedings of XVI Convegno ANIDIS*, 13-17 September, L'Aquila, Italy (in Italian).

Calderoni B, Cordasco EA, Musella C, Sandoli A (2017) La modellazione delle pareti murarie in relazione alle irregolarità geometriche: problemi aperti. Proceedings of *XVII Convegno ANIDIS*, 17-21 September, Pistoia, Italy (in Italian).

Caliò I, Cannizzaro F, Marletta M, Pantò B (2009) 3DMacro, Il software per le murature (3D computer program for the seismic assessment of masonry buildings), Gruppo Sismica s.r.l., Catania, Italy, Release 3.0, March 2014 (www.3dmacro.it).

Caliò I, Marletta M, Pantò B (2012) A new discrete element model for the evaluation of the seismic behavior of unreinforced masonry buildings, *Engineering Structures*, 40**,** pp: 327–338.

Calvi GM, Magenes G (1994) Experimental research on response of URM building system. *Proceedings of U.S.-Italy workshop on guidelines for seismic evaluation and rehabilitation of unreinforced masonry buildings*, D. P. Abrams, G. M. Calvi (Eds), State University of New York at Buffalo, NCEER-94-0021, 3-41/57, Pavia.

Cappi A, Castellani A, Gradori G, Locatelli P. (1975) Strengthening and repairing of masonry walls damaged by shear actions in their own planes. Publication N. 701, Politecnico di Milano, Istituto di Scienza e Tecnica delle Costruzioni.

Casagrande D, Giongo I, Pederzolli F, Franciosi A, Piazza M (2018) Analytical, numerical and experimental assessment of vibration performance in timber floors, *Engineering Structures*, 168, pp – 748-758.

Casolo S, Diana V, Uva G (2016) Influence of soil deformability on the seismic response of a masonry tower, *Bulletin of Earthquake Engineering*, 15(5), pp: 1991–2014.

Casolo S, Peña F (2007) Rigid element model for in-plane dynamics of masonry walls considering hysteretic behaviour and damage, *Earthquake Engineering and Structural Dynamics*, 36(8), pp: 1029-1048.

Castellazzi G, D'Altri AM, de Miranda S, Chiozzi A, Tralli A (2018) Numerical Insights on the Seismic Behavior of a Non-Isolated Historical Masonry Tower, *Bulletin of Earthquake Engineering*, 16 (2), pp: 933–961.

Cattari S, Curti E, Galasco A, Resemini S (2005) Analisi sismica lineare e non lineare di edifici in muratura. Esempi di applicazione secondo OPCM 3274/2003 E 3431(2005). Sistemi Editoriali, Napoli, ISBN 88-513-0305-3 (In Italian).

Cattari S (2007) Modellazione a telaio equivalente di strutture esistenti in muratura e miste muratura-c.a.: formulazione di modelli sintetici. PhD Thesis, University of Genoa (In Italian).

Cattari S, Lagomarsino S (2008) A strength criterion for the flexural behavior of spandrel in un-reinforced masonry walls. *Proceedings of the 15th World Conference on Earthquake Engineering*, Beijing, China.

Cattari S, Resemini S, Lagomarsino S (2008) Modelling of vaults as equivalent diaphragms in 3D seismic analysis of masonry buildings. *Proceedings of 6th International Conference on Structural Analysis of Historical Construction*, Bath, UK.

Cattari S, Lagomarsino S (2009) Modelling the seismic response of unreinforced existing masonry buildings: a critical review of some models proposed by codes. *Proceedings of 11th masonry symposium*, 31 May – 3 June, Toronto, Ontario.

Cattari S, Degli Abbati S, Ferretti D, Lagomarsino S, Ottonelli D, Rossi M (2012) The seismic behavior of ancient masonry buildings after the earthquake in Emilia (Italy) on May 20th and 29th. *Ingegneria Sismica*, pp. 87–111.

Cattari S, Lagomarsino S (2013a) Masonry structures, pp.151-200, in: *Developments in the field of displacement based seismic assessment*, Edited by T. Sullivan and Calvi GM, Ed. IUSS Press (PV) and EUCENTRE, pp.524, ISBN:978-88-6198-090-7.

Cattari S, Lagomarsino S (2013b) Analisi nonlineari per la simulazione del danno di un fabbricato in San Felice sul Panaro (Emilia, 2012). *Proceedings of XV Convegno ANIDIS*, 30 June – 4July, Padua, Italy (in Italian).

Cattari S, Lagomarsino S, Milani G, Rossi M., Simoni M, Tralli A (2014a) Non Linear Modelling of Fornasini Tower After the 2012 Emilia Earthquake (Italy). In: *Proceedings of the 9th International Conference on Structural Analysis of Historical Constructions*, F. Pena & M. Chavez (Eds.), Mexico City, Mexico.

Cattari S, Chioccariello A, Degée H, Doneaux C, Lagomarsino S, Mordant C (2014b) Seismic assessment of masonry buildings from shaking table tests and nonlinear dynamic simulations by the Proper Orthogonal Decomposition (POD). *Proceedings of the 2nd European Conference on Earthquake Engineering and Seismology (ECEES)*, 25-29 August, Istanbul, Turkey.

Cattari S, Karatzetzou A, Degli Abbati S, Pitilakis D, Negulescu C, Gkoktsi K (2015), Seismic performance based assessment of the Arsenal de Milly of the Medieval City of Rhodes. In: Psycharis IN, Pantazopoulou SJ, Papadrakakis M (Eds.), *Seismic Assessment, Behavior and Retrofit of Heritage Buildings and Monuments*, Springer International Publishing, pp. 365–392.

Cattari S, Beyer K (2015) Influence of spandrel modelling on the seismic assessment of existing masonry buildings. *Proceedings of the 10th Pacific Conference on Earthquake. Engineering Building an Earthquake-Resilient Pacific*, 6-8 November, Sydney, Australia

Cattari S, Camilletti D, Magenes G, Manzini CF, Morandi P, Spacone E, Camata G, Marano M, Caliò I,Pantò B, Cannizzaro F, Occhipinti G, Calderoni B, De Luca A, Cordasco EA, Brandonisio G, Sandoli A, Casapulla C, Portioli F, De Felice G, Malena M, Lasciarrea G (2016) Definizione di strutture benchmark di riferimento (semplici) e della metodologia di validazione/confronto dei risultati tra diversi modelli/software, Prodotto 2.1.g nell'ambito del della Linea Strutture in Muratura del progetto DPC-ReLUIS (accordo quadro 2014-2018), Scientific Report (in Italian).

Cattari S, Camilletti D, Magenes G, Manzini CF, Morandi P, Spacone E, Camata G, Corrado M, Caliò I, Pantò B, Cannizzaro F, Occhipinti G, Calderoni B, De Luca A, Cordasco EA, Brandonisio G, Sandoli A, Casapulla C, Portioli F, De Felice G, Malena M, Lasciarrea G (2017) Analisi di strutture benchmark per la valutazione dell'affidabilità di codici di calcolo sismico degli edifici in muratura. *Proceedings of XVII Convegno ANIDIS*, 17-21 September, Pistoia, Italy (in Italian).

Cattari S, Camilletti D, Magenes G, Manzini CF, Morandi P, Spacone E, Camata G, Marano C, Caliò I, Cannizzaro F, Pantò B, Occhipinti G, Calderoni B, Cordasco EA, Sandoli A (2018a) On the reliability of URM modelling approaches targeted to nonlinear seismic analysis: a comparative study on a two-storey benchmark case study. *Proceedings of 16° European Conference on Earthquake Engineering*, 18-21 June, Thessaloniki,18, Greece.

Cattari S, Camilletti D, Lagomarsino S, Bracchi S, Rota M, Penna A (2018b) Masonry Italian code-conforming buildings. Part 2: nonlinear modelling and time-history analysis, *Journal of Earthquake Engineering*, 22, pp: 2010-2040.

CDSWin in OpenSees© (2018).

CEN (2004a) Eurocode 8: Design of structures for earthquake resistance - Part 1: General rules, seismic actions and rules for buildings. EN1998 – 1, Comité Européen de Normalisation, Brussels.

CEN (2004b) Eurocode 6: Design of masonry structures, Part 1: General rules for reinforced and unreinforced masonry structures. EN 1996-1-1, Comité Européen de Normalisation, Brussels.

CEN (2005) Eurocode 8: Design of structures for earthquake resistance – Part 3: Assessment and retrofitting of buildings. EN1998 – 3, Comité Européen de Normalisation, Brussels.

Chen SY, Moon FL, Yi T (2008) A macroelement for the nonlinear analysis of in-plane unreinforced masonry piers, *Engineering Structures*, 44, pp. 3625–41.

CNR-DT 212/2013 (2014) Guide for the Probabilistic Assessment of the Seismic Safety of Existing Buildings, National research council of Italy.

Costley AC, Abrams DP (1996) Dynamic response of unreinforced masonry buildings with flexible diaphragms. NCEER-96-0001, University of Buffalo, Buffalo, N.Y., USA.

D'Altri AM, Castellazzi G, de Miranda S, Tralli A (2017) Seismic-Induced Damage in Historical Masonry Vaults: A Case-Study in the 2012 Emilia Earthquake-Stricken Area, *Journal of Building Engineering*, 13, pp: 224–243

D'Asdia P, Viskovic A (1994) L'analisi sismica degli edifici in muratura, *Ingegneria Sismica*, XI(1), 32-42 (in Italian).

D'Ayala DF, Speranza E (2003) Definition of collapse mechanisms and seismic vulnerability of historic masonry buildings, *Earthquake Spectra*, 19, pp: 479-509.

D'Ayala DF, Paganoni S (2011) Assessment and analysis of damage in L'Aquila historic city centre after 6th April 2009, *Bulletin of Earthquake Engineering*, 9(1), pp: 81–104.

De Borst R, Sluys LG, Mulhaus HB, Pamin J (1993) Fundamental issues in finite element analyses of localization of deformation, *Engineering Computations*, 10, pp: 99-121.

De Falco A, Guidetti G, Mori M, Sevieri G (2017) Model uncertainties in seismic analysis of existing masonry buildings: the Equivalent-Frame Model within the Structural Element Models approach. *Proceedings of XVII Convegno ANIDIS*, 17-21 September, Pistoia, Italy (in Italian).

Degli Abbati S, D'Altri AM, Ottonelli D, Castellazzi G, Cattari S, De Miranda S, Lagomarsino S (2019) Seismic assessment of interacting structural units in complex historical masonry constructions by nonlinear static analyses, *Computers & Structures*, 213, pp: 51 – 71.

Di Ludovico M, Fico R, Cordasco EA, Prota A, Verderame G, Manfredi G (2011) Some considerations on the use of the technical software in the reconstruction of the Abruzzo Region. *Convegno AIST/SAIE 2011 "Il Calcolo delle Strutture Esitenti: Software e Normativa",* Bologna, Italy.

Dolce M (1991) Schematizzazione e modellazione degli edifici in muratura soggetti ad azioni sismiche, *L'industria delle costruzioni*, 25 (242), pp. 44-57 (in Italian).

ESECMaSE (2005–2007) Enhanced safety and efficient construction of masonry structures in Europe, http://www.esecmase.org

Esposito R, Safari S, Ravenshorst GJP, Rots JG (2018). Characterisation of calcium silicate brick and element masonry structures. *Proceedings of 10th Australasian Masonry Conference*, 11-14 February, Sidney, Australia.

Fajfar P (2000) A nonlinear analysis method for performance-based seismic design, *Earthquake Spectra*,16(3), pp:573–591.

Fathi A, Mobadersany P, Fathi R (2012) A Simple Method to Solve Quartic Equations, *Australian Journal of Basic and Applied Sciences*, 6(6), pp: 331-336.

Fehling E, Stuerz J, Emami A (2007) Test results on the behaviour of masonry under static (monotonic and cyclic) in-plane lateral loads, ESECMaSE deliverable D7.1a, University of Kassel.

FEMA 306 (1998) Evaluation of earthquake damaged concrete and masonry wall buildings. Basic procedures manual, Applied Technology Council (ATC), Washington D.C.

FEMA 356 (2000) Pre-standard and commentary for the seismic rehabilitation of buildings, Applied Technology Council (ATC), Washington D.C.

Ferrari method. *Encyclopedia of Mathematics.*

Fortunato G, Funari MF, Lonetti P (2017) Survey and seismic vulnerability assessment of the Baptistery of San Giovanni in Tumba (Italy), *Journal of Cultural Heritage*, 26, pp. 64-78.

Fragomeli A, Galasco A, Graziotti F, Guerrini G, Kallioras S, Magenes, G, Malomo D, Mandirola M, Manzini CF, Marchesi B, Milanesi RR, Morandi P, Penna A, Rossi A, Rosti A, Rota M, Senaldi IE, Tomassetti U, Cattari S, da Porto F, Sorrentino L (2017) Comportamento degli edifici in muratura nella sequenza sismica dell'Italia centrale del 2016 - Parte 2: Esempi di centri colpiti, *Progettazione Sismica*, 8(3), pp: 75-98 (in Italian).

Franchin, P, Ragni L, Rota M, Zona A (2018) Modelling uncertainties of Italian code-conforming structures for the purpose of seismic response analysis, *Journal of Earthquake Engineering*, 22, pp: 1964 – 1989.

Freeman SA (1998) The capacity spectrum method as a tool for seismic design. *Proceedings of 11th European conference of earthquake engineering*, Paris, France.

Gambarotta L, Lagomarsino S (1996) On the dynamic response of masonry panels. *Proceedings of the National Conference "Masonry Mechanics Between Theory and Practice"*, Messina, Italy, 1996 (in Italian).

Gambarotta L, Lagomarsino S (1997a) Damage models for the seismic response of brick masonry shear walls. Part 1: the mortar joint model and its applications, *Earthquake Engineering and Structural Dynamics*, 26, pp. 423-439.

Gambarotta L, Lagomarsino S (1997b) Damage models for the seismic response of brick masonry shear walls. Part 2: the continuum model and its applications, *Earthquake Engineering and Structural Dynamics*, 26, pp. 441-462.

Giongo I, Rizzi E, Ingham JM, Dizhur D (2018) Numerical modelling strategies for the in-plane behavior of straight sheathed timber diaphragms, *Journal of Structural Engineering*, 144 (10).

Giuffré, A (1993), Sicurezza e conservazione dei centri storici – Il caso Ortigia, Editori Laterza, Italy.

Grande E, Imbimbo M, Sacco E (2011) A beam finite element for nonlinear analysis of masonry elements with or without fiber-reinforced plastic (FRP) reinforcements, *International Journal of Architectural Heritage*, 5, pp. 693–716.

Graziotti F, Magenes G, Penna A (2012) Experimental cyclic behaviour of stone masonry spandrels. *Procedeeings of the 15th World Conference on Earthquake Engineering*, Lisboa. Portugal.

Graziotti F, Tomassetti U, Kallioras S, Penna A, Magenes G (2017) Shaking table test on a full scale URM cavity wall building, *Bulletin of Earthquake Engineering*, 15, pp: 5329–5364.

Grünthal G (1998) European macroseismic scale 1998: EMS-98. Chaiers du Centre Européen de Géodynamique et de Séismologie, vol. 15, Luxembourg.

Hassan M, Ei-Tawil S (2003). Tension Flange Effective Width in Reinforced Concrete Shear Walls, *ACI Structural Journal*, 100 (3), pp: 349-356.

Iervolino I, Spillatura A, Bazzurro P (2018) Seismic structural reliability of code-conforming Italian buildings, *Journal of Earthquake Engineering*, 22, pp: 5-27.

Jalayer F, Cornell CA (2002) Alternative nonlinear demand estimation methods for probability-based seismic assessments, *Earthquake Engineering & Structural Dynamics*, 38(8), pp: 951-972.

Kappos AJ, Penelis GG, Drakopoulos CG (2002) Evaluation of simplified models for lateral load analysis of unreinforced masonry buildings, *Journal of Structural Engineering*, 128 (7), pp: 890–7.

Khanmohammadi M, Benham H, Marefat MS (2014) Seismic behavior prediction of flanged Unreinforced Maosnry (FURM) walls, *Journal of Earthquake Engineering*, 18, pp: 759-784.

Kržan M, Gosti˘c S, Cattari S, Bosiljkov V (2015) Acquiring reference parameters of masonry for the structural performance analysis of historical buildings, *Bullettin of Earthquake Engineering*, 13, pp: 203–236.

Lagomarsino S, Magenes G (2009) Evaluation and reduction of the vulnerability of masonry buildings. In: Manfredi G, Dolce M (Eds), *The state of earthquake engineering research in Italy: the ReLUIS-DPC 2005–2008 project*. Doppiavoce, Napoli.

Lagomarsino S, Penna A, Galasco A, Cattari S (2013) TREMURI program: an equivalent frame model for the nonlinear seismic analysis of masonry buildings, *Engineering structures*, 56, pp: 1787-1799.

Lagomarsino S, Cattari S (2015a), Seismic performance of historical masonry structures through pushover and nonlinear dynamic analyses, *Perspectives on European Earthquake Engineering and Seismology*, 39, pp: 265–292.

Lagomarsino S, Cattari S (2015b), PERPETUATE guidelines for seismic performance based assessment of cultural heritage masonry structures, *Bulletin of Earthquake Engineering*, 13, pp: 13–47.

Lee J, Fenves GL (1998) Plastic-Damage Model for Cyclic Loading of Concrete Structures, *Journal of Engineering Mechanics*, 124(8), pp: 892–900.

Liu Z, Crewe A (2018) Effect of position and size of the openings on in-plane behavior of unreinforced masonry (URM) walls. *Proceedings of 16ECEE*, 18-21 June, Thessaloniki, Greece.

Lourenço PB, Borst R, Rots JG (1997) A plane stress softening plasticity model for orthotropic materials, *International Journal for Numerical Methods in Engineering*, 40, pp: 4033-4057.

Lourenço PB, Rots JG, Blaauwendraad J (1998) Continuum model for masonry: Parameter estimation and validation, *Journal of Structural Engineering*, 124(6), pp: 642-652.

Lourenço PB (2002) Computations on historic masonry structures, *Progress in Structural Engineering and Mat.*, 4(3), pp:301-319

Lubliner J, Oliver J, Oller S, Onate E (1989) A Plastic-Damage Model for Concrete, *International Journal of Solids and Structures*, 25, pp: 299–329.

Magenes G, Calvi GM (1997) In plane seismic response of brick masonry walls, *Earthquake Engineering and Structural Dynamics*,26, pp: 1091-1112.

Magenes G, Della Fontana A (1998) Simplified non-linear seismic analysis of masonry buildings. *Proceedings of the British Masonry Society*, 8, pp.190–195.

Magenes (2006) Masonry building design in seismic areas: Recent experiences and prospects from a European standpoint. *1st European Conference on Earthquake Engineering and Seismology*, 3-8 September, Geneva, Switzerland.

Magenes G, Manzini CF, Morandi P, Remino M, Bolognini D (2006) SAM II, Software for the Simplified Seismic Analysis of Masonry buildings, Università degli Studi di Pavia and EUCENTRE.

Magenes G, Morandi P, Penna A (2008) Experimental in-plane cyclic response of masonry walls with clay units. *Proceeding of the 14th WCEE*, Beijing, China, Paper No. 95, 8 pages.

Magenes G (2010) Earthquake resistant design of masonry structures: rules, backgrounds, latest findings. In: *Prooceedings of 8th international masonry conference*, Dresden, Germany.

Magenes G, Penna A, Senaldi IE, Rota M, Galasco A (2014) Shaking Table Test of a Strengthened Full-scale Stone Masonry Building with Flexible Diaphragms, *International Journal of Architectural Heritage*: *Conservation, Analysis, and Restoration*, 8(3), pp: 349-375.

Mann W, Müller H (1980) Failure of shear-stressed masonry – An enlarged theory, tests and application to shear walls. *International Symposium on Loadbearing Brickwork*, London.

Manzini CF, Morandi P, Magenes G, Calliari R (2006) ANDILWall - Software di calcolo e verifica di edifici in muratura ordinaria, armata o mista - Manuale d'uso (in Italian), Università di Pavia, EUCENTRE e CRSoft S.r.l. (www.andilwall.it).

Manzini CF, Magenes G, Penna A, da Porto F, Camilletti D, Cattari S, Lagomarsino S, Masonry Italian code-conforming buildings. Part 1: case studies and design methods (2018), *Journal of Earthquake Engineering*, 22, pp: 54-73.

Marino S, Cattari S, Lagomarsino S, Ingham J, Dizhur D (2016) Modelling of two damaged unreinforced masonry buildings following the Canterbury earthquakes. *Proceedings of Reducing risk raising resilience – 2016 NZSEE Conference*, 1-3 April, Christchurch, New Zealand.

Marino S (2018) Nonlinear Static Procedures for the seismic assessment of irregular URM buildings, PhD Thesis, Univ. of Genoa.

Marino S, Cattari S, Lagomarsino S (2019) Are the nonlinear static procedures feasible for the seismic assessment of irregular existing masonry buildings?. *Engineering Structures* (submitted).

Marques R, Lourenço PB (2011) Possibilities and comparison of structural component models for the seismic assessment of modern unreinforced masonry buildings, *Computers & Structures*, 89, pp: 2079-2091.

Marques R, Lourenço PB (2014) Unreinforced and confined masonry buildings in seismic regions: Validation of macro-element models and cost analysis, *Engineering Structures*, 64, pp: 52−67.

Messali F, Rots JG (2018) In-plane drift capacity at near collapse of rocking unreinforced calcium silicate and clay masonry piers, *Engineering Structures*, 164 (1), pp: 183-194.

MIDAS Gen© (2018). MIDAS Information Technology Co., http://en.midasuser.com, www.cspfea.net.

Milani G, Beyer K, Dazio A (2009) Upper bound limit analysis of meso-mechanical spandrel models for the pushover analysis of 2D masonry frames, *Engineering Structures*, 31(11), pp: 2696- 2710.

Milani G, Valente M. (2015) Failure analysis of seven masonry churches severely damaged during the 2012 Emilia-Romagna (Italy) earthquake: non-linear dynamic analyses vs conventional static approaches, *Engineering Failure Analysis*,54: 13–56.

Milani G, Valente M, Alessandri C (2017) The Narthex of the Church of the Nativity in Bethlehem: A Non-Linear Finite Element Approach to Predict the Structural Damage, *Computers & Structures*, 207, pp: 3-18.

MIT (2009) Ministry of Infrastructures and Transportation Circ. C.S.Ll.Pp. No. 617 of 2/2/2009 ‘‘Istruzioni per l’applicazione delle nuove norme tecniche per le costruzioni di cui al D.M. 14 Gennaio 2008,’’ Cons. Sup. LLPP. S.O. n.27 alla G.U. del 26.02.2009, No. 47 (in Italian).

MIT (2019) Ministry of Infrastructures and Transportation Circ. C.S.Ll.Pp. No. 7 of 21/1/2019 ‘‘Aggiornamento delle ‘Norme Tecniche per le costruzioni’ di cui al D.M. 17 Gennaio 2018,’’ Cons. Sup. LLPP. S.O. n.27 alla G.U. del 11.02.2019, No. 35 (in Italian).

Moon FL, Yi T, Leon RT, Kahn LF (2006) Recommendations for Seismic Evaluation and Retrofit of Low-Rise URM Structures, *Journal of Structural Engineering*, 132 (5), pp: 663-672.

Morandi P, Albanesi L, Magenes G (2016) In-plane test campaign on different load-bearingURM typologies with thin shell and web clay units. *Proceedings of 16th International Brick and BlockMasonry Conference*, Padua, Italy.

Morandi, P, Albanesi L, Graziotti F, Piani TL, Penna A, Magenes G (2018) Development of a dataset on the in-plane experimental response of URM piers with bricks and blocks, *Construction and Building Materials*, 190, pp: 593-611.

Mordant C (2016) Unreinforced clay masonry structures: advanced characterization of the seismic behavior including acoustic issues. PhD Thesis, University of Liege, Belgium.

MSJC (2008) Building Code Requirements for Masonry Structures (TMS 402/ACI 530/ASCE 5). American Concrete Institute; Structural Engineering Institute; The Masonry Society (Masonry Standard Joint Committee) Boulder, CO, USA.

NTC08 (2008) Decreto ministeriale 14/1/2008: norme tecniche delle costruzioni. Ministero delle Infrastrutture e dei trasporti, S.O. No. 30 alla G.U. No. 29 del 4/2/2008, Ministero delle Infrastrutture e dei Trasporti, Rome, Italy (in Italian).

NTC18 (2018) Decreto ministeriale 20/2/2018: norme tecniche delle costruzioni. Ministero delle Infrastrutture e dei trasporti, S.O. No. 8 alla G.U. No. 42 del 20/2/2018, Ministero delle Infrastrutture e dei Trasporti, Rome, Italy (in Italian)

NZSEE (2006) Assessment and improvement of the structural performance of buildings in earthquakes. New Zealand Society for Earthquake Engineering, Wellington, New Zealand.

NZSEE (2015) Assessment and Improvement of the Structural Performance of Buildings in Earthquakes - Section 10 Revision. Seismic Assessment of Unreinforced Masonry Buildings. New Zealand Society for Earthquake Engineering, Corrigendum n° 4, 9 April 2015, Russell.

Orlando M, Salvatori L, Spinelli P, Stefano M (2016) Displacement capacity of masonry piers: parametric numerical analyses versus international building codes, *Bulletin of Earthquake Engineering* 14(8), pp: 2259-2271.

Pagani C, Salvatori L, Maurizio O, Spinelli P (2017) Irregular opening layouts in unreinforced Masonry Walls: Equivalent Frame and Finite Elements Simulations. *Proceedings of XVII Convegno ANIDIS*, 17-21 September, Pistoia, Italy (in Italian).

Paquette J, Bruneau M (2003) Pseudo-dynamic testing of unreinforced masonry building with flexible diaphragm, *Journal of Structural Engineering*, 129(6), pp: 708-716.

Parisi F, Augenti N (2013) Seismic capacity of irregular unreinforced masonry walls with openings, *Earthquake Engineering and Structural Dynamics*, 42, pp: 101–121.

Parisi F, Lignola GP, Augenti N, Prota A, Manfredi G (2013) Rocking response assessment of in-plane laterally-loaded masonry walls with openings, *Engineering Structures*, 56, pp: 1234–1248.

Parisi F, Augenti N, Prota A (2014) Implications of the spandrel type on the lateral behavior of unreinforced masonry walls, *Earthquake Engineering and Structural Dynamics*, 43, pp: 1867–1887.

Parisi F, Sabella G, Augenti N (2015) Seismic Capacity Prediction for Irregular Masonry Walls with Opening Offsets. *Proceedings of the 15th Intern. Conf. on Civil, Structural and Environmental Engineering Computing*, Prague, 1-4 Sept., Czech Republic.

Pasticier L, Amadio C, Fragiacomo M (2008) Non-linear seismic analysis and vulnerability evaluation of a masonry building by means of the SAP2000 V.10 code, *Earthquake Engineering and Structural Dynamics*, 37(3), pp: 467–85.

Penelis GR G (2006) An efficient approach for pushover analysis of unreinforced masonry (URM) structures, *Journal of Earthquake Engineering*, 10 (3), pp: 359-379.

Penna A, Galasco A (2013) A macro-element model for the nonlinear analysis of masonry members including second order effects, *Proceedings of 4th COMPDYN Conference*, 12-14 June, Kos Island, Greece.

Penna A, Morandi P, Rota M, Manzini CF, da Porto F, Magenes G (2014a) Performance of masonry buildings during the Emilia 2012 earthquake, *Bulletin of Earthquake Engineering*, 12, pp: 2255–2273.

Penna A, Lagomarsino S, Galasco A (2014b) A nonlinear macroelement model for the seismic analysis of masonry buildings, *Earthquake Engineering and Structural Dynamics*, 43(2), pp: 159–179.

Penna A, Senaldi IE, Galasco A, Magenes G (2015) Numerical simulation of shaking table tests on full-scale stone masonry buildings, *International Journal of Architectural Heritage: Conservation, Analysis and Restoration*, 10, pp: 146-163.

Petry S, Beyer K (2014) Influence of boundary conditions and size effect on the drift capacity of URM walls, *Engineering Structures*, 65, pp: 76-88.

Piazza M, Baldessari C, Tomasi R (2008) The role of in-plane floor stiffness in the seismic behavior of traditional buildings. *Procedeeings of 14th World Conference on Earthquake Engineering*, 12–17 October, Beijin, China.

Priestley MJ, He L (1995) Seismic Response of T-Section Masonry Shear Walls, *The Masonry Society Journal*, 9 (1), pp: 10-19.

Quagliarini E, Maracchini G, Clementi F (2017) Uses and limits of the Equivalent Frame Model on existing unreinforced masonry buildings for assessing their seismic risk: A review, *Journal of Building Engineering*,10, pp: 166–182.Raka E, Spacone E, Sepe V, Camata G (2015) Advanced frame element for seismic analysis of masonry structures: model formulation and validation, *Earthquake Engineering and Structural Dynamics*, 44 (14), pp: 2489-2506.

Rees EL (1922) Graphical Discussion of the Roots of a Quartic Equation, *American Mathematical Monthly*, 29 (2), pp: 51–55.

Rinaldin G, Amadio c, Macorini L (2016) A macro-model with nonlinear springs for seismic analysis of URM buildings, *Earthquake Engineering and Structural Dynamics*, 45, pp: 2261,2281.

RINTC Workgroup (2018) Results of the 2015-2017 Implicit seismic risk of code-conforming structures in Italy (RINTC) project. ReLUIS report, Rete dei Laboratori Universitari di Ingegneria Sismica (ReLUIS), Naples, Italy, available at http://www.reluis.it/

Roca P, Cervera M, Griup G, Pelà L (2010) Structural analysis of masonry historical constructions. Classical and advanced approaches, *Archives of Computational Methods in Engineering*, 17 (3), pp: 299-325.

Rota M, Penna A, Magenes G (2014) A framework for the seismic assessment of masonry buildings taking into account different sources of uncertainty, *Earthquake Engineering and Structural Dynamics*, 43(7), pp:1045–1066.

Russell AP, Ingham JM (2008) Flange effects of an unreinforced masonry wall subjected to pseudo-static in-plane seismic forces, *Proceedings of 14th World Conference on Earthquake Engineering*, 12-17 October, Beijing, China.

Russell AP, Ingham JM (2010) The influence of flanges on the in-plane seismic performance of URM walls in New Zealand buildings. In: *New Zealand society of Earthquake Engineering Conference*, paper n.38.

Russell AP, Elwood KJ, Ingham JM (2014) Lateral force-displacement response of Unreinforced Masonry walls with flanges, *Journal of Structural Engineering*, 140(4).

Sajid HU, Mohammad A, Qaisar A, Sikandar HS (2018) Effects of vertical stresses and flanges on seismic behavior of unreinforced brick masonry, *Engineering structures*, 155, pp: 394-409.

Salonikos T, Karakostas C, Lekidis V, Anthoine A (2003) Comparative inelastic pushover analysis of masonry frames, *Engineering Structures*, 25, pp: 1515–23.

SAP2000 v.18 (2015), distributed by CSI italia srl, developed by CSI Computer and Structures, Inc., http://www.csi-italia.eu/software/sap2000.

Shi QX, Wang B (2016) Simplified calculation of effective flange width for shear walls with flange, *The structural design of tall and special buildings*, 25, pp. 558-577.

Siano R, Sepe V, Camata G, Pelà L (2017a) Analysis of the performance in the linear field of Equivalent-Frame Models for Regular and Irregular Masonry Walls, *Engineering Structures*, 145**,** pp: 190–210.

Siano R, Camata G, Sepe V, Spacone E, Roca P, Pelà L (2017b) Finite Elements vs. Equivalent-Frame Models for URM walls' in-plane behavior. *Proceedings of 16th World Conference on Earthquake Engineering*, 9-13 January, Santiago, Chile.

Siano R, Roca P, Camata G, Pelà L, Sepe V, Spacone E, Petracca M (2018) Numerical Investigation of Non-Linear Equivalent-Frame Models for Regular Masonry Walls, *Engineering Structures*, 173, pp: 512-529.

Sorrentino L, Cattari S, da Porto F, Magenes G, Penna A (2018) Seismic behaviour of ordinary masonry buildings during the 2016 central Italy earthquake. *Bulletin of Earthquake Engineering*.

Spacone E, Filippou FC, Tourcer EF (1996) Fiber Beam-Column Model for Nonlinear Analysis of R/C Frames. I: Formulation, *Earthquake Engineering and Structural Dynamics*, 25(7), pp: 711-725.

Spacone E, Camata G (2007) Cerniere Plastiche sviluppate per telai in cemento armato e implementate nel programma di calcolo Aedes, *Issued by GC*, October 2007 (in Italian).

STA Data (2017) 3Muri computer program, Release 11.4.0, www.3muri.com

Tomaževič M (1978) The computer program POR, Report ZRMK, 1978 (in Slovenian).

Turnšek V, Cačovic F (1971) Some experimental results on the strength of brick masonry walls. *Proceedings of the 2nd international brick masonry conference*, Stoke on Trent, pp. 149-156.

Turnšek V, Sheppard P (1980) The shear and flexural resistance of masonry walls. Some experimental results on the strength of brick masonry walls. *Proceedings of the 2nd international brick masonry conference*, Stoke on Trent, pp. 149-156.

Valente M, Milani G (2016) Non-linear dynamic and static analyses on eight historical masonry towers in the North-East of Italy, *Engineering Structures*, 114, pp: 241–70.

Van der Pluijm R (1993) Shear behaviour of bed joints. In: *6th North American Masonry Conference*, 6-9 June, Philadelphia, Pennsylvania, USA.

Vanin F, Zaganelli D, Penna A, Beyer K (2017) Estimates for the stiffness, strength and drift capacity of stone masonry walls based on 123 quasi-static cyclic tests reported in the literature, *Bulletin of Earthquake Engineering*, 15(12), pp: 5435-5479.

Yi T (2004) Experimental investigation and numerical simulation of an unreinforced masonry structure with flexible diaphragms. PhD Thesis, Georgia Institute of Technology, Atlanta, GA, USA.

Yi T, Moon FL, Leon RT, Kahn LF (2006) Lateral load tests on a two-story unreinforced Masonry building, *Journal of Structural Engineering*, 132, pp: 643–652.

Zilch K, Finckh W, Grabowski S, Schermer D, Scheufler W (2008) Test results on the behaviour of masonry under static cyclic in-plane lateral loads, ESECMaSE deliverable D7.1b, Technical University of Munich.

APPENDIX A

A – MESH SIZE OBJECTIVITY STUDY AND SENSITIVITY TO THE VISCOSITY PARAMETER

In this Appendix the mesh size objectivity study carried out in order to check the robustness of the mesh dimension adopted in the FE analyses is illustrated.

In particular, the convergence analyses were performed both at the scale of the single panel (described in the following section A.1) and at the scale of the wall (described in the following section A.2). In this way it was possible to ensure the reliability of the results obtained in the calibration of the constitutive laws (section 3.2), realized through lateral load analyses on masonry panels, and also in the pushover analyses performed on the regular wall (section 3.3) and on the irregular walls (Chapter 4).

It is recalled that in the FE models 8-node linear brick elements are used and the masonry material is modelled through the CDP model.

In addition to the outcomes of the mesh size objectivity study, in section A.2 also the results of some sensitivity analyses performed on the regular wall and aimed to evaluate the role on the structural response of the regularization introduced by the viscosity parameter η included in the CDP model are presented.

A.1 - Analyses at panel scale

For each one of the masonry panels introduced in Chapter 3 (section 3.2.1, Table 3.3) the convergence analyses were carried out by considering three possible mesh dimensions and by fixing all the other parameters (applied axial load, parameters used in the CDP model).

In the following, by way of example, the results obtained for panel 2 (λ = 1.35) in terms of associated base shear – top displacement (V_b-d_{top}) curves and of occurred damage pattern are discussed. The results refer to an axial load N=100 kN (σ/f_c = 0.065) and to one of the possible combination of the mechanical parameters of the CDP model considered in the calibration process. In particular, in this case the adopted values of the different parameters are: for the tensile behavior f_t = 0.22 MPa and ε_{tu}^{in} = 0.001, while for compression an A-type behavior (i.e. without hardening and with a linear softening branch, see Figure 3.7) was assumed, with ε_{cu}^{in} = 0.008.

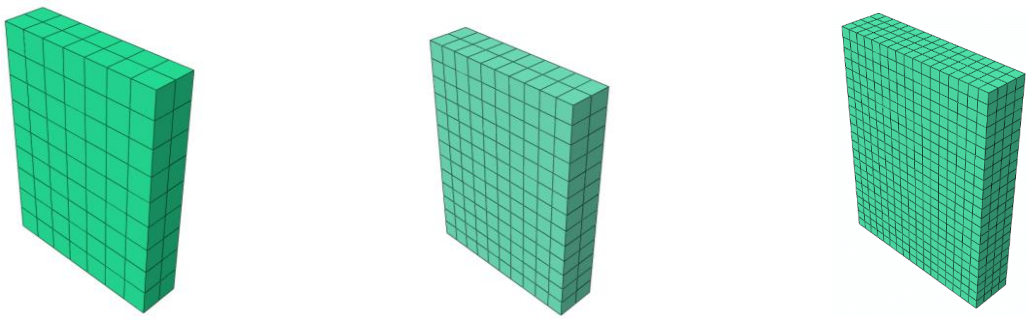

Mesh_0 ***Mesh_1*** ***Mesh_2***

Figure A.1 - Different mesh dimensions adopted for the panel in the sensitivity analyses (*Mesh_0*: 240 nodes and 126 brick elements; *Mesh_1*: 462 nodes and 260 brick elements; *Mesh_2*: 2160 nodes and 1564 brick elements).

The different considered dimensions for the mesh are shown in Figure A.1, while the related V_b - d_{top} curves and the occurred damage patterns (in terms of tensile damage contour plots) are represented in Figure A.2 and in Figure A.3, respectively.

By examining the V_b-d_{top} curves it is possible to see that in the initial elastic phase, as expected, no significant differences are detected in the obtained results. However, when considering a more advanced nonlinear phase, the response of the panel associated to *Mesh_0* (coarse mesh) presents a higher global stiffness and a higher maximum strength with respect to the other 2 cases; moreover, the strength decay associated to the failure of the panel occurs for a higher top displacement. On the other hand, regarding the other two analyses, it is observed that the global response activated by the panel is almost the same in terms of stiffness, maximum strength and top displacement associated to the main drop of strength ($d_{top} \approx$ 2mm) . Considering the post-peak phase, more differences can be detected, which can be explained by considering that the convergence process in the post-peak phase, in presence of high levels of nonlinearity, is particularly critical; however, almost similar trends can be observed in the 2 examined curves.

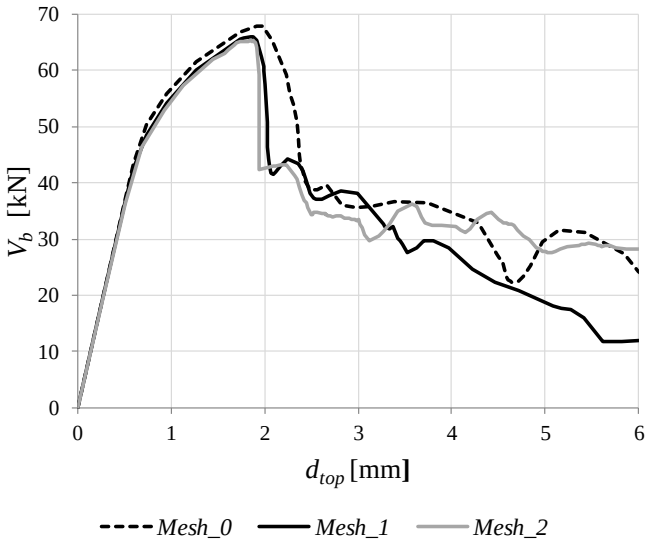

Figure A.2 - Sensitivity of the results obtained in terms of base shear (V_b) – top displacement (d_{top}) curves associated to the different considered mesh dimensions for panel 2.

By looking at the results in terms of occurred damage (in correspondence of d_{top} = 4mm), it is possible to observe that, in general, all the considered mesh dimensions are able to capture the same failure mode (hybrid failure mode), characterized by both a parzialization of the end sections and the development of a diagonal shear crack.

The analyses on the other panels confirm in general these results, both in terms of global curves and in terms of damage.

In the light of these considerations, it was decided to adopt for all the panels the *Mesh_1*(brick elements of approximatively 10x10x12 mm), which provides almost the same results in terms of global response and occurred damage of a more refined mesh (*Mesh_2*), guaranteeing at the same time a higher computational efficiency.

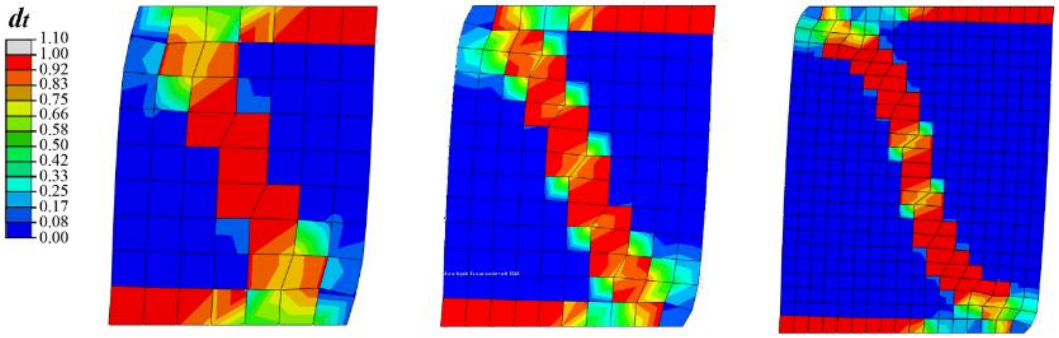

Figure A.3 - Sensitivity of the results obtained in terms of tensile damage (d_{top} = 4 mm) associated to the different considered mesh dimensions for panel 2.

A.2 - Analyses at wall scale

The convergence analyses at the wall scale were performed on the regular wall configuration (introduced in section 3.3). In particular, in this case the criteria adopted for checking the robustness of the mesh were aimed to evaluate the influence of the mesh dimension on the parameters of the structural response that are considered in the comparisons with the EF models (introduced in section 3.3.4: comparisons in terms of global response, damage pattern and local response).

Three different mesh dimensions were considered for the examined wall, referred to as *Mesh A*, *Mesh B* and *Mesh C* (Figure A-4), with decreasing reference dimensions for the brick elements (moving from *Mesh A* to *Mesh C*). In particular, *Mesh A* is characterized by brick elements with dimensions approximatively equal to 20x20 cm in the plane of the wall and by the presence of two elements in the wall thickness, while in case of *Mesh C* the dimensions of the brick elements are approximatively equal to 8x8 cm in the plane of the wall and four elements are present in the wall thickness. Finally, the mesh indicated as *Mesh B* is characterized by brick elements with a dimension approximatively equal to 10x10 cm in the plane of the wall and by two elements in the wall thickness; this last mesh dimension corresponds to the one adopted as reference, after the convergence analyses, in the case of the panels previously analysed (see previous section A.1). The resulting total number of nodes is: 2983 nodes for *Mesh A*, 9972 nodes for *Mesh B* and 25893 nodes in case of *Mesh C*.

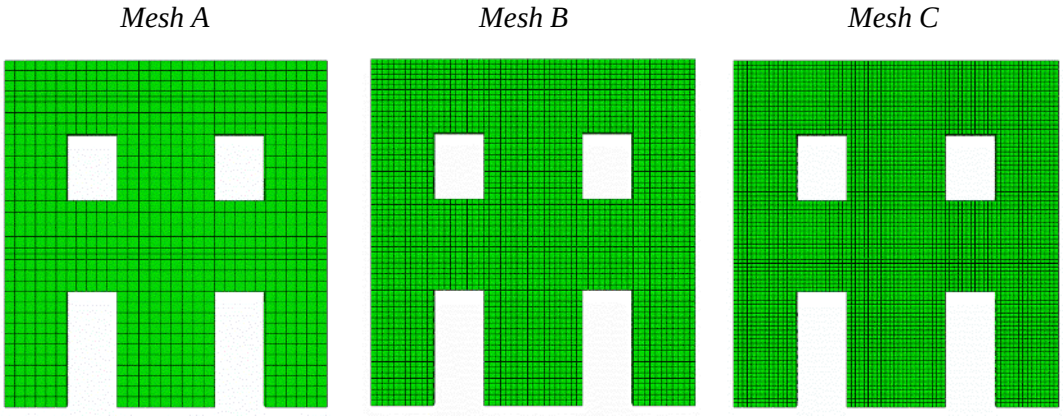

Figure A.4 - Different mesh dimensions adopted for the regular wall in the sensitivity analyses.

The nonlinear static analyses were performed on each one of the three FE models obtained for the wall, according to the procedure described in section 3.3.2.

In Figure A.5 the pushover curves obtained with the three different FE models of the wall are represented. It is possible to observe that the curve associated to the coarser mesh (*Mesh A*) presents some differences with respect to the pushover curves obtained through the use of a more refined mesh (*Mesh B* and *Mesh C*). These differences concern both the stiffness degradation and the maximum strength: indeed, the FE model associated to the coarser mesh presents a slightly less pronounced stiffness degradation and a slightly higher maximum strength with respect to the other two FE models of the wall. This is confirmed also by the data reported in Table A.1, which indicate, for each pushover curve, the corresponding maximum strength V_{max} and also the parameter R_k, (defined as the ratio between the secant stiffness $k_{s,70}$ corresponding to the 70% of the maximum strength and the secant stiffness $k_{s,35}$ corresponding to the 35% of the maximum strength), which allows to have a measure of the stiffness degradation phenomenon.

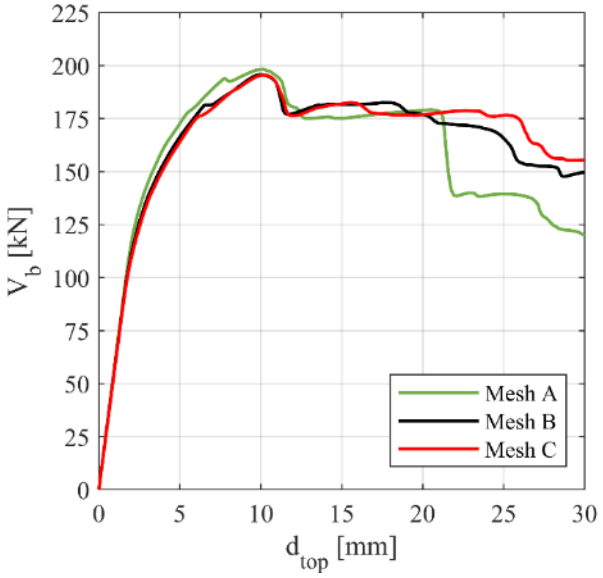

Figure A.5 - Global pushover curves obtained with the FE models of the regular wall associated to the three adopted mesh dimensions.

Moreover, quite significant differences are present also in the post-peak response: differently from the curves of the other two models, in the pushover curve associated to the model with *Mesh A* a drop of strength is observed in correspondence of a top displacement approximatively equal to 22 mm. This sudden strength degradation, in particular, is related to the failure of one of the piers at the ground floor, as it will be explained in the following discussion on the damage pattern.

Table A.1 - Values of the maximum strength (V_{max}) and of the parameter R_k associated to the pushover curves of the three FE models characterized by different mesh dimensions

	Mesh A	***Mesh B***	***Mesh C***
$\boldsymbol{R_k}$ **[-]**	0.846	0.777	0.767
$\boldsymbol{V_{max}}$ **[kN]**	198.20	195.68	195.48

On the contrary, the curves associated to the FE models with *Mesh B* and *Mesh C* are almost coincident in terms of both stiffness and strength (see also Table A.1 for the comparison in terms of R_k and V_{max} parameters). Moreover, also the post-peak phase is similar, at least until a top displacement equal to 20 mm; after that, slight differences are detected between the two models, probably related to convergence issues in advanced nonlinear phase.

In Figure A.6 the comparison in terms of damage pattern (tensile damage) associated to a top displacement equal to 30 mm is reported. It can be seen that all the models predict a concentration of damage at the ground floor of the wall; however, while the damage pattern associated to *Mesh B* and *Mesh C* is substantially the same, some differences can be highlighted when comparing it with the predictions of the FE model associated to *Mesh A*. This last, in particular, does not capture the damage characterizing the masonry piers at the second floor and the damage in the left spandrel at the first floor, which are instead visible when considering the other two models. Moreover, the FE model associated to *Mesh A* predicts the shear failure of the central pier at the ground floor, which occurs for a top displacement approximatively equal to 22 mm, thus producing a sudden drop of strength which is clearly visible, as highlighted before, in the global pushover curve. On the contrary, in the FE models associated to *Mesh A* and *Mesh B*, the failure of the central pier at the ground floor occurs only for higher values of top displacement (d_{top} approximatively equal to 50 mm).

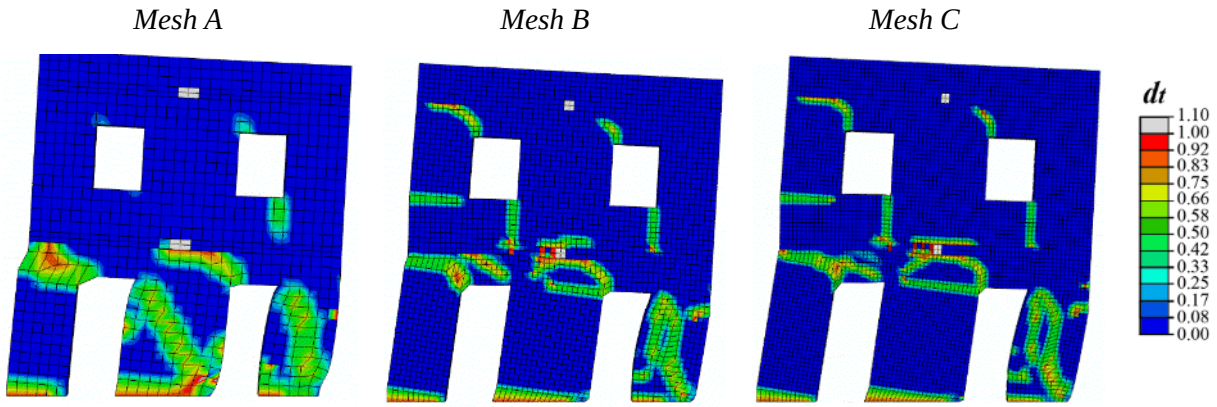

Figure A.6 - Damage pattern (tensile damage) in correspondence of a top displacement equal to 30 mm obtained with the FE models of the regular wall associated to the three adopted mesh dimensions.

In Figure A.7 the evolution of the generalized forces acting in correspondence of the three base sections of the wall is represented. It is possible to see that the results provided by the three models are substantially in agreement until a value of top displacement approximatively equal to 22 mm, even if slight discrepancies can be detected in case of the results obtained with the model with the coarser mesh. Then, for higher values of top displacement the results associated to the model with *Mesh A* deviate from the values of generalized forces derived from the other two models, as it is particularly evident in the central pier at the ground floor (S2 in Figure A.7), thus implying a different redistribution of the vertical and horizontal loads among the masonry portions at the ground floor of the wall. On the contrary, the evolution of the normal force, bending moment and shear force obtained with the models associated to *Mesh B* and *Mesh C* are almost coincident for all the considered sections, except for specific cases where slight discrepancies can be detected when considering high values of top displacement.

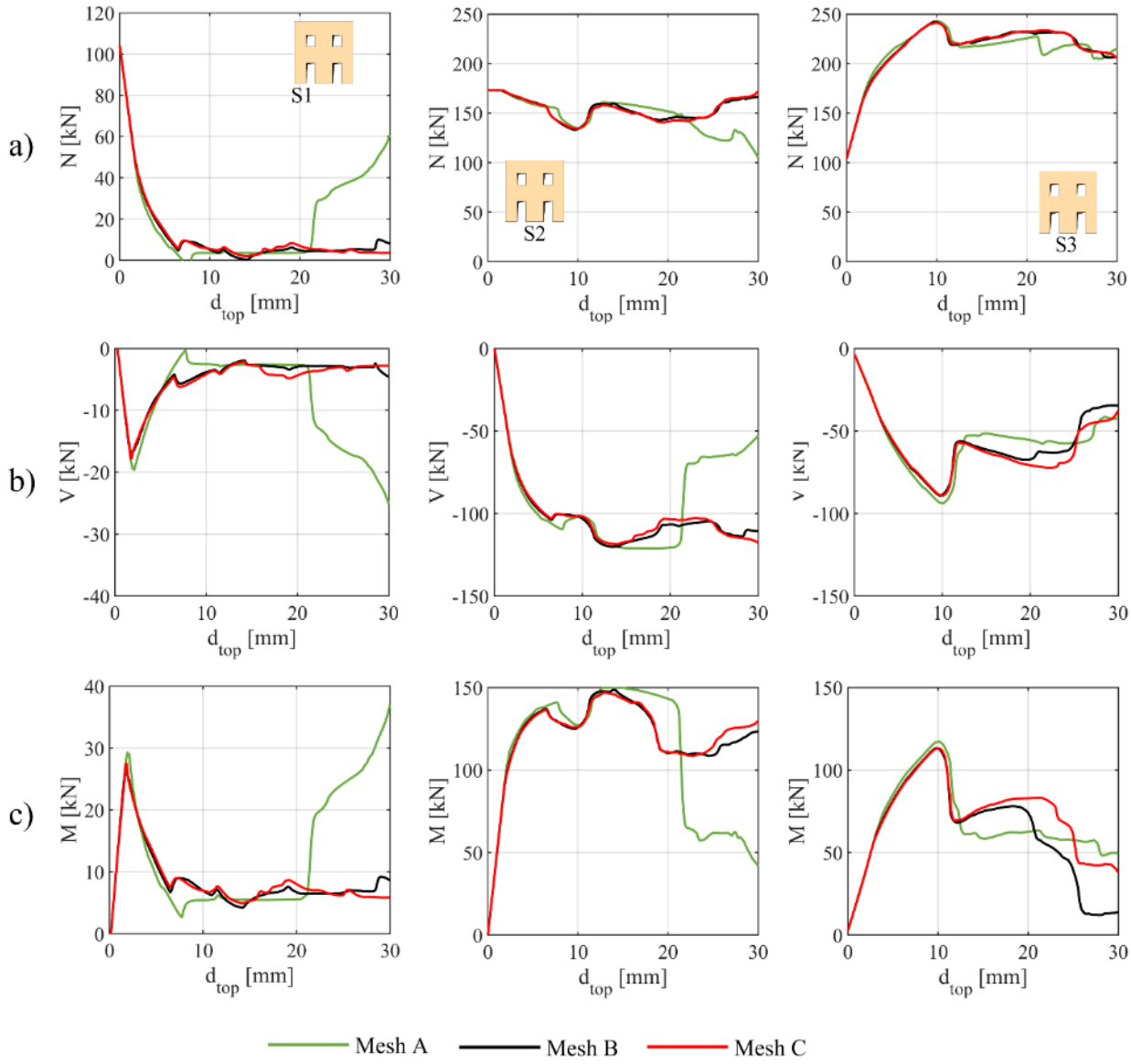

Figure A.7 - Evolution of the generalized forces at the three base sections (S1, S2, S3) of the wall (a) normal force; b) shear force; c) bending moment): comparison between the FE models of the regular wall associated to the three adopted mesh dimensions

All the results above illustrated show that *Mesh A* is actually too coarse to provide a good description of the wall response. On the contrary, the FE model associated to *Mesh B* provides robust results when considering the parameters that are adopted as the reference solution in the comparisons with the EF models. Indeed, it is able to provide results which are almost coincident to the ones obtained with a more refined mesh (*Mesh C*), guaranteeing, at the same time, a significantly reduced computational burden. For this reason, this mesh dimension was adopted in the FE model of the regular wall (section 3.3) and then also in the case of the irregular walls (Chapter 4).

Moving to the investigation of the effect of the viscosity parameter on the structural response obtained for the regular wall, the sensitivity analyses were conducted by varying the values adopted for η (see the

Table in Figure A.8) and by fixing all the other parameters of the numerical model, including the mesh size (in particular, the one came out from the above illustrated study was employed). In the following Figure A.8 the global pushover curves obtained by considering 5 different values of the viscosity parameter are reported. It is possible to see that by progressively reducing the values of the viscosity parameter the obtained pushover curves present differences which are definitely not negligible, especially when moving from Analysis 1 (η = 0.001) to Analysis 3 (η =0.0001). In particular, these differences involve the stiffness degradation in the ascending branch of the curve (which is more significant the lower is the value of η), the peak strength (that decreases as η reduces) and also the softening phase (which becomes more pronounced when adopting lower values of η). However, the curve obtained by further reducing η (Analysis 4 - η = 0.00001) is substantially similar in terms of initial response and peak strength to the one obtained with a higher value of the viscosity parameter (Analysis 3 - η =0.0001), with only slight differences in the post-peak phase.

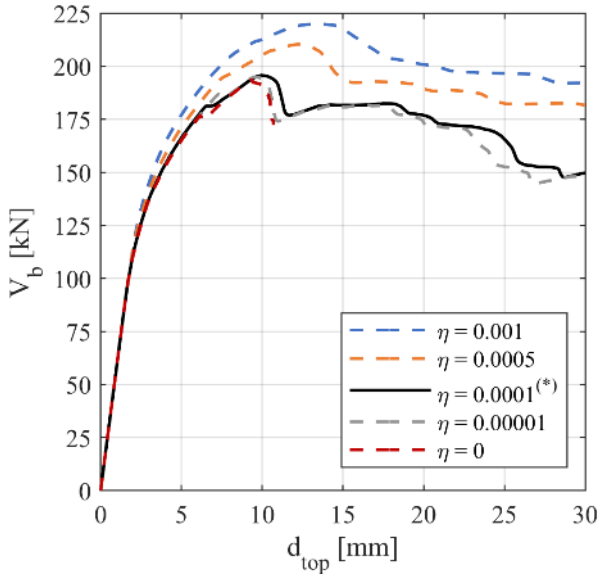

Analysis	η	Time required (°)
Analysis 1	0.001	00:56:53
Analysis 2	0.0005	01:14:02
Analysis 3(*)	0.0001	01:50:24
Analysis 4	0.00001	02:40:27
Analysis 5	0	Diverged

(o) on a desktop computer equipped with a processor Intel® Core™ Duo CPU E8400 @ 3.00 GHz and 4.00 GB RAM

Figure A.8 – Results in terms of global pushover curves of the sensitivity analyses on the viscosity parameter η performed on the regular wall and times required by each numerical analysis (*) analysis finally adopted as reference).

Furthermore, when the viscosity parameter is set equal to zero (Analysis 5), which means that the viscoplastic regularization is not working at all, the obtained curve is again similar to the one obtained through Analysis 3 and 4, where slightly higher values of η are adopted. However, in this case convergence problems arise after the reaching of the maximum strength, thus making not possible to catch the softening phase of the curve.

In Figure A.9 the tensile damage contour plots (d_{top} = 20 mm) emerging from the analyses performed with three different values of η (Analysis 1,3 and 4, see Table in Figure A.8) are illustrated. From these pictures it is possible to see that the three damage scenarios are consistent in terms of propagation of tensile cracks and type of damage occurred in the different masonry portions. However, it is evident that the effect

of the viscoplastic regularization (which is higher the higher is the value of η adopted in the analysis) is to emphasize the smearing of the tensile cracks over the masonry material.

In particular, by looking at the results obtained in case of Analysis 1(η = 0.001) it is possible to see that the tensile cracks tend to interest a slightly larger portion of the material with respect to what happens in the other two analyses here considered. Indeed, both in case of Analysis 3 and analysis 4, where the value of η is lower (η = 0.0001 and η = 0.00001, respectively) a higher localization of the tensile damage is observed, which indicates a better result of the analysis. This effect is particularly evident by looking, as for example, at the shear crack occurring in the right pier at the ground floor. In addition, the damage pattern obtained from Analysis 3 is substantially the same as the one emerging from Analysis 4, thus confirming what previously observed in terms of global pushover curves. This further confirms that the results obtained from these two analyses are totally comparable, which means that the adoption of η = 0.0001 or η =0.00001 does not significantly change the final outcome, except for the time required for the analysis (see the table in Figure A.8).

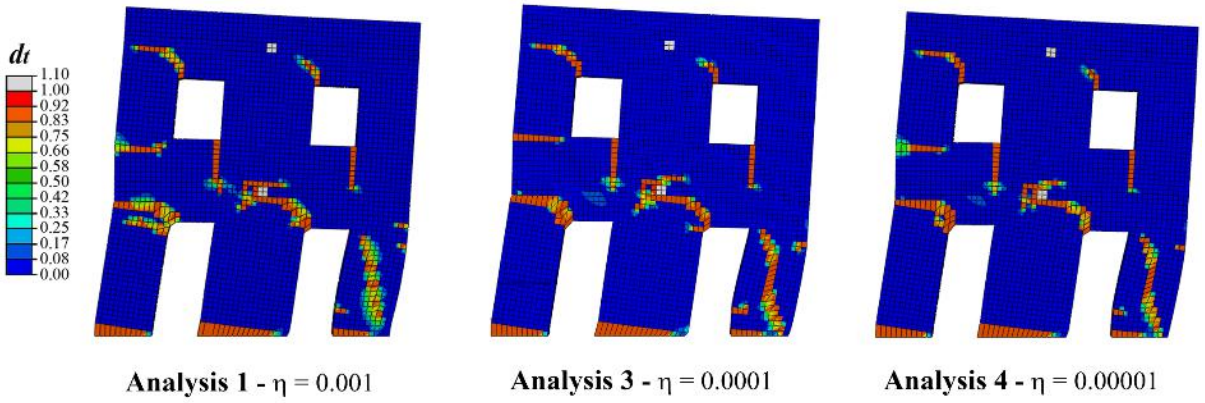

Figure A.9 – Results of the sensitivity analyses on the viscosity parameter η in terms of tensile damage contour plots (d_{top} = 20 mm) detected in the regular wall.

Concluding, the results of the sensitivity analyses now illustrated show that the adoption of a viscosity parameter η equal to 0.0001 allows to obtain a good compromise between accuracy, good convergence and time required by the numerical analyses. This value has been therefore adopted as reference for all the performed analyses.

APPENDIX B

B - DETERMINATION OF THE "CRITICAL" AXIAL LOAD RATIO

When adopting an Equivalent Frame approach the modelling is faced at the structural element scale, and the failure of masonry panels is described through specific strength criteria associated to the failure type which may occur (mainly shear or flexural failures). These failure criteria are in general functions of the geometry of the panel, of the mechanical properties of masonry and of the applied axial load.

Within this framework, the compression rate associated to the transition between a prevailing shear failure and a prevailing flexural failure is referred to in the following as the "critical" axial load ratio $(\sigma/f_c)_{CR}$; the determination of such value is interesting with reference to the modelling rule proposed in Chapter 5 (section 5.1, equation 5.1).

In particular, once defined the criteria to adopt for describing the shear and the flexural failure of masonry panels, the exact value of σ_{CR} (which normalized to f_c leads to $(\sigma/f_c)_{CR}$), can be analytically evaluated by equating their analytical expressions. In the following, it is assumed to adopt in case of shear failure the criterion proposed by Turnšek and Cačovic (1971) with the modification introduced in Turnšek and Sheppard (1980), which describes the diagonal shear failure, and in case of flexural failure the rule proposed in the Italian building code (NTC08), as summarized in Figure B.1.

Shear strength

$$V_s = \frac{1.5\tau_0 Bt}{b}\sqrt{1+\frac{\sigma}{1.5\tau_0}}$$

Flexural strength

$$V_f = \frac{\sigma B^2 t}{2}\left(1-\frac{\sigma}{0.85 f_c}\right)\frac{1}{H_0}$$

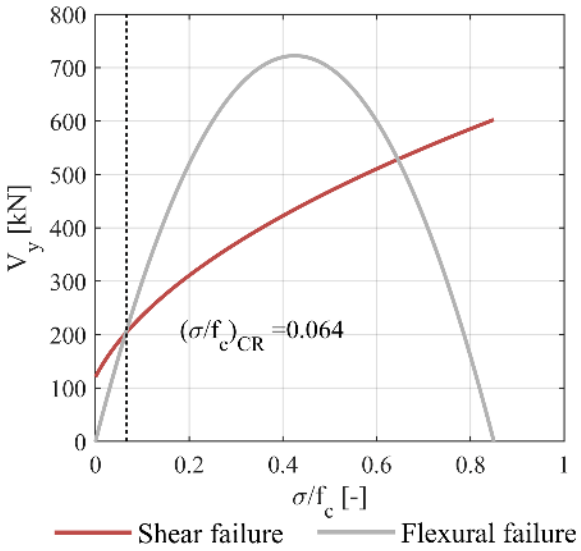

Figure B.1 – Failure criteria adopted as reference and associated failure domain for a given masonry panel with the identification of the value of $(\sigma/f_c)_{CR}$.

With reference to the formulae reported in Figure B.1, B and t are the width and the thickness of the panel, σ the mean normal stress acting on the cross section of the panel, f_c the masonry compressive strength, τ_0 the masonry shear strength, H_0 the shear span ($H_0 = H$ for the cantilever scheme and $H_0 = H/2$ for the fixed-fixed scheme, being H the height of the panel), b: shape factor depending on the aspect ratio $\lambda = H/B$ of the panel; according to MIT (2009): b = 1.5 for $\lambda \geq 1.5$, b=1 for $\lambda \leq 1$ and $b = \lambda$ in the other cases.

By looking at the strength domain obtained for a given panel through the application of these two failure criteria (Figure B.1), it is possible to see that there are two intersection points between the associated curves, corresponding to two different values of σ/f_c. However, it is worth noting that, since in almost all the cases the masonry panels included in the common masonry buildings are subjected to compression rates not so high and, in general, quite far from the ultimate compressive strength of the material, the point of most interest for what usually concerns the analysis of the behaviour of masonry panels is the minimum between these two values, as indicated with the dashed vertical line in Figure B.1. Therefore, in the following the attention is focused on the description of the procedure for the analytical determination of this specific value.

By equating the analytical formulae of the two strength criteria the following equation is obtained (equation B.1), where the unknown is σ_{CR} (i.e. the mean normal stress acting on the cross section of the panel that leads to the intersection between the two examined failure criteria):

$$\frac{\sigma_{CR}B^2t}{2}\left(1-\frac{\sigma_{CR}}{0.85f_m}\right)\frac{1}{H_0}=\frac{1.5\tau_0Bt}{b}\sqrt{1+\frac{\sigma_{CR}}{1.5\tau_0}} \qquad (B.1)$$

First of all, with the aim to remove the square root in the factor on the right-hand side, the square of both members is done, thus leading to equation B.2:

$$\left[\frac{\sigma_{CR}B^2t}{2}\left(1-\frac{\sigma_{CR}}{0.85f_c}\right)\frac{1}{H_0}\right]^2=\left[\frac{1.5\tau_0Bt}{b}\sqrt{1+\frac{\sigma_{CR}}{1.5\tau_0}}\right]^2 \qquad (B.2)$$

It is recalled that in this way a new equation is obtained which has the same roots of the starting equation but for which, in general, also further roots are possible; for this reason, it will be necessary, at the end, to impose specific acceptability conditions on the obtained solutions.

By expanding the left-hand and the right-hand sides, equation B.2 becomes:

$$\left(\frac{\sigma_{CR}B^2t}{2H_0}\right)^2+\left(\frac{{\sigma_{CR}}^2B^2t}{2\cdot 0.85f_cH_0}\right)^2-2\cdot\frac{\sigma_{CR}B^2t}{4H_0}\cdot\frac{{\sigma_{CR}}^2B^2t}{0.85f_cH_0}=\left(\frac{1.5\tau_0Bt}{b}\right)^2\left(1+\frac{\sigma_{CR}}{1.5\tau_0}\right) \qquad (B.3)$$

By further expanding both members:

$$\left(\frac{\sigma_{CR}B^2t}{2H_0}\right)^2+\left(\frac{{\sigma_{CR}}^2B^2t}{2\cdot 0.85f_cH_0}\right)^2-\frac{2{\sigma_{CR}}^3B^4t^2}{4\cdot 0.85f_c{H_0}^2}=\left(\frac{1.5\tau_0Bt}{b}\right)^2+\left(\frac{1.5\tau_0Bt}{b}\right)^2\frac{\sigma_{CR}}{1.5\tau_0} \qquad (B.4)$$

Then, after regrouping the terms containing $\sigma_{CR,}$ the following equation is obtained*:*

$$\left(\frac{B^2t}{2H_0\cdot 0.85f_c}\right)^2{\sigma_{CR}}^4-2\frac{(B^2t)^2}{(2H_0)^2 0.85f_c}{\sigma_{CR}}^3+\left(\frac{B^2t}{2H_0}\right)^2{\sigma_{CR}}^2-\frac{1.5\tau_0(Bt)^2}{b^2}\sigma_{CR}-\left(\frac{1.5\tau_0Bt}{b}\right)^2=0 \qquad (B.5)$$

which is a quartic (fourth degree polynomial) equation with real coefficients where the unknown is σ_{CR}.

Through a proper substitution of the coefficients, equation B.5 can be rewritten as follows, which is the form of a general quartic equation:

$$a_1{\sigma_{CR}}^4 + a_2{\sigma_{CR}}^3 + a_3{\sigma_{CR}}^2 + a_4\sigma_{CR} + a_5 = 0 \qquad (B.6)$$

where:

$$a_1 = \frac{(B^2t)^2}{0.85f_c(2H_0)^2}; \qquad (B.7)$$

$$a_2 = -2\frac{(B^2t)^2}{(2H_0)^2 0.85f_c} \qquad (B.8)$$

$$a_3 = \left(\frac{B^2t}{2H_0}\right)^2 \qquad (B.9)$$

$$a_4 = \frac{1.5\tau_0(Bt)^2}{b^2} \qquad (B.10)$$

$$a_5 = -\left(\frac{1.5\tau_0 Bt}{b}\right)^2 \qquad (B.11)$$

In the following, the formulae which are necessary in order to solve an equation of this type are presented. In particular, when considering a general quartic equation in the form:

$$a_1x^4 + a_2x^3 + a_3x^2 + a_4x + a_5 = 0 \qquad (B.12)$$

its four roots x_1, x_2, x_3, x_4 can be obtained by applying a method (developed by the mathematician L. Ferrari – published in 1545 (Fathi et al (2012)) based on the idea to convert the quartic into a depressed quartic (i.e. without the cubic term) by a simple change of variables; then, the method leads, through a series of passages, to a resolvent cubic of the quartic equation. At this point, by using the formulae for solving quadratic and cubic equations it is possible to obtain the final solutions of the original quartic equation (see *Encyclopedia of Mathematics* in the references for further details).

In the following, the final explicit formulae obtained for the four roots of the initial quartic equation by applying this procedure are provided (equations B.13 and B.14):

$$x_{1,2} = \frac{a_2}{4a_1} - Q \pm \frac{1}{2}\sqrt{-4Q^2 - 2p + \frac{S}{Q}} \qquad (B.13)$$

$$x_{3,4} = -\frac{a_2}{4a_1} + Q \pm \frac{1}{2}\sqrt{-4Q^2 - 2p - \frac{S}{Q}} \qquad (B.14)$$

where p and S are the coefficients of the second and of the first degree, respectively, in the associated depressed quartic:

$$p = \frac{8a_1a_3 - 3{a_2}^2}{8{a_1}^2}; \qquad (B.15)$$

$$S = \frac{{a_2}^3 - 4a_1a_2a_3 + 8{a_1}^2a_4}{8a^3} \qquad (B.16)$$

and where:

$$Q = \frac{1}{2}\sqrt{-\frac{2}{3}p + \frac{1}{3a_1}\left(\Delta_0 + \frac{q}{\Delta_0}\right)} \qquad (B.17)$$

$$\Delta_0 = \sqrt[3]{\frac{s + \sqrt{s^2 - 4q^3}}{2}} \qquad (B.18)$$

with:

$$q = 12a_1a_5 - 3a_2a_4 + {a_3}^2 \qquad (B.19)$$

$$s = 27a_1{a_4}^2 - 72a_1a_3a_5 + 27{a_2}^2 - 9a_2a_3a_4 + 2{a_3}^3 \qquad (B.20)$$

By applying the formulae from (B.13) to (B.20), taking into account that in our case the expressions for the coefficients a_1, a_2, a_3, a_4 and a_5 are those indicated in equations from B.7 to B.11, it is possible find the values of σ_{CR} which satisfy the initial equation (equation B.5). Then, in order to obtain $(\sigma/f_c)_{CR}$ it is sufficient to normalize it to f_c.

It is worth noting that, given the general quartic equation with real coefficients expressed as in equation B.6, the nature of its roots is mainly determined by the sign of its discriminant Δ, which can be expressed as follows:

$$\begin{aligned}\Delta = {} & 256{a_1}^3{e_5}^3 - 192{a_1}^2a_2a_4{a_5}^2 - 128{a_1}^2{a_3}^2{a_5}^2 + 144{a_1}^2a_3{a_4}^2a_5 - 27{a_1}^2{a_4}^4 + 144a_1{a_2}^2a_3{a_5}^2 - \\ & + 6a_1{a_2}^2{a_4}^2a_5 - 80a_1a_2{a_3}^2a_4a_5 + 18a_1a_2a_3{a_4}^3 + 16a_1{a_3}^4a_5 - 4a_1{a_3}^3{a_4}^2 - 27{a_2}^4{a_5}^2 + \\ & 18{a_2}^3a_3a_4a_5 - + 4{a_2}^3{a_4}^3 - 4{a_2}^2{a_3}^3a_5 + {a_2}^2{a_3}^2{a_4}^2 \end{aligned} \qquad (B.21)$$

This may be refined by considering the signs of two other polynomials *P* and *D*:

$$P = 8a_1a_3 - 3{a_2}^2 \qquad (B.22)$$

$$D = 64{a_1}^3a_5 - 16{a_1}^2{a_3}^2 + 16a_1{a_2}^2a_3 - 16{a_1}^2a_2a_4 - 3{a_2}^4 \qquad (B.23)$$

The possible cases for the nature of the roots are as follows (Rees (1922)):

- if $\Delta < 0$ then the equation has two distinct real roots and two complex conjugate non-real roots;
- if $\Delta > 0$:
  - if $P < 0 \wedge D < 0$ the all four roots are real and distinct;
  - if $P > 0 \vee D > 0$ then there are two pairs of non-real complex conjugate roots;
- if $\Delta = 0$ then (and only then) the polynomial has a multiple root; the different possibilities about the nature of the four roots in this case are discussed in detail in Rees (1922).

After having computed the four roots of the quartic equation according to the formulae expressed in B.13 and B.14, it is necessary, as aforementioned, to impose specific acceptability conditions on the obtained solutions. In particular, by remembering that the solution σ_{CR} we are looking for has to be real, positive and also lower than the maximum compressive strength of masonry multiplied for the coefficient 0.85 (on the

basis of the criterion adopted for the flexural failure, see Figure B.1), these conditions can be expressed as follows:

$$\sigma_{CR} \in \mathbb{R} \quad \wedge \quad \sigma_{CR} > 0 \ \wedge \ \sigma_{CR} < 0.85 f_c \qquad \text{(B. 24)}$$

If, by imposing such conditions, two acceptable solutions can be found, they represent the two intersection points between the functions associated to the strength criterion for shear failure and to the one for flexural failure. According to what explained before, among these two points the one of our interest is the one corresponding to the first intersection (see Figure B.1); therefore, in these cases a further condition that has to be imposed is to choose the minimum between the two acceptable solutions.

However, it is also possible that only one acceptable solution can be found or that no one of the computed roots fulfils all the required conditions. In particular, the first case refers to the limit situation in which the curve associated to the shear failure intersects the one associated to the flexural failure only in one point (tangent curves), while the second one refers to the situation in which the two curves do not intersect at all.

With reference to a practical example, some of the possible cases are shown in Figure B.2 and in Figure B.3, where both the representation of the quartic function $f(\sigma) = a_1\sigma^4 + a_2\sigma^3 + a_3\sigma^2 + a_4\sigma + a_5$, whose intersections with the *x* axis ($f(\sigma) = 0$) represent the solutions of equation B.5, and the associated situation in terms of strength domain of the examined panel are illustrated.

In particular, the two illustrated situations refer to a panel with the same geometry and boundary conditions (B = 5.18 m, t= 0.25m, H=2.85m, cantilever boundary condition) and in which only the shar strength of masonry is changed (f_c =6.2 MPa): in the first case, referred to in the following as "Panel 1" (Figure B.2) τ_0 = 0.167 MPa, while in the second case, referred to in the following as "Panel 2", τ_0= 0.367 MPa..

By examining the case of Panel 1, illustrated in Figure B.2, the representation of $f(\sigma)$ clearly shows that in this case there are four real roots (i.e. the crossings of the *x* axis), and thus no complex roots; indeed, as reported in the graph, Δ>0, D<0, P<0. However, only two of them fulfil the imposed acceptability conditions (equation B.24), which are individuated in the graph through the area highlighted with the red filling. These two acceptable solutions represent the two intersection points between the shear and the flexural failure criteria that define the strength domain, as shown in Figure B.2-b; among them, the point of our interest is the minimum (which is indicated in this Figure with the dashed vertical line).

In the second case (Figure B.3, Panel 2), on the contrary, the graph of the quartic function shows that there are only two real roots (the other two are complex conjugates, indeed in this case Δ<0); moreover, among these two real roots, no one satisfies the acceptability conditions, since both of them are outside of the red filling, which represents the range of the acceptable solutions. When looking at the corresponding situation in the strength domain of the panel, it is possible to see that actually there are no intersection points between the two failure criteria, being the shear strength always higher than the flexural one, which therefore always prevails, whatever is the applied axial load.

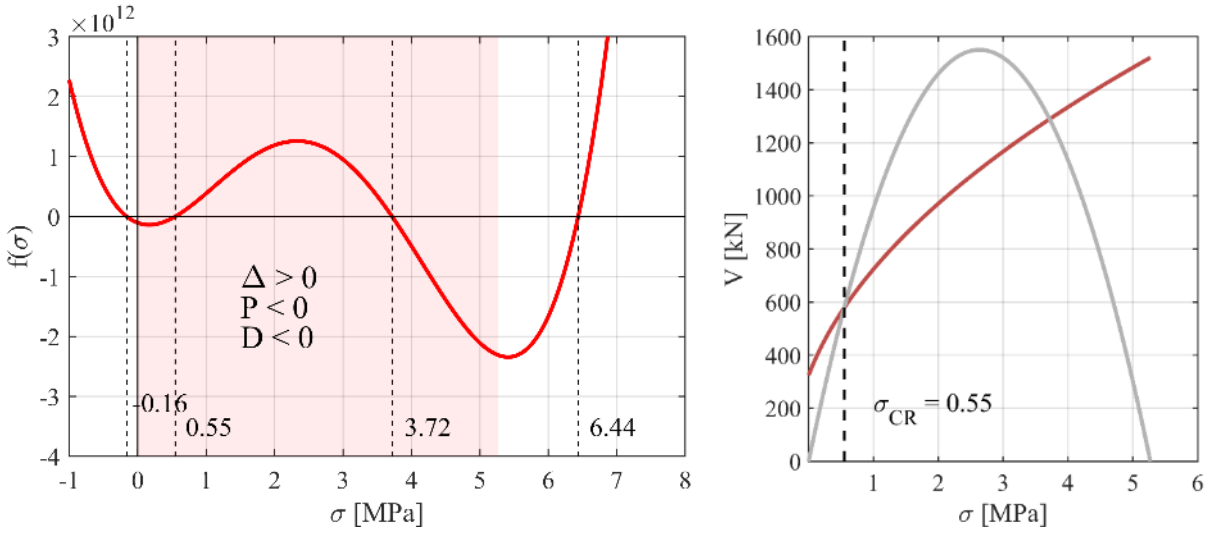

(a) **(b)**

Figure B.2 – Panel 1: representation of (a) the quartic function *f(σ)* and (b) of the strength domain *V-σ* of the examined panel, with the identification of the value of σ_{CR}.

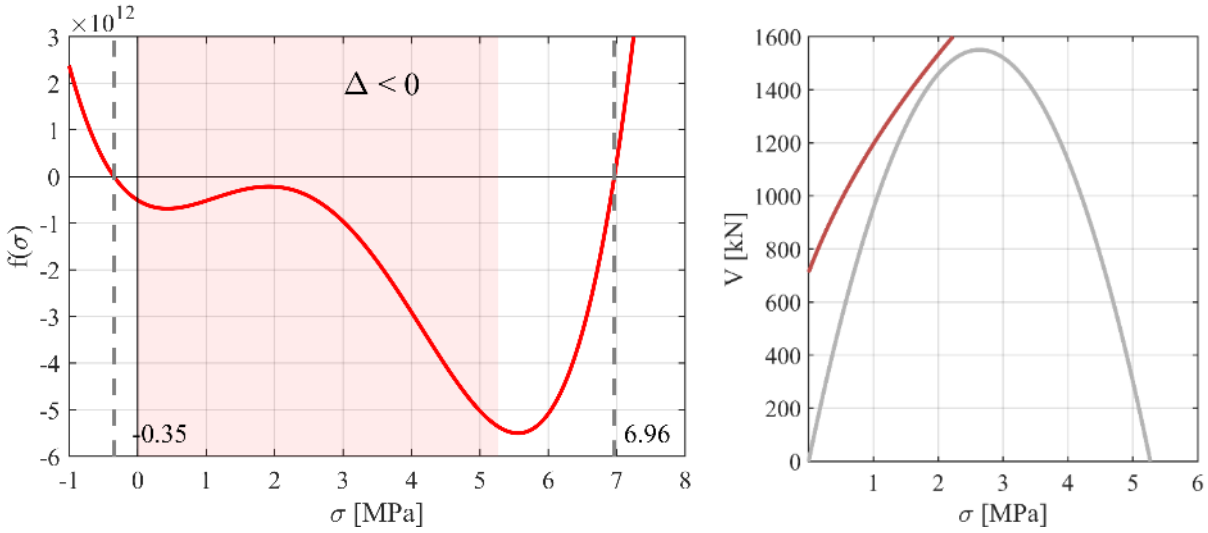

(a) **(b)**

Figure B.3 - Panel 2: representation of (a) the quartic function *f(σ)* and (b) of the strength domain *V-σ* of the examined panel (in this case σ_{CR} does not exist).

APPENDIX C

C - VERTICAL LOAD REDISTRIBUTION IN I-SHAPED FLANGED SECTIONS

Given a cantilever beam subjected to a combined vertical (*N*) and horizontal (*V)* load and provided with an I-shaped cross section (see Figure C.1), the analytical calculations illustrated in the following allows to evaluate the redistribution of the vertical load which occurs due to the application of the horizontal force between the three rectangular panels composing the cross section (the web and the two flanges).

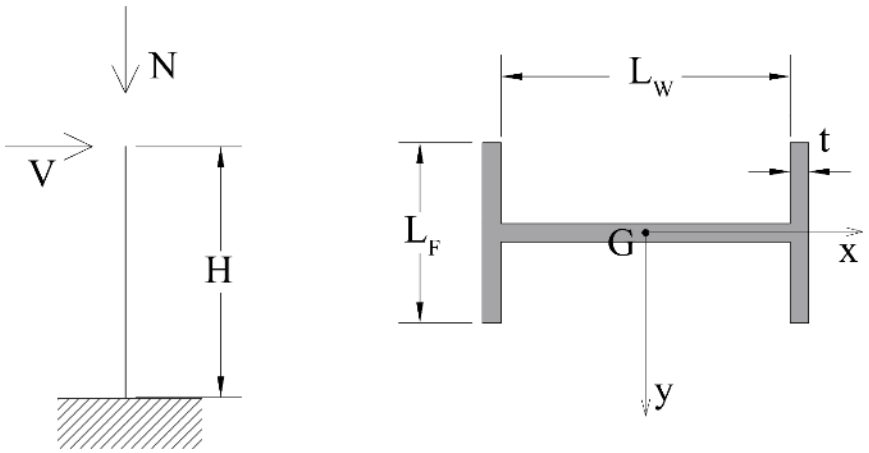

Figure C.1 – Cantilever beam subjected to combined vertical and horizontal loads and its I-shaped cross section

The objective is to reproduce the predictions of an EF model in which the flanged section, which may be representative of a URM panel with flanges, is modelled as three perfectly coupled rectangular section beams.

First of all, the axial load acting after the application of the dead loads in the web ($N_{W,dl}$) and in the flanges ($N_{F,dl}$) is computed as a function of the axial stiffness of each panel (this is the strategy adopted in the EF models when the hypothesis of perfect coupling between the panels is assumed), as indicated in the following equations, which refer to the values of N acting at the base section of each panel:

$$N_{F,dl} = N_{TOT}\frac{A_F}{A_W + 2A_F} \qquad (C.1)$$

$$N_{W,dl} = N_{TOT}\frac{A_W}{A_W + 2A_F} \qquad (C.2)$$

where N_{TOT} is the total axial load acting in correspondence of the base section of the structure (including the applied vertical load and the total weight of the structure), A_F is the area of the cross section of one flange and is the area of the cross section of the web.

Then, by assuming that the horizontal action is applied through an incremental procedure, since the axial load in the web is remains constant and equal to the initial value $N_{W,dl}$, for each incremental step *i* the redistribution of the axial load between the two flanges can by computed by assuming that the value of the applied horizontal load V_i at the i-th step is known.

In particular, for the I-shaped cross section reported in Figure C.1, the moment of inertia J_F of one flange (by considering only the transfer contribution) and the moment of inertia of the web panel *Jw* with respect to y-axis are:

$$J_W = \frac{1}{12} t {L_W}^3 \qquad (C.3)$$

$$J_F = L_F t \left(\frac{L_W}{2}\right)^2 = \frac{1}{4} t L_F {L_W}^2 \qquad (C.4)$$

Then, when considering the i-th step of the incremental procedure, the bending moment acting on one flange $M_{F,i}$ can be obtained as:

$$M_{F,i} = M_{TOT,i} \frac{J_F}{J_W + 2J_F} \qquad (C.5)$$

where $M_{TOT,i}$ is the total bending moment acting in the structure at step *i*; therefore, with reference to the base section of the structure, it can be determined as:

$$M_{TOT,i} = V_i H \qquad (C.6)$$

However, $M_{F,i}$ can be expressed also as the product of the axial load variation occurring in one flange with respect to $N_{F,dl}$, ($\Delta N_{F,i}$) multiplied for its distance with respect to the centroid G of the section:

$$M_{F,i} = \Delta N_{F,i} \frac{L_W}{2} \qquad (C.7)$$

By equating the two expressions of $M_{F,i}$ (equations C.5 and C.7) and by substituting $M_{TOT,i}$ with the expression in equation C.6 it is possible to make explicit the value of ΔN_{Fi}:

$$\Delta N_{F,i} = \frac{2V_i H}{L_W} \cdot \frac{J_F}{J_W + 2J_F} \qquad (C.8)$$

By substituting C.3 and C.4 and by doing further simplifications:

$$\Delta N_{F,i} = \frac{2V_i H}{L_W} \cdot \frac{\frac{1}{4} t L_F {L_W}^2}{\frac{1}{12} t {L_W}^3 + 2 \cdot \frac{1}{4} t L_F {L_W}^2} = \frac{6V_i H L_F L_W}{{L_W}^3 + 6L_F {L_W}^2} = \frac{6V_i H L_F}{{L_W}^2 + 6L_F L_W} \qquad (C.9)$$

Therefore, the axial load variation acting in one flange at the i-th incremental step can be expressed as:

$$\Delta N_{F,i} = \frac{6V_i H L_F}{{L_W}^2 + 6L_F L_W} \qquad (C.10)$$

Concluding, by considering that in one of the flange the axial load increases an in the other it decreases, the value $N_{F,i}$ of the vertical load acting on the two flanges of the I-shaped cross section at the i-th incremental step of the application of the horizontal load *V* can be evaluated as:

$$N_{F,i} = N_{F,dl} \pm \Delta N_{F,i} = N_{F,dl} \pm \frac{6V_i H L_F}{{L_W}^2 + 6L_F L_W} \qquad (C.11)$$

LIST OF SYMBOLS AND ACRONYMS

Symbol	Unit	Description
b	[-]	Shape factor associated to the shear stress distribution in the mid-section of a masonry panel
B	[L]	Width of a masonry panel
d_c	[-]	Damage variable accounting for compressive damage (CDP Model)
d_t	[-]	Damage variable accounting for tensile damage (CDP Model)
$d_{top,n}$	[L]	d_{top} corresponding to a n% reduction of V_{max} detected from the pushover curve of the FE model
d_{top}	[L]	Top displacement (in a masonry wall: horizontal displacement of the top floor; in a masonry panel: horizontal displacement of the top section)
$d_{u,s}$	[L]	Ultimate displacement of the equivalent bilinear curve
E_c	[F/L^2]	Concrete Young modulus
E_m	[F/L^2]	Masonry Young modulus
E_s	[F/L^2]	Steel rebars Young Modulus
E_0	[F/L^2]	Young modulus of the undamaged material (CDP Model)
f_c	[F/L^2]	Masonry compressive strength
$f_{c,hd}$	[F/L^2]	Masonry compressive strength in the horizontal direction
f_{cc}	[F/L^2]	Concrete compressive strength
f_{ch}	[F/L^2]	Uniaxial compressive stress at the point of initial yield (CDP Model)
f_{cu}	[F/L^2]	Residual uniaxial compressive strength at the end of the softening branch
f_t	[F/L^2]	Masonry tensile strength
f_{tc}	[F/L^2]	Concrete tensile strength
f_{tu}	[F/L^2]	Residual uniaxial tensile strength at the end of the softening branch
f_{ys}	[F/L^2]	Steel rebars yielding strength
G_m	[F/L^2]	Masonry shear modulus
h_{eff}	[L]	Pier effective height
h_o	[L]	Height of an opening in a pier panel
h_w	[L]	Interstorey height
h'	[L]	Geometrical parameter included in the formulation of h_{eff} according to Dolce (1991): distance between the midpoints of the lines connecting the vertices of two consecutive openings
H	[L]	Length of a masonry panel

H_0	[L]	Shear span (height of the point of contraflexure in an element)
K_c	[-]	Ratio of the second stress invariant on the tensile meridian to that on the compressive meridian at initial yield (CDP Model)
$k_{A,F}$	[F/L]	In a flanged section, the axial stiffness of the flange
$k_{A,W}$	[F/L]	In a flanged section, the axial stiffness of the web
$k_{F,F}$	[F/L]	In a flanged section, the flexural stiffness of the flange
$k_{F,W}$	[F/L]	In a flanged section, the flexural stiffness of the web
$k_{s,35}$	[F/L]	Secant stiffness corresponding to the 35% of V_{max}
$k_{s,70}$	[F/L]	Secant stiffness corresponding to the 70% of V_{max}
K_s	[F/L]	Stiffness of the equivalent bilinear curve
L_{eff}	[L]	Spandrel effective length
L_o/L_p	[-]	Ratio between the width of an opening in a pier panel and the width of the panel
M	[F]	Bending moment
N	[F]	Axial load
N_{app}	[F]	In a flanged section, axial load applied at the top section of the web
$N_{W,eff}$	[F]	In a flanged section, actual axial load acting in the mid-section of the web
$N_{W,dl}$	[F]	In a flanged section, axial load acting after the application of the vertical load in the web
R_k	[-]	Ratio between $k_{s,70}$ and $k_{s,35}$
S_a	[L/T^2]	Spectral acceleration
t	[L]	Thickness of a masonry panel
u	[L]	Horizontal displacement
v	[L]	Vertical displacement
V	[F]	Shear force
V_b	[F]	Base shear
V_f	[F]	Strength of a masonry panel with respect to flexural failure
V_{max}	[F]	Maximum base shear
V_s	[F]	Strength of a masonry panel with respect to shear failure
V_y	[F]	Maximum strength of a masonry panel
$V_{y,s}$	[F]	Maximum base shear of the equivalent bilinear curve
$V_{y\,tot}$	[F]	In a flanged section, maximum total base shear computed by considering the reaction forces at the base of the whole section (including flanges)
$V_{y,W}$	[F]	In a flanged section, maximum base shear computed by considering only the reaction forces associated to the web panel

Y_{LS}	[-]	Limit state function (for UPD and GC limit states)
w	[F/L^3]	Masonry specific weight
x_o/x_p	[-]	Ratio between the position of the centroid of an opening in a panel and the total length of the panel
β_{Ei}	[-]	Strength decay in an element at the attainment of the i^{th} DL
ε_c	[-]	Uniaxial compressive total strain (CDP Model)
ε_c^p	[-]	Uniaxial compressive plastic strain (CDP Model)
ε_c^{in}	[-]	Uniaxial compressive inelastic strain (CDP Model)
ε_{0c}^{el}	[-]	Uniaxial compressive elastic strain corresponding to the undamaged material (CDP Model)
ε_{cm}	[-]	Uniaxial compressive total strain corresponding to f_c
ε_{cm}^{in}	[-]	Uniaxial compressive inelastic strain corresponding to f_c
ε_{cu}	[-]	Uniaxial compressive total strain at the end of the softening branch
ε_{cu}^{in}	[-]	Uniaxial compressive inelastic strain at the end of the softening branch
ε_t	[-]	Uniaxial tensile total strain (CDP Model)
ε_t^p	[-]	Uniaxial tensile plastic strain (CDP Model)
ε_t^{in}	[-]	Uniaxial tensile inelastic strain (CDP Model)
ε_{0t}^{el}	[-]	Uniaxial tensile elastic strain corresponding to the undamaged material (CDP Model)
ε_{tu}	[-]	Uniaxial tensile total strain at the end of the softening branch
ε_{tu}^{in}	[-]	Uniaxial tensile inelastic strain at the end of the softening branch
η	[-]	Viscosity parameter (CDP Model)
θ	[-]	Drift in a masonry panel
θ_{Ei}	[-]	Drift threshold corresponding to the attainment of the i^{th} DL in an element
$\theta_{S,i}$	[-]	Drift threshold corresponding to the attainment of the ith DL (shear response)
$\theta_{F,i}$	[-]	Drift threshold corresponding to the attainment of the ith DL (flexural response)
Θ_{max}	[-]	Maximum interstorey drift
Θ_R	[-]	Roof drift
λ	[-]	Aspect ratio of a masonry panel
μ	[-]	Mean value of a parameter with respect to its defined range of variation
ν_c	[-]	Poisson's ratio of concrete
ν_s	[-]	Poisson's ratio of steel rebars

ν_m	[-]	Poisson's ratio of masonry
σ_c (σ_t)	[F/L^2]	Uniaxial compressive (tensile) stress (CDP Model)
σ_0	[F/L^2]	Average normal stress acting on the whole cross section of a masonry panel
$(\sigma/f_c)_{CR}$	[-]	Critical axial load ratio: compression level corresponding to the first intersection between the shear and flexural failure criteria defining the domain of a panel
$(\sigma/f_c)_{dl}$	[-]	Axial load ratio acting in a panel after the application of the dead loads
τ_0	[F/L^2]	Masonry shear strength
φ	[-]	Rotation
ψ	[°]	Dilatancy angle
ϵ	[-]	Smoothing parameter (CDP Model)

Acronyms:

CCLM	Continuum Constitutive Law Models
CDP	Concrete Damaged Plasticity
DIM	Discrete Interface Models
DL	Damage Level
EDP	Engineering Demand Parameter
EF	Equivalent Frame
FE	Finite Element
GC	Global Collapse
IM	Intensity Measure
LS	Limit State
LSA	Linear Static Analysis
MBM	Macro Block Models
NLDA	Non-Linear Dynamic Analysis
NLSA	Non-Linear Static Analysis
PGA	Peak Ground Acceleration
r.c.	Reinforced concrete
SB	Simple Building
SEM	Structural Element Models
SSWP	Strong Spandrel Weak Pier
UPD	Usability-Preventing Damage
URM	Unreinforced Masonry
WSSP	Weak Spandrel Strong Pier

ACKNOWLEDGMENTS

The author gratefully acknowledges the financial support to the research provided by the Italian Network of Seismic Laboratories (ReLUIS), in the frame of the 2014 – 2018 ReLUIS III Projects (Topic: *Masonry* Structures) and of the joint research program DPC-ReLUIS-EUCENTRE 2014–2018, funded by Presidenza del Consiglio dei Ministri – Dipartimento della Protezione Civile. Moreover, the author acknowledges the whole research group that participated to the activities of Task 4.3- *Analysis of Benchmark Structures*, which, starting from 2014, has involved over the years several research units of different Italian universities: in addition to the University of Genoa - UniGE (Coord. S. Cattari), also the University of Pavia - UniPV (Coord. Prof. G. Magenes), the University of Chieti-Pescara - UniCH (Coord. Proff. E. Spacone and G. Camata), the University of Catania - UniCT (Coord. Prof. I. Caliò), the University of Naples – UniNA b/d (Coord. Proff. B. Calderoni and A. De Luca) and UniNA-c (Coord. Proff. C. Casapulla and F. Portioli), the University of Rome - UniRM3 (Coord. Prof. G. De Felice), the University of Venice - IUAV (Coord. by Prof. A. Saetta) and the University of Bologna - UniBO (Coord. by Prof. S. De Miranda).

The author acknowledges also the research group of the University of Bologna (Prof. G. Castellazzi, Prof. S. De Miranda and Ing. A.M. D'Altri), whose collaboration provided an important support for the development of the nonlinear Finite Element analyses, allowing to execute them by means of the software ABAQUS.

In these last pages I wish to thank all of them who, through their work, commitment and trust have allowed and helped the development and the realization of this thesis.

First of all, I wish to thank my supervisors, Prof. Sergio Lagomarsino and Prof. Serena Cattari, for the opportunity they gave me with this thesis and for the hours of discussion and review (sometimes fruitful and encouraging, other times hard and challenging) which fed in these years my passion and enthusiasm for research. Thanks to them and to their passion and dedication to work I learnt a lot in this period, including the humility to say "I don't know" ("*even if to understand is not possible, at least to know is necessary*").

Then, I wish to thank the external reviewers of the thesis, Prof. Jan Rots and Prof. Vincenzo Sepe, whose careful reviews and comments helped to improve the quality of this work.

A very special thank is for my beautiful and wonderful family, which gave me the possibility to reach this, for me important and (as those who were close to me in this period know very well) hard-earned achievement, providing me all the support I needed and, above all, helping me to find self-confidence and to believe in what I was doing.

A special thank is also for Alfonso, who was always with me, giving love, affection, comfort, support and all what I needed in the most difficult moments, making me smiling almost anytime, even when he himself was having hard time. Both him and my family helped me to grow up and gave me more than what I was able to give them; if I am who I am today, I owe a lot to them.

Also, these three (now almost four) years of PhD taught me a lot, both from a professional point of view, about work and research, extending and improving my knowledge on seismic engineering and masonry structures, and about life. I really liked my research topic and I wish to keep on dealing with these themes in my future work. However, I am aware that sometimes it is not possible to do what you like and wish; anyway, I am sure that this experience will be part of me forever, and I will always bring it in my heart.

At last, but non least, I would like to thank all my friends, the "historical" ones (especially Laura, Simona, Marika, Carola and Maria) and the ones I met during the last years. I also wish to say thank to all the colleagues and other PhD students of this department and of other universities, who accompanied me along the path, helping me when I had troubles in research and always available for both "technical discussions" and "coffee breaks".

All of you are and did a lot for me, and I have not enugh words to explain how much you are important in my life.